

**MEASURING AND MODELING
THE MECHANICAL PROPERTIES OF BICYCLE TIRES**

by

Andrew Erwin Dressel

A Dissertation Presented in
Partial Fulfillment of the
Requirements of the Degree of
Doctor of Philosophy
in Engineering

at

The University of Wisconsin-Milwaukee

May 2013

ABSTRACT

MEASURING AND MODELING

THE MECHANICAL PROPERTIES OF BICYCLE TIRES

by

Andrew Erwin Dressel

The University of Wisconsin-Milwaukee, 2013

Under the Supervision of Professor Adeeb Rahman

It has been shown that tire deformation can play an important role in the stability and handling of a bicycle. It is expected that an accurate understanding of tire behavior is necessary for correct understanding of rider behavior and that correct understanding of rider behavior is necessary for optimizing bicycle design. That certainly has been the case for motorcycles.

Several instances of published bicycle tire stiffness data exist, but they seldom agree with each other, do not all measure the same properties, and often are missing key pieces of test configuration data, such as tire size, rim width, inflation pressure, or vertical load.

In this project, three different test devices specific to bicycle tires were developed. Measured bicycle tire stiffnesses are presented for 14 different tires ranging from 22 to 50 mm wide, at inflation pressures from 2 to 11 bar (29 to 160 psi), under vertical loads from 304 to 731 Newtons (68 to 164 lb); for a total of about 120 different parameter combinations.

Normalized cornering stiffness was found to vary from below 0.15 to over 0.35, which is $\pm 40\%$ from the average, and normalized camber stiffness varies from below 0.0075 to over 0.015, which is $\pm 33\%$ from the average. Based on numerical simulations, this is more than sufficient to influence bicycle stability and handling.

Tires approach the camber stiffness necessary, without slip, for the net ground reaction force to be in the plane of the wheel, obeying the so-called tangent rule, but most tires with most inflation pressures and under most loads presented here fall below that.

A numerical model, based on an analysis developed by Rotta for slender toroidal tire cross sections in contact with the ground, was also developed to provide insight into how the tires generated the forces they do and attempt to predict them from simpler measurements.

Although actual values generated by the model do not exactly match measured values, the trends in contact patch size and lateral stiffness values generated do correspond well with measured data as parameters vary, such as inflation pressure, vertical load, and rim width.

© Copyright by Andrew Erwin Dressel, 2013

All Rights Reserved

DEDICATION

I dedicate this work to my wife, Anne Dressel, and my mom and dad, Ellen and Erwin Dressel, for their years of unwavering support and encouragement.

TABLE OF CONTENTS

ABSTRACT.....	i
DEDICATION.....	iv
LIST OF FIGURES	xvi
LIST OF TABLES.....	xxv
GLOSSARY	xxvii
LIST OF SYMBOLS	xxxiii
ACKNOWLEDGMENTS	xxxvii
EPIGRAPH.....	xxxix
CHAPTER 1 INTRODUCTION	1
1.1 Bicycle dynamics.....	1
1.1.1 The Whipple Model.....	1
1.2 The role of tires in bicycle dynamics.....	3
1.2.1 Previous physical testing.....	4
1.2.2 Previous numerical simulation.....	6
1.3 Problem Statement.....	6

1.4	Objectives	6
1.4.1	Additional contributions	7
1.4.2	Scope.....	7
1.4.3	Setting	8
CHAPTER 2 BACKGROUND		9
2.1	Tire coordinate system.....	9
2.2	Tire parameters	10
2.3	Tire mechanical properties.....	12
2.4	Camber stiffness and the “tangent rule”	13
2.5	Previous bicycle tire measurements.....	16
2.5.1	Roland, 1972-1973.....	18
2.5.2	Davis, 1975	19
2.5.3	Man and Kane, 1979	20
2.5.4	Kyle, 1987, 1988, 1995.....	20
2.5.5	Cole and Khoo, 2001	23
2.5.6	Cossalter, 2006.....	24

2.5.7	Sharp, 2008	25
2.5.8	Doria <i>et al.</i> , 2012	25
2.5.9	Motorcycle tires	26
CHAPTER 3 EXPERIMENTATION.....		29
3.1	Tires tested	29
3.2	Rims used.....	32
3.3	Wheels used	34
3.4	Pavement surface	34
3.5	Contact patch ink prints	35
3.6	Test devices.....	35
3.7	Test device number 1	37
3.7.1	Description.....	38
3.7.2	Contacts and force transmission	39
3.7.3	Forward speeds and actuation rates	41
3.7.4	Instrumentation	41
3.7.5	Advantages and disadvantages of design.....	42

3.8	Test device number 2	44
3.8.1	Geometry.....	45
3.8.2	Contacts and force transmission	49
3.8.3	Instrumentation	49
3.8.4	Uncertainty propagation.....	52
3.8.5	Forward speeds and actuation rates	52
3.8.6	Additional tests performed with device number 2.....	53
3.8.6.1	Radial stiffness	53
3.8.6.2	Static lateral stiffness.....	54
3.8.6.3	Decay length	55
3.8.7	Advantages and disadvantages to design.....	59
3.9	Test device number 3.....	60
3.9.1	Geometry.....	63
3.9.2	Actuation.....	64
3.9.3	Instrumentation	66
3.9.4	Uncertainty Propagation	69

3.9.5	Forward speeds and actuation rates	70
3.9.6	Advantages and disadvantages of design.....	71
3.10	Test data capture and processing	72
3.10.1	MATLAB®.....	72
3.10.2	Detection and subtraction of periodic noise in force data.....	76
3.10.3	Wheel lateral stiffness.....	80
3.10.4	Lateral force sensor misalignment	81
3.11	Other testing.....	81
3.11.1	Instron compression stiffness.....	81
3.11.2	Rate-dependent lateral stiffness	82
3.11.3	Stress relaxation	83
3.11.4	Decay length	84
3.11.5	Confirming slip angle during camber	86
3.12	Test protocols.....	88
3.12.1	Instrument warm up and calibration	88
3.12.2	Tire break in and warm up	88

3.12.3 Forward rolling rate 89

3.12.4 Test device angle actuation rate 89

3.12.5 Operating temperature 89

3.12.6 Steps for test device number 3 89

CHAPTER 4 EXPERIMENTAL RESULTS 91

4.1 Physical measurements 91

4.1.1 Ink prints of contact patch..... 91

4.1.1.1 Drum vs. Plate 93

4.1.2 Forces and moments 93

4.1.3 Lateral stiffness 94

4.1.4 Cornering stiffness 94

4.1.5 Camber stiffness..... 95

4.1.6 Self-aligning torque 95

4.1.7 Twisting torque 96

4.1.8 Pneumatic trail 96

4.1.9 Relaxation length, decay length, and relaxation distance 98

4.1.9.1	Decay length	100
4.1.9.2	Relaxation distance.....	106
4.1.10	Summary.....	108
4.2	Repeatability	112
4.3	Tire described as “radial” does not stand out	113
4.4	Physical measurements compared between three test devices	113
4.4.1	TU Delft drum vs. UWM cart.....	113
4.4.2	TU Delft drum vs. UWM flat track	114
4.5	Physical measurements compared to previous results	115
4.5.1	Doria <i>et al.</i> , 2012	117
CHAPTER 5 MODELING.....		119
5.1	Rotta’s model.....	120
5.2	Expanding Rotta’s model in 3D.....	131
5.3	Drums and disks.....	140
5.3.1	Drums.....	140
5.3.2	Disks	142

5.4	Contact patch ellipse	144
5.5	Calculating forces generated.....	145
5.6	Friction.....	145
5.7	Extending Rotta's model beyond the ends of the contact patch	146
5.8	Decay rate and length	150
5.9	Taut beam on an elastic foundation	154
5.9.1	Differential equation	154
5.9.2	Numerical implementation.....	154
5.9.3	Constants.....	155
5.9.3.1	Area Moment of Inertia	155
5.9.3.2	Modulus of Elasticity.....	156
5.9.3.3	Tension	156
5.9.4	Integration with Rotta model	156
CHAPTER 6 MODELING RESULTS.....		158
6.1	Model predictions	158
6.1.1	Contact patch	158

6.1.2	Sinkage.....	158
6.1.3	Stiffness.....	159
6.1.4	Tangent rule	160
6.2	Physical measurements compared to model predictions	161
6.2.1	Contact patch size and shape	162
6.2.2	Variation in stiffness with rim width	163
6.2.3	Variation in stiffness with tire arc length.....	164
6.2.4	Other stiffnesses.....	165
CHAPTER 7 DISCUSSION.....		167
7.1	Difficulties in the physical testing	167
7.1.1	Difficulty detecting edges of contact patch in ink prints	167
7.1.2	Difficulty in setting one angle to zero while second angle is swept.....	167
7.1.3	Flexibility.....	168
7.1.4	Headset bearing in test device number 3	168
7.1.5	Resonance	168
7.2	The difference between measured camber stiffness presented here and values from Padua published by Doria <i>et al.</i>	169

7.2.1	Reasons that the data presented here may be correct.....	169
7.2.2	Possible problems with the data presented here	170
7.2.3	Possible problems with the data presented by Doria <i>et al.</i>	170
7.3	Shortcomings of the model	171
7.3.1	Contact patch shape	171
7.3.2	Flatness and straightness of contact patch in cambered tire	171
7.3.3	The bending of a beam might not be the best analogy for the lateral deflection of an inflated bicycle tire.....	171
7.3.4	Difficulty with convergence	171
CHAPTER 8 CONCLUSIONS AND FUTURE WORK.....		172
8.1	Conclusions.....	172
8.1.1	Contributions.....	172
8.1.2	Tire properties should matter to bicycle stability and handling.....	173
8.1.3	Tangent rule for camber stiffness	174
8.1.4	Model fidelity.....	174
8.2	Future Work	175
8.2.1	Measuring	175

8.2.1.1	Measure sinkage directly	175
8.2.1.2	Measure contact patch pressure distribution	175
8.2.1.3	Measuring slip angle directly during camber to confirm camber force.....	175
8.2.2	Modeling.....	176
8.2.2.1	Extract analytical relationships from numerical model.....	176
8.2.2.2	Find proper model for lateral displacement of tire centerline for non-zero slip and camber angles	176
8.2.2.3	Enhance numerical model of bicycle with force generating tires	176
8.2.3	Validation of tire properties by measuring bicycle behavior	177
8.2.4	Design a better bicycle tire	177
APPENDIX A	Individual Tire Contact Patches	178
APPENDIX B	Individual Tire Test Results	285
APPENDIX C	MATLAB® Source Code for Numerical Model.....	443
APPENDIX D	Additional Test Device Designs	467
BIBLIOGRAPHY	468
CURRICULUM VITAE	473

LIST OF FIGURES

Figure 1-1: Schematic of the Whipple Model bicycle.....	1
Figure 1-2: Stability eigenvalues for benchmark bicycle from FastBike motorcycle simulation[3] and from JBike6[4] bicycle simulation.	2
Figure 1-3: Root-locus plot from FastBike[3] showing wobble mode becoming unstable as tire cornering stiffness varies.	5
Figure 2-1: Tire coordinate system.....	10
Figure 2-2: Radial cross section of rim and rim with bicycle tire.	11
Figure 2-3: Flattened carcass, with outer tread up and inside down, showing arc length s_0 and thickness t of a bicycle tire.....	11
Figure 2-4: A wheel in camber and net ground reaction force orientation.....	14
Figure 2-5: Plot of true value vs. approximation of the normalized camber stiffness that produces a net ground reaction force parallel to the plane of the wheel.....	16
Figure 2-6: Normalized cornering and camber forces from previous bicycle tire measurements.....	17
Figure 2-7: Roland, 1973, "typical bicycle tire at a vertical load of 75 pounds".	19

Figure 2-8: Cole and Khoo "bicycle tyres, size 20" diameter and 2.125" tyre width". ...	23
Figure 2-9: Cossalter bicycle tire data	24
Figure 2-10: Doria <i>et al.</i> , 2012, tire force data.	25
Figure 2-11: Summary of motorcycle tire normalized cornering and camber stiffness ..	28
Figure 3-1: Test devices 1-3	29
Figure 3-2: Ink prints of contact patches of a Maxxis radial.	35
Figure 3-3: Schematic of test device number 1.	40
Figure 3-4: Plane view of test device number 1 showing external lateral forces.	41
Figure 3-5: Raw force data captured from test device number 1.....	42
Figure 3-6: Photograph of final test device number 1 on its concrete track.....	43
Figure 3-7: Photograph of test device number 2. The forward pivot is on the far left, and the flat-top chain track is under the wheel on the right.....	45
Figure 3-8: Schematic of test device number 2.	46
Figure 3-9: Test device number 2 flat-top chain with anti-skid tape also showing one rim displacement sensor contacting the braking surface of the wheel rim.	47
Figure 3-10: Finite Element Analysis of test device 2 frame deformation under load....	48

Figure 3-11: Raw force and displacement data captured from test device number 2.....	51
Figure 3-12: Radial stiffness of a Bontrager All Weather 28-622 mm tire at various inflation pressures and under vertical loads of 30.3, 42.2, 54.2, 78.5, 102.7, and 114 lb.....	54
Figure 3-13: Measuring static lateral stiffness with test device number 2.	55
Figure 3-14: Measuring tire centerline lateral deflection beyond the contact patch.	56
Figure 3-15: Measuring tire centerline lateral deflection on a HED Cycling carbon tri-spoked wheel.....	57
Figure 3-16: Paired displacement sensors.	58
Figure 3-17: Schematic diagram of test device number 3	62
Figure 3-18: Photograph of test device number 3.....	64
Figure 3-19: Camber angle actuator installed on test device number 3 before non- skid tape is installed on the drum.....	65
Figure 3-20: Instrumentation before installation on test device number 3.....	66
Figure 3-21: Vertical load created by attaching additional masses to frame of test device number 3.....	69
Figure 3-22: Inflation pressure gauge integrated with tire pump.	69
Figure 3-23: Raw force and displacement data captured from test device number 3.....	71

Figure 3-24: Formatted data from test device number 3.	76
Figure 3-25: Fourier analysis of raw lateral force data showing signal from irregularity in the Roller shoe wheels and the Inline skate wheel.	77
Figure 3-26: Power spectrum of force data collected from test device number 2. The vertical blue line at 83 inches is the circumference of the bicycle wheel with tire.	78
Figure 3-27: Raw data and data corrected by subtracting out the signal with period equal to the circumference of the bicycle wheel.....	79
Figure 3-28: Vertical deflection vs. vertical load showing rate-independent hysteresis.....	82
Figure 3-29: Lateral stiffness dependence on lateral displacement rate.....	83
Figure 3-30: Force and displacement vs. time demonstrating stress relaxation.	84
Figure 3-31: Schwalbe Durango 23-622 at 80 psi. Undeformed above, and deformed by a 25 lb localized lateral load (by red cord at far right) below.....	85
Figure 3-32: Bontrager All Weather 28-622 at 50 psi. Undeformed above, and deformed by a 25 lb localized lateral load (by red cord at far right) below.....	86
Figure 3-33: Extracting slip angle from sequential video frames.....	87
Figure 3-34: Contact-less optical sensor for measuring sideslip angle.	88

Figure 4-1: Contact patch on the plate analyzed in MATLAB®. 91

Figure 4-2: Contact patch on the drum analyzed in MATLAB®..... 92

Figure 4-3: Comparison of vertical load divided by measured contact patch area vs. inflation pressure. The assumption that they are equal is represented by the black diagonal line. 92

Figure 4-4: Lateral stiffness for Schwalbe Big Apple 55-622 on rim of width 18.7 mm at 3 bar (44 psi) and under 450 N (55 kg, 121 lb) vertical load..... 94

Figure 4-5: Cornering stiffness for Schwalbe Big Apple 55-622 on rim of width 18.7 mm at 3 bar (44 psi) and under 450 N (55 kg, 121 lb) vertical load..... 94

Figure 4-6: Camber stiffness for Schwalbe Big Apple 55-622 on rim of width 18.7 mm at 3 bar (44 psi) and under 450 N (55 kg, 121 lb) vertical load..... 95

Figure 4-7: Self-aligning torque stiffness for Schwalbe Big Apple 55-622 on rim of width 18.7 mm at 3 bar (44 psi) and under 450 N (55 kg, 121 lb) vertical load..... 95

Figure 4-8: Twisting torque stiffness for Schwalbe Big Apple 55-622 on rim of width 18.7 mm at 3 bar (44 psi) and under 450 N (55 kg, 121 lb) vertical load..... 96

Figure 4-9: Pneumatic trail for Schwalbe Big Apple 55-622 on rim of width 18.7 mm at 3 bar (44 psi) and under 450 N (55 kg, 121 lb) vertical load..... 97

Figure 4-10: Summary of pneumatic trail for all Schwalbe Big Apple tests.....	98
Figure 4-11: Recorded tire centerline lateral deflection non-zero and zero slip angles.	101
Figure 4-12: Recorded tire centerline lateral deflection for non-zero slip angle.....	101
Figure 4-13: Recorded tire centerline lateral deflection for zero camber and slip angles.	102
Figure 4-14: Tire centerline lateral displacement with zero slip and zero camber angles.	103
Figure 4-15: Tire centerline lateral displacement with non-zero slip angle.	104
Figure 4-16: Tire centerline lateral displacement with non-zero camber angle.	105
Figure 4-17: Tire centerline lateral displacement with non-zero slip and camber angles.	106
Figure 4-18: Graph of data from Table 4-3	112
Figure 4-19: Comparing results from test device 2 at UWM and test device 3 at TU Delft.	115
Figure 4-20: Comparison of all known bicycle tire normalized cornering stiffnesses at 1 degree slip angle.....	116
Figure 4-21: Comparison of all known bicycle tire normalized camber stiffnesses at 10 degree camber angle.	117

Figure 5-1: Rotta model coordinate system. The y-axis is into the page.....	121
Figure 5-2: Geometric parameters of tire cross section.	122
Figure 5-3: Geometric parameters of cambered and displaced tire cross section.	124
Figure 5-4: Geometric parameters of one side of cambered and displaced tire cross section.....	126
Figure 5-5: Plot of sample tire cross section calculated using the Rotta model.	131
Figure 5-6: Location of lowest point on tire, first point to touch ground, on cambered tire.....	132
Figure 5-7: Side view of wheel dimensions as the tire is pressed into the ground.....	133
Figure 5-8: Side view of tire calculated with 3D Rotta model showing flat contact patch.	134
Figure 5-9: Flatness of contact patch developed by the 3D Rotta model.	135
Figure 5-10: Straightness of contact patch developed by the 3D Rotta model (part 1).	136
Figure 5-11: Plots showing horizontal and vertical displacement of contact patch.	137
Figure 5-12: Straightness of contact patch developed by the 3D Rotta model (part 2).	138
Figure 5-13: 3D representation of cambered tire modeled by Rotta.	139
Figure 5-14: Side view schematic of wheel and drum.....	141

Figure 5-15: Rotta model contact patch fitted with an ellipse.....	144
Figure 5-16: Geometric argument that displaced tire cannot have constant radius.....	148
Figure 5-17: Continuously varying radius in laterally displaced tire cross sections.	149
Figure 5-18: Comparison of constantly varying radius vs. two discrete radii.....	149
Figure 5-19: Rotta model of tire with 2 mm lateral displacement blended smoothly back to undisplaced over nearly half the wheel circumference with a 0.993 relaxation rate.....	151
Figure 5-20: Graph showing lateral displacement of each cross section, the lateral and vertical forces generated in each cross section, and the average lateral force applied in the contact patch for a tire with 2 mm lateral displacement blended smoothly back to undisplaced over nearly half the wheel circumference with a 0.993 relaxation rate.	152
Figure 5-21: Graph showing same values and for same tire as Figure 5-21 , but now with a 0.5° slip angle. Note similarity with measured lateral displacement shown in Figure 4-15	153
Figure 5-22: Graph showing same values and for same tire as Figure 5-21 , but now with a 10° camber angle. Note similarity with measured lateral displacement shown in Figure 4-16	154
Figure 5-23: Lateral displacement, in blue, of a taut beam on an elastic foundation subject to a concentrated load at the midspan.....	155

Figure 5-24: Camber force results of iteration between Rotta model and model of taut beam on elastic foundation.	157
Figure 6-1: Lateral force vs. sinkage for constant inflation pressure and constant vertical load.....	159
Figure 6-2: Plot of Rotta model prediction of % agreement with tangent vs. ratio of tire radius over rim width.....	161
Figure 6-3: Comparison of contact patch area vs. length and width between Rotta model and measured physical tires.	163
Figure 6-4: Variation in lateral stiffness with rim width, measure and modeled.	163
Figure 6-5: Rims and their widths used to generate data in Figure 6-4	164
Figure 8-1: Alternate test device design for TU Delft drum.....	467

LIST OF TABLES

Table 2-1: Kyle, 1987, Small tire.....	21
Table 2-2: Kyle, 1988, Moulton 17x1¼	22
Table 3-1: Tires tested on third device at TU Delft.	30
Table 3-2: Dimensions of tires tested, published, measured, and calculated.....	31
Table 3-3: Rims on which the tires were mounted for stiffness testing.....	33
Table 3-4: Sensors for test device number 2.....	50
Table 3-5: Sensors for test device number 3.....	67
Table 3-6: Published wheel lateral stiffnesses	80
Table 4-1: Summary of contact patch length, width, and area for plate and drum.....	93
Table 4-2: Correlations between stiffnesses.	110
Table 4-3: True size and normalized lateral stiffnesses for four different 37-622 tires mounted on the same 18.7 mm wide rim.	111
Table 4-4: Example of repeatability of results from test device number 3.....	112
Table 4-5: Comparing results of test device 1 at UWM[37] and test device 3 at TU Delft.....	113

Table 4-6: Comparison of stiffness found by Doria <i>et al.</i> at Padua with tires tested on device number 3 at TU Delft.	118
Table 5-1: Sample calculations for tire cross section geometry (part 1).	122
Table 5-2: Sample calculations for tire cross section geometry (part 2).	124
Table 5-3: Sample calculations for tire cross section geometry (part 3).	125
Table 5-4: Sample calculations for tire cross section geometry (part 4).	129

GLOSSARY

bead: the portion of the tire in contact with the rim.

bead seat diameter: twice the distance parallel to the midplane of the wheel from the center of its axle to where the tire bead contacts the rim. Governed by ISO standard 5775.

Calspan Corporation: a science and technology company located in Buffalo, NY that specializes in aerospace and transportation research and testing. According to their website, “Calspan is known the world over for its unrivaled tire test capability. Our machine can handle all types of tires, including truck, passenger, utility, race and even aircraft tires.”[1] It was previously called the Cornell Aeronautical Laboratory.

camber angle: the angle between the midplane of the wheel and the vertical.

camber force: the portion of lateral force generated in the contact patch due to non-zero camber angle. Also known as camber thrust.

camber stiffness: the ratio of camber force over camber angle.

capsize mode: one of two fundamental modes predicted by the Whipple model and named by Sharp, in which the bike slowly leans and steers to one side until the side of the bike contacts the ground.

contact patch: the portion of the tire in contact with the pavement.

cornering force: the portion of lateral force generated in the contact patch due to non-zero slip angle.

cornering stiffness: the ratio of cornering force over slip angle.

DataStudio: the software that accompanies PASCO® instrumentation hardware.

decay length: the length along the circumference of the wheel over which a lateral displacement of the tire centerline decays to $1/e$ ($\sim 36.8\%$) of its original magnitude (Pacejka's relaxation length σ [2]).

FastBike: numerical simulation software designed for motorcycles. Its capabilities include modeling frame, fork, wheel, rider, and tire flexibility.[3]

JBike6: software to calculate the stability eigenvalues of the Whipple model for any geometry and mass distribution and at a range of forward speeds.[4]

LabVIEW: software by National Instruments for data acquisition.

lateral force: the force generated in the contact patch in the ground plane perpendicular to the intersection of the wheel midplane and the ground plane.

lateral stiffness: the ratio of lateral force over lateral displacement.

lean angle: the angle between the midplane of the bike and the vertical. Also known as roll angle.

MATLAB®: software by MathWorks for numerical computing.

PASCO®: brand of instrumentation offering plug-and-play simplicity.

pneumatic trail: the distance by which the net lateral force trails behind the center of the contact patch.

rim: the outer edge of the wheel that facilitates mounting a tire, characterized by two parallel flanges to support tire beads.

self-aligning torque: the moment about the vertical axis through the contact patch associated with non-zero slip angle. Tends to rotate wheel so that it points in the direction in which it is rolling.

sliding: the movement of tire tread relative to the pavement with which it is in contact. Requires the friction coefficient between the two materials to be less than infinite.

slip or side slip: the phenomenon by which a tire can roll in a direction other than the direction in which it is pointed due solely to deformation even if friction is infinite and no part of the tire tread slides relative to the pavement.

slip angle: the angle between wheel midplane and velocity vector (usually expressed in degrees). At low angles, this is primarily due to tire deformation and occurs even if friction is infinite. In practice, there may be a zone, starting at the rear of the contact patch in which sliding between the tire tread and pavement may occur. This sliding zone increases in size toward the front of the contact patch as slip angle increases or friction decreases.

steer angle: the angle between the midplane of the bike and the midplane of the steered wheel.

steering axis: the axis about which the steered wheel rotates.

steering axis angle: the angle between the steering axis and the horizontal, in the case of bicycles, which have steering axis angles near 70° , or the vertical, in the case of motorcycles, which have steering axis angles near 25° .

relaxation rate: rate at which lateral deflection of tire centerline returns to zero.

relaxation distance: the distance long the pavement that a wheel rolls after a step change in slip angle before for the lateral force reaches $1 - 1/e$ ($\sim 63.2\%$) of its steady-state value (also Pacejka's relaxation length σ , [2] and Cossalter's L [5]).

relaxation length: either the decay length or the relaxation distance, depending on author and context.

rim width: the distance between parallel flanges of rim that contact the tire beads.

sinkage: the distance that an uncambered wheel moves vertically toward ground plane relative to when it is just touching ground plane and undeformed as it supports a load.

tire: the layer at the outer edge of a wheel that protects the wheel, provides suspension, and improves traction. Usually implemented by enclosing a compressed gas in a flexible torus.

tire arc radius: radius of circular arc formed by a radial cross section of the tire.

tire arc length: the arc length of a radial cross section of the tire, from bead to bead.

tire size: the manufacturer's stated size: approximately the diameter of a radial cross section.

trail: the distance by which the center of the contact patch of the steered wheel trails behind the intersection of the steering axis and the pavement.

TU Delft: Delft University of Technology, located in Delft, The Netherlands. Location of two, side-by-side 2.5 meter tire testing drums and home institution of Prof. Hans Pacejka, author of *Tire and Vehicle Dynamics* and the so-called "Magic Formula" empirical tire model.

twisting torque: the moment about a vertical axis through the contact patch associated with non-zero camber angle. Tends to rotate the wheel toward the direction in which it is cambered.

UWM: University of Wisconsin-Milwaukee. Location of test devices 1 and 2.

weave mode: one of the two fundamental modes predicted by the Whipple model and named by Sharp in which the bike alternately steers and then rolls from side to side.

wheel: a disk that enables a vehicle to roll over ground surface.

Whipple model of a bicycle: simplified model that consists of just four rigid bodies connected by frictionless revolute joints: rear frame, front frame, rear wheel, and front wheel. The wheels have knife edges that roll without slip.[6]

wobble mode: a fundamental mode of bikes that is not predicted by the Whipple model and is characterized by a relatively high frequency oscillation of the steering assembly about the steering axis. This mode, also known as shimmy, is only predicted by bike models that have some type of compliance: in the frame, in the tires, or between a rider and the frame.[7][8]

LIST OF SYMBOLS

- x For entire tire: coordinate axis forward from the contact patch at intersection of ground plane and wheel plane. For just tire cross section: coordinate axis to right in plane of section. See **Figure 2-1**.
- y For entire tire: coordinate axis to the right from the contact patch, perpendicular to x and in ground plane. For just tire cross section: coordinate axis normal to plane of section and into page. See **Figure 2-1**.
- z For entire tire: coordinate axis up from the contact patch, perpendicular to both x and y axes. For just tire cross section: coordinate axis straight up and in plane of section. See **Figure 2-1**.
- v velocity vector, direction in which the center of the wheel is moving. See **Figure 2-1**.
- α slip angle: the angle between wheel x -axis and velocity vector v (usually expressed in degrees). See **Figure 2-1**.
- γ camber angle: the angle between the vertical and the wheel midplane (Rotta's σ) (usually expressed in degrees). See **Figure 2-1**.
- F_x rolling resistance force. See **Figure 2-1**.
- F_y cornering force if due to non-zero slip angle, or "camber thrust" if due to non-zero camber angle. See **Figure 2-1**.

- M_α self-aligning torque: moment about vertical axis through the contact patch associated with non-zero slip angle α . See **Figure 2-1**.
- M_γ twisting torque: moment about vertical axis through the contact patch associated with non-zero camber angle γ . See **Figure 2-1**.
- M_z total torque about z -axis generated in contact patch: sum of self-aligning torque and twisting torque. See **Figure 2-1**.
- C_{F_y} lateral stiffness: ratio of lateral force F_y over lateral displacement δ_h .
- C_{F_α} cornering stiffness: ratio of lateral force F_y over slip angle α .
- C_{F_γ} camber stiffness: ratio of lateral force F_y over camber angle γ .
- w rim width (usually expressed in mm). See **Figure 2-2**.
- r tire arc radius. Subscripts 0, 1, and 2 represent entire tire, left side bulge, and right side bulge, respectively (usually expressed in mm). See **Figure 2-2**.
- s tire carcass arc length: cross section arc length. Subscripts 0, 1, and 2 represent entire tire, left side bulge, and right side bulge, respectively (usually expressed in mm). See **Figure 2-3**.
- t thickness of the tire carcass. See **Figure 2-3**.
- θ angle swept by tire arc. Subscripts 0, 1, and 2 represent entire tire, left side bulge, and right side bulge, respectively ($s = r \theta$) (usually expressed in radians).

- φ angle of tire cross section from vertical (bottom) cross section (usually expressed in radians).
- h height of rim: vertical distance between the lowest point on the undeflected tire to the lowest point on the uncambered rim (usually expressed in mm). See **Figure 5-2**.
- R Wheel radius, height of axle above undeflected tire (usually expressed in mm).
- R_e Effective wheel radius, height of axle above ground plane (usually expressed in mm).
- δ displacement of contact patch with respect to rim, or rim with respect to contact patch, depending on context. Subscripts w , v , h , represent in the plane of the wheel, vertically with respect to the ground, and horizontally with respect to the ground, respectively. $\delta_v = R - R_e$.
- e horizontal distance to the edge of the contact patch from the center of the tire. Subscripts 1 and 2 represent left side, and right side, respectively.
- p inflation pressure.
- dy distance between tire cross sections.
- dS contribution to horizontal force from one cross section.
- dN contribution to vertical force, normal to ground plane, from one cross section.
- μ coefficient of friction between the tire and the pavement.

- i relaxation rate at which deflection of tire centerline returns to zero.
- ℓ decay length (Pacejka's relaxation length σ).
- κ relaxation distance (also Pacejka's relaxation length σ , and Cossalter's L).
- E modulus of elasticity of the tire carcass.
- I area moment of inertia of the tire carcass.
- T circumferential tension in the tire carcass.
- k foundation stiffness rate on a beam.
- f force rate on a beam.
- u lateral displacement of a beam.

ACKNOWLEDGMENTS

Many individuals generously gave time and advice which helped me with this research.

From UWM, I would like to thank my advisor Prof. Adeeb Rahman for his nearly infinite patience and support; Prof. Chris Papadopoulos who recruited me back to academia; Rahim Reshadi, who hosted me in his lab; John, Mark, and Ray in the machine shop; Betty Warras, who always shepherded my paperwork flawlessly; Andrew Fronek, who helped with testing one summer; Kyle Jacobson, who provided the HED Cycling tri-spoke carbon wheel; Prof. Konstantin Sobolev, who helped me with concrete admixtures; and Ali Shrih, my ever-dependable lab, teaching, and degree-seeking partner. I would also like to thank Prof. Anoop Dhingra, Prof. Rani El-Hajjar, and Prof. Habibollah Tabatabai, who served on my final committee; and Prof. Yaoyu Li, and Prof. George Papaioannou, who served on my initial committee.

From TU Delft, I would like to thank Prof. Arend Schwab for inviting and hosting me, Dr. Edwin de Vries and Dr. Jodi Koojiman for help with tire testing, Prof. Hans Pacejka for help with the design, Karwan Hamamurad for help in the machine shops, Jos van Driel for help with the instrumentation, Jurian for welding, Hans, and the guys in the other two machine shops I visited.

From industry, I would like to thank Dr. Jim Brendelson, who suggested applying motorcycle dynamics understanding to bicycles, and Dr. Tim Hunter at Harley Davidson; Mike Weber at Trek, who provided tires to test; Harry Peppelman at Vredestein, who

provided tires to test; Rob van Regenmortel at Batavus, who provided wheels to test with; Prof. Matteo Massaro, Prof. Roberto Lot, and Prof. Vittore Cossalter at Padua University, for granting access to FastBike; Landelijk Bureau Fietsersbond, for funding some of the tire testing; and Damon Rinard, who wrote “stiffness is among the easiest properties to measure so go for it!”

I would also like to thank the less-easily categorized Tom Muro, who first suggested graduate school to me; Prof. Andy Ruina, who provided me with the first opportunity to study bicycles; Dr. Jim Papadopoulos, who suggested the design used in test devices 2 and 3, the Rotta model, served on my committee, and patiently discussed all aspects of tire theory, experimentation, and implications. I also thank Prof. Robin Sharp for encouraging me to publish my initial results without delay; Dr. Jason Moore for blazing a trail in Delft and providing key historical documents; Dan Boehm, Mark Kapij, and Mike Miller for numerous technical consultations; Roger Hajny, at the MSOE machine shop; Erwin Dressel, for flying out to Milwaukee in December to help me machine parts; and Dr. Anne Dressel, my wife, for continuously reminding me that a negative result is still a result.

EPIGRAPH

"If we knew what it was we were doing,
it would not be called research, would it?"

-- Albert Einstein[9]

CHAPTER 1

INTRODUCTION

1.1 Bicycle dynamics

1.1.1 The Whipple Model

The Whipple model of a bicycle is simplified and idealized to facilitate the derivation of equations of motion without losing key dynamic characteristics, such as self-stability. It consists of four rigid bodies, two wheels, a rear frame, and a front fork. These are connected by three frictionless revolute joints, a steering axis between the frame and fork and two wheel axles. The wheels have knife edges and roll without slip on a flat surface.[6]

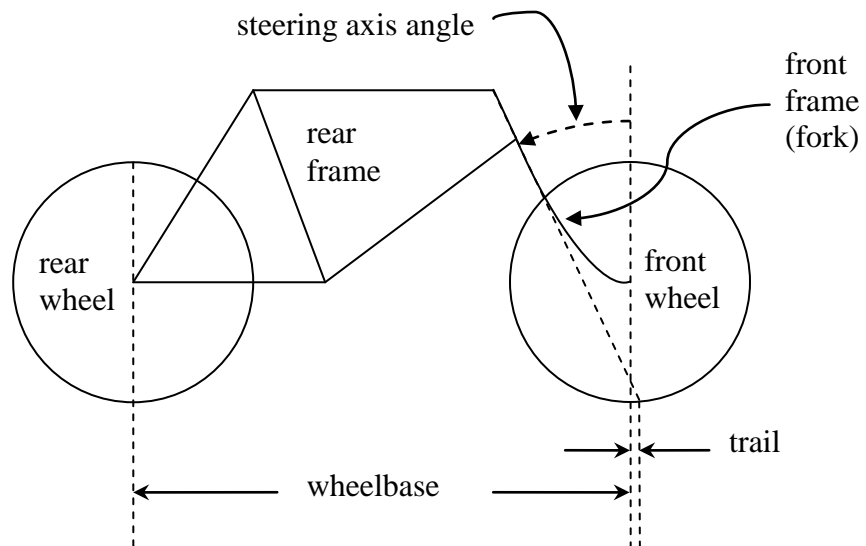


Figure 1-1: Schematic of the Whipple Model bicycle.

The linearized model can be characterized by as few as 17 parameters specifying geometry and mass distribution. The linearized equations have just four state variables, lean angle, steer angle, and their rates, and so can be used to generate four stability eigenvalues, [6] as shown in the right half of **Figure 1-2**.

A bike is self stable at any forward speed at which all its real eigenvalues and the real components of its complex eigenvalues are negative. The bike whose eigenvalues are shown in the right half of **Figure 1-2** is self-stable at forward speeds between about 4.5 and 6.0 m/s.

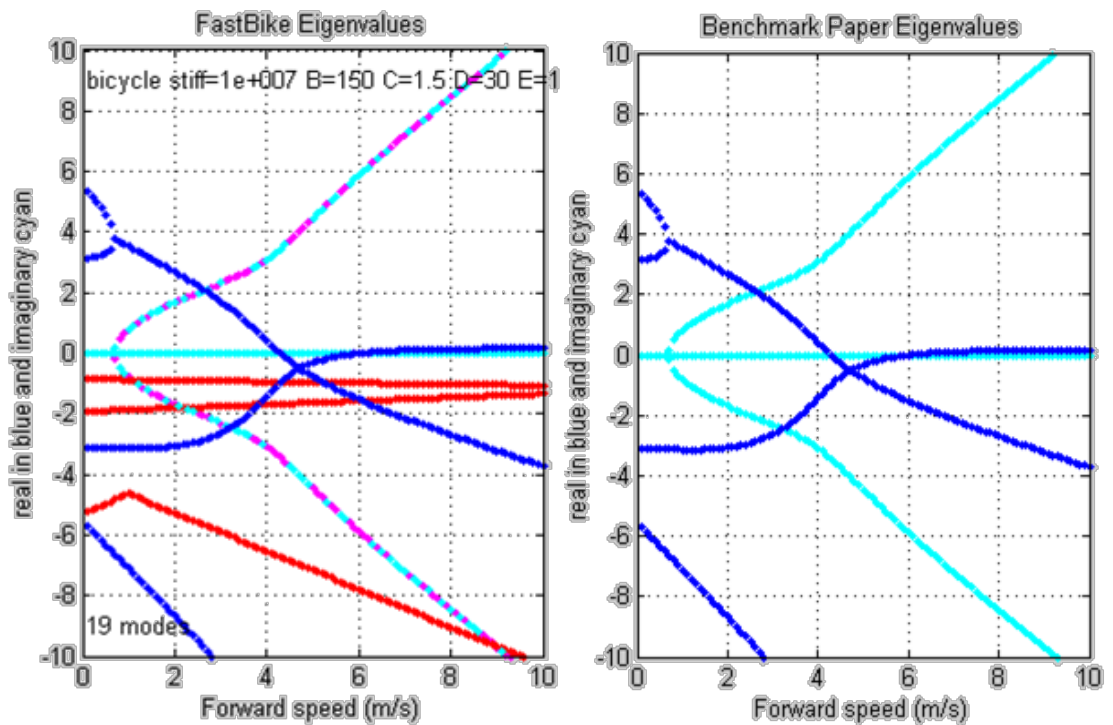


Figure 1-2: Stability eigenvalues for benchmark bicycle from FastBike motorcycle simulation[3] and from JBike6[4] bicycle simulation.

1.2 The role of tires in bicycle dynamics

It has been shown that the Whipple model of a bicycle, with knife-edge wheels that roll without slip, accurately predicts behavior under certain low-speed and controlled circumstances,[10] however it has also been shown that tire deformation can play an important role in more complicated or higher-speed behavior, such as wobble, a well-documented mode not predicted by the Whipple model.[8] Tires are also understood to play a large role in motorcycle dynamics.[11]

When Robin Sharp, author of the landmark 1971 paper, “The Stability and Control of Motorcycles”, in which he coins “wobble” and “weave” for two of the fundamental oscillatory modes of bikes,[12] turned his attention to the control of bicycles, he selected bicycle tire data published by Roland.[13] Sharp used an average of the reported cornering stiffness, rejected the reported camber stiffness for being unreasonable, and had to estimate the missing torque stiffness about the vertical axis, M_z . Never-the-less, he reports that “one of the low-speed modes is much altered” and “oscillatory behavior of the bicycle may be predicted badly by the [Whipple model] and rather better by including [tire] slip, as is well known in the case of motorcycles.”[7]

It is also expected that an accurate understanding of tire behavior is necessary for correct understanding of rider behavior, and that a correct understanding of rider behavior is necessary for optimizing bicycle design. That certainly is the case for motorcycles.

1.2.1 Previous physical testing

In 2006, Kooijman, *et al.*, showed that the Whipple model does accurately predict weave frequencies for an uncontrolled and very light bicycle at speeds below 6 kph.[10] At 19.2 kg on tires inflated to 3.5 bar, and assuming an even weight distribution, the test bicycle would have a contact patch area under each tire of about 270 mm². The measured contact patches presented in Appendix B have a ratio of length to area of about 0.076, so a contact patch of 270 mm² would be about 20 mm long, or just under 20% of the average contact patch measured. That is about equivalent to a 32 kg (70 lb) rider on a 6 kg (14 lb) bike with tires inflated to 7 bar (100 psi), which is not a likely combination in the real world. Most real tires support a larger load and so have larger contact patches. Thus the influence of tires was minimized. A more-likely 68 kg (150 lb) rider on a 9 kg (20 lb) bike at the same inflation pressure would have contact patches just about twice that size.

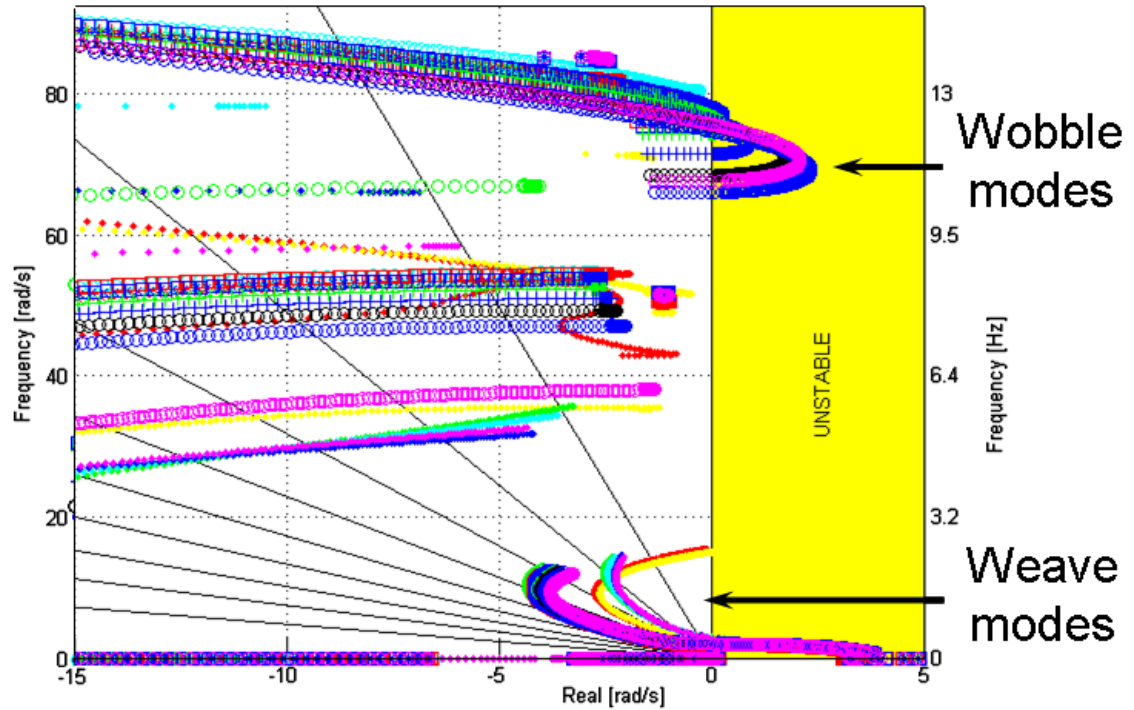


Figure 1-3: Root-locus plot from FastBike[3] showing wobble mode becoming unstable as tire cornering stiffness varies.

In 2012, Jason Moore, in his National Science Foundation (NSF)-funded Ph.D. dissertation, reports that in his attempts at bicycle and rider system identification, “the deficiencies are most likely due to un-modeled effects, with the knife-edge, no side-slip wheel contact assumptions being the most probable candidate.” He also notes that “as pointed out by many, in particular the motorcycle researchers, there is very good reason to question [the] assumption [of] knife-edge no side-slip wheels, especially when under a rider’s weight. Specifically, the Whipple model does not predict correct steer torque magnitudes required for a given steer angle and roll angle.”[14]

1.2.2 Previous numerical simulation

Simulations with FastBike,[3] using a bicycle model validated against a benchmark bicycle,[15] predict that small changes in tire stiffness can cause the wobble mode to transition from stable to unstable, as shown in **Figure 1-3**. The bicycle tire stiffnesses used were developed from existing motorcycle tire stiffness provided with the software and augmented with the few bicycle tire stiffness numbers published by Cossalter.[5]

1.3 Problem Statement

Although some bicycle tires have been previously tested, the measured stiffnesses vary by more than two orders of magnitude in some cases, and many test parameters, such as tire size, inflation pressure, or vertical load, are not included with the published results. This makes it difficult to select stiffness values for modeling bicycle stability and handling and to validate the results of that modeling by testing a physical proximity of the model.

1.4 Objectives

The objectives of this project were to determine bicycle tire stiffness values that can be used to improve the fidelity of bicycle numerical modeling. To that end,

- the literature was surveyed to find all available previously existing bicycle tire test data;
- additional tires were tested to broaden the range of tested tires and to provide values for comparison between similar tires;

- all stiffnesses were compared to identify outliers and improve the likelihood that stiffness values used in future modeling represent reality; and
- a model was developed to gain insight into how a tire generates the forces and moments it does.

1.4.1 Additional contributions

In addition to achieving the objectives stated above, it will be shown that:

- The so-called tangent rule, based on the radial brush model, does not accurately predict bicycle tire camber stiffness.
- Bicycle tires exhibit a long decay length beyond the ends of the contact patch as the laterally deflected tire centerline returns to equilibrium and this needs to be considered for accurate modeling.
- The lateral stiffness of bicycle tires depends upon the width of the rim on which they are mounted.
- Bicycle tires exhibit rate-independent and rate-dependent hysteresis, which may contribute to rolling resistance.

1.4.2 Scope

This project is limited to measuring the lateral stiffnesses, and related values, of pneumatic bicycle tires with smooth or semi-smooth tread intended for on-road use.

Items and values that were not measured include tires with knobby treads, solid tires,

motorcycle tires, rolling resistance, friction between tire and pavement, loose, soft, or bumpy ground surfaces, operating temperature, or the effects of tread wear.

1.4.3 Setting

Bicycle tire testing was performed both at the University of Wisconsin-Milwaukee (UWM), with devices number 1 and 2, described in sections 3.7 and 3.8; and at Delft University of Technology (TU Delft) with device number 3, described in section 3.9. The testing began in April 2010 and continued through April 2013.

Test device construction occurred at UWM, TU Delft, and at the Milwaukee School of Engineering (MSOE). It began in March 2010 on test device number 1, and modifications for specialized tests continued on test device number 2 through April 2013.

CHAPTER 2

BACKGROUND

2.1 Tire coordinate system

The coordinate system used for a tire is described by Pacejka[2] and Cossalter[5] and has its origin at the intersection of three planes: the wheel midplane, the ground plane, and a vertical plane through the hub. The x -axis is in the ground plane and oriented forward, in the direction of travel; the y -axis is also in the ground plane and rotated 90° clockwise from the x -axis when viewed from above; and the z -axis is normal to the ground plane and downward from the origin.

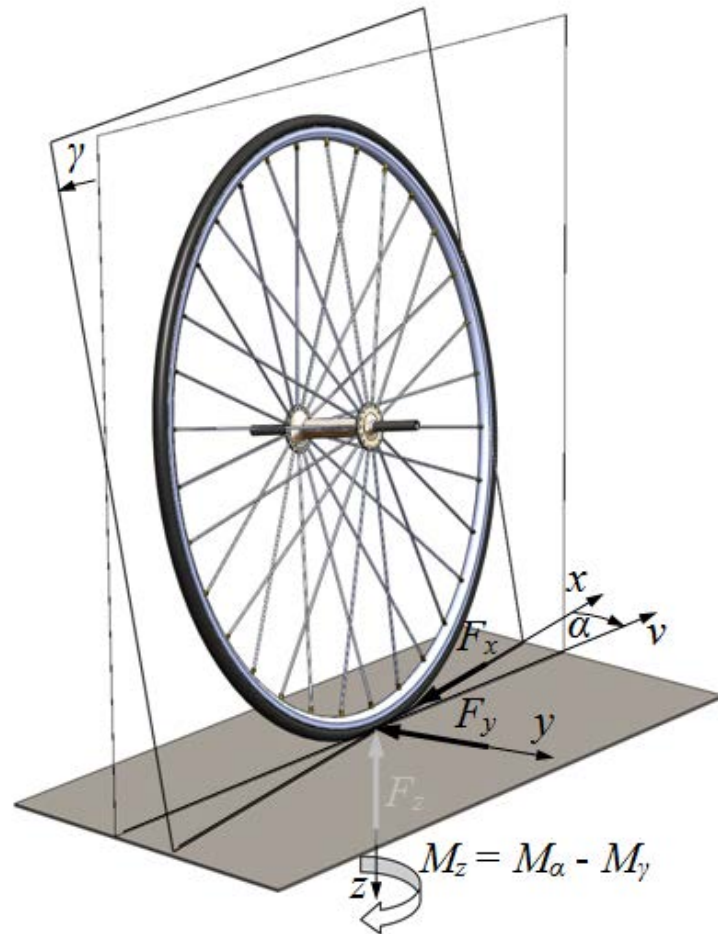


Figure 2-1: Tire coordinate system.

2.2 Tire parameters

A bicycle tire can be characterized by its bead seat diameter (ISO 5775); carcass arc length from bead to bead (s_0 in **Figure 2-3**); ply orientation, either bias or radial; and tread thickness (t in **Figure 2-3**) and composition (smooth, semi smooth, knobby), flat prevention layer, and tread compound. It has also been found that the width of the rim onto which a tire is mounted and the actual width of the tire on that rim are both

important parameters. The latter can be calculated from carcass arc length and rim width, w , as shown in **Figure 2-2**.

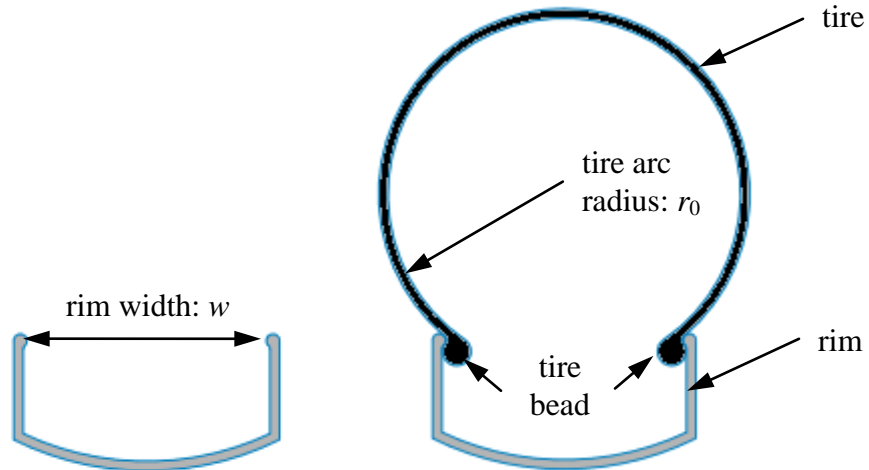


Figure 2-2: Radial cross section of rim and rim with bicycle tire.

Actual rim profiles used for testing are shown in **Table 3-3**.

The carcass circumference, s_0 , or arc length was measured by pressing a portion of the tire onto a flat surface and then measuring the distance between the two beads, as shown in **Figure 2-3**.

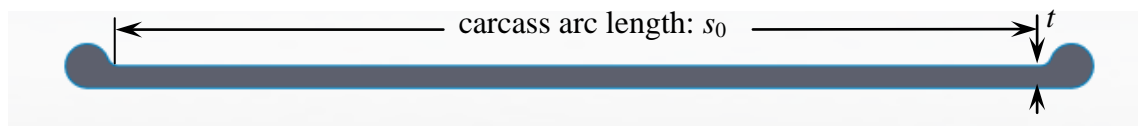


Figure 2-3: Flattened carcass, with outer tread up and inside down, showing arc length s_0 and thickness t of a bicycle tire

2.3 Tire mechanical properties

The mechanical properties of a tire that have been found to affect vehicle dynamics include:

- i) lateral stiffness: Pacejka's C_{Fy} on page 234 of 2006 edition [2]
- ii) cornering or lateral slip stiffness: Pacejka's $C_{F\alpha}$ on page 12 of 2006 edition [2]
- iii) camber stiffness: Pacejka's $C_{F\gamma}$ on page 12 of 2006 edition [2]
- v) torques and moments: Pacejka's M_z [2] and the sum of Cossalter's Twisting and Self-aligning torques[5]
- vi) pneumatic trail, the distance between the net horizontal ground reaction force and origin of the tire coordinate system. Pacejka's t , page 5 of 2006 edition [2] and Cossalter's a_t on page 59 of second edition [5].
- iv) relaxation lengths: Pacejka's σ , page 222 of 2006 edition[2] also Sharp[7] and Uil[16]. Separated here for clarity into decay length, ℓ , the distance around the circumference of the wheel over which a lateral displacement decays, and relaxation distance, κ , the distance along the ground required for lateral force to build up in response to a step change in orientation.

In order better to correct for variations in the data caused by the testing devices and to help construct and validate the model, these additional parameters were also measured:

- i) Contact patch size and shape, both on a 2.5 meter drum and a flat plate, as in **Figure 4-1** and **Figure 4-2**
- ii) Hysteresis, both rate-independent and rate-dependent.
 - (1) Force due to deformation depending on previous state of deformation, as shown in **Figure 3-12**. This was specifically confirmed with an Instron® Universal Test Instrument, as shown in **Figure 3-28**.
 - (2) Force due to deformation depending on speed of deformation: lateral stiffness at various deformation rates, as in **Figure 3-29**.
- iii) Lateral deflection of the tire center line due to a static point load, and as the tire rolls forward under various configurations of vertical load, inflation pressure, slip angle, and camber angle.

2.4 Camber stiffness and the “tangent rule”

For a bicycle tire rolling forward with non-zero camber angle and zero slip angle, the conventional multi-spoke or “brush” tire model, based on a continuous distribution of linear springs, predicts that the net ground reaction force should be in the plane of the wheel, without the need for supplementary cornering force due to a non-zero slip angle.[17] Since the camber force then equals the vertical load times the tangent of the camber angle, Sharp calls this the “tangent rule,”[7] and Sakai *et al.* call this “neutral” camber thrust.[18] There are a variety of different ways to express this condition mathematically.

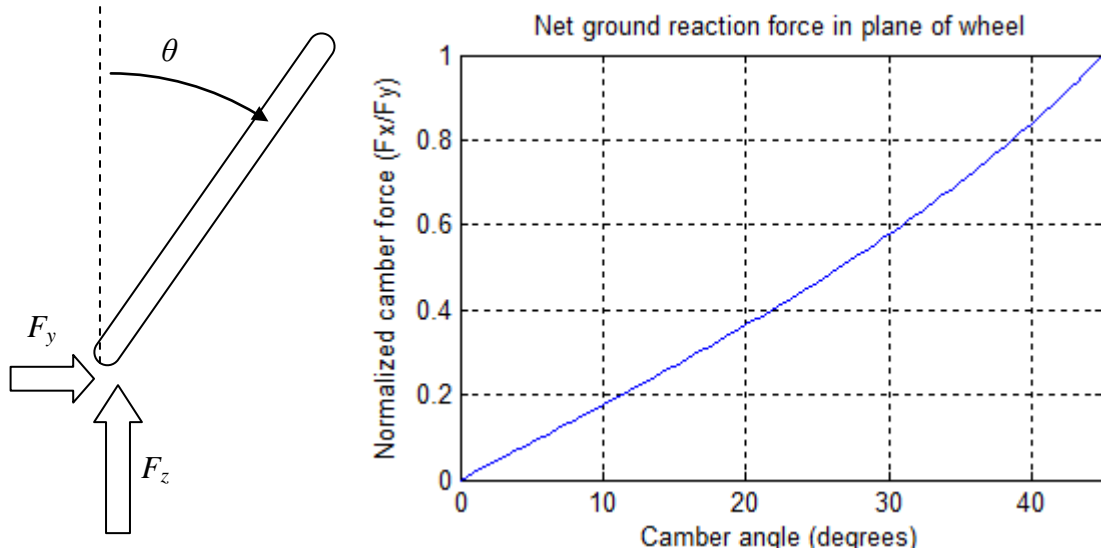


Figure 2-4: A wheel in camber and net ground reaction force orientation.

First, relate forces and angle (in degrees) such that the net ground reaction force is in the plane of a cambered wheel (plotted to right in **Figure 2-4** above):

$$\frac{F_y}{F_z} = \tan\left(\theta \frac{\pi}{180}\right) \Rightarrow \tan^{-1}\left(\frac{F_y}{F_z}\right) \frac{180}{\pi} = \theta \quad \text{Eq. 2-1}$$

Then define camber stiffness and normalized camber stiffness:

$$C_{F\gamma} = \frac{F_y}{\theta} \quad \text{and} \quad \overline{C}_{F\gamma} = \frac{C_{F\gamma}}{F_z} = \frac{F_y}{F_z \theta} \Rightarrow \theta = \frac{F_y}{F_z \overline{C}_{F\gamma}} \quad \text{or} \quad \theta \overline{C}_{F\gamma} = \frac{F_y}{F_z} \quad \text{Eq. 2-2}$$

Combine the two expressions above, in **Eq. 2-2**, to eliminate the angle, isolate the inverse tangent and take tangent of both sides:

$$\tan^{-1}\left(\frac{F_y}{F_z}\right) \frac{180}{\pi} = \frac{F_y}{F_z C_{F\gamma}} \Rightarrow \frac{F_y}{F_z} = \tan\left(\frac{F_y}{F_z C_{F\gamma}} \frac{\pi}{180}\right) \quad \text{Eq. 2-3}$$

Plug this back into expressions for normalized camber stiffness from **Eq. 2-2** above:

$$\theta \overline{C_{F\gamma}} = \tan\left(\frac{F_y}{F_z} \frac{F_z \theta}{F_y} \frac{\pi}{180}\right) = \tan\left(\theta \frac{\pi}{180}\right) \quad \text{Eq. 2-4}$$

Thus, the “tangent rule” can be expressed as

$$\overline{C_{F\gamma}} = \frac{1}{\theta} \tan\left(\theta \frac{\pi}{180}\right) \quad \text{Eq. 2-5}$$

Since $\tan(\theta) = \theta$ for small angles in radians, **Eq. 2-5** above can be approximated by

$$\overline{C_{F\gamma}} = \tan\left(\frac{\pi}{180}\right) = 0.017455064928218 \quad \text{Eq. 2-6}$$

This approximation, plotted below, is within about 1% of the true value, also plotted below, in **Figure 2-5**, for angles up to 10° and is about 21% too low at 45°.

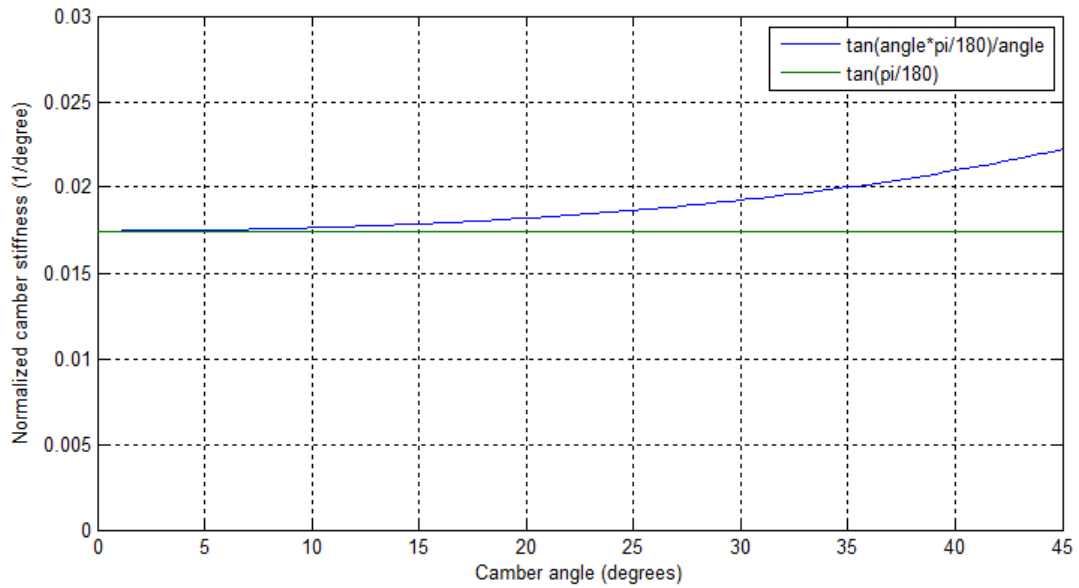


Figure 2-5: Plot of true value vs. approximation of the normalized camber stiffness that produces a net ground reaction force parallel to the plane of the wheel

2.5 Previous bicycle tire measurements

Several instances of published bicycle tire force data exist, and they are summarized below in **Figure 2-6**.

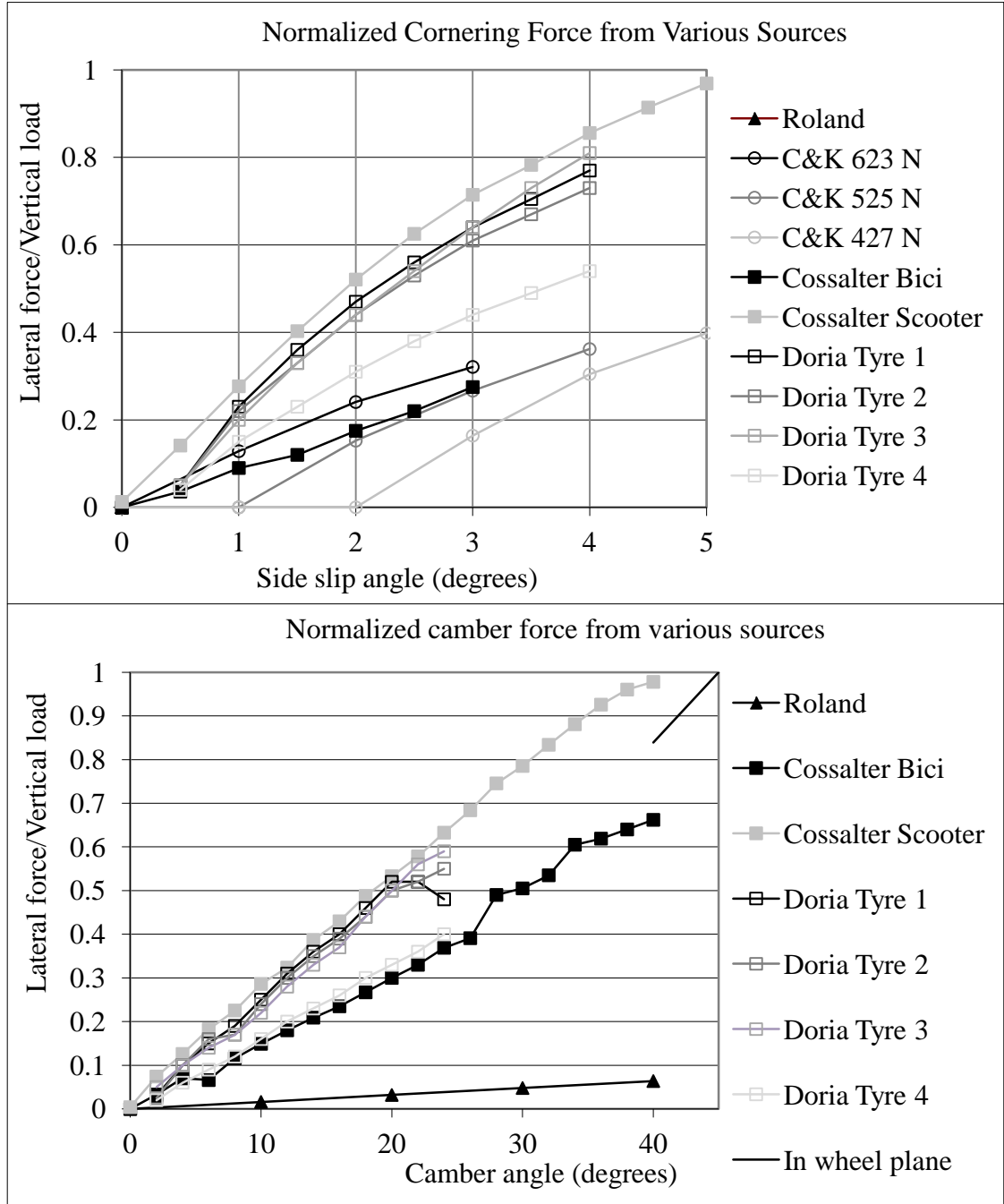


Figure 2-6: Normalized cornering and camber forces from previous bicycle tire measurements.

The sets of existing tire force and moment data seldom agree with each other, do not all measure the same values, and often are missing key pieces of test configuration data, such as tire size, inflation pressure, or vertical load.

2.5.1 Roland, 1972-1973

Roland reports that “a thorough review of the published bicycle research literature revealed no investigation of the side force characteristics of bicycle tires.” He measured bicycle tires at Calspan Corporation with a single-wheel trailer towed behind an automobile.[19][13] Eleven different tires were tested, from 24 to 27 inches in diameter with rated inflation pressures from 55 to 110 psi. He reports a range of cornering stiffness from 0.15 to 0.35 “lb/lb/deg” and a camber stiffness of 0 to 0.1 “lb/lb/deg”. The 1972 report contains detailed tire data, and the 1973 report contains sample data for one tire: “normalized side force vs. slip angle and inclination angle for a typical bicycle tire at a vertical load of 75 pounds.” This is shown below in **Figure 2-7**.

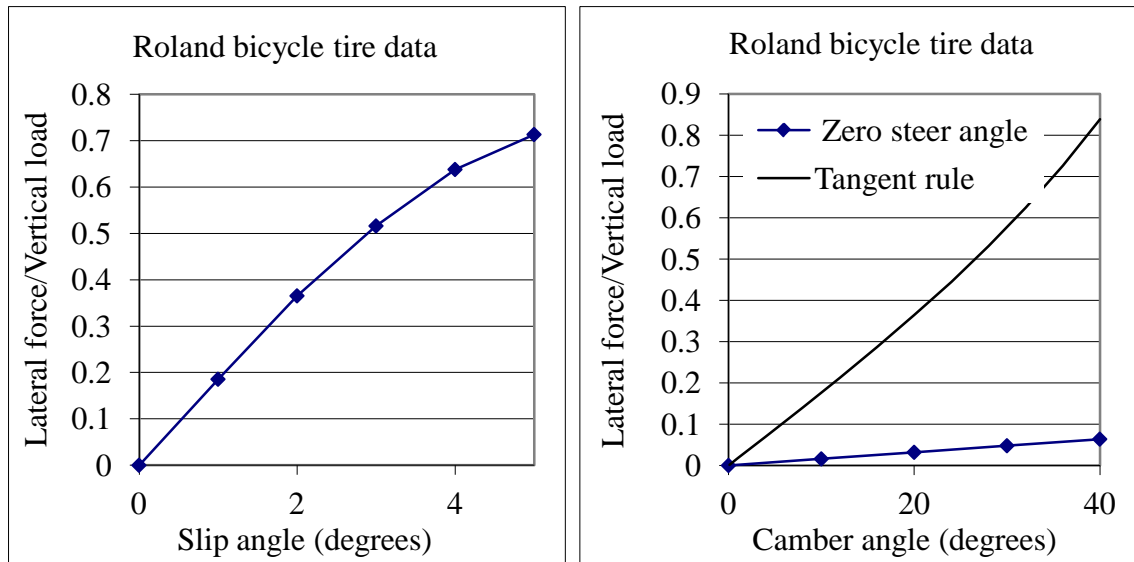


Figure 2-7: Roland, 1973, "typical bicycle tire at a vertical load of 75 pounds".

The size of the particular tire, its inflation pressure, and the forward speed of the testing are not provided. [13]

2.5.2 Davis, 1975

Davis continues the Calspan bicycle tire testing, but on a 4-foot (1.2192 meter) diameter drum, and focuses on wet pavement and low inflation pressures. He reports values similar to Roland under dry conditions for the Schwinn Puff Road Racer 27x1-1/4 (ETRTO 32-630) at 75 psi (5.171 bar) under a vertical load of 100 lb (444.822 N): a cornering stiffness of 0.17 1/° at 1° slip angle, and a camber force of 2 lb (8.896 N) at a 10° camber angle, which converts to a camber stiffness of 0.002 1/°.[20]

Davis also shows an unusual curve for camber force as a function of camber angle. By the time camber angle has increased to 20 degrees, the lateral force is 16 lb (75.62 N),

which increases the normalized camber stiffness to 0.008 1/° , about 48% of the tangent rule, although by 20 degrees, the tangent rule requires a stiffness of 0.0182 1/° , as explained in section 2.4.

2.5.3 Man and Kane, 1979

Guy Man and Thomas Kane, at the Mechanical Engineering Department of Stanford University use values of 12.949 1/rad and 0.1862 1/rad for bicycle tire cornering and camber stiffness, respectively.[21] That is a cornering stiffness of 0.2260 1/° , which is similar to other published values, and a camber stiffness of $0.003250 \text{ 1/}^\circ$, which is about twice Roland's value, and Roland's 1973 paper is cited in the bibliography, but only 18.4% of the value predicted by the tangent rule.

Basu-Mandal *et al.* suggest that their surprising results, "that turn radius at a given speed is independent of the steer angle ... may be due to details of tyre slip modelling." [22]

2.5.4 Kyle, 1987, 1988, 1995

Chester R. Kyle, Ph.D., Adjunct Professor of Mechanical Engineering at California State University, Long Beach, tested a variety of tires, mostly for rolling resistance, at General Motors facilities in the late 1980s and 1990s. It is not clear that he ever published his results in a journal or conference proceedings, but Jason Moore at UC Davis has posted four PDF documents and 3 XLS spreadsheets online at biosport.ucdavis.edu/blog/bicycle-tire-data.

In a 1987 document titled "General Motors, Detroit 4/13/87", Kyle presents data for a "small" tire, with an outside diameter of 0.44 m ($\approx 20 \text{ in}$), possibly a Moulton on a 1.7 m

drum at 3.5 kph. The data is described as “corrected to flat surface”, but without further explanation. The stiffness data is summarized below in **Table 2-1**. [23]

Table 2-1: Kyle, 1987, Small tire

Normalized Lateral Force @ 1 deg slip				
		Load N		
		300	450	600
Press. (psi)	75	0.213	0.179	0.157
	100	0.244	0.216	0.183
	113	0.201	0.173	0.156

Normalized Aligning Torque @ 1 deg slip (mm)				
		Load N		
		300	450	600
Press. (psi)	75	2.37	2.78	2.83
	100	2.23	2.4	2.53
	113	2	2.2	2.33

Normalized Camber @ 1 deg camber				
		Load N		
		300	450	600
Press. (psi)	100	0.0166	0.0156	0.0142

In a 1988 document titled “Society of Automotive Engineers, Warrendale, PA”, Kyle reports on a tire rolling resistance for “the race across Australia.” The report includes some stiffness values for a “17 in x 1¼ in” Moulton tire, which is summarized below in **Table 2-2**.^[24]

Table 2-2: Kyle, 1988, Moulton 17x1¼

Normalized Cornering @ 1 deg slip				
		Load N		
		300	450	600
Press. (psi)	113	0.202	0.175	0.161

He also reports some observations on how stiffness varies with vertical load and inflation pressure. In particular “cornering force on a rough stable surface will increase with higher tire loads... However higher tire pressure can have varying results ... Cornering force can reach a maximum and decline with increasing pressure ... Slick treads have a higher cornering force than patterned treads on dry roads ... The effect of tire width on cornering force is unclear.”

In a 1995 document titled “GM Flat Track Rolling Road Test”, Kyle presents raw data in tables for a variety of tires. There is also a spreadsheet with a graph labeled “Lateral Force Vs. Steering Angle 700C Continental, 180 psi, 3.5 mph”. Then some of the data in the document is incomplete, because the pages were misaligned in the scanner, and data in the document and the spreadsheet are questionable, because of the surprisingly high lateral forces reported: up to 2.5 times the vertical load. For example, the last line of page

26 reads: camber angle (deg) = 9.03, slip angle (deg) = 0, radial load (N) = -350, and lateral force (N) = 859. This agrees approximately with the spreadsheet.

Two documents from 1996 and two other spreadsheets appear only to contain rolling resistance data.[25][26]

2.5.5 Cole and Khoo, 2001

Cole and Khoo used a back-to-back tire test device to measure cornering stiffness.[27] They tested 57-406 "20" diameter and 2.125" tyre width" at 240 kN/m^2 and under 132-623 N vertical load. A summary of their results, both as presented and normalized, is provided below in **Figure 2-8**. They explain that "the graph is in the form of a carpet plot, where the origins of the six curves are spaced at one degree intervals along the horizontal axis."

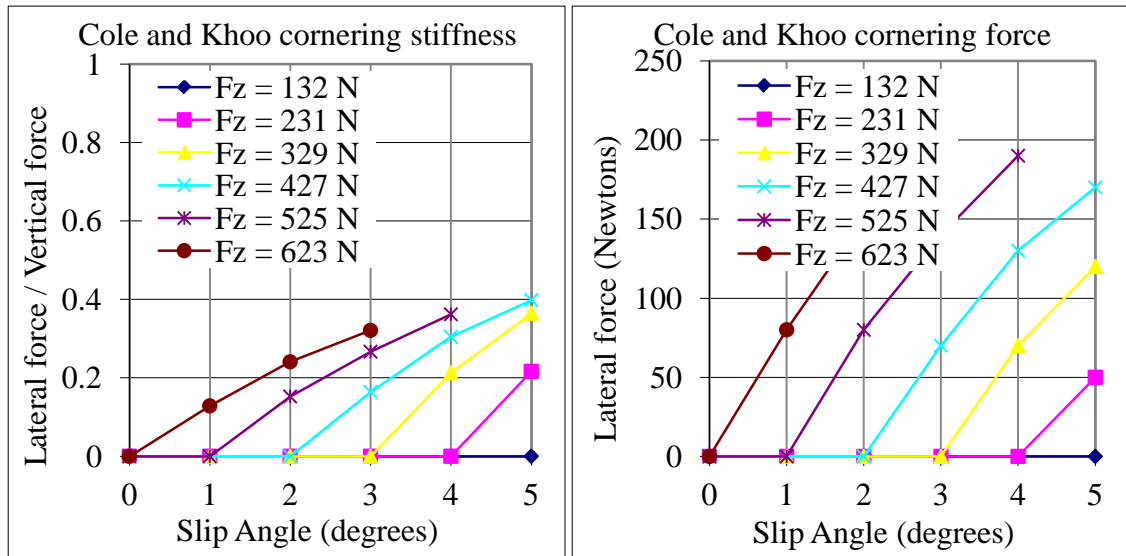


Figure 2-8: Cole and Khoo "bicycle tyres, size 20" diameter and 2.125" tyre width".

The forward speed is not specified, and the camber angle “was set to zero for all the tests.” It also appears that for all but the largest vertical load, the lateral force was at or below zero at non-zero slip angles. [27]

2.5.6 Cossalter, 2006

Cossalter measured at least one bicycle tire on his rotating disk test device, [5] designed for motorcycle tires, at the University of Padua.[11] The data he published is presented below in **Figure 2-9**.

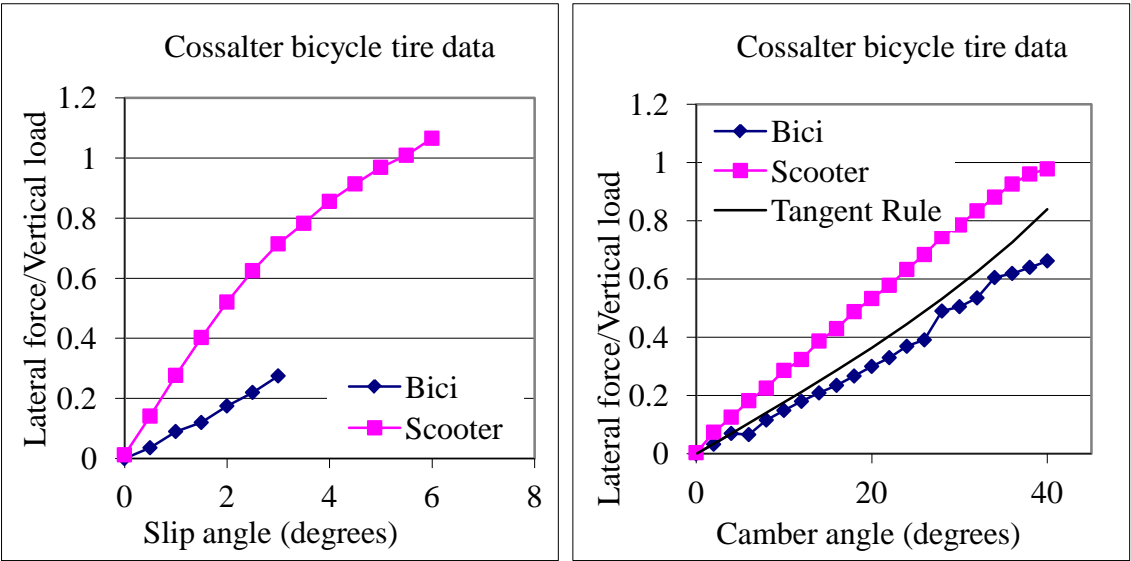


Figure 2-9: Cossalter bicycle tire data

He does not indicate which tire it was, the rim it was on, the inflation pressure, the vertical load, nor the forward speed at which it was tested. [5]

2.5.7 Sharp, 2008

Sharp uses “the side-forces developed by a number of different types of bicycle tires” measured by Roland and estimates the aligning moments.[7] Sharp uses a value 0.25 for normalized cornering stiffness. It is less clear what exactly he uses for camber stiffness. First he observes that “Roland’s camber stiffnesses vary from zero to unreasonably large.” Then he invokes the “tangent rule”. Finally he states that “ C_ϕ is taken to be equal to the tire load,” where C_ϕ is a term in his expression for F_y .

2.5.8 Doria et al., 2012

Doria et al. measure properties of four bicycle tires, three 37-622 and one 35-622, all on the rotating disk test device designed for motorcycle and scooter tires at Padua.[28]

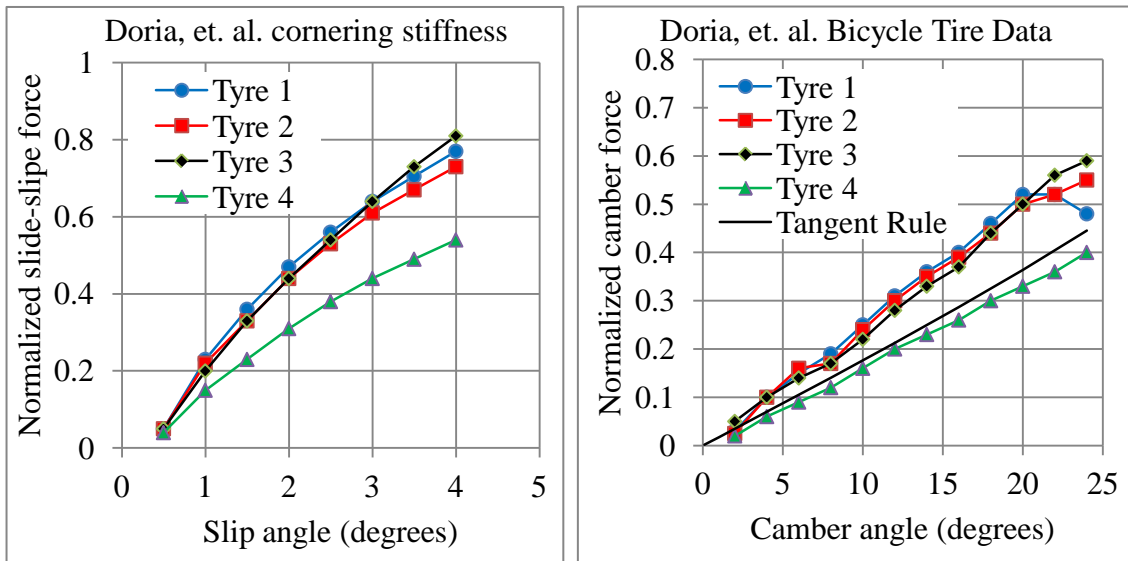


Figure 2-10: Doria et al., 2012, tire force data.

They applied two vertical loads, 400 and 600 N, and two inflation pressures, 2 and 4 bar. They report the results for the tires under “normal conditions”, but do not state explicitly what those are. It is likely that they mean 400 N and 4 bar.[28] This is shown below in **Figure 2-10**.

They do not indicate the width of the rim on which the tires were mounted,[28] but responded to an inquiry that it was 18.5 mm.

2.5.9 Motorcycle tires

While motorcycle tires and bicycle tires share many similarities, such as the need to allow large camber angles and an approximately toroidal shape, they also have important differences, such as inflation pressure, vertical load, carcass stiffness and rigidity, and cross section profile. For example, the Rotta model, presented below in section 5.1 assumes a circular cross section profile, but the *FTire* motorcycle tire simulation application allows for multiple radii to define the cross section profile,[29] and the Michelin Power One series of racing motorcycle tires have a pronounced v-shaped profile.[30]

Sharp, in 1971, models a motorcycle with tires that have normalized cornering stiffness of 0.191 to 0.195 $1/^\circ$ and normalized camber stiffness of 0.0161 to 0.0163 $1/^\circ$. He specifically neglects pneumatic trail.[12]

Rice, in 1975, reported on measuring “triangular, universal, and ribbed” motorcycle tires at Calspan Corporation's Tire Research Facility (TIRF).[31] With tires inflated “according to manufacturer's recommendation” and with a vertical load of “nominal value with a 200

lb. rider and and 120% of the nominal value”, he measured a normalized cornering stiffness of 0.33 to 0.15 1° , normalized camber stiffness of 0.009 to 0.21 1° , and pneumatic trail between 0.5 to 1.0 inches (13 – 25 mm). He also reports that “For a given tire, the value of the cornering stiffness coefficient decreased with increasing normal load; the value of camber stiffness coefficient was relatively unaffected by normal load.”

Sakai, Kanaya, and Iijima, in 1979, report normalized camber force to be slightly higher than the tangent rule of 0.0176 1° . [18]

de Vries and Pacejka, in 1991, report for a 120/70 front tire under 1600 – 3200 N vertical load a normalized cornering stiffness of 0.125 to 0.225 1° and normalized camber stiffness of 0.0268 to 0.069 1° . [32]

Kageyama and Kuwahara, in 2002, report experimental normalized cornering stiffness of 0.47 to 0.5 1° and normalized camber stiffness of 0.0122 to 0.0127 1° . [33]

Berritta, Cossalter, Doria, and Lot, in 2002, report on their motorcycle tire testing device, [34] and Cossalter, in 2006, presents a variety of stiffnesses. [5] Depending on tire, vertical load, and inflation pressure, normalized cornering stiffness varies from 0.1 to 0.25 1° , and normalized camber stiffness varies from 0.015 to 0.020 1° . Cossalter specifically describes how it is common for motorcycle tires to exceed the tangent rule in camber stiffness, up to a camber angle of about 30° , and a negative slip angle is required to achieve equilibrium.

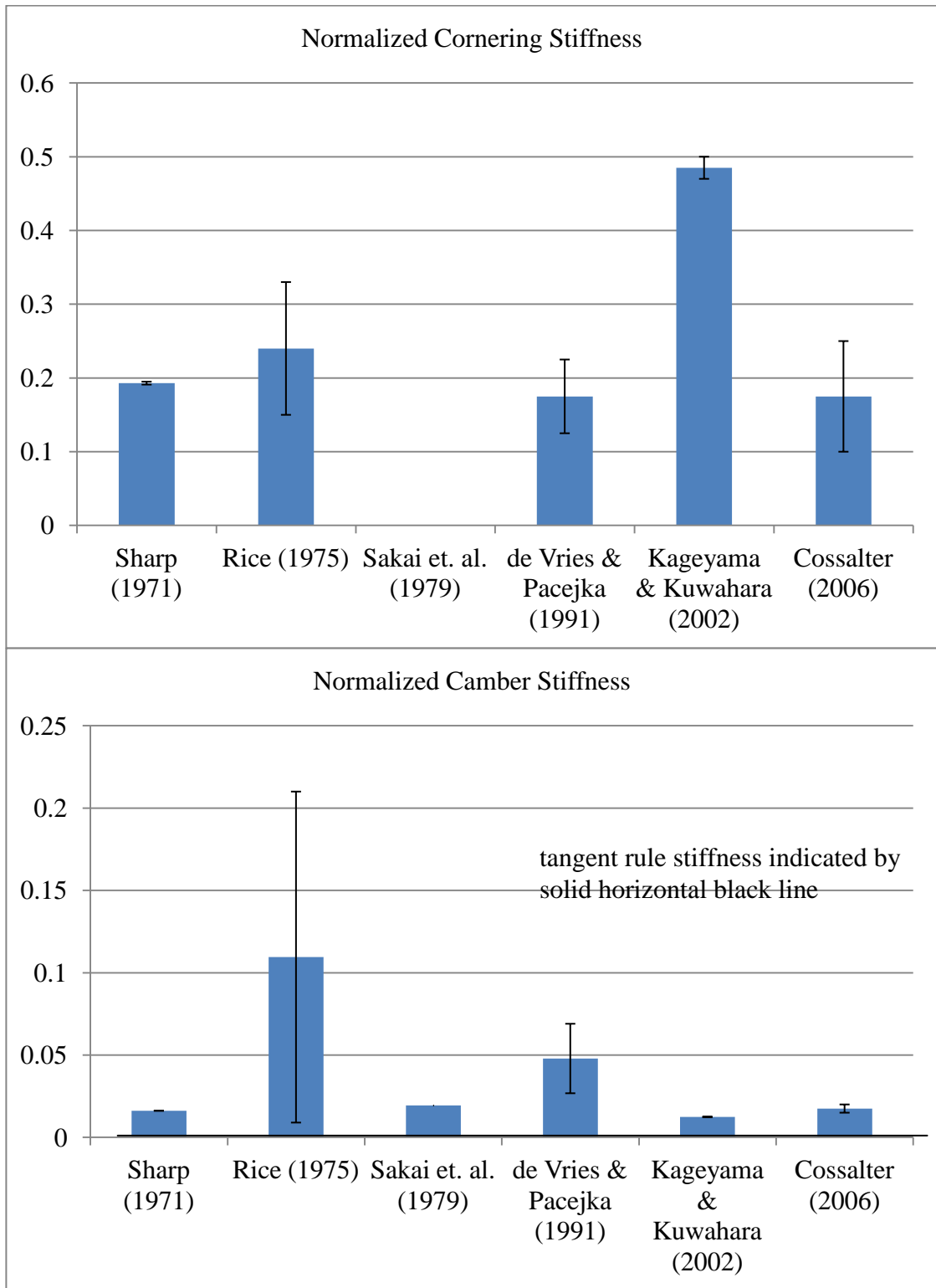


Figure 2-11: Summary of motorcycle tire normalized cornering and camber stiffness

CHAPTER 3

EXPERIMENTATION

Three different test devices were developed, as shown in **Figure 3-4**, one that rolls along a guide fence on a stationary flat track, one that remains stationary over a moving flat track, and one that remains stationary over a rotating drum. They were used to measure bicycle tire stiffness for 14 different tires from 22 to 50 mm in size, at up to four different inflation pressures per tire from 2 to 11 bar (29 to 160 psi), and under three different vertical loads from 304 to 731 Newtons (68 to 164 lb): about 120 different parameter combinations in all.



Figure 3-1: Test devices 1-3

3.1 Tires tested

A variety of tires was chosen, as listed in **Table 3-1**, in order to gain wider understanding from the test results. Most are bias ply, with casing cords oriented diagonally, at about

45° from the normal to the tire beads, but one is described as a radial, with casing cords oriented at about 15° from normal to the beads. All have a bead seat diameter of 622 mm and all were tested with vertical loads between 304 and 736 N (31 and 75 kg). Since the behavior of the carcass is the subject of this study, thick tread, especially knobby tires, were avoided.

Table 3-1: Tires tested on third device at TU Delft.

ID	Brand	Model	Size	Tread	Bead
1	Bontrager	All Weather	23	Semi-smooth	Foldable
2	Bontrager	All Weather	25	Semi-smooth	Foldable
3	Bontrager	All Weather	28	Semi-smooth	Foldable
4	Cheng Shin	Classic Zeppelin	50		Wire
5	Continental	Top Contact Winter	37		Wire
6	Maxxis	Radial Prototype	22	Smooth	Foldable
7	Michelin	Dynamic	23	Semi-smooth	Wire
8	Schwalbe	Big Apple	55		Wire
9	Schwalbe	Kojak	35		Foldable
10	Schwalbe	Marathon Plus	37		Wire
11	Vittoria	Randonnear Hyper	37		Foldable
12	Vredestein	Perfect Tour	37	Semi-smooth	Wire
13	Vredestein	Fortezza DuoComp	23	Smooth	Foldable
14	Vredestein	Fortezza TriComp	23	Smooth	Foldable

As the results of testing and modeling were compared, it was discovered that the rim width, w , and the resulting true tire arc radius, r_0 , influences stiffnesses. Thus, the arc length of each tire carcass was measured, from bead to bead when pressed flat, as shown in **Figure 2-3**, and calculated a true tire radius from that. In this document, “arc length” is used to mean this measurement, and “size” is used to mean the manufacturer’s stated size, which is approximately the diameter of the mounted tire.

Sheldon Brown discusses some practicalities of tire sizes and widths, including a tendency by manufacturers to under report tire sizes during the 1970s and 1980s, the sizing standards of the European Tyre and Rim Technical Organisation (ETRTO) and International Organization for Standardization (ISO), and some guidelines and rules of thumb for tire size and rim width combinations. Specifically, “if you flatten out a tire and measure the total [arc length] from bead to bead, it should be approximately 2.5 x the ISO [size],” and “the tire [size] should be between 1.45/2.0 x the inner rim width.”[35]

As reported in **Table 3-2**, the tires tested have a ratio of arc length to size between 1.99 and 2.43, with an average of 2.27, which is 0.23 below Brown’s target. The ratio of true size to rim width, w , is between 1.43 and 2.51, with an average of 1.78, which is right in the middle of the target range.

Table 3-2: Dimensions of tires tested, published, measured, and calculated.

ID	Mfr’s Size (mm)	Arc length s_0 (mm)	Radius (mm)	Rim width w (mm)	“True size” (mm)	Size diff. (%)	Arc length over size	True size over rim width
1	23	51.5	10.5	13.4	21.0	-8.6	2.24	1.57



2	25	60.0	11.8	13.4	23.6	-5.5	2.40	1.76
3	28	65.0	12.6	13.4	25.2	-10.0	2.32	1.88
4	50	119.5	22.1	18.7	44.2	-11.6	2.39	2.36
5	37	78.0	15.6	18.7	31.2	-15.6	2.11	1.67
6	22	45.0	9.5	13.4	19.1	-13.4	2.05	1.43
7	23	53.5	10.8	13.4	21.6	-6.0	2.33	1.61
8	55	128.2	23.5	18.7	46.9	-14.7	2.33	2.51
9	35	78.5	15.7	18.7	31.4	-10.4	2.24	1.68
10	37	73.5	14.9	18.7	29.8	-19.4	1.99	1.59
11	37	90.0	17.5	18.7	34.9	-5.6	2.43	1.87
12	37	85.7	16.8	18.7	33.6	-9.2	2.32	1.80
13	23	52.5	10.7	13.4	21.3	-7.3	2.28	1.59
14	23	54.0	10.9	13.4	21.8	-5.3	2.35	1.63

All tires sized 22-28 mounted on a 13.4 mm wide rim and sized 37-50 on a 18.7 mm wide rim. Sample calculations provided below in **Table 5-1** and **Table 5-2**

3.2 Rims used

All the tires tested on the third device at TU Delft were mounted on one of two 32-spoke wheels provided by Batavus: one with a narrow “sport” rim, and the other with a wider, touring or commuting rim. Details are provided in **Table 3-3**.

Table 3-3: Rims on which the tires were mounted for stiffness testing.

Model	Size	measure width	profile
Aero XR1 exel	622-13	13.4 mm	 <p>The image shows the profile of the Aero XR1 exel rim. On the left is a cross-sectional diagram with a width dimension of 13,4 mm and a height dimension of 20 mm. On the right is a photograph of the actual rim, which is dark green and black, with 'AERO XR1 exel' printed on it.</p>
exal	622-19	18.7 mm	 <p>The image shows the profile of the exal rim. On the left is a cross-sectional diagram with a width dimension of 19 mm and a height dimension of 21,5 mm. On the right is a photograph of the actual rim, which is black and yellow, with 'exal' and 'Alloy Double Wall' printed on it.</p>

3.3 Wheels used

In nearly all cases, a standard wire-spoked front wheel was used for testing. They naturally have significant lateral compliance, but Prof. Pacejka at TU Delft urged measuring bicycle tires in as realistic a setting as possible. Thus, instead of a solid bicycle wheel made to be especially stiff, a displacement sensor was used to record the deflection of the rim relative to the fork. The resulting change in camber angle due to wheel flex was found to be negligible, as described in section 3.10.3. Twisting of the rim with respect to the wheel midplane, however, was not measured.

The one exception is the carbon tri-spoked rear wheel by HED Cycling. This was used when measuring the lateral displacement of the tire centerline with respect to the rim, as explained in section 3.8.6.3 to eliminate slight lateral deflections of the rim caused by decreasing tension in non-vertical wire spokes over the contact patch.

3.4 Pavement surface

In all cases, when lateral forces were measured, the surface against which the tire was pressed was covered with non-skid tape. For devices 1 and 2 at UWM, that was implemented with National Floor Safety Institute (NFSI) certified “Safety Grit Tape” by LifeSafe® with a grit designation of 60 and an average particle size of 0.265 millimeters.[36] This was intended to insure maximum friction between the tire and the pavement so that tire stiffness can be measured instead of the friction coefficient between the tire and the pavement. Without this, the cornering and camber stiffness decrease

much more quickly as slip and camber angles increase than they do in the data presented in **Figure 4-5**, **Figure 4-6**, and Appendix B.

3.5 Contact patch ink prints

Ink prints were made of several bicycle tires under various vertical loads and inflation pressures. Once inflated, mounted in the test device, and loaded, the wheel was simply lifted off the drum, placed on an ink pad, and then placed back on a sheet of white paper, first on the drum, and then on a flat plate. A description of how the resulting ink prints were analyzed is presented below in section 4.1.1.



Figure 3-2: Ink prints of contact patches of a Maxxis radial.

In **Figure 3-2**, the top ink print is on the 2.5 meter drum at TU Delft and the bottom is on a flat plate, both supporting a 31 kg vertical load and at 100 psi (0.6895 N/mm²) inflation pressure.

3.6 Test devices

The motivating principles behind all three test devices constructed were:

1. Hold the wheel at some approximate orientation, either fixed or actuated so that a range of orientation angles can be swept during testing. Only an approximate orientation is sufficient because the actual orientation is measured directly from the rim braking surfaces to allow for flex in the bicycle wheel and test device frame.
2. Apply a vertical load (dead weight) that results in a known vertical force in the contact patch: F_z .
3. Roll the wheel forward over the pavement, either by moving the wheel or moving the pavement. The wheel must be constrained from moving laterally relative to the forward direction.
4. As lateral force builds up in the contact patch between the tire and the pavement, measure the force required to do so. This is F_y .
5. As a moment about the steering axis builds up in the contact patch, measure the torque required to constrain the wheel rotating about this axis. This is M_z .
6. Minimize geometries and mechanisms that complicate or interfere with these two measurements.
7. Measure the orientation of the rim with respect to the direction the wheel is moving with a pair of displacement sensors located symmetrically about the center of the contact patch. The angle calculated from arctangent of the difference between the two displacements over the distance between them is the slip angle α .

8. Measure the orientation of the rim with respect to the vertical, either with a pair of displacement measurements or with an inclinometer mounted on the fork and a displacement sensor on an extension of one fork blade to measure the lateral displacement of the rim over the center of the contact patch. The resulting angle is the camber angle γ .
9. Adjust slip angle by pivoting about a vertical axis through the center of the contact patch, either by rotating the wheel above the pavement, or rotating the pavement under the wheel. This minimizes lateral forces due to wheel lateral motion, and keeps the contact patch on the narrow strip of non-skid tape described above in section 3.4.
10. Adjust camber angle by pivoting the wheel about a horizontal axis through the center of the contact patch. This minimizes lateral forces due to wheel lateral motion, and keeps the contact patch on the narrow strip on non-skid tape described above in section 3.4.
11. Vertical load is implemented by the mass of the frame. Additional mass can be mounted near the contact patch, as desired.

3.7 Test device number 1

A description of this device and the data it generated has been previously published in *Vehicle System Dynamics* by Dressel and Rahman.[37]

3.7.1 Description

The device consists of a wooden cart to hold a bicycle wheel in the desired orientation as it is towed forward along a straight guide fence and a flat and stationary track. The cart can be adjusted to change the camber and slip angles of the wheel. Actual wheel orientation is measured by hand with a separate jig placed on the track for measurements and removed for testing. Setting and measuring wheel orientation are all performed by hand when the cart is stationary. Sweeping of angles is not possible. A schematic of the instrumented test cart is provided in **Figure 3-3**, and a photograph of test device number 1 on its final track is provided in **Figure 3-6**.

The track went through several iterations in an attempt to improve its level, flatness, and straightness in order to remove the influence of imperfections on the measured forces:

1. Flat and level section of floor in hallway adjacent to straight wall.
2. Flat and level section of floor in hallway adjacent to straight aluminum beam against straight wall.
3. Laminate counter top reinforced for stiffness and shimmed to be level.
4. Self-leveling concrete poured onto the web of a large, steel I-beam lying on its side and shimmed to be level.

The towing mechanism also evolved over several iterations:

1. Pulling on a cord directly by hand.

2. Pulling on a bicycle chain with a sprocket and hand crank.
3. Pulling on a chain with a sprocket driven by an electric motor and gearbox.

3.7.2 Contacts and force transmission

The bicycle wheel and the frame that holds it have a total of six contacts with the external world:

- The tire contact patch.
- Two casters that roll on the horizontal track to provide camber stability.
- Two casters that roll against a vertical surface along the edge of the track to prevent lateral motion.
- One point of attachment for a towing chain.

The lateral force generated in the contact patch is transmitted through the bicycle wheel to the fork to the test device frame. From the frame, the force is transmitted through the force sensors to the casters that roll against the vertical surface along the edge of the track.

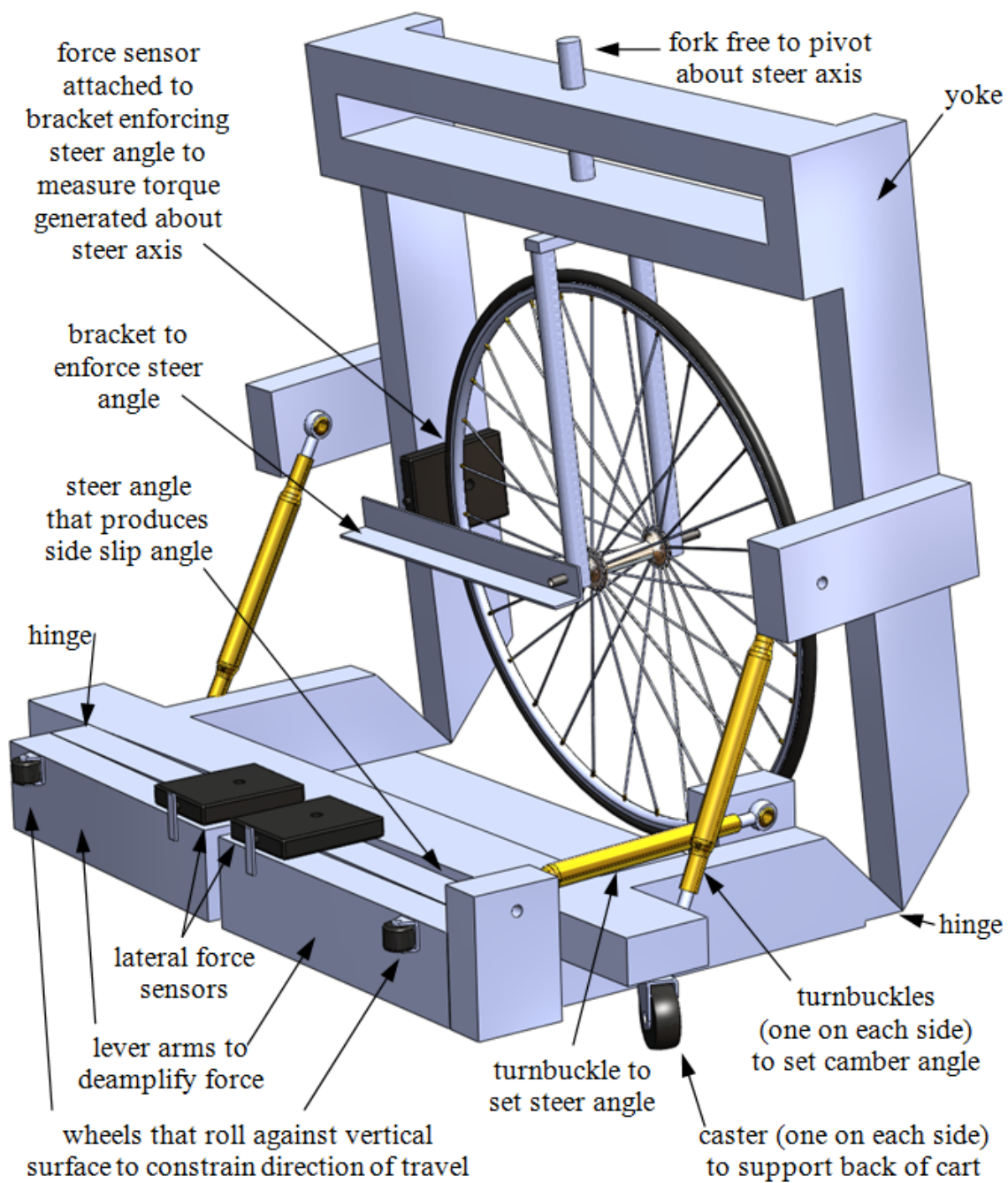


Figure 3-3: Schematic of test device number 1.

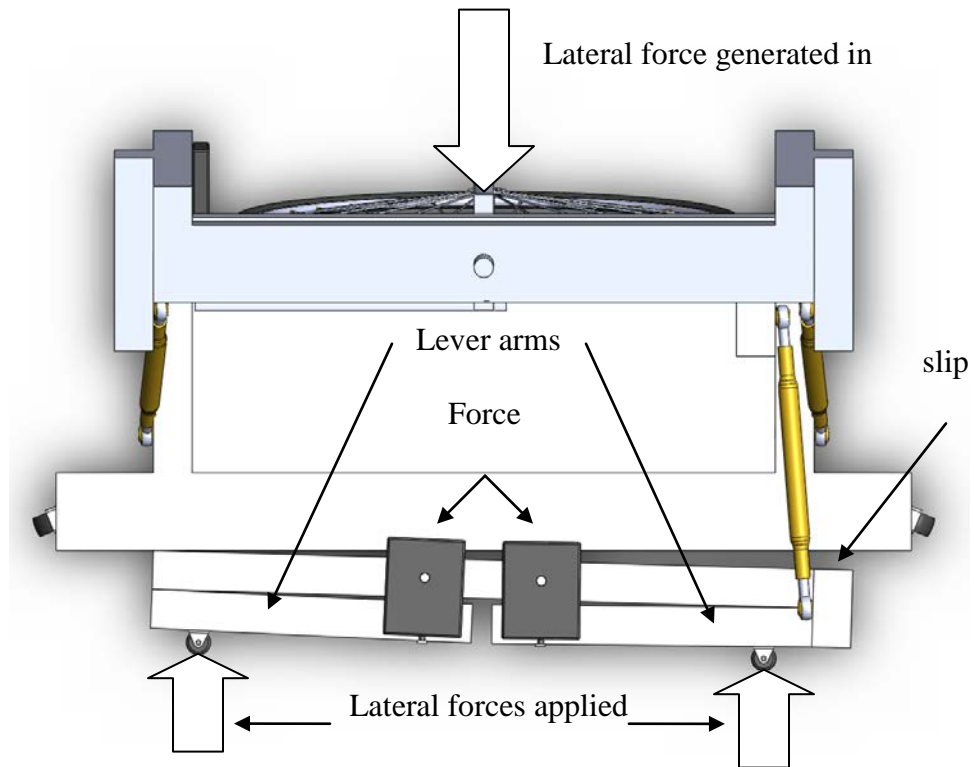


Figure 3-4: Plane view of test device number 1 showing external lateral forces.

3.7.3 Forward speeds and actuation rates

A forward towing speed of only 0.07 m/s was used, and all the angles were always fixed during an entire test run, so there was no actuation rate.

3.7.4 Instrumentation

The instrumentation and data collection system consisted entirely of proprietary plug-and-play components from PASCO®. The data is uploaded to a laptop computer to be read, presented, and saved with DataStudio, a proprietary software application also by

PASCO®. More details are provided about the PASCO® equipment below in section 3.8.3.

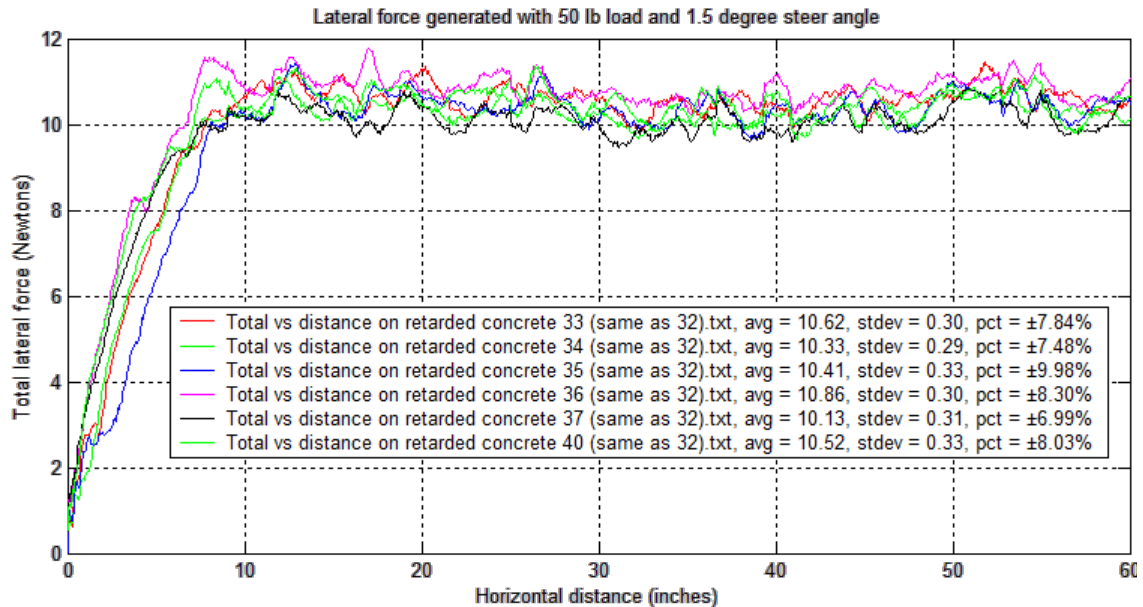


Figure 3-5: Raw force data captured from test device number 1

3.7.5 Advantages and disadvantages of design

The main goal of this design was to be inexpensive and portable, and it was that initially. After the search for a sufficiently flat, smooth, and level track resulted in a massive I-beam lying on the floor, the portability was lost.

Testing tires with this device was very time consuming and labor intensive. The only data automatically recorded was the lateral force. The tire orientation had to be set and recorded by hand for each combination of slip and camber angles tested. Because changes in the tire orientation could not be detected as forces built up and the bicycle wheel flexed, the wheel was supported by small bearings that ran on the braking surface.

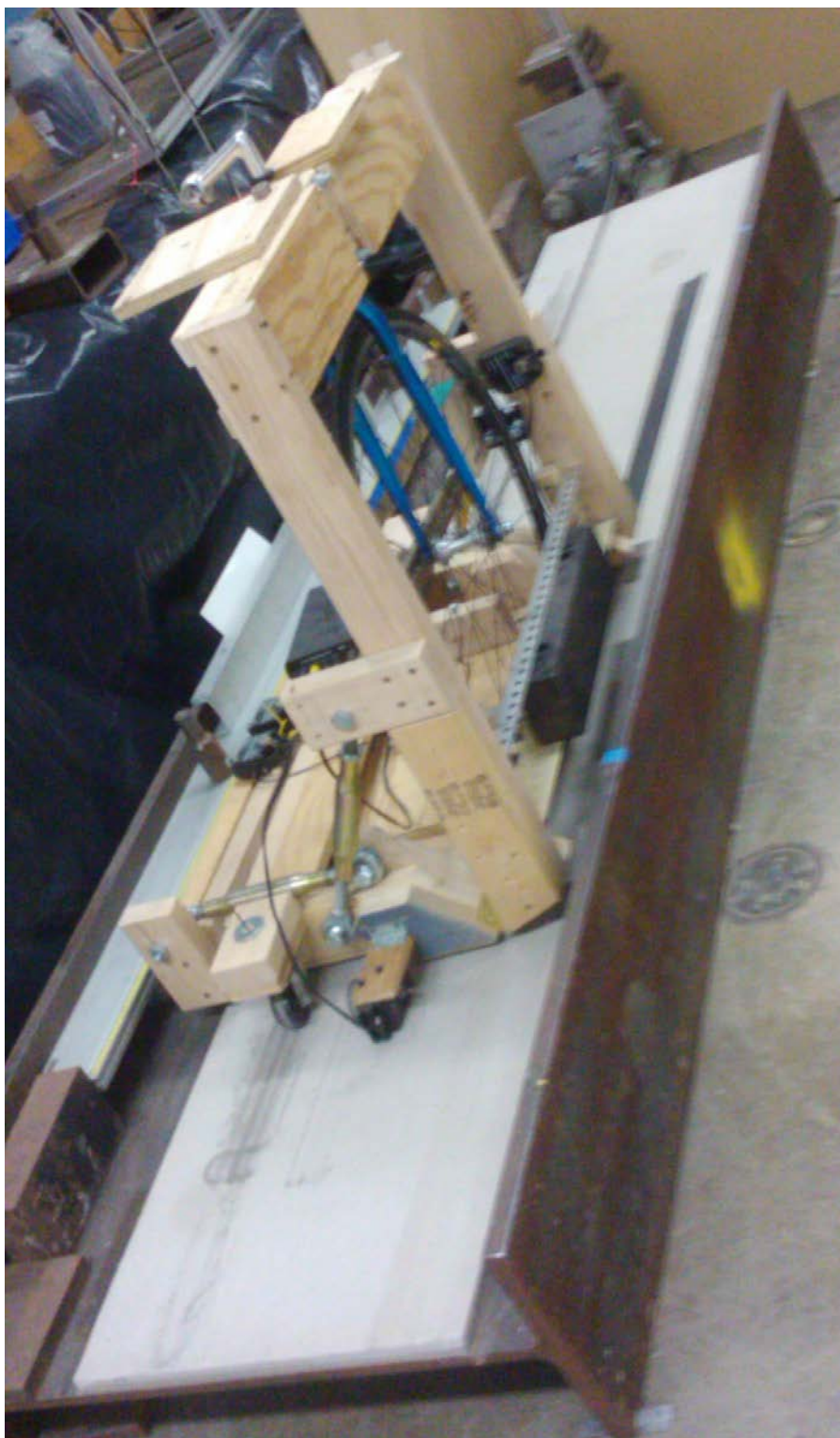


Figure 3-6: Photograph of final test device number 1 on its concrete track.

Finally, test runs were constrained by the length of the track. It was never possible to record the force data generated for an entire rotation of the wheel. Thus, the pattern in the force data with the same period as the wheel circumference was never detected.

3.8 Test device number 2

The second test device consists of a welded steel frame to hold the wheel stationary in a desired orientation, as shown below in **Figure 3-7**, on top of a small track of flat-top chain, as shown below in **Figure 3-9**. It is based on a design recommended by Jim Papadopoulos which has a two-degrees of freedom pivot, implemented with an automobile universal joint, far forward of the bicycle tire so that slight variations in vertical or horizontal position produce negligible variations in orientation angle. Potential sources of variations in vertical or horizontal position include any out-of-roundness of the bicycle wheel or tire and deflections of the lateral force sensor or frame due to lateral force generated in the contact patch. The forward pivot is implemented with needle-bearings in an automotive universal joint approximately 1.3 meters forward of the contact patch, so that any friction in the bearings or seals generates a negligible lateral force at the contact patch.



Figure 3-7: Photograph of test device number 2. The forward pivot is on the far left, and the flat-top chain track is under the wheel on the right.

3.8.1 Geometry

This device allows for sweeping slip and camber angles while measuring the lateral force, F_y , and vertical moment, M_z , generated in the contact patch. It uses one or more force sensors, depending on expected load, to maintain the lateral location of the contact patch and a second force sensor to prevent rotation of the fork that holds the bicycle wheel about its steering axis.

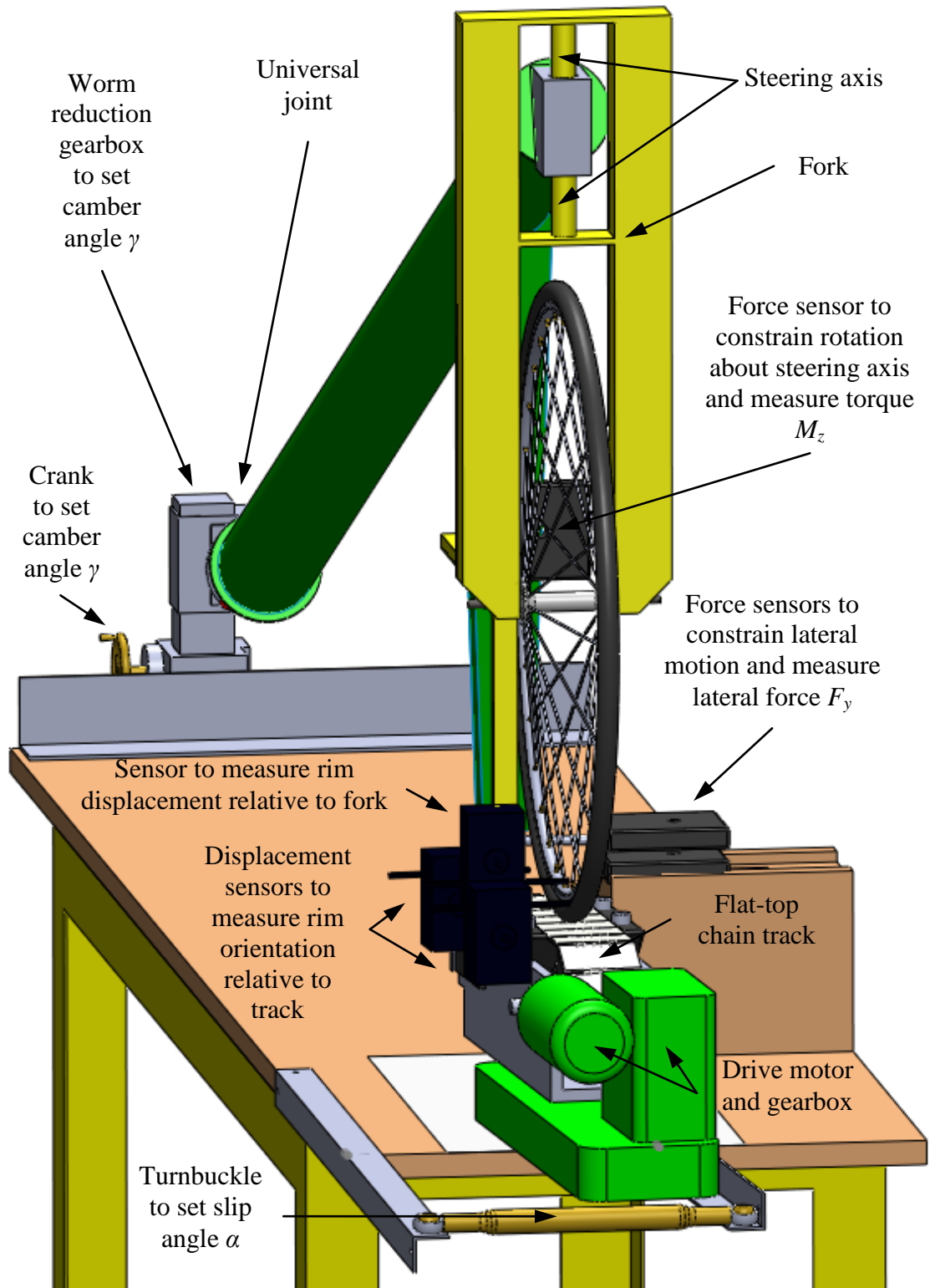


Figure 3-8: Schematic of test device number 2.

In order to allow for the inevitable flexibility of the test frame and the bicycle wheel, the slip orientation of the bicycle rim is measured with a pair of position sensors mounted rigidly to the support platen for the flat-top chain near each end of the contact patch, one of which is shown below in **Figure 3-9**. Similarly, the camber orientation of the rim is measured with an accelerometer on the fork and a position sensor mounted rigidly to an extension of the fork to measure displacement of the rim relative to the fork.

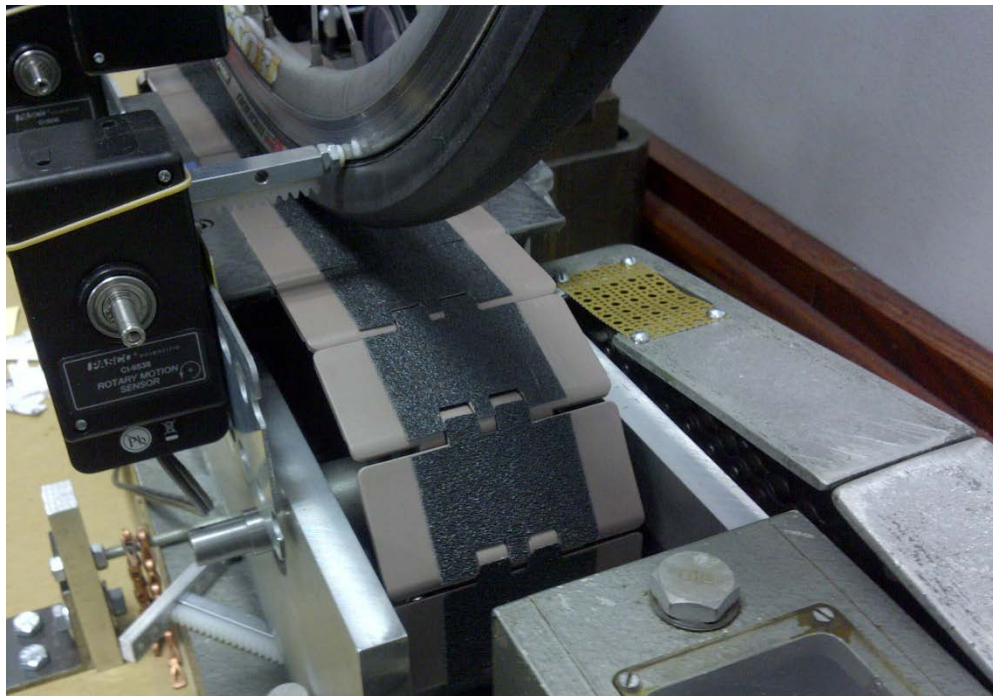


Figure 3-9: Test device number 2 flat-top chain with anti-skid tape also showing one rim displacement sensor contacting the braking surface of the wheel rim.

The forward pivot point is fixed, and slip angle is altered by pivoting the small flat-top chain track about a vertical axis under the center of the contact patch, with a turnbuckle as shown below in **Figure 3-9**. Camber angle is altered by rotating the universal joint about its longitudinal axis, which passes through the contact patch, with a 300:1 worm

reduction gear box. Since the track moves slowly, and the entire device sits on a table top, the angle sweeps are easily implemented by hand cranks.

The vertical load borne by the tire is generated simply by the weight of the frame.

Additional mass can be added above the fork as desired. The frame was designed in SolidWorks® and analyzed with the finite element method in ANSYS® Workbench, as shown in **Figure 3-4**, in a effort to create the most stiffness with the least weight. The goal was to have a light enough frame so that the desired vertical loads could be tested without need of some kind of counter-balancing system.

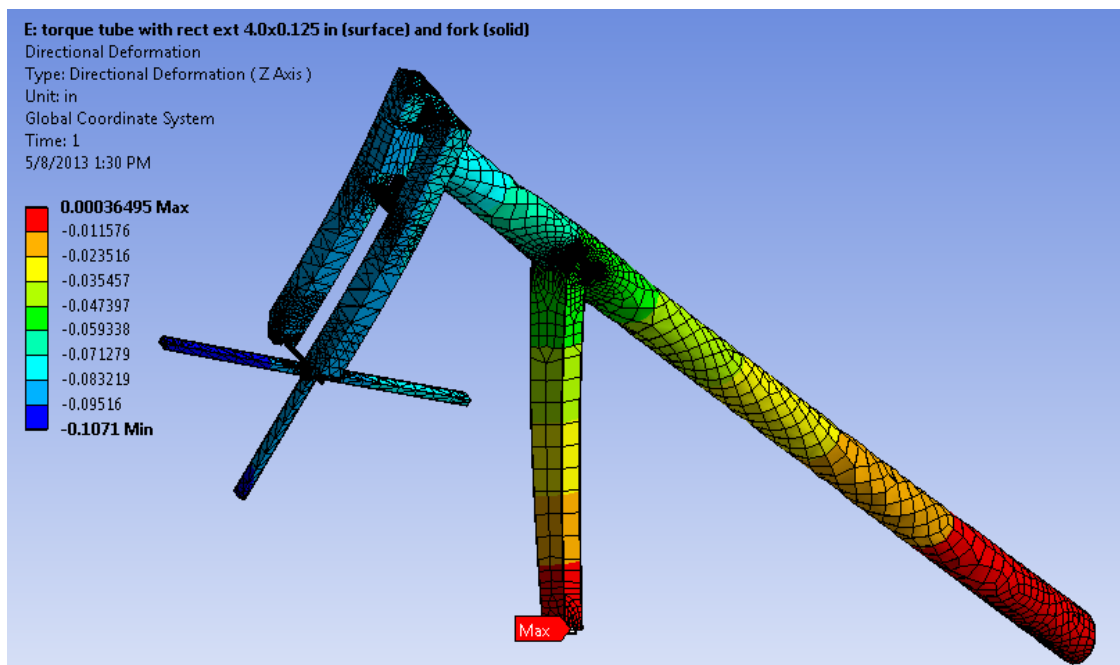


Figure 3-10: Finite Element Analysis of test device 2 frame deformation under load

3.8.2 Contacts and force transmission

The bicycle wheel and the frame that holds it have a total of three contacts with the external world:

- The tire contact patch.
- A force sensor, which constrains lateral motion of the wheel.
- The universal joint, which allows lateral and vertical motion of the wheel, but constrains rotation about the camber axis.

The lateral force generated in the contact patch is transmitted through the bicycle wheel to the fork to the test device frame. From the frame, the force is transmitted to both the lateral force sensor and the universal joint. A simple static summing of the moments about a vertical axis through the universal joint provides a relationship between the lateral force generated in the contact patch and the lateral force measured by the sensor. The mounting point on the frame for the lateral force sensor is positioned on the same axis through the center of the contact patch as the universal joint so that changes in camber angle have no effect on the lateral force sensor geometry.

3.8.3 Instrumentation

As with test device number 1, the instrumentation and data collection system consisted entirely of proprietary plug-and-play components from PASCO®.

Table 3-4: Sensors for test device number 2

Sensor	Use.
Force	Measure lateral force generated in the contact patch by constraining frame from moving laterally.
Force	Measure torque about a vertical axis generated in the contact patch by constraining fork from rotating in head bearing.
Acceleration	Measure camber angle of fork.
Displacement	Measure slip angle of wheel relative to flat-top chain by comparing measurements from one sensor near the front of the contact patch and another near the rear.
Displacement	Measure displacement of rim relative to fork.

The data is fed via USB port to a laptop computer to be read, presented, and saved with DataStudio, a proprietary software application also by PASCO®. A PASCO® rotary motion sensor with a linear motion track pressed lightly to the braking surface of the bicycle wheel with a thin rubber band, can be seen in the upper left of the photograph in **Figure 3-9**.

The individual force sensors, described by PASCO® as having a 1% accuracy, 0.03 N (0.006744 lb) resolution, and up to a 1000 Hz sample rate, are rated for only ± 50 N (11.24 lb). The force sensors “employ four strain gauges epoxied to a binocular dual-beam made from annealed aluminium. The strain gauges are wired to form a full-bridge

circuit that is driven by a constant voltage source. The voltage across the bridge circuit is proportional to the applied force.”[38]

All three displacement sensors require contact and are implemented by converting linear motion to rotary motion with a rack and pinion. PASCO® describes their rotary motion sensor as having an optical encoder with a resolution of 0.25° and accuracy of ±0.09°. The pinion has a radius of 12.72 mm (0.500 in) and thus a resolution of 0.0554 mm (0.0022 in) ±0.02 mm (0.0008 in).

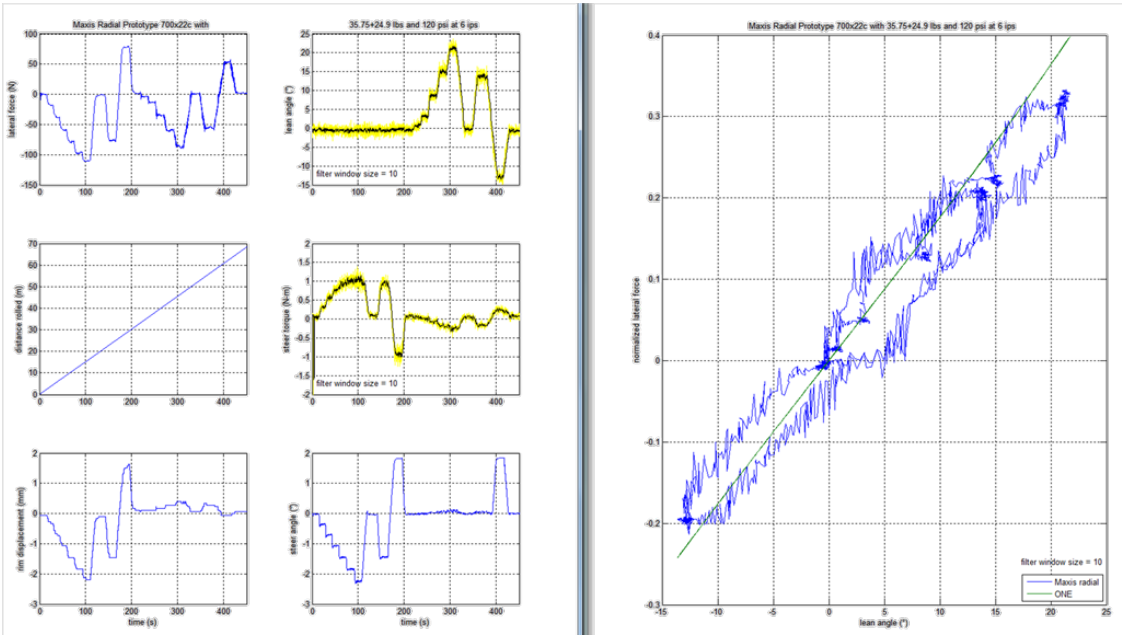


Figure 3-11: Raw force and displacement data captured from test device number 2.

The plot on the right side of **Figure 3-11** shows camber force vs. camber angle, and the source of the apparent hysteresis was not discovered. It was not observed in the same data collected from device number 3, as shown below in the bottom right plot in **Figure 3-23**.

3.8.4 Uncertainty propagation

Propagation of uncertainty from the sensors to a final value can be calculated with **Eq. 3-1**, where f is the function to evaluate the final value y , the x_i are the measured values that contribute to it, Δx_i is the uncertainty in x_i , and Δy is the uncertainty in the final value.

$$\Delta y_{\max} = \sum_{i=1}^n \left| \frac{\partial f}{\partial x_i} \Delta x_i \right| \quad \text{Eq. 3-1}$$

For lateral stiffness, **Eq. 3-1** expands into **Eq. 3-2**.

$$C_{F_y} = \frac{F}{\delta_h} \Rightarrow \Delta C_{F_y} = \left| 1 \cdot \delta_h^{-1} \cdot \Delta F \right| + \left| -F \cdot \delta_h^{-2} \cdot \Delta \delta_h \right| \quad \text{Eq. 3-2}$$

For a lateral stiffness of 41 N/mm, **Eq. 3-2** yields **Eq. 3-3**.

$$\Delta C_{F_y} = \left| 1 \cdot (1 \text{ mm})^{-1} \cdot 0.01(41 \text{ N}) \right| + \left| -(41 \text{ N}) \cdot (1 \text{ mm})^{-2} \cdot (0.02 \text{ mm}) \right| = 1.23 \text{ N/mm} \quad \text{Eq. 3-3}$$

Thus, the lateral stiffness is 41 N/mm \pm 1.23 N/mm (3%).

3.8.5 Forward speeds and actuation rates

A forward speed of only 0.15 m/s was used, approximately twice the speed of test device number 1. Higher speeds are prohibited by the limited power of the electric motor used to drive the flat-top chain. Camber angle was varied at 1 deg/sec and slip angle at 0.25

deg/sec. Camber angle could be varied more quickly, but slip angle variation rate is limited by the rate at which the controlling turnbuckle can be rotated by hand.

Thus the tires experienced change rates of 1.5 deg/m in slip angle and 6.5 deg/m in camber angle on test device number 2.

3.8.6 Additional tests performed with device number 2

Test device number 2 was also repurposed to perform several additional tests, as described in the following sections.

3.8.6.1 Radial stiffness

To compare with the model, presented below in CHAPTER 5, radial stiffness data was collected, in the form of vertical sinkage due to a sequence of increasing versus decreasing dead weights, as shown below in **Figure 3-12**. Slopes of horizontal segments reflect creep or relaxation (rate dependence).

The rate-independent hysteresis, described in section 2.3 can be seen in the difference in deflection under the same load depending on whether the previous load was larger or smaller. The difference in heights could be because of additional creep taking place between loading and unloading.

Vertical displacement was measured by a PASCO® rotary motion sensor with a small cord wrapped around its axle, over a pulley above the rim between two spokes, and straight down to a single spoke nipple.

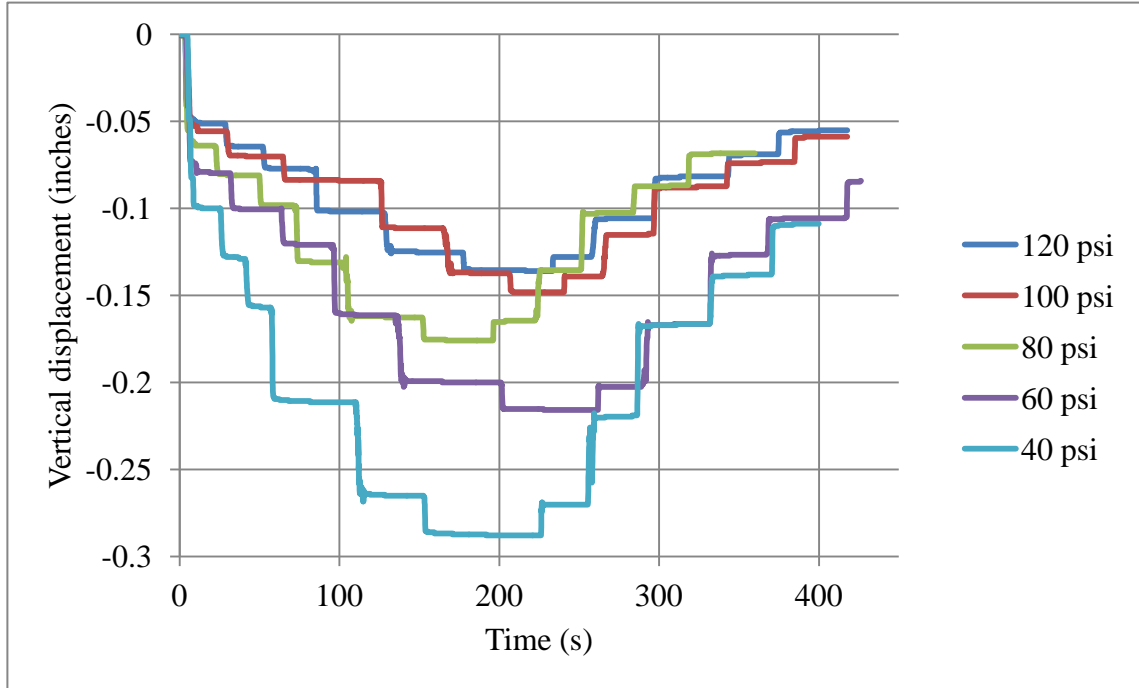


Figure 3-12: Radial stiffness of a Bontrager All Weather 28-622 mm tire at various inflation pressures and under vertical loads of 30.3, 42.2, 54.2, 78.5, 102.7, and 114 lb.

3.8.6.2 *Static lateral stiffness*

To improve accuracy of the static lateral stiffness values obtained, a method was devised to pull directly on the rim slowly and precisely while measuring the force required and the resulting deflection, as shown in **Figure 3-13**. The results were used to measure the sensitivity of tire stiffness to rim width presented in **Figure 6-4** below.

The lateral displacement was provided by a PASCO® Stress-Strain Apparatus, the force was measured with a PASCO® force sensor, and the lateral displacement was measured with a pair of PASCO® rotary motion sensors equipped with the PASCO® linear motion accessory, as shown in **Figure 3-13**.

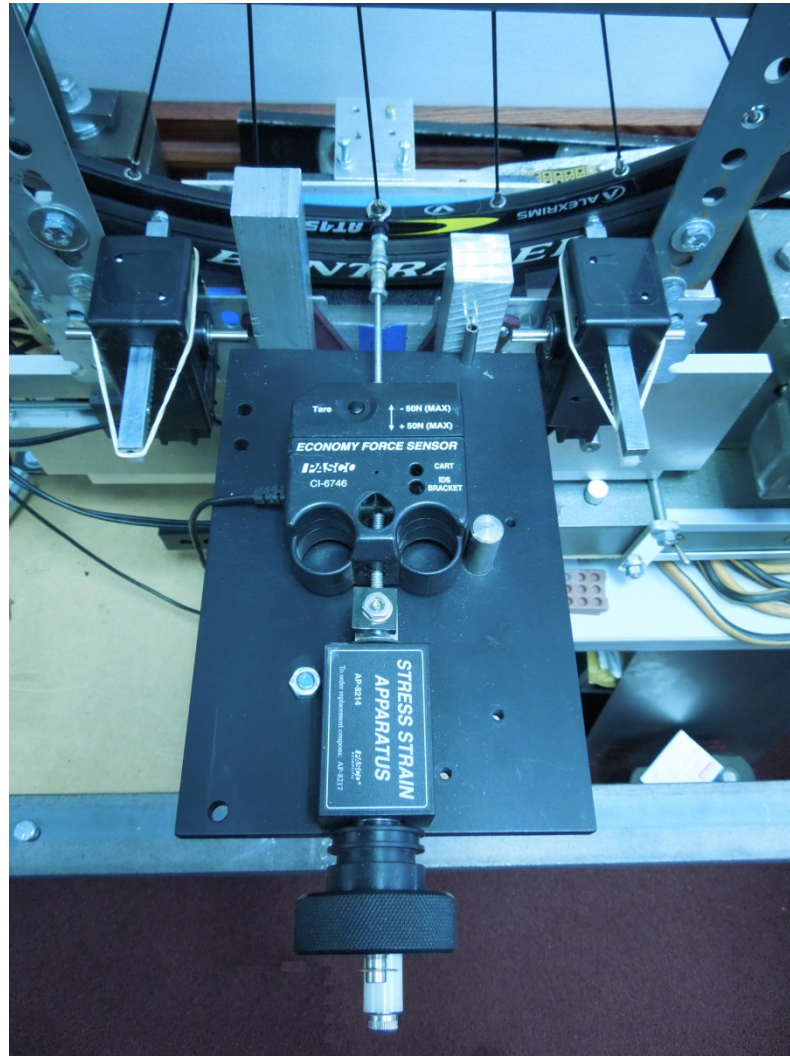


Figure 3-13: Measuring static lateral stiffness with test device number 2.

3.8.6.3 Decay length

In order to measure deflection of the tire centerline beyond the contact patch, a PASCO® rotary motion sensor was attached to the rim so that it rotates with the wheel, as shown in **Figure 3-14**. A fine cord, dental floss, is run from a pin-hole in the centerline of the tire, over a pulley, a common “608” inline skate or skateboard bearing, to the rotary motion

sensor. The bracket that holds the pulley extends 150 mm (nearly 6 inches) so that vertical fluctuations as the tire compresses above the contact patch, will have a minimal effect on the length of the cord and therefore the measured location of the centerline of the tire.



Figure 3-14: Measuring tire centerline lateral deflection beyond the contact patch.

As can be seen in **Figure 4-11**, the lateral deflection looks as might be expected from a non-zero slip angle, but is oddly S-shaped when the tire is not generating a side force.

A wire-spoked wheel, however, under a vertical load experiences a vertical deflection of the rim over the contact patch, it will also deflect laterally “away from the spoke where the load is applied.”[39] To confirm that this effect is contributing to the tire centerline lateral deflection data, the same tests were performed with the same tire mounted on a HED Cycling carbon tri-spoke wheel, as pictured below in **Figure 3-15**.



Figure 3-15: Measuring tire centerline lateral deflection on a HED Cycling carbon tri-spoked wheel.

The sensor of **Figure 3-14** and **Figure 3-16** can be seen at the 6 o'clock position of the wheel in **Figure 3-15**.

The particular wheel available for testing was a rear wheel with a 130 mm wide hub. The drive side is implemented as a cassette hub, which integrates the axle bearing into part of the ratchet mechanism and cannot be trivially removed or replaced. A spacer from the non-drive side could be removed, however, which reduced the hub width to about 105 mm. This is only slightly wider than the 100 mm width of front wheels that the test device fork was designed to accommodate. The fork blades could be spread by unbolting the connection at the top of the fork tubes, but this reduced lateral stiffness, and probably caused the actual camber angle of the wheel to be significantly more than the camber

angle of the frame. In **Figure 4-12**, multiple test runs are superimposed to demonstrate the robust repeatability of the measurement.

Finally, to gain a better understanding of what exactly is happening in the contact patch with zero slip angle, a pair of sensors were mounted directly to a spoke of the carbon tri-spoke wheel, one on each side of the wheel, to confirm either the symmetry or asymmetry of the measured displacement.

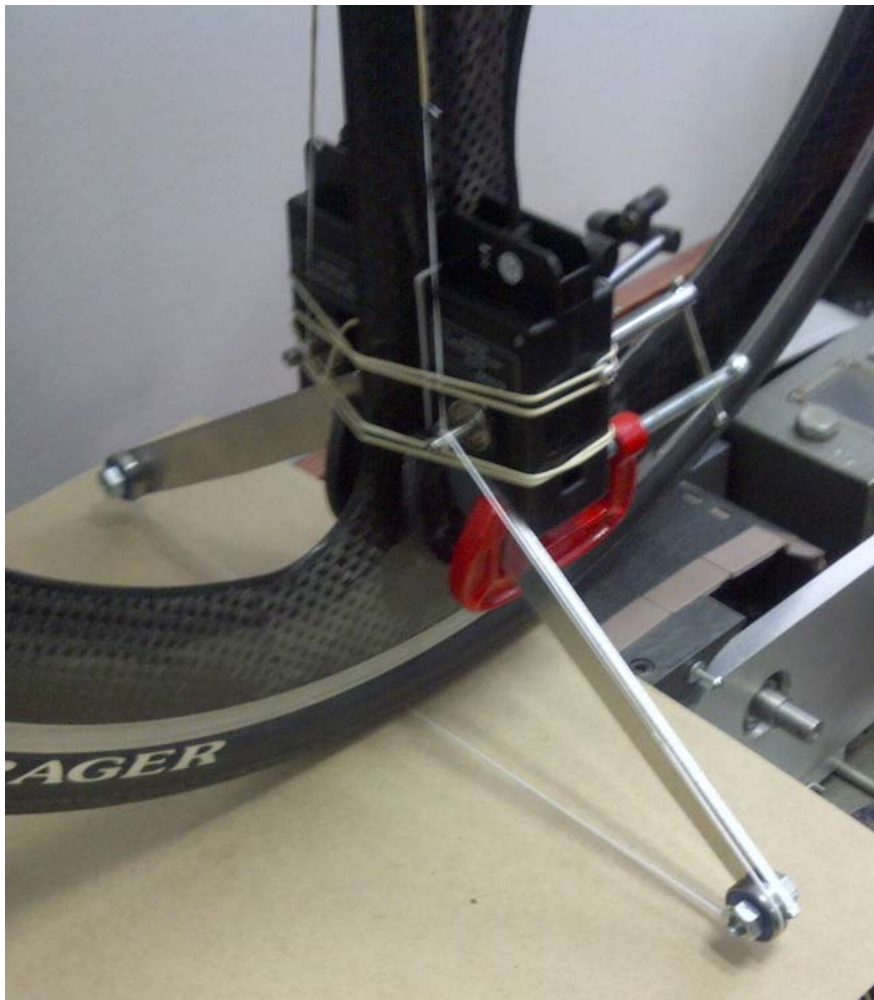


Figure 3-16: Paired displacement sensors.

The data presented in **Figure 4-14** confirm that the small, ~0.1 mm, lateral displacement of the centerline actually occurs, is asymmetric, and is not just some artifact of the measuring technique. Instead, it is likely due to slightly non-zero camber or slip angles, even tire or rim non-uniformity, or some combination of these conditions.

The sensors mounted on the wheel to measure lateral displacement of the tire centerline prevent the use of the pair of sensors mounted to the track and that measure the displacement of the rim, which are used to measure slip angle. Instead, zero slip angle was set for these tests by adjusting the track orientation until the measured lateral force generated by the tire was zero. It is possible that modifications to the test apparatus fork assembly, which were necessary for it to accept the wider hub of the rear tri-spoke wheel, could have caused the wheel to be slightly out of vertical alignment with the fork, and zero camber angle is set with a level mounted to one of the fork blades. Thus, even though the measured lateral force was zero, the camber angle might have been slightly non-zero, and that was countered by a slightly non-zero slip angle in the other direction. Finally, the fact that slip angle has a larger effect on centerline lateral displacement could explain the small lateral displacement measured when the measured lateral force was zero.

3.8.7 Advantages and disadvantages to design

Being able to record wheel orientation automatically and thus sweep slip and camber angles during a single test run was a huge improvement over the previous design. The wheel and frame could be allowed to flex because the true orientation was being recorded along with the force data. Being located on top of a table make working on it far less

arduous. The design also proved to be quite adaptable, as evidenced by the variety of additional experiments performed with it.

The electric motor that drives the flat-top chain is too little power to drive it at speeds anywhere near to those commonly experienced by bicycle tires, however, and it is not clear that the flat-top chain would perform well at those speeds if it could.

The system by which the steering axis is adjusting to be vertical over the contact patch is awkward. Placing the additional weights at the top of the fork ensures that they are centered over the contact patch, but is an ungainly operation to perform.

The PASCO® sensor system is at its limits to capture all the desired signals. The force sensors are limited to 50 Newtons, and so a group of three are used to measure the lateral force. Altogether, 4 force sensors, an accelerometer, and three rotary motion sensors were used. This required using two separate PASCO® interfaces that connect to the PC via two separate USB ports. The only way to collect data through the two ports with the PASCO® DataStudio software is to run two separate instances of it, and there is no way to start them recording data simultaneously. Instead, a synchronizing signal must be generated in the recorded data.

3.9 Test device number 3

Upon the invitation of Prof. Arend Schwab, at Delft University of Technology (TU Delft) in Delft, the Netherlands, three separate visits were made to the tire testing facility there to design, build, and operate a bicycle tire test device that works with one of the existing 2.5 meter diameter tire testing drums.

The device consists of a welded steel frame to hold the wheel stationary in a desired orientation on top of the drum, as shown below in **Figure 3-17** and **Figure 3-18**, and is based on the same design recommendation by Jim Papadopoulos as was used for test device number 2 described above in section 3.8.

The wheel is mounted on a steerable fork held by a frame whose roll is prevented by a front universal joint. The slip angle is achieved by holding the contact patch in a fixed horizontal location, while the universal joint assembly is displaced to alter the angle. Steering torque is measured by a load cell constraining rotation about the steering axis. Only a small section of the large drum penetrates through the laboratory floor.

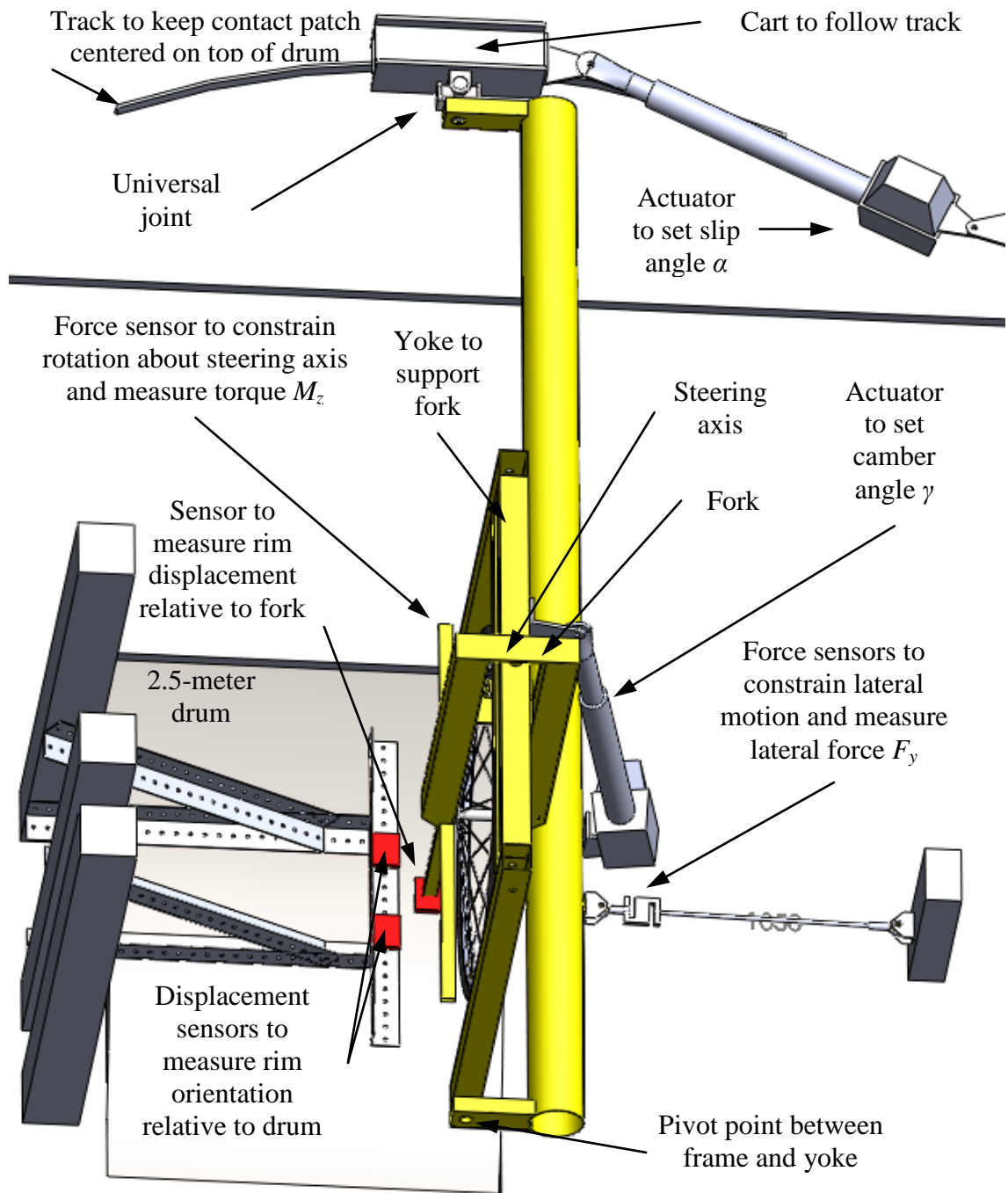


Figure 3-17: Schematic diagram of test device number 3

3.9.1 Geometry

In order to create the desired slip angle between the bicycle tire and the drum, which rotates on a fixed axle, the forward pivot point moves on a curved track, just visible in the lower left corner of **Figure 3-18** above and at the top of **Figure 3-17** below, that keeps the tire contact patch stationary on the crown of the drum. Camber angle is implemented by a yoke that holds the bicycle fork and pivots relative to the rest of the frame about an axis that passes through the contact patch, as shown below in **Figure 3-19**. As with test device number 2, there are only three contact points with the fixed ground, the tire contact patch on the drum, the forward pivot point, and the ball-jointed mount for the lateral force sensor. The forward pivot is implemented with needle-bearings in an automotive universal joint approximately 1.3 meters forward of contact patch, so that any friction in the bearings or seals generates a negligible lateral force at the contact patch.

As with test device number 2, the frame was designed in SolidWorks® and analyzed with the finite element method in ANSYS® Workbench in an effort to create the most stiffness with the least weight.



Figure 3-18: Photograph of test device number 3.

3.9.2 Actuation

Because access to the room that contains the drum is prohibited for safety reasons when it is rotating, actuators were installed to sweep slip and camber angles. LiftMaster® ECO400K electric gate openers were found with the necessary 400-mm travel, 250-N force, 12-13-mm/s rate, and dimension and used as actuators. They were set to run in a “manual” mode and connected to a pair of switches in the control room. In hind-sight, their 8 cycles/hour duty cycle proved to be on the light side, and care had to be taken to prevent them from over heating. The camber angle actuation is pictured below in **Figure 3-19**.



Figure 3-19: Camber angle actuator installed on test device number 3 before non-skid tape is installed on the drum.

3.9.3 Instrumentation

The instrumentation and data collection system consists of an ad-hoc arrangement of sensors connected to a National Instruments DAQ controlled by National Instruments LabVIEW running on a laptop computer, as pictured in **Figure 3-20**.

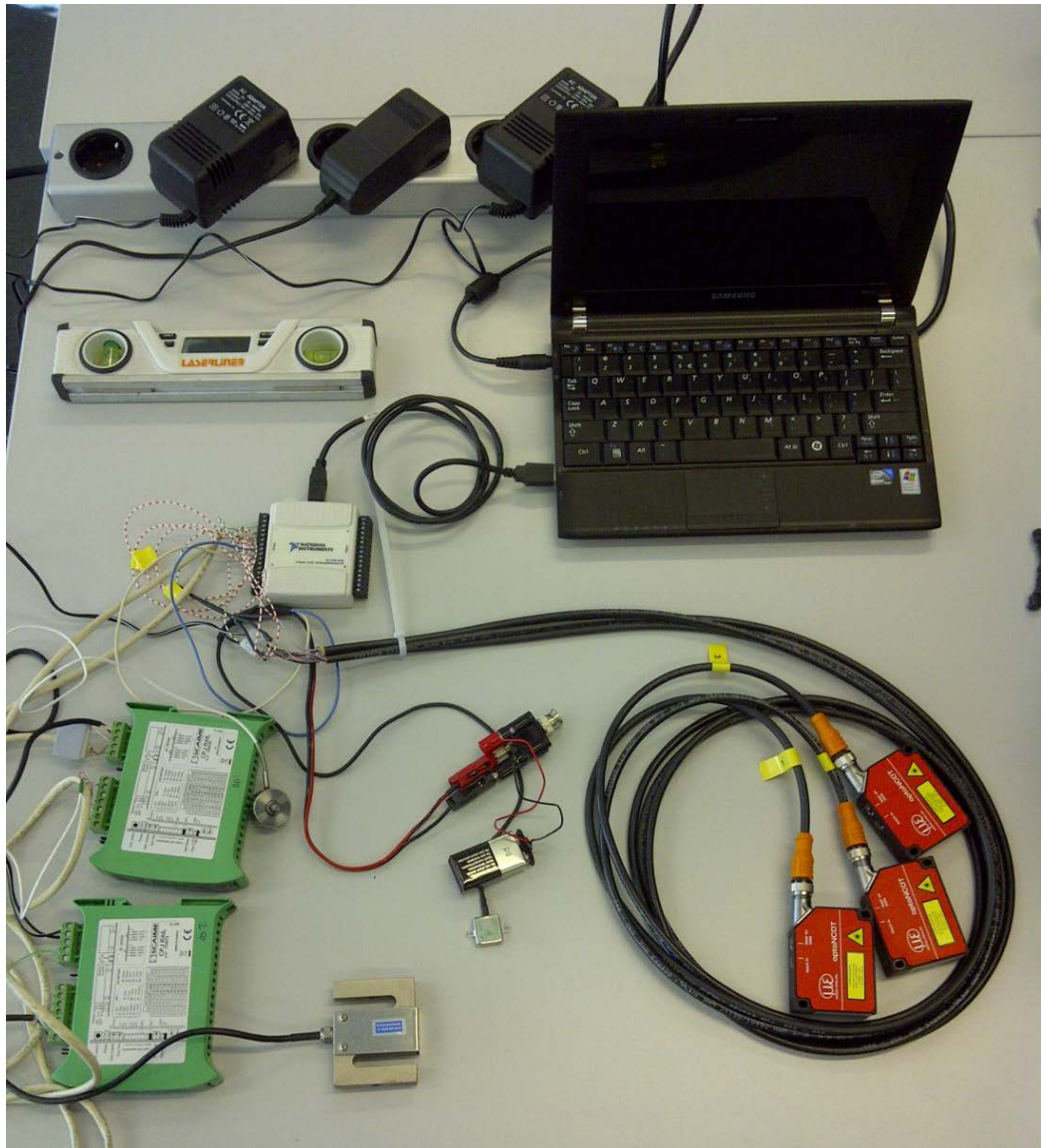


Figure 3-20: Instrumentation before installation on test device number 3.

The lateral force, generated by either slip angle or camber angle, is measured with a single force sensor mounted collinear with the center of the contact patch between two ball joints to minimize torques and off-axis loads. It is in either tension or compression, depending on the sign of the applied slip or camber angle.

The camber angle is measured with an accelerometer mounted on the fork blade. Visual observation during testing was in agreement with recorded values. A laser displacement sensor mounted rigidly to the fork and aimed at the rim directly above the center of the contact patch shows only small displacements during camber angle sweeps that would produce only small variations in actual camber angle experienced by the tire and rim.

All three displacement sensors are contactless and use a laser beam which can be aimed precisely at the point whose displacement needs to be measured. That is the braking surface of the wheel rim in all three cases.

Table 3-5: Sensors for test device number 3.

Sensor	Make and model	Use
Force	Scaime ZFA 100 kg Loadcell with “combined sensor error : 0.03 % full scale” so ± 0.29 N	Measure lateral force generated in the contact patch by constraining frame from moving laterally.
Force	Scaime ZFA 25 kg Loadcell with “combined sensor error : 0.03 % full scale” so ± 0.074	Measure torque about a vertical axis generated in the contact patch by constraining fork from rotating in

	N	head bearing.
Acceleration/ Inclination		Measure camber angle of fork.
Displacement	Micro-Epsilon OptoNCDT ILD 1300-50 Laser displacement sensor with 50 mm range, 10 μ m resolution, and “linearity $\pm 0.2\%$ FSO” so ± 0.1 mm	Measure slip angle of wheel relative to drum by comparing measurements from one sensor near the front of the contact patch and another near the rear.
Displacement	Micro-Epsilon OptoNCDT ILD 1300-20 Laser displacement sensor with 20 mm range, 10 μ m resolution, and “linearity $\pm 0.2\%$ FSO” so ± 0.04 mm	Measure displacement of rim relative to fork.

The vertical load is applied simply with the mass of the test frame and additional masses attached to the frame near the contact patch. The vertical force at the contact patch is measured by placing the tire directly on a scale located immediately beside and at the same level as the drum. See readings for three different vertical loads in the three images shown in **Figure 3-21**.



Figure 3-21: Vertical load created by attaching additional masses to frame of test device number 3.

The tire inflation pressure is measured by two different gauges on two different tire pumps. See reading of second gauge, on the second pump in the image shown in **Figure 3-22**.



Figure 3-22: Inflation pressure gauge integrated with tire pump.

3.9.4 Uncertainty Propagation

For a lateral stiffness of 41 N/mm, **Eq. 3-2** from section 0 yields **Eq. 3-4**.

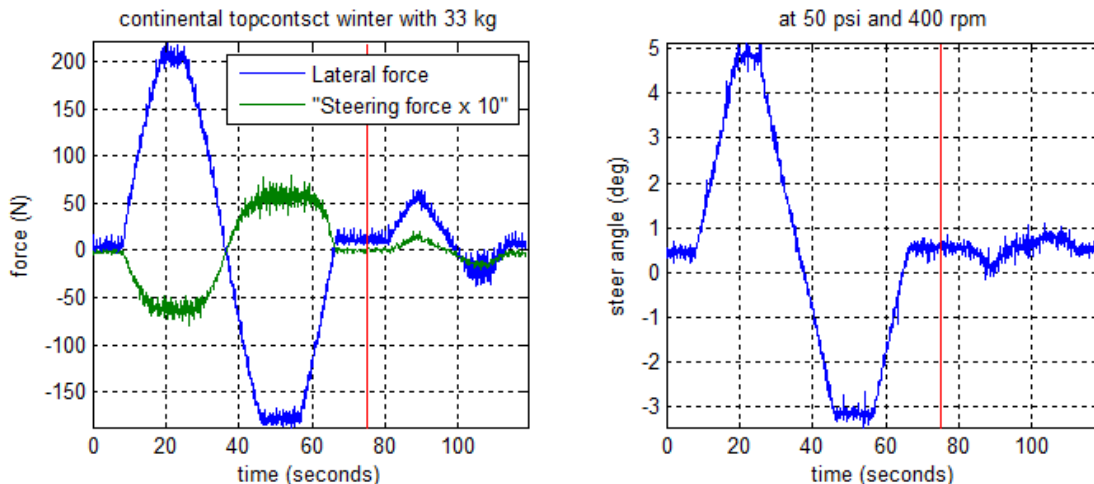
$$\Delta C_{Fy} = \left| 1 \cdot (1 \text{ mm})^{-1} \cdot (0.29 \text{ N}) \right| + \left| -(41 \text{ N}) \cdot (1 \text{ mm})^{-2} \cdot (0.1 \text{ mm}) \right| = 4.39 \text{ N/mm} \tag{Eq. 3-4}$$

Thus, the lateral stiffness is 41 N/mm ± 4.39 N/mm (10.7%).

3.9.5 Forward speeds and actuation rates

The 2.5 meter drum at TU Delft can be driven at nearly any forward speed likely to be experienced by an automobile tire. A speed was selected compatible with the fixed actuation rate of the electric gate openers used to sweep slip and camber angles: 22 m/s (~8 kph, ~5 mph), far faster than the two test devices at UWM.

Slip angle was swept at 0.33 deg/sec, and camber angle was swept at 2.33 deg/sec. The difference in rates, from identical actuators, is caused by the different geometries of their installation on the test device frame. Thus the tires on test device number 3 experienced change rates of 0.015 deg/m in slip angle (about 1/100 the rate of test device number 2) and 0.11 deg/m in camber angle (about 1/60 the rate of test device number 2).



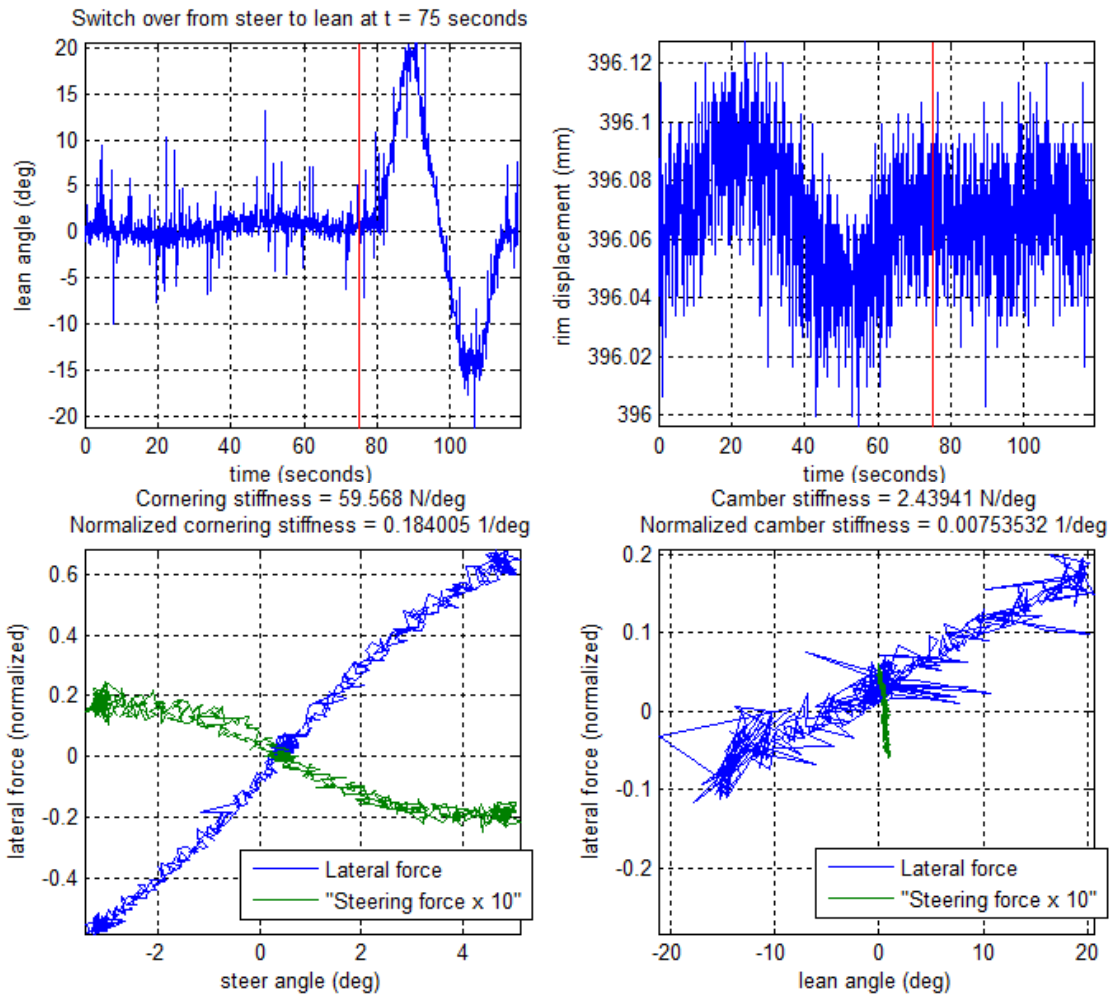


Figure 3-23: Raw force and displacement data captured from test device number 3.

3.9.6 Advantages and disadvantages of design

The 2.5 meter drum at TU Delft was designed for testing automobile and even truck tires, and so is well suited to this task. Any forward speed that a bicycle tire might reasonably encounter is easily producible. Its curvature of the drum, however, changes the length and width of the contact patch slightly. As with test device number 2, the wheel and frame

could be allowed to flex because actual tire orientation was recorded along with the force data.

Also, the safety precautions required for working with such a powerful system can be limiting. All testing must be performed from an adjacent room, behind a glass window. Close examination of the tire or test device during operation was not possible. The room is not well ventilated, and electronic equipment would sometimes fail when the air temperature rose during testing.

The drum is nearly flush to the floor, so working on the test frame, especially raising and lowering it repeatedly to make contact patch ink prints, was exhausting. The simple, manual control developed for the angle actuators meant that it was difficult to zero one angle exactly while sweeping the other.

3.10 Test data capture and processing

The first two systems, both at UWM, use an integrated system of proprietary sensors and data acquisition hardware and software by PASCOS[®]. The third system, at TU Delft, uses an ad-hoc arrangement of sensors connected to a National Instruments DAQ controlled by LabVIEW.

3.10.1 MATLAB[®]

In all cases, data from force, displacement, and acceleration sensors was captured on a laptop computer and then manipulated with MATLAB[®].

Read data from the *.xls file with a MATLAB® application and extract tire name, inflation pressure, and vertical load from the file name.

Apply calibration to sensor data.

```
% calibrate lateral force
masses = [0 2 2 2 2 2 2 2 2];
masses = cumsum(masses);
volts = [0 0.2 0.4 0.6 0.79 0.99 1.19 1.39 1.59];
p = polyfit(volts, masses, 1);
f1 = f1*p(1)*9.81;
% + p(2); %zeroed amplifier 'in situ' after calibration
% calibrate lean angle: 0.811 = -12 and %-1.706 = 25.5
% 0.7290 = -(90-77.2) and -1.8390 = +(90-59.3)
p = polyfit([0.7290 -1.839],[-(90-77.2) +(90-59.3)], 1);
a1 = a1*p(1) + p(2);
```

Prompt for time that separates slip angle sweep from camber angle sweep.

Combine appropriate force data with corresponding displacement or angle data.

Plot “raw” data, as seen in a sample image in **Figure 3-23** above.

Fit a first-order polynomial to data near the origin to extract stiffness and offset values.

```
p1 = polyfit(a2s, f1s, 1);
cornering_stiffness = p1(1);
cornering_stiffness_offset = p1(2);
p1 = polyfit(a1s, f1s, 1);
camber_stiffness = p1(1);
```

```
camber_stiffness_offset = p1(2);
```

Smooth data and shift data to so that zero force occurs at zero angle.

Plot smoothed and shifted data along with straight lines to indicate extracted stiffness values.

```
window_size = 100;
sorted_data = sortrows([(a2(1:switch_over_time_idx)) , ...
                        (f1(1:switch_over_time_idx))] );
filtered_data(:,1) = filter(ones(1,window_size)/window_size, ...
                            1, sorted_data(:,1));
filtered_data(:,2) = filter(ones(1,window_size)/window_size, ...
                            1,sorted_data(:,2));
slip_angle = abs(filtered_data(window_size:end,1));
normalized_cornering_force = ...
    abs(filtered_data(window_size:end,2) - ...
        cornering_stiffness_offset)/w;
plot(slip_angle, normalized_cornering_force, '-k', ...
     slip_angle_disp_range, ...
     slip_angle_disp_range*cornering_stiffness/w, '-k');

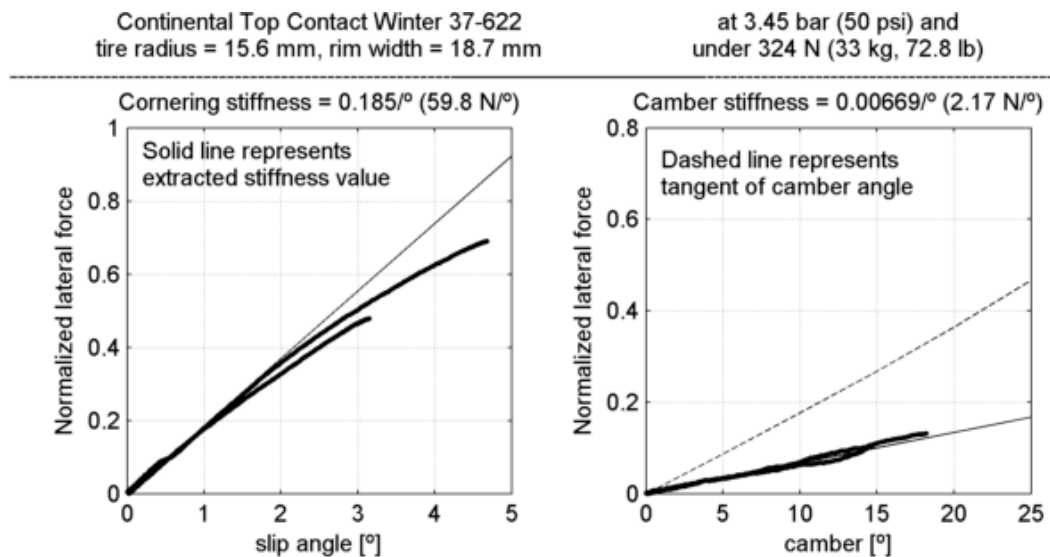
window_size = 50;
sorted_data = sortrows([(a1(switch_over_time_idx:end)), ...
                        (f1(switch_over_time_idx:end))] );
filtered_data(:,1) = filter(ones(1,window_size)/window_size, ...
                            1, sorted_data(:,1));
filtered_data(:,2) = filter(ones(1,window_size)/window_size, ...
                            1, sorted_data(:,2));
```

```

normalized_camber_force = ...
    abs(filtered_data(window_size:end,2) - ...
        camber_stiffness_offset)/w;
plot(abs(filtered_data(window_size:end,1)), ...
    normalized_camber_force, '-k', ...
    camber_angle_disp_range, ...
    camber_angle_disp_range*camber_stiffness/w, '-k', ...
    [0 5 10 15 20 25], tand([0 5 10 15 20 25]), '--k' );

```

Perform similar manipulations on data from second force sensor, multiply it by the fixed moment arm, and plot self-aligning torque and twisting torque. Plot straight line to indicate stiffnesses found for both forces and both torques. Look for lateral stiffness data for same tire configuration saved in separate file. Calculate pneumatic trail as simply self-aligning torque divided by cornering force and plot that. Plots of the same data used in the image above can be seen in the sample image below.



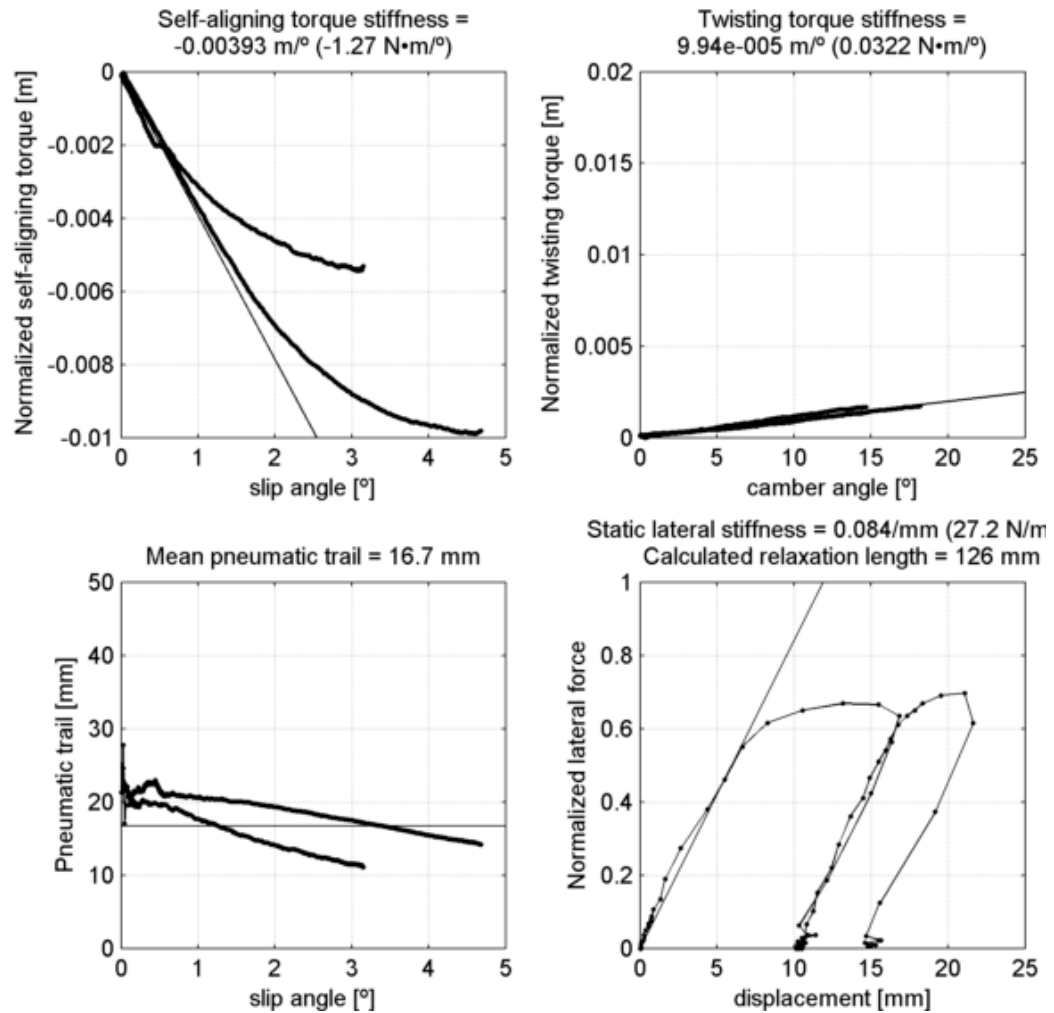


Figure 3-24: Formatted data from test device number 3.

3.10.2 Detection and subtraction of periodic noise in force data

With test device number 1, besides issues with the horizontal and vertical tracks, several other sources of noise in the data were identified. A fast Fourier transform of the data, shown below in **Figure 3-25**, reveals periodic signals with periods that closely match the circumferences of the wheels that run against the vertical track and the support wheel that runs against the braking surface of the rim. The original inexpensive casters were

replaced with neoprene wheels on ball bearings: off-the-shelf in-line skate and roller shoe wheels and bearings.

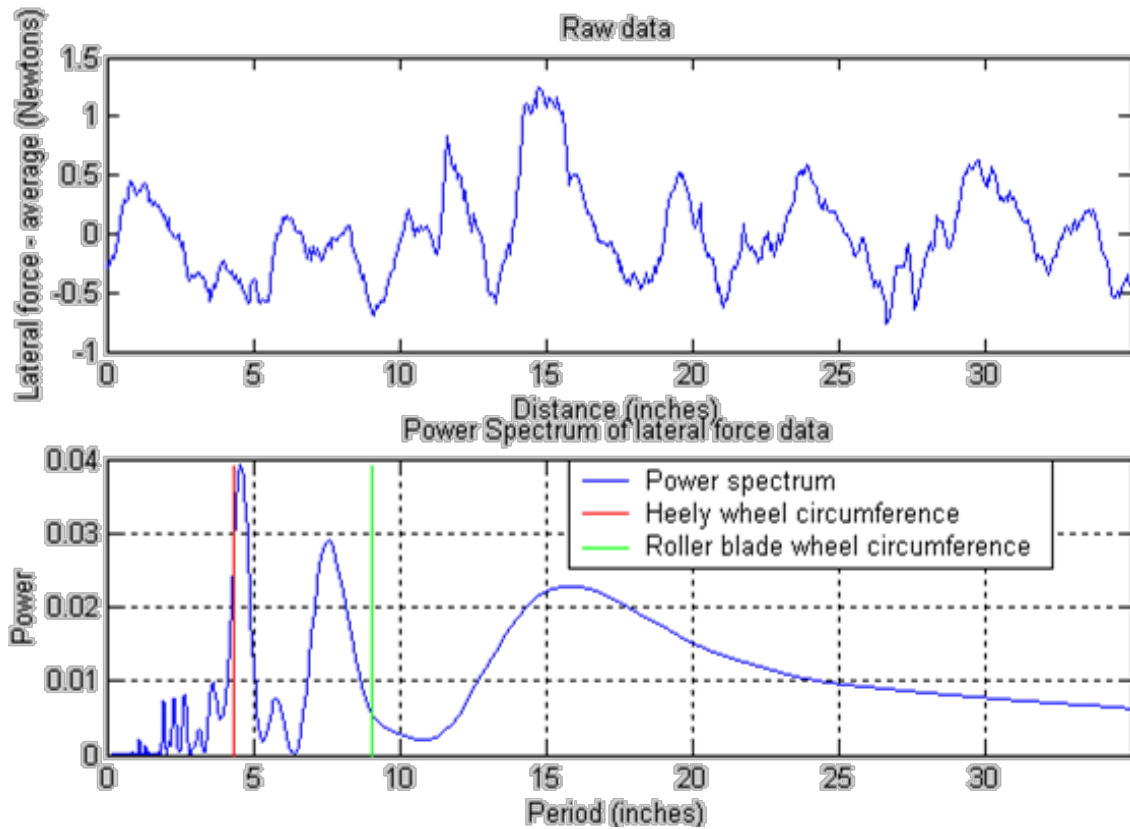


Figure 3-25: Fourier analysis of raw lateral force data showing signal from irregularity in the Roller shoe wheels and the Inline skate wheel.

For test device number 2, because it was able to collect data over multiple rotations of the bicycle wheel, the same analysis finds the largest signal has a period equal to the bicycle wheel circumference, as shown below in **Figure 3-26**.

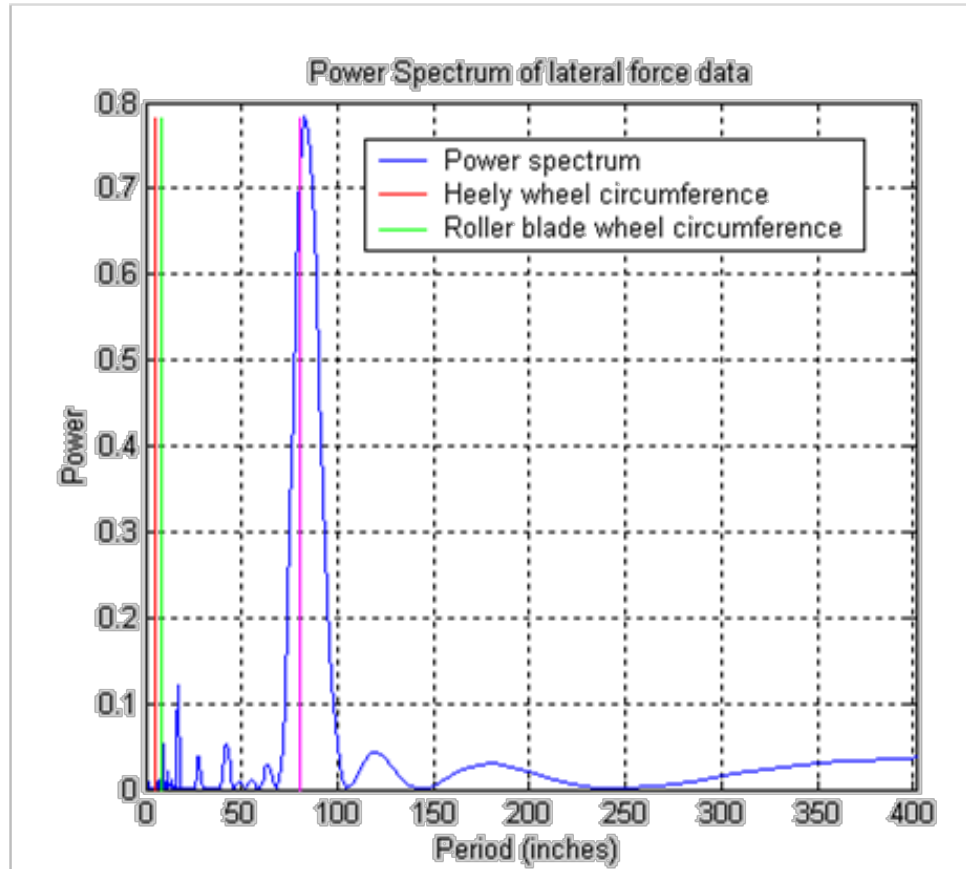


Figure 3-26: Power spectrum of force data collected from test device number 2. The vertical blue line at 83 inches is the circumference of the bicycle wheel with tire.

Once identified, this sinusoidal signal could be subtracted from the force data to smooth it out dramatically, as shown below in **Figure 3-27**.

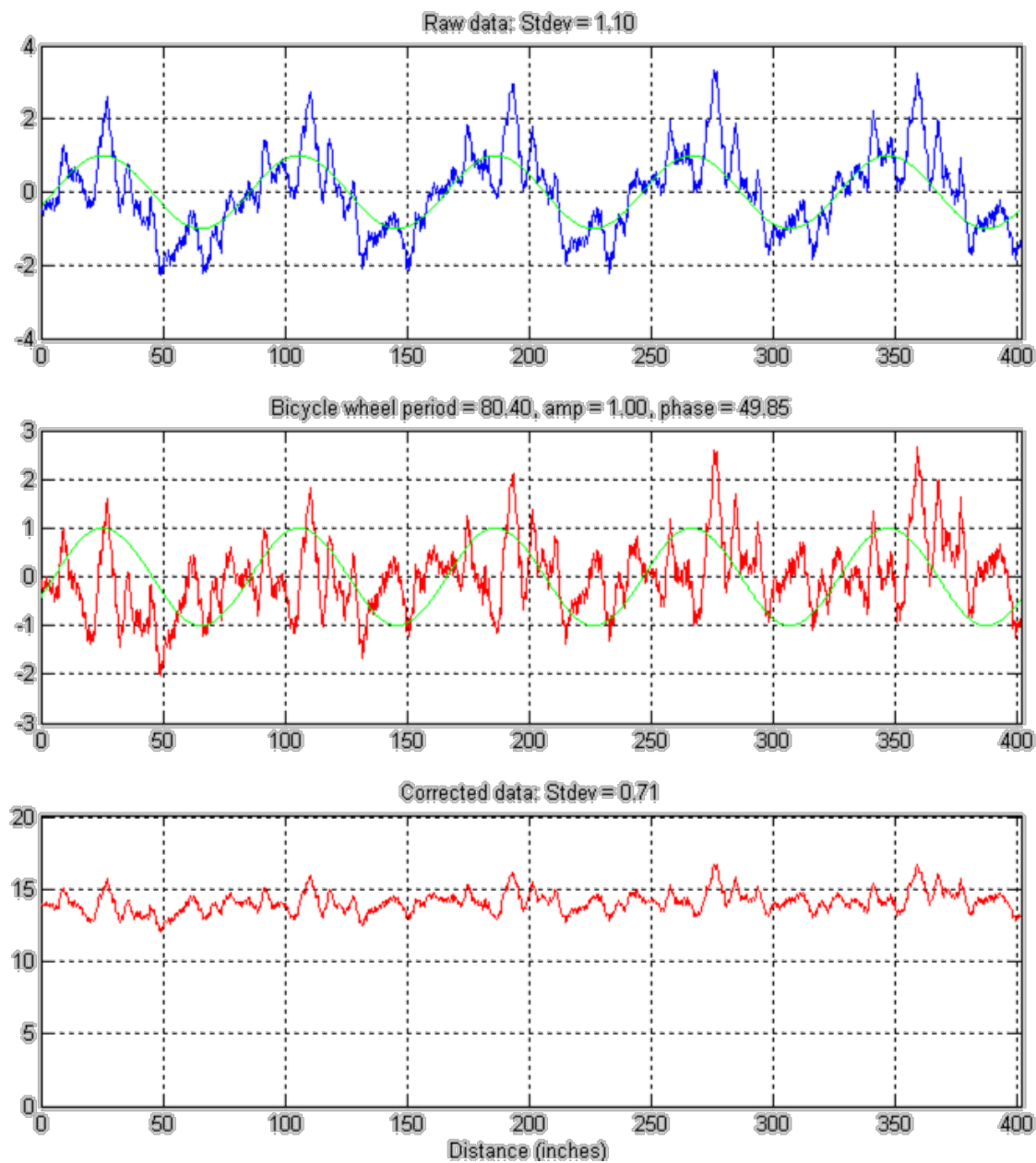


Figure 3-27: Raw data and data corrected by subtracting out the signal with period equal to the circumference of the bicycle wheel.

3.10.3 Wheel lateral stiffness

A displacement sensor was mounted rigidly to the fork to measure wheel rim deflection relative to the fork.

Published values for wheel stiffness include the maximum, minimum, and average presented below in **Table 3-6**. [40]

Table 3-6: Published wheel lateral stiffnesses

maximum	78 N/mm	2006 Shimano WH-7801 Carbon 50
minimum	27 N/mm	2007 Xentris Mark 1 TT
average	52.7 N/mm	2005/2008 Campagnolo Bora G3 2008 Mavic Cosmic Carbone SL Premium 2007 Mavic Ksyrium Equipe

The measured values are approximately 50 N/mm, close to the published average, which translates to about 0.3685 degrees per 100 N. Thus, a maximum variation in camber angle from the values measured at the fork of less than 1 degree can be expected for the range of forces encountered during testing, up to 250 N. That, in turn, represents only a 0.01 variation in normalized lateral force, based on an approximate average normalized camber stiffness of 0.01 1/°.

3.10.4 Lateral force sensor misalignment

The original design called for the fixed end of the lateral force sensor to also move on a curved track along with the forward pivot point to maintain a constant geometry during slip angle sweeps, but this was eliminated to simplify and speed up the construction.

As it turns out, the slip angle was usually limited to less than $\pm 3^\circ$, so as not to exceed the limitations of the lateral force sensor, and so the distortion of the recorded lateral force is minimized. Even at 5° , the force value recorded is overstated by less than 0.5%

$$error = \frac{1}{\cos(5^\circ)} - 1 = 0.00382 < 0.5\% \quad \text{Eq. 3-5}$$

3.11 Other testing

3.11.1 Instron compression stiffness

Rate-independent hysteresis was observed in bicycle tires similar to that described by Foale in motorcycle tires.[41] The force required to create a given deflection in a tire depends on the history of force and deflection. If deflection is increasing, the required force is higher than if the deflection is decreasing, as shown below in **Figure 3-28**.

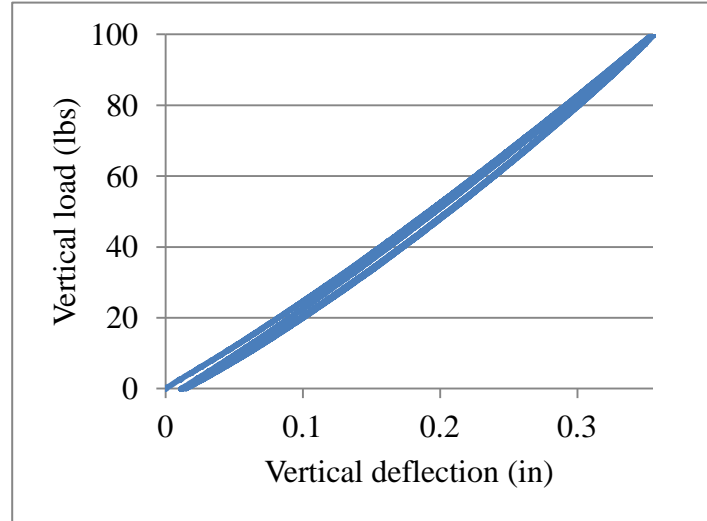


Figure 3-28: Vertical deflection vs. vertical load showing rate-independent hysteresis.

This property of the tires will affect the lateral stiffness measured by simply displacing a tire laterally and measuring the force required to do so.

3.11.2 Rate-dependent lateral stiffness

The lateral stiffness value was found to depend on the rate at which the tire is laterally displaced: rate dependent hysteresis. **Figure 3-29** shows the different stiffness obtained by applying a lateral displacement at varying rates, as shown in **Figure 3-30**.

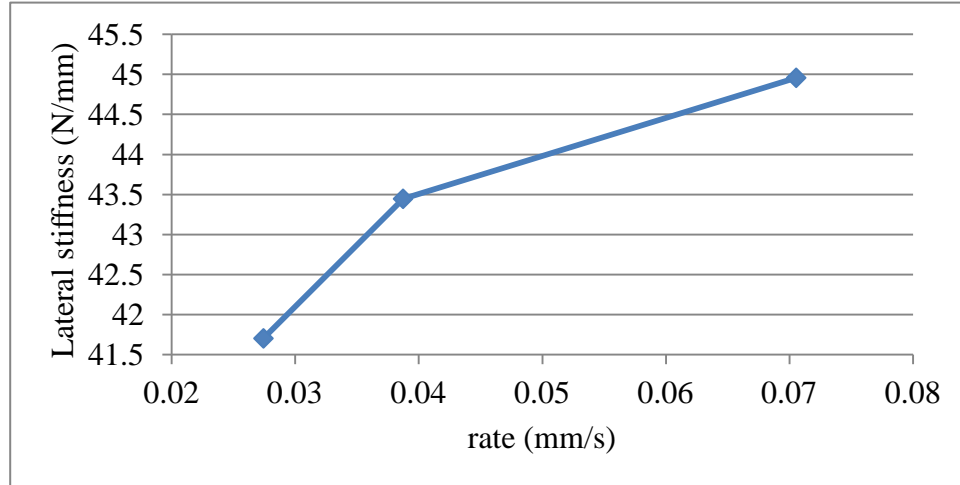


Figure 3-29: Lateral stiffness dependence on lateral displacement rate.

3.11.3 Stress relaxation

Another viscoelastic behavior observed was stress relaxation: stiffness decreases with time.

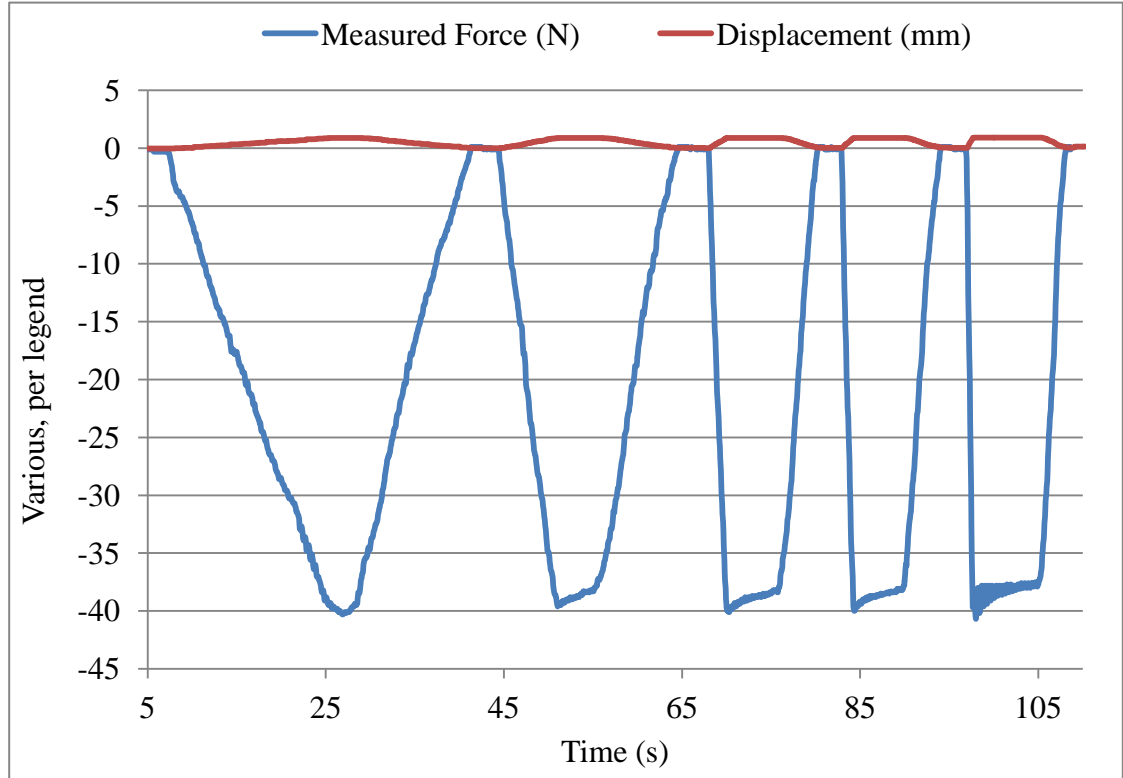


Figure 3-30: Force and displacement vs. time demonstrating stress relaxation.

This behavior, along with the rate dependent hysteresis graphed in **Figure 3-29**, have implications for stiffness testing. Applying a displacement too quickly or slowly will result in a value different from the value that the tire would exhibit when used on a bicycle.

3.11.4 Decay length

The displacement of a tire subjected to a point lateral load was measured to better understand how a tire transitions from being laterally displaced in the contact patch to being undisplaced far from the contact patch.

As shown below in **Figure 3-31**, deflection of $1/20''$ (half of white square at right, calibrated to scale in middle) appears to be completely gone after 3 inches (white dot just under edge of ruler at about 2.4 on the scale towards the left), so the decay length is $3(1 - 0.36788) \approx 1.9$ inch.

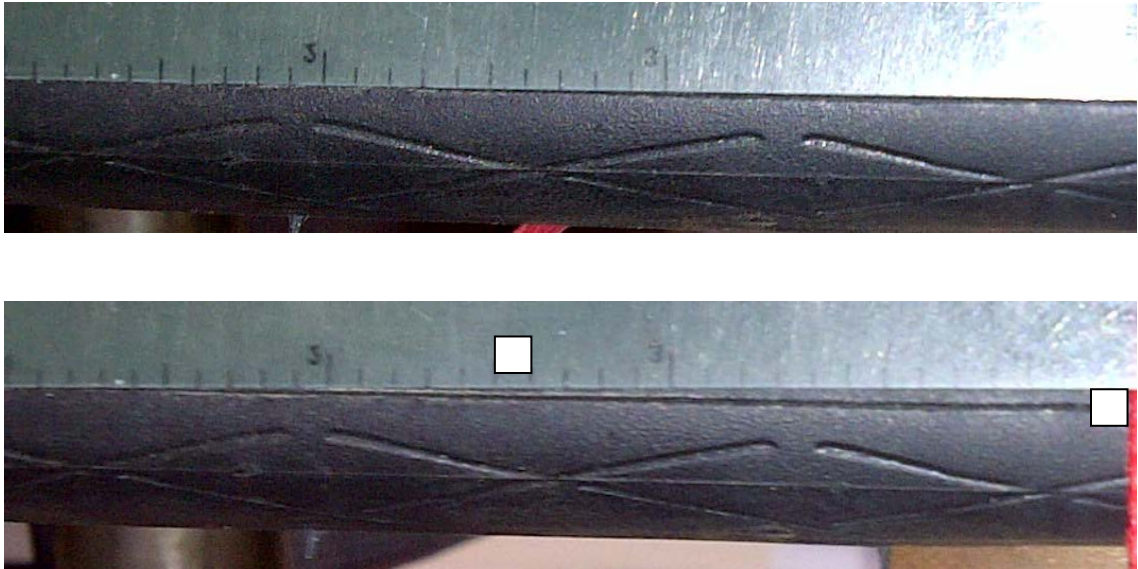
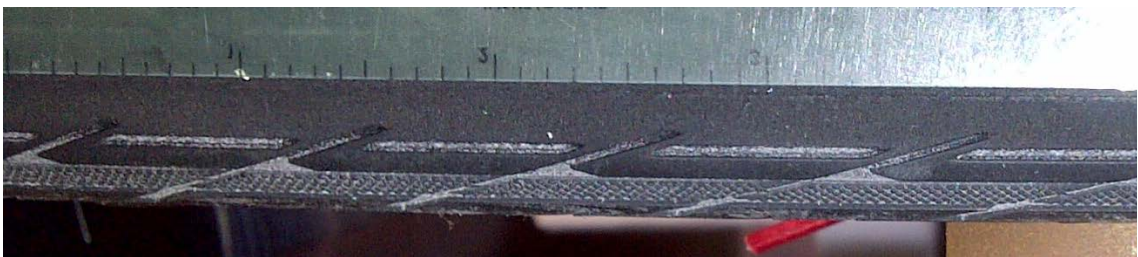


Figure 3-31: Schwalbe Durango 23-622 at 80 psi. Undeformed above, and deformed by a 25 lb localized lateral load (by red cord at far right) below.

As shown below in **Figure 3-32**, deflection of $1/10''$ (white square at right, calibrated to scale in middle) appears to have reduced to 0.036788 (white square at left) by 3.9 inches.



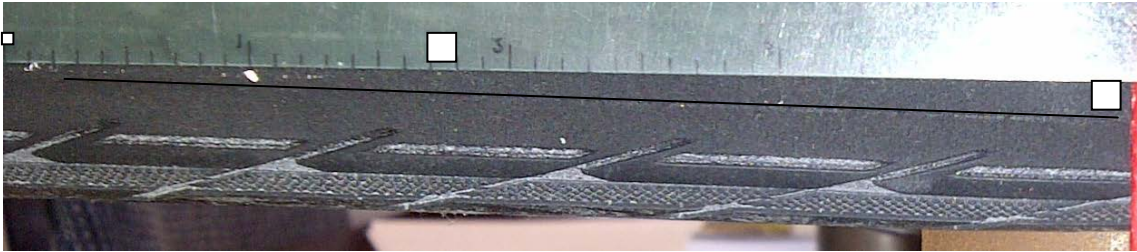


Figure 3-32: Bontrager All Weather 28-622 at 50 psi. Undeflected above, and deflected by a 25 lb localized lateral load (by red cord at far right) below.

3.11.5 Confirming slip angle during camber

Attempts were made to confirm the slip angle that occurs during pure camber, in order to validate or invalidate the “tangent rule”, described above in section 2.4. A video recording device was mounted at the rear axle of a bicycle and aimed at the ground. Then the bicycle was rolled straight forward while kept vertical on pavement with a lateral slope. The idea was to measure the motion of the pavement, relative to the rear wheel, by tracking the trajectory of identifiable points on the pavement, in order to measure the side slip angle, as shown below in **Figure 3-33**.



Figure 3-33: Extracting slip angle from sequential video frames.

Unfortunately, uncertainty in attempts to extract the relative velocity of the pavement from the resulting video was too large to confirm or deny the presence of small slip angles, on the order of 1° . A better approach might be to use an existing device, such as the Correvit Non-Contact Optical Sensor, pictured below in **Figure 3-34**, but corrections would have to be made for camber angle. Such a device was beyond the budget of this project, however, and attempts to borrow one from the manufacturer were unsuccessful.[42]



Figure 3-34: Contact-less optical sensor for measuring sideslip angle.

3.12 Test protocols

3.12.1 Instrument warm up and calibration

Instruments were powered on and allowed to warm up for about a half hour before calibration or testing began. Calibration was performed by applying several known, independently measured inputs, forces or displacements, and recorded the reported voltages. These value pairs were then fitted to a first order polynomial with the polyfit() function in MATLAB®, and the resulting two constants, a slope and an offset, are used in MATLAB® to interpret the recorded values.

3.12.2 Tire break in and warm up

Tires were run on the drum at varying orientations for several minutes after being mounted on the rim to ensure that they were seated on the rim fully and to scuff off any die-release agent left over from the manufacturing process.

3.12.3 Forward rolling rate

Since testing has shown that the horizontal force generated in the contact patch decreases with time, see section 3.11.3, it is necessary to roll the wheel at a forward rate sufficient to minimize this effect.

3.12.4 Test device angle actuation rate

Since horizontal force due to side slip takes a finite time to develop,[16] it is necessary, in the case of continuous force and angle measurement, to modify the slip angle slowly enough, relative to the forward rolling rate, so that an accurate measure of the horizontal force can be taken.

3.12.5 Operating temperature

All tests were performed at “room temperature”.

3.12.6 Steps for test device number 3

- 1 Inflate tire to desired pressure.
- 2 Attach desired vertical load to test frame.
- 3 Lift frame and place wheel on ink pad.
- 4 Lift frame and place inked tire on sheet of paper on top of the drum.
- 5 Lift frame and place wheel on ink pad.
- 6 Lift frame and place inked tire on sheet of paper on top of a flat plate.

- 7 Lift frame and place wheel on strip of non-skid tape on drum.
- 8 Detach lateral force sensor from fixed mounting point.
- 9 Start recording sensor data with LabVIEW application.
- 10 Pull on far end of lateral force sensor horizontally to create lateral deflection in tire.
- 11 Stop recording data with LabVIEW application.
- 12 Save data recorded by LabVIEW into an *.xls file whose name encodes the tire name, the inflation pressure, the vertical load, and drum rotation rate of zero.
- 13 Reattach lateral force sensor to fixed mounting point.
- 14 Start drum rotation.
- 15 Start recording sensor data with LabVIEW application.
- 16 Sweep orientation angles, first slip and then camber.
- 17 Stop recording data with LabVIEW application.
- 18 Stop drum rotation.
- 19 Save data recorded by LabVIEW into an *.xls file whose name encodes the tire name, the inflation pressure, the vertical load, and drum rotation rate.
- 20 Return to step one and repeat with next configuration.

CHAPTER 4

EXPERIMENTAL RESULTS

4.1 Physical measurements

4.1.1 Ink prints of contact patch

The contact patch images were scanned into PDF documents, cut and pasted into JPEG format images, and analyzed in MATLAB® to extract their length, width, and area. First, the image is converted from grey-scale to black-and-white. Then groups of pixels are identified and a convex hull is constructed around them. Finally, an ellipse is fitted to the convex hull, as shown below in **Figure 4-1** and **Figure 4-2**.

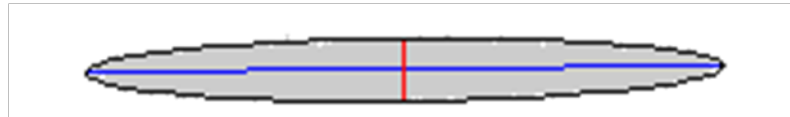


Figure 4-1: Contact patch on the plate analyzed in MATLAB®.

Contact patch on the plate image area = 15479 square pixels (461.7 mm^2), which, when assuming a uniform pressure, yields a pressure of 0.6587 N/mm (95.5% of inflation pressure). A fitted ellipse has a length = 453 pixels (78.2 mm) and width = 43.9 pixels (7.57 mm) for an ellipse area of 15588 pixels (464.9 mm^2), which yields a pressure of 0.6541 N/mm_2 (94.9% of inflation pressure).

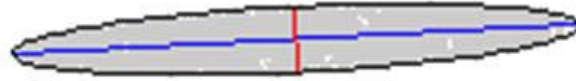


Figure 4-2: Contact patch on the drum analyzed in MATLAB®.

Contact patch on the drum analyzed in MATLAB®: image area = 14252 square pixels (425.1 mm²), which yields a pressure of 0.7155 N/mm (104% of inflation pressure). A fitted ellipse has a length = 404 pixels (68.8 mm) and width = 45.6 pixels (7.87 mm) for an ellipse area of 14463 pixels (431.3 mm²), which yields a pressure of 0.705 N/mm² (102% of inflation pressure).

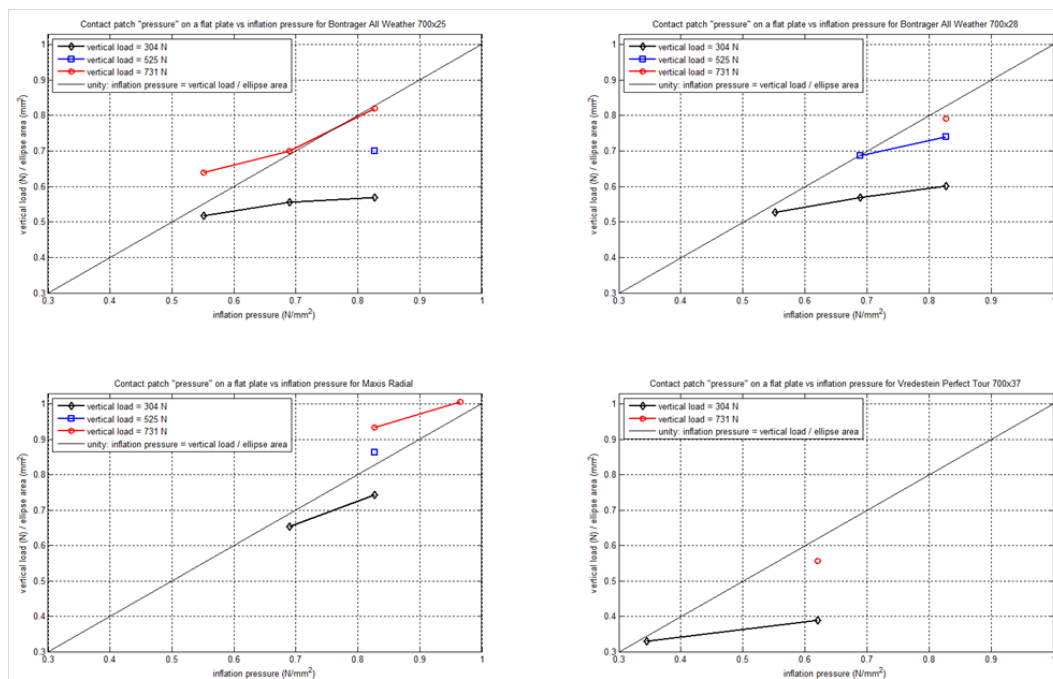


Figure 4-3: Comparison of vertical load divided by measured contact patch area vs. inflation pressure. The assumption that they are equal is represented by the black diagonal line.

4.1.1.1 Drum vs. Plate

As expected, the contact patches taken on the drum are slightly shorter and wider than those taken on the plate. The data is summarized below in **Table 4-1**.

Table 4-1: Summary of contact patch length, width, and area for plate and drum.

	Max	Min	Mean	Stdev
drum/plate length	105%	81%	92%	3.1%
drum/plate width	132%	83%	112%	8.5%
drum/plate area	119%	68%	104%	8.2%

4.1.2 Forces and moments

Despite the finite curvature radius of the drum, and the measurable effect it has on contact patch length and width, it is expected to have a negligible effect on forces and moments measured. A Calspan report from 1975 on testing bicycle tires on a 4-foot diameter (1.2192 meter, a little less than half the diameter of the 2.5 meter drum used at TU Delft) explicitly states “Since the bicycle tire contact patch is small, the drum closely approximates a flat surface.”[20] This is confirmed by the good agreement between the measurements from test device number 2 at UWM and test device number 3 at TU Delft, described below in section 4.4.2, and by the Rotta model, described below in section 5.3.1.

4.1.3 Lateral stiffness

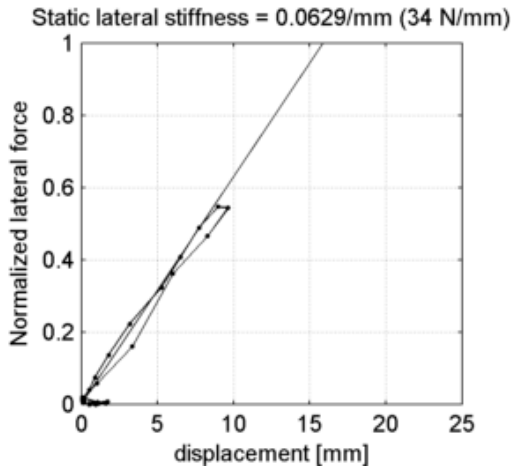


Figure 4-4: Lateral stiffness for Schwalbe Big Apple 55-622 on rim of width 18.7 mm at 3 bar (44 psi) and under 450 N (55 kg, 121 lb) vertical load.

4.1.4 Cornering stiffness

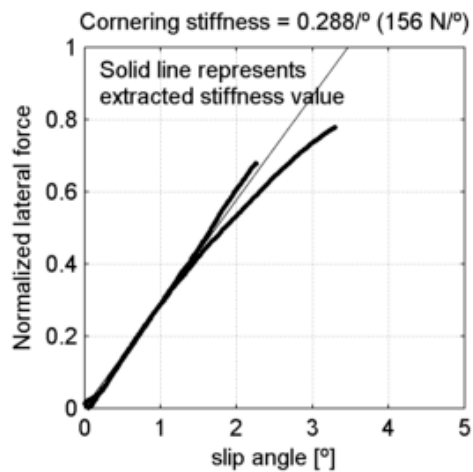


Figure 4-5: Cornering stiffness for Schwalbe Big Apple 55-622 on rim of width 18.7 mm at 3 bar (44 psi) and under 450 N (55 kg, 121 lb) vertical load.

4.1.5 Camber stiffness

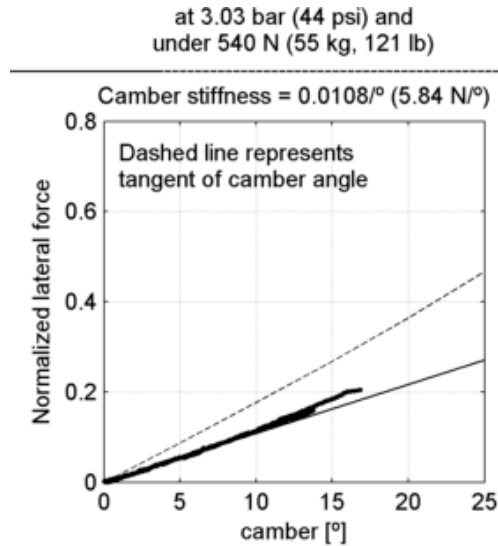


Figure 4-6: Camber stiffness for Schwalbe Big Apple 55-622 on rim of width 18.7 mm at 3 bar (44 psi) and under 450 N (55 kg, 121 lb) vertical load.

4.1.6 Self-aligning torque

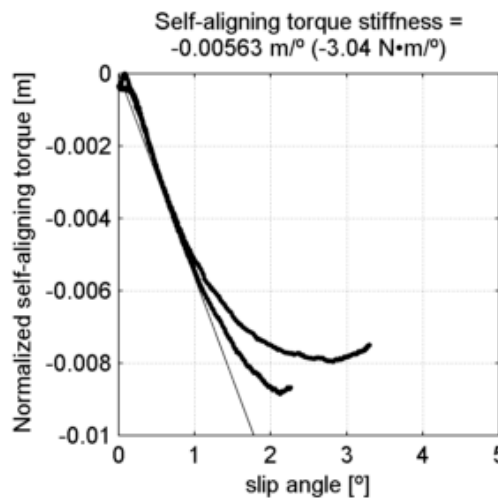


Figure 4-7: Self-aligning torque stiffness for Schwalbe Big Apple 55-622 on rim of width 18.7 mm at 3 bar (44 psi) and under 450 N (55 kg, 121 lb) vertical load.

4.1.7 Twisting torque

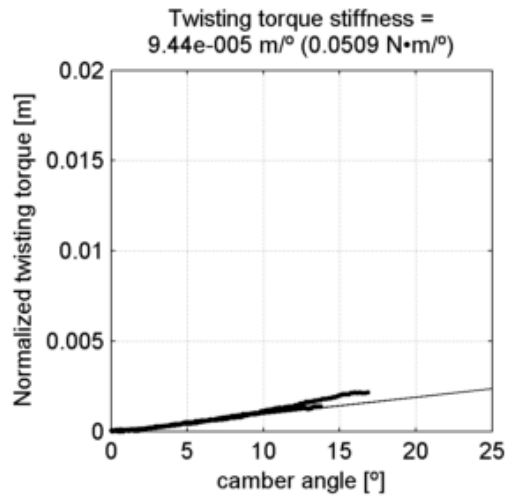


Figure 4-8: Twisting torque stiffness for Schwalbe Big Apple 55-622 on rim of width 18.7 mm at 3 bar (44 psi) and under 450 N (55 kg, 121 lb) vertical load.

4.1.8 Pneumatic trail

Calculate pneumatic trail from experimentally measured cornering force and self-aligning torque via Pacejka's formula 1-87:[2]

$$t(\alpha) = \frac{M_z(\alpha)}{F_y(\alpha)} \quad \text{Eq. 4-1}$$

The calculated value varies with slip angle due to the variation in cornering force and self-aligning torque, and so an arithmetic mean is calculated and reported.

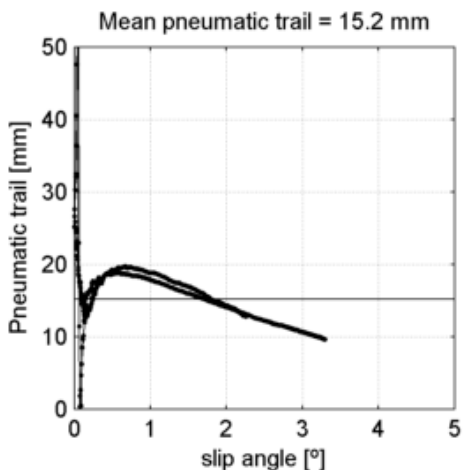
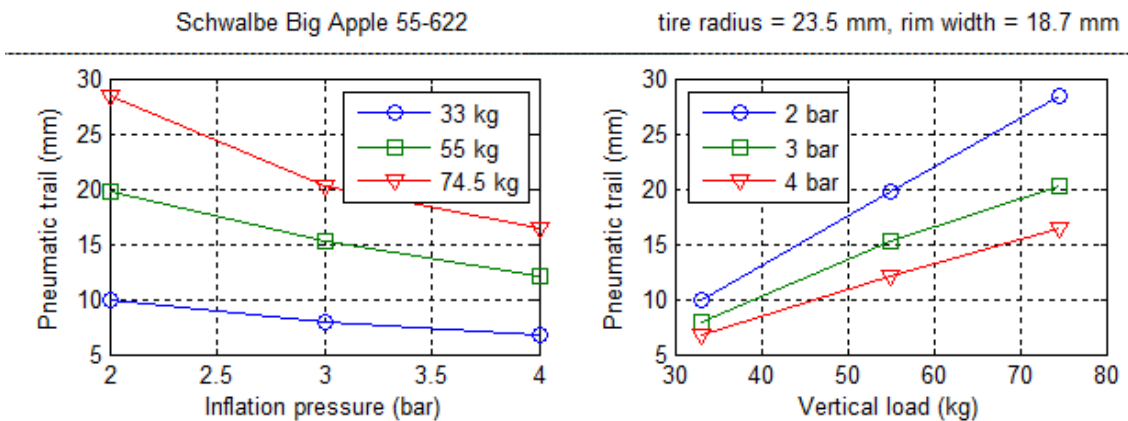


Figure 4-9: Pneumatic trail for Schwalbe Big Apple 55-622 on rim of width 18.7 mm at 3 bar (44 psi) and under 450 N (55 kg, 121 lb) vertical load.

The 15.2 mm mean pneumatic trail reported in **Figure 4-9** is 14.76% of the 103 mm contact patch length on the drum. The average ratio of mean pneumatic trail over contact patch length for all tires and configurations tested was 12.76%.



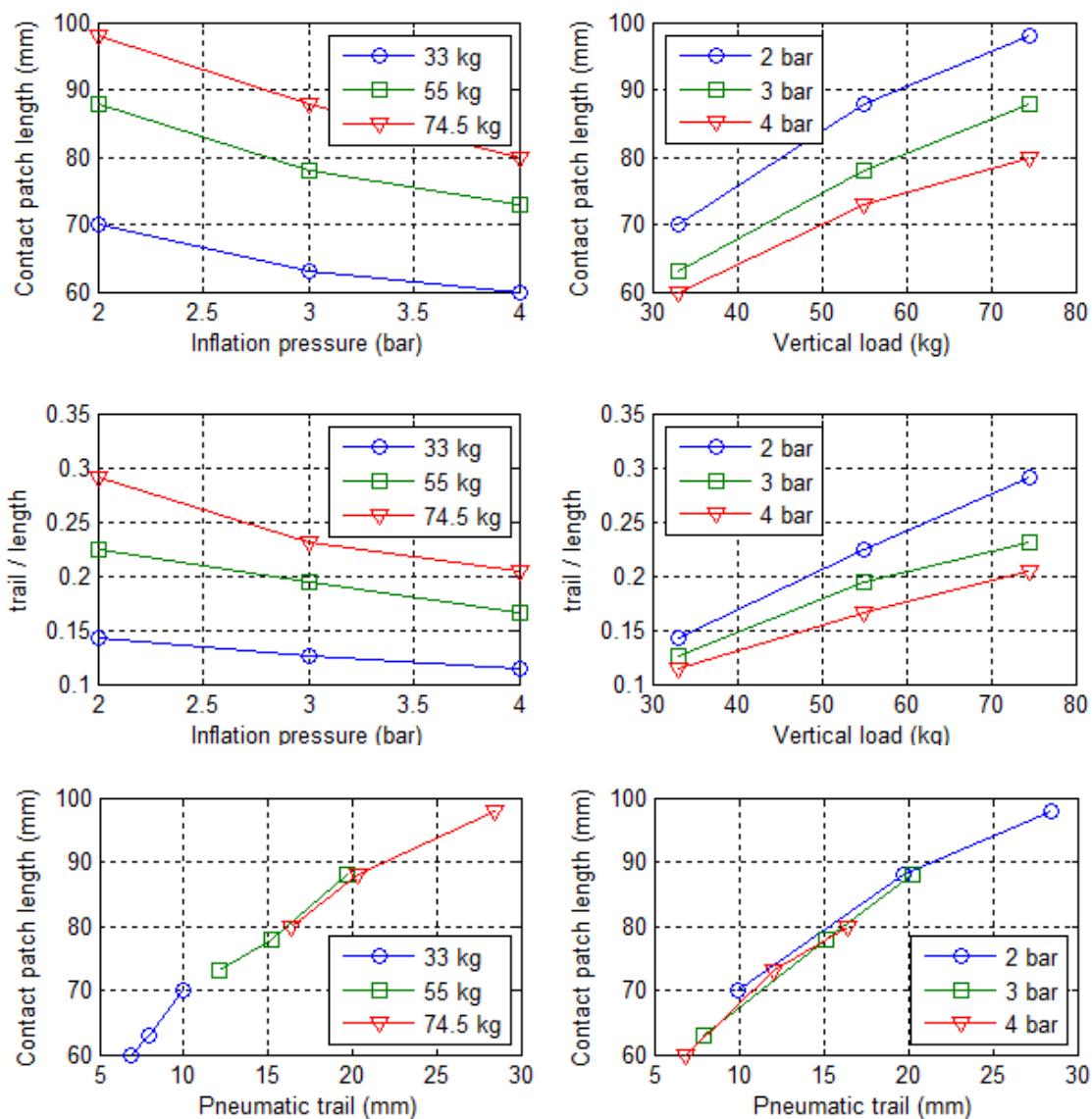


Figure 4-10: Summary of pneumatic trail for all Schwalbe Big Apple tests.

4.1.9 Relaxation length, decay length, and relaxation distance

Pacejka defines “relaxation length” as “an important parameter that controls the lag of the response of the side force to the input slip angle.” He also uses the term to indicate the length of laterally deflected tire beyond the end of the contact patch: “The length σ ,

designated as the relaxation length.” For a “non-steady-state out-of-plane string-based” tire model, he calculates it in his equation 5.5 as [2]

$$\sigma = \sqrt{\frac{S}{c_c}} \quad \text{Eq. 4-2}$$

where c_c is the lateral carcass stiffness per unit length, and S is the circumferential component of the total tension force.

He also provides another expression (7.6) for calculating it in “single contact point transient” tire models. [2]

$$\sigma_\alpha = \frac{C_{F\alpha}}{C_{Fy}} \quad \text{Eq. 4-3}$$

The values calculated from the collected data agree with the rules of thumb Pacejka provides: “of the order of magnitude of the wheel radius” and “approximately equal to half the contact length of the tyre.”[2]

It is not clear, however, that these two different parameters, the distance a tire rolls after a step change in slip angle before the side force reaches 63% of its steady-state, and the length along the tire beyond the end of the contact patch that is deflected laterally, are equivalent.

Therefore, in this document, “decay length”, ℓ , will be used exclusively to mean the length along the tire beyond the end of the contact patch that is deflected laterally, and “relaxation distance”, κ , will be used exclusively to mean the distance a tire rolls after a step change in slip angle before the side force reaches 63% of its steady-state.

4.1.9.1 Decay length

Pacejka develops a decay length, given in **Eq. 4-2** above, for the string model of a tire.

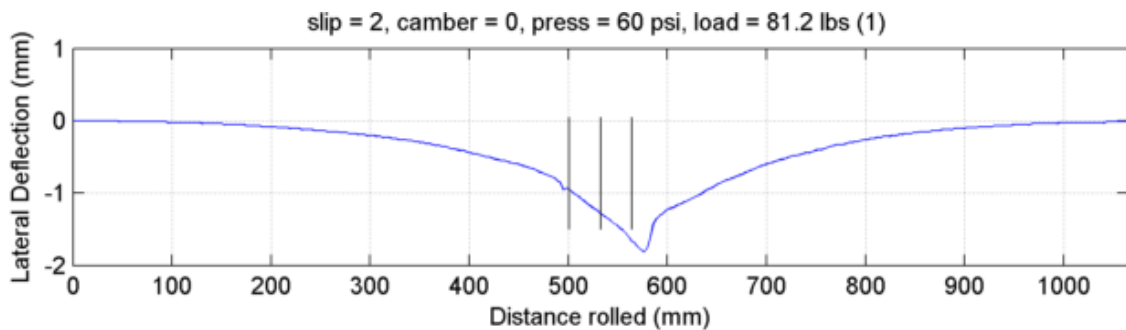
The Rotta model for the stiffness of a single cross section has been combined with the model of a beam on an elastic foundation to describe the deflection of the centerline of the tire beyond the ends of the contact patch.

The fourth-order differential equation of a beam on an elastic foundation has a

characteristic length $\frac{1}{\ell} = \sqrt[4]{\frac{k}{4EI}}$, where k is the stiffness of the foundation, E is the

modulus of elasticity of the beam material, and I is the area moment of inertia of the beam cross section.

As can be seen in **Figure 4-11** below, the lateral deflection looks as might be expected from a non-zero slip angle, but is oddly S-shaped when the tire is not generating a side force.



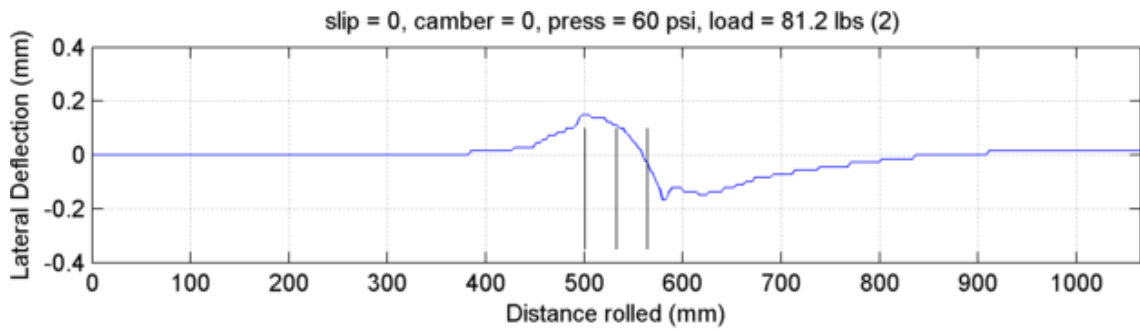


Figure 4-11: Recorded tire centerline lateral deflection non-zero and zero slip angles.

A wire-spoked wheel, however, under a vertical load experiences a vertical deflection of the rim over the contact patch, it will also deflect laterally “away from the spoke where the load is applied.”[39] To confirm that this effect is contributing to the tire centerline lateral deflection data, the same tests were performed with the same tire mounted on a carbon tri-spoke wheel by HED Cycling, as pictured in **Figure 3-15**.

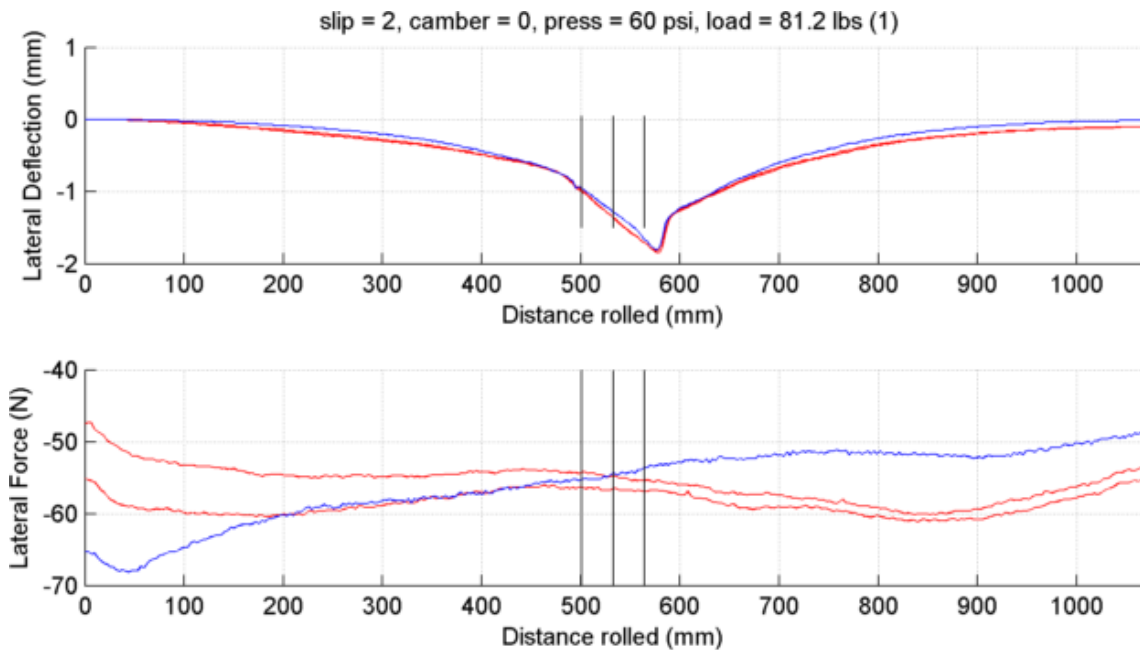


Figure 4-12: Recorded tire centerline lateral deflection for non-zero slip angle.

It appears, in **Figure 4-12** above, that the spoke arrangement to support the rim has negligible influence on tire centerline displacement during non-zero slip angles.

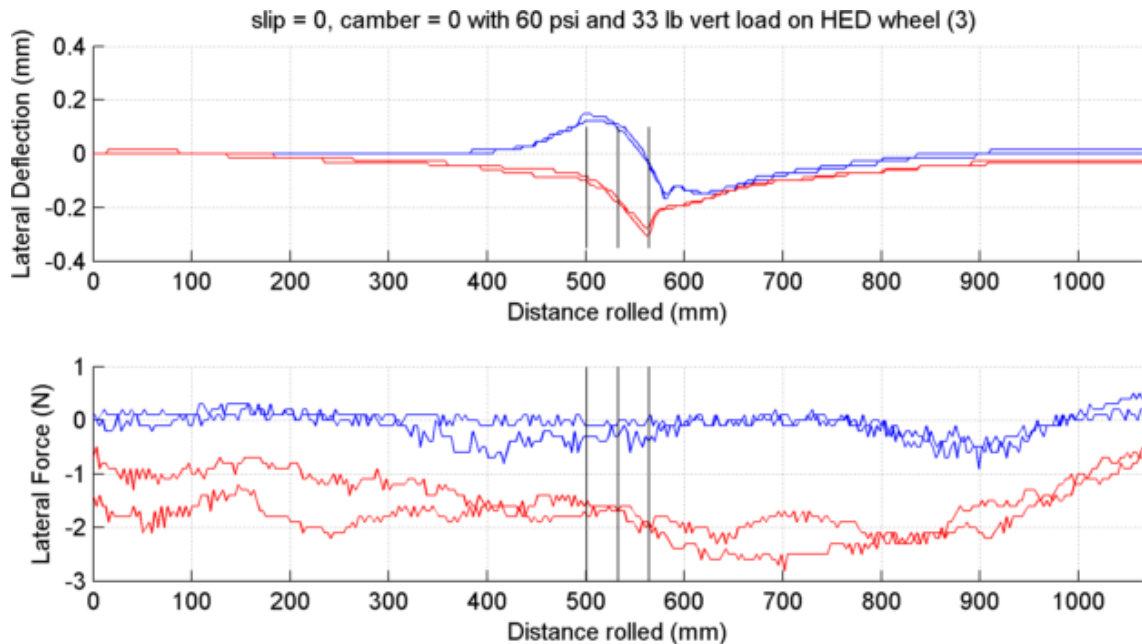


Figure 4-13: Recorded tire centerline lateral deflection for zero camber and slip angles.

In **Figure 4-13** above, the crude S-shape seen in the deflection of the wire-spoked rim (in blue) is completely absent in the deflection of the tri-spoked wheel (in red), and the remaining small deflection ($0.3 \text{ mm} \approx 0.012 \text{ in}$) is likely due to some other deformation of the now-unsupported rim or due to the widening tire pressing the sensor string onto the non-skid tape.

The data presented below in **Figure 4-14** confirm that the small, $\sim 0.1 \text{ mm}$, lateral displacement of the centerline actually occurs, is asymmetric, and is not just some artifact of the measuring technique. Instead, it is likely due to slightly non-zero camber or slip angles, even tire or rim non-uniformity, or some combination of these conditions.

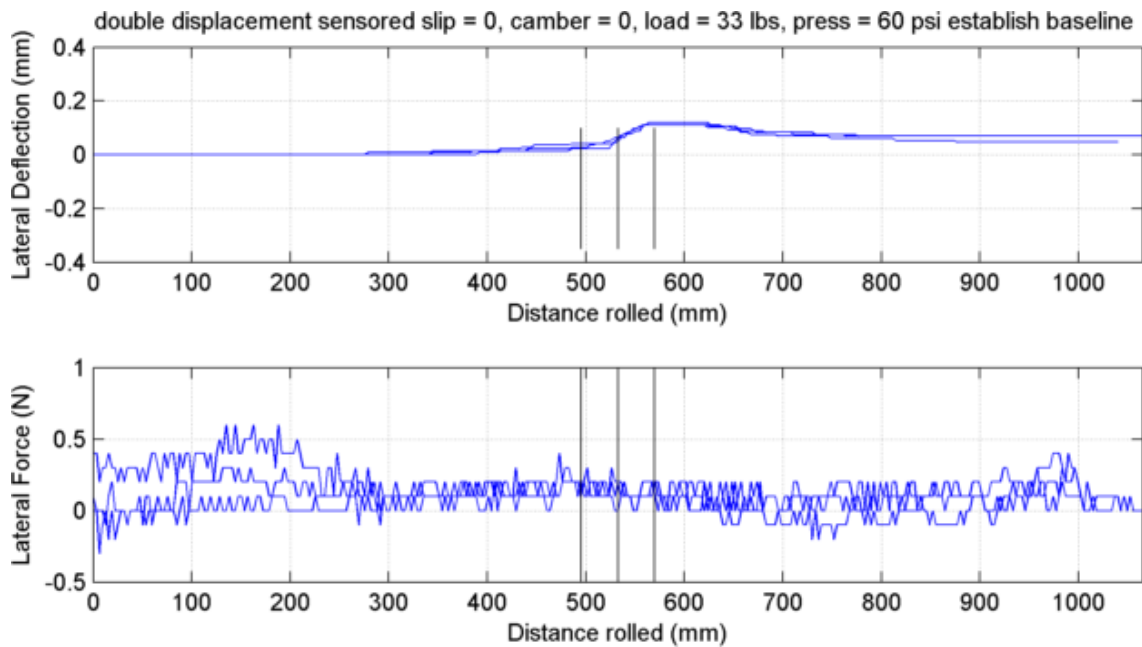


Figure 4-14: Tire centerline lateral displacement with zero slip and zero camber angles.

The sensors mounted on the wheel to measure lateral displacement of the tire centerline prevent the use of the pair of sensors mounted to the track and that measure the displacement of the rim, which are used to measure slip angle. Instead, zero slip angle was set for these tests by adjusting the track orientation until the measured lateral force generated by the tire was zero. It is possible that modifications to the test apparatus fork assembly, which were necessary for it to accept the wider hub of the rear tri-spoke wheel, could have caused the wheel to be slightly out of vertical alignment with the fork, and zero camber angle is set with a level mounted to one of the fork blades. Thus, even though the measured lateral force was zero, the camber angle might have been slightly non-zero, and that was countered by a slightly non-zero slip angle in the other direction.

Finally, the fact that slip angle has a larger effect on centerline lateral displacement could explain the small lateral displacement measured when the measured lateral force was zero.

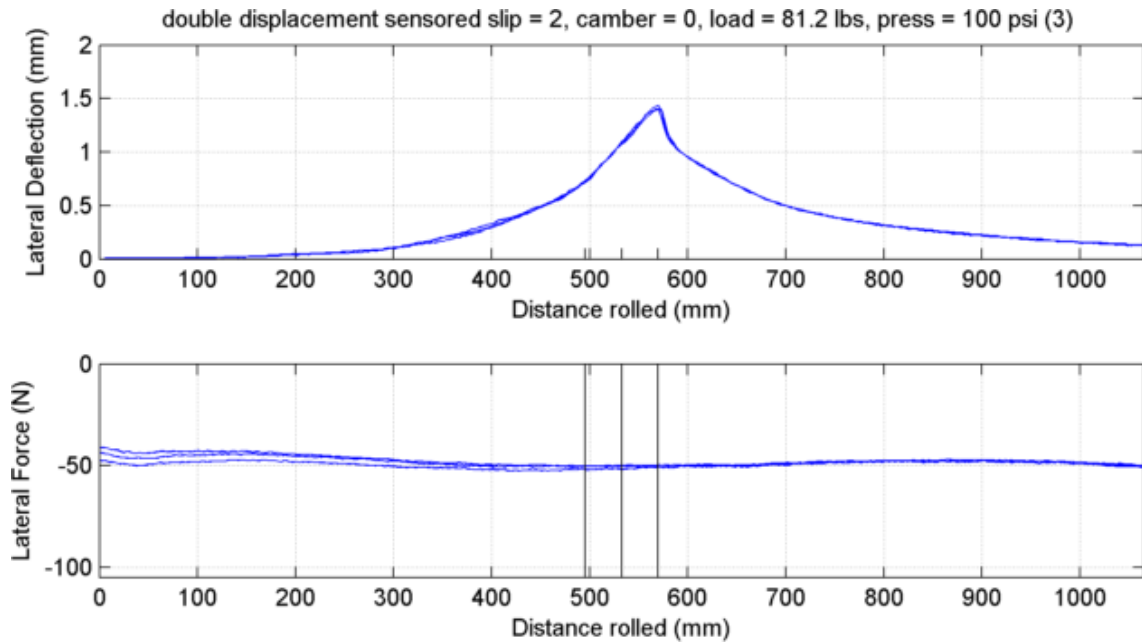


Figure 4-15: Tire centerline lateral displacement with non-zero slip angle.

The long decay length, ~3 times the length of the contact patch, can clearly be seen before and after the nearly straight track through the contact patch in **Figure 4-15** above.

Three separate test runs are superposed to show excellent repeatability of experiment.

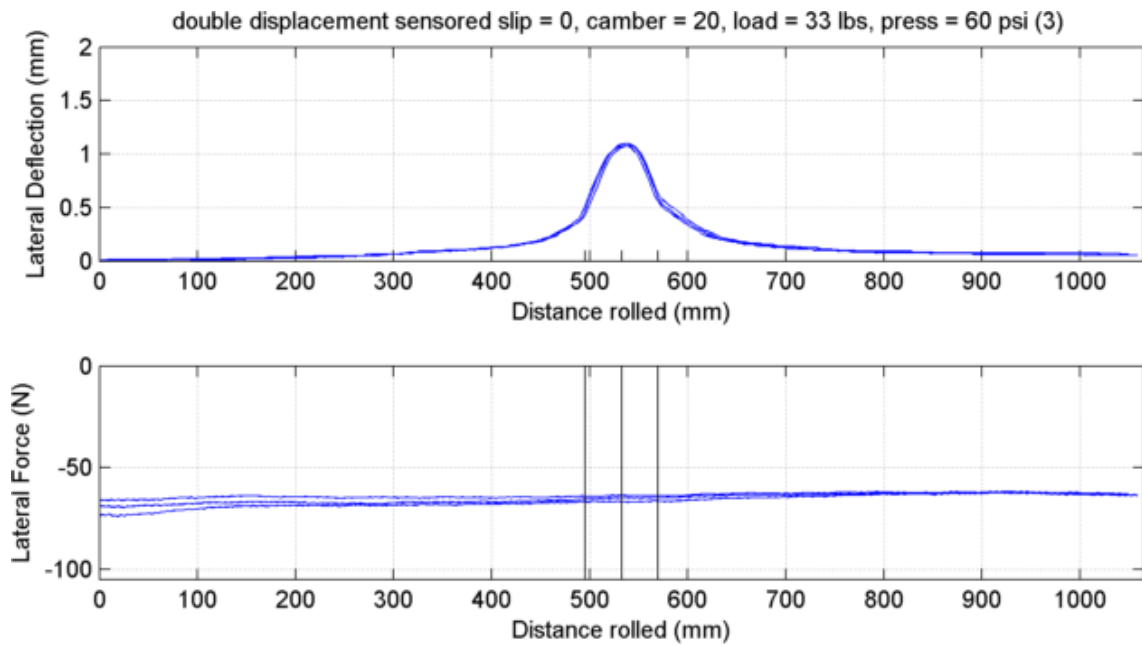


Figure 4-16: Tire centerline lateral displacement with non-zero camber angle.

The curved trajectory of the tire centerline through the contact patch of a cambered tire can clearly be seen in **Figure 4-16** above. The smaller lateral displacement required by the tire in camber to produce a larger lateral force than the tire in slip can be seen by comparing **Figure 4-16** with **Figure 4-15**.

Finally, the assumption that force and displacement due individually to non-zero camber and non-zero slip angles can be superposed to yield a good approximation of the combined effects of both is confirmed in **Figure 4-17** below. The slight misalignment of the peak lateral displacement is most likely due to experimental error: not starting each test run with identical wheel orientations.

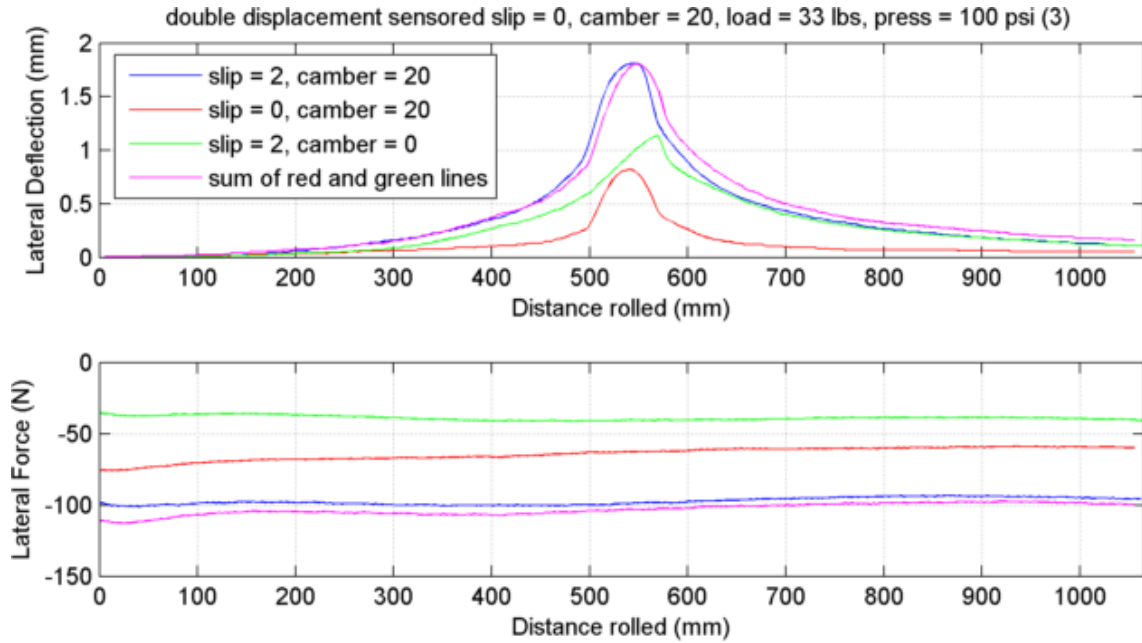


Figure 4-17: Tire centerline lateral displacement with non-zero slip and camber angles.

4.1.9.2 Relaxation distance

Pacejka's expression 7.6 for relaxation distance, **Eq. 4-3** above, can be derived from developing a differential equation that describes the lateral displacement of a tire in terms of lateral forces and stiffness constants. This derivation will use u for longitudinal displacement, in the x direction, and v for lateral displacement, in the y direction, after Pacejka, for example, equation 7.2.

Start with the definition of pure lateral displacement $F_y = vC_{Fy}$ (Pacejka's equation 7.5).

Rearrange slightly and take time derivative of both sides.

$$\frac{dv}{dt} = \frac{1}{C_{Fy}} \frac{dF_y}{dt} \quad \text{Eq. 4-4}$$

Next, combine the definition for pure slip displacement $F_y = \alpha C_{F\alpha}$ (Pacejka's equation

7.3) or $\alpha = \frac{F_y}{C_{F\alpha}}$, and the definition of slip angle α , $\tan \alpha = -\frac{V_y}{V_x}$ (Pacejka equation 1.3).

For small angles α , $\tan \alpha = \alpha$ so $\alpha = -\frac{V_y}{V_x} \Rightarrow \alpha V_x = -V_y$, which can be written as

$\frac{du}{dt} \alpha = -\frac{dv}{dt}$. Combine this last expression with the expression for pure slip to eliminate

$$\alpha: \frac{du}{dt} \frac{F_y}{C_{F\alpha}} = -\frac{dv}{dt}.$$

$$\frac{dv}{dt} = -\frac{du}{dt} \frac{F_y}{C_{F\alpha}} \quad \text{Eq. 4-5}$$

Then, combine lateral displacement, **Eq. 4-4**, with slip displacement, **Eq. 4-5**, to

eliminate $\frac{dv}{dt}$ and time altogether:

$$\frac{1}{C_{Fy}} \frac{dF_y}{dt} = -\frac{du}{dt} \frac{F_y}{C_{F\alpha}} \Rightarrow \frac{dt}{du} \frac{dF_y}{dt} = -\frac{C_{Fy}}{C_{F\alpha}} F_y \Rightarrow \frac{dF_y}{du} = -\frac{C_{Fy}}{C_{F\alpha}} F_y \quad \text{Eq. 4-6}$$

Rewrite **Eq. 4-6** as a homogeneous first-order, ordinary differential equation, which describes how lateral force varies with distance rolled.

$$\frac{dF_y}{du} + \frac{C_{Fy}}{C_{F\alpha}} F_y = 0 \quad \text{Eq. 4-7}$$

Add a forcing function to **Eq. 4-7**, such as $A \cdot H(u)$, a constant lateral force A applied to the tire by the rim, for example, by a change in slip angle such that $A = \alpha C_{F\alpha}$, multiplied by the Heaviside step function $H(u)$, and let $\kappa = \frac{C_{F\alpha}}{C_{Fy}}$:

$$\frac{dF_y}{du} + \frac{1}{\kappa} F_y = \frac{A}{\kappa} \cdot H(u) \quad \text{Eq. 4-8}$$

Eq. 4-8 has the form of a first order linear time-invariant system differential equation, but is in terms of forward distance rolled, instead of time. It has solutions, by Laplace transform, for example, of the form:[43]

$$F_y(u) = F_y(0)^{-u/\kappa} + A(1 - e^{-u/\kappa}) \quad \text{Eq. 4-9}$$

If the initial force value is allowed to go to zero, $F_y(0) = 0$, then at the forward distance

$$u = \kappa = \frac{C_{F\alpha}}{C_{Fy}} \quad \text{Eq. 4-10}$$

the lateral force generated by the tire against the pavement $F_y(\kappa) = A(1 - e^{-1}) = 0.632A$, or about 63% of its steady-state value, the input lateral force applied to the tire by the rim. The constant in **Eq. 4-10** has units of length, and is called the *relaxation distance*.

4.1.10 Summary

In summary, notable results from the physical experimentation include:

1. *Cornering and camber stiffness* depend on lateral displacement of tire centerline both in and beyond the ends of contact patch. This is predicted by the Rotta model when extended into 3D and confirmed by physical testing.
2. *Normalized lateral stiffness* increases as rim width increases for the same tire at the same inflation pressure and under the same vertical load. A 24% increase in rim width was observed to produce a 23% increase in stiffness. Tires marked as the same size vary in arc length by as much as 20%. To correctly characterize the size of a tire, it is necessary to incorporate the rim width and the arc length or carcass circumference.
3. *Normalized lateral stiffness* decreases as vertical load increases and increases as inflation pressure increases for any given tire on a given rim. It decreases as vertical load divided by inflation pressure, which approximately equals the contact patch area, decreases, for all tires, independent of size.
4. *Normalized cornering stiffness* decreases as vertical load increases and appears to either increase or decrease as inflation pressure increases, depending on the tire and the vertical load.
5. *Normalized camber stiffness increases* as vertical load increases and decreases as inflation pressure increases, but less clearly than either lateral stiffness or cornering stiffness. The values measured tend to be insufficient to produce a net ground reaction force that is in the plane of the wheel and agree with the tangent

rule, but not always. They are very seldom excessive and then only to a small degree.

6. *Correlations between stiffnesses*: As summarized in **Table 4-2**, there is a strong correlation between lateral stiffness and cornering stiffness, that remains even when all tires are considered together. There is a weaker anticorrelation between camber stiffness and both cornering stiffness and lateral stiffness, but this disappears when all tires are considered together.

Table 4-2: Correlations between stiffnesses.

Stiffnesses compared	Cornering and camber	Cornering and lateral	Camber and lateral
average of tire by tire	-0.711	0.922	-0.848
all tires combined	0.052	0.633	0.129

7. *Pneumatic trail* increases as vertical load increases and decreases as inflation pressure increases. Its ratio with contact patch length for a given tire is nearly a constant as vertical load and inflation pressure vary.
8. *Contact patch* area tends to be less than the value of vertical load divided by inflation pressure. The length is 6.7 times the width, on average, with a standard deviation of 1.2, a max of 9.8 times and a minimum of 4.7 times.
9. *Decay length*, the distance beyond the end of the contact patch over which a lateral displacement decreases to $1/e$ or 36.8% of its original value, exists and contributes to the total lateral stiffness, cornering stiffness, and possibly camber stiffness of the tire.

10. *Hysteresis*, both rate-independent and rate-dependent occurs, in both vertical and lateral deflection. Measured force at any given deflection depends both on previous deflection, rate at which current deflection was induced, and time spent at that current deflection.

11. *True tire size*, the actual diameter of the tire when mounted on the rim, correlates well with lateral stiffness, as can be seen in the last row of **Table 4-3** and in the graph in **Figure 3-4**.

Table 4-3: True size and normalized lateral stiffnesses for four different 37-622 tires mounted on the same 18.7 mm wide rim.

ID	Size (mm)	Arc length (mm)	Radius (mm)	“True size” (mm)	Size diff. (%)	max norm lat stiffness	min norm lat stiffness	average norm lat stiffness
5	37	78.0	15.6	31.2	-15.6	0.0979	0.0445	0.0664
10	37	73.5	14.9	29.8	-19.4	0.107	0.0417	0.0681
11	37	90.0	17.5	34.9	-5.6	0.149	0.0517	0.0888
12	37	85.7	16.8	33.6	-9.2	0.149	0.0492	0.0679
						0.896	0.9999	0.736

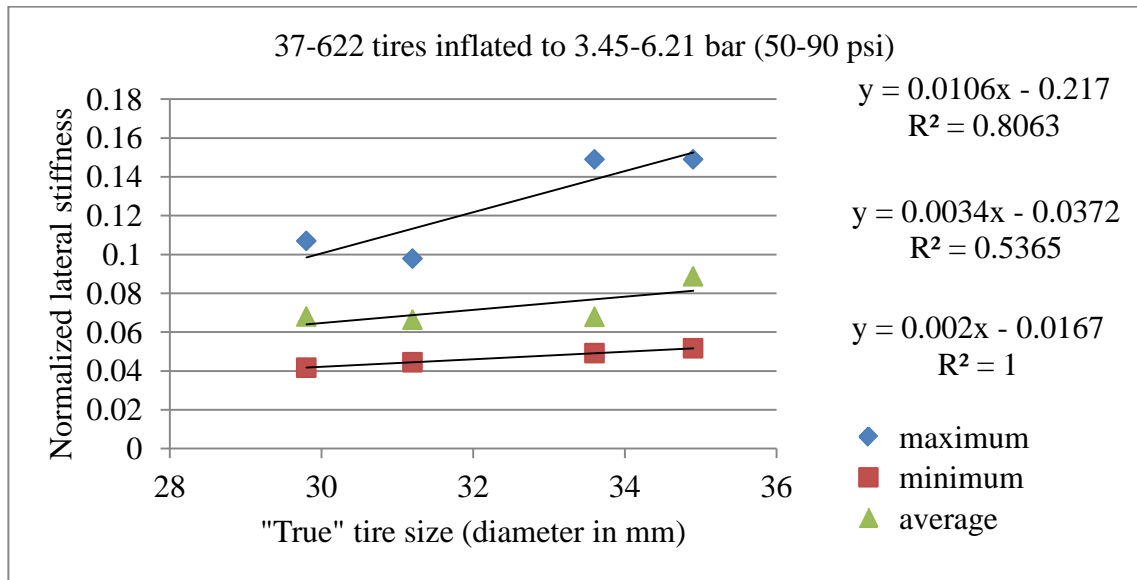


Figure 4-18: Graph of data from **Table 4-3**.

4.2 Repeatability

Test device number 3 provides good repeatability, except for the twisting torque, a very small value. For example, the Bontrager All Weather 23-622 measured twice at 5.52 bar (80 psi) and with a 304 N (31 kg, 68.3 lb) vertical load yields the results shown below in **Table 4-4**.

Table 4-4: Example of repeatability of results from test device number 3.

Property	Test #1	Test #2	% Difference
Normalized cornering stiffness [$1/^\circ$]	0.259	0.260	-0.39
Normalized camber stiffness [$1/^\circ$]	0.0120	0.0119	0.84
Normalized self-aligning torque [$m/^\circ$]	-0.00309	-0.00312	-0.97
Normalized twisting torque [$m/^\circ$]	3.77E-05	8.91E-05	-81.07
Pneumatic trail [mm]	5.33	5.11	4.21

4.3 Tire described as “radial” does not stand out

The Maxxis prototype, which is described as “radial” and does appear to have cords aligned at about 22.5°, instead of the 45° usually associated with bias-ply, does not have stiffnesses noticeably different from other tires of similar size.

4.4 Physical measurements compared between three test devices

To a certain extent, the three different test devices represent an evolution in testing technique over two years, especially in the rate at which testing can be performed. Therefore, there is little overlap in the data collected. Never-the-less, in the cases where overlap exists, good agreement can be found.

4.4.1 TU Delft drum vs. UWM cart

Because of how testing protocols evolved from test device number 1 to test device number 3, no tire ended up being tested under the same configuration on both devices. Two tires, however, were tested under similar conditions so that a comparison can be made.

Table 4-5: Comparing results from test device 1 at UWM[37] and test device 3 at TU Delft.

Tire	Bontrager RL All Weather 23-622			Maxxis Radial Prototype 22-622		
	1	3	3	1	3	3
Test device						
Load (N)	402.6	303.8	524.9	378.1	303.8	524.9
Inflation pressure (bar)	6.895	6.895	8.274	6.895	6.895	9.653

Normalized cornering stiffness	0.198	0.252	0.193	0.212	0.217	0.174
Normalized camber stiffness (1/°)	0.0138	0.0117	0.0135	0.0168	0.0158	0.0168

As can be seen in **Table 4-5** above, both devices yield similar stiffnesses for the two tires. Notably, camber stiffness approaches but does not exceed the tangent rule value of 0.0172 1/°.

4.4.2 TU Delft drum vs. UWM flat track

As can be seen in the plots below in **Figure 4-19**, the few data points collected for the Maxxis 22-622 radial tire at UWM fit well with the data points collect at TU Delft for the same tire. The sample size is small, but it was all that time permitted. Unfortunately, the UWM data was collected on different rims and before the dependence on rim width was discovered, so that parameter was not recorded, although all the rims are still available and can still be measured.

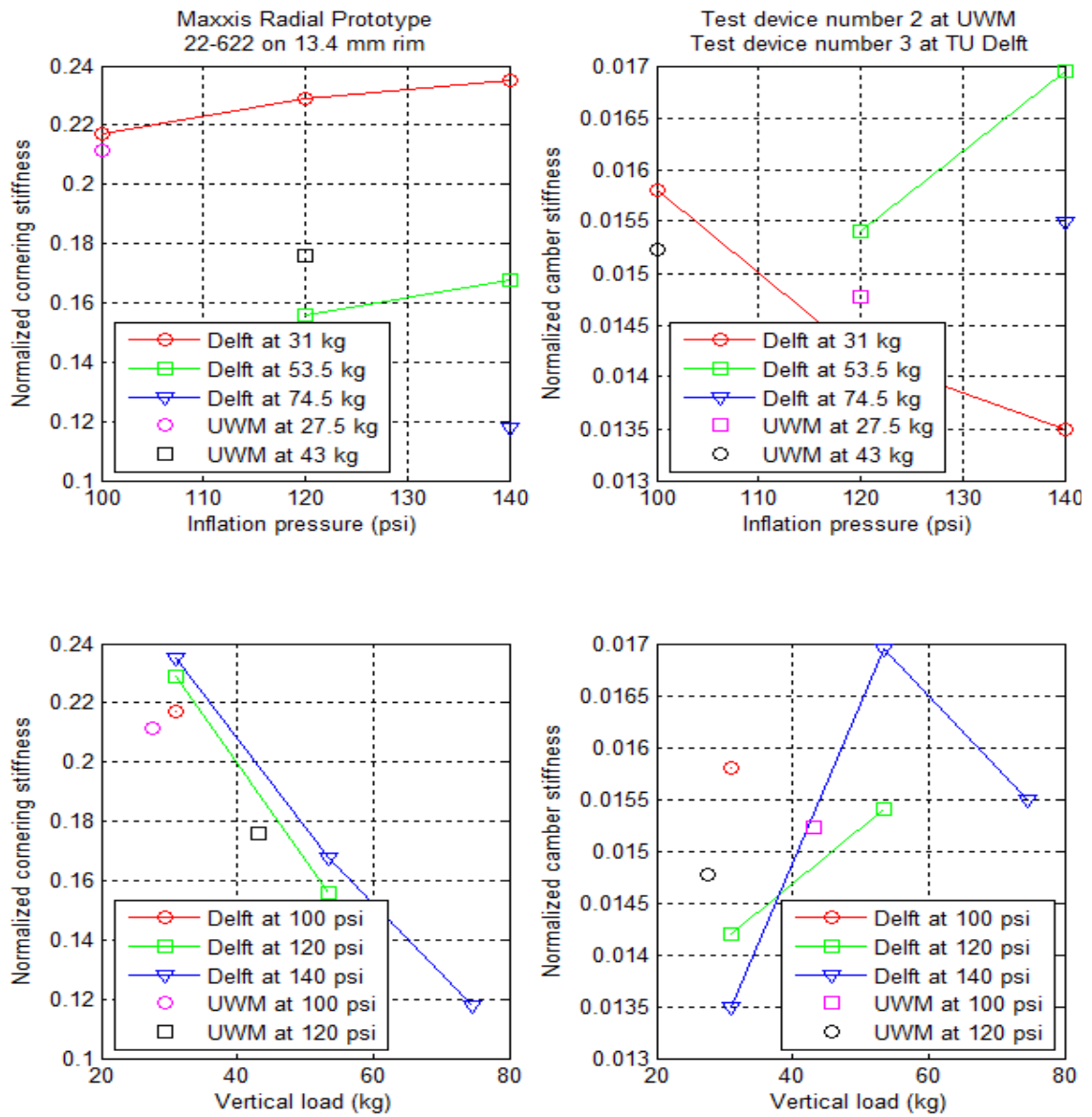


Figure 4-19: Comparing results from test device 2 at UWM and test device 3 at TU Delft.

4.5 Physical measurements compared to previous results

For cornering stiffness, there is reasonable agreement between the several sources, as can be seen in **Figure 4-20**.

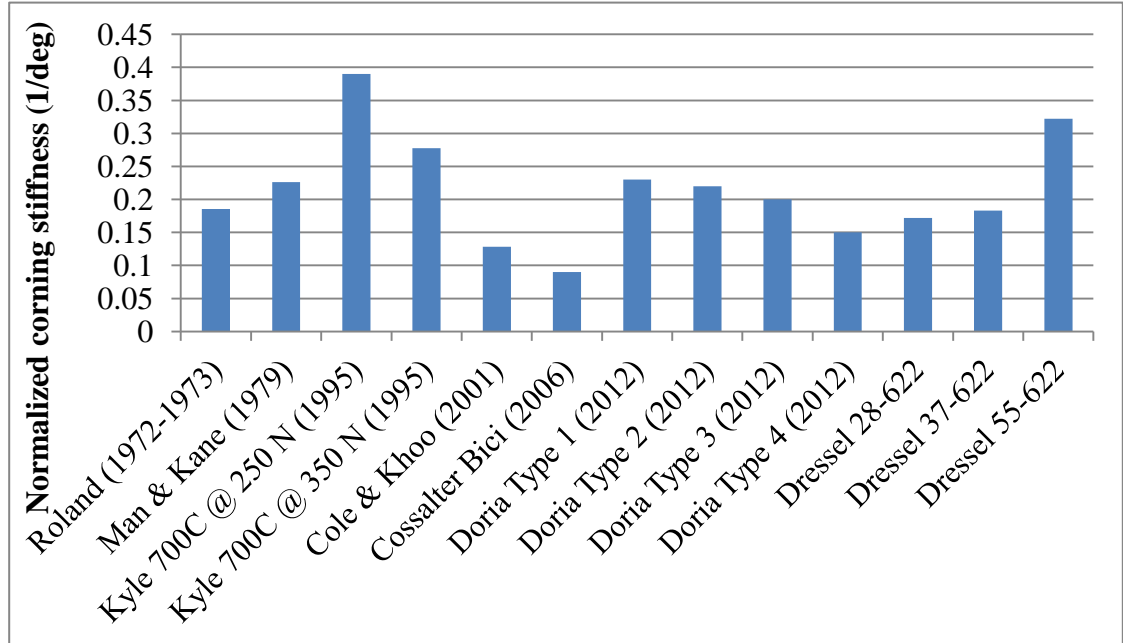


Figure 4-20: Comparison of all known bicycle tire normalized cornering stiffnesses at 1 degree slip angle.

For camber stiffness, there is much greater disagreement between the several sources, as can be seen in **Figure 3-4**. In particular, the values from Kyle stand out for far exceeding a friction coefficient of 1. Roland and Man and Kane fall far below the tangent rule, and Doria *et al.* exceed the tangent rule by as much as 45%.

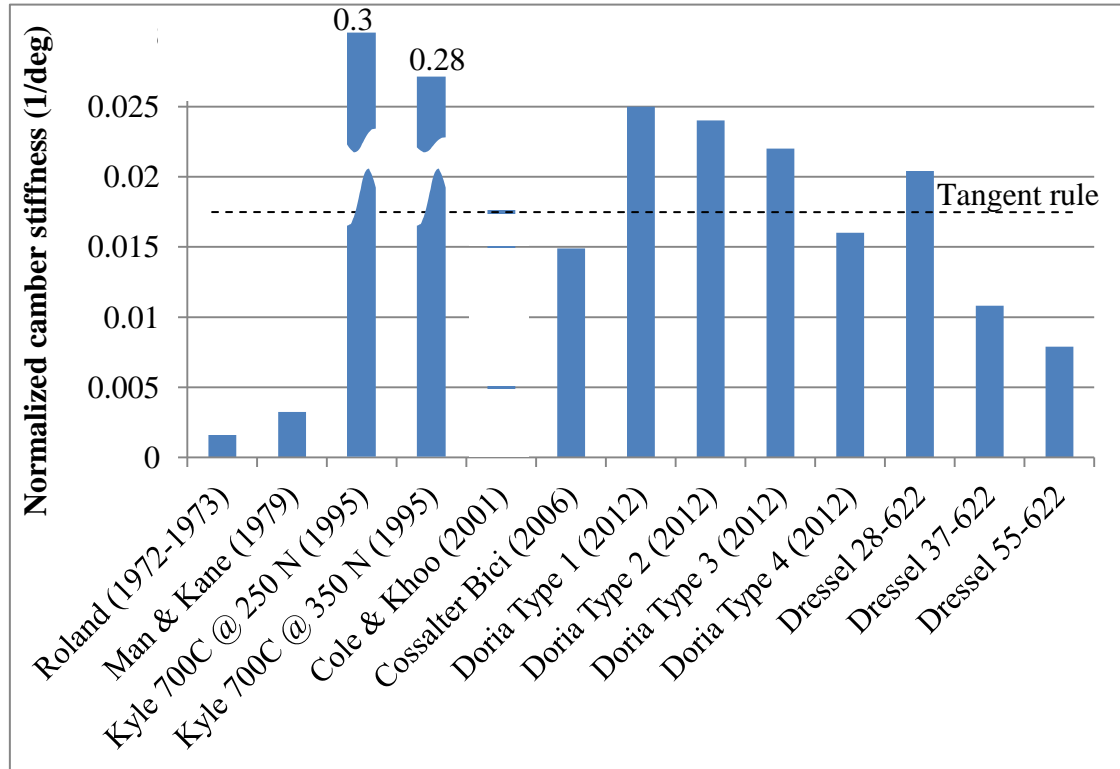


Figure 4-21: Comparison of all known bicycle tire normalized camber stiffnesses at 10 degree camber angle.

4.5.1 Doria et al., 2012

Because the results reported recently by Doria *et al.* have so many details, [28] a more-detailed comparison can be made, as seen below in **Table 4-6**. In general, for similar tires, there is good agreement between the cornering stiffness values, but the camber stiffnesses measured at Padua are much higher than those found at TU Delft. A more-detail discussion of the differences is presented below in section 7.2.

Table 4-6: Comparison of stiffness found by Doria *et al.* at Padua with tires tested on device number 3 at TU Delft.

	Tire number	Tire name	Tire "size"	Vertical load [kg]	Inflation pressure [psi]	Normalized Cornering Stiffness [$1/\text{°}$] at 1°	Difference between Padua and Delft values	Normalized Camber Stiffness [$1/\text{°}$] at 10°	Difference between values and tangent rule
at Padua	1	unknown	37	41	58	0.247		0.0242	37%
	2	Vredestein Perfect Tour	37	41	58	0.220	-18%	0.0232	31%
	3	Schwalbe Marathon Plus	35	41	58	0.200	11%	0.0211	19%
	4	Continental Top Contact Winter	37	41	58	0.147	-11%	0.0153	-13%
Normalized Camber stiffness of tangent rule								0.0176	
at TU Delft	5	Continental Top Contact Winter	37	33	58	0.183		0.0067	-62%
				44	58	0.165	11%	0.0077	-56%
				55	58	0.146		0.0087	-51%
	9	Schwalbe Kojak	35	33	58	0.315		0.0085	-52%
				44	58	0.270		0.0088	-50%
				55	58	0.224		0.0091	-48%
	10	Schwalbe Marathon Plus	37	33	58	0.197		0.0056	-68%
				44	58	0.179	-11%	0.0064	-64%
	11	Vittoria Randonneur Hyper	37	55	58	0.161		0.0072	-59%
				33	58	0.350		0.0105	-40%
				44	58	0.305		0.0114	-35%
	14	Vredestein Perfect Tour	37	55	58	0.260		0.0123	-30%
				31	60	0.292		0.0079	-55%
				42	60	0.265	18%	0.0087	-51%
			54	60	0.237		0.0094	-47%	

The inflation pressure used in Padua is nearly halfway between two of the inflation pressures used in Delft, so a simple average is calculated for comparison in **Table 4-6**.

CHAPTER 5

MODELING

Collecting force and moment values for all interesting combinations of tire, size, inflation pressure, vertical load, and orientation is a time- and labor-intensive operation that requires specialized testing equipment. A model that can predict these values from a few simple static measurements is desirable.

A variety of predictive models have been developed for pneumatic tires in general, and some have been specific to motorcycle tires. Wanatabe describes a motorcycle tire specific finite element model for investigating camber thrust, but it predicts a net ground reaction force orientation of only about a half of his measured data, which in turn is only about 60% of the value predicted by the tangent rule.[44]

The simplest existing tire model available, the original 'brush' model of Fromm and of Julien,[2] was chosen as a place to start, and it was enhanced only as necessary to predict the values found from physical experiments. The Rotta model was used to find the bristle stiffness from just inflation pressure, vertical load, rim width, and tire radius.[45] Finally, the relaxation rate of the tire was accounted for with a model of a taut beam on an elastic foundation. The tension can be found as a function of inflation pressure and cross section area; the area moment of inertia can be found from the cross section radius and casing thickness; the modulus of elasticity can be estimated from published data; and the foundation stiffness can be calculated with Rotta's model.

5.1 Rotta's model

Bicycle tires, by virtue of their relatively thin carcass and relatively high inflation pressure, are expected to behave differently than automobile and even motorcycle tires. They assume a toroidal shape, as do motorcycle tires, but the stiffness of their much-thinner carcass plays a reduced role in their total stiffness.

There is a model developed by Rotta for toroidal tires, specifically aircraft tires, that predicts the forces generated in the contact patch and that might be applicable to bicycles.[45]

Rotta's premise is simply that, in the plane of a cross section that is perpendicular to the midplane of the wheel and collinear with a radius, the two side bulges of a tire that is pressed against a flat surface form constant-radius circular arcs on either side of the contact patch and that those arcs are tangent to the ground plane.

Thus, the total arc length of the carcass, from bead to bead, is divided between a straight line representing the contact patch, and two circular arcs between the rim and the contact patch, which are tangent to the ground at the contact patch. For a given position and angle of the rim relative to the ground contact of the tire centerline, there is no closed-form solution, but the radii of the arcs can be calculated by a simple iteration.

Forces generated in each cross section can be calculated from the air pressure and resulting geometry. Vertical force is just contact patch width times distance to next cross section times inflation pressure. Horizontal force is the difference between the radii of the circular arcs tangent to the ground, times inflation pressure.

Vertical displacement of the wheel may be specified directly or found by iteration to support a given vertical load at a given inflation pressure.

The calculation of the size of these arcs and the corresponding width of the contact patch, can be started with the known constants:

- the width of the rim, w ;
- the arc length of the tire from bead to bead, s_0 , and
- the distance that the particular cross section is pressed into the surface. If the tire is vertical, the cross section is vertical, and the surface is horizontal, this is the vertical displacement of the wheel, δ_w .

Note that, in this discussion, dimensions for the entire tire have a subscript of 0 and dimensions for the left and right sides have subscripts of 1 and 2, respectively. Also note that Rotta uses a different coordinate system for the cross section of a tire, shown below in **Figure 5-1**, than that for an entire tire described above in **Figure 2-1**. [45]

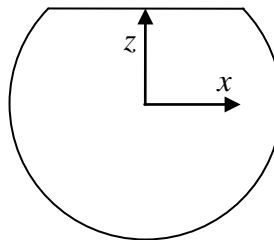


Figure 5-1: Rotta model coordinate system. The y-axis is into the page.

First, a quick detour to calculate the necessary arc length of the undeformed tire from bead to bead, s_0 , from the rim width, w , and the undeformed tire radius, r_0 :

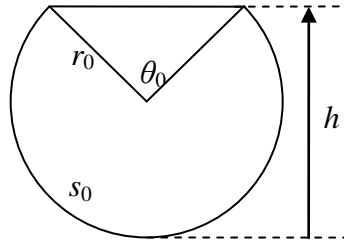


Figure 5-2: Geometric parameters of tire cross section.

$$w = 2r_0 \sin\left(\frac{1}{2}\theta_0\right) \quad \text{Eq. 5-1}$$

$$\theta_0 = 2 \sin^{-1}\left(\frac{w}{2r_0}\right) \quad \text{Eq. 5-2}$$

One more value that will be needed below is rim height, h , which can be calculated directly:

$$h = r_0 + r_0 \cos\left(\frac{1}{2}\theta_0\right) = r_0 \left(1 + \cos\left(\frac{1}{2}\theta_0\right)\right) \quad \text{Eq. 5-3}$$

For example: a tire with a “size” of 28 mm tire on a 15 mm wide rim

(assuming that tire size = 2 * tire radius).

Table 5-1: Sample calculations for tire cross section geometry (part 1).

rim_width	given	15 mm
-----------	-------	-------

tire_size	given	28 mm
tire_radius	tire_size / 2	14 mm
rim_angle	2 * asin(rim_width / (2 * tire_radius))	1.1307 rad
arc_length	tire_radius * (2*pi - rim_angle)	72.1347 mm
rim_height	tire_radius * (1 + cos(rim_angle / 2))	25.8216 mm

If, instead of starting with the specified tire size and assuming that it equals the tire diameter, which is rarely the case, an actual measurement of the carcass arc length is used:

$$w = 2r_0 \sin\left(\frac{1}{2}\theta_0\right) \text{ and } s_0 = r_0(2\pi - \theta_0) \quad \text{Eq. 5-4}$$

$$r_0 = \frac{w}{2\sin\left(\frac{1}{2}\theta_0\right)} \text{ and } r_0 = \frac{s_0}{2\pi - \theta_0} \quad \text{Eq. 5-5}$$

$$\frac{w}{2\sin\left(\frac{1}{2}\theta_0\right)} = \frac{s_0}{2\pi - \theta_0} \text{ so } \frac{w}{s_0} = \frac{2\sin\left(\frac{1}{2}\theta_0\right)}{2\pi - \theta_0} \quad \text{Eq. 5-6}$$

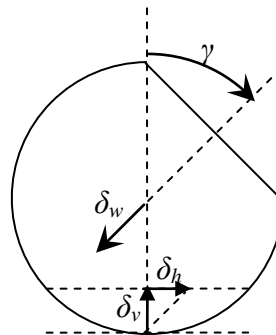
It appears that there is no closed-form solution, but it can be found by iteration, with the `fzero()` function in MATLAB®, for example:

```
rim_angle = fzero(@(theta) (rim_width/arc_length -  
    (2*sin(0.5*theta))/(2*pi - theta)), pi/4)
```

Table 5-2: Sample calculations for tire cross section geometry (part 2).

rim_width		15 mm
arc_length		72.1347 mm
rim_angle	$fzero(@(theta)$ $(rim_width/arc_length -$ $(2*\sin(0.5*theta))/(2*pi - theta)),$ $pi/4)$	1.1307 rad
tire_radius	$rim_width / (2*\sin(0.5*rim_angle))$	14 mm
rim_height	$tire_radius *(1 + \cos(rim_angle / 2))$	25.8216 mm

There may also be a known horizontal displacement relative to the rim, δ_h , of the part of a cross section in the contact patch. This displacement may simply be imposed on the contact patch, but in the case of a camber angle, σ , this displacement is based on the premise that once a section of tire touches the pavement, it remains stationary as the wheel rolls forward over it, until it is lifted back off the pavement.

**Figure 5-3:** Geometric parameters of cambered and displaced tire cross section.

As the cambered tire rolls forward, the rim moves both horizontally and vertically with respect to the lowest point of a section of tire once it is in the contact patch and therefore stationary. Since the rim remains centered about the midplane of the wheel, by definition, the parts of the tire in the contact patch move relative to the rim in a line parallel to the midplane of the wheel, and the horizontal displacement of any point in the contact patch, δ_h , can be calculated from the vertical displacement of that point, δ_v , simply as:

$$\delta_h = \delta_v \tan(\sigma) \quad \text{Eq. 5-7}$$

The vertical displacement of the lowest cross section, δ_v , the one perpendicular to the horizontal ground, in turn can be calculated from the displacement of the entire wheel in the plane of the wheel, δ_w by:

$$\delta_v = \delta_w \cos(\sigma) \quad \text{Eq. 5-8}$$

Together, of course, they sum to the total displacement of the wheel in the plane of the wheel:

$$\delta_w = \sqrt{\delta_h^2 + \delta_v^2} \quad \text{Eq. 5-9}$$

Thus, continuing the numerical example from above in **Table 5-3** below.

Table 5-3: Sample calculations for tire cross section geometry (part 3).

wheel_vert_d	given (in the plane of the wheel)	5 mm
wheel_horz_d	Given	0 mm

camber_angle	$45 * \text{pi} / 180$	0.7854 rad
slice_vert_d	$\text{wheel_vert_d} * \cos(\text{camber_angle})$	3.5355 mm
slice_horz_d	$\text{slice_vert_d} * \tan(\text{camber_angle})$	3.5355 mm
wheel_vert_d	$\text{sqrt}(\text{slice_horz_d}^2 + \text{slice_vert_d}^2)$	5 mm

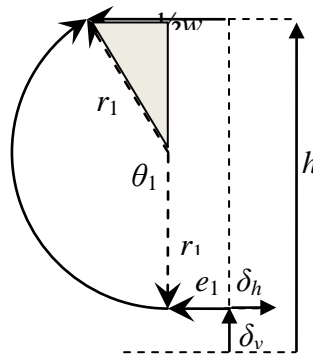


Figure 5-4: Geometric parameters of one side of cambered and displaced tire cross section.

The arc length of the left side bulge s_1 can be related to the total arc length s_0 , horizontal displacement δ_h , and the horizontal distance to the edge of the contact patch from the center of the undeformed tire, e_1 :

$$s_1 = \frac{1}{2} s_0 - e_1 - \delta_h \quad \text{and} \quad s_2 = \frac{1}{2} s_0 - e_2 + \delta_h \quad \text{Eq. 5-10}$$

For a tire of original rim height h and vertical displacement δ_v , the shaded right triangle can be analyzed with Pythagoras's theorem to find the radius of the left side bulge r_1 :

$$\begin{aligned}
 r_1^2 &= \left(\frac{1}{2}w - e_1\right)^2 + (h - \delta_v - r_1)^2 \\
 r_1^2 &= \left(\frac{1}{2}w - e_1\right)^2 + (h - \delta_v)^2 - 2(h - \delta_v)r_1 + r_1^2 \\
 r_1 &= \frac{\left(\frac{1}{2}w - e_1\right)^2 + (h - \delta_v)^2}{2(h - \delta_v)}
 \end{aligned}
 \tag{Eq. 5-11}$$

The same shaded triangle can be analyzed to find the angle swept by the left side bulge

θ_1 :

$$\begin{aligned}
 \frac{1}{2}w - e_1 &= r_1 \sin(\pi - \theta_1) \\
 \theta_1 &= \pi - \sin^{-1}\left(\frac{\frac{1}{2}w - e_1}{r_1}\right)
 \end{aligned}
 \tag{Eq. 5-12}$$

Since the width of the contact patch, the radius of the side bulge, and the angle that it sweeps out are all unknown, and there is no closed-form solution for them, they also must be found by iteration. For example: increment e_1 , calculate s_1 , r_1 , and θ_1 , and then check to see if $\text{abs}(r_1\theta_1 - s_1) > \text{tolerance}$.

This is slow, however, and can be sped up with a zero finding algorithm that finds the

zeros of $(r_1\theta_1 - s_1)$, where $s_1 = \frac{1}{2}s_0 - e_1 - \delta_h$, $r_1 = \frac{\left(\frac{1}{2}w - e_1\right)^2 + (h - \delta_v)^2}{2(h - \delta_v)}$, and

$\theta_1 = \pi - \sin^{-1}\left(\frac{\frac{1}{2}w - e_1}{r_1}\right)$. Combine into a single expression to eliminate r_1 and θ_1 , leaving

just e_1 .

$$\frac{(\frac{1}{2}w - e_1)^2 + (h - \delta_v)^2}{2(h - \delta_v)} \left[\pi - \sin^{-1} \left(\frac{\frac{1}{2}w - e_1}{\frac{(\frac{1}{2}w - e_1)^2 + (h - \delta_v)^2}{2(h - \delta_v)}} \right) \right] - (\frac{1}{2}s_0 - e_1 - \delta_h) \quad \text{Eq. 5-13}$$

Again, the `fzero()` function in MATLAB® works well.

One detail remains, however, and it is that the horizontal displacement δ_h , due to camber angle, used in the above expression needs to be adjusted by a delta for how much additional length of tire cross section is pulled towards this side by the cambering. This delta is approximately the tire radius times the tangent or the sine of the camber angle, but really depends on the radius of the side bulge which has not yet been calculated. All attempts to find this delta value correctly with a closed-form expression have failed, and a two step iteration has been developed that works well:

1. Estimate the delta value with `tire_radius * sin(camber_angle)`.
2. Calculate the geometry of the deformed tire in the cross section, as explained above, and add to this delta value the difference between the found contact patch center and the originally-calculated horizontal displacement.

The delta value needs to be calculated only once, for the vertical cross section, at the center of the contact patch, and then can be used on all the cross sections in the contact patch.

Lastly, it is useful to calculate where in the contact patch the lowest point of the cross section has ended up. When plotted in 3D, this provided visual confirmation that all the

above calculations do not contain some gross error, if this point from all the cross sections in the contact patch forms a straight line from one tip of the contact patch to the other. Also, the value must be the same when calculated from the left side and from the right.

Finally, continuing the example of a 28 mm tire on a 15 mm wide rim with 5 mm vertical displacement at 45° further, in **Table 5-4** below:

Table 5-4: Sample calculations for tire cross section geometry (part 4).

rim_width		15 mm
tire_radius		14 mm
rim_height		25.8216 mm
arc_length		72.1347 mm
camber_angle		0.7854 rad
slice_vert_d		3.5355 mm
slice_horz_d		3.5355 mm
delta	$\text{tire_radius} * \sin(\text{camber_angle})$	9.8995
delta	$\text{delta} + (\text{cp}(1,2) - \text{slice_horz_ds}(\text{slice}))$	10.9956
cp_edges(1)	$\text{fzero}(@(\text{cp_edge}) (((\text{rim_widths}(1) - \text{cp_edge})^2 + (\text{rim_heights}(1) + \text{tire_radius} - \text{slice_vert_d})^2) / (2 * (\text{rim_heights}(1) + \text{tire_radius} - \text{slice_vert_d}))) * (\text{pi} - \text{asin}((\text{rim_widths}(\text{side}) - \text{cp_edge}) /$	-0.7780 mm

	$\left(\left(\left(\text{rim_widths}(1) - \text{cp_edge} \right)^2 + \left(\text{rim_heights}(1) + \text{tire_radius} - \text{slice_vert_d} \right)^2 \right) / \left(2 * \left(\text{rim_heights}(1) + \text{tire_radius} - \text{slice_vert_d} \right) \right) \right) - \left(\text{arc_length}/2 + \text{cp_edge} - \left(\text{slice_horz_d} - \text{delta} \right) \right), x0$	
cp_edges(2)	$\text{fzero}(@(\text{cp_edge}) \left(\left(\left(\text{rim_widths}(2) - \text{cp_edge} \right)^2 + \left(\text{rim_heights}(2) + \text{tire_radius} - \text{slice_vert_d} \right)^2 \right) / \left(2 * \left(\text{rim_heights}(2) + \text{tire_radius} - \text{slice_vert_d} \right) \right) \right) * \left(\text{pi} - \text{asin} \left(\left(\text{rim_widths}(\text{side}) - \text{cp_edge} \right) / \left(\left(\text{rim_widths}(2) - \text{cp_edge} \right)^2 + \left(\text{rim_heights}(2) + \text{tire_radius} - \text{slice_vert_d} \right)^2 \right) / \left(2 * \left(\text{rim_heights}(2) + \text{tire_radius} - \text{slice_vert_d} \right) \right) \right) \right) - \left(\text{arc_length}/2 - \text{cp_edge} + \left(\text{slice_horz_d} - \text{delta} \right) \right), x0$	9.7218 mm
cp_mids(1)	$\text{cp_edges}(1) - \left(r(1) * a(1) - \text{tire_radius} * \left(\text{pi} - 0.5 * \text{rim_angle} + \text{camber_angle} \right) \right)$	3.5355 mm
cp_mids(2)	$\text{cp_edges}(2) + \left(r(2) * a(2) - \text{tire_radius} * \left(\text{pi} - 0.5 * \text{rim_angle} + \text{camber_angle} \right) \right)$	3.5355 mm

The resulting geometry is depicted below in **Figure 5-5**.

Tire radius = 14 mm, rim width = 15 mm, rim diameter = 622 mm,
 rim height = 25.82 mm, inflation pressure = 0.8274 N/mm² (120 psi)
 vertical displacement = 5 mm (19.36% sinkage), horizontal displacement = 0 mm,
 camber angle = 45°, slip angle = 0°, adjusted relaxation rate = 0.977

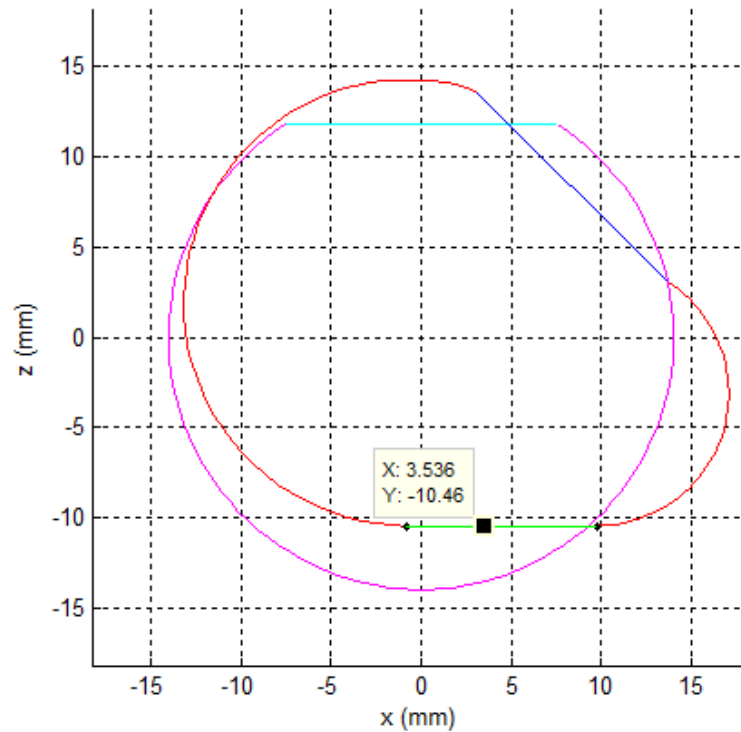


Figure 5-5: Plot of sample tire cross section calculated using the Rotta model.

So far, all calculations have been limited to a single cross section, the one that is vertical, at the lowest point on the rim, and at the center of the contact patch, if it is symmetrical.

5.2 Expanding Rotta's model in 3D

In order to calculate the forces and moments generated over the entire contact patch, it is necessary to consider multiple cross sections. Each tire carcass cross section is oriented perpendicular to the midplane of the wheel and parallel to wheel radii.

For a tire with radius r_0 , finite sinkage δ_w , and non-zero camber angle γ , the lowest point of the tire as it touches the ground, at the leading and trailing edges of the contact patch, is at a distance around the cross section of $s = r_0 * \gamma$ from the centerline of the tire.

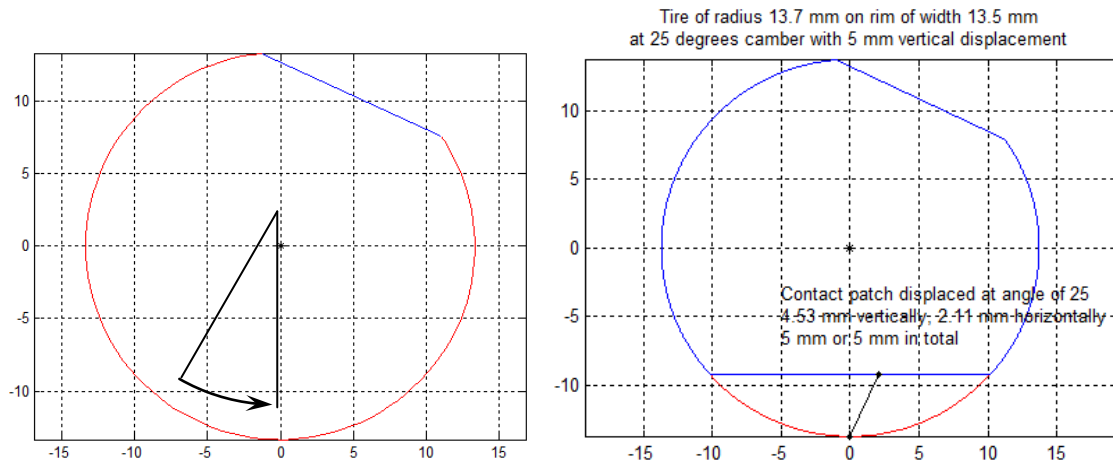


Figure 5-6: Location of lowest point on tire, first point to touch ground, on cambered tire.

Then, as the wheel rolls forward, this point on the cross section remains stationary with respect to the pavement and so moves relative to the rim both vertically, towards the rim, and horizontally in the direction of camber. This occurs independent of the bulging modeled by Rotta, and is depicted on the right in **Figure 5-6** above, for the sake of simplicity, as though the tire were a solid material with Poisson's ratio of zero, cork for example, and thus compresses in one direction without a corresponding bulge in the perpendicular directions.

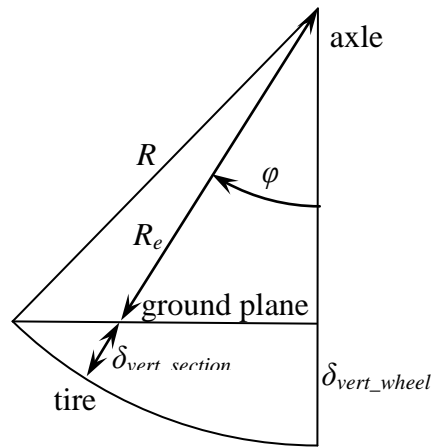


Figure 5-7: Side view of wheel dimensions as the tire is pressed into the ground.

In the plane of each radial cross section, the plane in which the Rotta geometry is determined, the vertical component of this displacement can be calculated as:

$$\begin{aligned}
 \delta_{vert_section} &= R - R_e \\
 R_e \cos(\varphi) &= R - \delta_{vert_wheel} \\
 \delta_{vert_section} &= \left(R - \frac{(R - \delta_{vert_wheel})}{\cos(\varphi)} \right)
 \end{aligned}
 \tag{Eq. 5-14}$$

Where **Figure 5-7** above shows dimensions on the side view of a portion of the entire wheel, R , is the height of the axle, also the radius of the wheel including the tire, and the distance from the axle to the farthest point on the tire; and $\theta_{section}$ is the angle of the cross section in question as measured from the bottom-dead-center of the wheel. The distance from the axle to the ground plane is R_e , and the displacement of the tire in the radial plane is $\delta_{vert_section}$.

Finally, to adjust for non-zero camber angle, multiply by cosine of the camber angle:

$$\delta_{vert_section} = \left(R - \frac{(R - \delta_{vert_wheel})}{\cos(\varphi)} \right) \cos(\gamma) \quad \text{Eq. 5-15}$$

When this vertical component of the displacement is applied to each radial cross section of the tire, and then each cross section is oriented correctly in 3D, their bottom edges form a plane, as shown below in **Figure 5-8**.

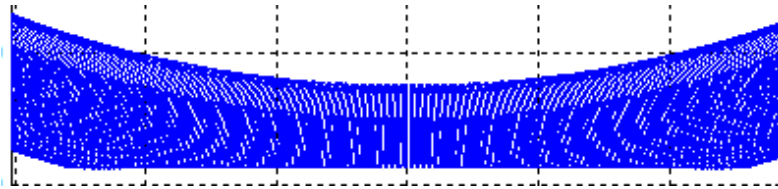


Figure 5-8: Side view of tire calculated with 3D Rotta model showing flat contact patch.

It is not, however, perfectly flat for non-zero camber angles. A tire with 5 mm vertical displacement on a 622 mm diameter wheel is modeled to have the small variations shown in **Figure 5-9** below, for two different camber angles.

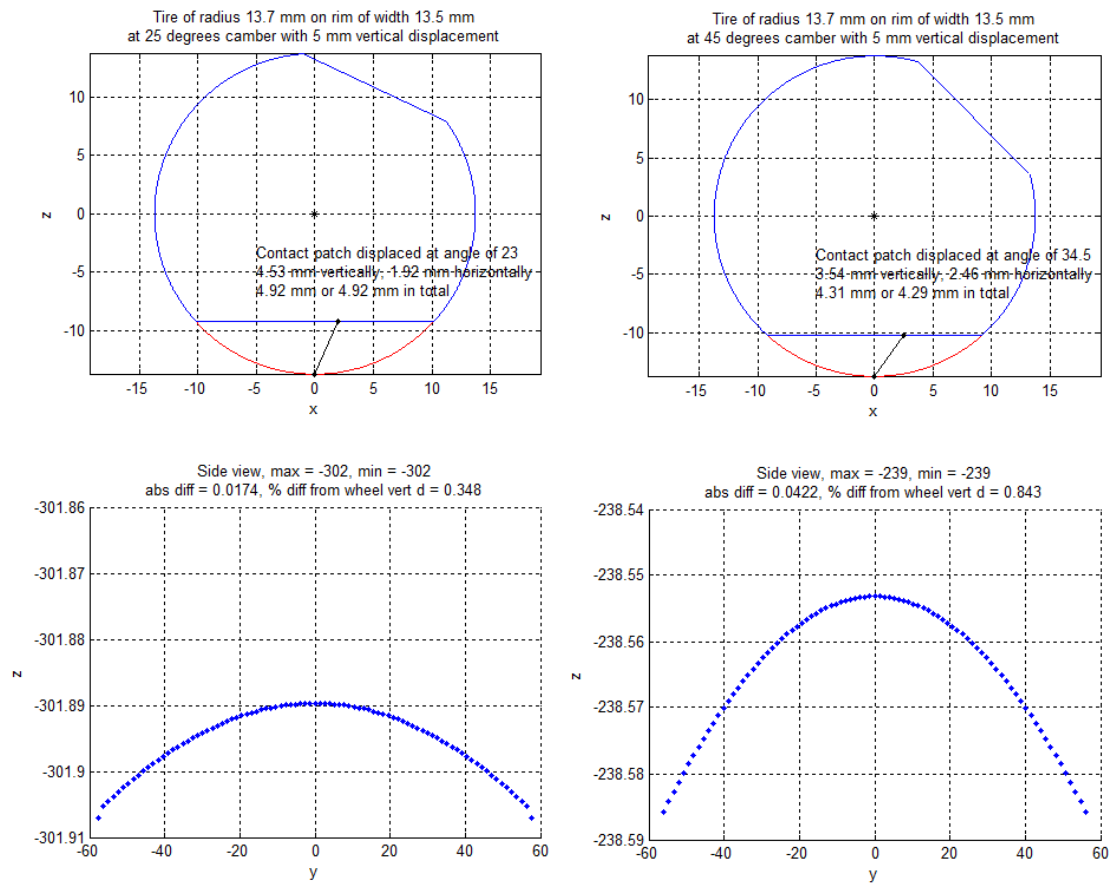


Figure 5-9: Flatness of contact patch developed by the 3D Rotta model.

The two lower plots in **Figure 5-9** above show an exaggerated side view of the calculated vertical location of the bottom, flattened part of each cross section, as plotted along the length of the contact patch.

The corresponding horizontal component of the displacement can be calculated, also in the plane of the radial cross section, by an expression that is actually more assembled through trial and error than derived:

$$\delta_{horz_section} = r_0 \gamma + r_0 \sin(\gamma) + \dots$$

$$\left(\begin{array}{l} -\left(R \left(1 - \frac{\delta_{vert_wheel}}{R} \right) \cos(\gamma) \right) + \dots \\ R \cos(\varphi) \cos(\gamma) \end{array} \right) \tan(\gamma) \quad \text{Eq. 5-16}$$

This too is not exactly correct and a tire with 5 mm vertical displacement on a 622 mm diameter wheel is modeled to have the variations shown below:

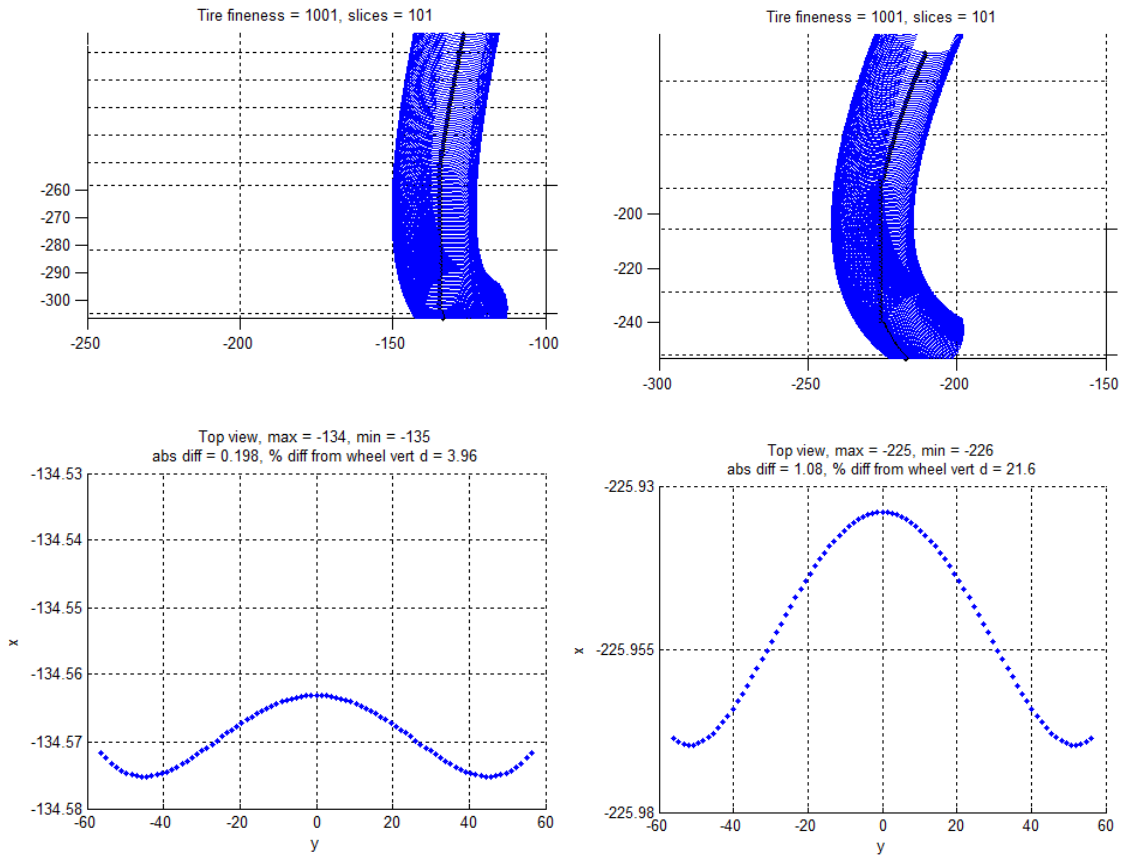


Figure 5-10: Straightness of contact patch developed by the 3D Rotta model (part 1).

The lower two plots in **Figure 5-10** above show an exaggerated top view of the calculated horizontal location of the point on each cross section that first touched the ground, as plotted along the length of the contact patch.

This variation in the horizontal displacement of each cross section, with respect to a straight line, can be improved by recognizing the desired relationship between the horizontal and vertical displacements, and so calculating the horizontal displacement directly from the vertical displacement:

$$\delta_{horz_section} = \delta_{vert_section} \tan(\gamma) \quad \text{Eq. 5-17}$$

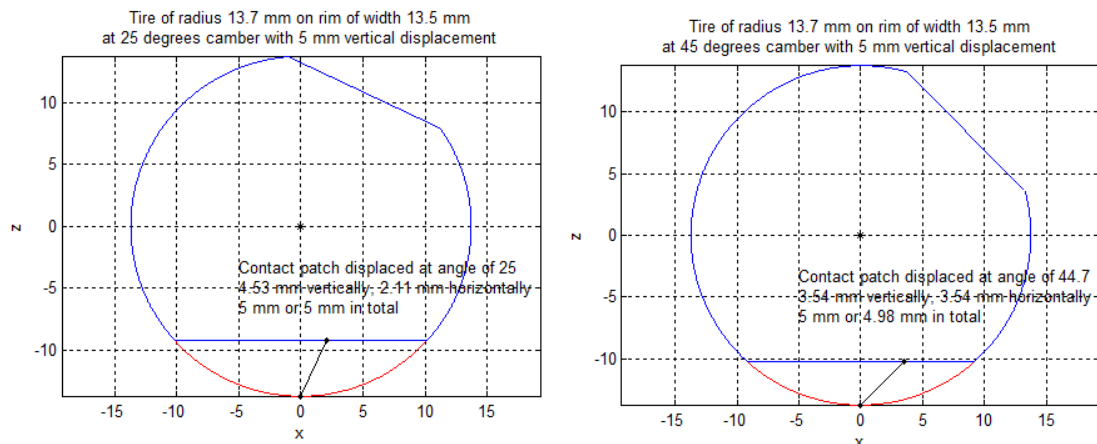


Figure 5-11: Plots showing horizontal and vertical displacement of contact patch.

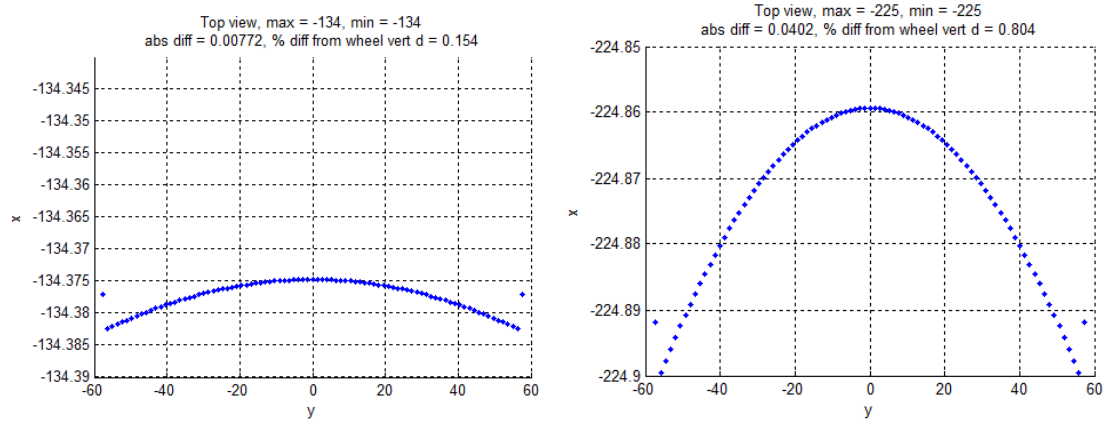


Figure 5-12: Straightness of contact patch developed by the 3D Rotta model (part 2).

This simplification shows a nice improvement, as can be seen in the difference between the lower two plots in **Figure 5-12** immediately above vs. the lower two plots in **Figure 5-10** on the previous page.

With this final version, the cross sections flattened in the contact patch, and modeled to bulge out on the sides with Rotta's method, now blend seamlessly with the undeformed cross sections beyond the ends of the contact patch, as shown in **Figure 5-13** on the next page and as expected in the case of vertical deflection, also called sinkage, and camber angle without additional horizontal deflection.

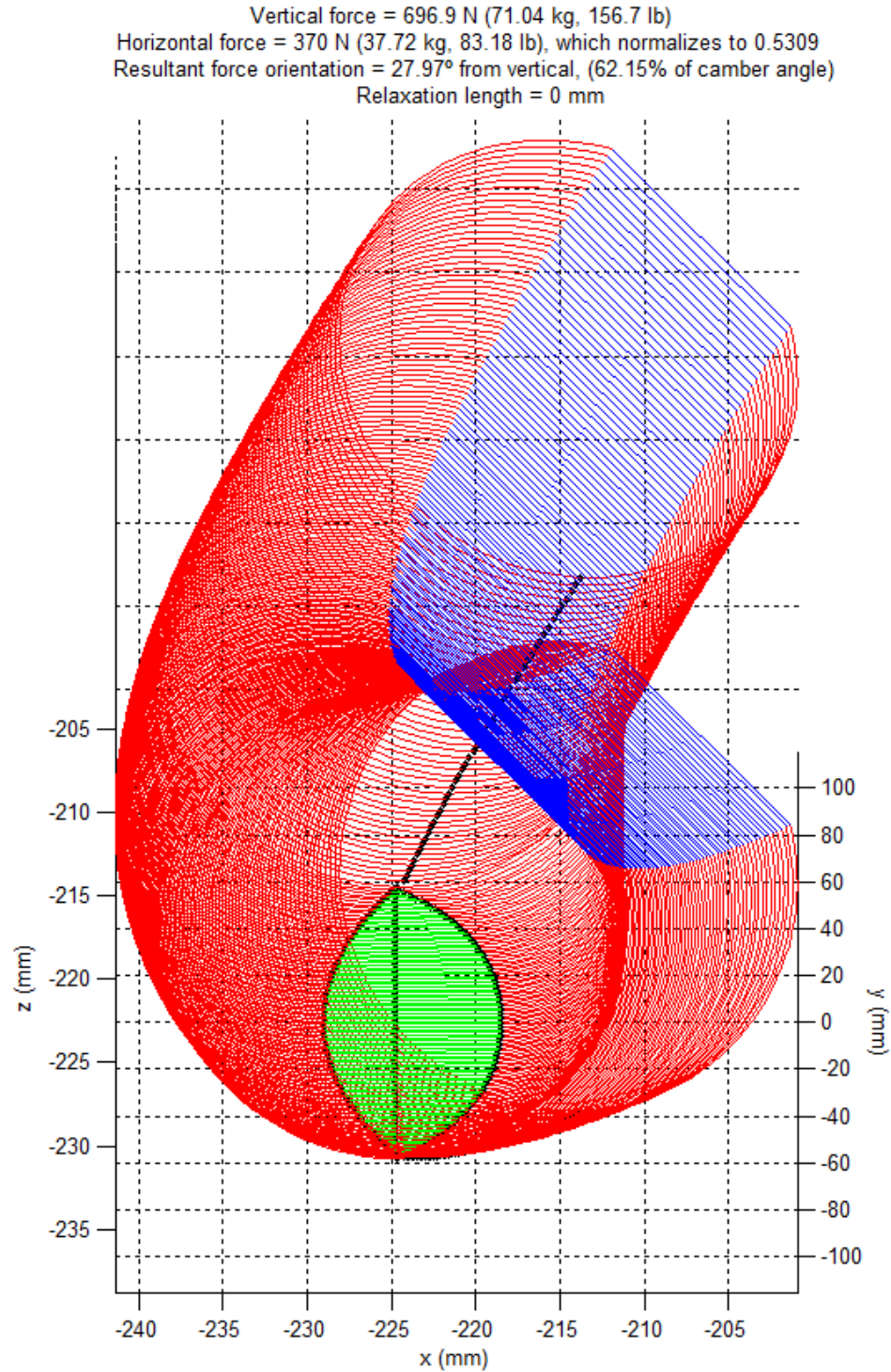


Figure 5-13: 3D representation of cambered tire modeled by Rotta.

5.3 Drums and disks

The above calculations can be adjusted to account for the curvature of various testing surfaces: such as the 2.5 meter drum at TU Delft and the 3 meter disk at Padua.

5.3.1 Drums

If the vertical displacement of the wheel, δ_{vert_wheel} , is taken to be with respect to the top of the drum, then the new radial deflection of each tire cross section due to the drum can be calculated as a decrease in the deflection already calculated above for the case of flat pavement.

$$\delta_{vert_section} = R - R_e - \delta_{drum_section} \quad \text{Eq. 5-18}$$

This change, $\delta_{drum_section}$, indicated below in **Figure 5-14**, can be calculated as in **Eq. 5-19**.

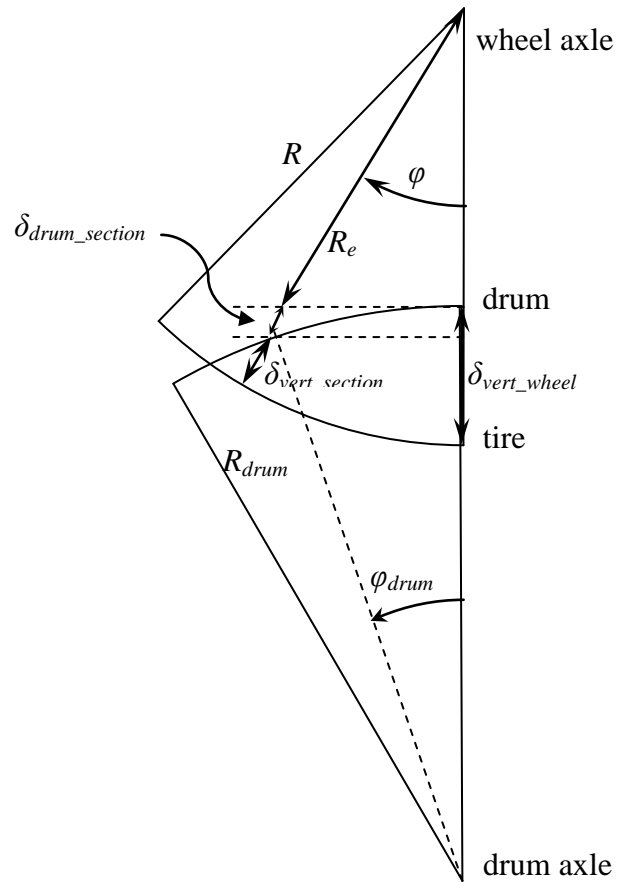


Figure 5-14: Side view schematic of wheel and drum.

$$\delta_{drum_section} = \frac{R_{drum} (1 - \cos(\varphi_{drum}))}{\cos(\varphi)} \quad \text{Eq. 5-19}$$

Finally, assuming that the wheel radius and the drum radius are both much larger than the wheel vertical displacement, which is the case for narrow bicycle tires, then the two angles can be approximately related for any radial cross section:

$$R_{drum} \sin(\varphi_{drum}) = R \sin(\varphi)$$

Eq. 5-20

$$\varphi_{drum} = \sin^{-1}\left(\frac{R}{R_{drum}} \sin(\varphi)\right)$$

All together:

$$\delta_{vert_section} = R - R_e - \frac{R_{drum} \left(1 - \cos\left(\sin^{-1}\left(\frac{R}{R_{drum}} \sin(\varphi)\right)\right)\right)}{\cos(\varphi)} \quad \text{Eq. 5-21}$$

This implementation of the Rotta model predicts only a 2% difference in camber force between flat pavement and the 2.5 meter drum at TU Delft. A 37 mm tire at 4 bar and under 400 N generates a 210 N horizontal force when cambered 45° on a straight track. If the track is a 2.5-meter diameter drum that curves away from the tire, then it generates 206 N.

5.3.2 Disks

In the case of a disk, the situation is nearly the same except that the curvature of the disk needs to be accounted for in the horizontal displacement of each cross section of the tire,

$\delta_{horz_section}$.

$$\delta_{disk_section} = \frac{R_{disk} (1 - \cos(\varphi_{disk}))}{\cos(\varphi)} \quad \text{Eq. 5-22}$$

Finally, assuming that the wheel radius and the disk radius are both much larger than the wheel vertical displacement, which is the case for narrow bicycle tires, then the two angles can be approximately related for any radial cross section:

$$R_{disk} \sin(\varphi_{disk}) = R \sin(\varphi)$$

Eq. 5-23

$$\varphi_{disk} = \sin^{-1}\left(\frac{R}{R_{disk}} \sin(\varphi)\right)$$

All together:

$$\delta_{disk_section} = \frac{R_{disk} \left(1 - \cos\left(\sin^{-1}\left(\frac{R}{R_{disk}} \sin(\varphi)\right)\right)\right)}{\cos(\varphi)}$$

Eq. 5-24

Lastly, the entire contact patch needs to be offset by the difference between $\delta_{disk_section}$ for the center section and $\delta_{horz_section}$ of the end section so that the ends of the contact patches are located where they would be if there were not a disk curvature.

This cannot be calculated in closed-form before hand, and simply needs to be calculated from the resulting contact patch and then used to create the contact patch again from scratch.

Modeling a tire, such as those tested by Doria *et al.*, with the 3 meter disk they describe,[28] confirms their assumption that averaging the lateral force from a tire first cambered one way and then cambered the same amount in the opposite direction does indeed yield the lateral force the tire generates on a flat surface.

For example, a size 37 mm tire at 4 bar and under 400 N generates a 210 N horizontal force when cambered 45° on a straight track. If the track is a 3-meter diameter disk that curves away from the camber, then it generates 206 N, and if the track curves toward the camber, then it generates 214 N. The average of 214 and 206, of course is 210, which matches the expected value.

5.4 Contact patch ellipse

The contact patch predicted by extending the Rotta model in 3D has pointed ends which are obviously different from the contact patches recorded in ink. One way to generate a more-realistic contact patch is to fit an ellipse to it, at least in the case of vertical displacement only, without slip or camber angles, when the contact patch is symmetrical. This tends to shorten the contact patch and reduce the area, as shown below in **Figure 5-15**, both of which better match the experimental results.

Contact patch length = 118.7 mm (4.674 in),	Fitted ellipse has length = 98.49 mm (3.878 in) 82.95%,
width = 9.917 mm (0.3904 in),	(in blue) width = 9.783 mm (0.3852 in) 98.65%,
area = 795.5 mm ² (1.233 in ²),	area = 756.8 mm ² (1.173 in ²) 95.13%

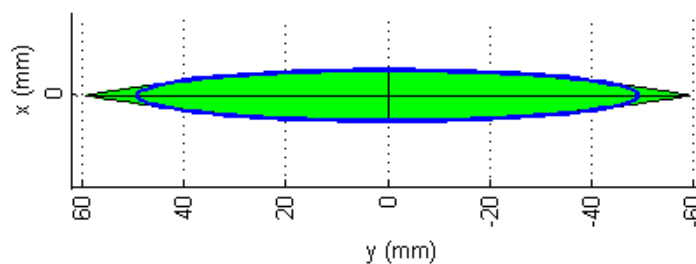


Figure 5-15: Rotta model contact patch fitted with an ellipse.

5.5 Calculating forces generated

In all cases, the lateral force generated, dS , in a cross section of depth dy is calculated from just the inflation pressure, p , and the radii of the two circular arcs, r_1 and r_2 , as shown below in **Eq. 5-25**. The lateral force generated by the entire tire is simply the sum of all the dS s.

$$dS = p(r_1 - r_2)dy \quad \text{Eq. 5-25}$$

Following the assumption that the vertical force between a piece of tire and the pavement is equal to the inflation pressure multiplied by the area of the piece of tire in question, the vertical force borne by each cross section can be calculated. The vertical force, dN , in a cross section of depth dy is simply the width of the contact patch in that cross section multiplied by its depth, the area dA , multiplied by the inflation pressure, p , as shown below in **Eq. 5-26**.

$$dN = p(e_2 - e_1)dy \quad \text{Eq. 5-26}$$

5.6 Friction

Dividing into the lateral force from **Eq. 5-25** by the vertical force from **Eq. 5-26** yields the minimum coefficient of friction necessary to prevent sliding, as shown in **Eq. 5-27**.

$$\mu_{\min} = \frac{dS}{dN} \quad \text{Eq. 5-27}$$

One solution to the problem of excessive coefficients of friction, for example $\mu > 1$, is to allow a cross-section to slide in the direction of the lateral force until the lateral force is

reduced enough to be withstood by the available friction, and the sliding can be implemented by simple iteration. In practice, however, because the cross-sectional slices are completely decoupled, it was found that cross-sectional slices near the ends of the contact patch would slide nearly all the way back to their undeflected location before friction became sufficient, and this causes an unlikely kink in the centerline of the tire.

Instead, it was found that limiting the sliding of any cross section to some fraction of its immediate neighbor produces much more realistic results. More details about how this fraction is decided and implemented are given below in section 5.8.

Another issue that arises once deflection of the tire beyond the ends of the contact patch is considered is the additional lateral force generated there that must be borne by friction in the contact patch. Since this cannot be known until those cross-sectional slices are considered, a simple iteration was implemented to calculate the lateral force generated by the entire tire by at first ignoring the additional force that must be applied to the contact patch, and then recalculating each cross-sectional slice and its possible sliding due to this additional force. This process usually converges to a stable total lateral force in just three or four iterations.

5.7 Extending Rotta's model beyond the ends of the contact patch

If a cross section does not intersect the contact patch, then its contact patch width can simply be set to zero, the radii of the two sides are equal, and it forms a single, constant-radius circular arc from bead to beam. If there is no lateral displacement of the tire centerline at this point, then the two zones blend together seamlessly. If there is a lateral

displacement of the tire centerline at the end of the contact patch, however, simply reverting to completely undeflected cross sections will result in a discontinuity.

The published Rotta analysis does mention displacement of the tire beyond the contact patch, but it does not predict that behavior, and it has been observed that a lateral displacement of even a point contact patch causes lateral displacement over a significant length of the tire. Here, the Rotta model is used to calculate a foundation stiffness for the model of a beam on an elastic foundation.

If the assertion that tire cross sections are displaced laterally beyond the ends of the contact patch is correct, and logical analysis and physical testing presented in section 3.8.6.3 suggests that it is, then it begs the question, what shape does it take? Rotta does not say, so additional models must be considered.

Choices are:

- Even displaced, it is a perfectly circular arc from bead to bead.
- The radius of curvature varies continuously in some way.
- The radius of curvature is constant for parts and there is a discontinuity, either in radius or the rate at which it changes.

The first choice, constant radius for the entire cross section, can be rejected by geometric analysis, as shown below in **Figure 5-16**. If the radius is constant from bead to bead, and the tire forms a perfect constant-radius circular arc, then it cannot be displaced laterally.

There is no way to draw a straight rim from one point on a circle to some other point on a circle so that it is not bisected by a radius:

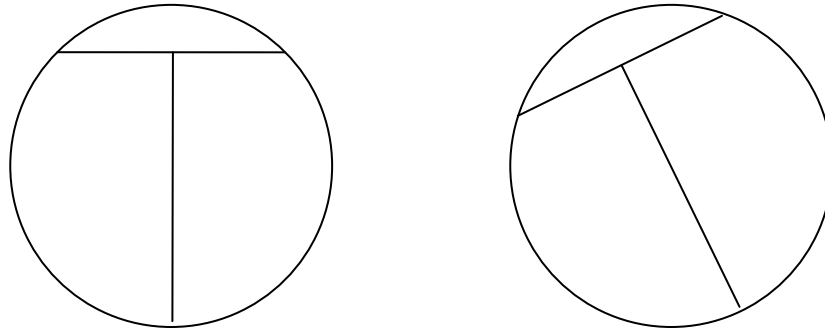


Figure 5-16: Geometric argument that displaced tire cannot have constant radius.

So that leaves a continuously varying radius or multiple distinct radii. Of the two, the former is more likely to match reality because it does not require something to create the discontinuity, as the contact patch does in the case of the Rotta model. Examples are shown in **Figure 5-17** below in green.

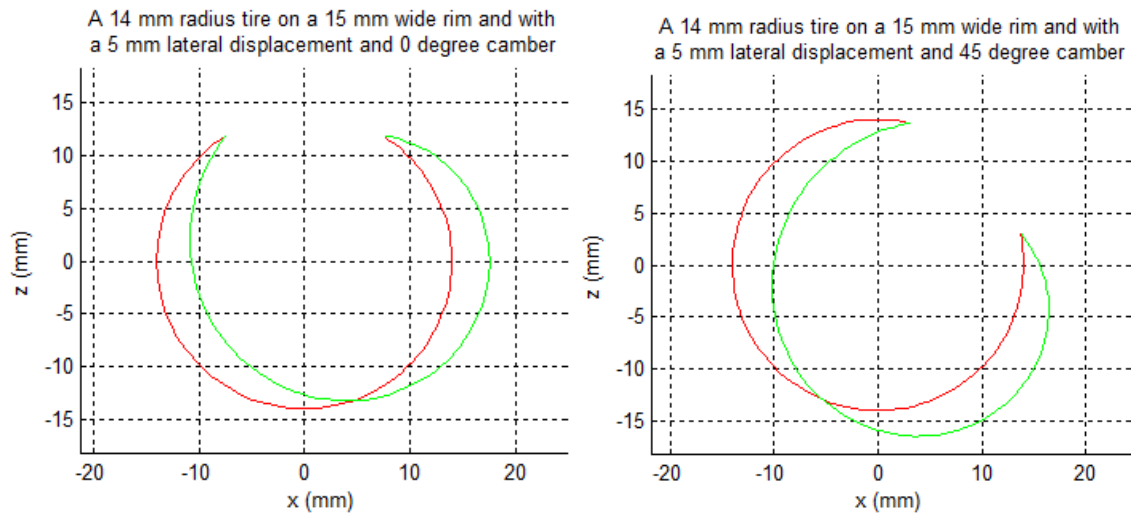


Figure 5-17: Continuously varying radius in laterally displaced tire cross sections.

This then begs the next question, however, of what two radii should be used to calculate the lateral force applied to the rim with Rotta's dS equation, **Eq. 5-25**? It can be argued that the difference between the angles at which the tire departs the two sides of the rim should be used instead of radii, but there is also another issue. There is not a closed-form solution to either configuration, and the variable radius configuration does not lend itself to speedy solution with the `fzero()` function in MATLAB®.

Instead, consider treating the problem as simply a zero-width contact patch and use the existing technology, which is already greatly speeded along with the `fzero()` function in MATLAB®, to calculate the radii of the two, distinct side bulges. As can be seen in **Figure 5-18** below, the results (in blue) are very similar to the continuously varying radius results (in green).

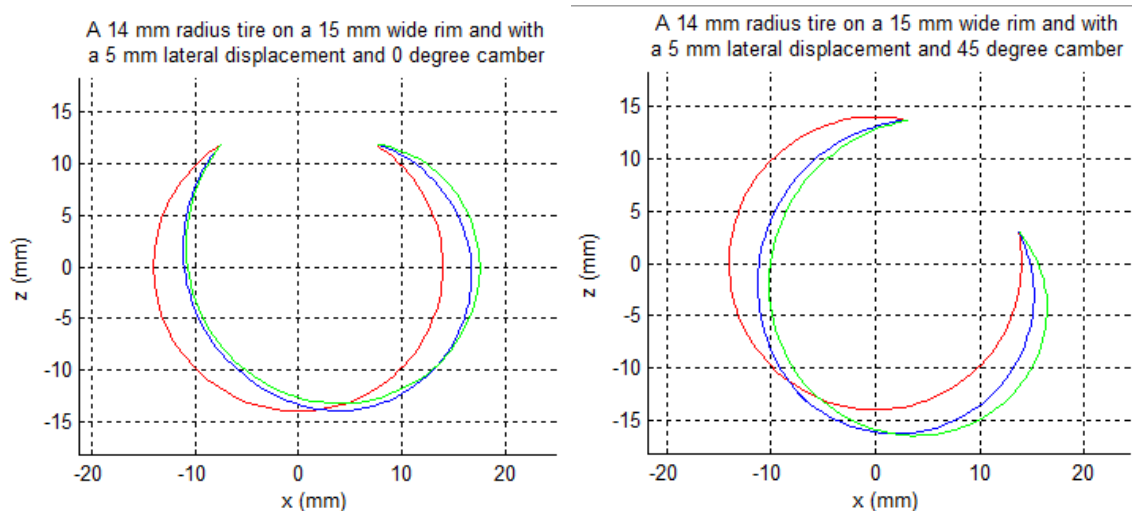


Figure 5-18: Comparison of constantly varying radius vs. two discrete radii.

5.8 Decay rate and length

The first method implemented to calculate the horizontal displacement of each cross section beyond the end of the contact patch is simply exponential decay. Each subsequent horizontal displacement is calculated by multiplying the previous horizontal displacement by a relaxation rate, i , in the range of 0.9 to 0.99.

$$\lambda = 1 - i \quad \text{Eq. 5-28}$$

This relaxation rate, i , can be converted to an exponential decay rate, λ , with **Eq. 5-28** above and the exponential decay rate, λ , can be converted to a decay length, ℓ , with **Eq. 5-29** below:

$$\ell = \frac{1}{\lambda} \quad \text{Eq. 5-29}$$

Vertical force = 490.3 N (49.98 kg, 110.2 lb)
 Horizontal force = 57.52 N (5.864 kg, 12.93 lb), which normalizes to 0.1173
 Resultant force orientation = 6.692° from vertical, (1n% of camber angle)
 Relaxation length = 131 mm, Static lateral stiffness = 28.76 N/mm (0.05866 1/mm)

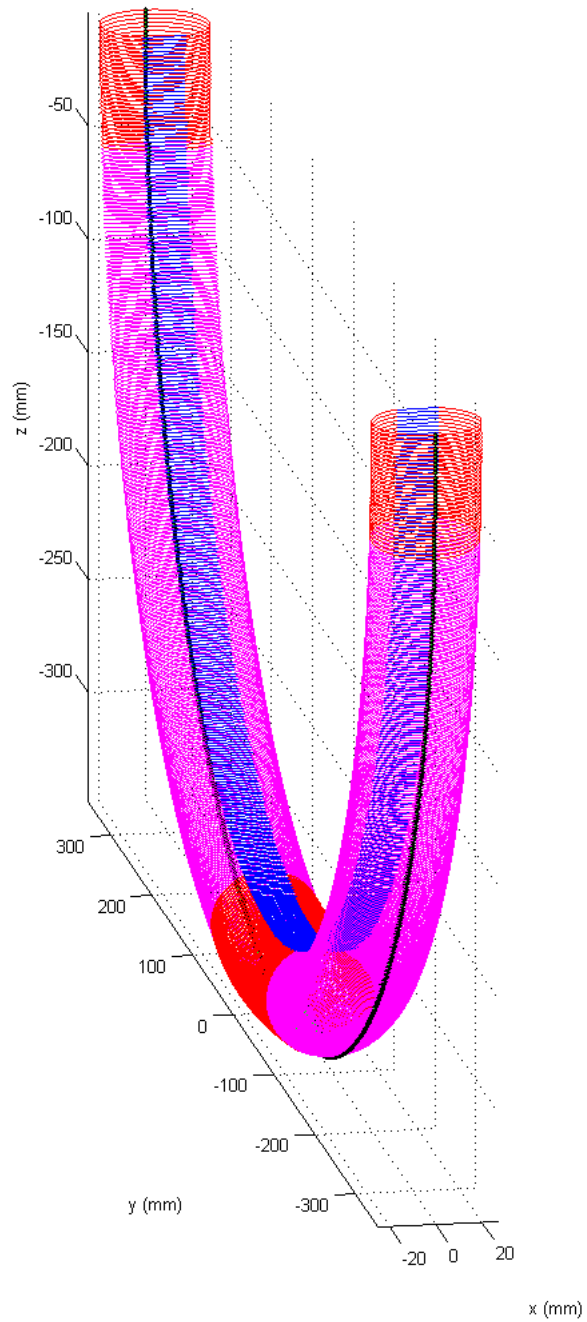


Figure 5-19: Rotta model of tire with 2 mm lateral displacement blended smoothly back to undisplaced over nearly half the wheel circumference with a 0.993 relaxation rate.

This produces reasonable looking results, as shown in **Figure 5-19** and **Figure 5-20**, but leaves the question of what rate to use unanswered. One method of determining the rate would be to measure the relaxation rate of an actual tire, but this is more easily said than done and goes against the motivation for the model in the first place.

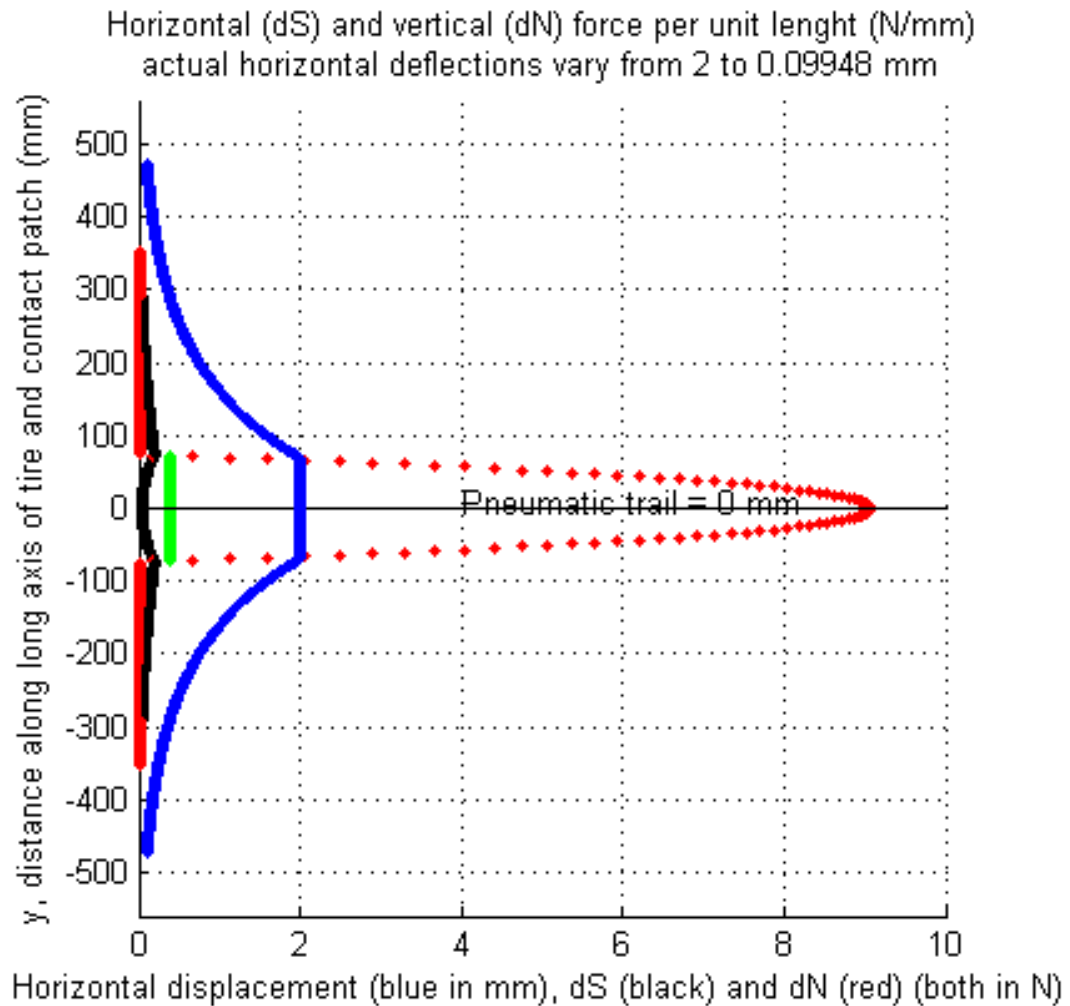


Figure 5-20: Graph showing lateral displacement of each cross section, the lateral and vertical forces generated in each cross section, and the average lateral force applied in the contact patch for a tire with 2 mm lateral displacement blended smoothly back to undisplaced over nearly half the wheel circumference with a 0.993 relaxation rate.

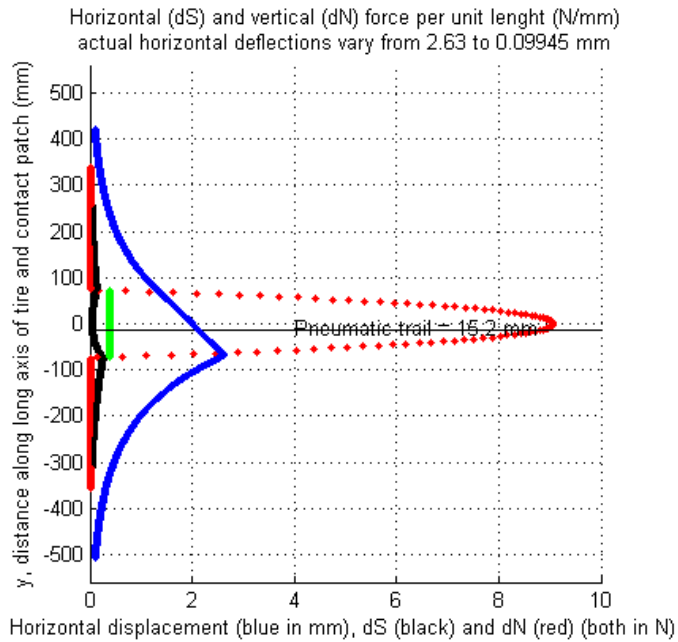


Figure 5-21: Graph showing same values and for same tire as **Figure 5-21**, but now with a 0.5° slip angle. Note similarity with measured lateral displacement shown in **Figure 4-15**.

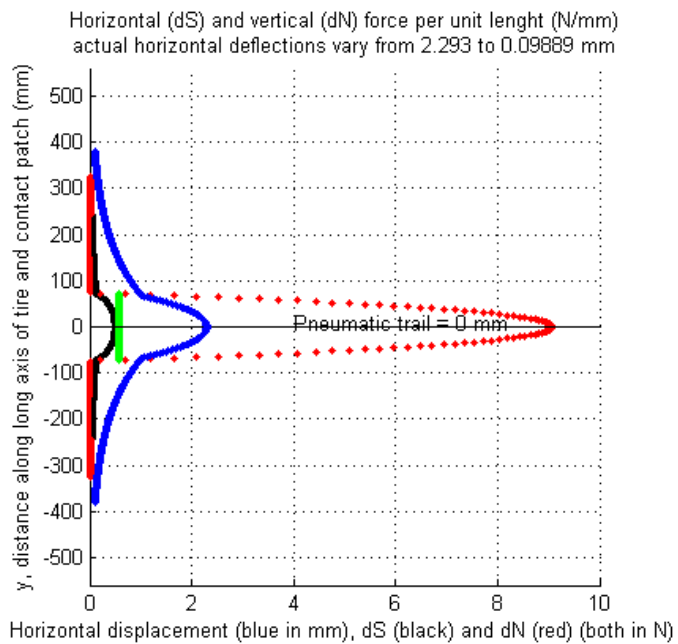


Figure 5-22: Graph showing same values and for same tire as **Figure 5-21**, but now with a 10° camber angle. Note similarity with measured lateral displacement shown in **Figure 4-16**.

5.9 Taut beam on an elastic foundation

In an effort to enhance the Rotta model so that it can provide a relaxation rate as output instead of require one as input, the model of a taut beam on an elastic foundation was considered. The resistance to lateral flexing of a tire is the beam lateral stiffness, the circumferential tension in the tire is the tension in the beam, and the lateral stiffness of each cross section according to the Rotta model is the elastic foundation.

5.9.1 Differential equation

The lateral displacement behavior of a taut beam on an elastic foundation can be modeled by a fourth-order ordinary differential equation, as shown in **Eq. 5-30**.

$$-\frac{\partial^2}{\partial x^2} \left(EI \frac{\partial^2 u}{\partial x^2} \right) + T \frac{\partial^2 u}{\partial x^2} - k(x)u(x) + f(x) = 0 \quad \text{Eq. 5-30}$$

5.9.2 Numerical implementation

The boundary value problem represented by this ordinary differential equation is solved by collocation with the `bvp4c()` function in MATLAB®,[46] as shown below in **Figure 5-23**. The length of the beam is some large fraction of the circumference of the wheel. Because the lateral stiffness of the tire causes any lateral displacement to eventually go to

zero beyond the ends of the contact patch, any length beyond the ends of this displacement is sufficient.

Beam with $I = 0.0169 \text{ in}^4$, $E = 5.48 \times 10^4 \text{ lb/in}^2$, $A = 0.644 \text{ in}^2$, and $L = 20.7 \text{ in}$
 on a foundation with stiffness rate $4 \times 10^3 \text{ lb/in/in}$ for a net stiffness of $8.26 \times 10^4 \text{ lb/in}$
 and subject to $T = 51.5191 \text{ lb}$ and a load rate of 200 lb/in over a contact patch length 0.125 in for a net force of 25 lb
 undergoes a maximum displacement of 0.05 in for a net stiffness of 500 lb/in (an increase of 0.01338%), and a relaxation length of 3.02 in

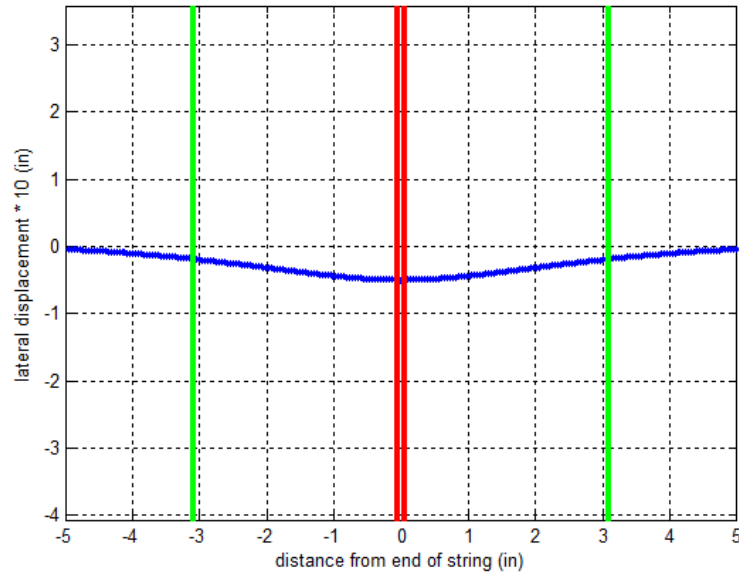


Figure 5-23: Lateral displacement, in blue, of a taut beam on an elastic foundation subject to a concentrated load at the midspan.

5.9.3 Constants

The governing equation for a taut beam on an elastic foundation requires several constants.

5.9.3.1 Area Moment of Inertia

An area moment of inertia can be calculated directly from the tire cross section geometry. As the lateral deflection of the tire decreases as the tire nears the rim, only the area of the

half of the tire cross section furthest from the rim is considered to approximate this reality, as shown in equation **Eq. 5-31**.

$$I = \frac{\pi}{4} \left(r^4 - (r-t)^4 \right) \quad \text{Eq. 5-31}$$

5.9.3.2 Modulus of Elasticity

An estimate of the modulus of elasticity for the composite material of nylon cords embedded in a rubber matrix that makes up the carcass can be found in the literature.[47]

5.9.3.3 Tension

The tension in the tire, normal to the cross section, can be estimated by simply multiplying the inflation pressure by the internal cross sectional area, as shown in **Eq. 5-32**.

$$T = p\pi r^2 \quad \text{Eq. 5-32}$$

Another estimation is to consider the radial pressure acting on the tire carcass over the wheel circumference,[2] as shown in **Eq. 5-33**.

$$T = p(R + 2r) \quad \text{Eq. 5-33}$$

For a 28-622 tire, **Eq. 5-32** predicts about twice the tension as does **Eq. 5-33**.

5.9.4 Integration with Rotta model

The integration of this model with the Rotta model begins by picking some small lateral displacement, scaled to the arc length of the tire, and calculating the contact patch length,

the stiffness rate, and the force rate with the Rotta model. In the case of zero displacement beyond the contact patch, which would give an infinite stiffness, use instead the maximum stiffness, found just inside the ends of the contact patch. Plug those values into the taut beam on elastic foundation model to calculate displacements. Plug those displacements into the Rotta model to calculate the contact patch length, the stiffness rate, and the force rate. Iterate until the orientation angle of the ground reaction force converges.

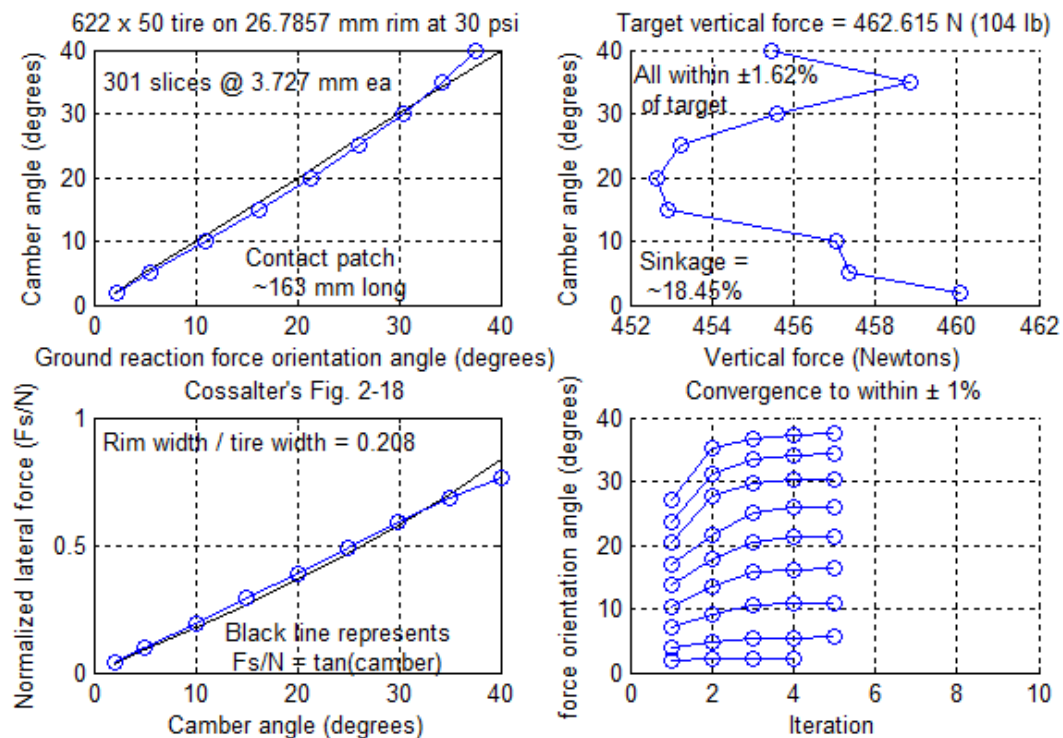


Figure 5-24: Camber force results of iteration between Rotta model and model of taut beam on elastic foundation.

CHAPTER 6

MODELING RESULTS

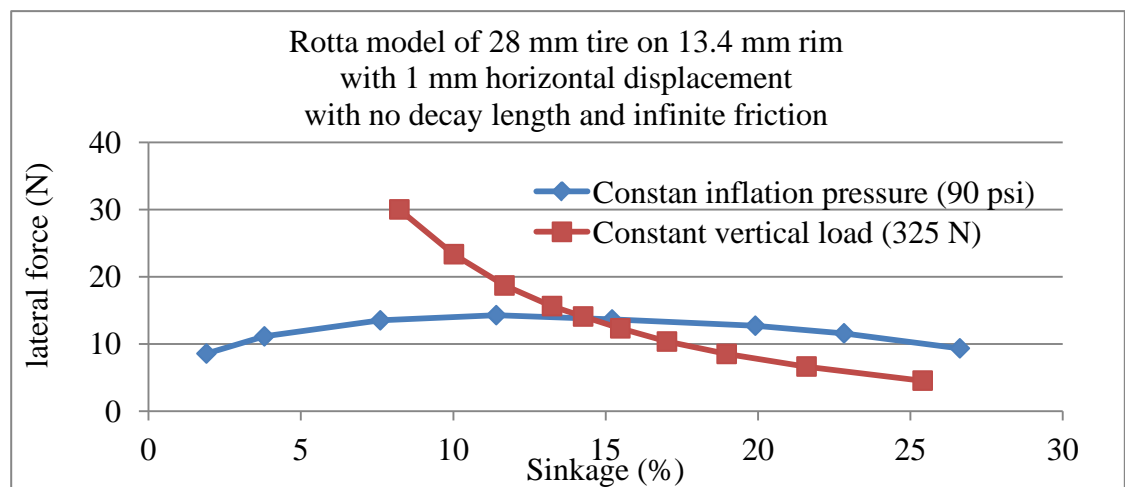
6.1 Model predictions

6.1.1 Contact patch

That the contact patch area equals the vertical load divided by the inflation pressure is an assumption intrinsic to the Rotta model, but all measured contact patches have slightly less area than this.

6.1.2 Sinkage

Increasing vertical load without changing inflation pressure increases sinkage. The Rotta model predicts that increasing sinkage has small effect on lateral stiffness, but the increasing load decreases normalized lateral stiffness.



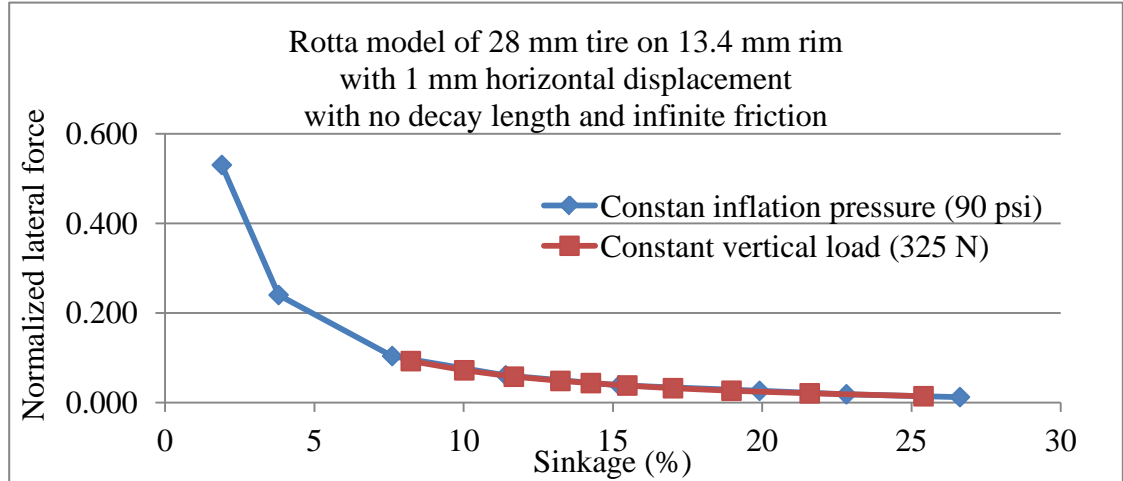


Figure 6-1: Lateral force vs. sinkage for constant inflation pressure and constant vertical load.

- Sinkage calculated by the Rotta model increases linearly ($R^2 = 0.999$) with vertical load, and decreases proportional to about the -0.7 power of inflation pressure ($R^2 = 1$).
- For values from the Rotta model, the ratio between sinkage and contact patch area raised to the 0.704 power is nearly constant ($+0.2\%$, -0.6%) for sinkages from 9% - 25% .

6.1.3 Stiffness

Increasing inflation pressure without changing vertical load decreases sinkage, and the Rotta model predicts that decreasing sinkage has small effect on lateral stiffness, but the increasing inflation pressure increases lateral stiffness and thus normalized lateral stiffness.

The lateral force calculated by the Rotta model increases linearly with the lateral displacement of the centerline of the tire.

6.1.4 Tangent rule

The Rotta model casts doubt on the applicability of the tangent rule derived from the radial spoke model to bicycle tires.[17][7] The Rotta model predicts that camber thrust deficiency tends to decrease as sinkage decreases, but there is no guarantee that it will go to zero before sinkage does. Instead, the model suggests that camber thrust deficiency appears to be sensitive also to the ratio of tire arc length over rim width, and a deficiency can be decreased, even to the point of becoming a surplus, by widening the rim on which the tire is mounted, as shown in **Figure 6-4**.

Limited physical testing of this prediction to date has proven inconclusive.

Jim Papadopoulos writes, “The deformation is only unchanged if you have a brush or spoke model of the world. Rotta calculations show us that the force aligns with the wheel only for very tiny radial deformations, otherwise it deviates more and more as deformation increases. That is the first flaw of the brush model: that it takes a linear approximation of the radial and lateral tire stiffness, and assumes that this is unaffected by camber. The second flaw of course is the lack of a belt or string, but of course that is not your discovery. (Except for finding that the decay length is of order half the contact length, for typical loadings.)”

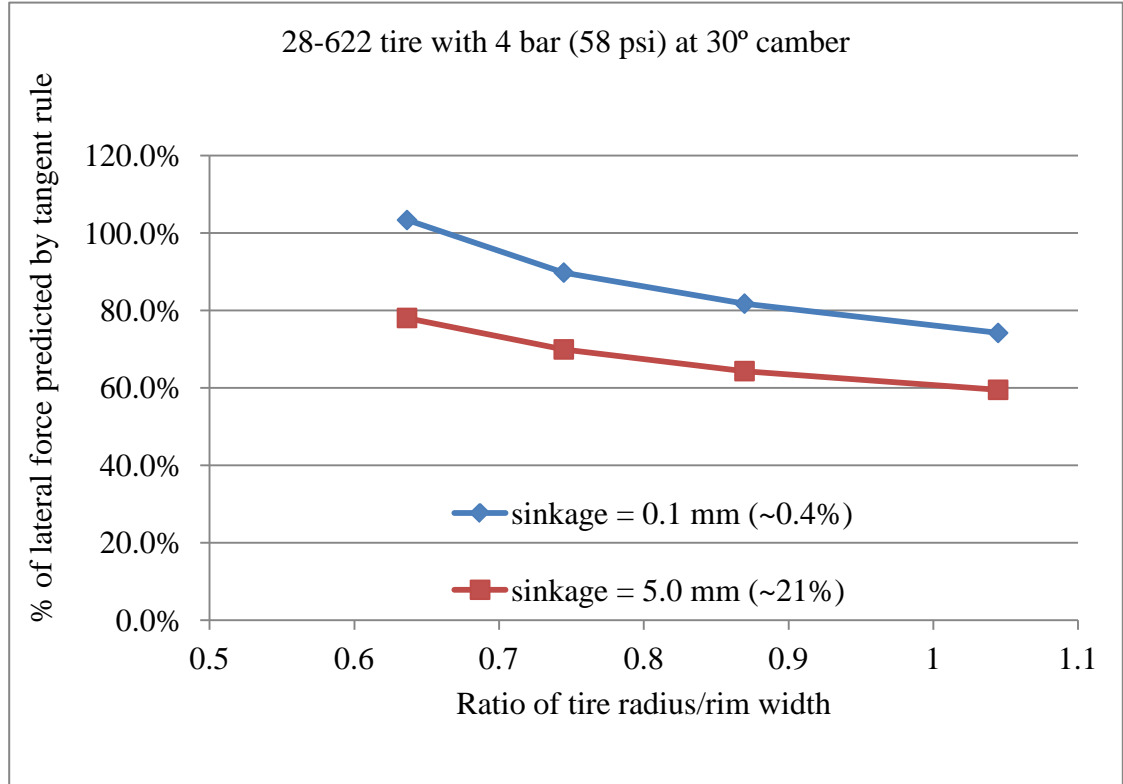


Figure 6-2: Plot of Rotta model prediction of % agreement with tangent vs. ratio of tire radius over rim width.

6.2 Physical measurements compared to model predictions

The length and width of the contact patch predicted by the Rotta model for a given contact patch area is compared against the lengths and widths of contact patches measured from physical tires under various vertical loads and at various inflation pressures. In general, as can be seen below in **Figure 6-3**, measured contact patch lengths are shorter and the widths are wider than those predicted by the Rotta model.

6.2.1 Contact patch size and shape

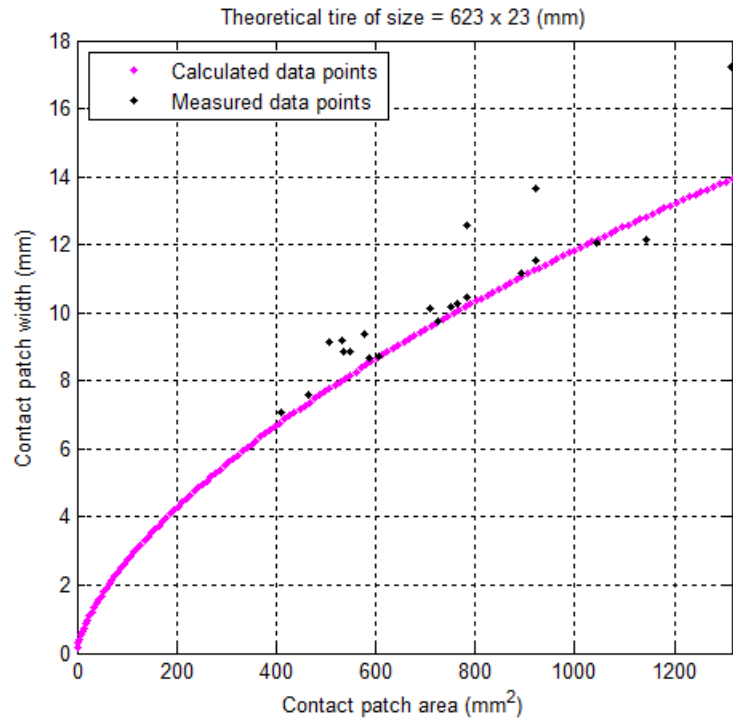
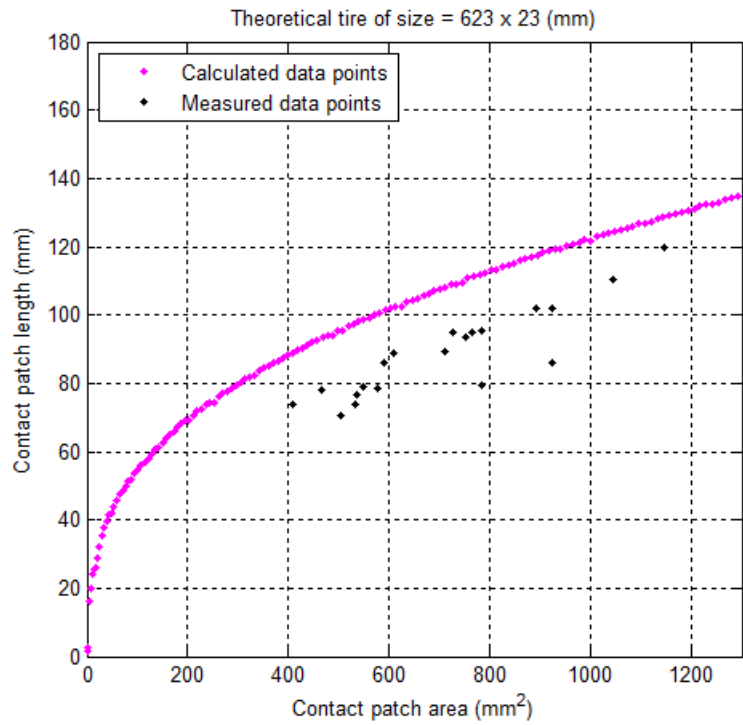


Figure 6-3: Comparison of contact patch area vs. length and width between Rotta model and measured physical tires.

6.2.2 Variation in stiffness with rim width

As can be seen in **Figure 6-4**, the lateral stiffness of a tire varies almost perfectly linearly with the width of the rim. The result is also seen in the Rotta model.

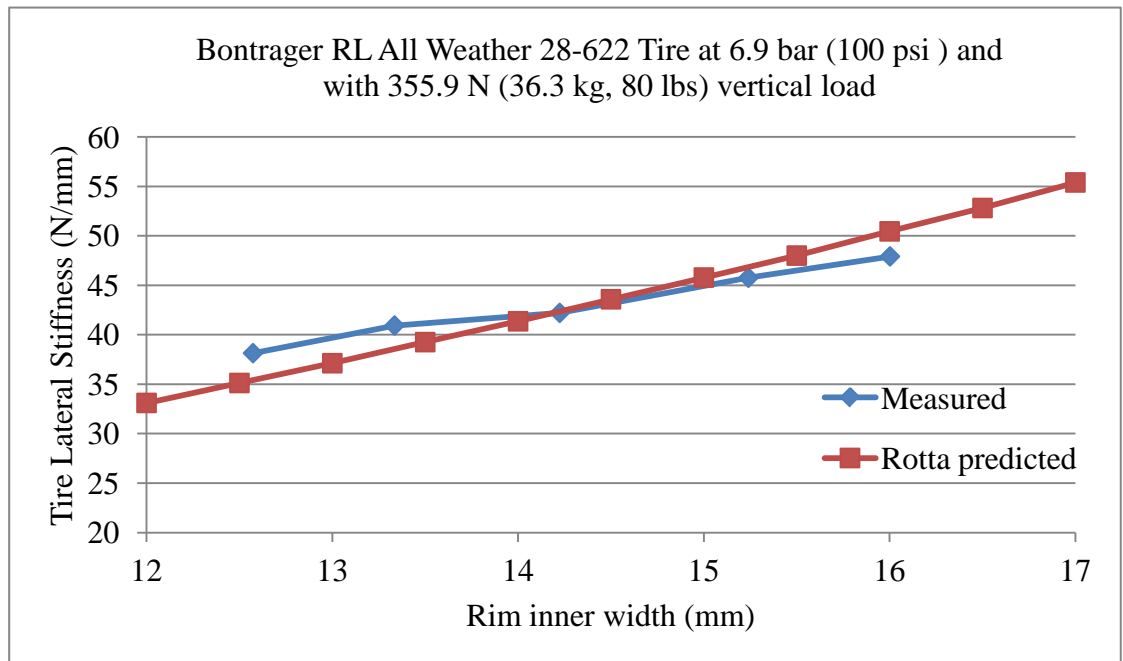


Figure 6-4: Variation in lateral stiffness with rim width, measure and modeled.

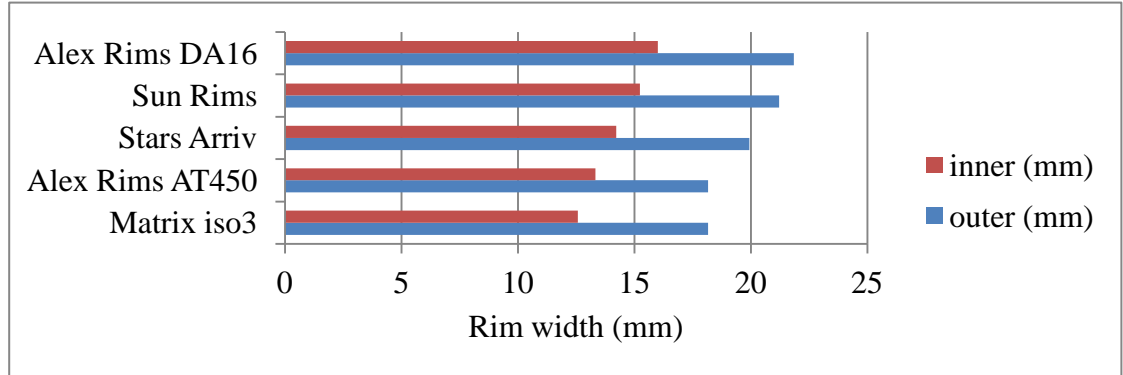


Figure 6-5: Rims and their widths used to generate data in **Figure 6-4**

6.2.3 Variation in stiffness with tire arc length

As shown above, in **Table 4-3** and **Figure 3-4**, four tires with the same 37-mm size designation were found to have actual carcass arc lengths that vary from 73.5 mm to 90 mm and stiffness tends to increase with carcass arc length. The Rotta model predicts the opposite, all else remaining the same. A wider tire, however, would have greater resistance to bending, all else remaining the same, simply due to having a greater area moment of inertia and greater circumferential tension, and thus could have a slower exponential decay of lateral displacement. This could cause more cross sections to be deflected and therefore generate more force. In the current implementation of a taut beam on an elastic foundation, however, as described above in section 0, this is not sufficient to overcome the decrease in stiffness of each cross section.

On the other hand, the trend seen in the measured data could just as well be due to other factors. The four tires in question are not known to be identical except for their carcass

arc length, and the observed increases stiffness with carcass arc length could be due to several other factors, such as increased carcass thickness or modulus of elasticity.

6.2.4 Other stiffnesses

1. Measured normalized lateral stiffness increases as inflation pressure increases in 11 of 11 cases and decreases as vertical load increases in 12 of 12 cases. The Rotta model predicts both of these trends.
2. Measured normalized cornering stiffness decreases as vertical load increases in 14 of 14 cases. The Rotta model predicts this trend for a fixed lateral displacement:
 - a. decreases as inflation pressure increases in 8 of 14 cases, ranging in size from 23-37 mm,
 - b. increases as inflation pressure increases in 2 of 14 cases, the Cheng Shin Classic Zeppelin at 50 mm and the Maxxis radial at 22 mm,
 - c. increases and decreases as inflation pressure increases in 4 of 14 cases, ranging in size from 35 mm to 55 mm.
3. Measured normalized camber stiffness:
 - a. decreases as inflation pressure increases and increases as vertical load increases in 13 of 14 cases, which is the opposite of what the Rotta model with no lateral displacement predicts,

- b. increases as inflation pressure increases and remains constant as vertical load increase in 1 of 14 cases.

CHAPTER 7

DISCUSSION

7.1 Difficulties in the physical testing

7.1.1 Difficulty detecting edges of contact patch in ink prints

Connecting isolated sections of tire treads was not too difficult, but determining which sections near the edge actually bore weight and which merely touched the paper was far more problematic.

Once a judgment was made on which isolated ink spots should be included, the convex hull algorithm worked well. The fitted ellipse, however, is slightly problematic because the true shape of the contact patch is not necessarily an ellipse.

7.1.2 Difficulty in setting one angle to zero while second angle is swept

Ideally, camber angle would be set to zero before sweeping slip angle in order to measure cornering stiffness. After sweeping slip angle, it should ideally be set to zero while camber angle is swept in order to measure camber stiffness. The remote actuators on test device number 3 at TU Delft were not designed to do this precisely. Instead, it was up to the operator to observe the reported slip and camber angles, and get them as close to zero as possible.

7.1.3 Flexibility

As with the bicycle wheels used, and mentioned in section 3.3, the frame of all three test devices are flexible, and the sensors used and their locations, especially the displacement sensors on the rim, were designed to accommodate this. The one measurement that could not easily be made, however, is relaxation distance (also Pacejka's relaxation length σ , and Cossalter's L), the distance the tire rolls after a step change in orientation before developing $1-1/e$ or about 63.2% of its steady-state force. Any measured value would be greatly exaggerated as the wheel and the frame flexed under the building lateral force.

One idea for overcoming this difficulty was to support the rim directly over the contact patch with a stiff mechanism that connected directly to a force sensor. Time did not permit implementing this, however.

7.1.4 Headset bearing in test device number 3

A poorly implemented headset in test device number 3 at TU Delft caused poorly recorded torques for thin tires. This was corrected before testing of the wide tires.

7.1.5 Resonance

Under some configurations, test device number 3 at TU Delft could be seen bouncing significantly. This, of course, was captured in the recorded force and displacement data.

7.2 The difference between measured camber stiffness presented here and values from Padua published by Doria *et al.*

7.2.1 Reasons that the data presented here may be correct

At TU Delft, the same sensor is used for cornering force, which mostly agrees with Padua values, as for camber force. Errors in measurement of lateral force, tire inflation pressure, or vertical load are not likely to produce a cornering stiffness that agrees with Padua and also a camber stiffness that does not.

The inability to zero slip angle accurately on test device number 3 could introduce noise to the camber stiffness values from configuration to configuration and tire to tire, but the recorded results do not show this inconsistency. If anything, an undetected non-zero slip angle should increase the measured camber stiffness, not decrease it.

The camber force measurements from test device number 3 are symmetrical about zero camber angle, as can be seen in the plots in Appendix B.

As shown above, in section 4.4.2, there is good agreement between the measured values from TU Delft and similar measurements made on the flat-track tester at UWM: The Maxxis Radial Prototype was found to have normalized camber stiffness between 0.0135 and 0.017 at TU Delft and 0.015 at UWM. These are both just below the 0.0174 that represents the net ground reaction force aligning with the plane of the wheel.

7.2.2 Possible problems with the data presented here

There is no correction applied for drum curvature, as explained in section 4.1.2. The implementation of the Rotta model with no decay length predicts only a 3% difference in camber force between flat pavement and the 2.5 meter drum at TU Delft.

The Rotta model predicts that a 37 mm tire at 4 bar and under 400 N, which is the best guess at what Padua used, generates a 214.3 N horizontal force when cambered 45° on a straight track. If the track is a 2.5-meter diameter drum that curves away from the tire, then it generates 208.5 N: a 2.7% decrease.

7.2.3 Possible problems with the data presented by Doria *et al.*

The finite radius and asymmetrical nature of the disk used is an obvious suspect, despite the correction for disk curvature they describe. This implementation of the Rotta model, however, completely agrees with them on this point, when not using any enhancements for tire deflections beyond the ends of the contact patch.

The Rotta model predicts that a 37 mm tire at 4 bar and under 400 N, which is the best guess at what Padua used, generates a 214.3 N horizontal force when cambered 45° on a straight track. If the track is a 3-meter diameter disk that curves away from the camber, then it generates 222.4 N, and if the track curves toward the camber, then it generates 208.1 N. The average is 215.25 N, just 0.44% high.

Another possibility is that Doria *et al.* used a much wider rim for their testing than the 18.7 mm wide rim used to test the 37-622 tires on device number 3. As described above in section 6.1.4, the Rotta model predicts a sensitivity in camber stiffness to rim width.

7.3 Shortcomings of the model

7.3.1 Contact patch shape

The modeled contact patches have sharp points at each end instead of the rounded shape of real contact patches captured in the ink prints. The fitted ellipse matches reality better, but it can only be applied when the contact patch is symmetrical about the centerline.

7.3.2 Flatness and straightness of contact patch in cambered tire

The contact patch generated by the model for non-zero camber angles is not perfectly flat and straight.

7.3.3 The bending of a beam might not be the best analogy for the lateral deflection of an inflated bicycle tire

Other options include the torsion of a thin-walled tube, although that is not perfect either.

7.3.4 Difficulty with convergence

Although initially promising, the integration of the model of a taut beam on an elastic foundation with the Rotta model has proven to be problematic, because the stiffness of the foundation predicted by Rotta is almost perfectly linear. It is possible to reach equilibrium between the foundation stiffness and the force applied in the contact patch at nearly any reasonable lateral displacement. Thus, the model quickly converges to some lateral displacement near the initial guess.

CHAPTER 8

CONCLUSIONS AND FUTURE WORK

8.1 Conclusions

8.1.1 Contributions

The contributions of this project include:

1. Collecting and comparing previously measured bicycle tire data. While a handful of published papers have been found with some bicycle tire data, few refer to another, and none summarizes all the data.
2. Developing three different test devices specific to bicycle tires. When this project began, it was explained that the motorcycle tire test device in Padua was too heavy and therefore unsuitable for testing bicycle tires. There appeared to be no other option available, but to create test devices from scratch.
3. Measuring all relevant properties from a wide variety of tires and under a wide variety of configurations. In most cases, the existing published bicycle tire data includes only one or two variables, and is missing many of the parameters, such as inflation pressure, vertical load, or tire size, necessary to duplicate it.
4. Documenting lateral stiffness dependence on rim width.
5. Documenting rate-independent and rate-dependent hysteresis, which may contribute to rolling resistance.

6. Documenting existence of long decay length beyond the ends of the contact patch as laterally deflected tire centerline returns to equilibrium which needs to be considered for accurate modeling.
 7. Documenting that the so-called tangent rule, based on the radial brush model, does not accurately predict bicycle tire camber stiffness.
 8. Developing a numerical model, implemented in MATLAB®, which suggests the capability of predicting hard-to-measure properties from properties which are easier to measure. A working predictive model minimizes the need for future testing.
 9. Additional observations from the collected data are enumerated above in section 4.1.10.
- 8.1.2 Tire properties should matter to bicycle stability and handling

The numerical simulation that showed how a change in tire stiffness can affect the wobble mode, shown above in **Figure 1-3**, was based on an assumption that a 10% difference in stiffness is possible. Much larger variations in stiffness than that can be seen in tire test results. Normalized cornering stiffness varies from below 0.15 to over 0.35, which is $\pm 40\%$ from the average, and normalized camber stiffness varies from below 0.0075 to over 0.015, which is $\pm 33\%$ from the average.

8.1.3 Tangent rule for camber stiffness

Tires approach the camber stiffness necessary for the net ground reaction force to be in the plane of the wheel, but most tires with most inflation pressures and under most loads presented here fall below that. Some possibilities for the difference between the results presented here and the results presented by Doria *et al.* are offered above in sections 7.2.2 and 7.2.3, but a conclusive reason has yet to be found.

8.1.4 Model fidelity

Although actual values generated by the model do not exactly match measured values, the trends in contact patch size and lateral stiffness values generated do correspond well with measured data as parameters vary, such as inflation pressure, vertical load, and rim width. Cornering stiffness is problematic because the measured value depends to a large extent on the lateral displacement of the tire centerline, and attempts to model this displacement have proven fruitless. Camber stiffness also depends in part on lateral displacement, but the displacement values are smaller. The trends in measured camber stiffness with vertical load and inflation pressure, however, are opposite those predicted by the Rotta model.

8.2 Future Work

8.2.1 Measuring

8.2.1.1 Measure sinkage directly

The current Rotta model implementation assumes that the vertical load divided by the contact patch area must equal the inflation pressure, but experimental results show that is only approximately true. If sinkage was measured physically, and that was used in the Rotta model, perhaps the contact patch dimensions predicted by the Rotta model would better match reality. It would also enable comparison with Lyasko's model relating sinkage, contact patch dimension, and tire dimensions.[48]

8.2.1.2 Measure contact patch pressure distribution

Pressure sensitive paper exists that that would enable measuring pressure throughout the contact patch. This would enable better calculation of contact patch area, and possibly enable enhancement of the model to better predict exceeding the limits of friction.

8.2.1.3 Measuring slip angle directly during camber to confirm camber force

Since an unexplained discrepancy remains between data collected for camber force at UWM and TU Delft and that most recently published by Doria, *et al.*[28], an independent method of confirming one or the other set of values is desired. One such method would be to measure the slip angle of a cambered bicycle tire.

8.2.2 Modeling

8.2.2.1 Extract analytical relationships from numerical model

The modeling results are more likely to be useful to more people if they are expressed as analytical relationships linking contact patch behavior to tire dimensions.

8.2.2.2 Find proper model for lateral displacement of tire centerline for non-zero slip and camber angles

Since the Rotta model depends on this value so much, predictions of cornering and camber stiffness can not be made from simple geometric tire parameters until this value is also well predicted.

One possibility is to examine the effect mentioned by Pacejka and Sharp in which “a structural interaction involving a tendency of the tyre tread to deflect laterally if an overturning moment M_x is applied to the tread occurs.”[17]

8.2.2.3 Enhance numerical model of bicycle with force generating tires

Before expending the time, money, and energy required for physical testing, as described below in the next point, the bike with the pair of tires that might reasonably be mounted on it should be modeled together to confirm that they will cause a detectable change in bicycle behavior.

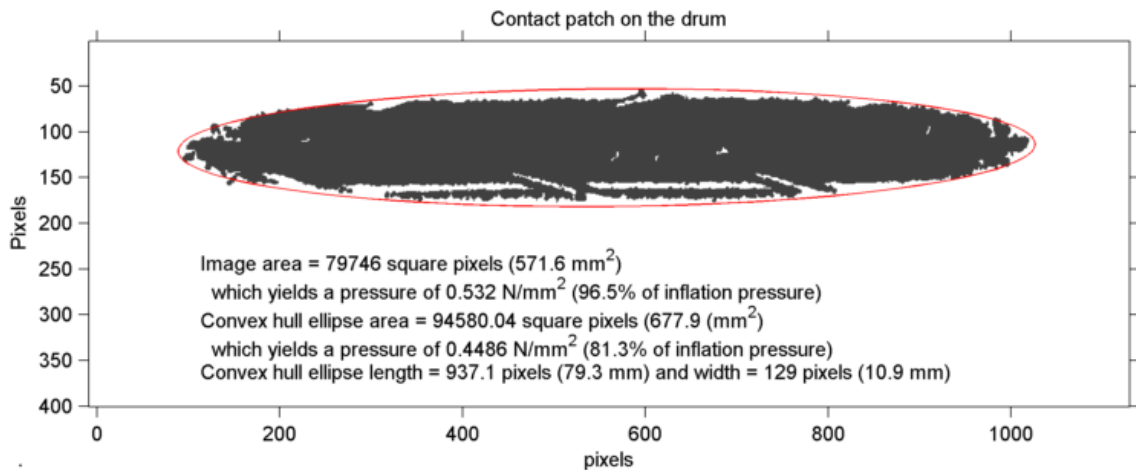
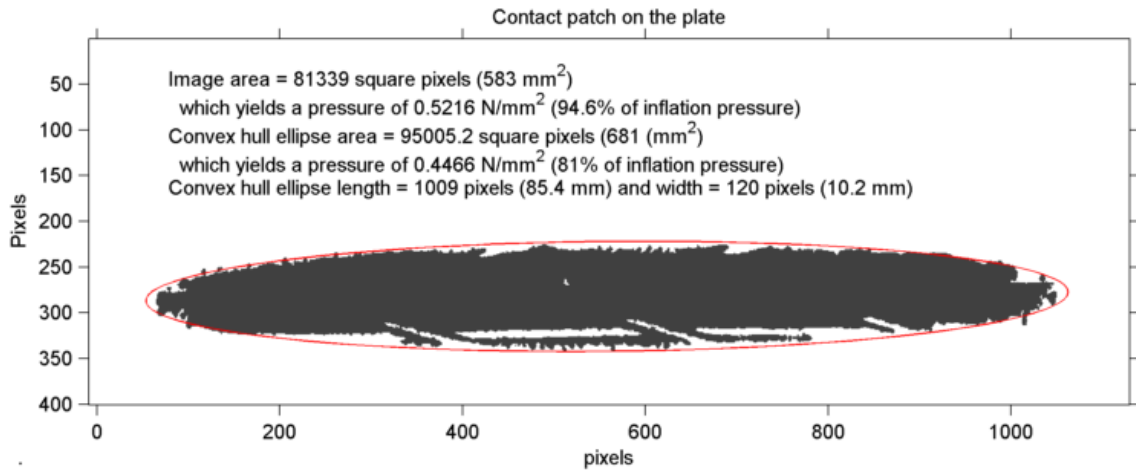
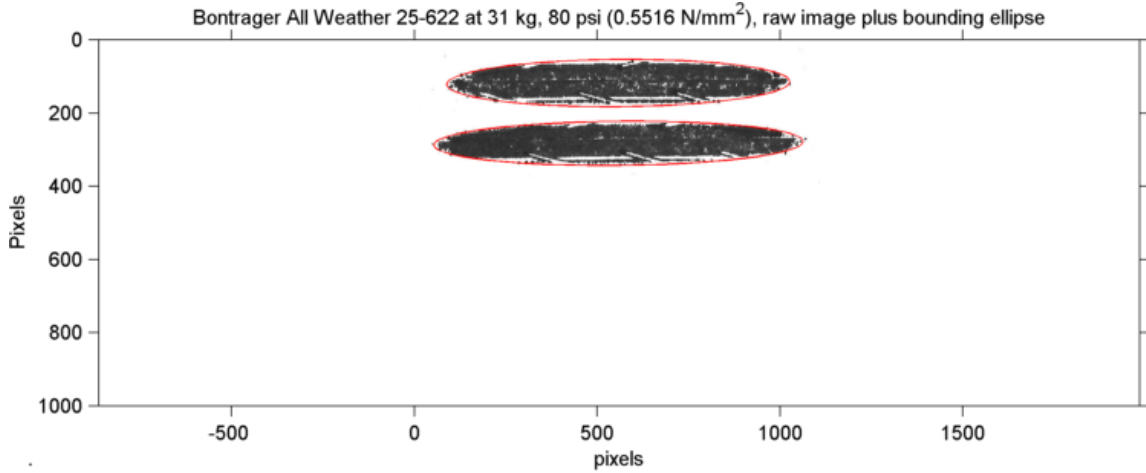
8.2.3 Validation of tire properties by measuring bicycle behavior

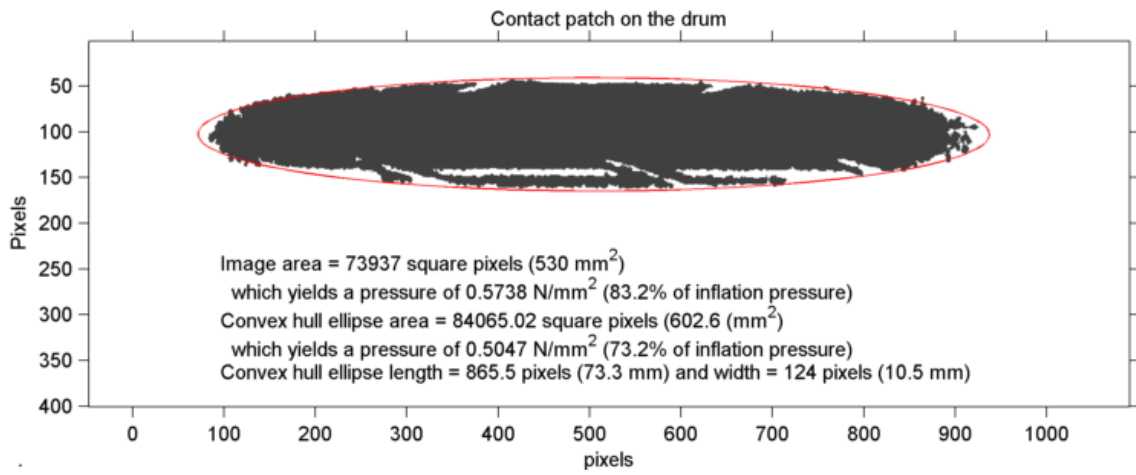
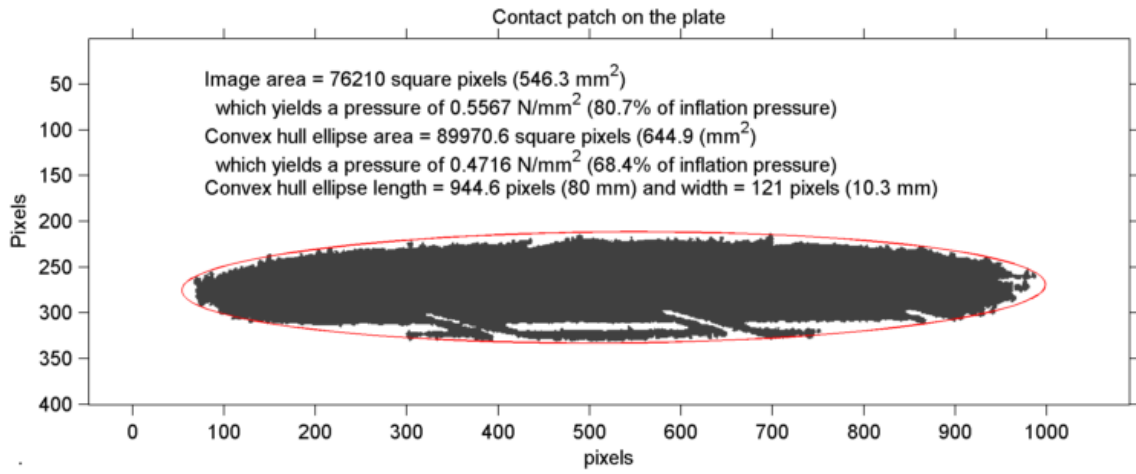
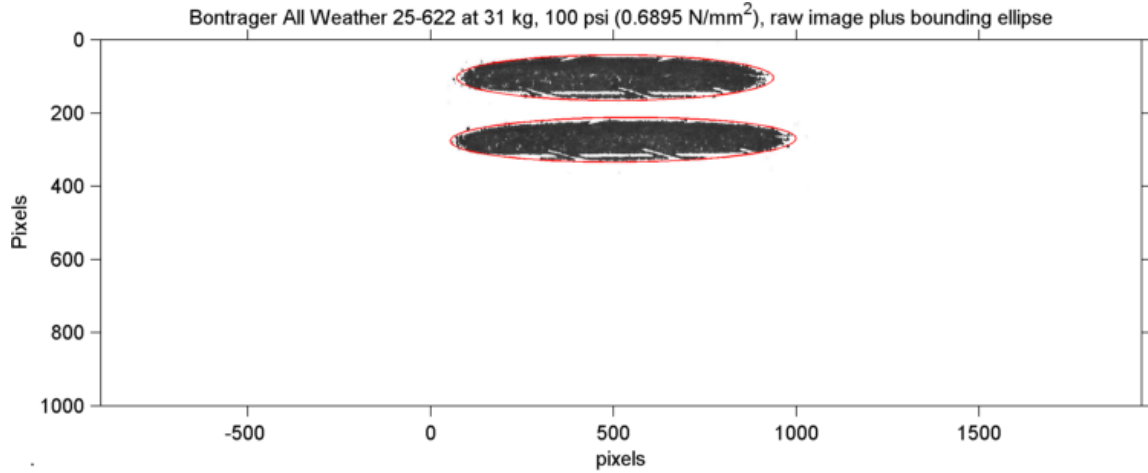
Since one of the purposes of collecting this data in the first place is to model bicycle behavior more accurately, the ideal validation of this data would be to model the behavior of a bicycle with these tires and then measure that behavior physically in a way similar to Kooijman, *et al.*[10]

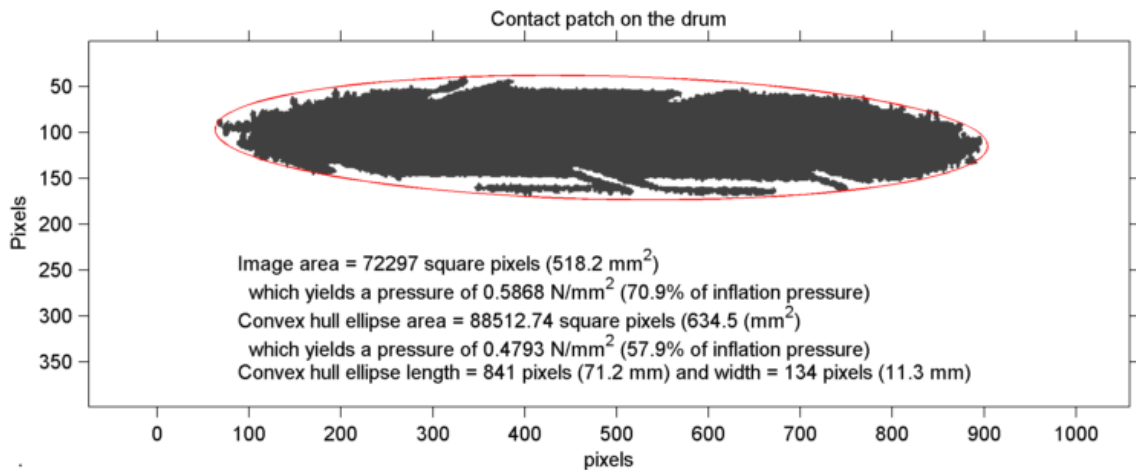
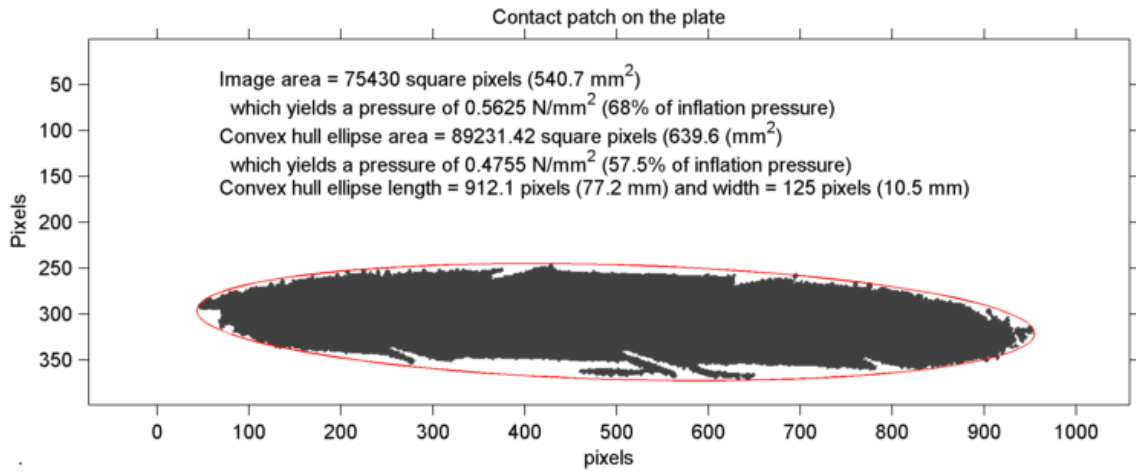
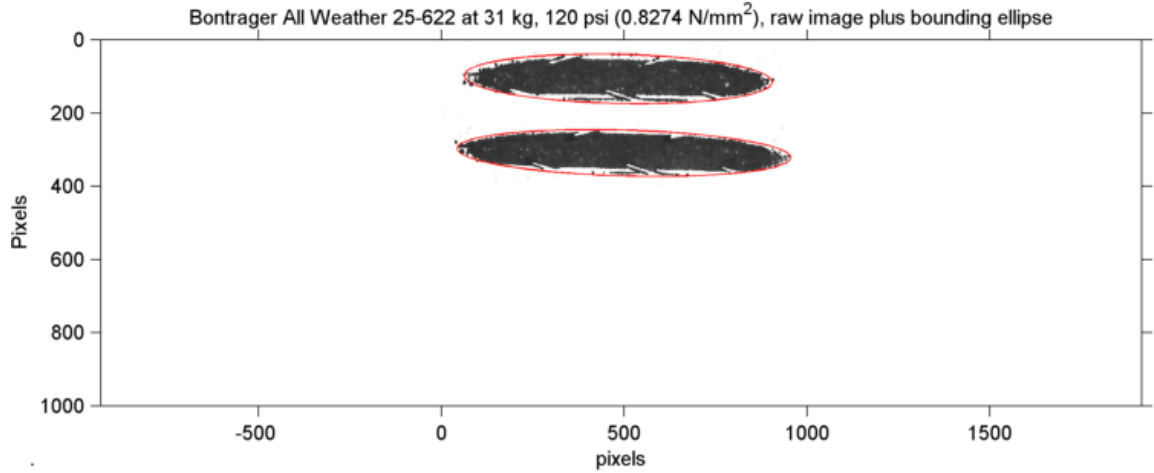
8.2.4 Design a better bicycle tire

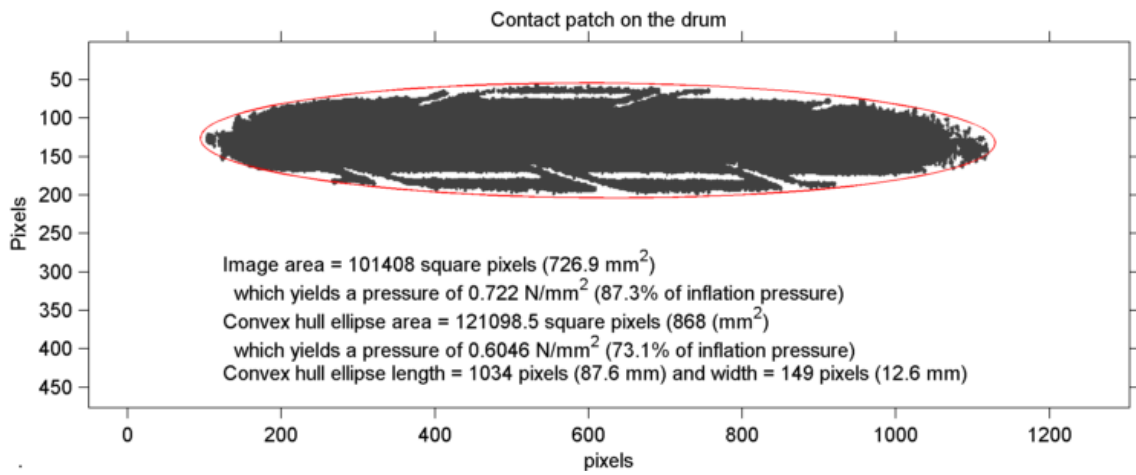
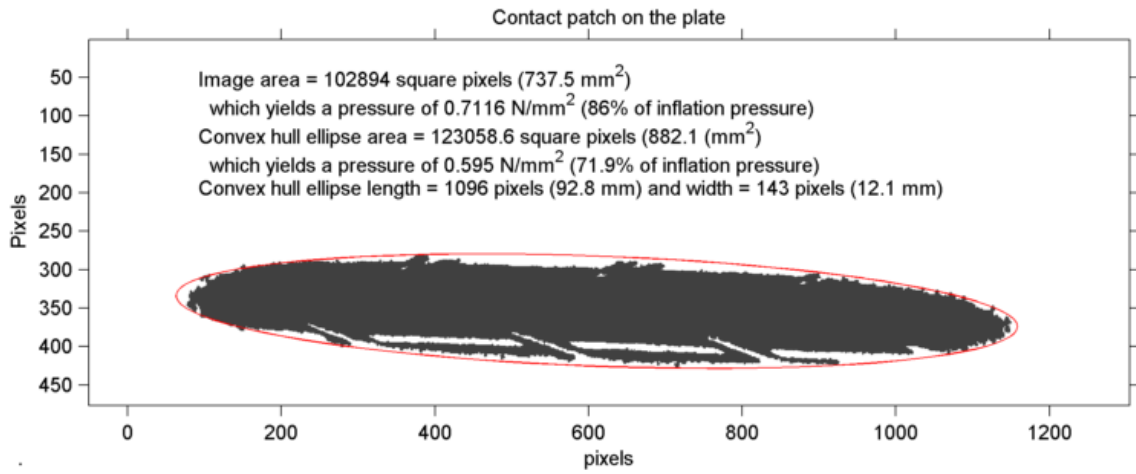
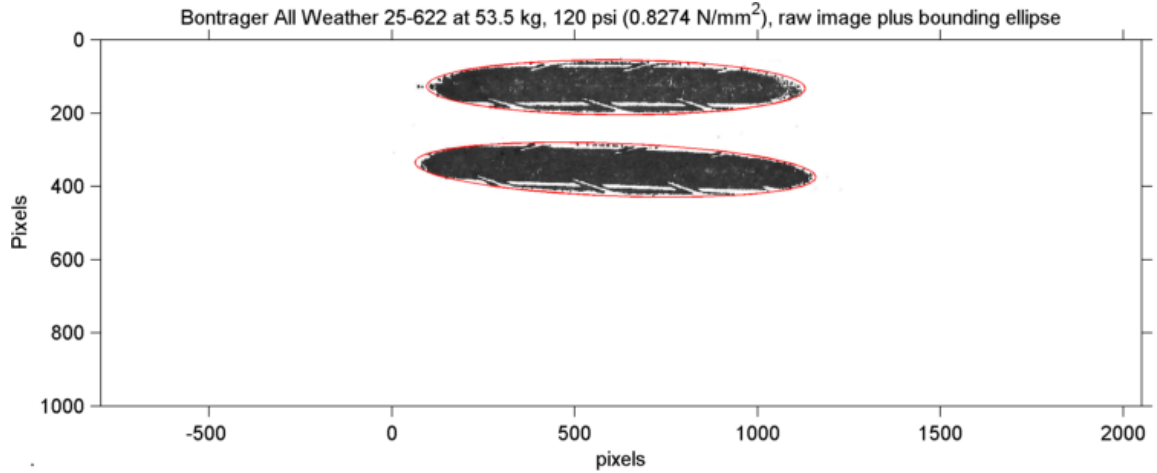
While modern pneumatic bicycle tires perform admirably in many situations, they continue to suffer from loss of inflation pressure, both slowly because of the finite permeability of the inner tube, or catastrophically because of a puncture. Meanwhile, non-pneumatic tires suffer from poor rolling resistance and poor handling characteristics. Perhaps a solid understanding of what forces and moments a tire generates and how it does so will enable the design of a non-pneumatic tire that would provide the best of both worlds.

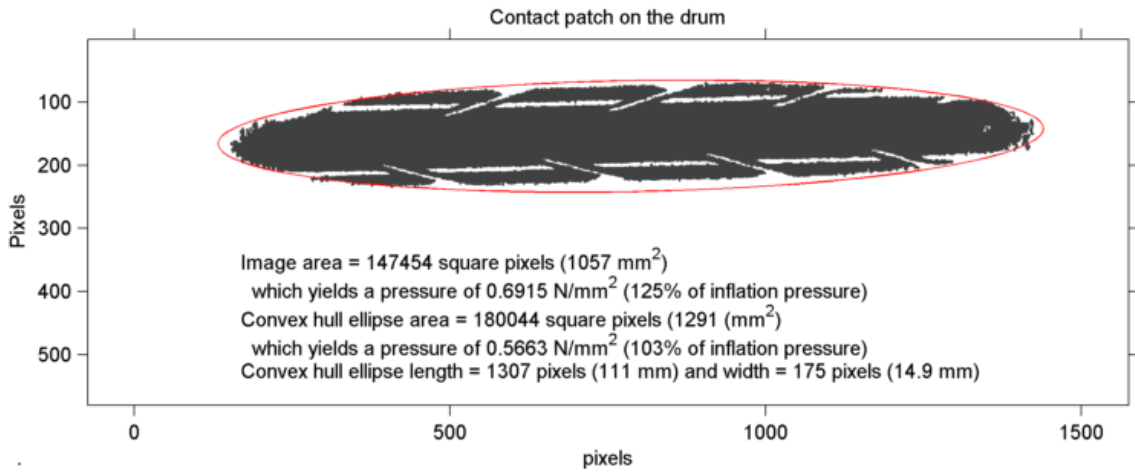
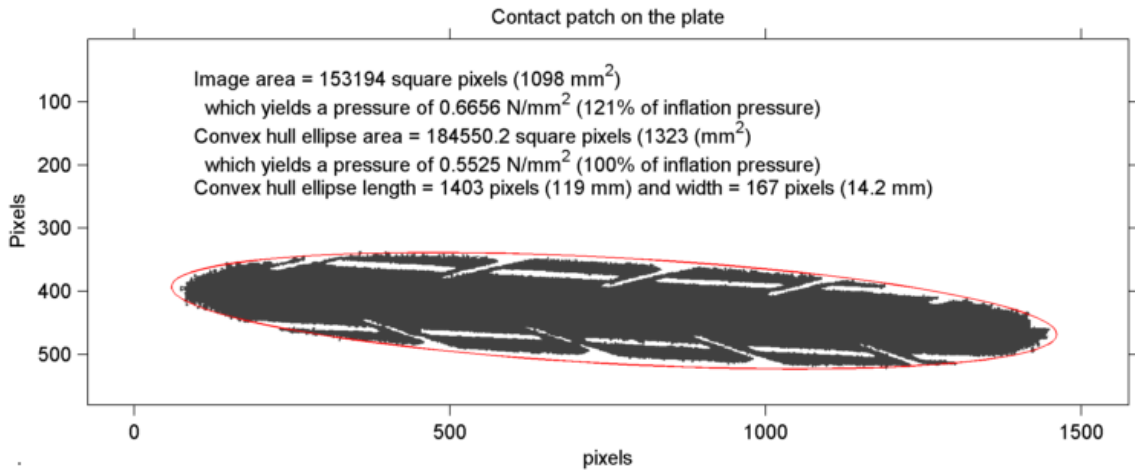
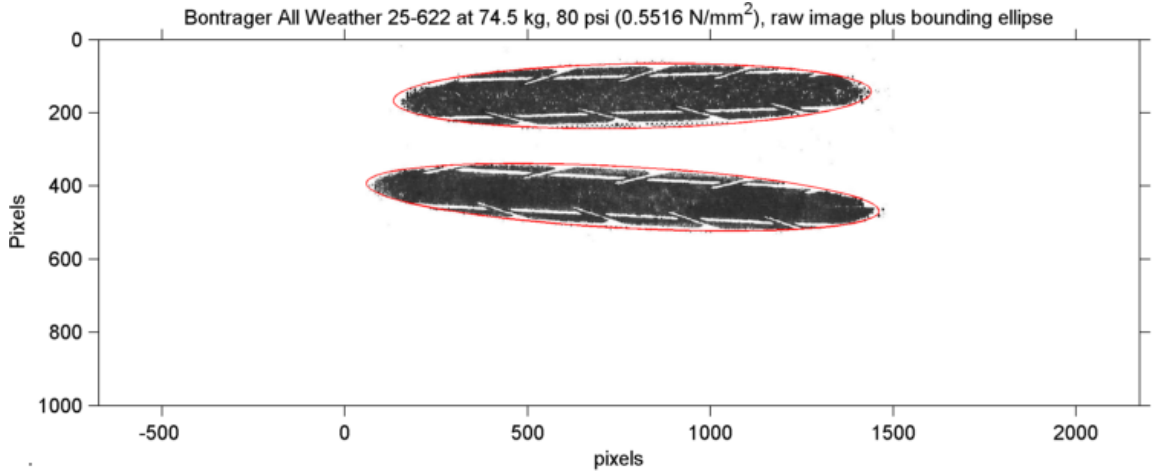
APPENDIX A
INDIVIDUAL TIRE CONTACT PATCHES

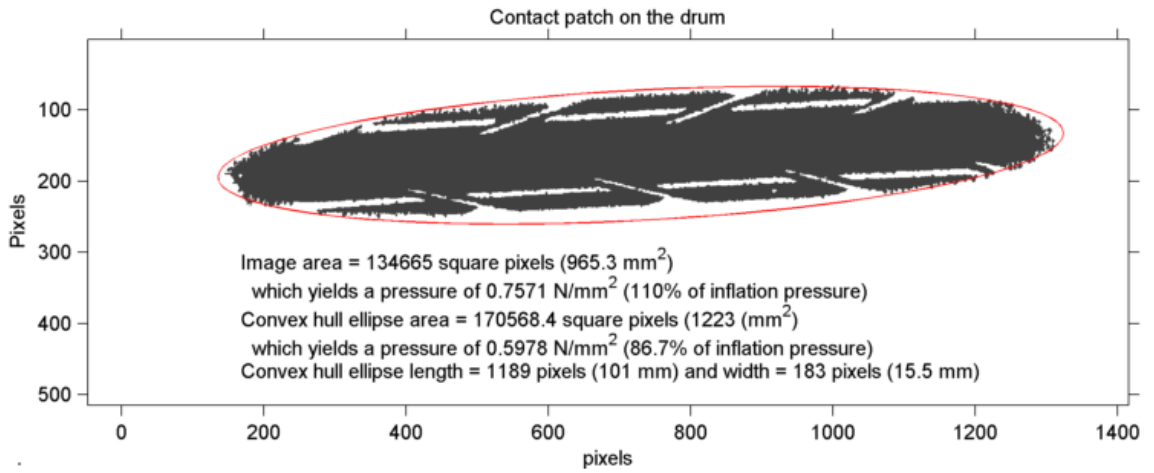
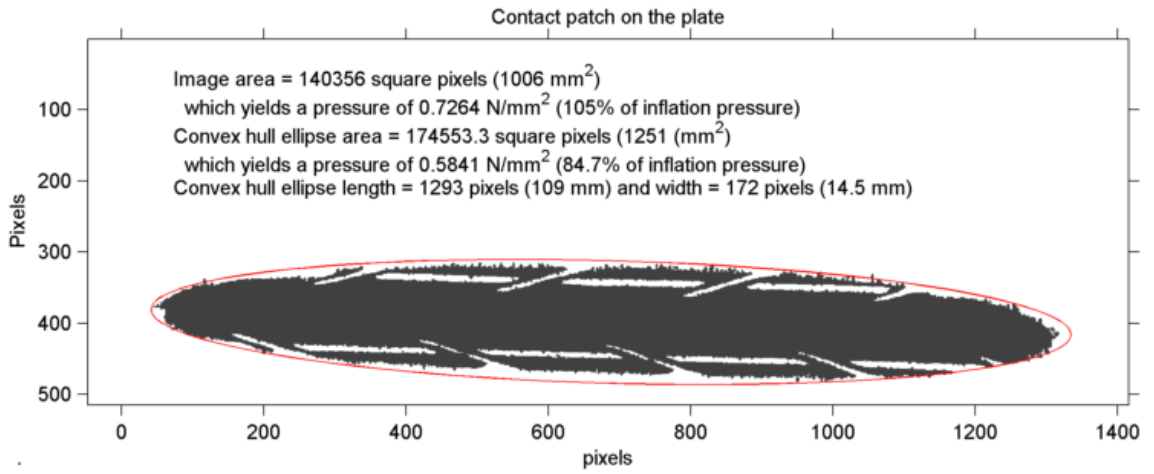
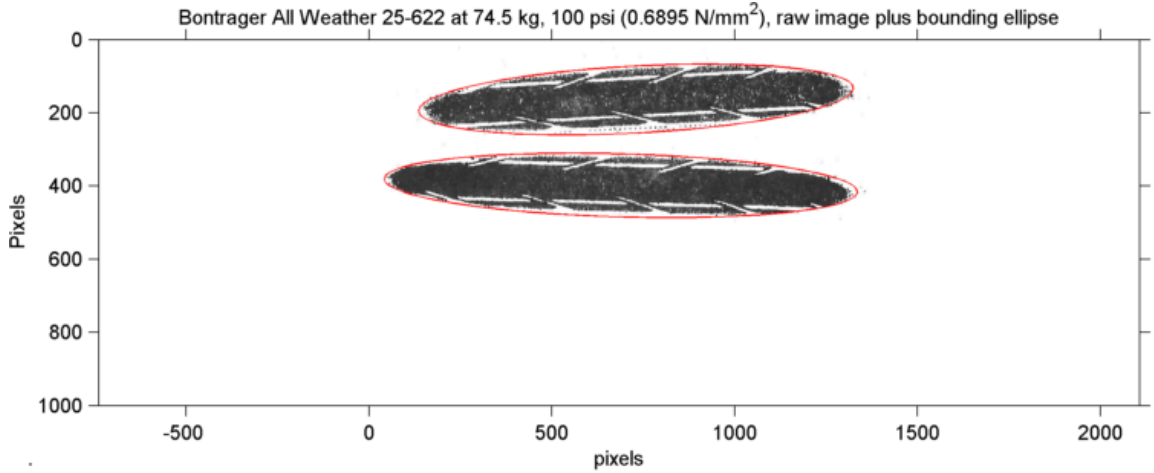


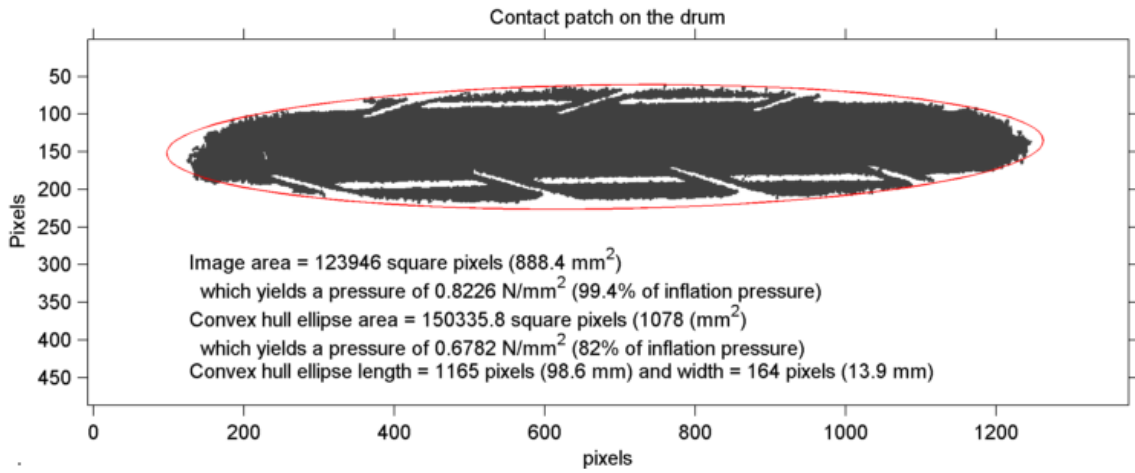
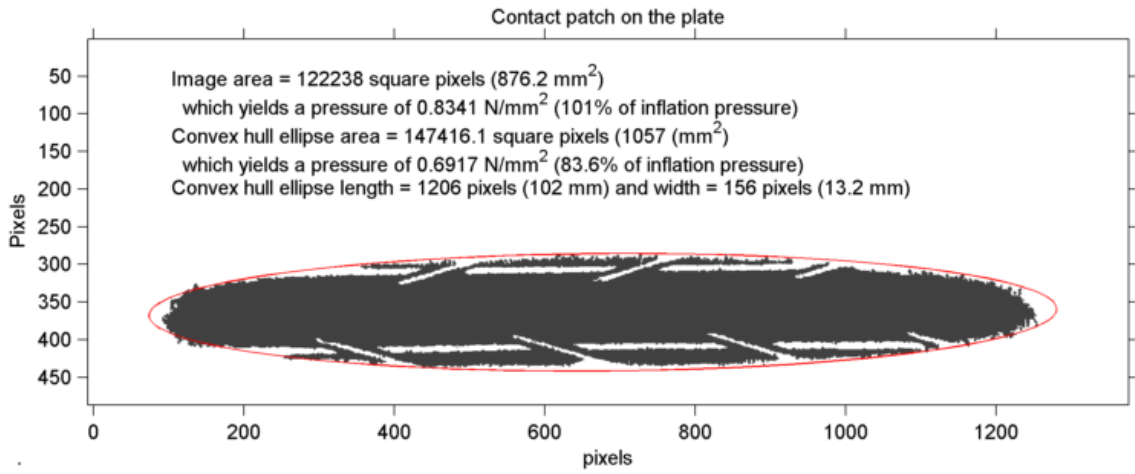
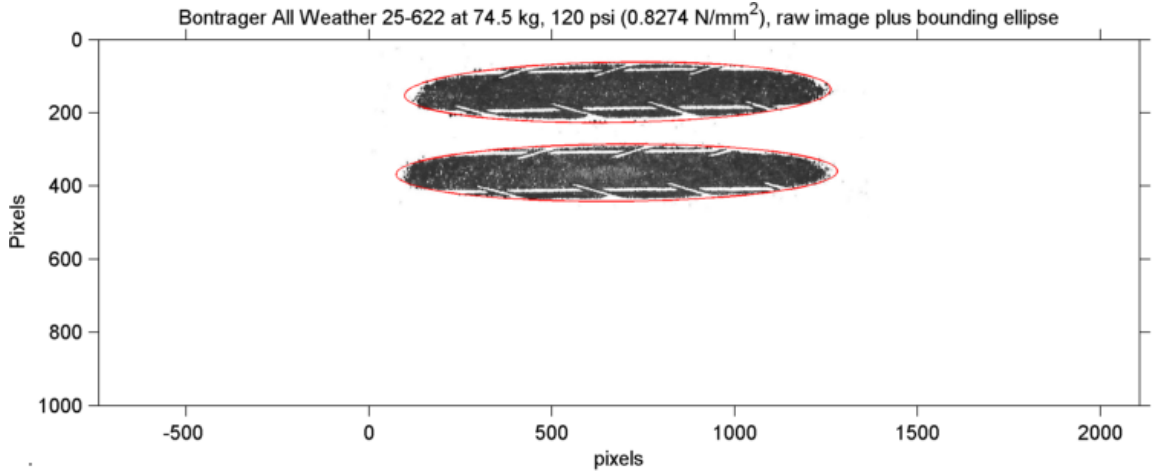


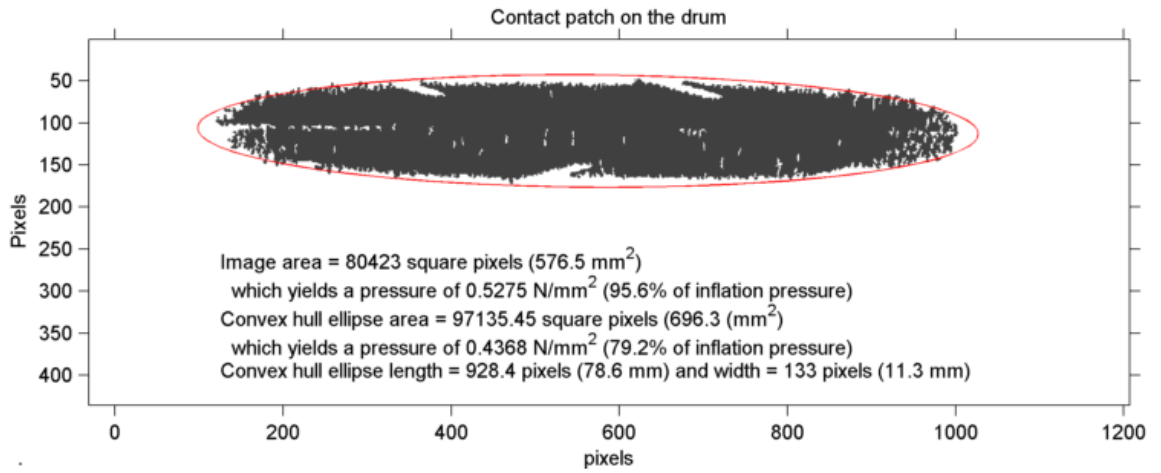
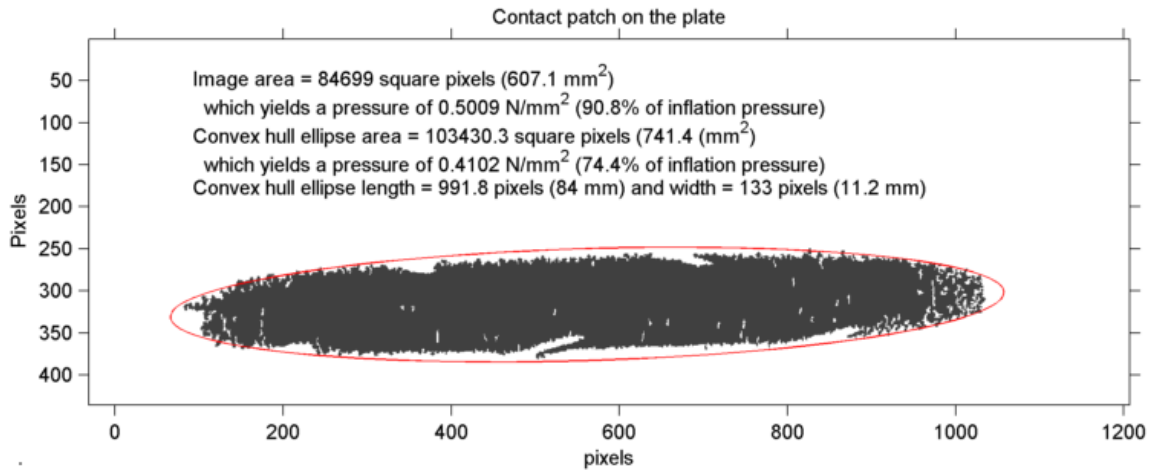
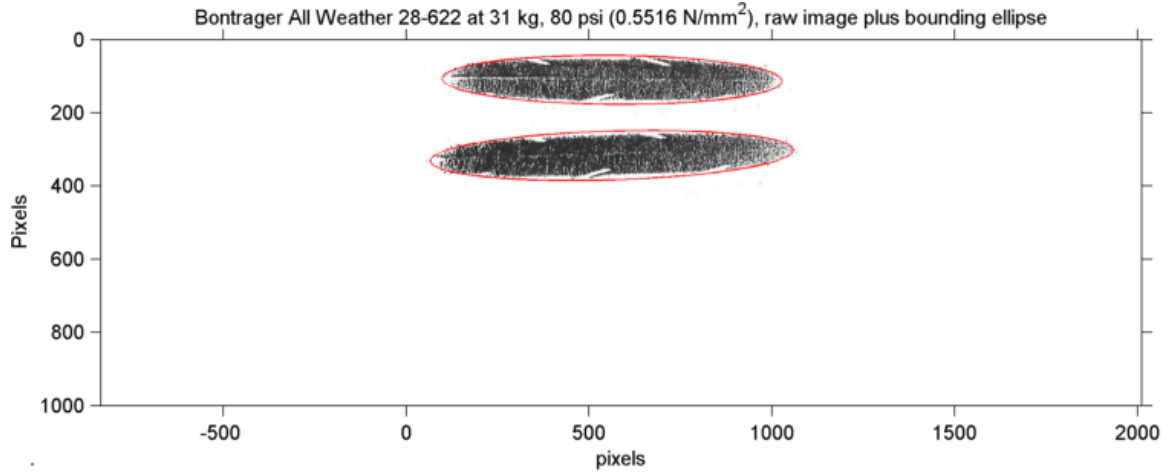


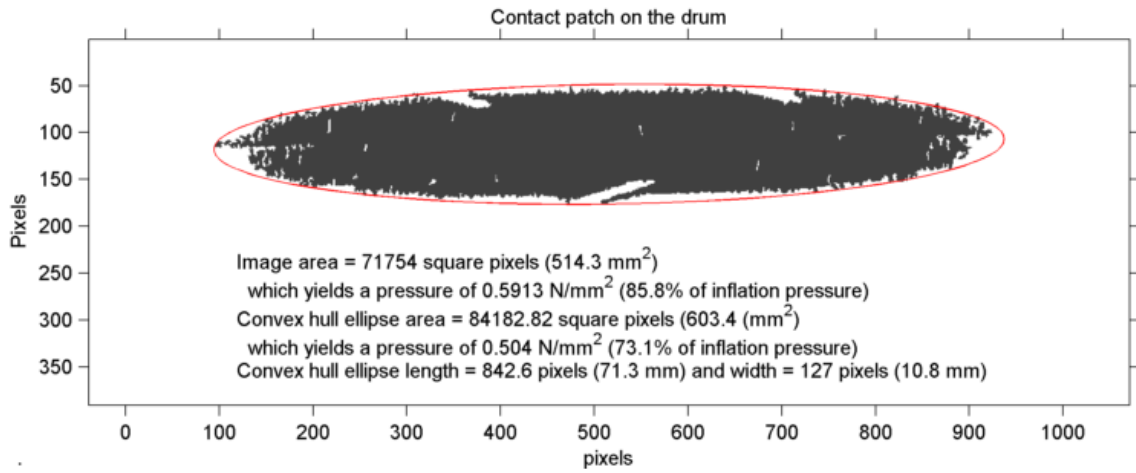
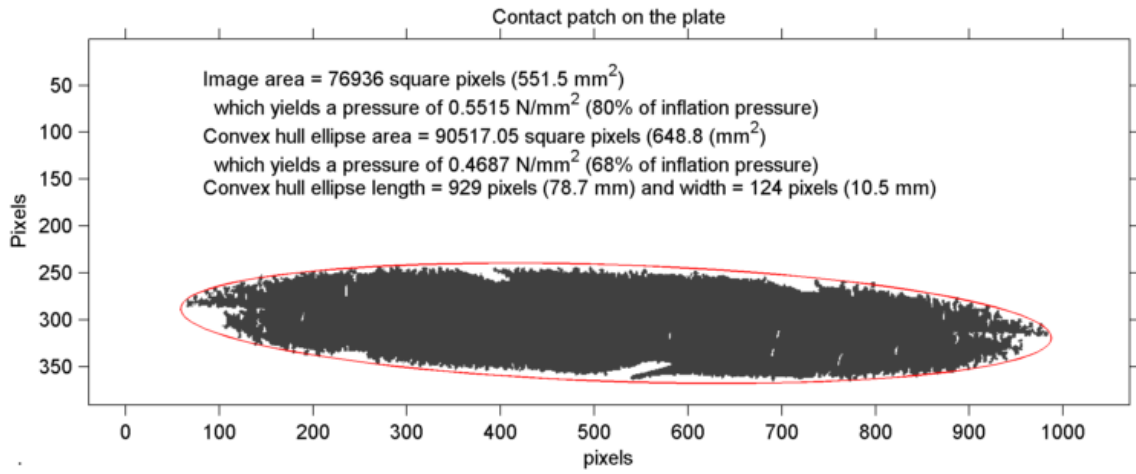
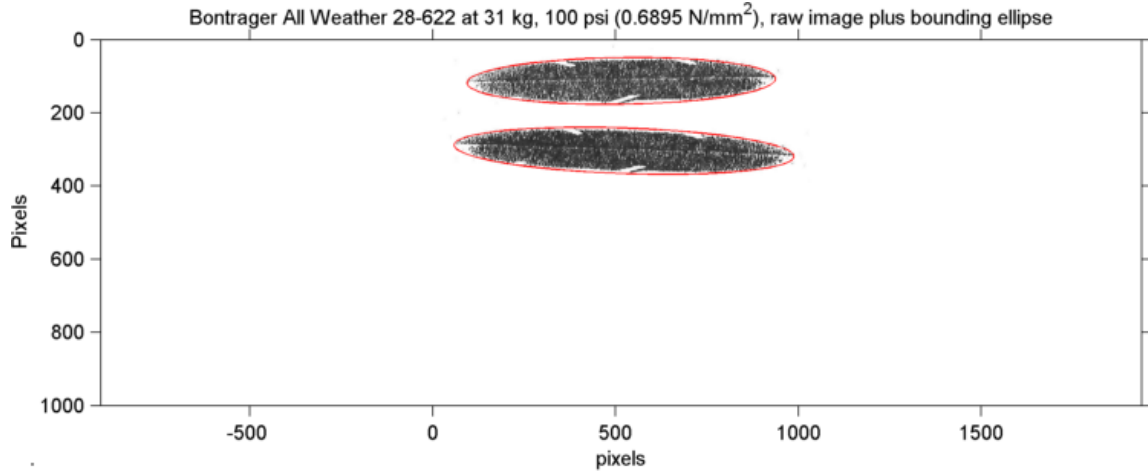


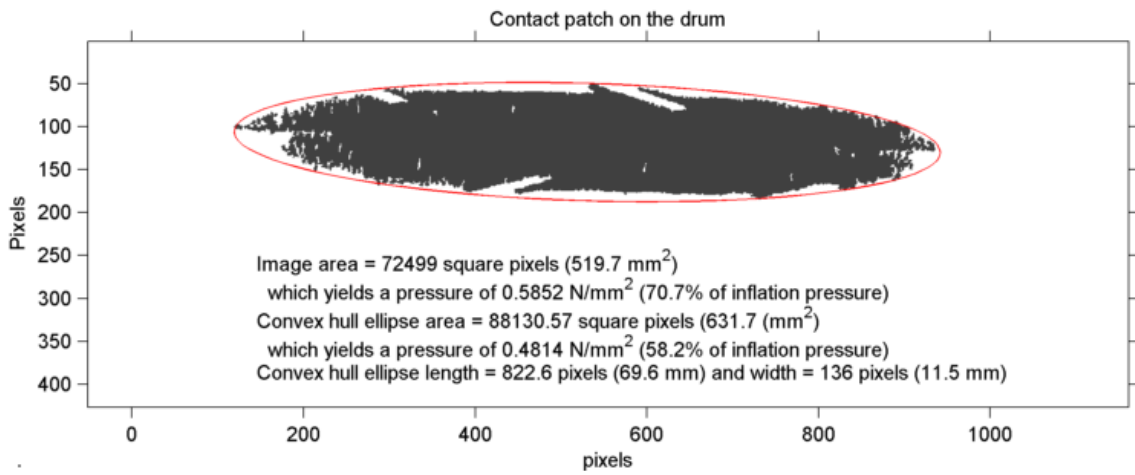
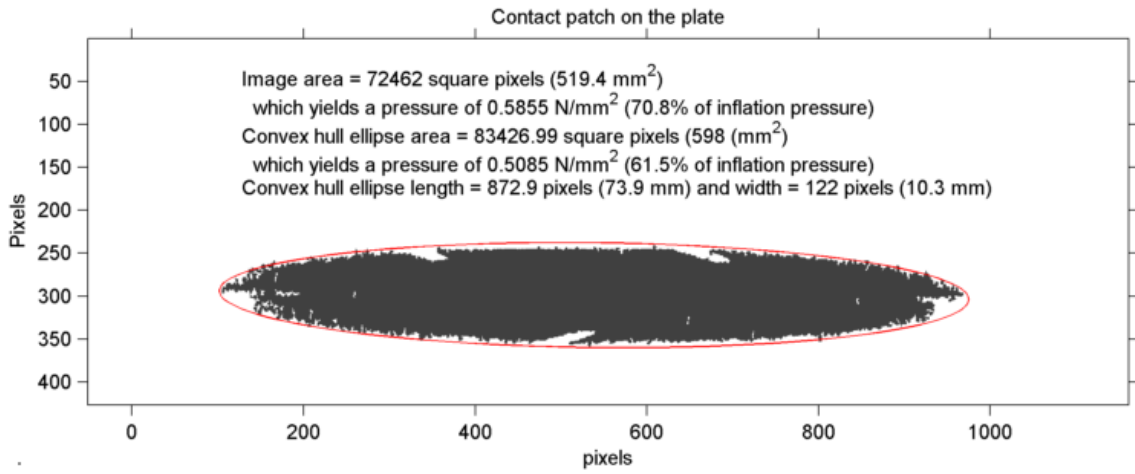
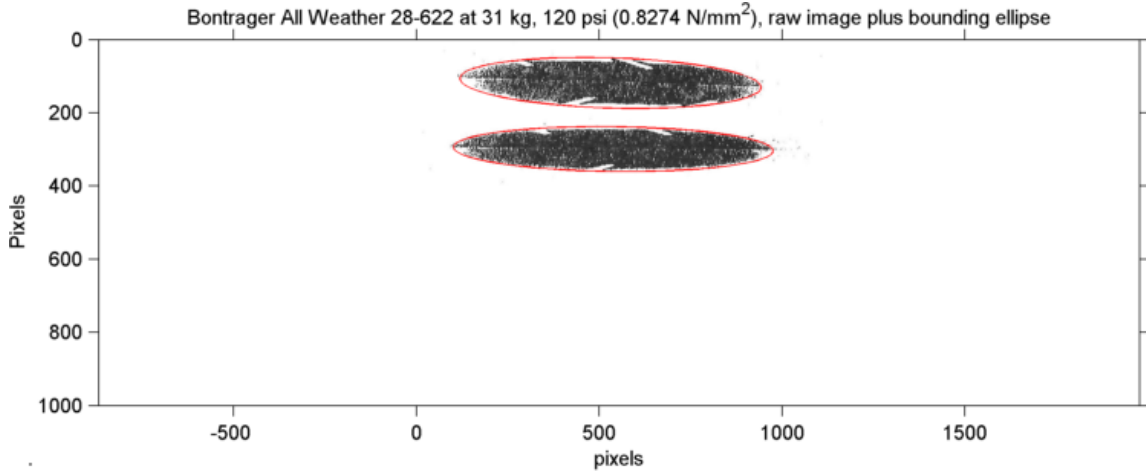


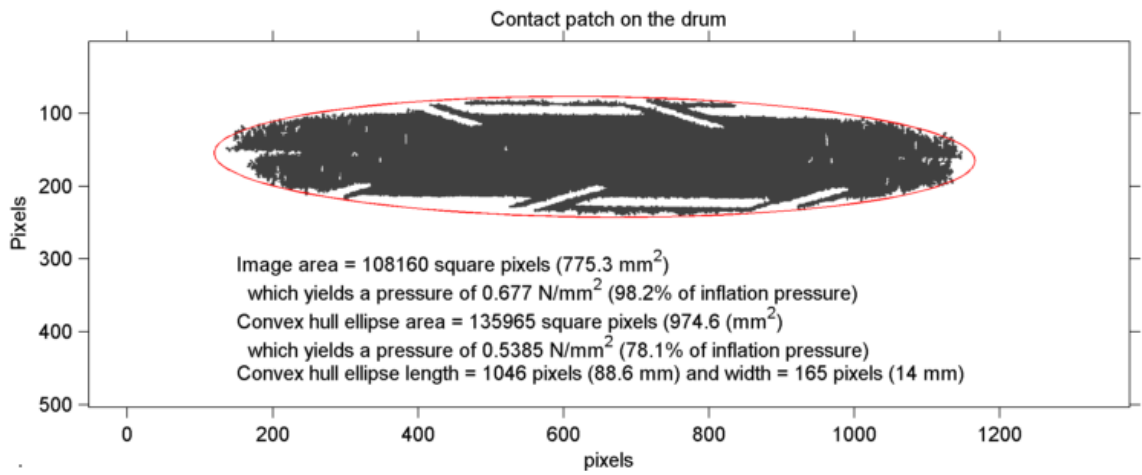
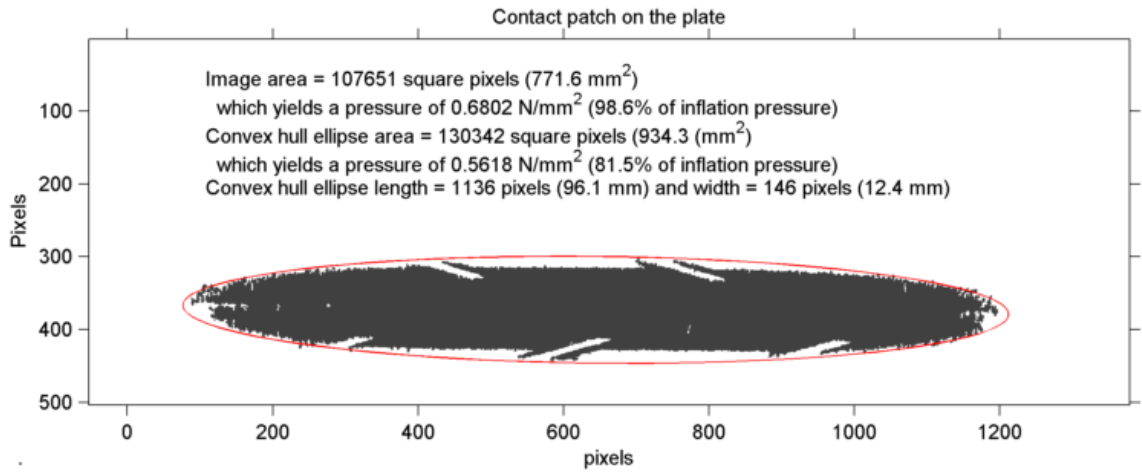
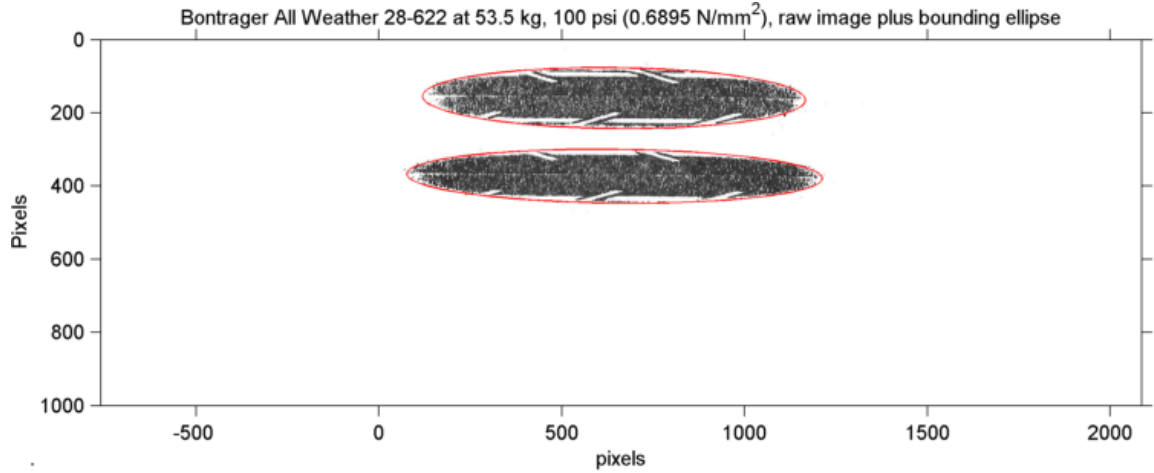


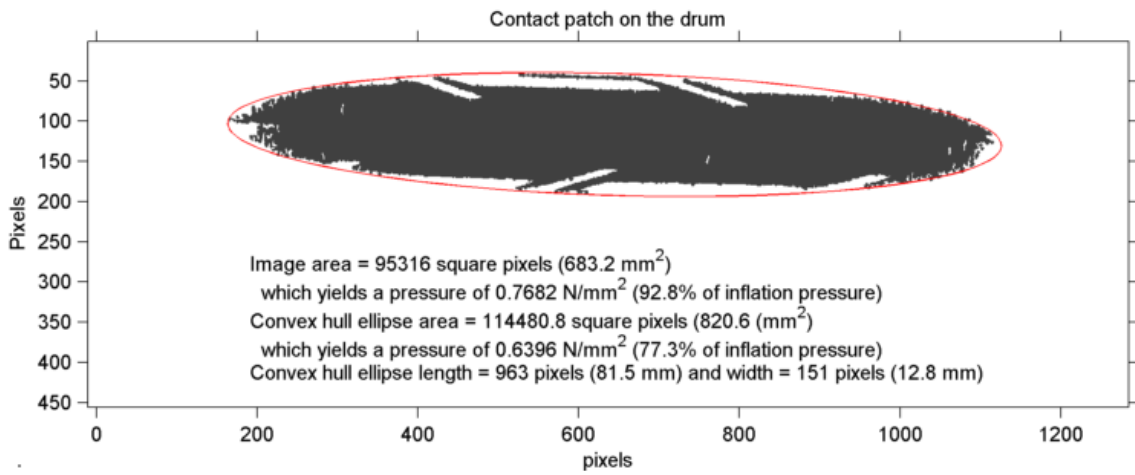
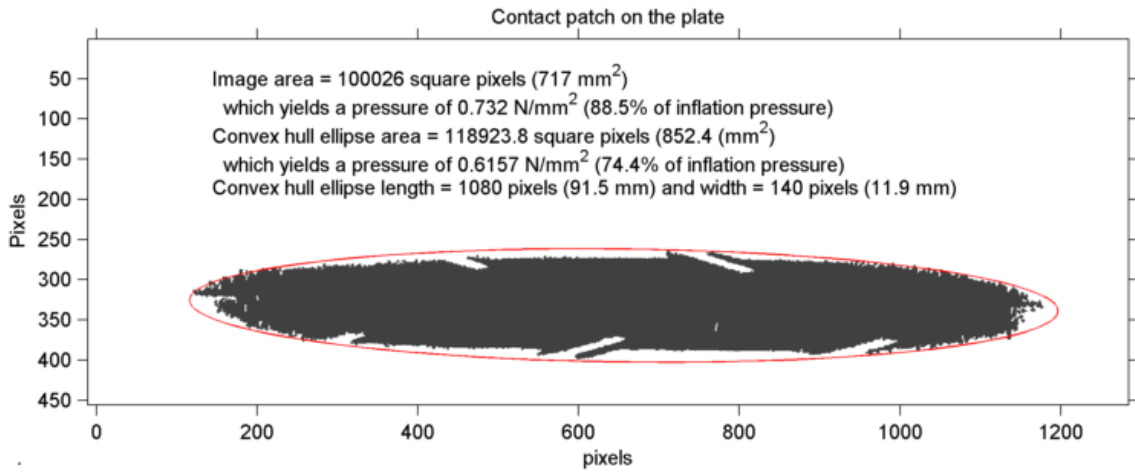
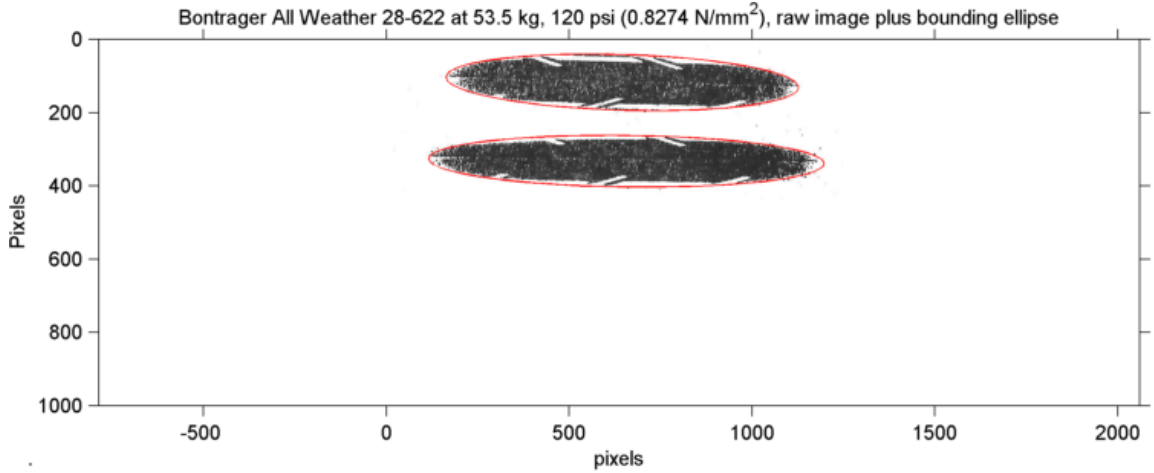


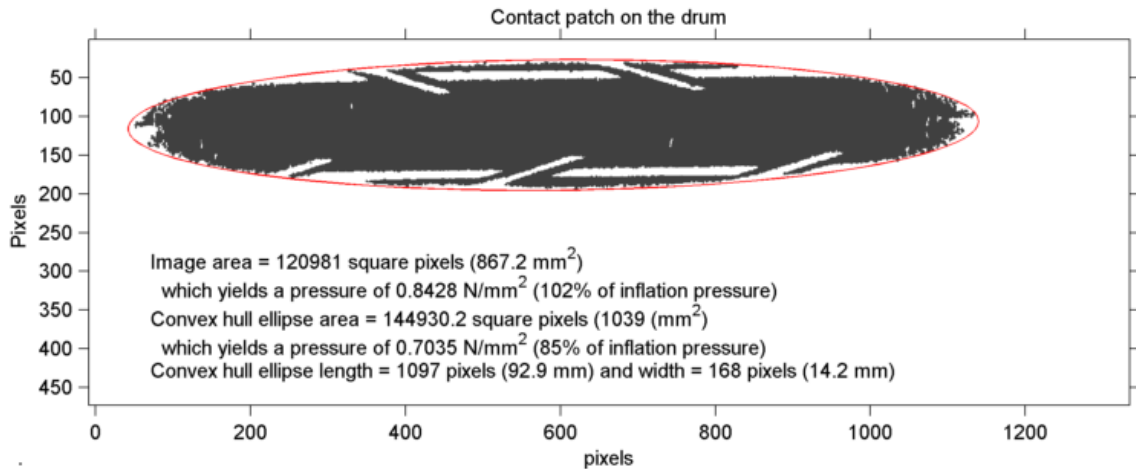
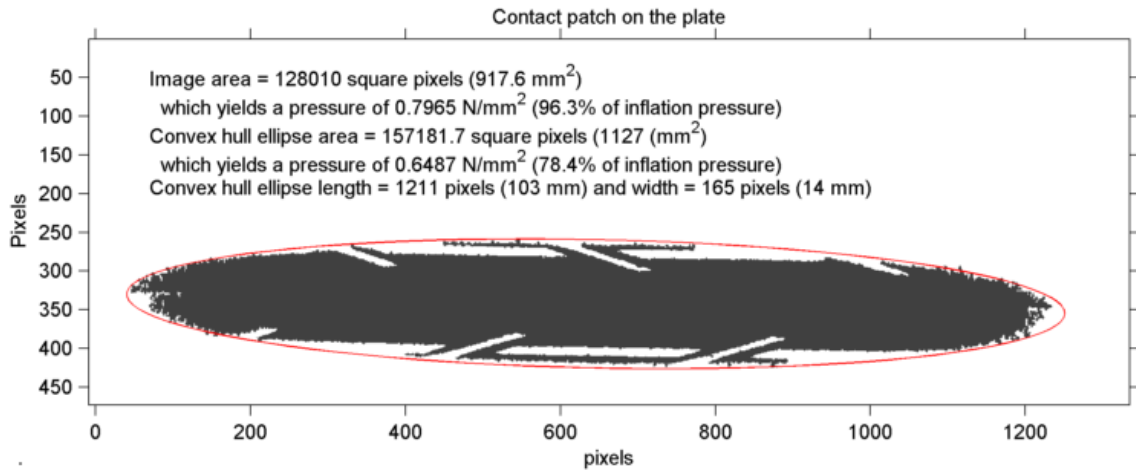
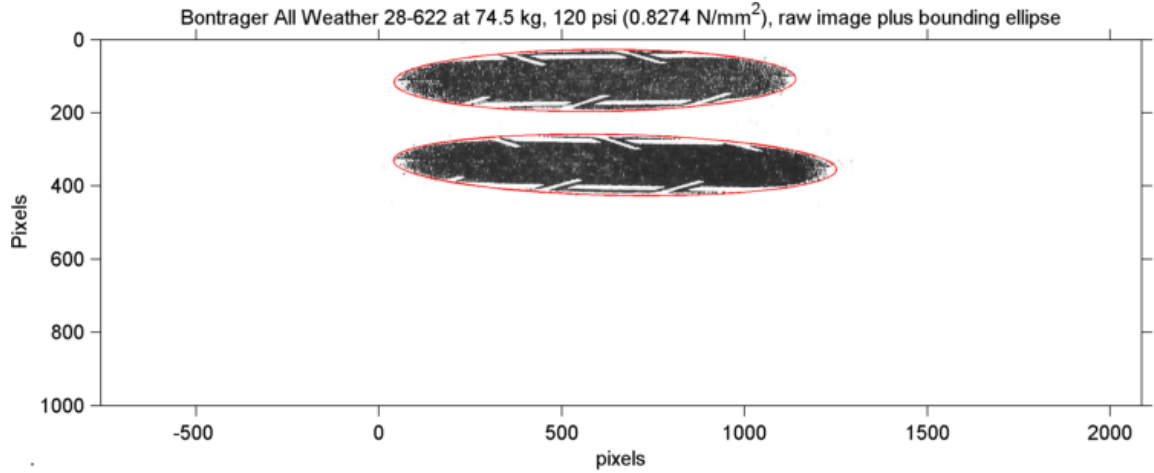


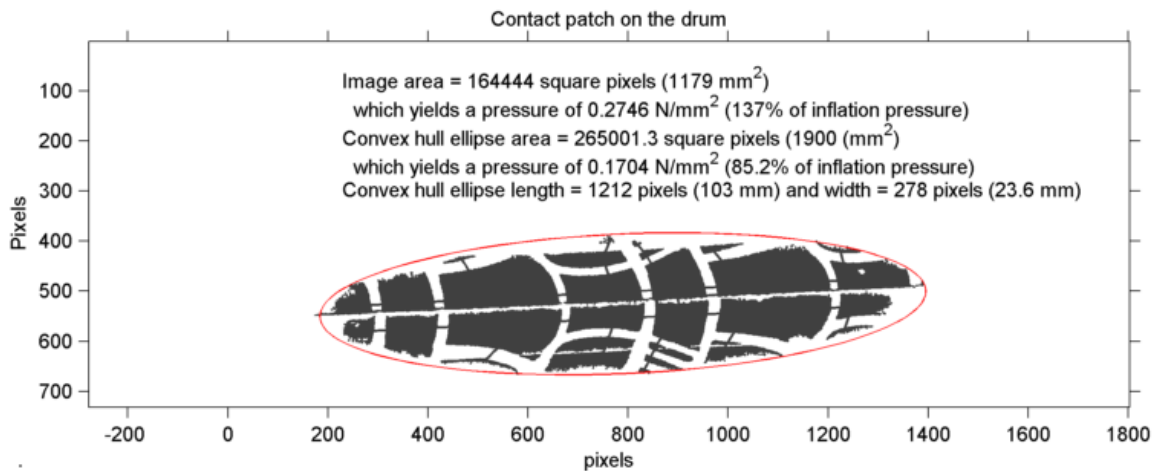
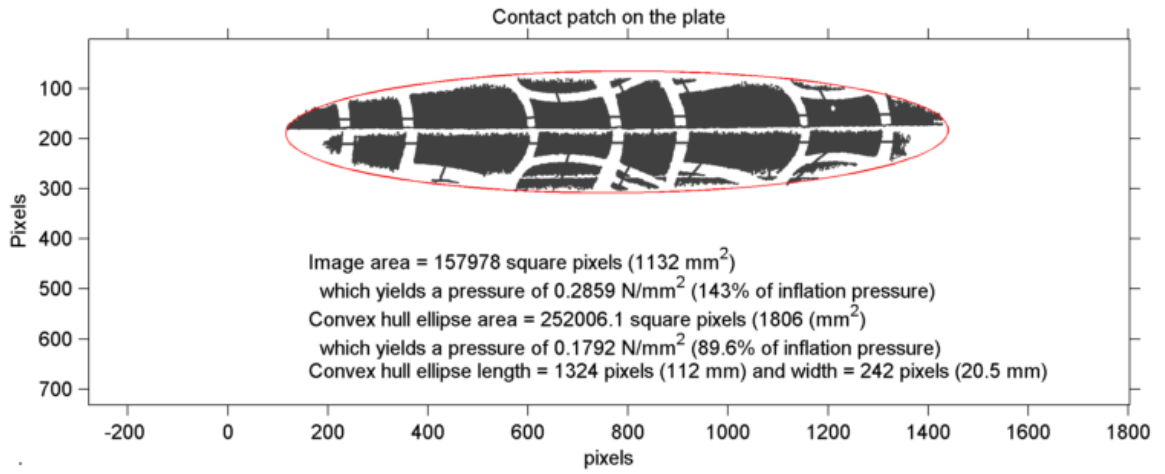
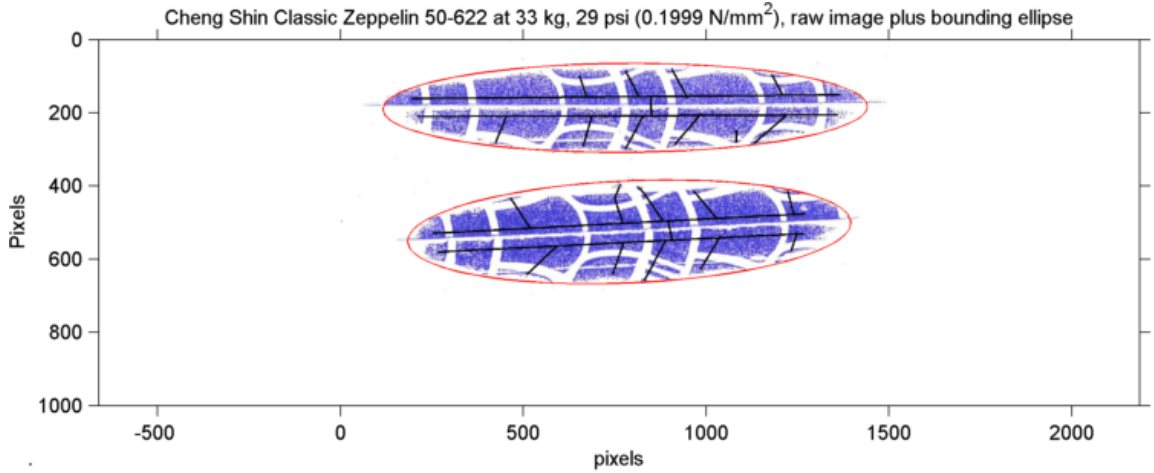


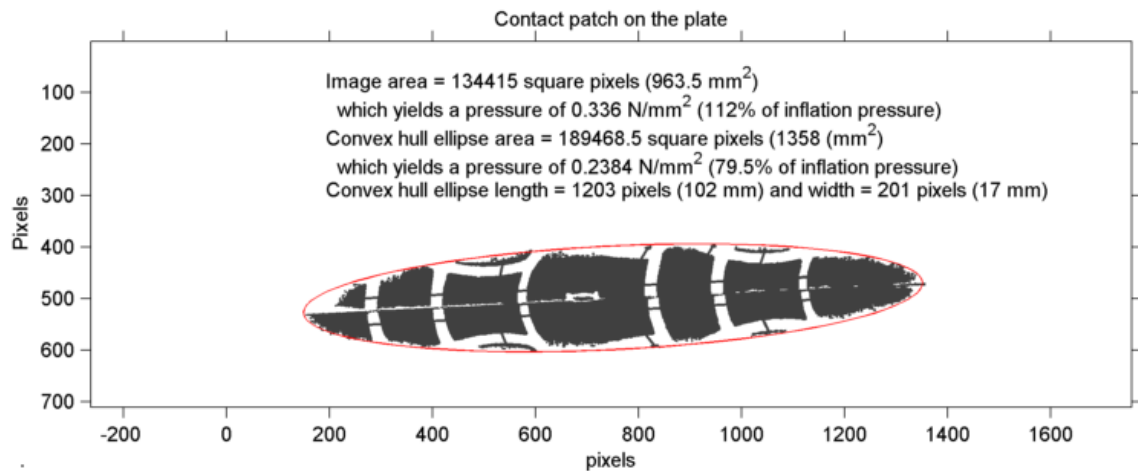
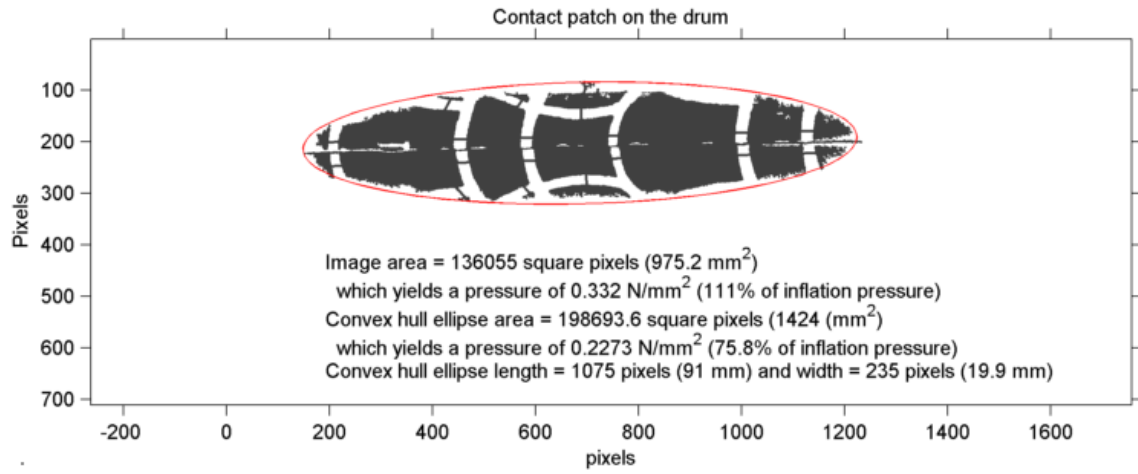
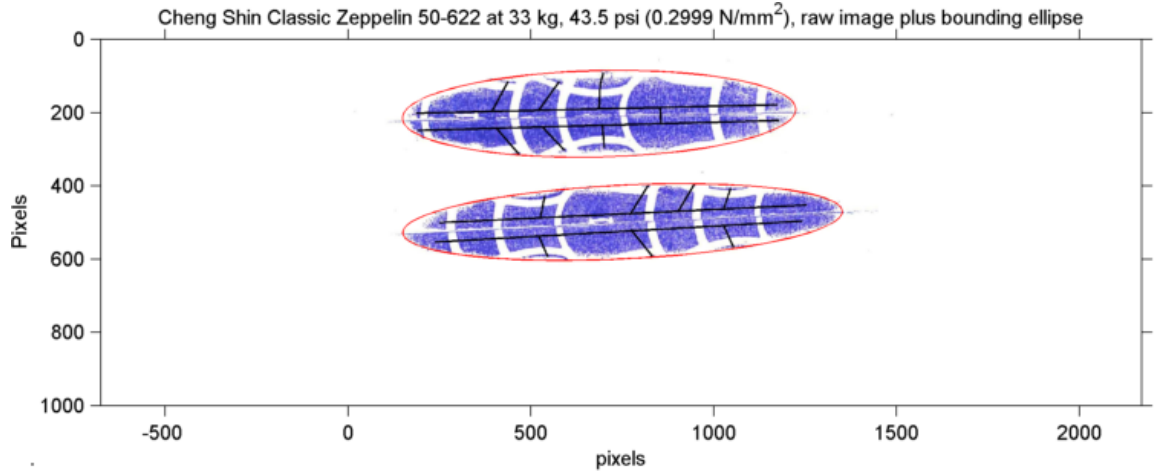


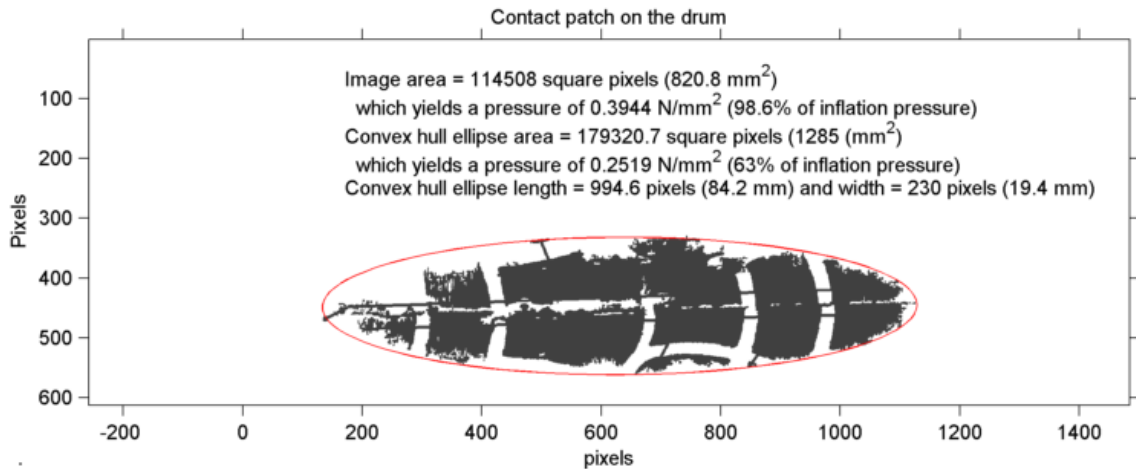
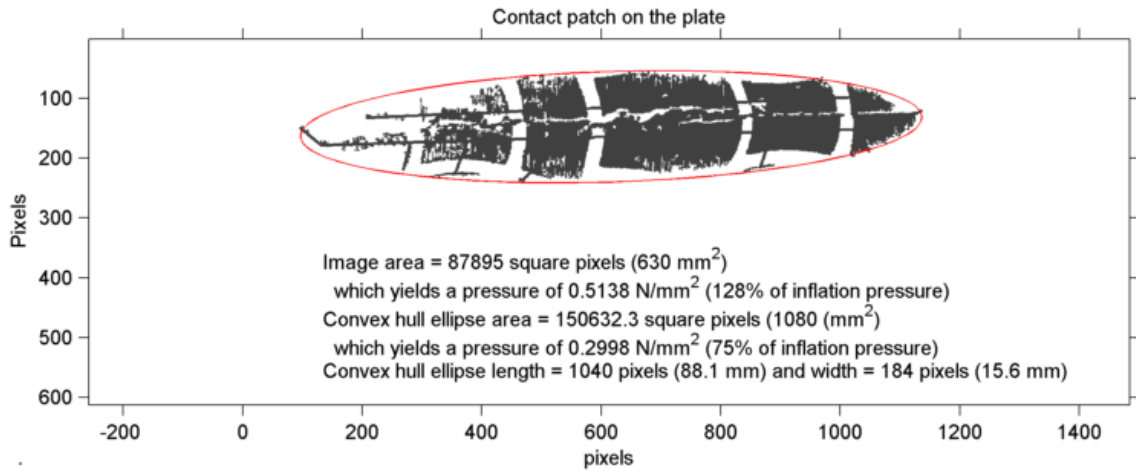
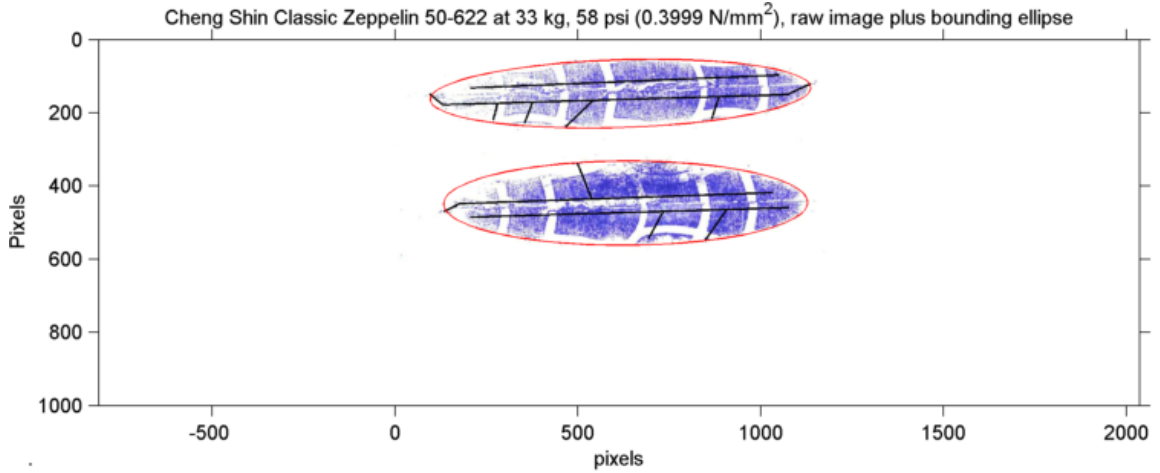


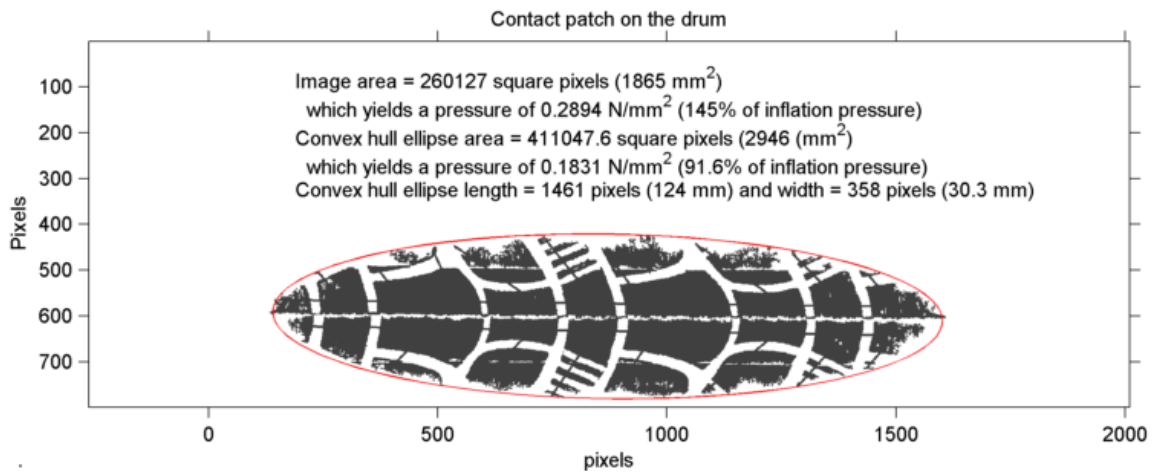
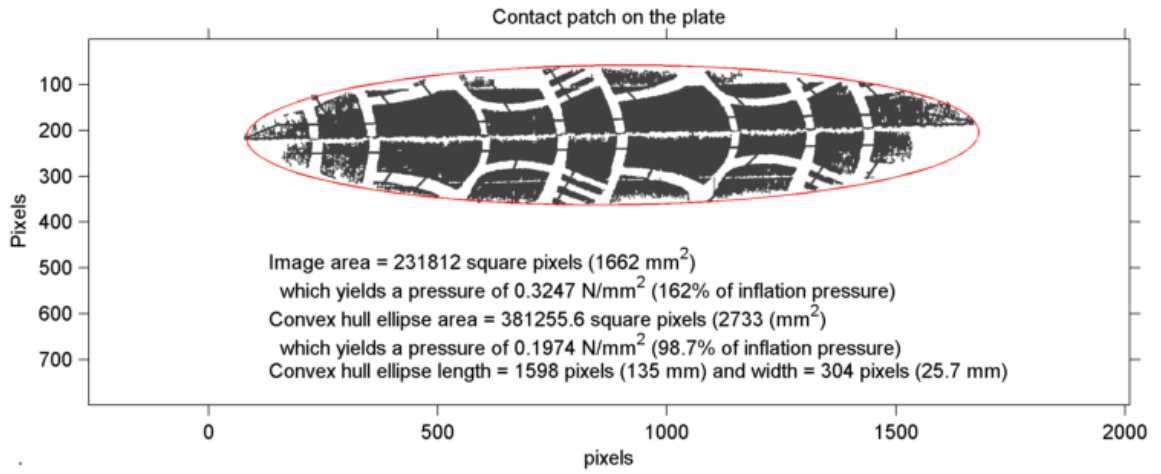
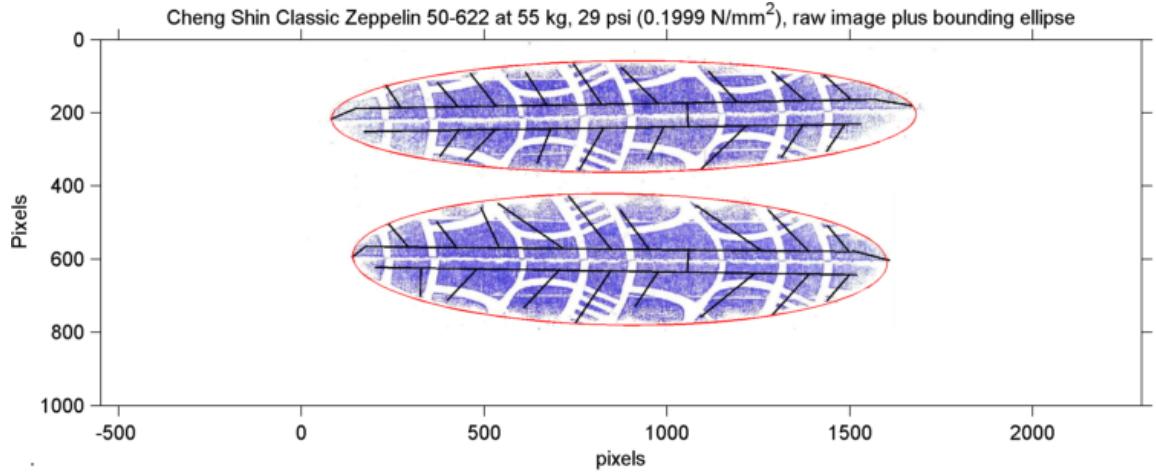


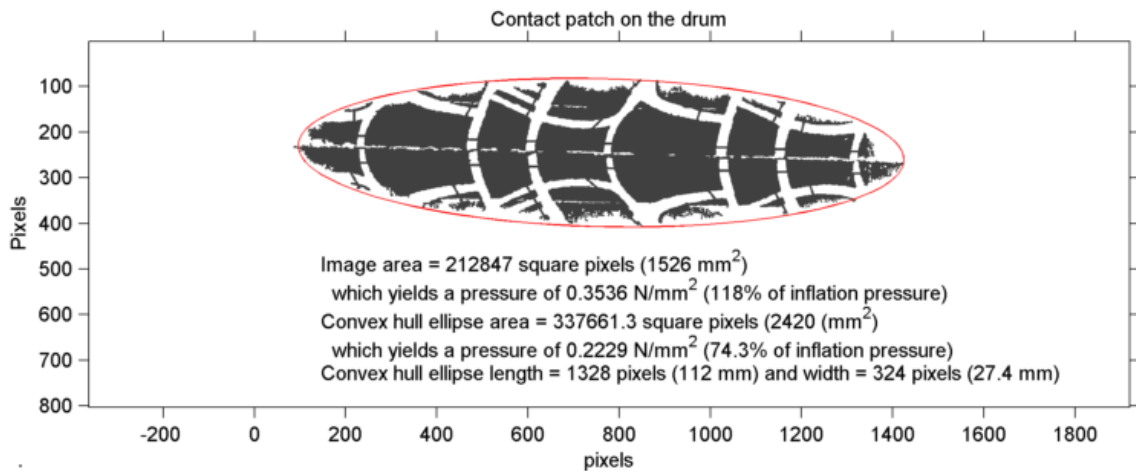
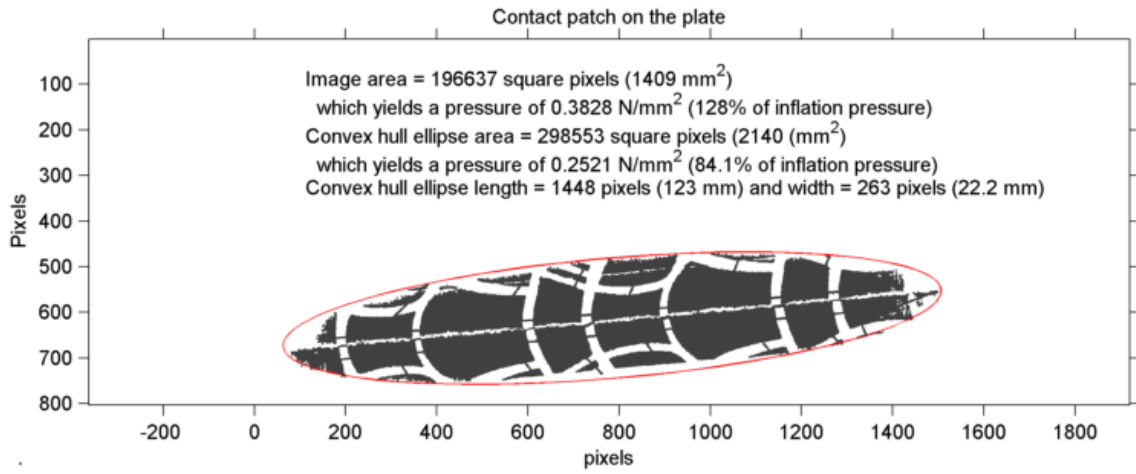
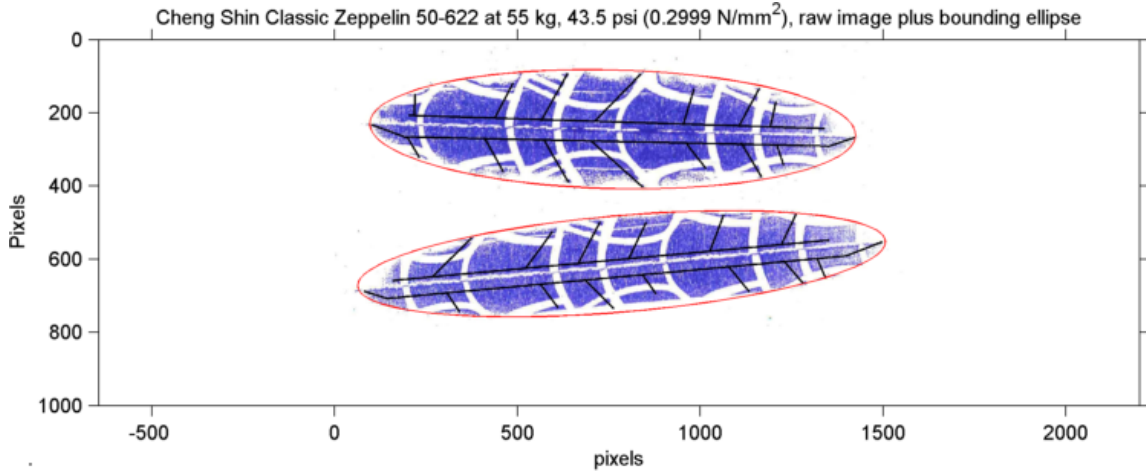


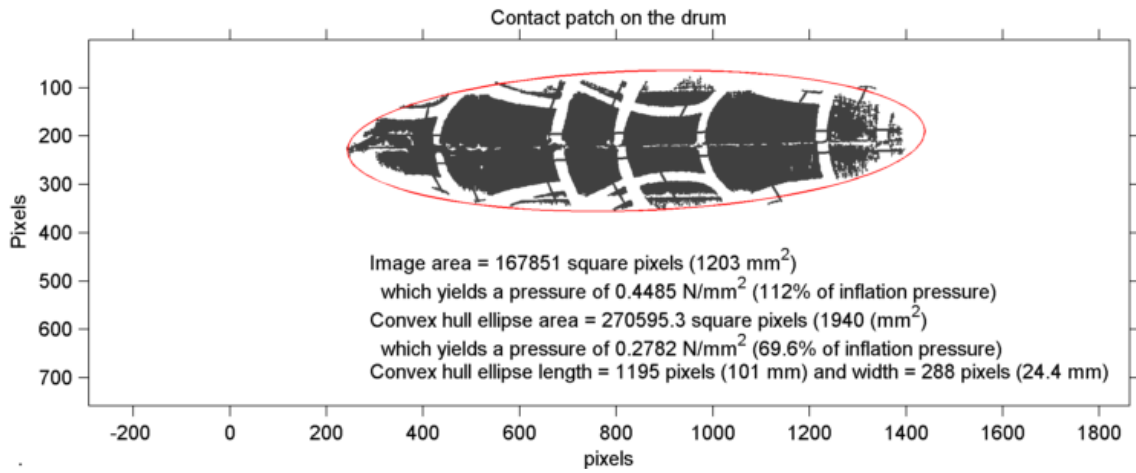
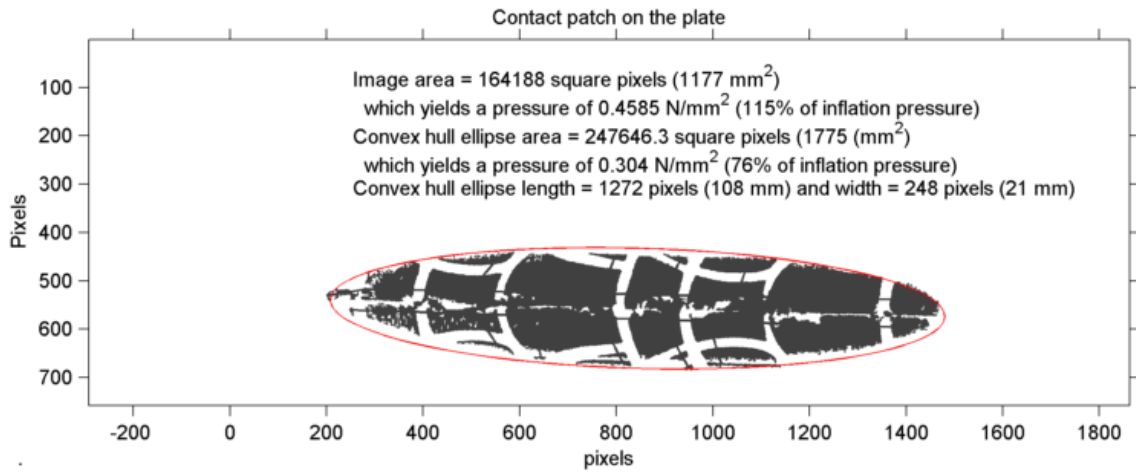
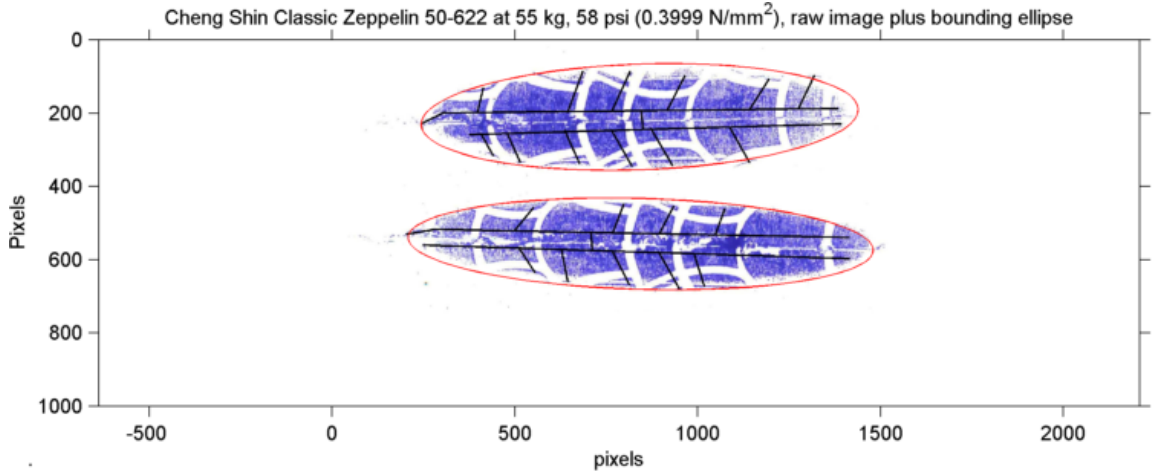


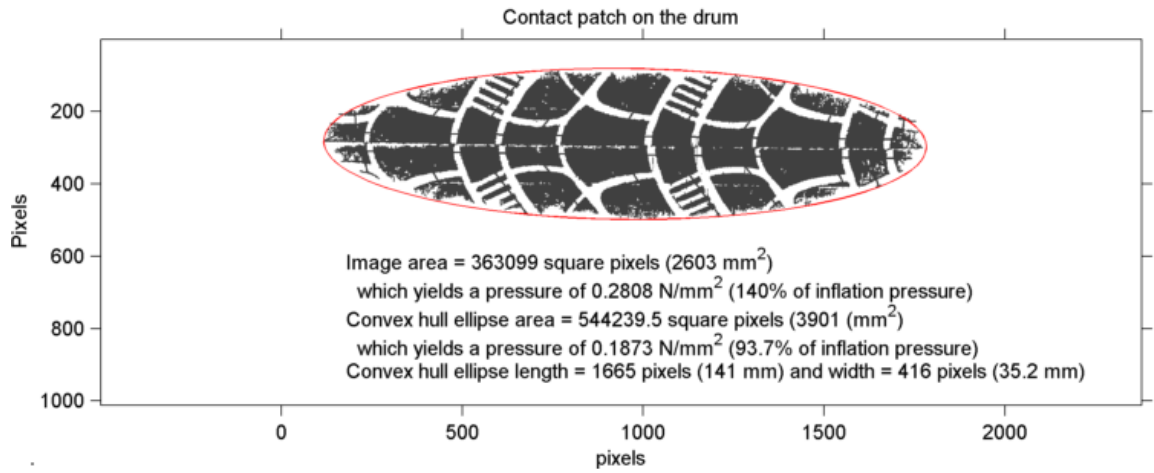
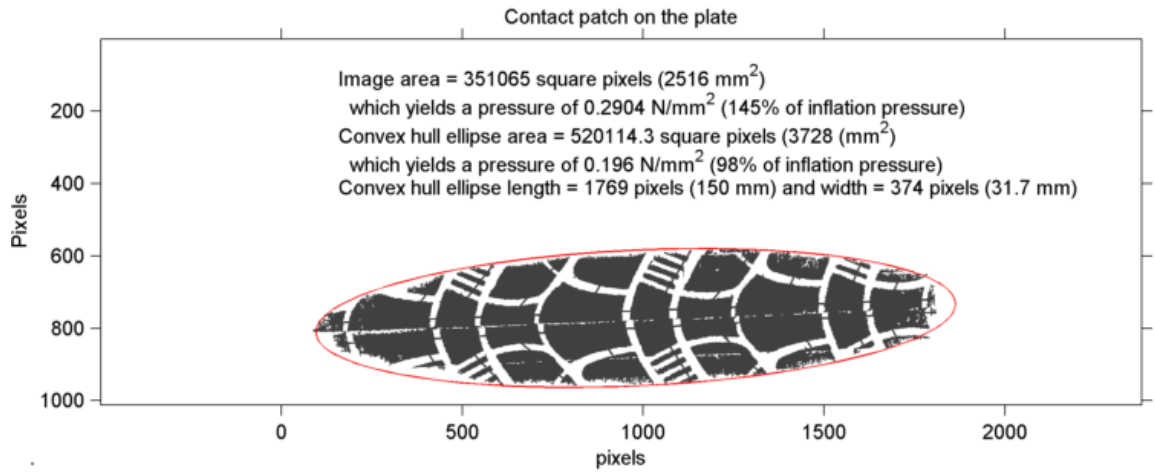
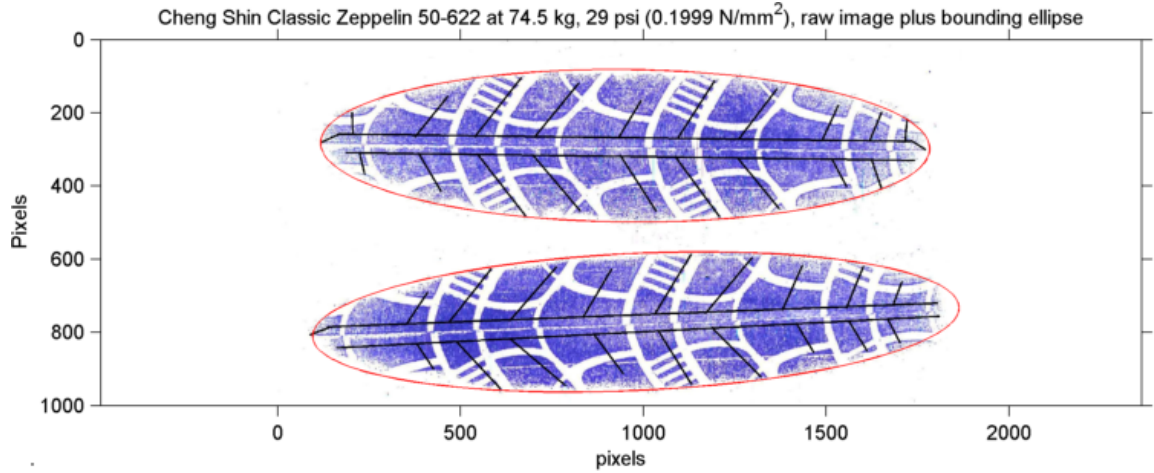


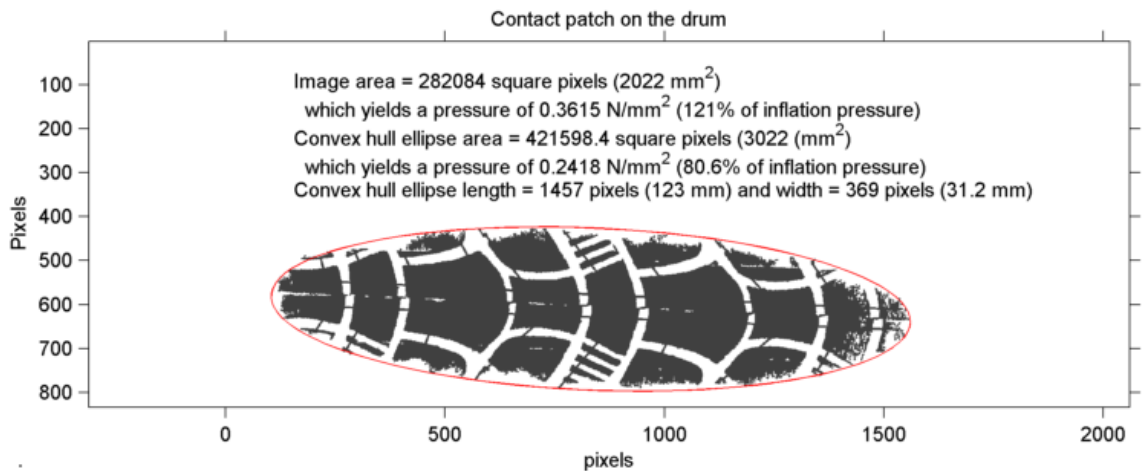
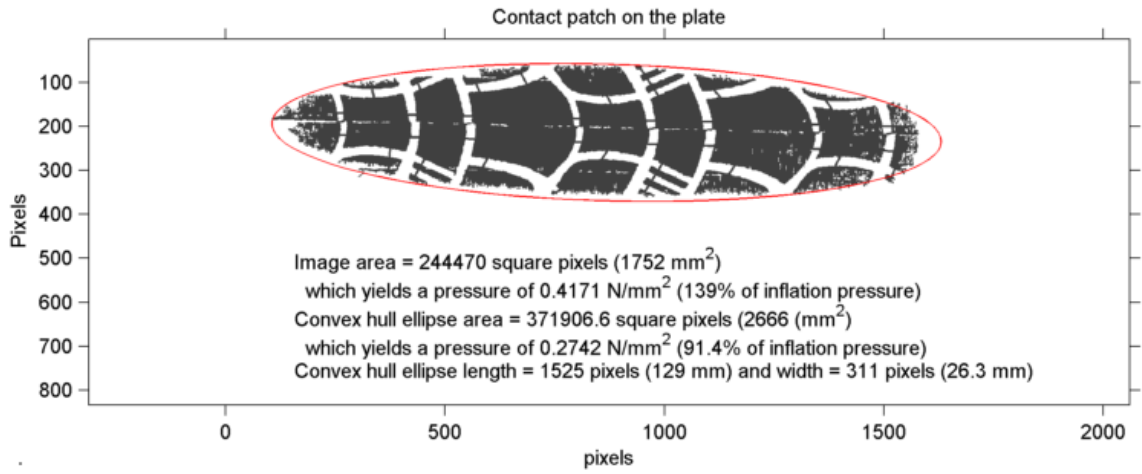
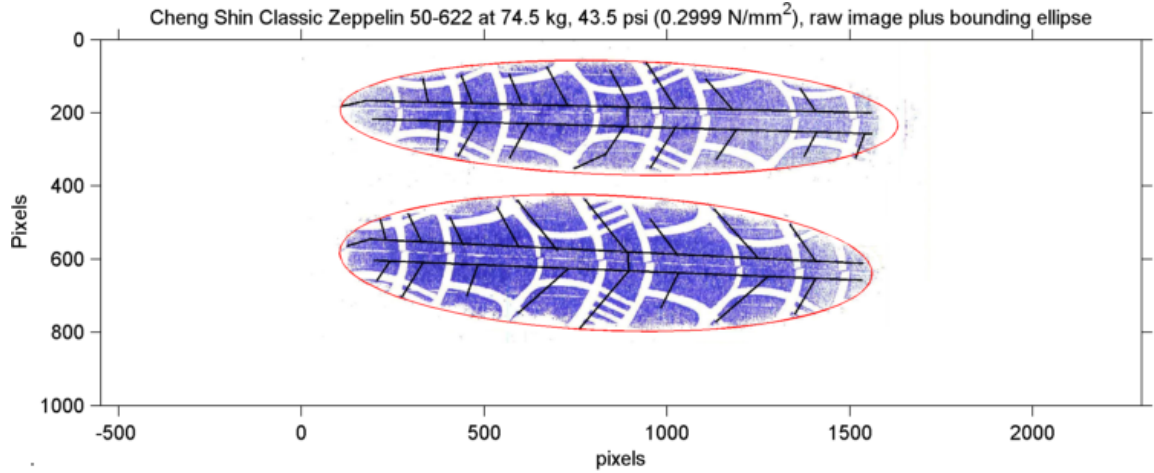


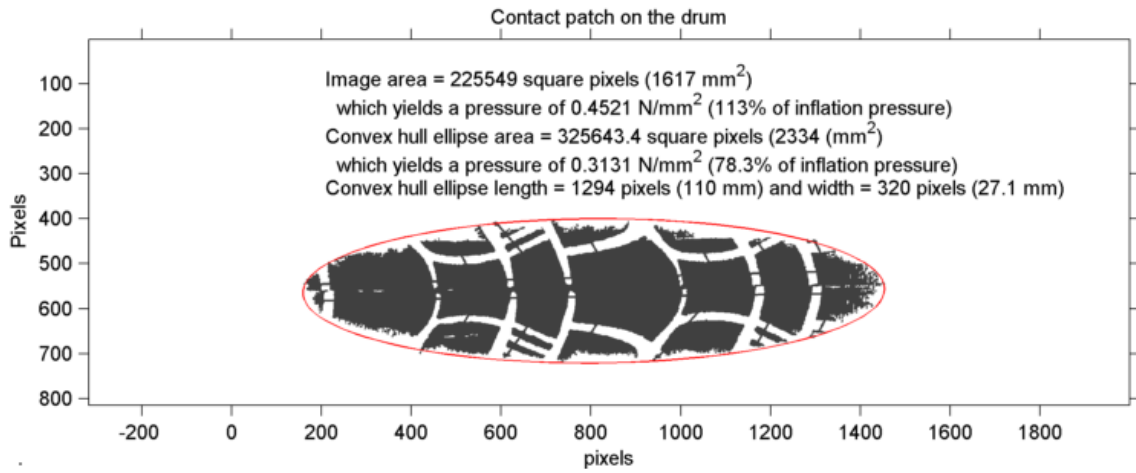
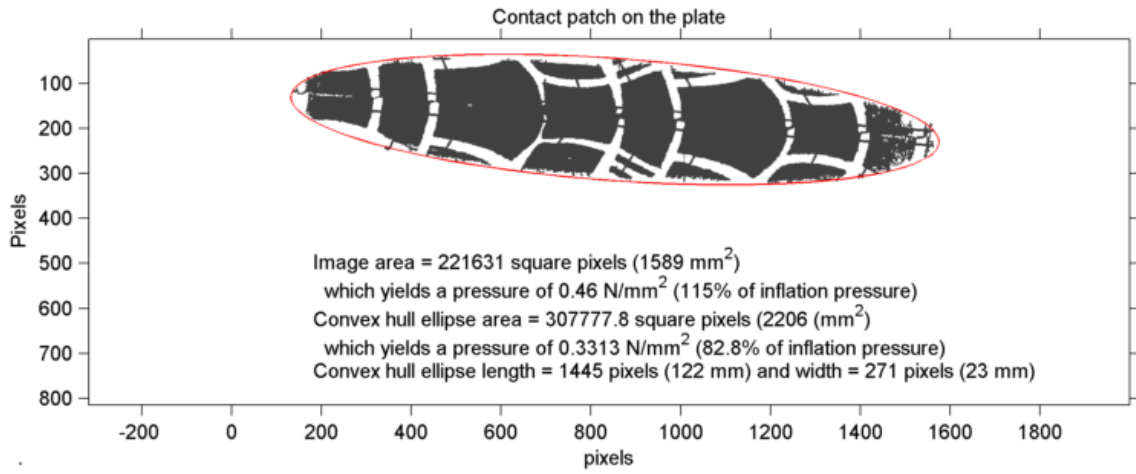
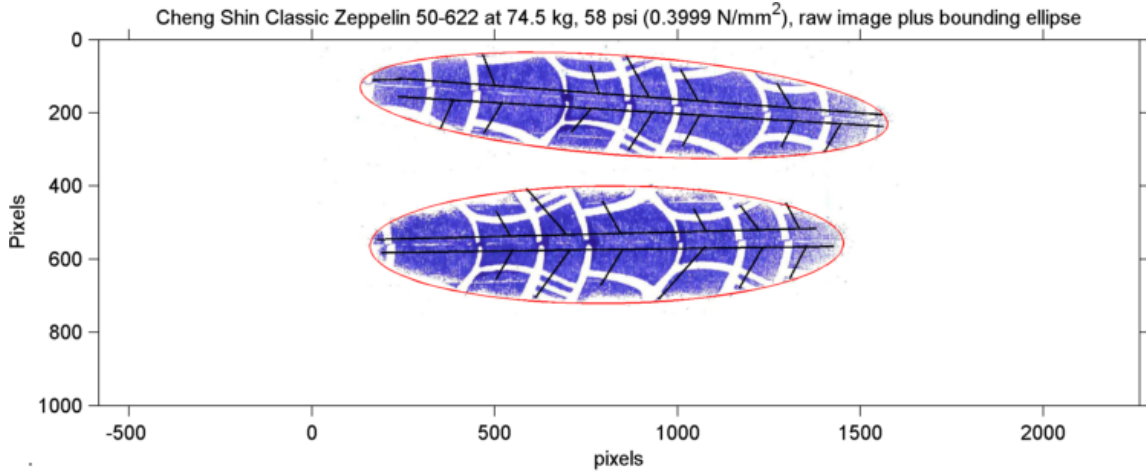


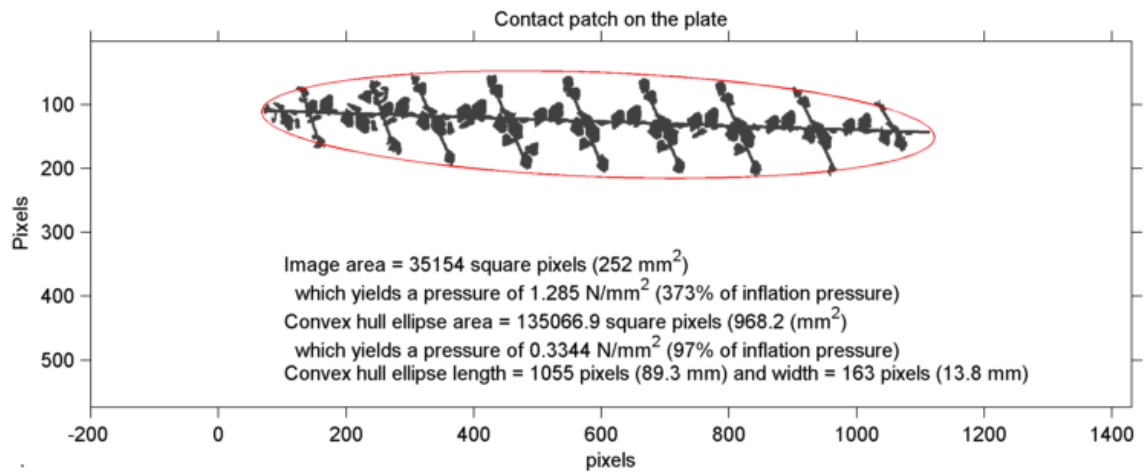
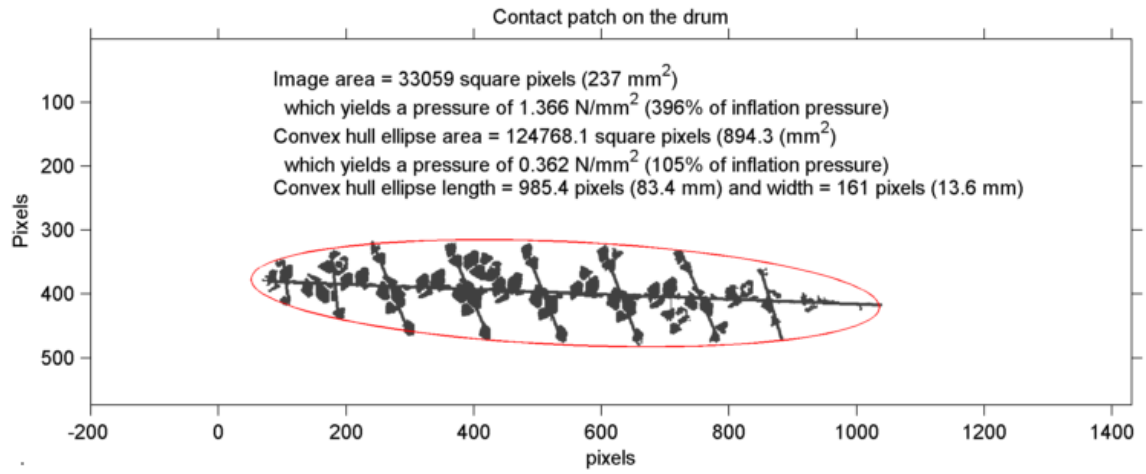
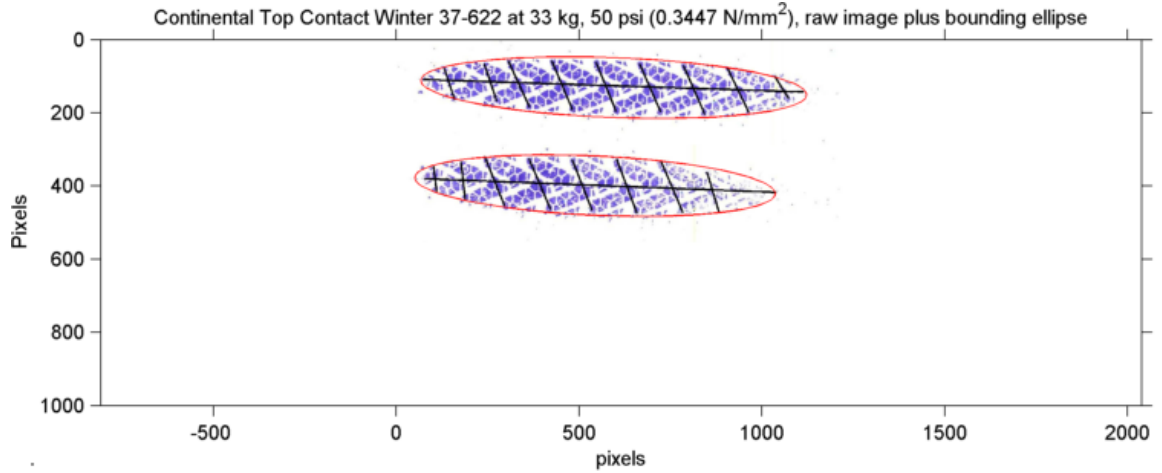


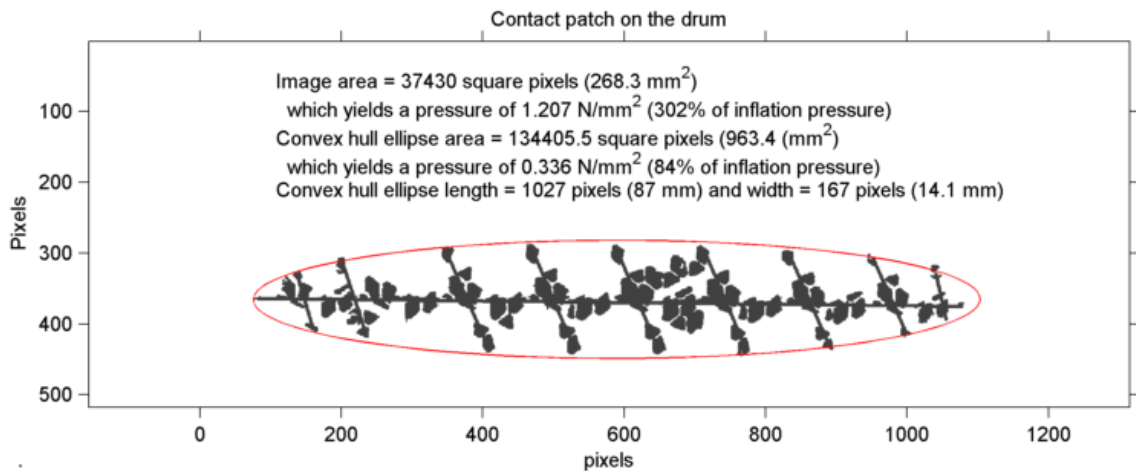
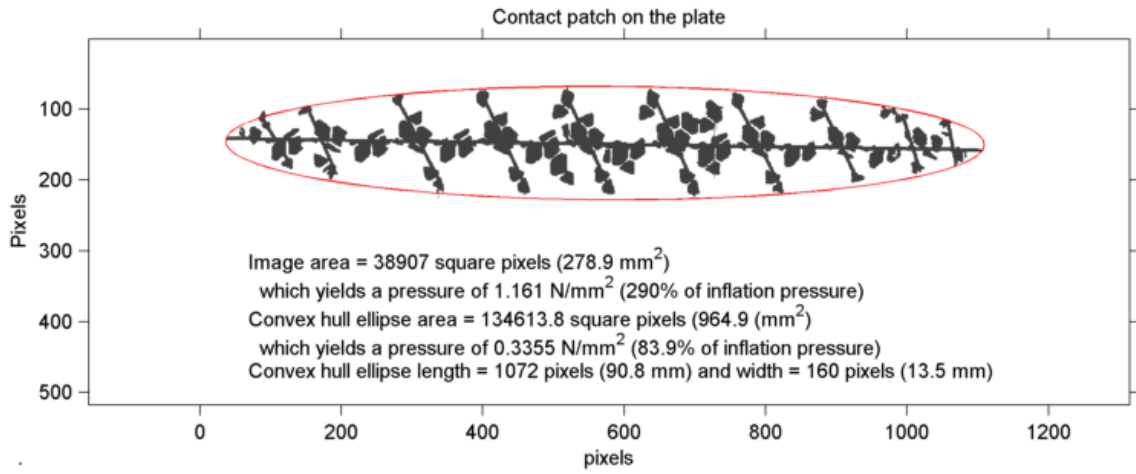
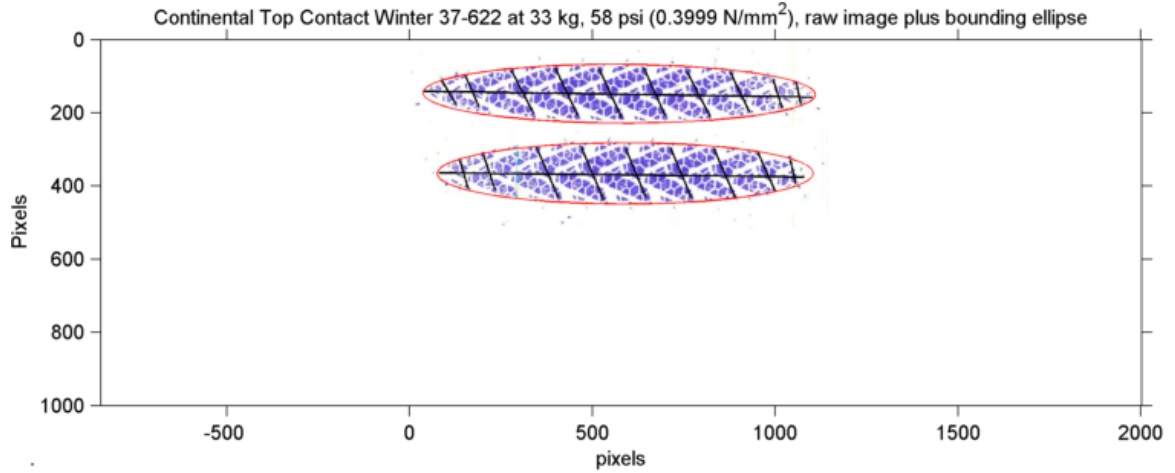


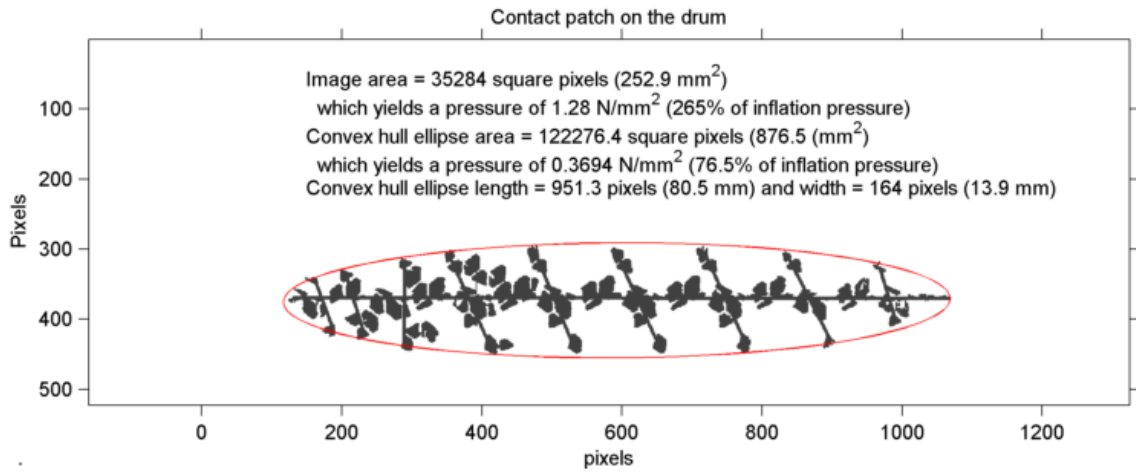
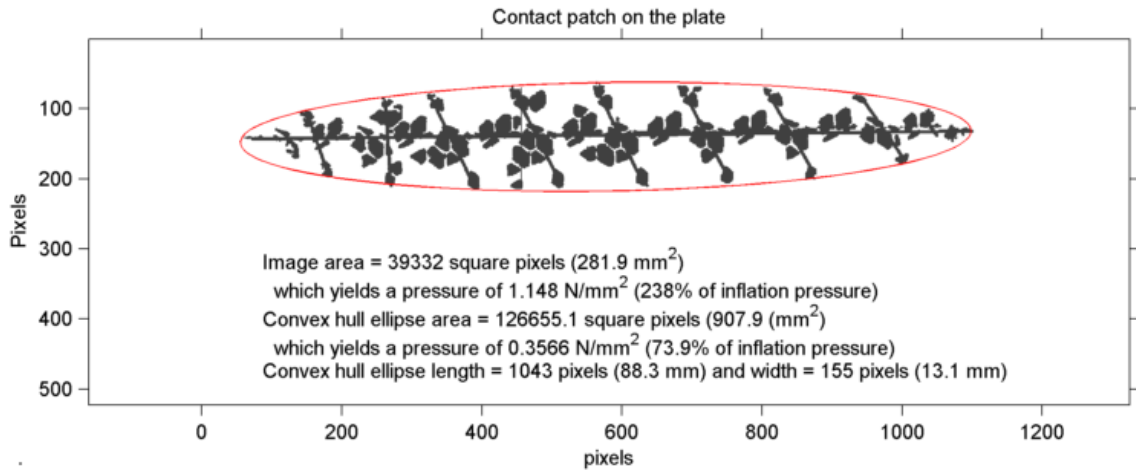
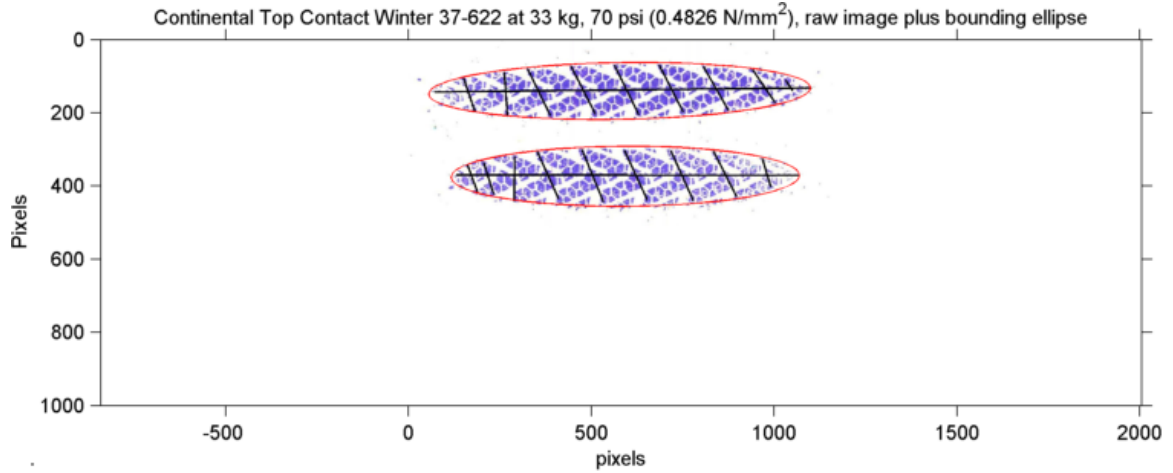


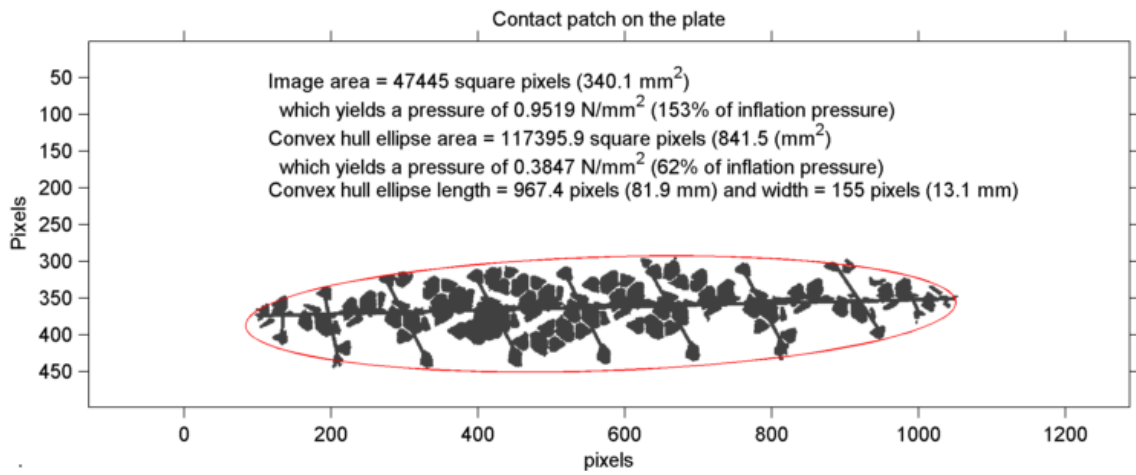
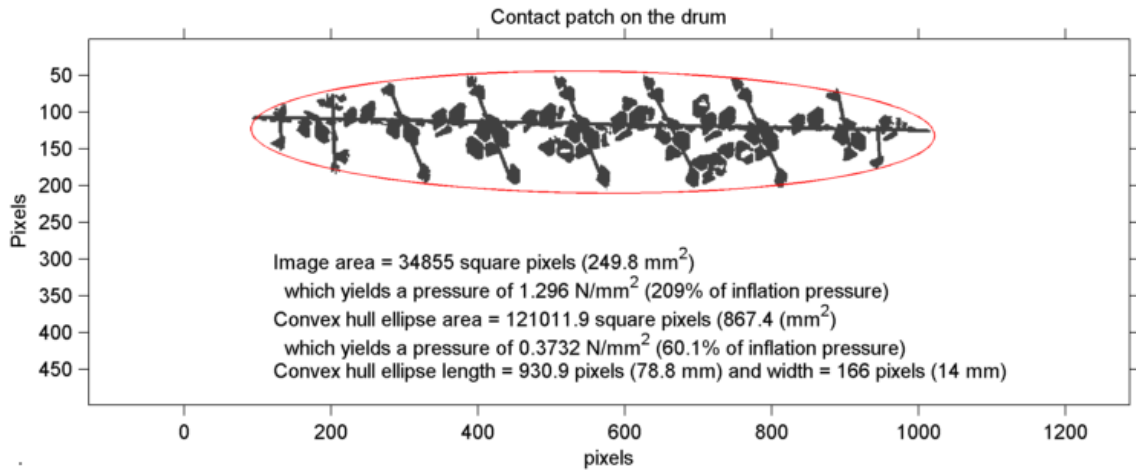
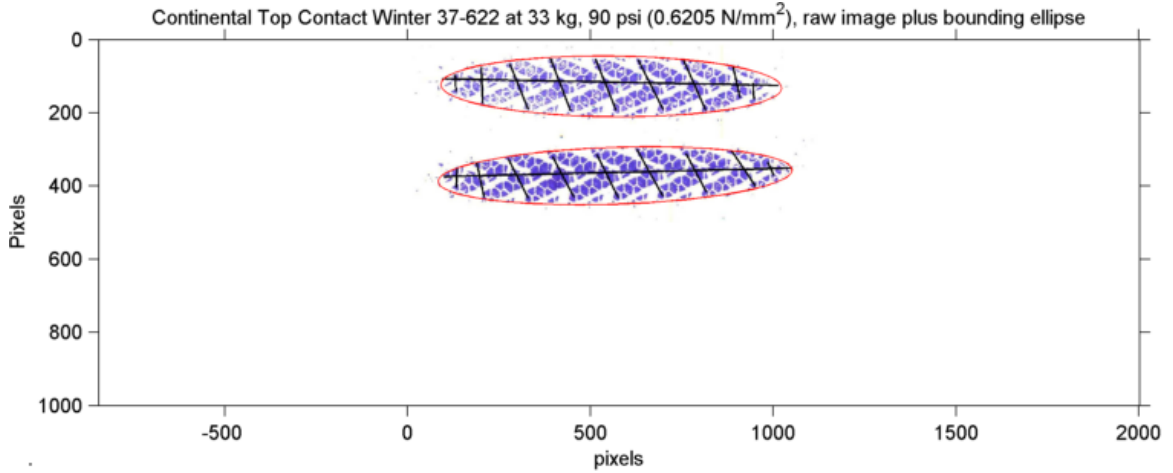


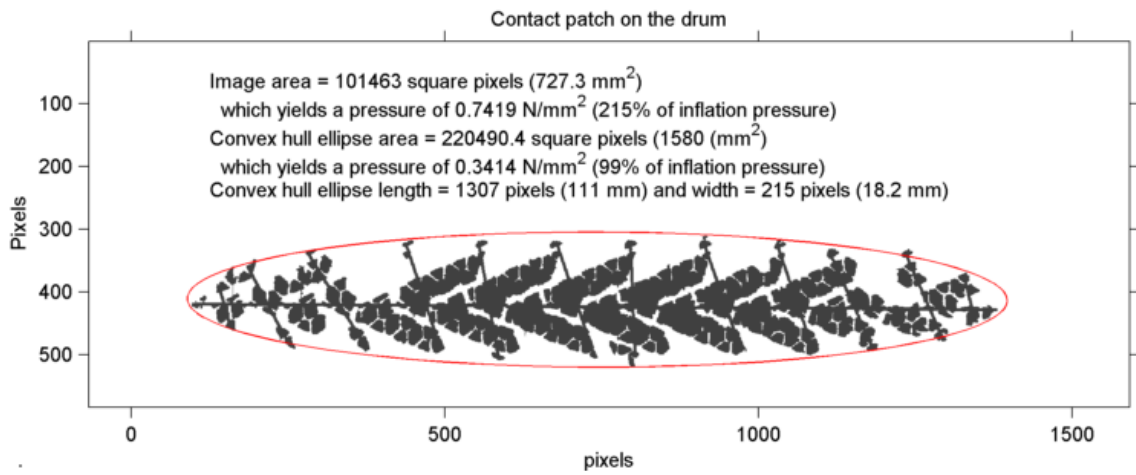
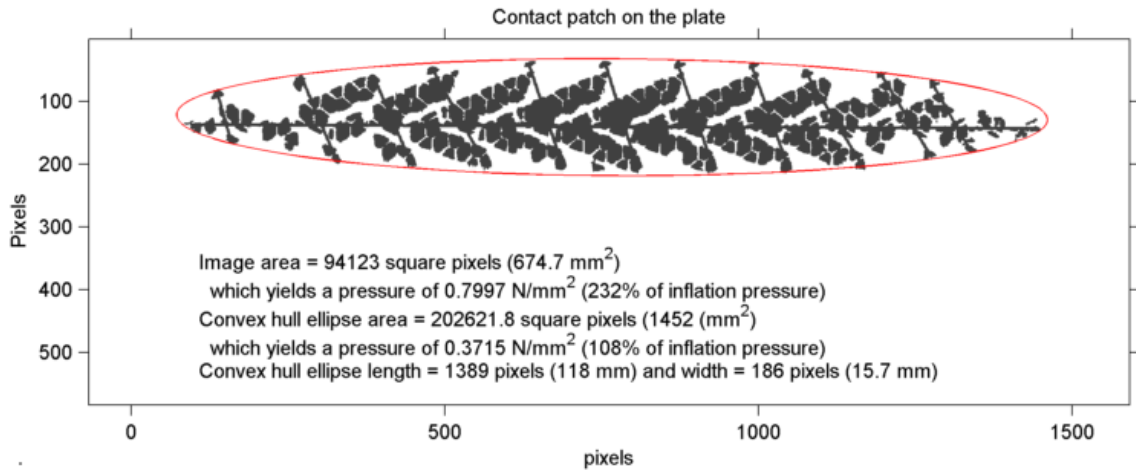
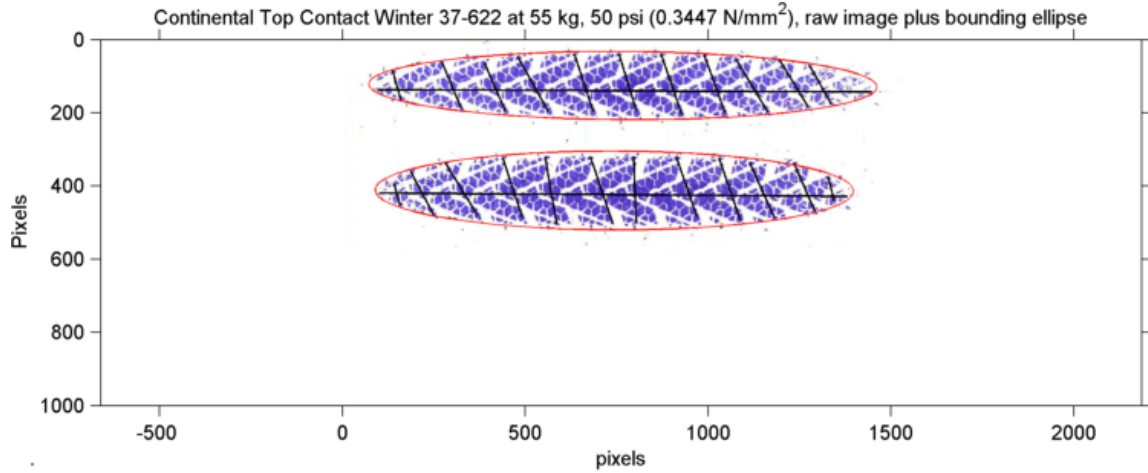


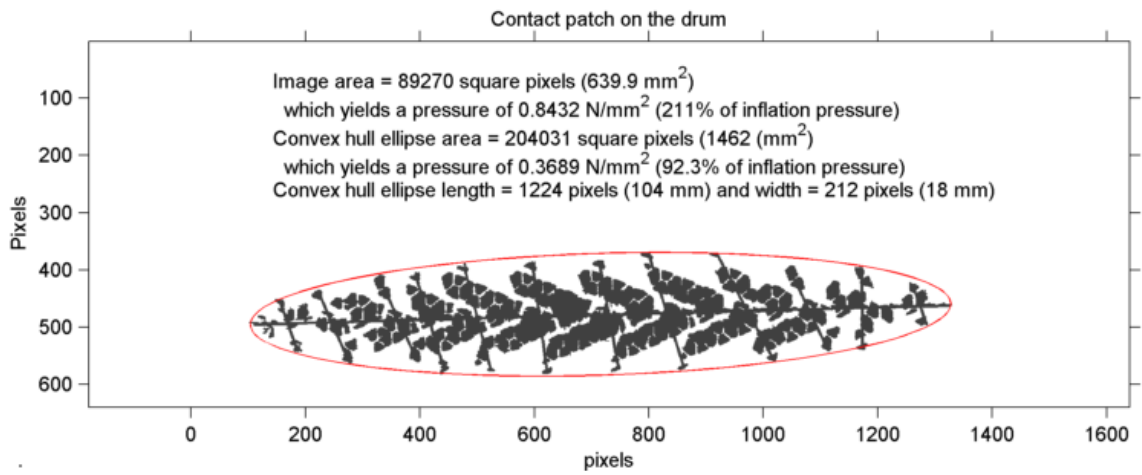
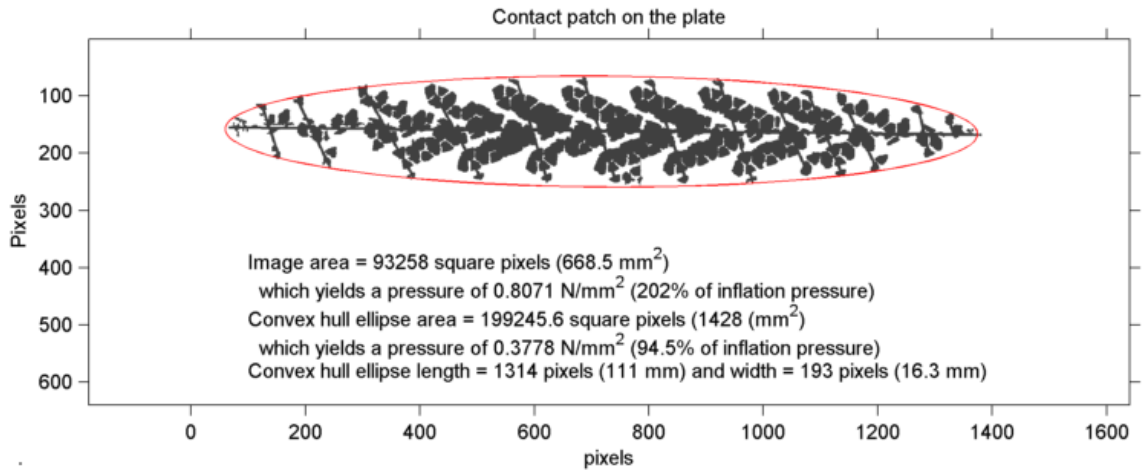
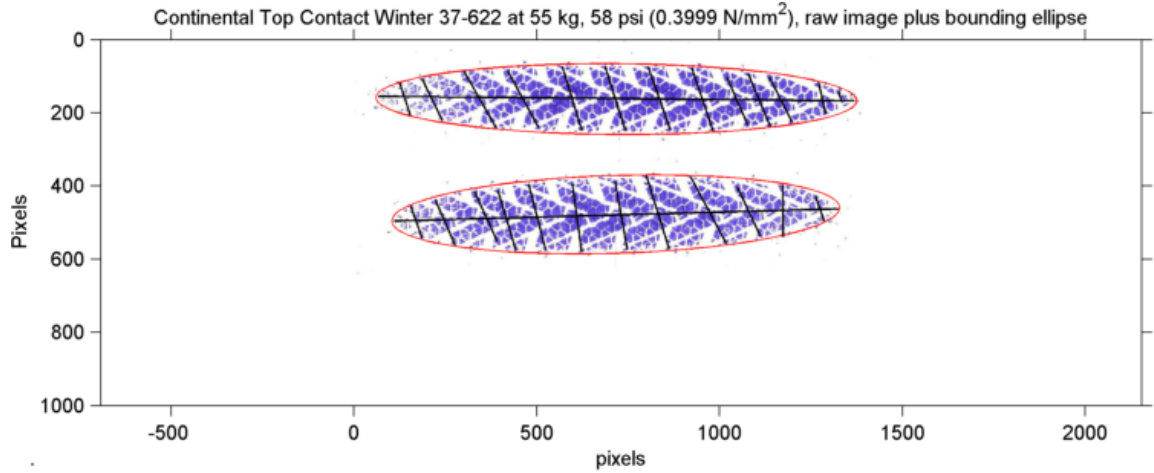


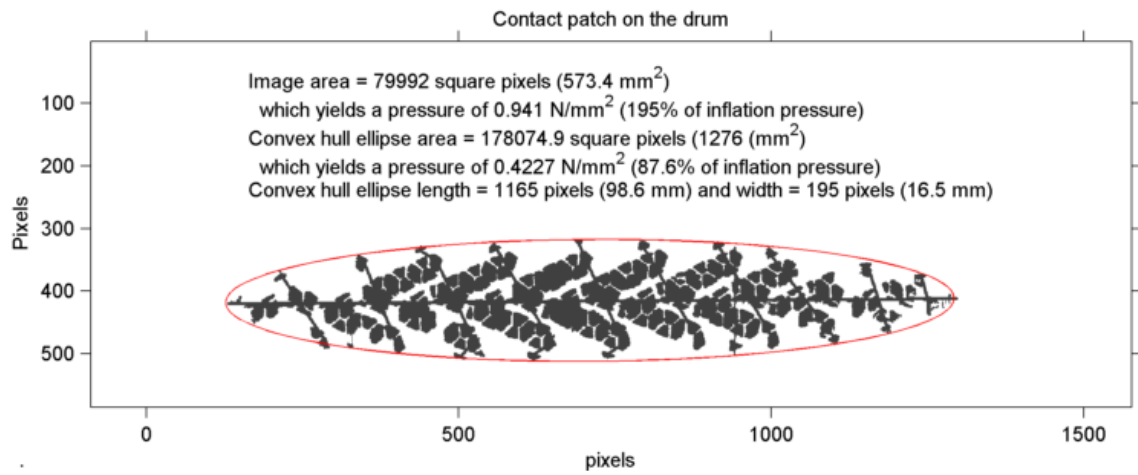
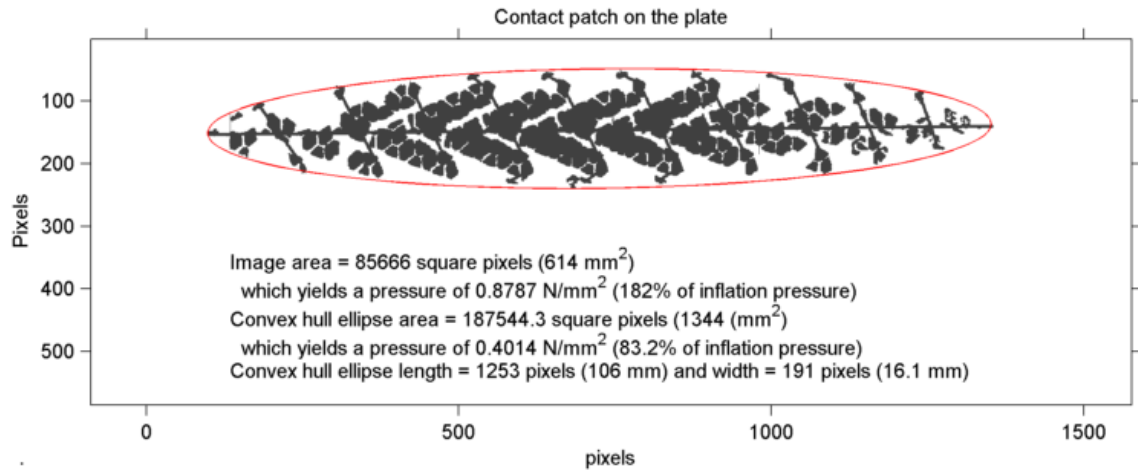
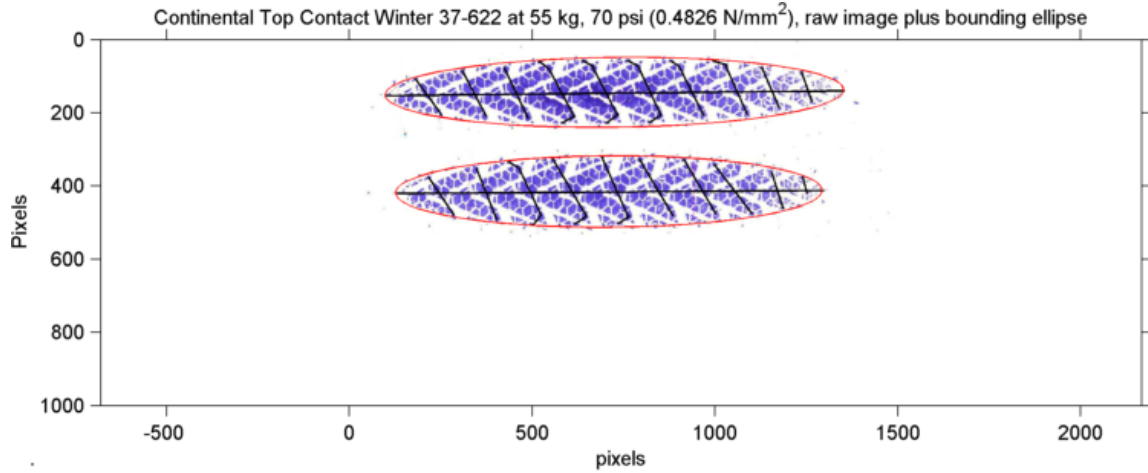


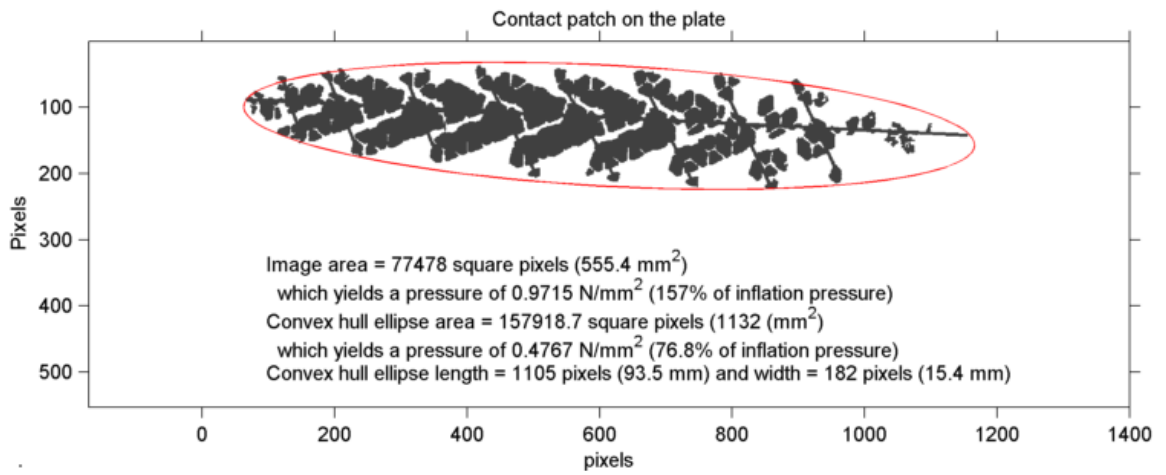
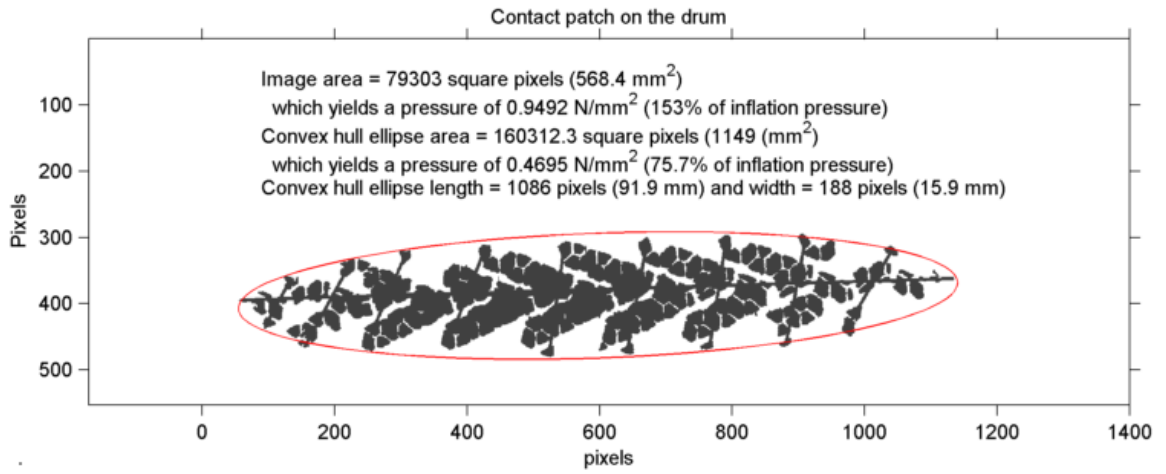
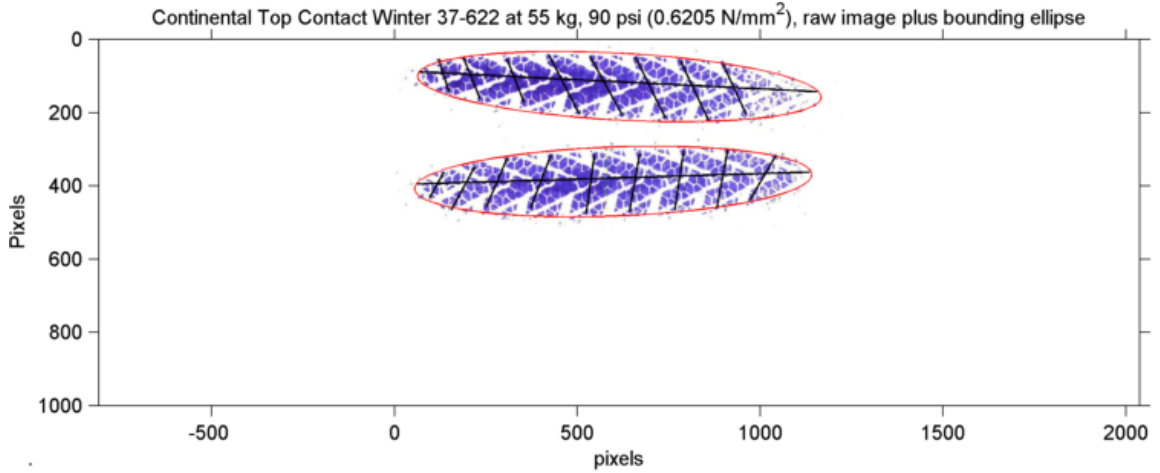


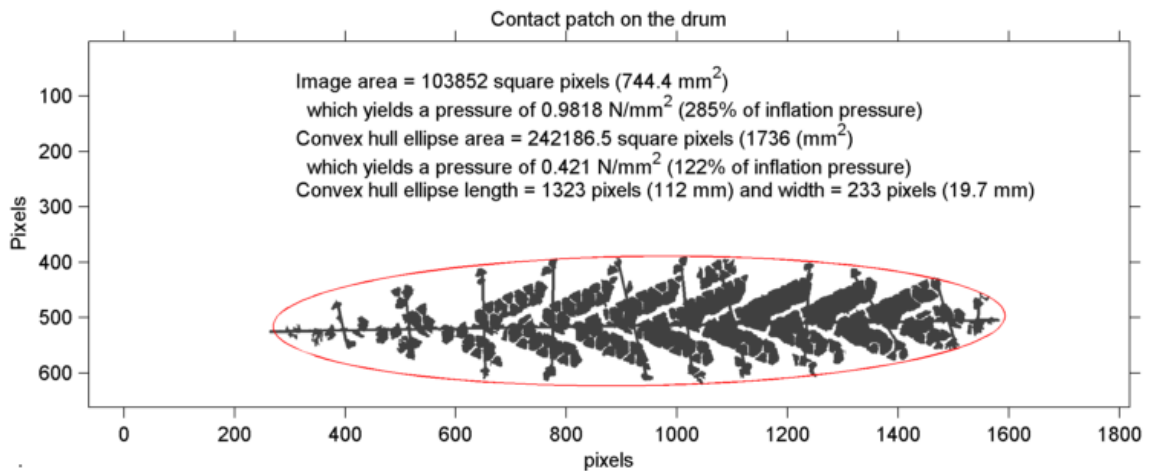
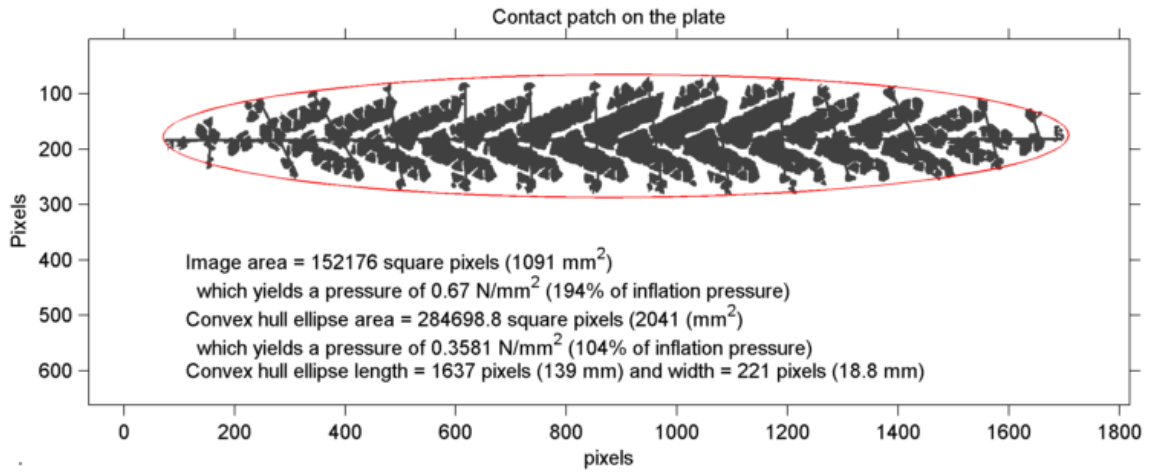
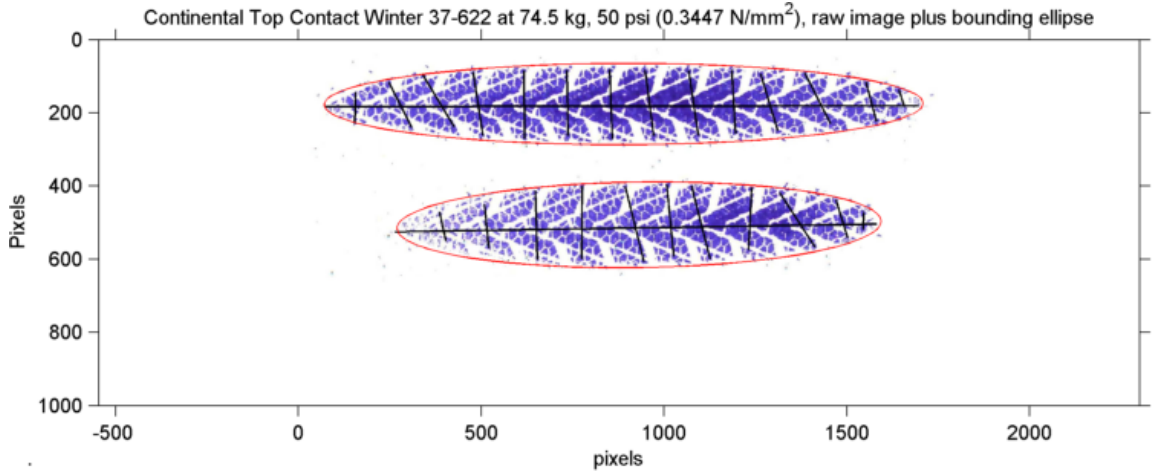


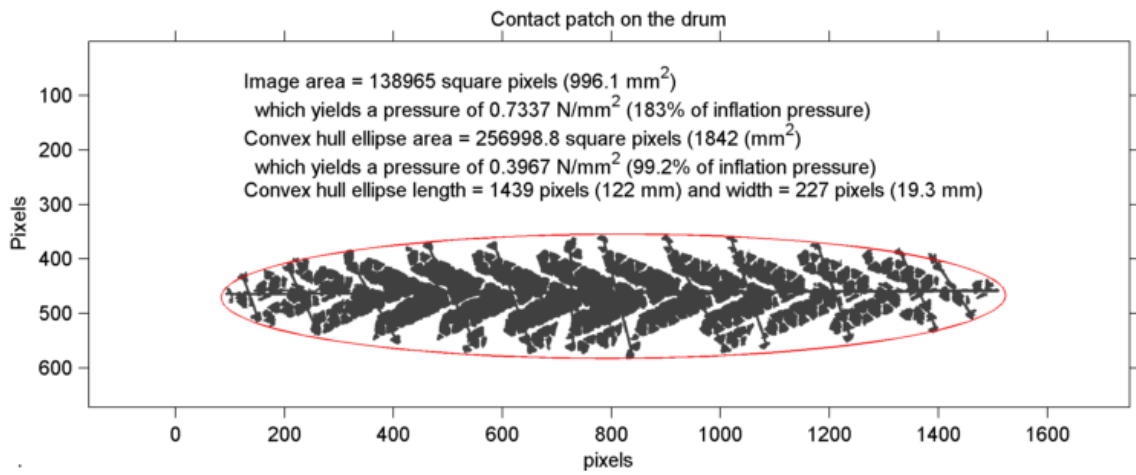
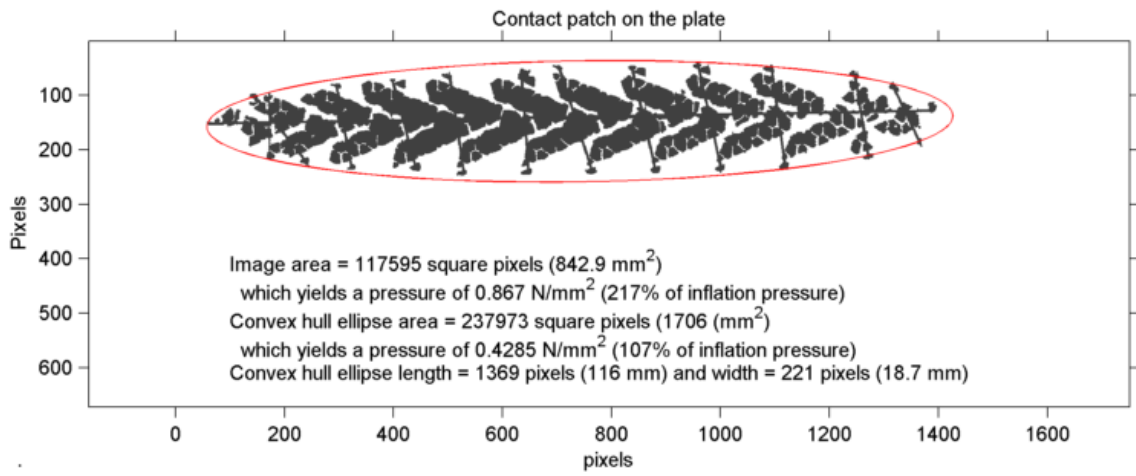
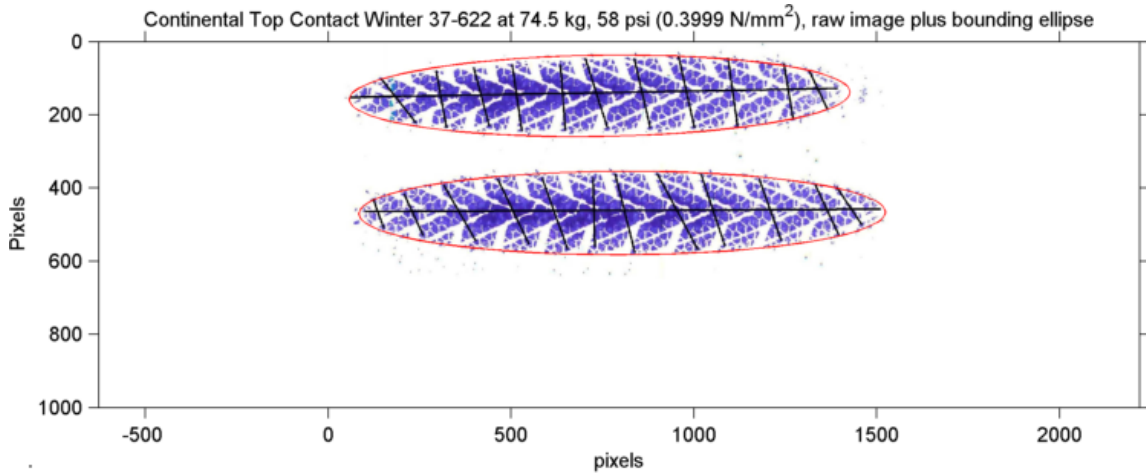


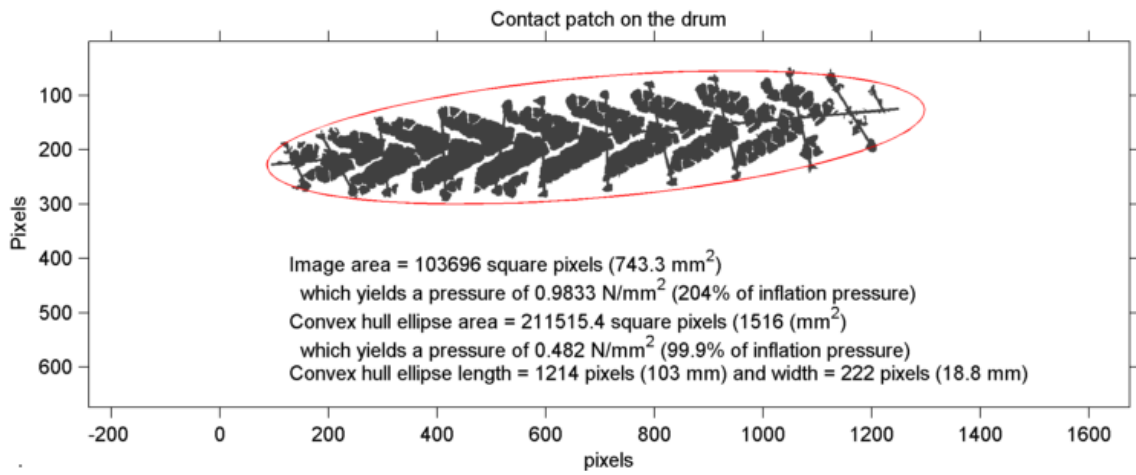
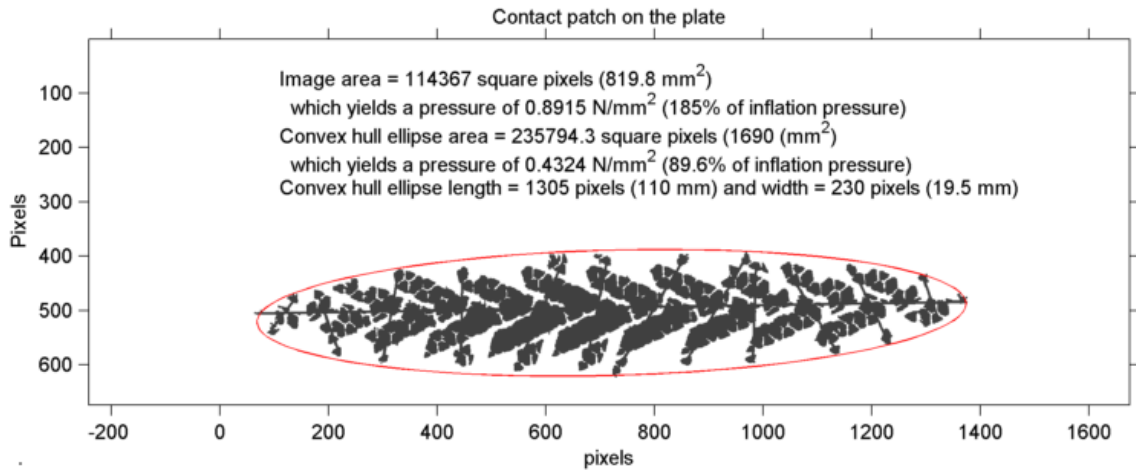
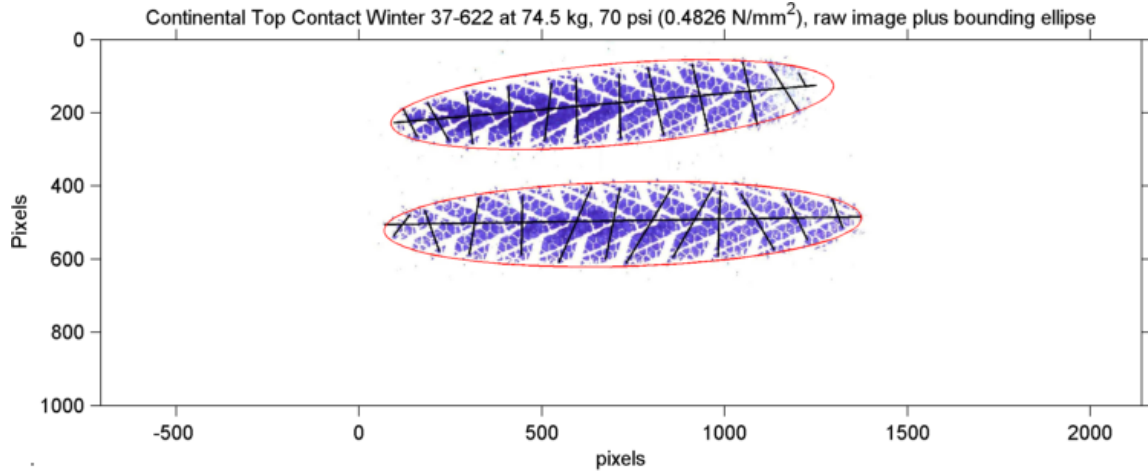


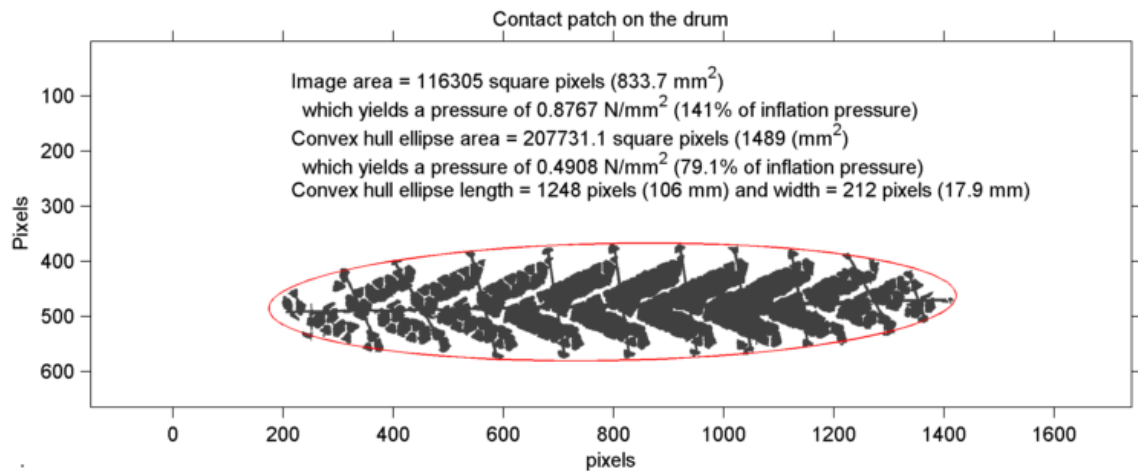
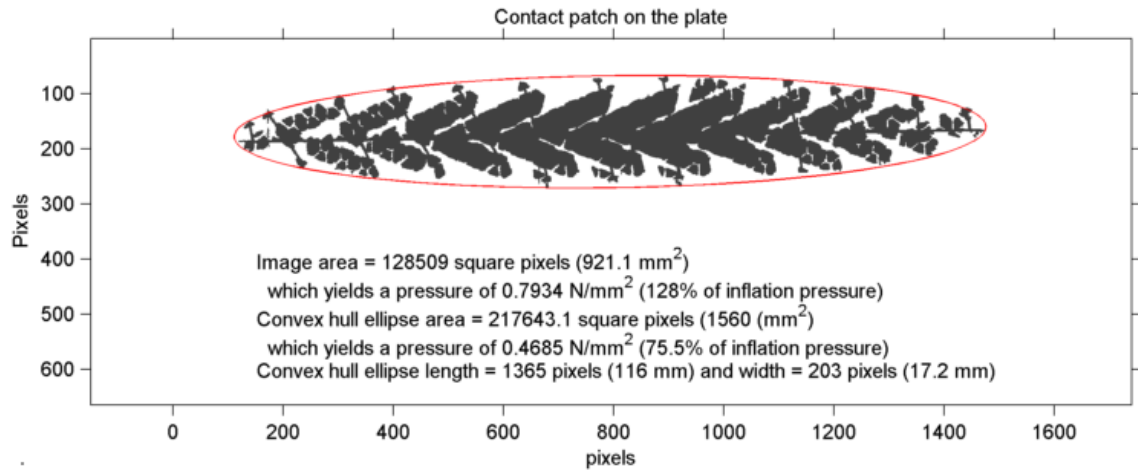
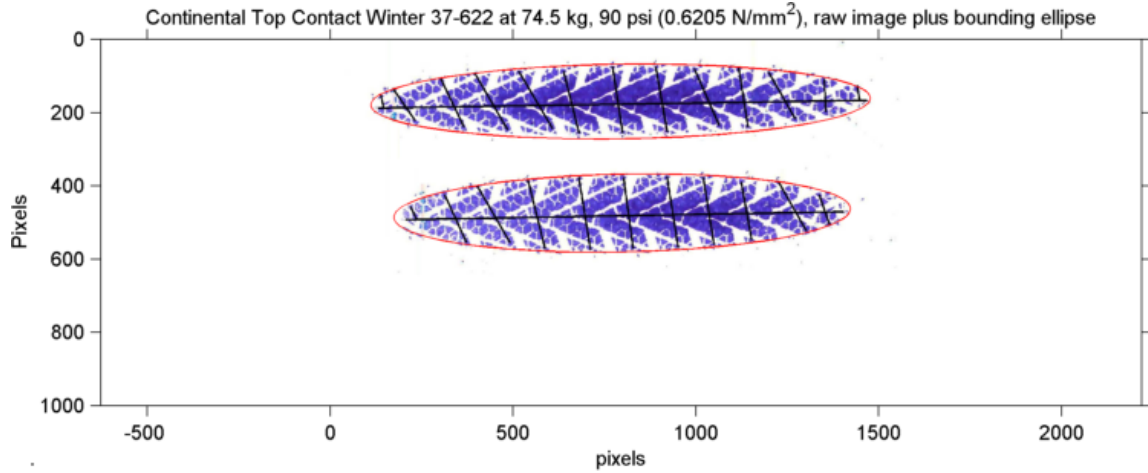


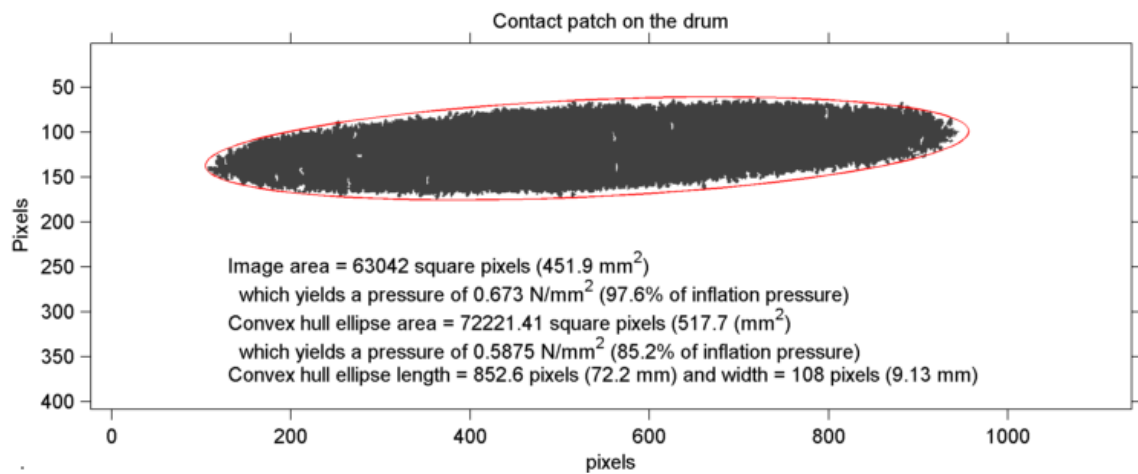
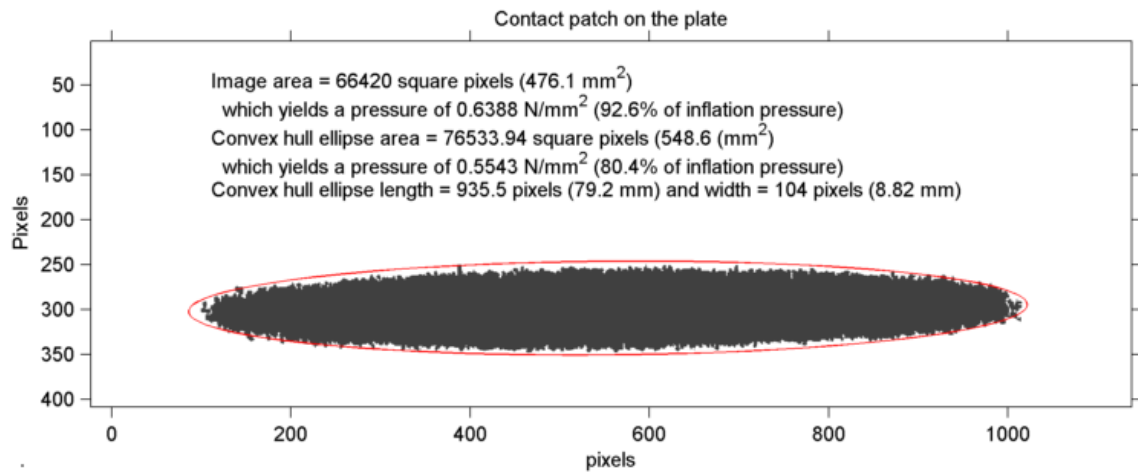
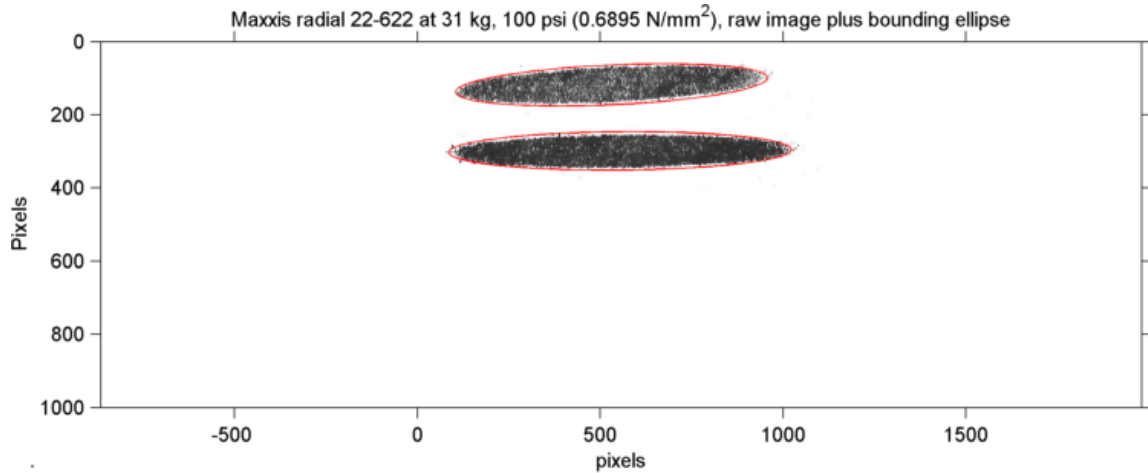


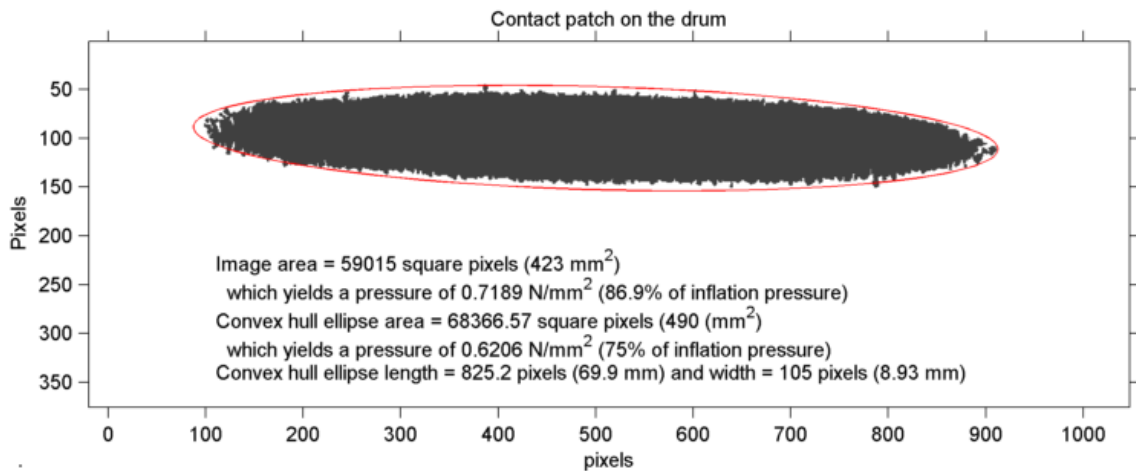
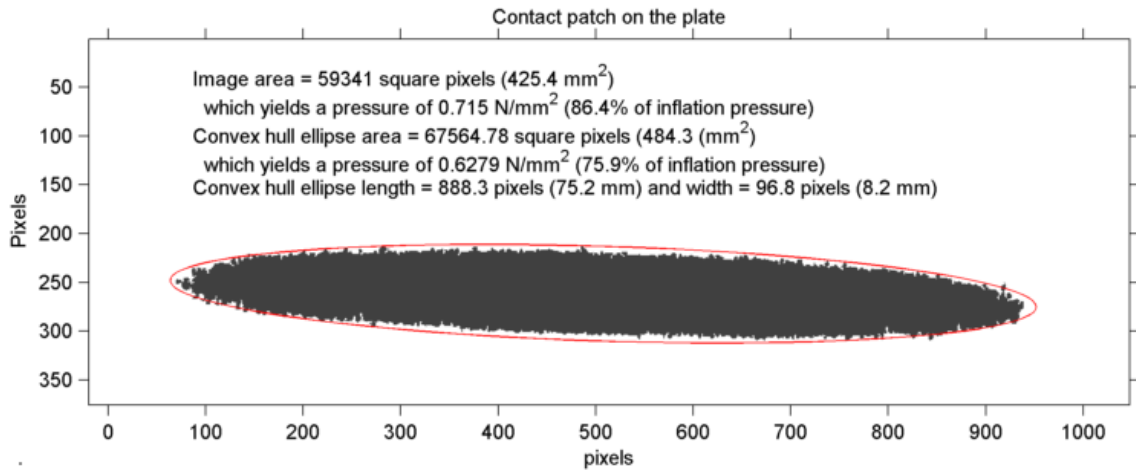
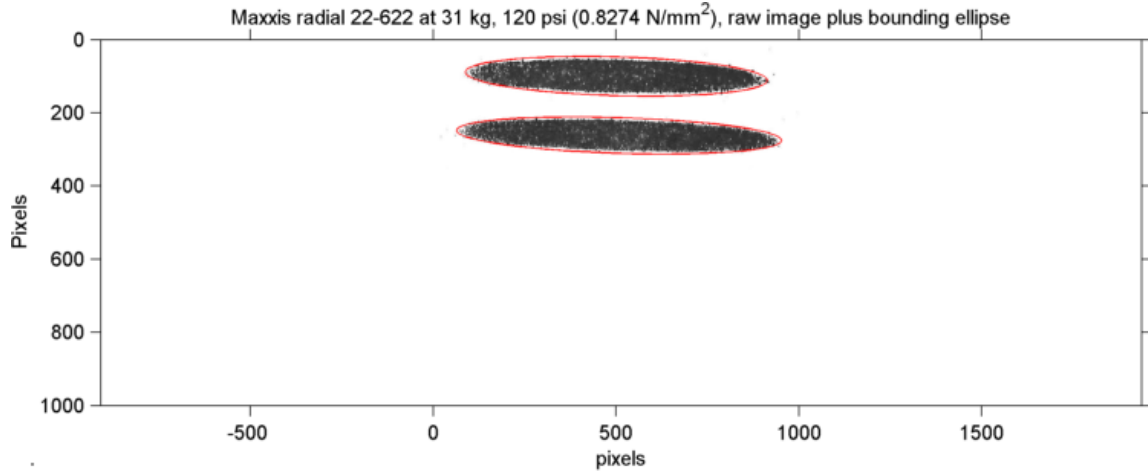


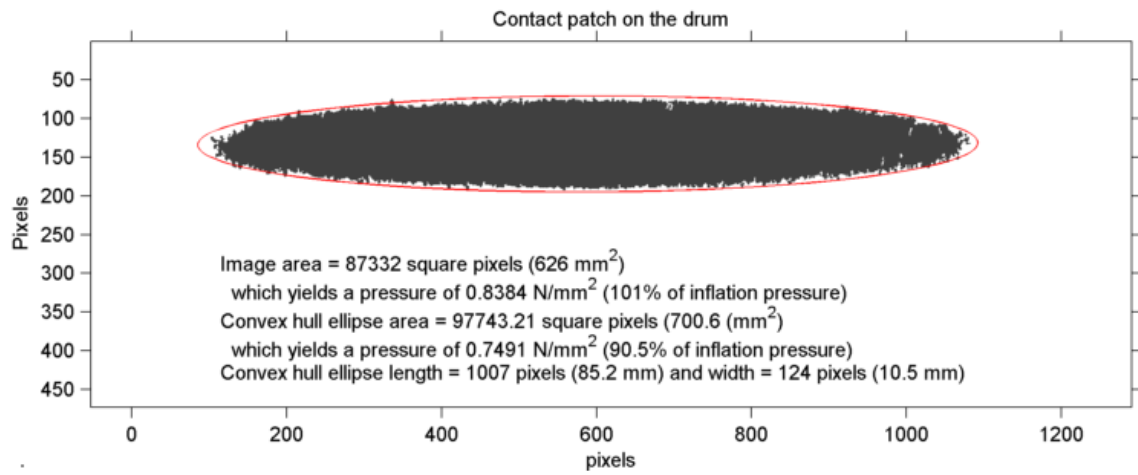
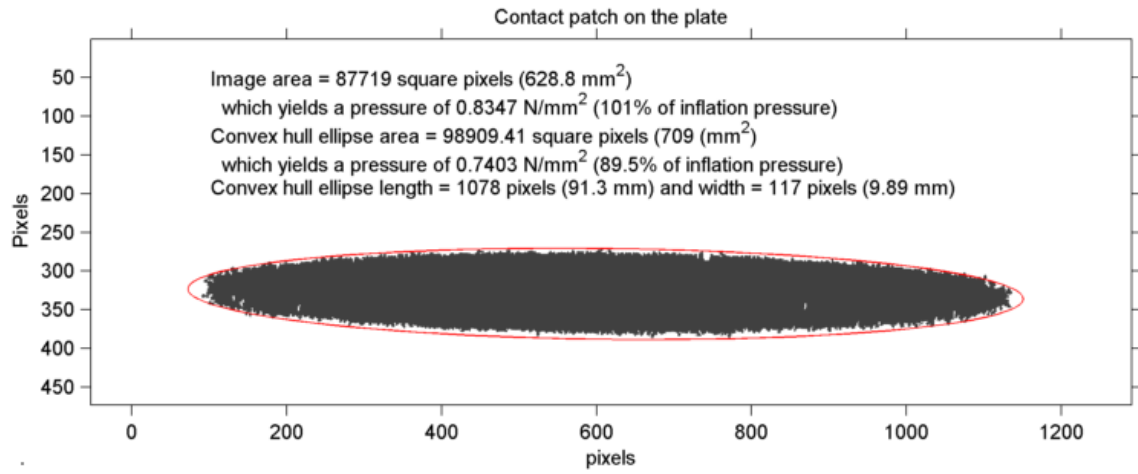
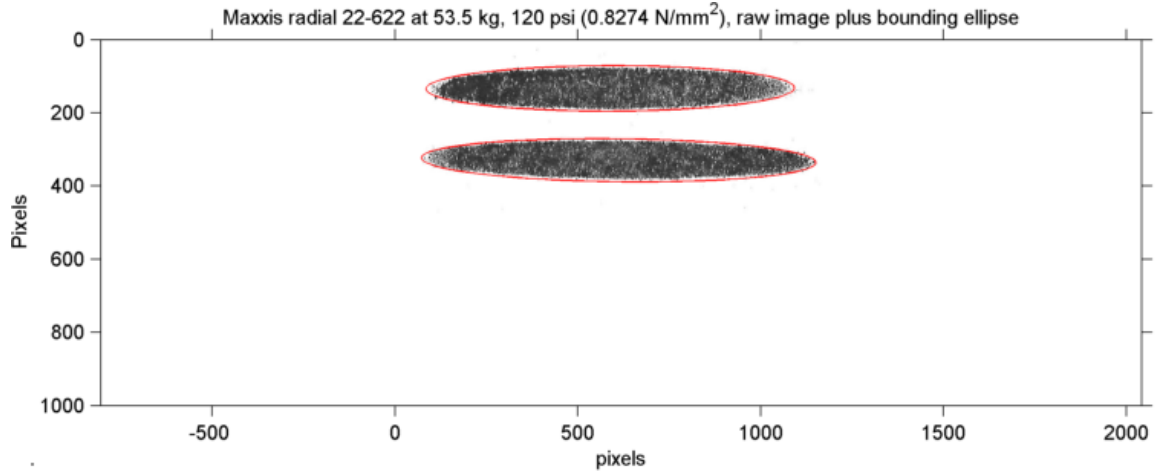


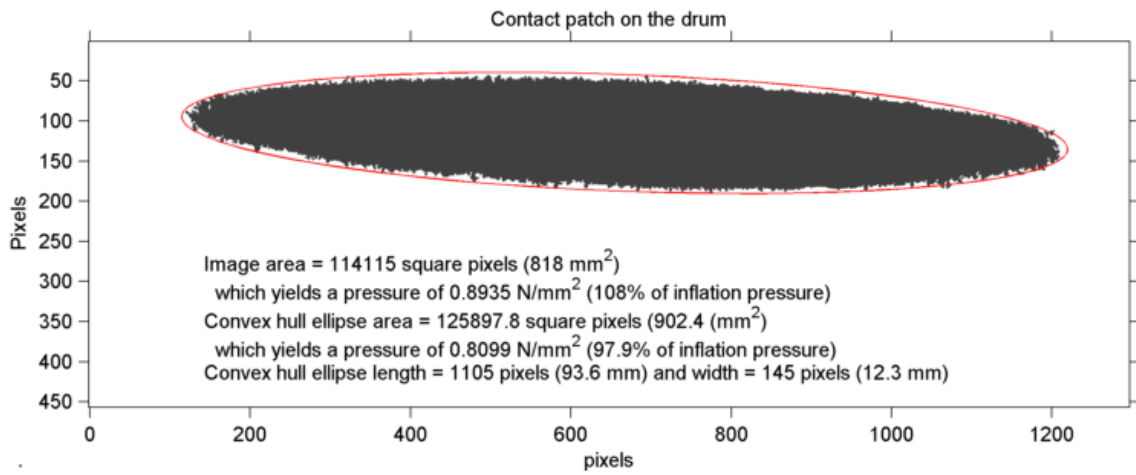
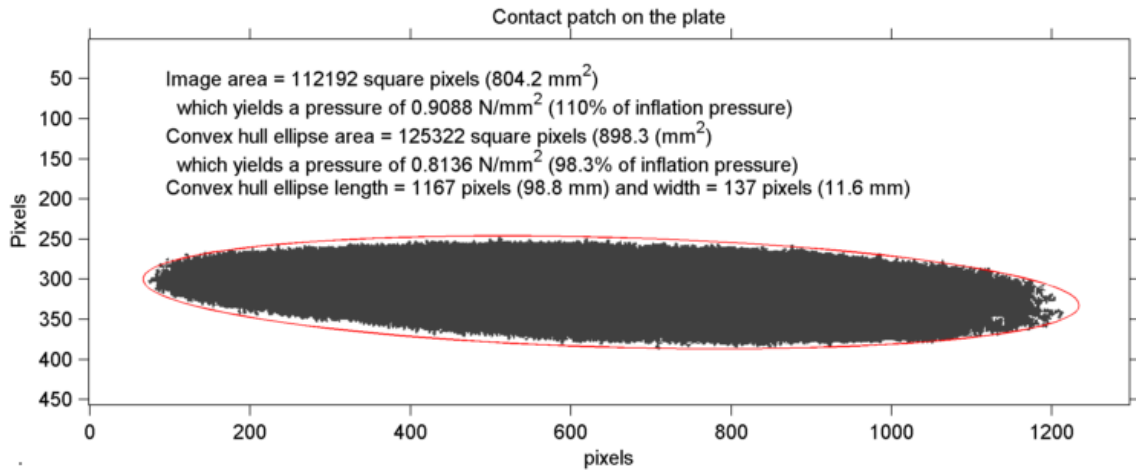
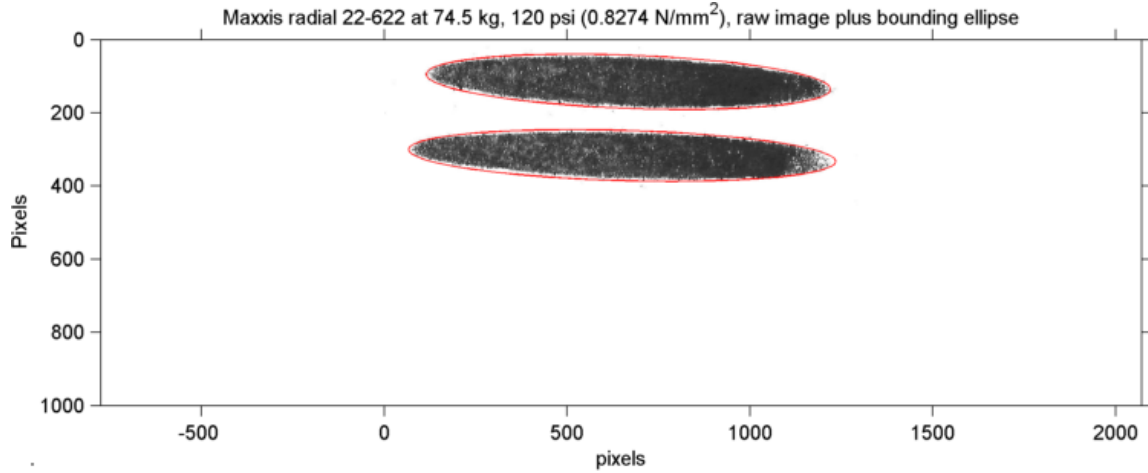


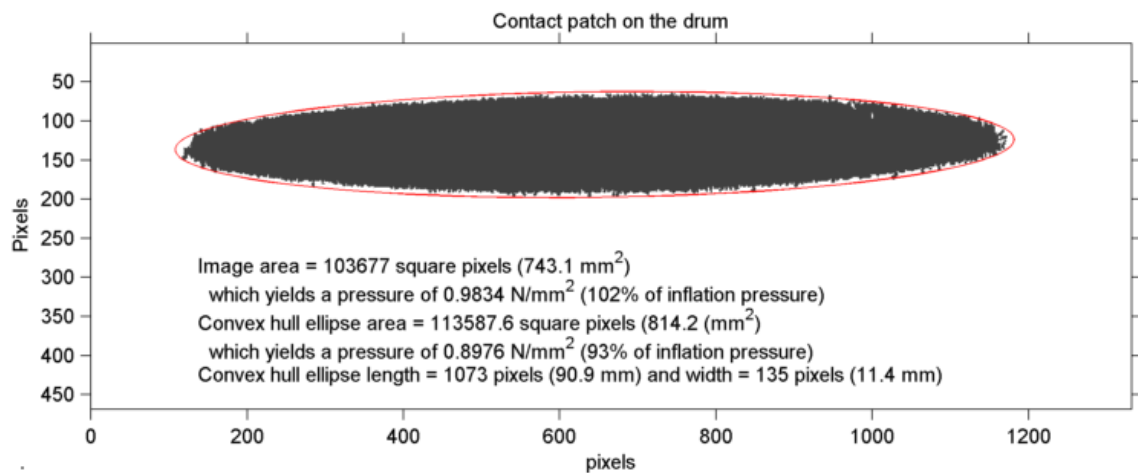
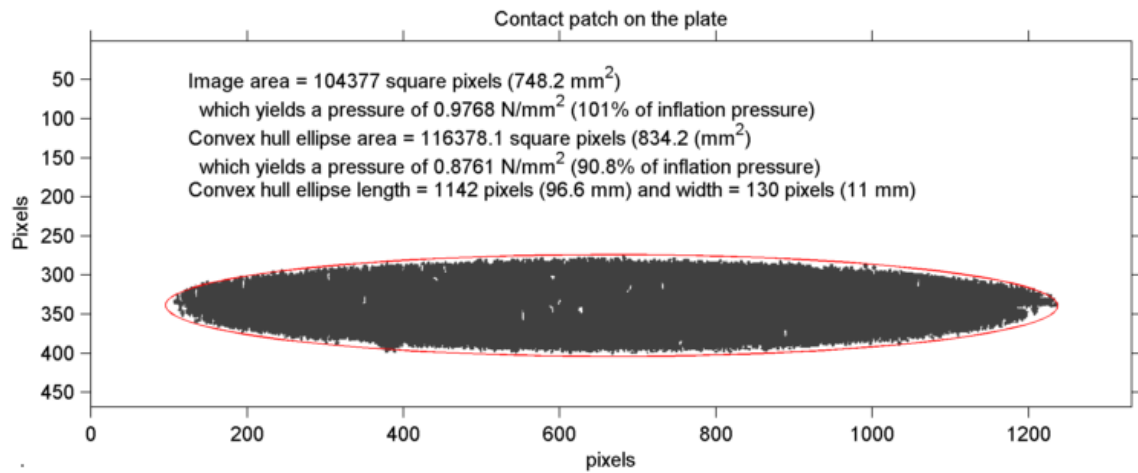
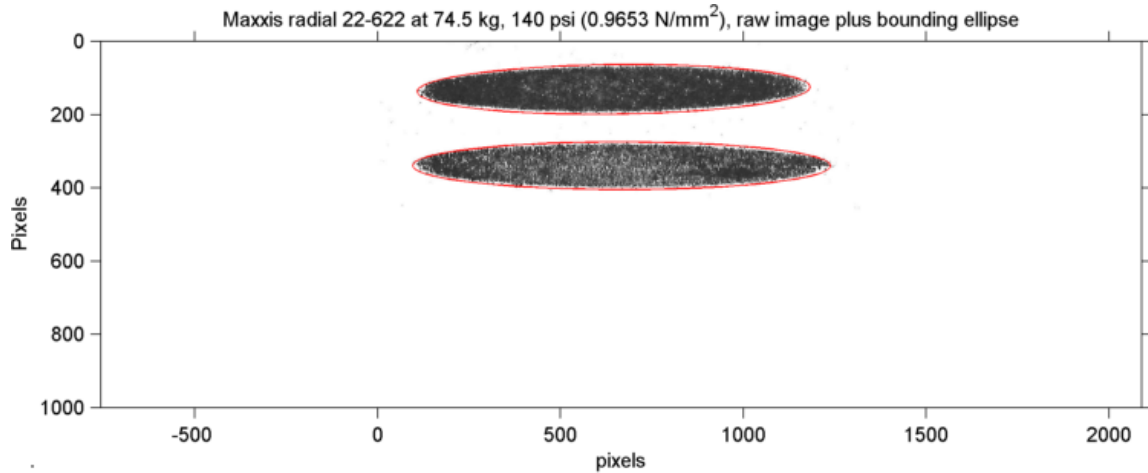


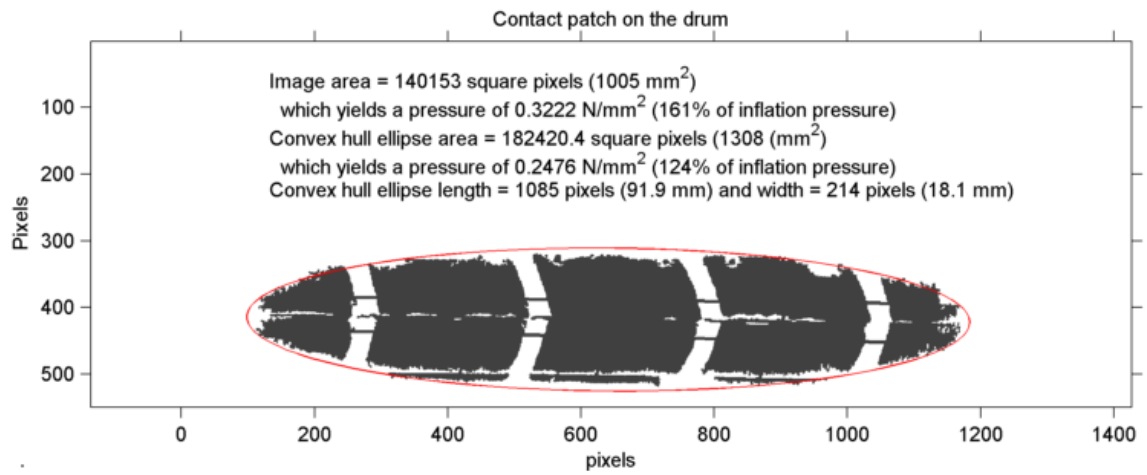
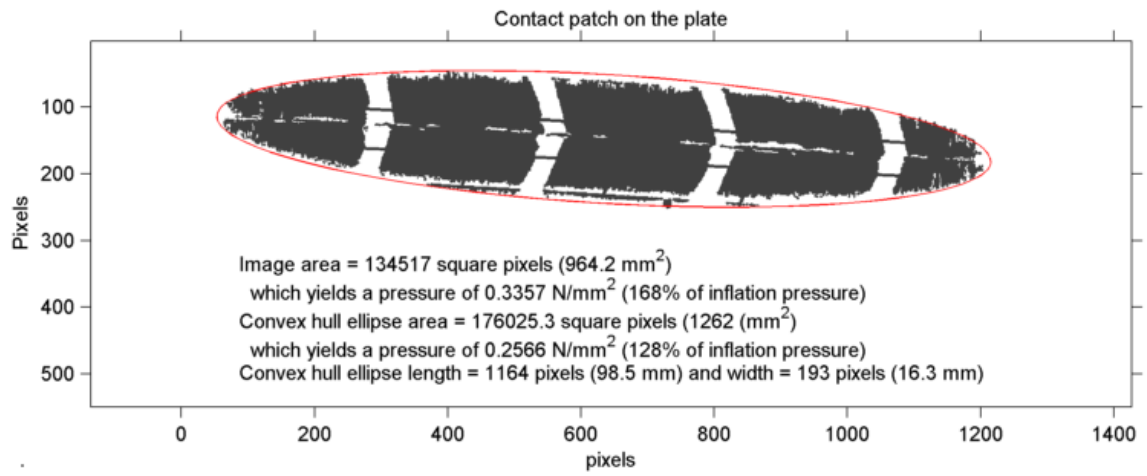
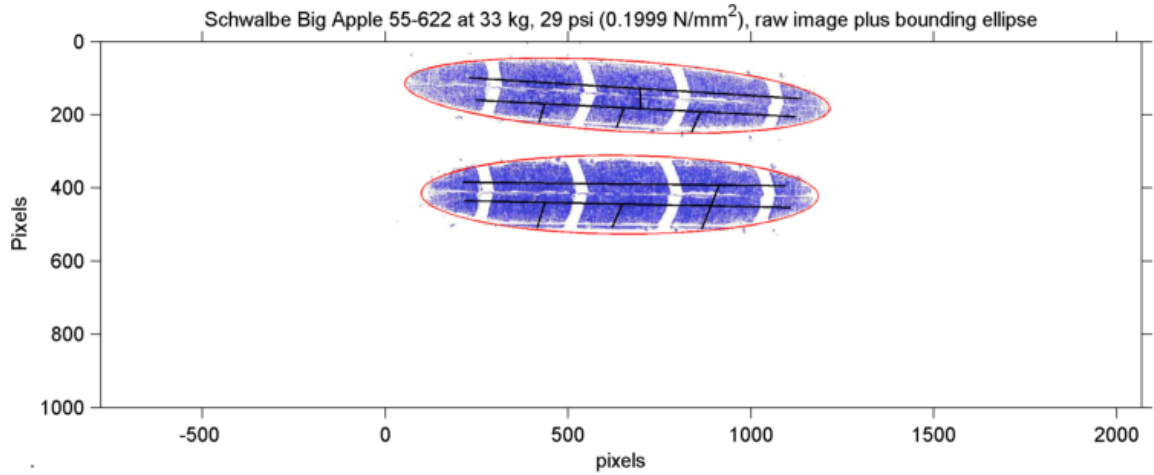


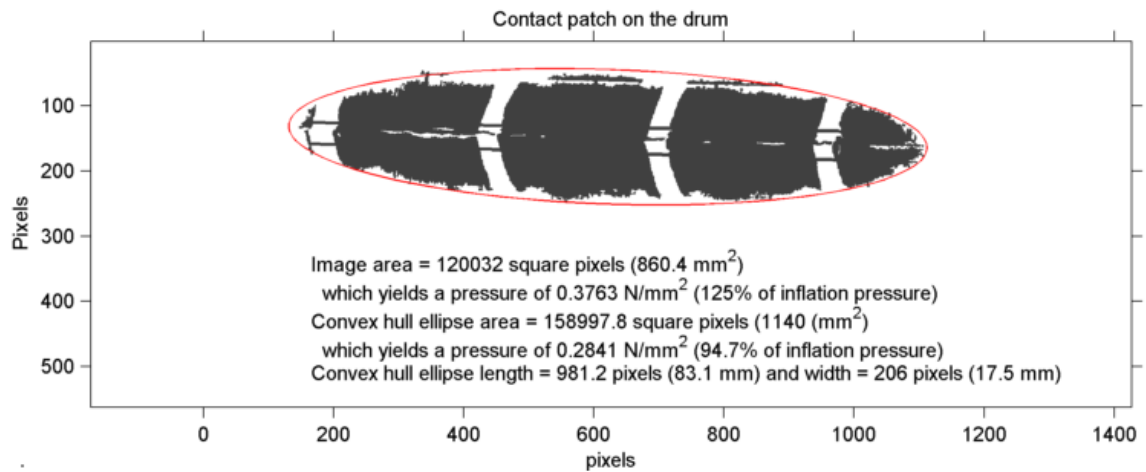
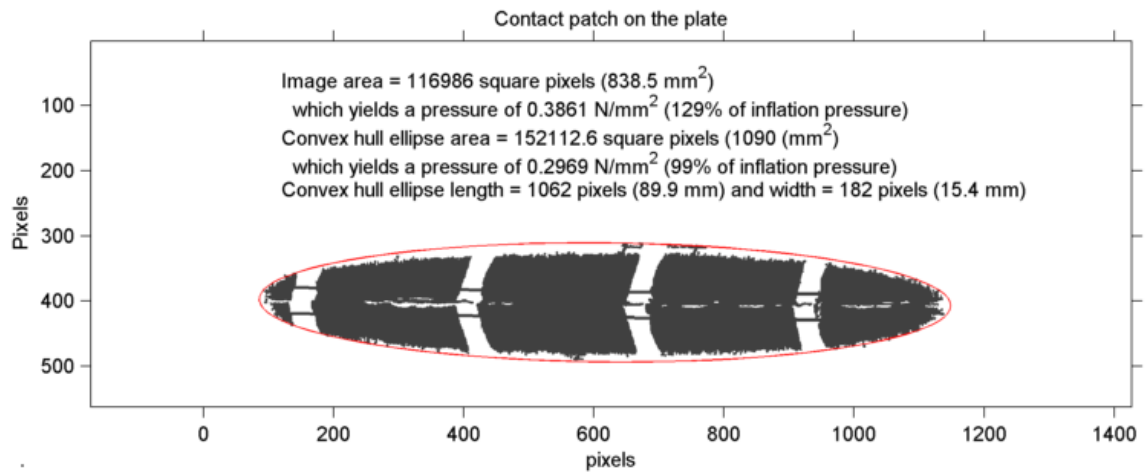
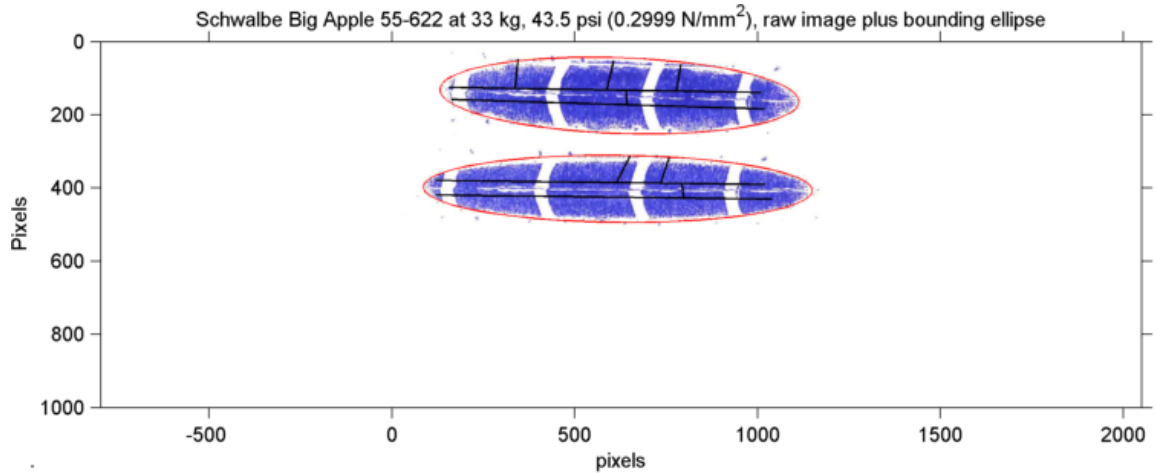


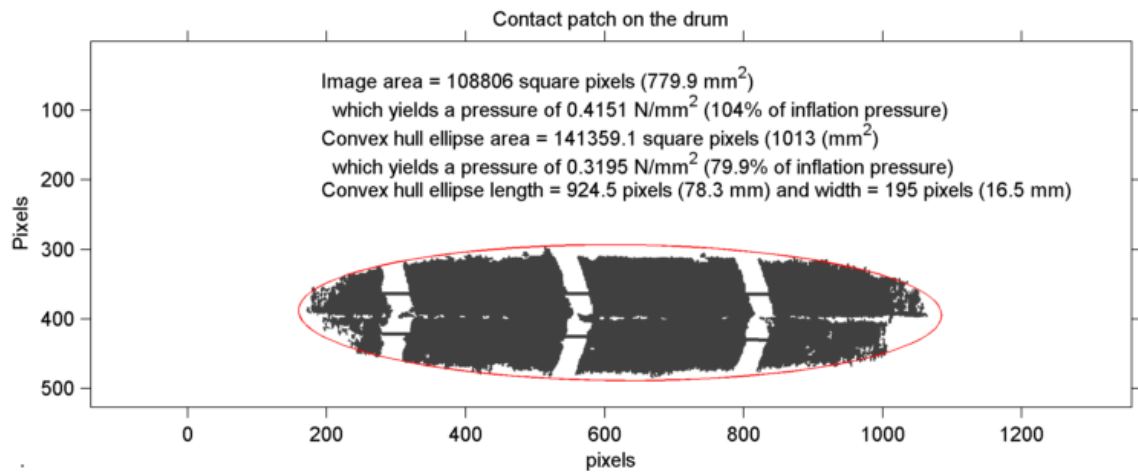
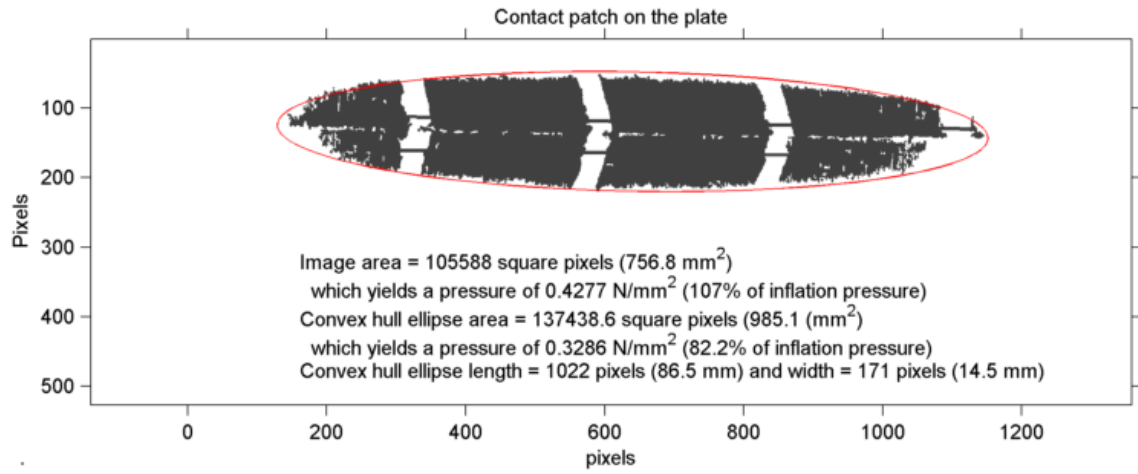
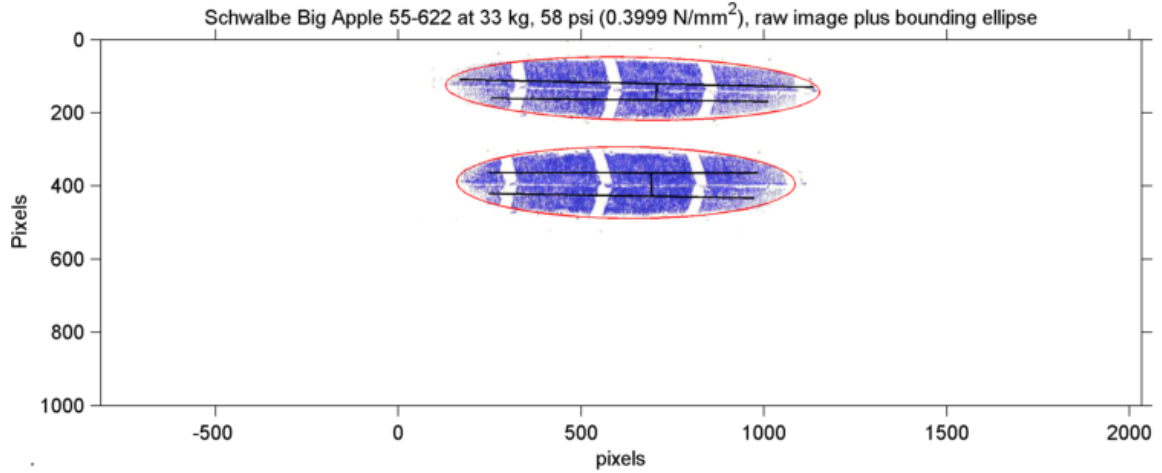


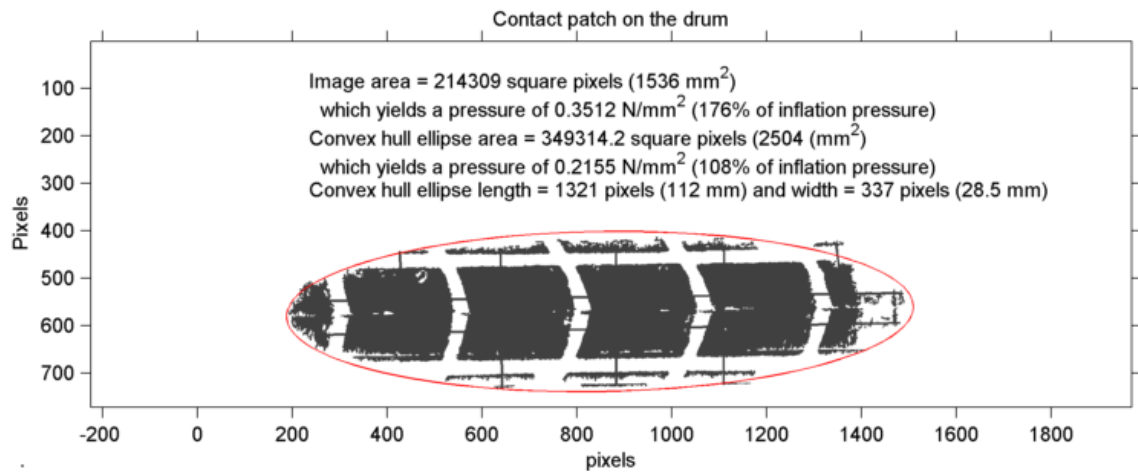
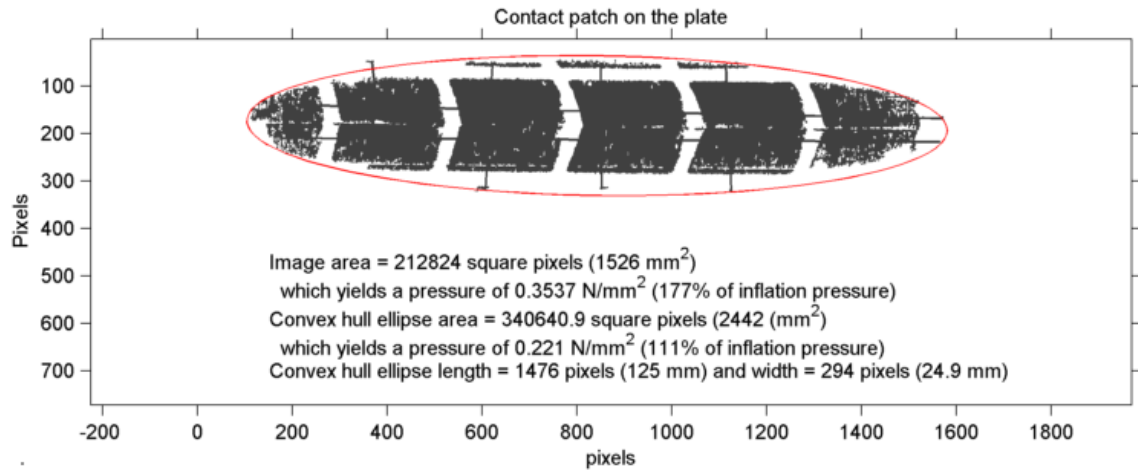
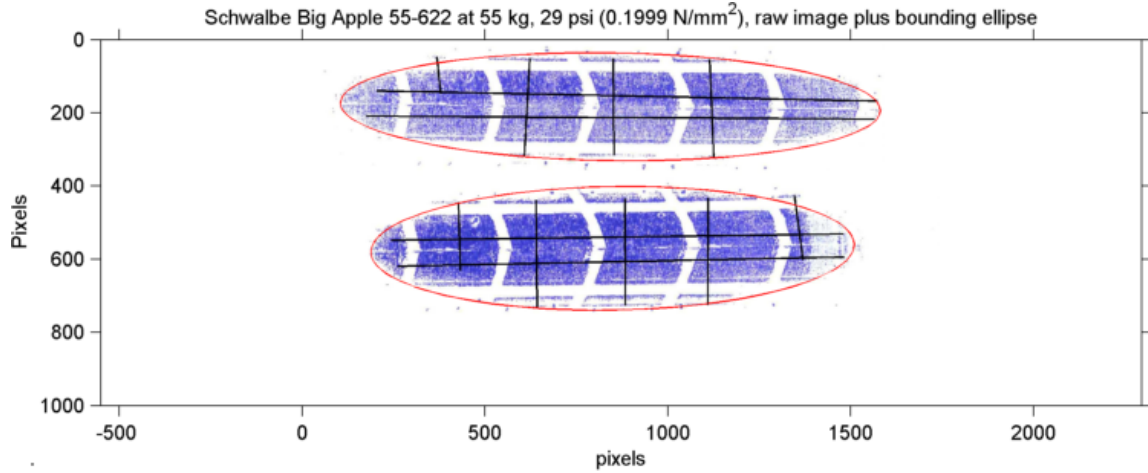


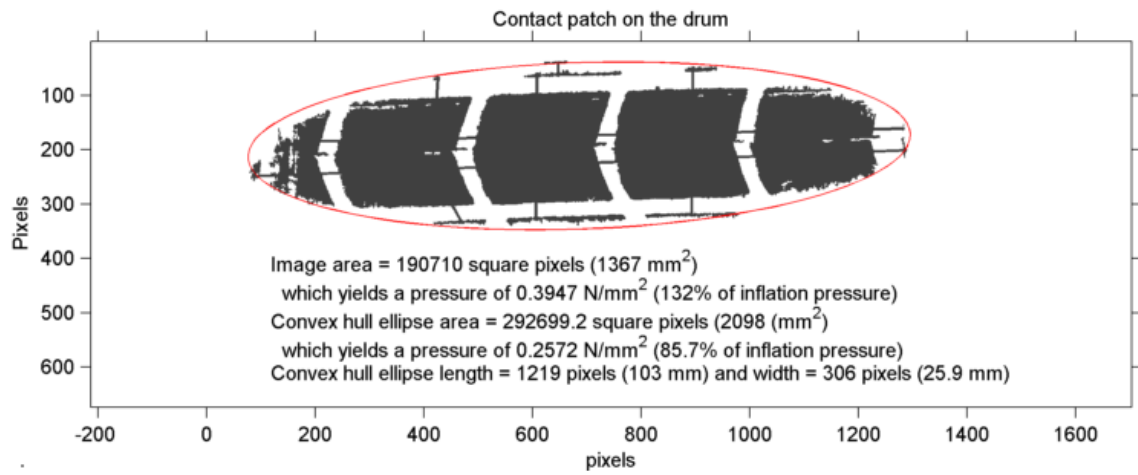
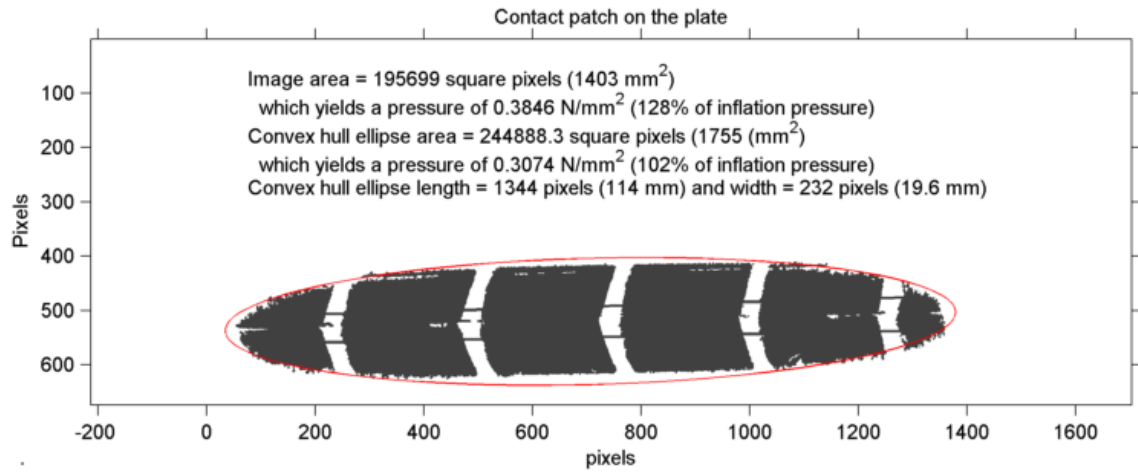
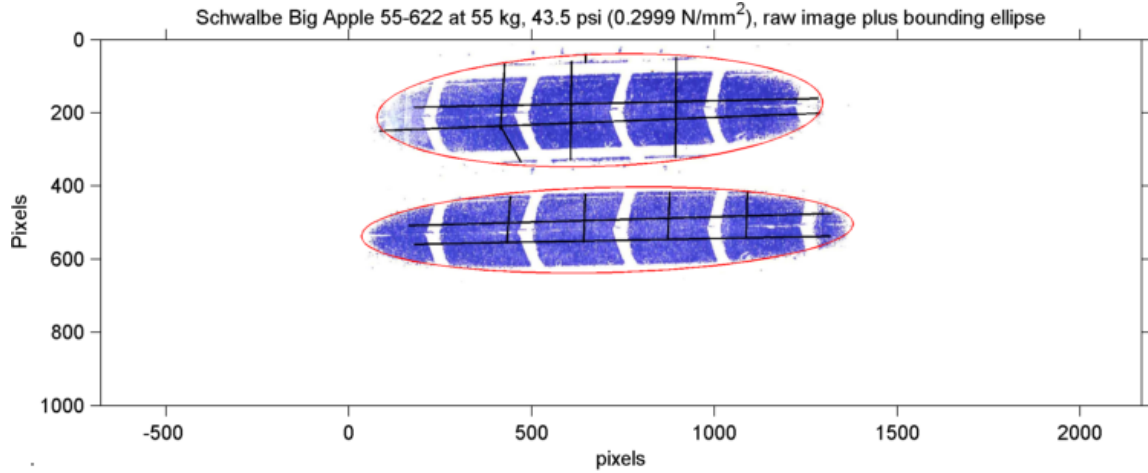


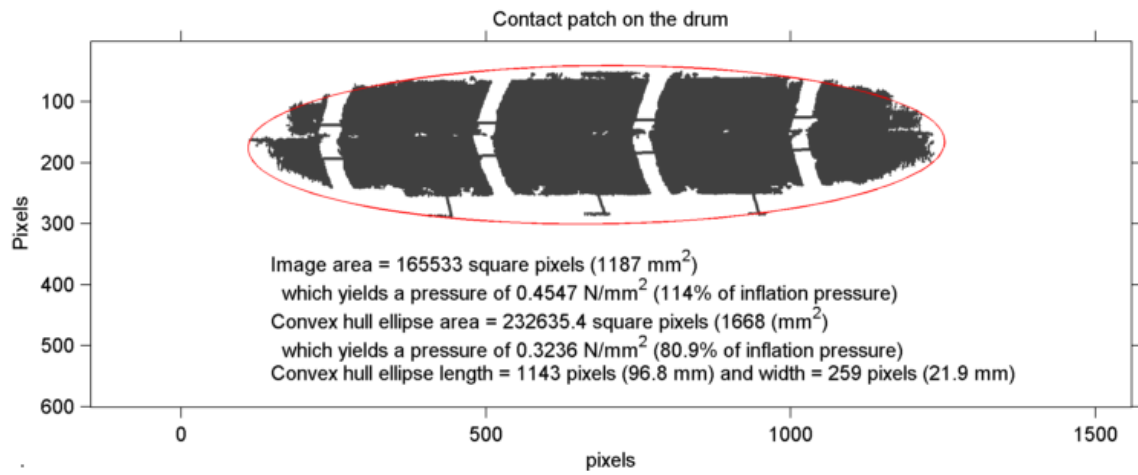
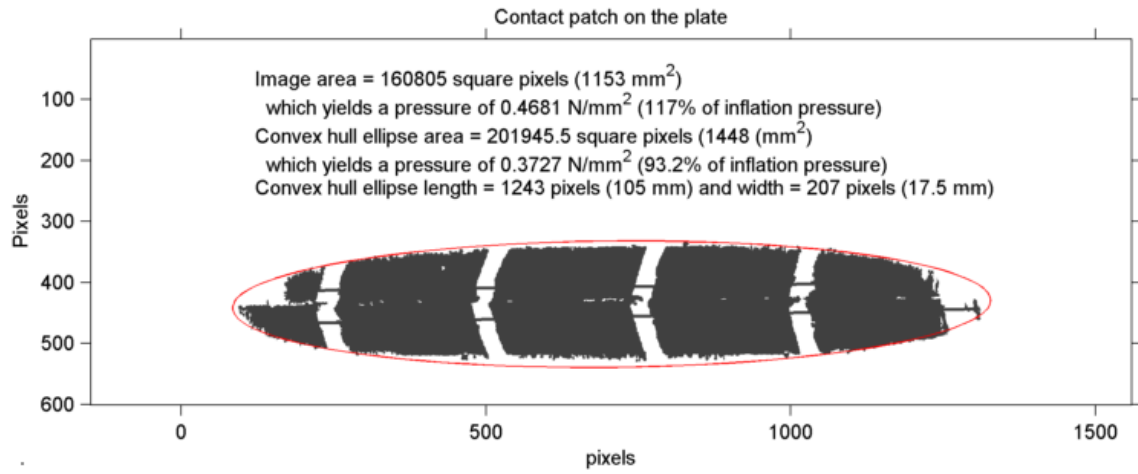
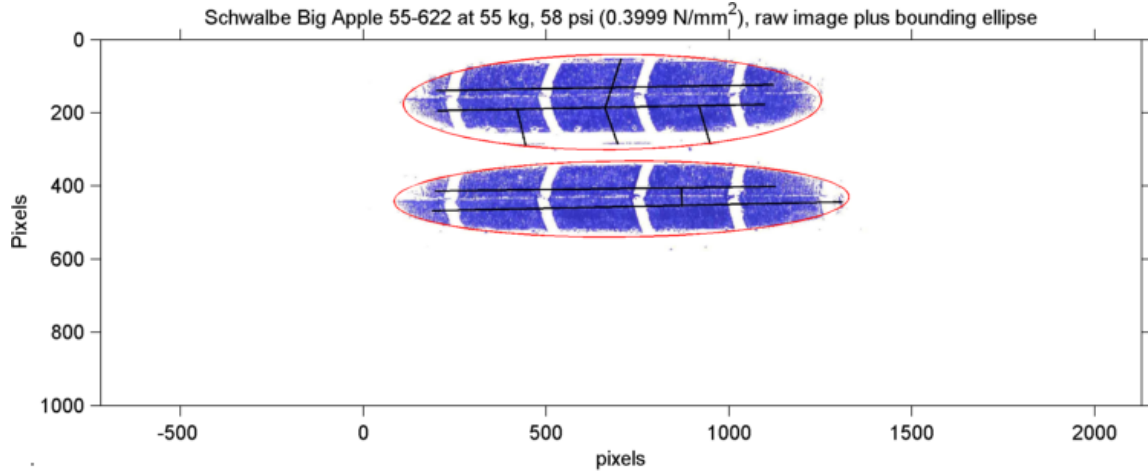


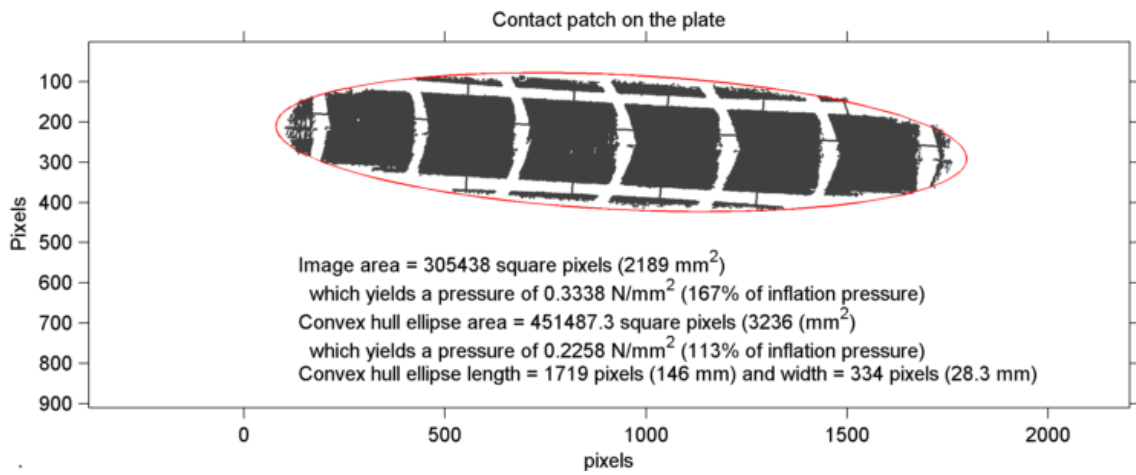
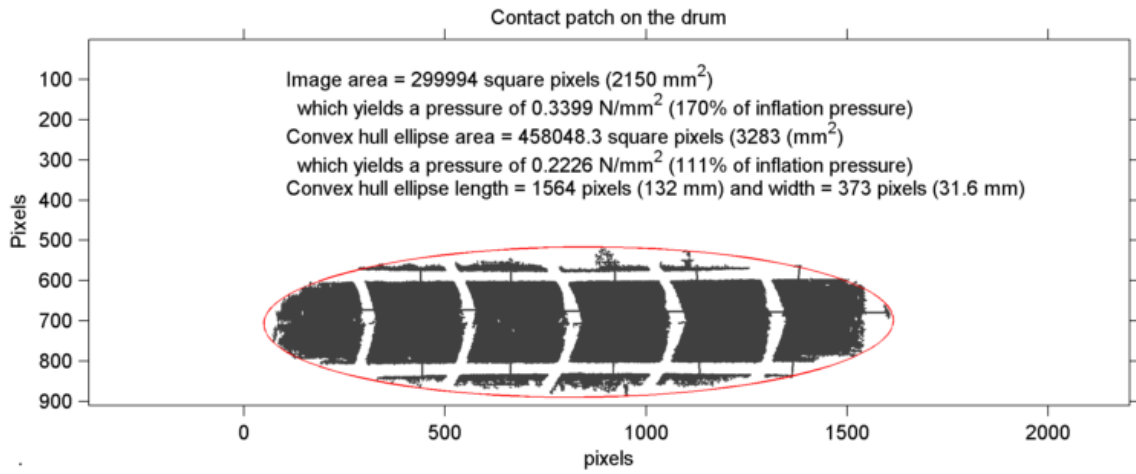
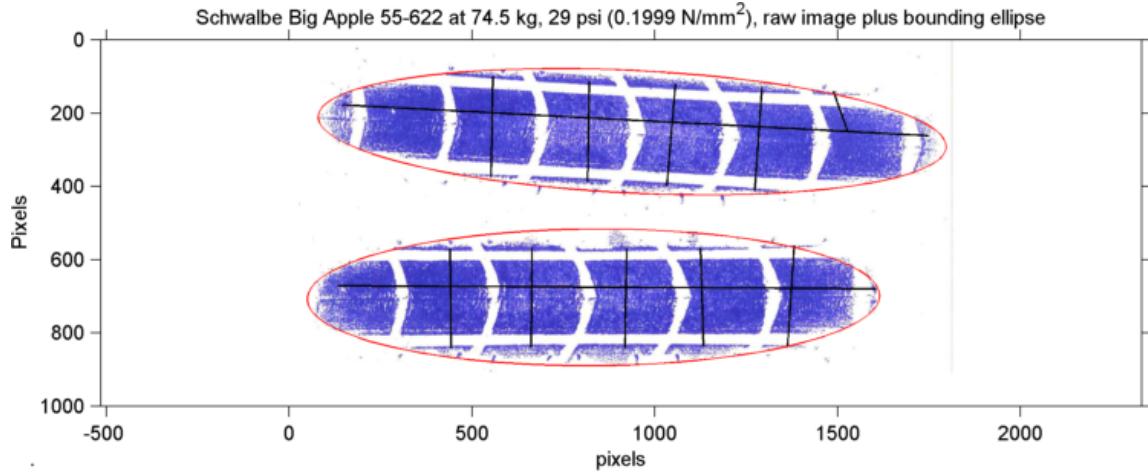


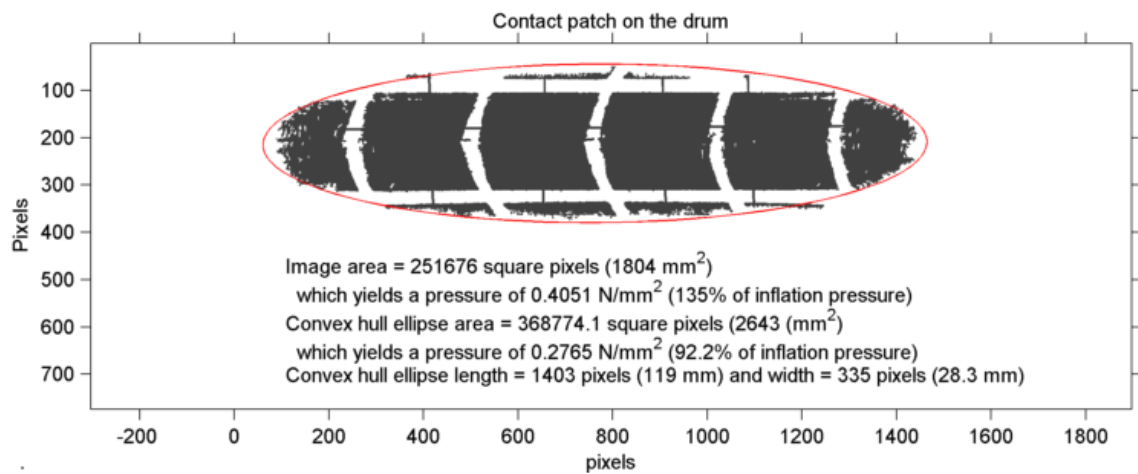
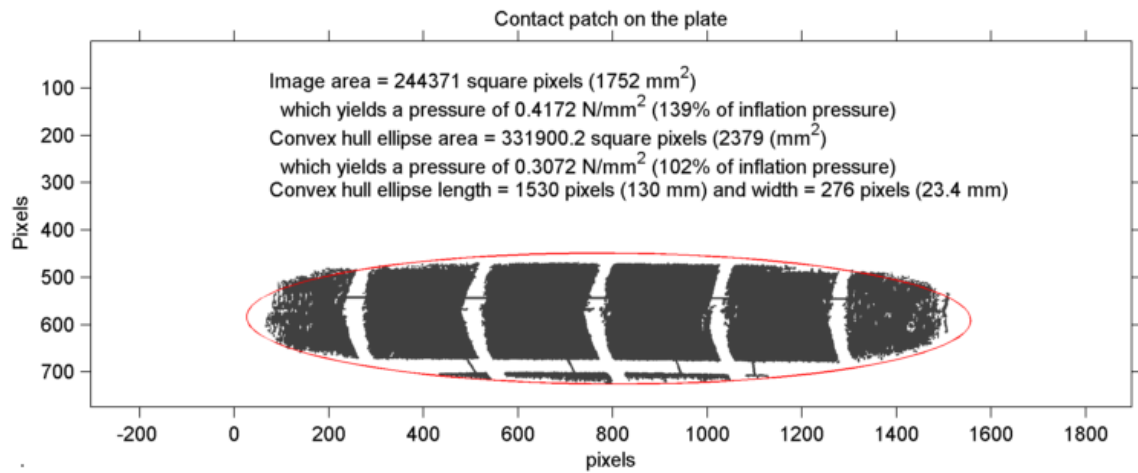
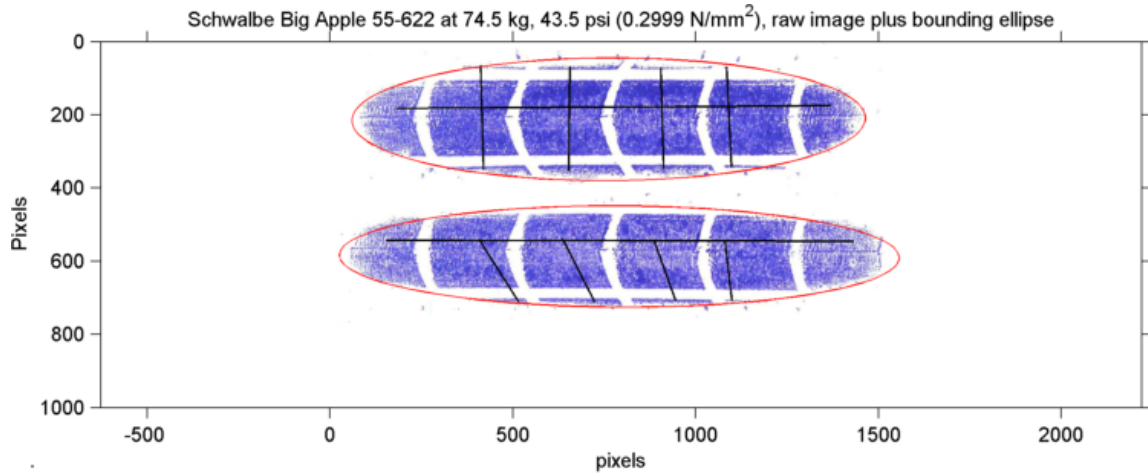


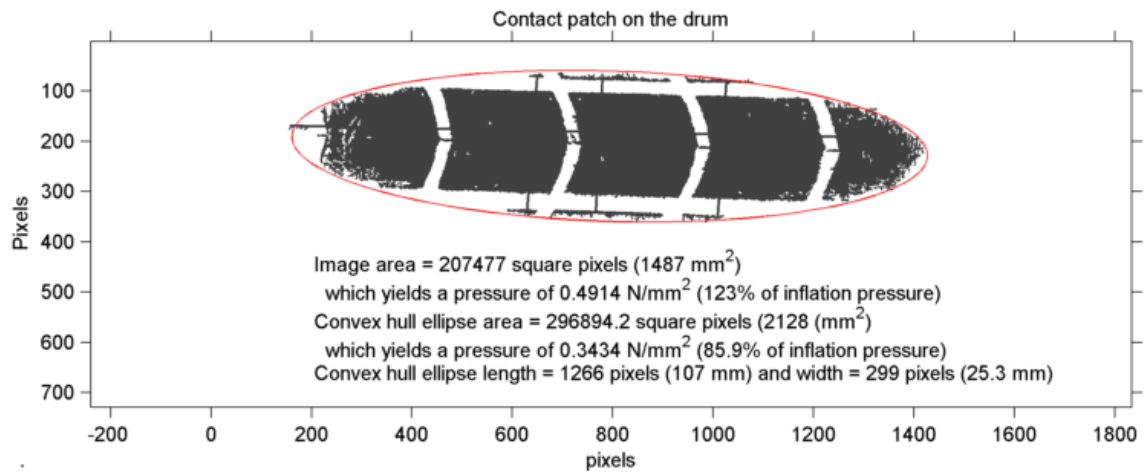
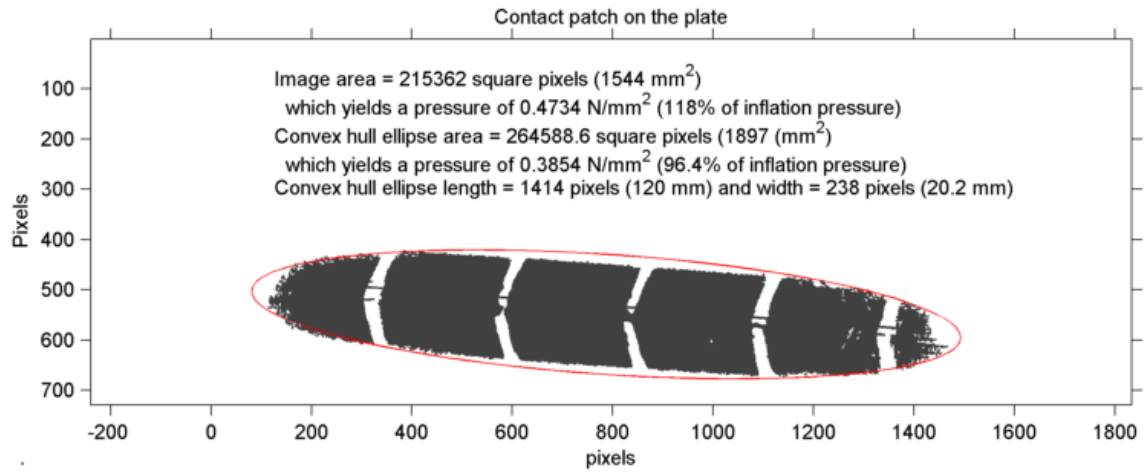
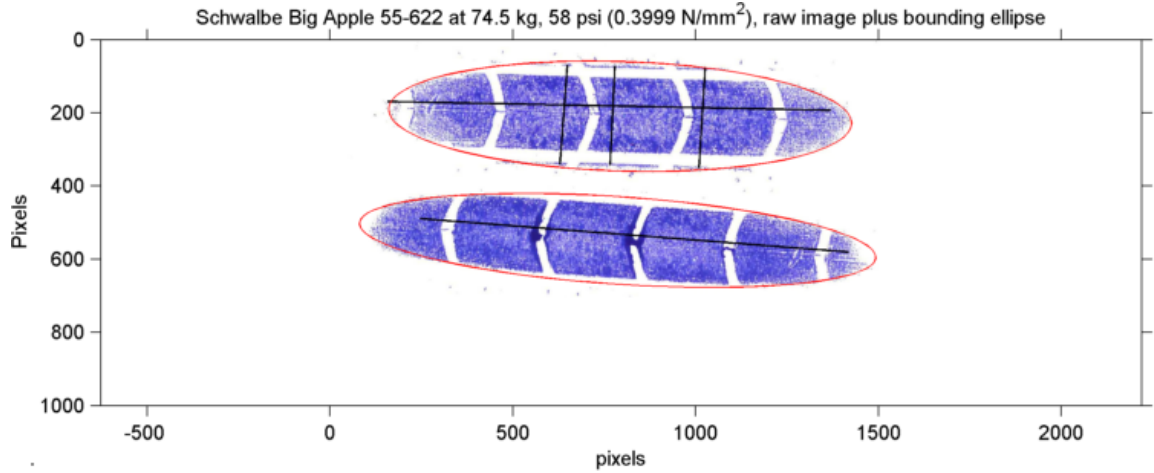


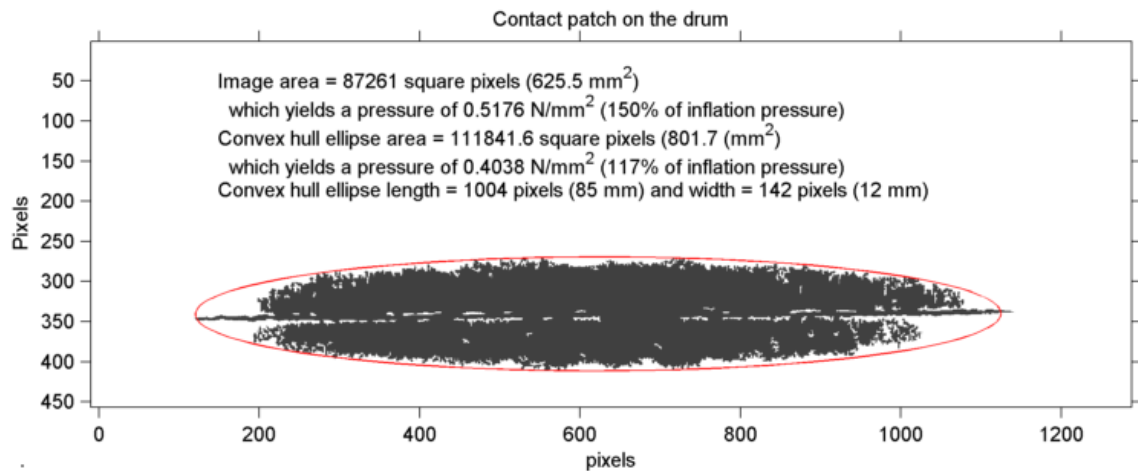
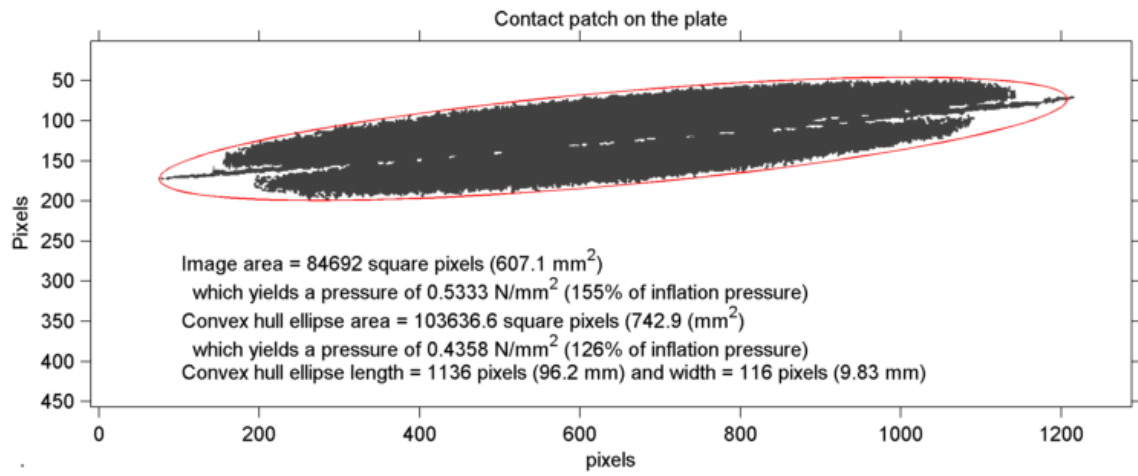
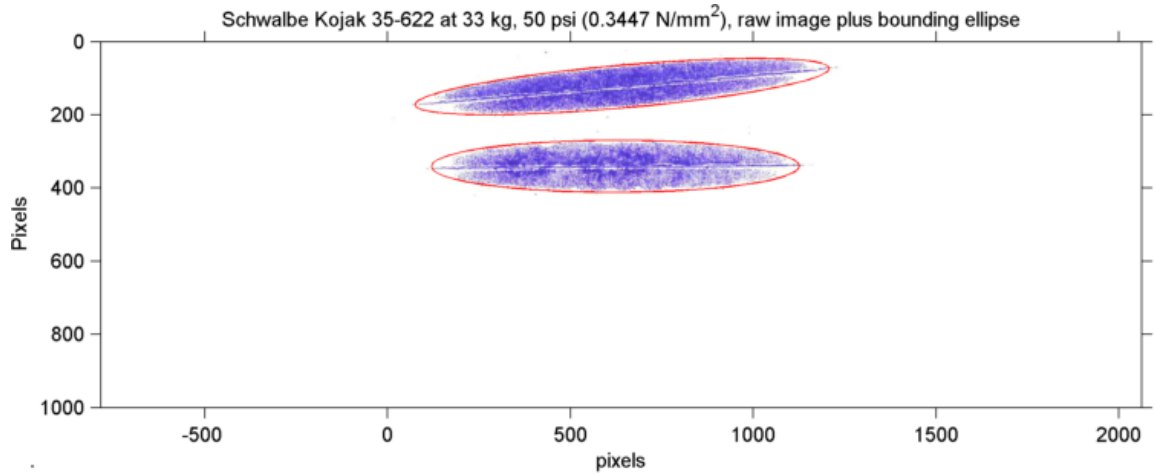


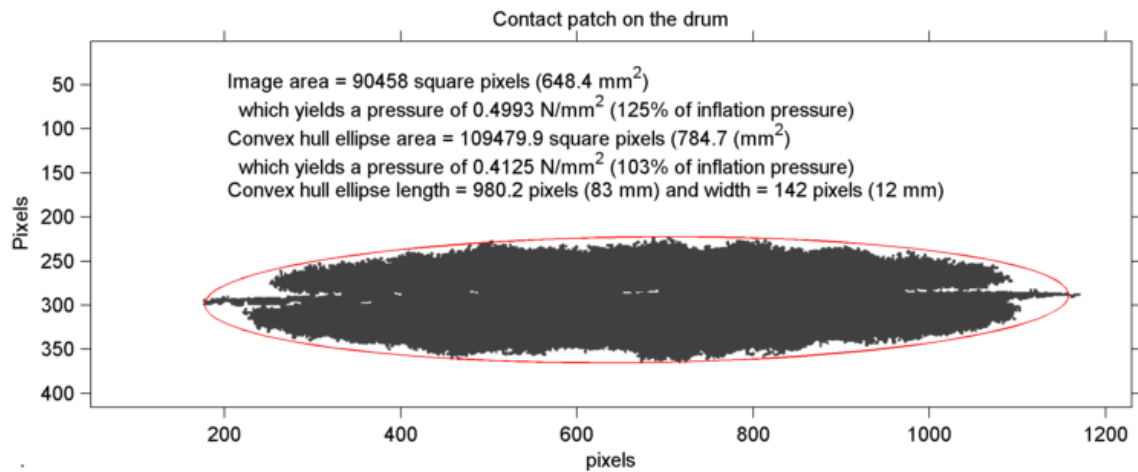
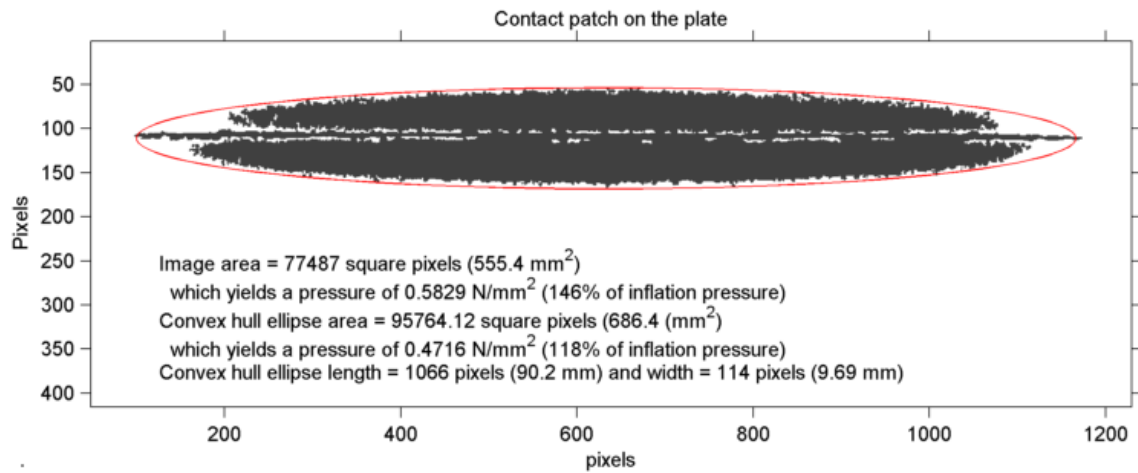
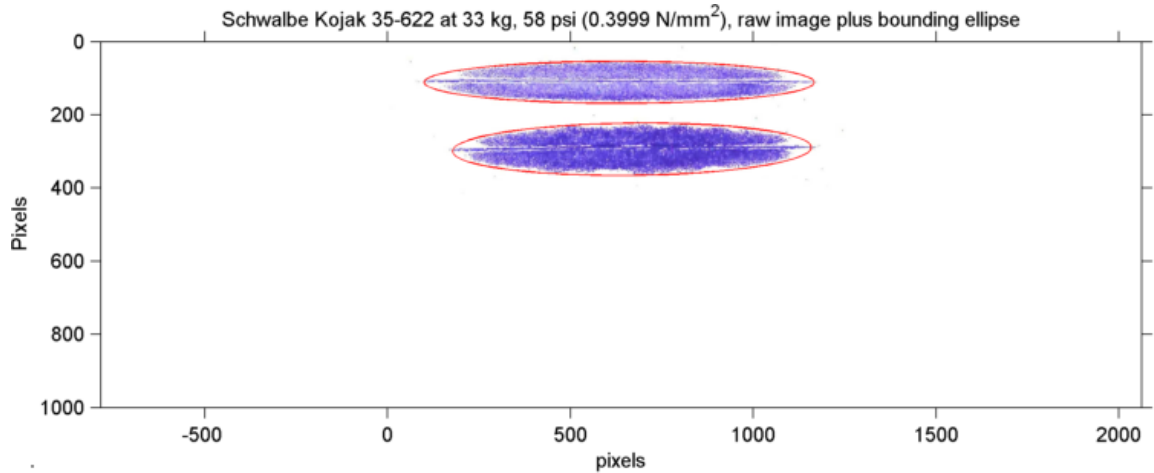


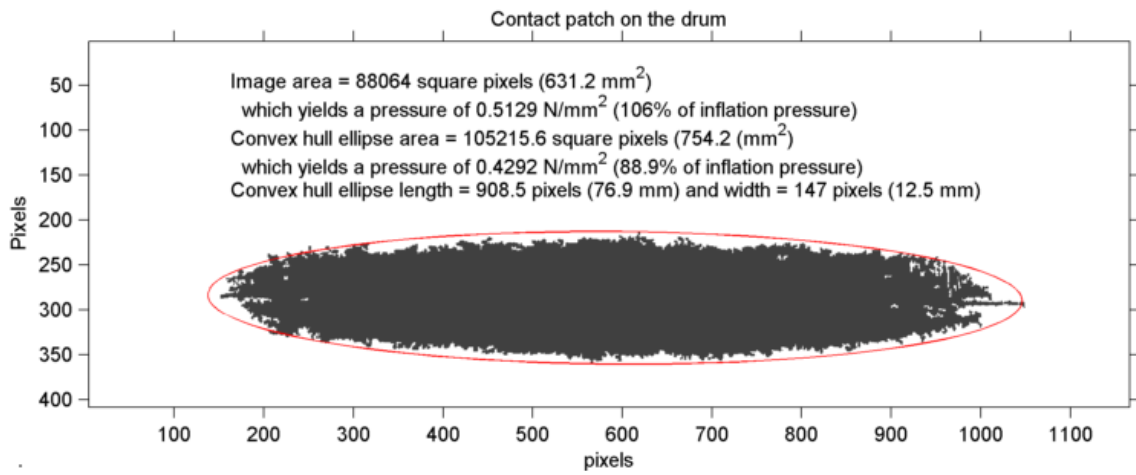
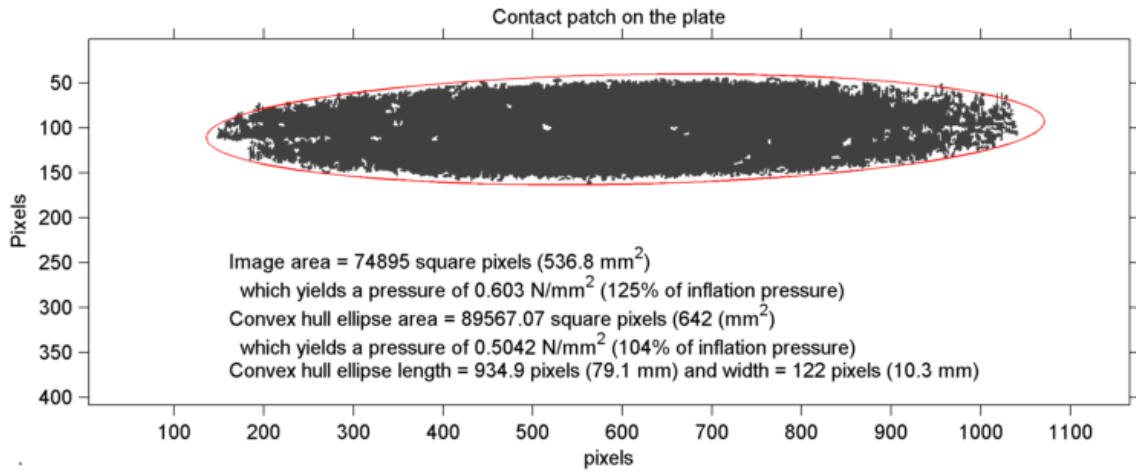
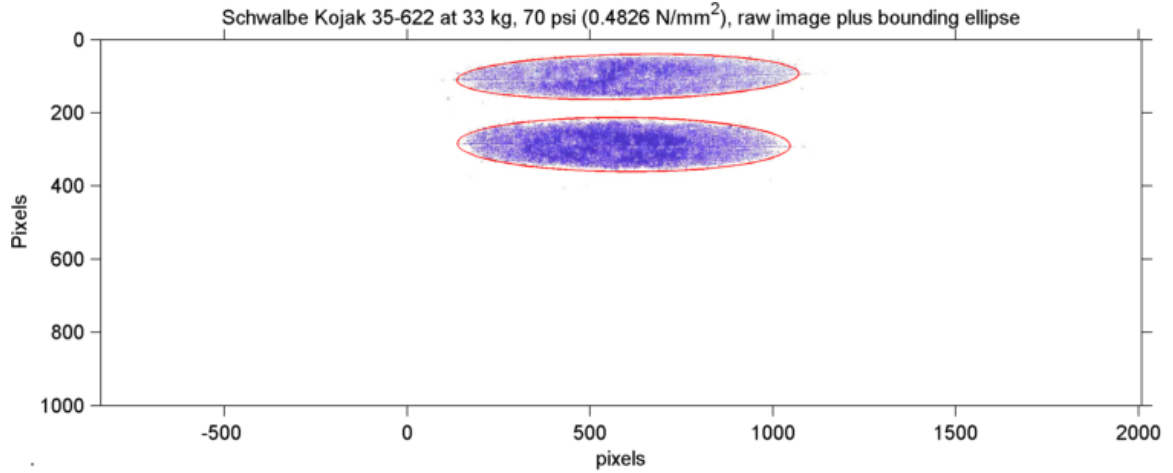


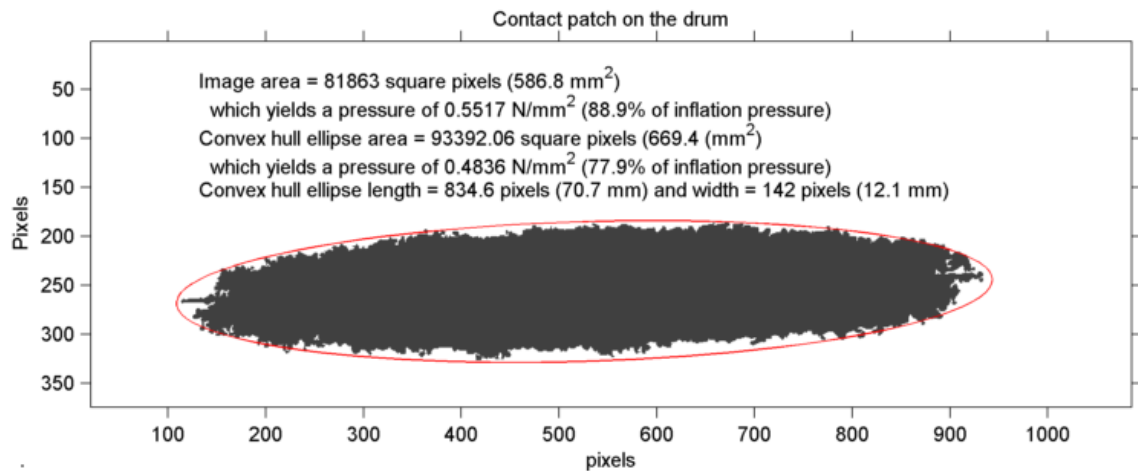
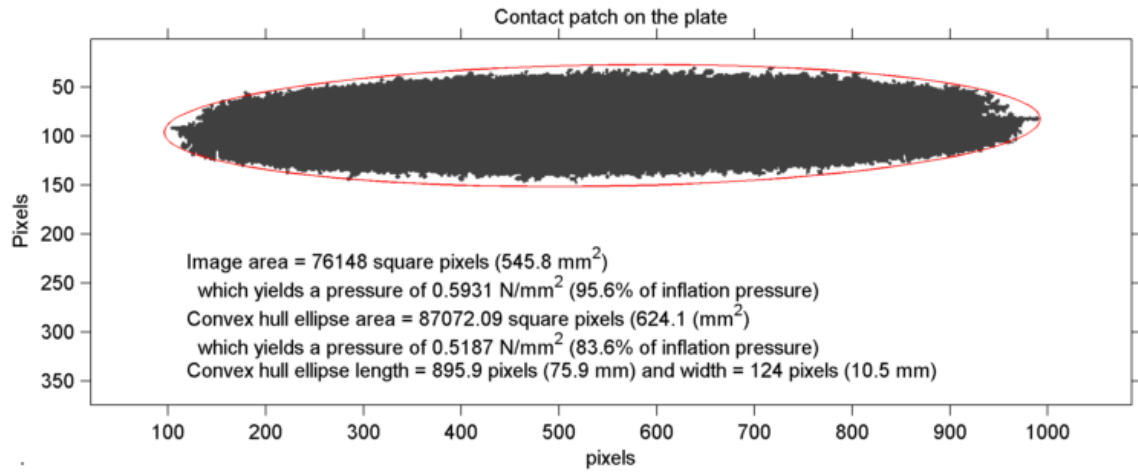
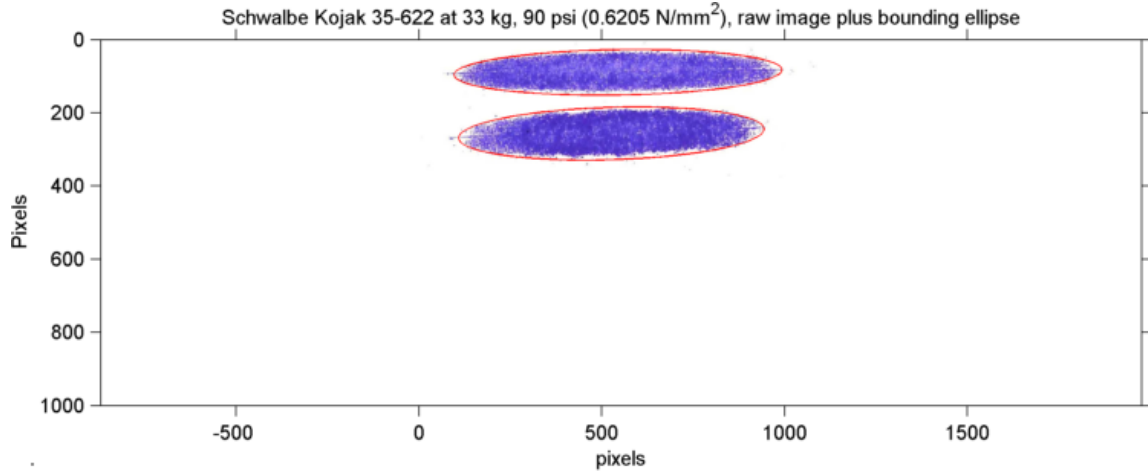


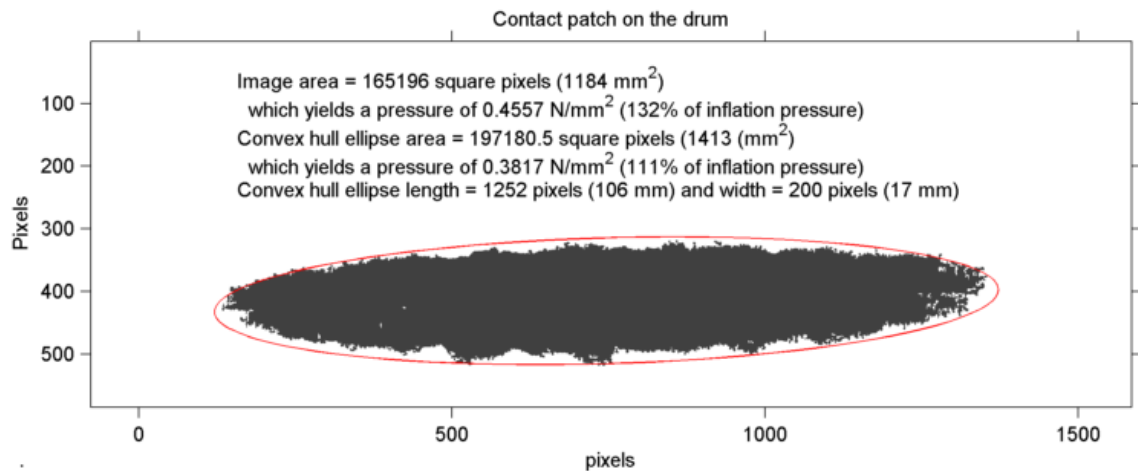
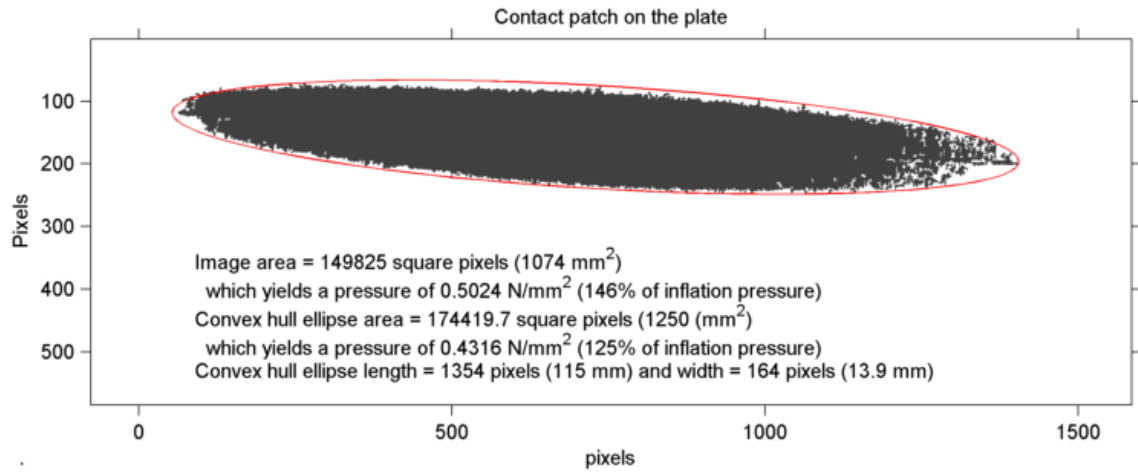
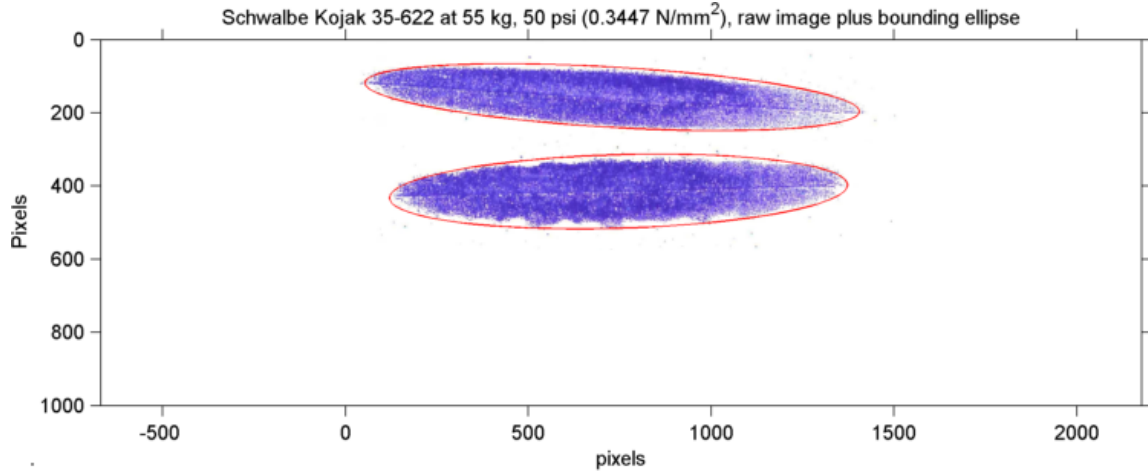


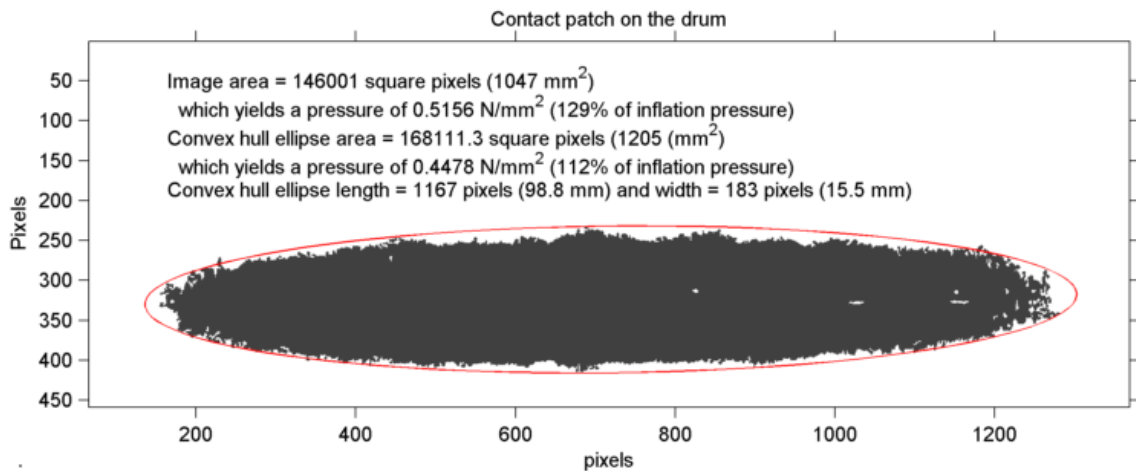
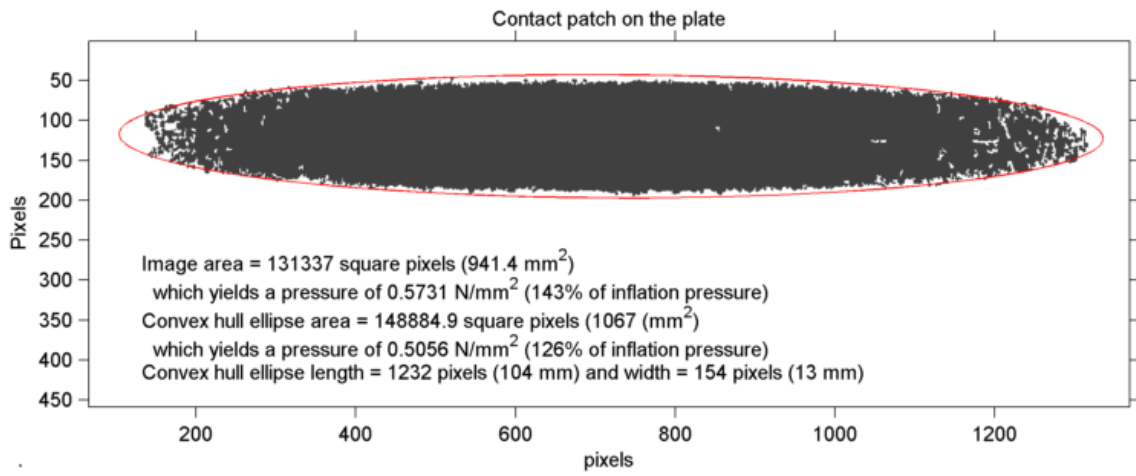
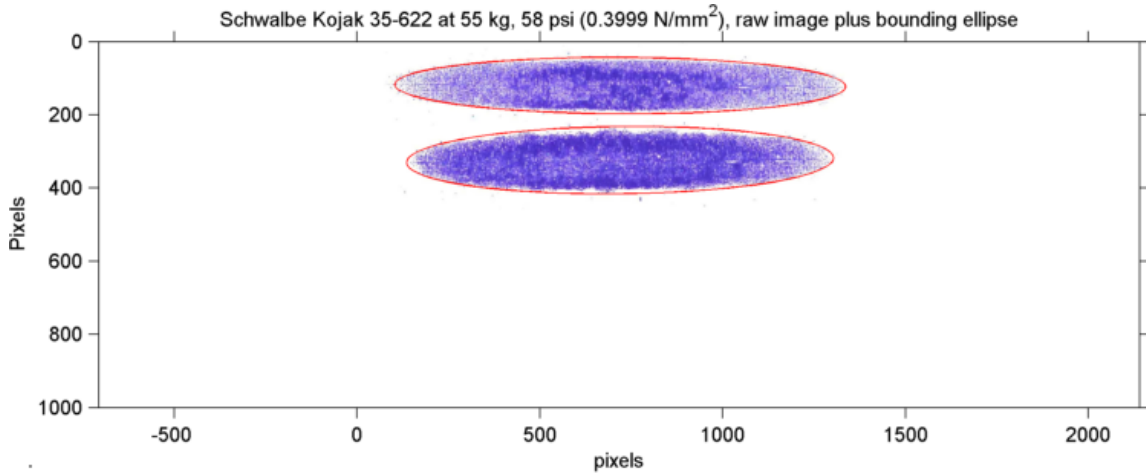


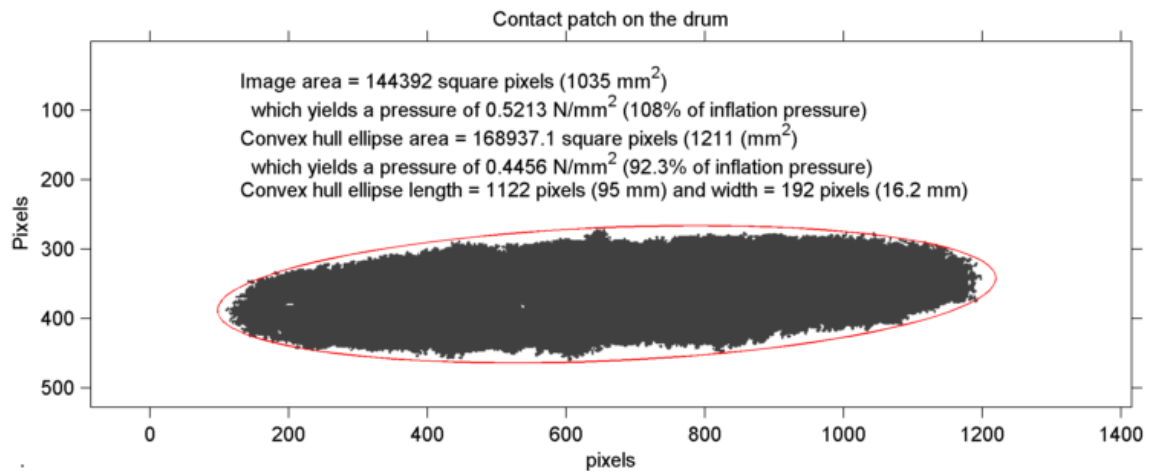
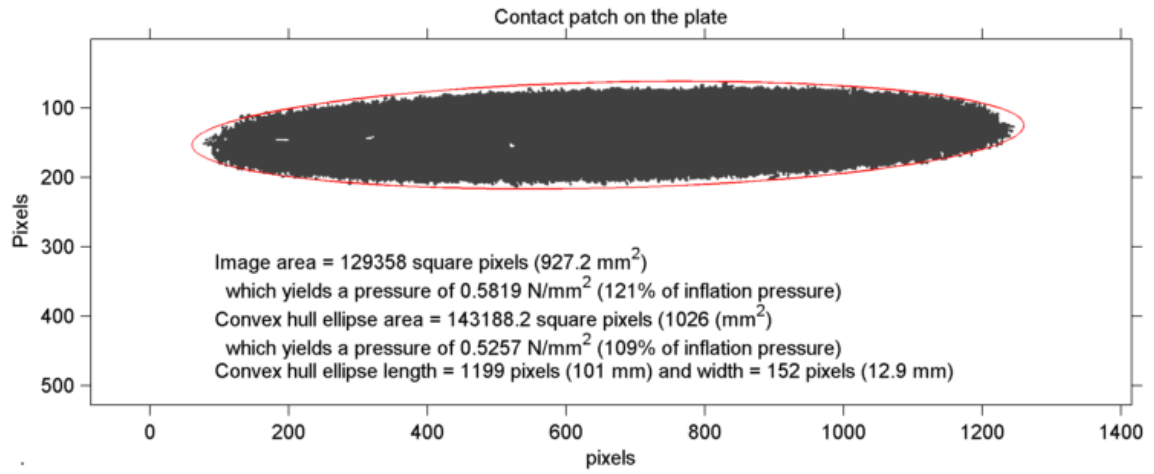
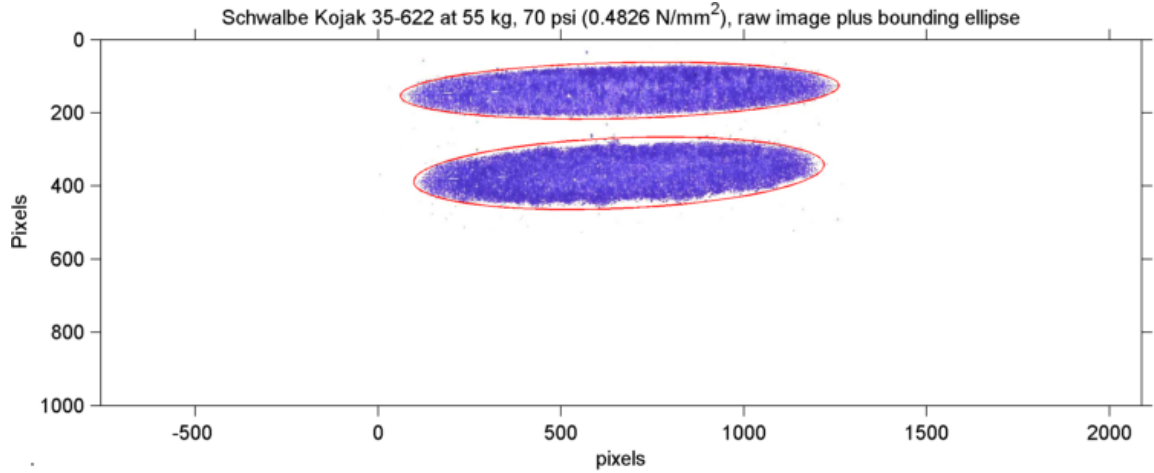


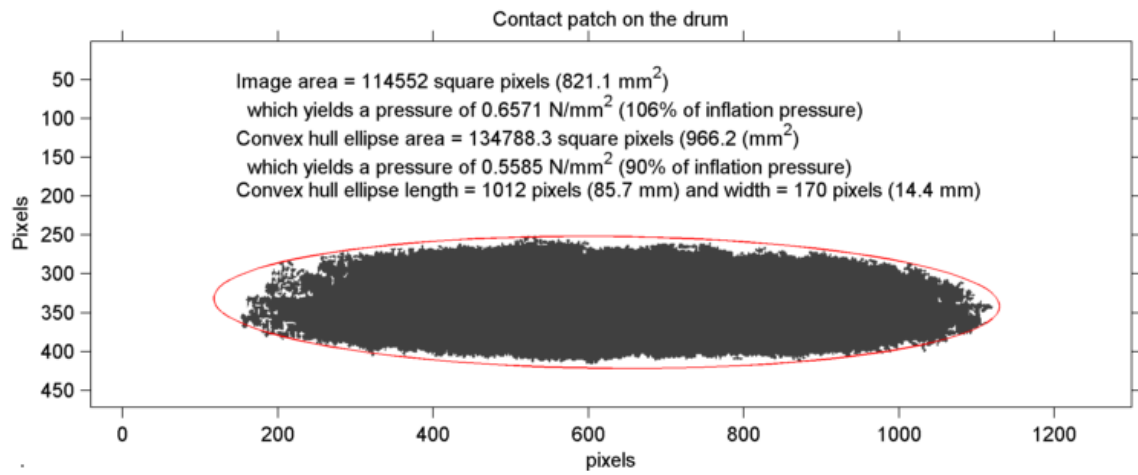
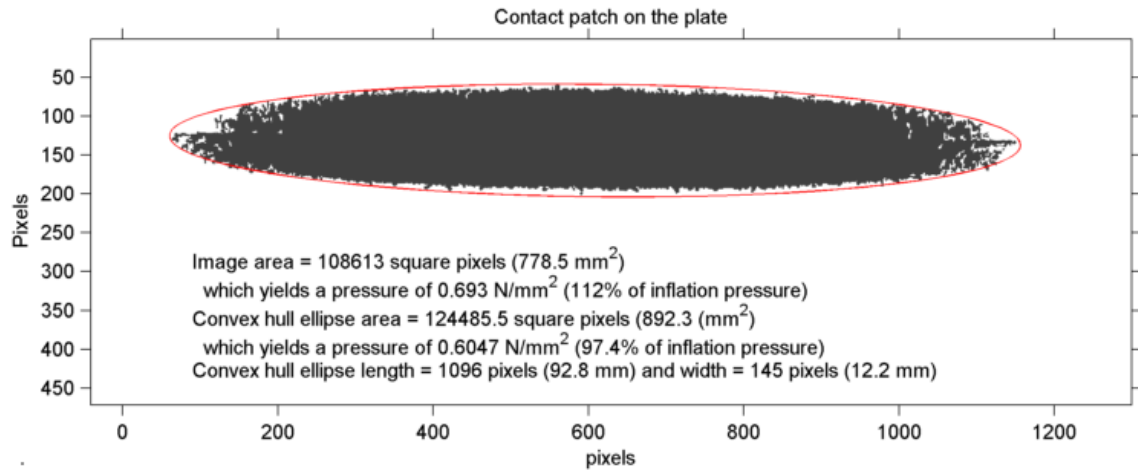
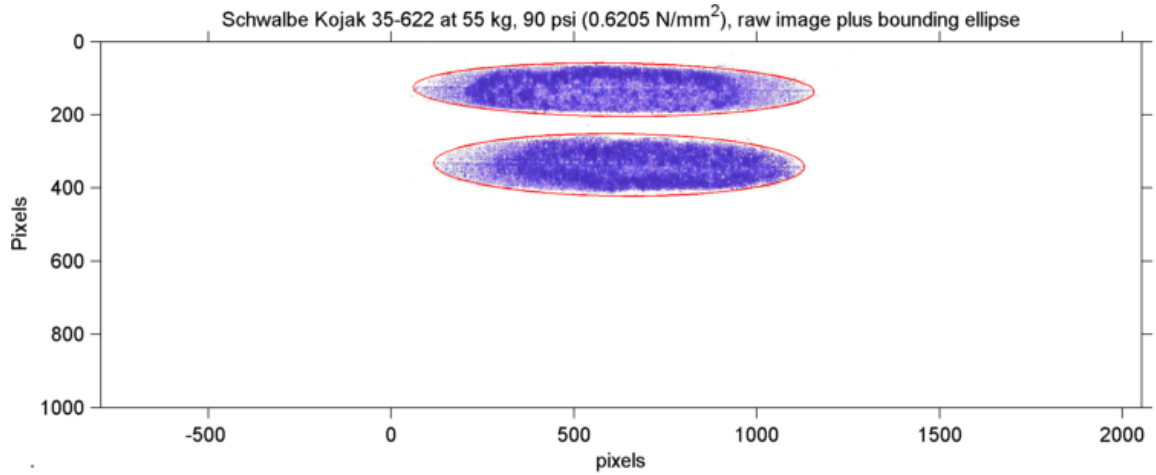


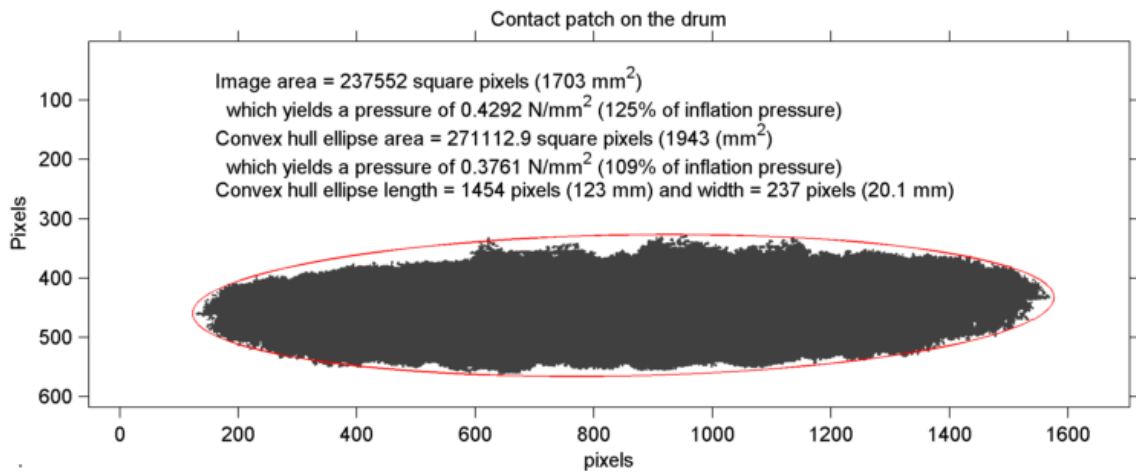
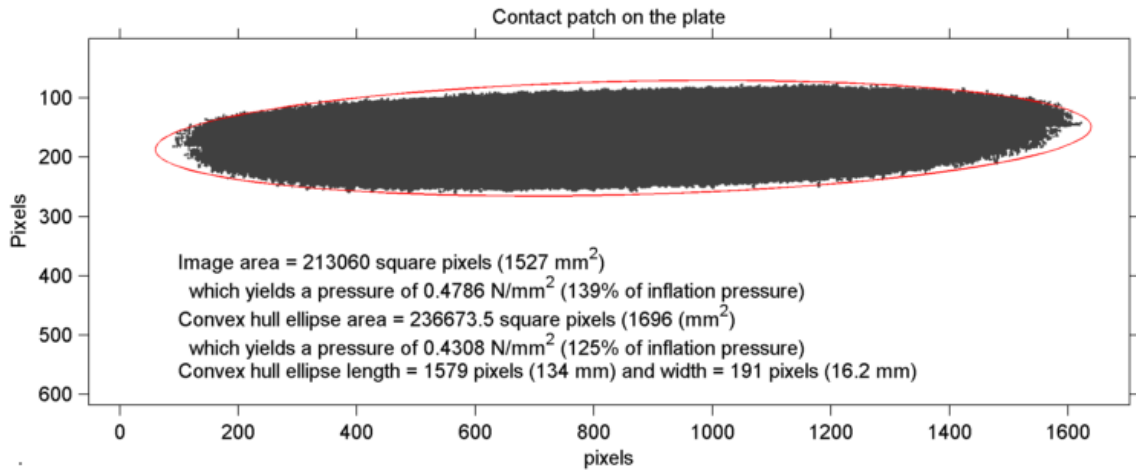
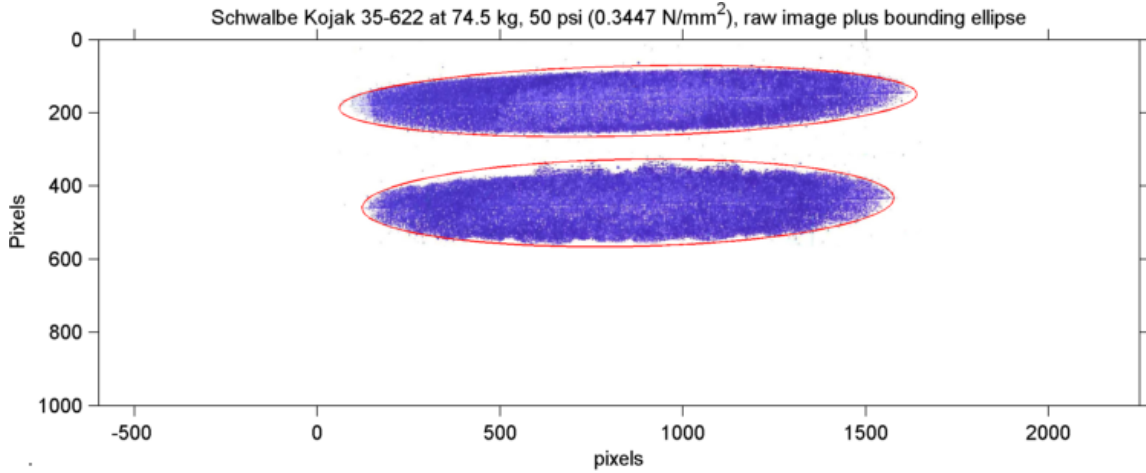


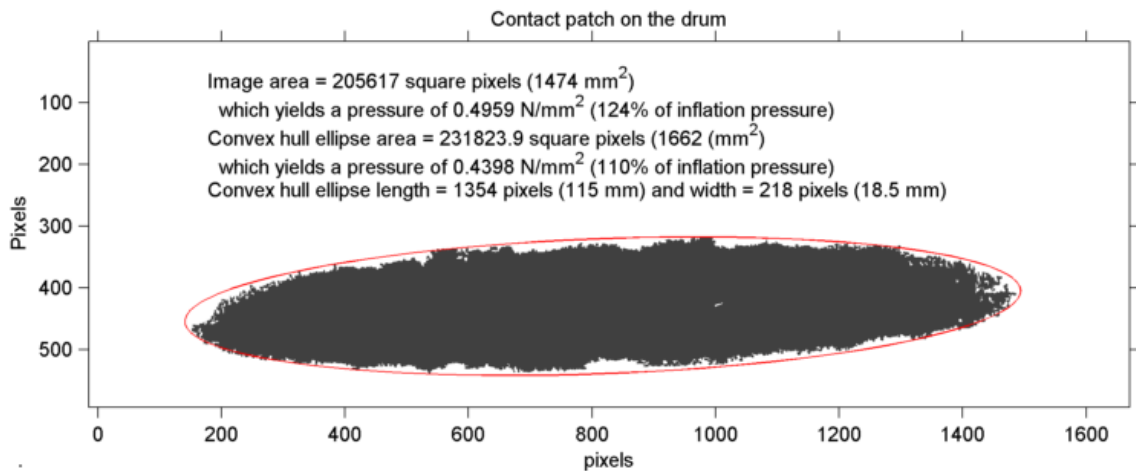
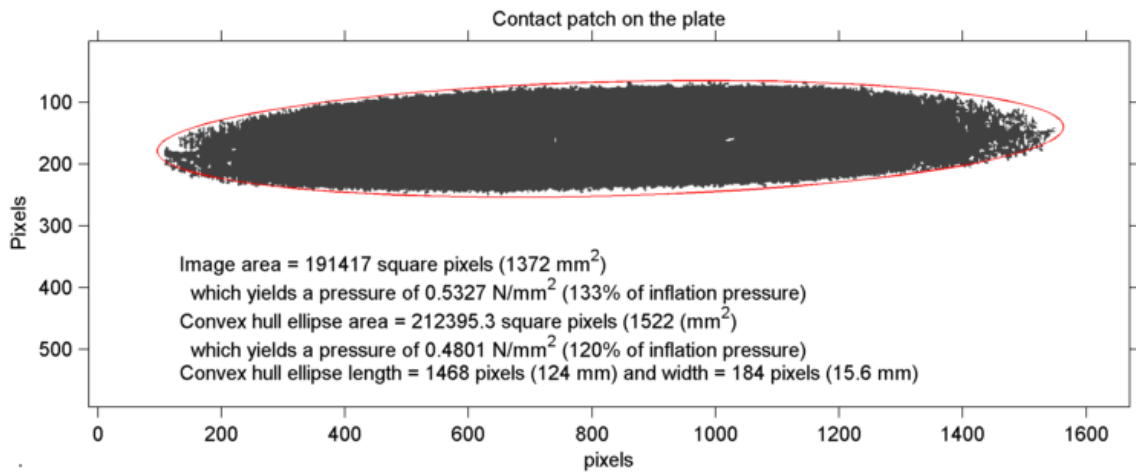
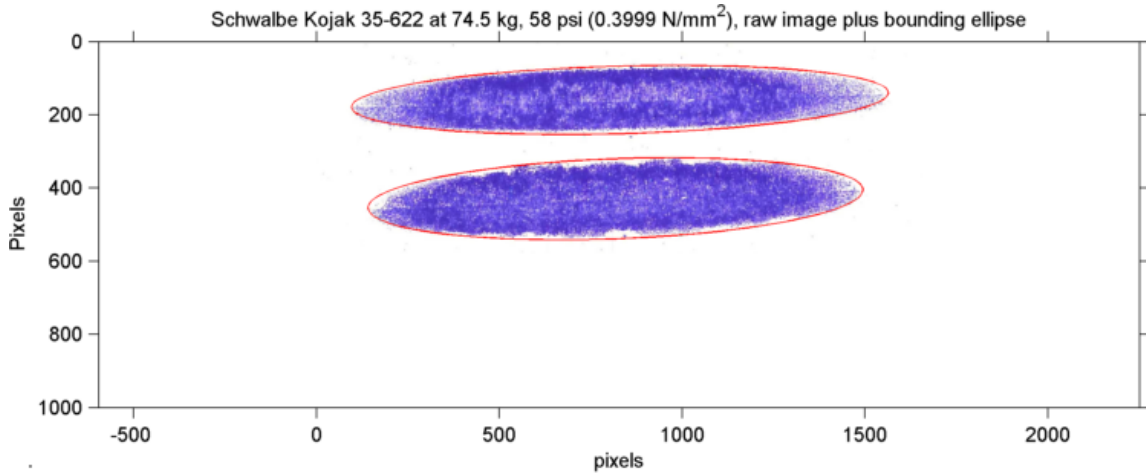


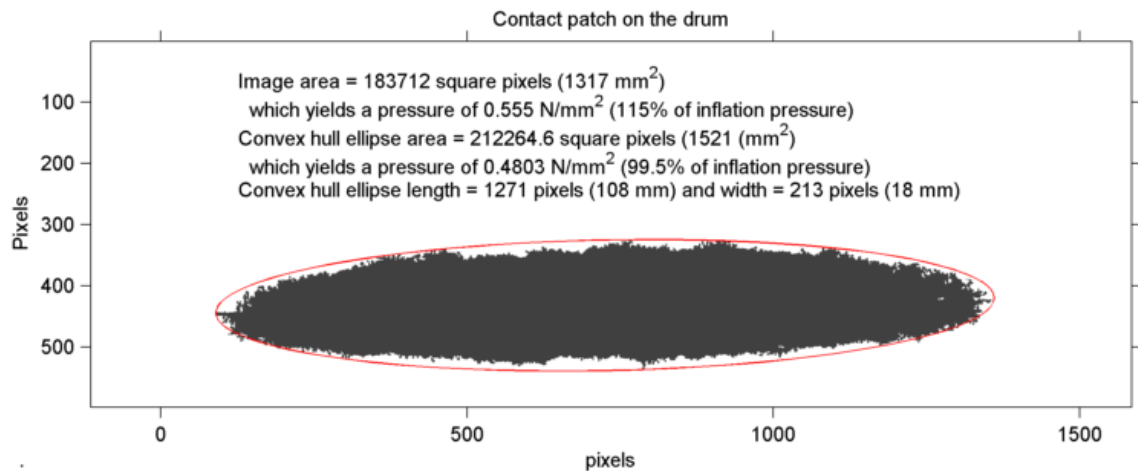
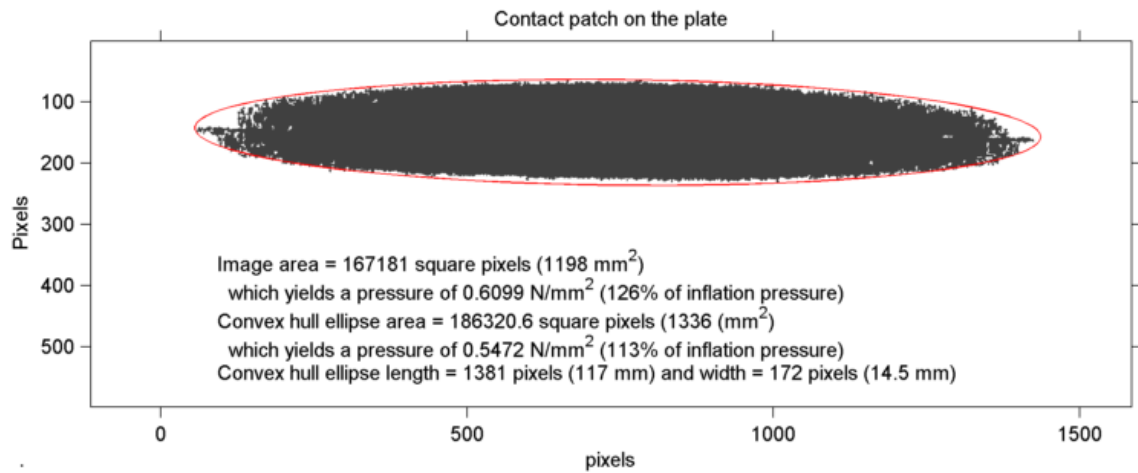
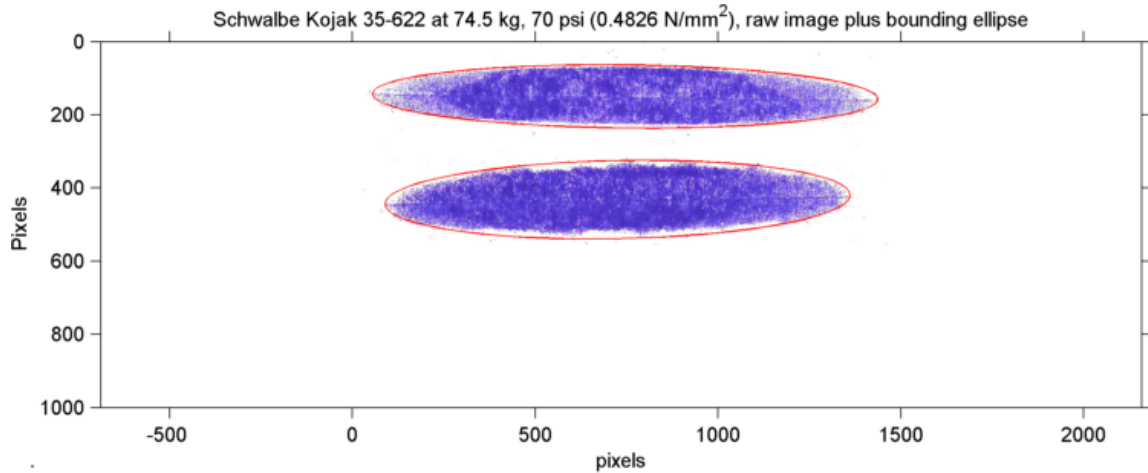


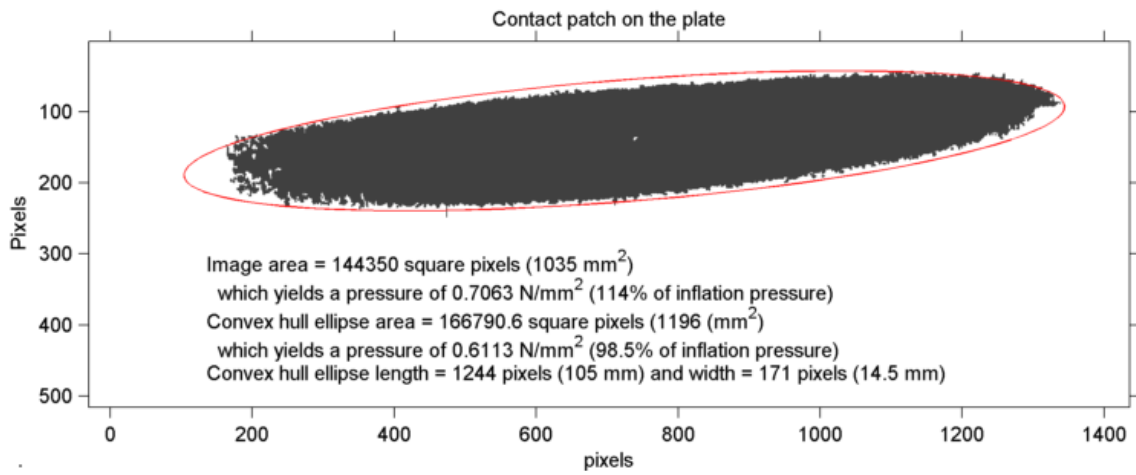
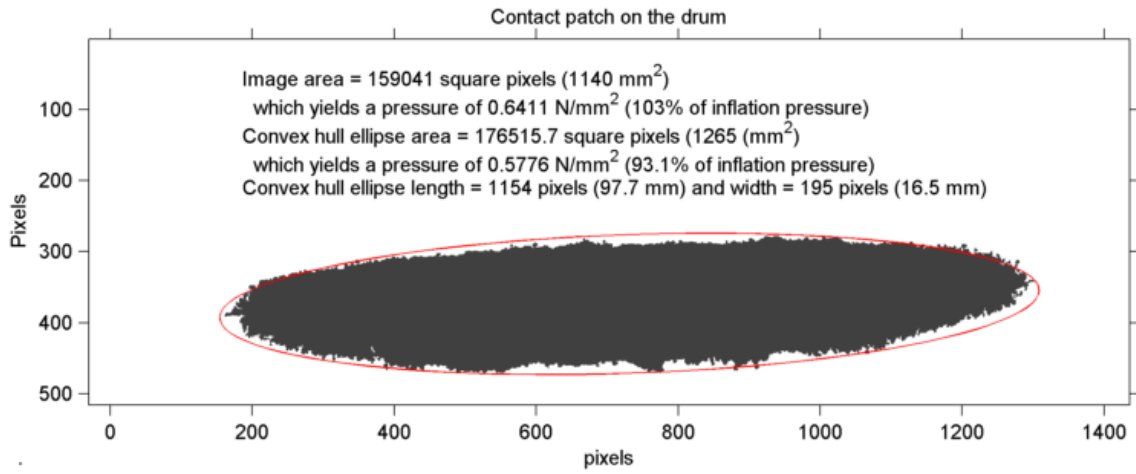
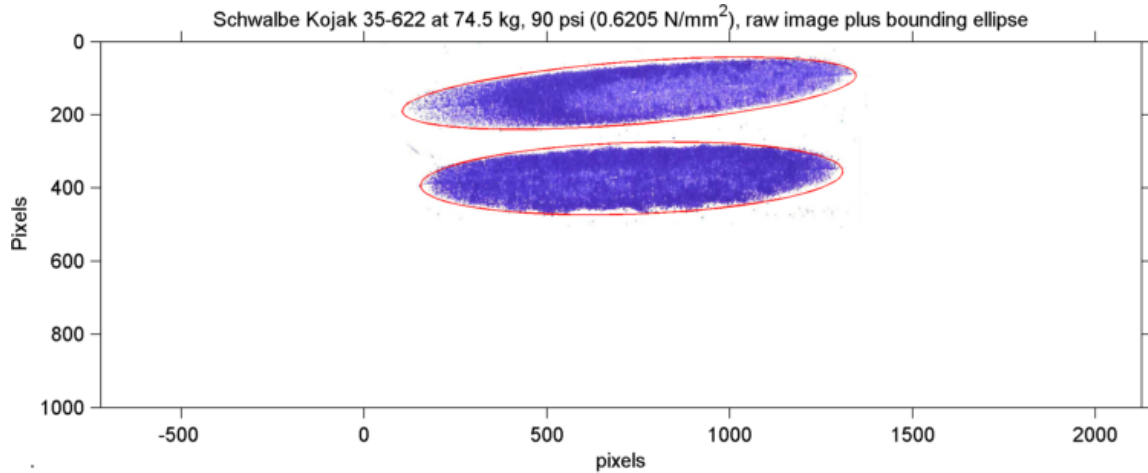


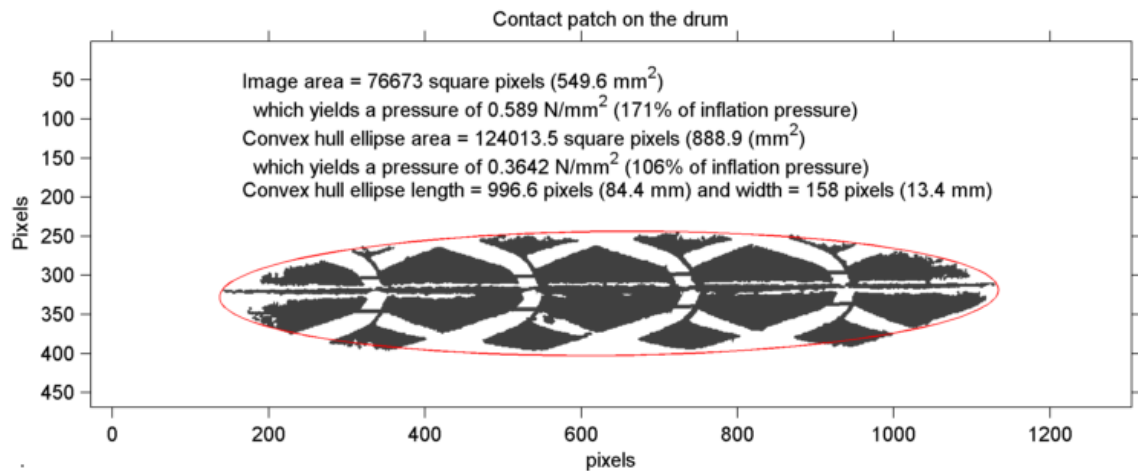
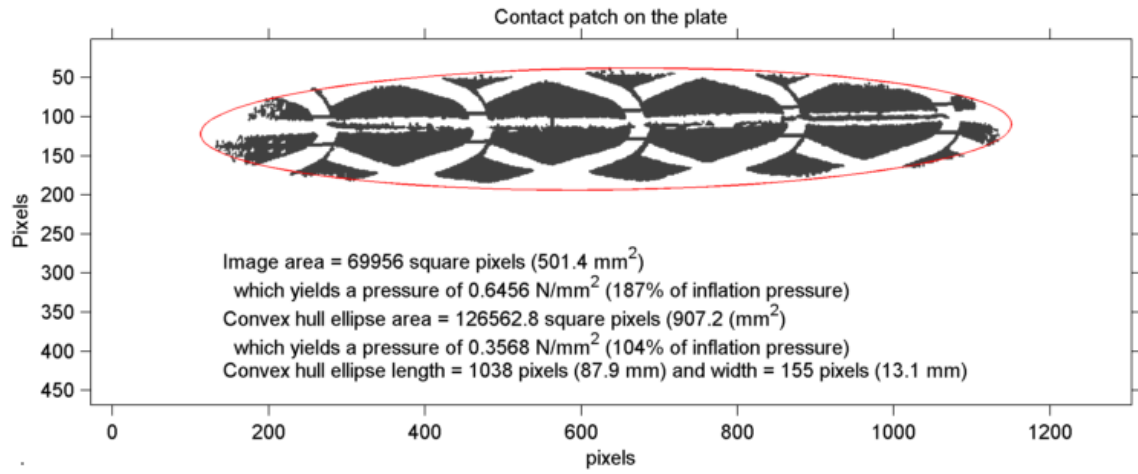
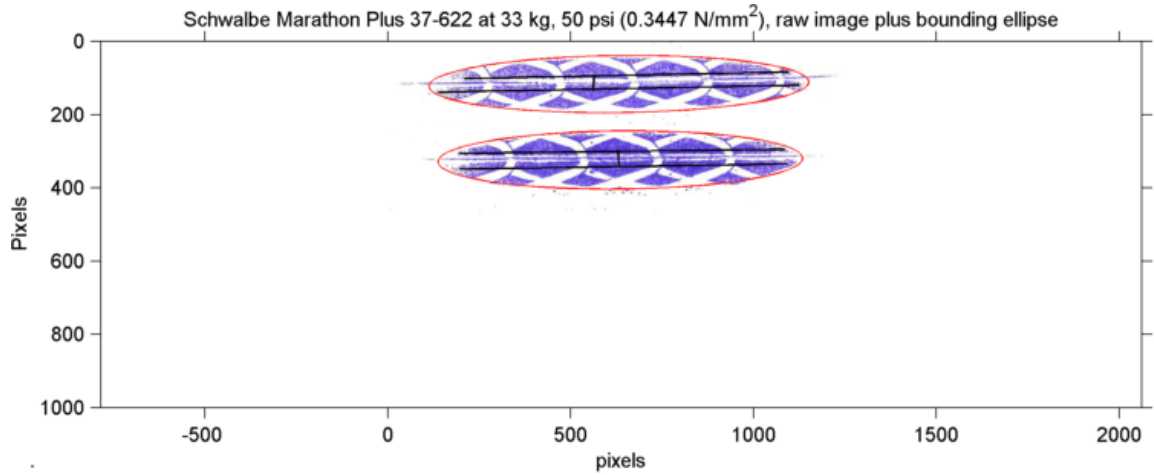


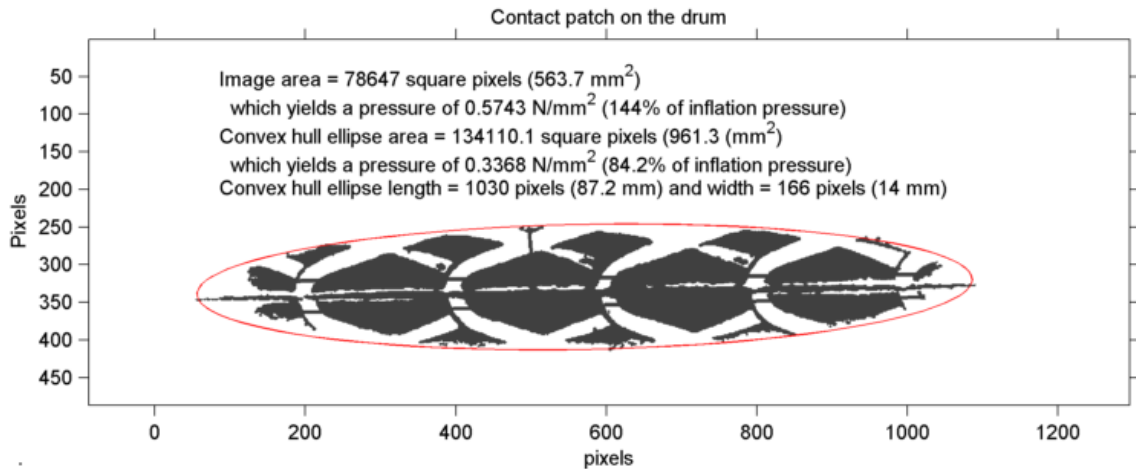
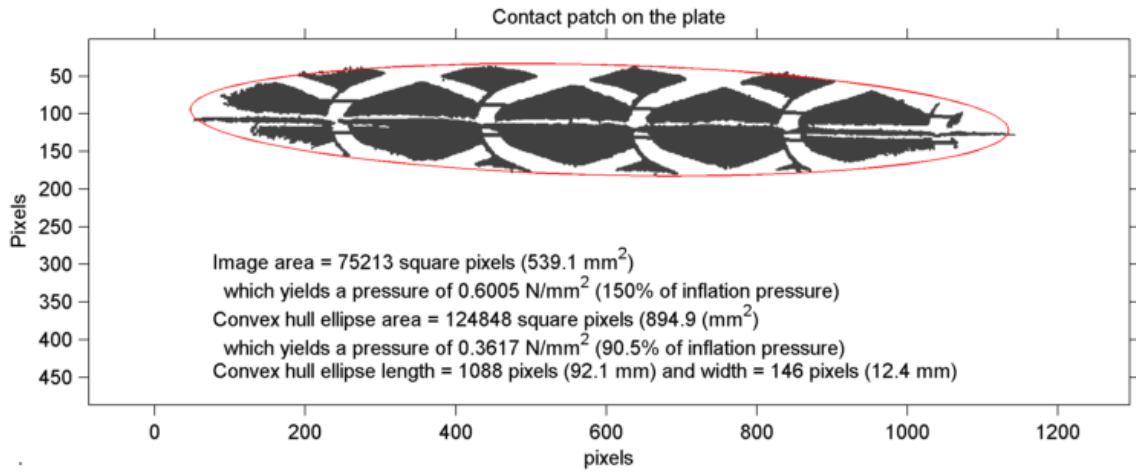
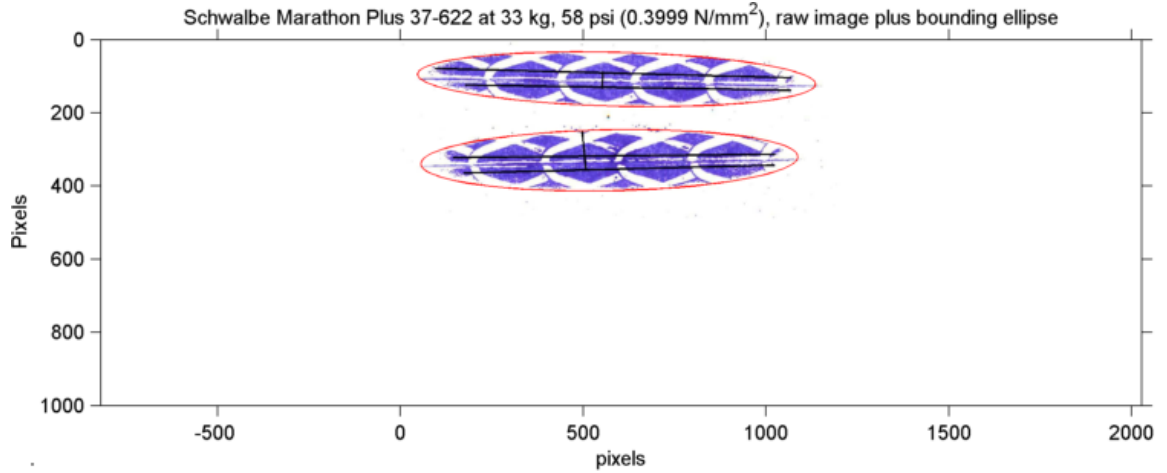


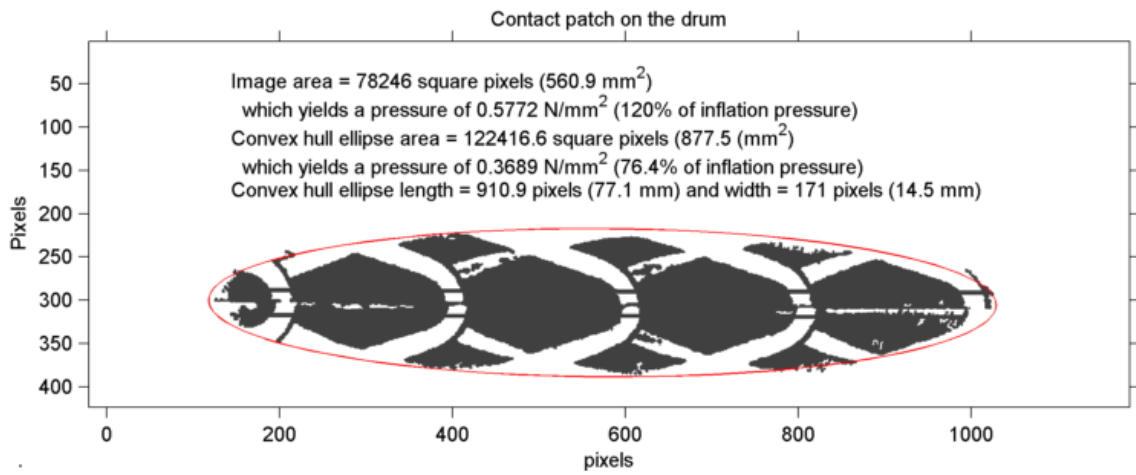
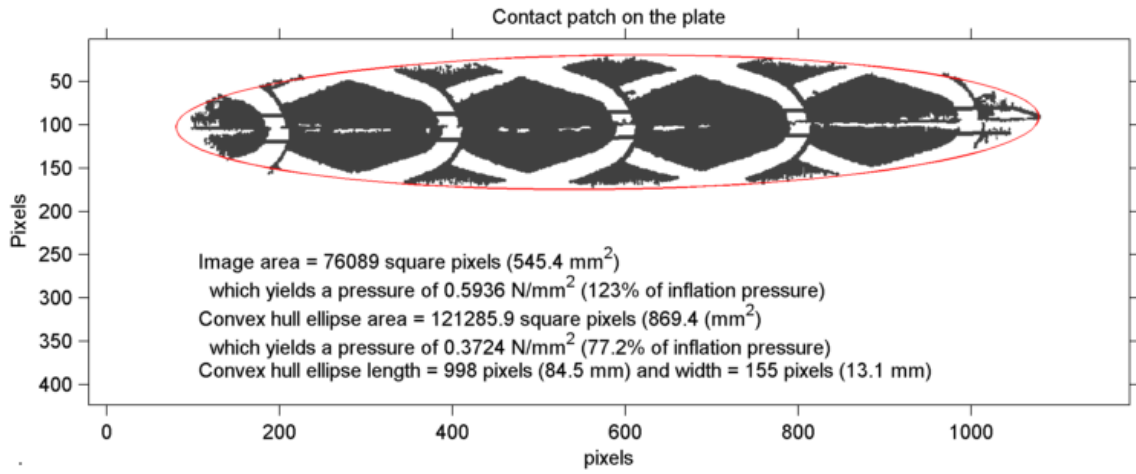
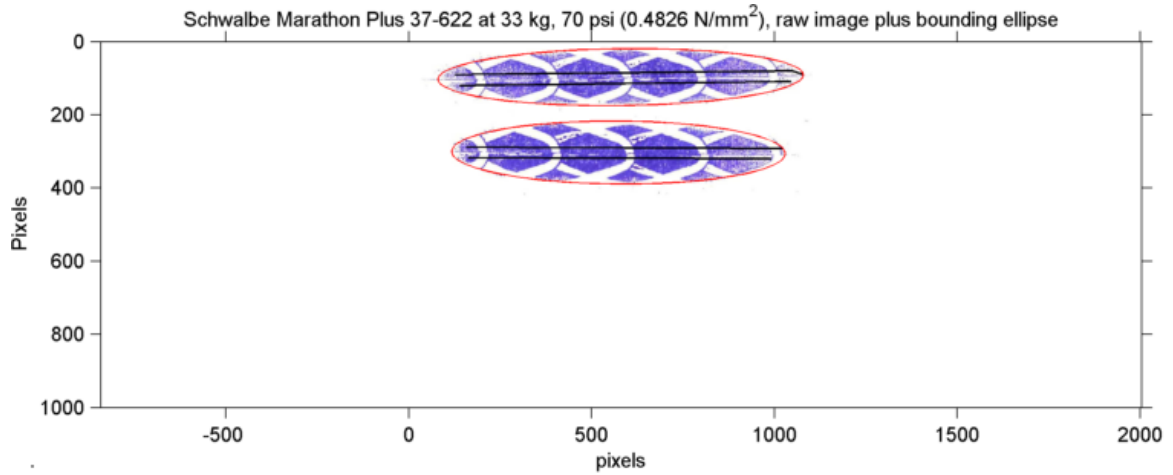


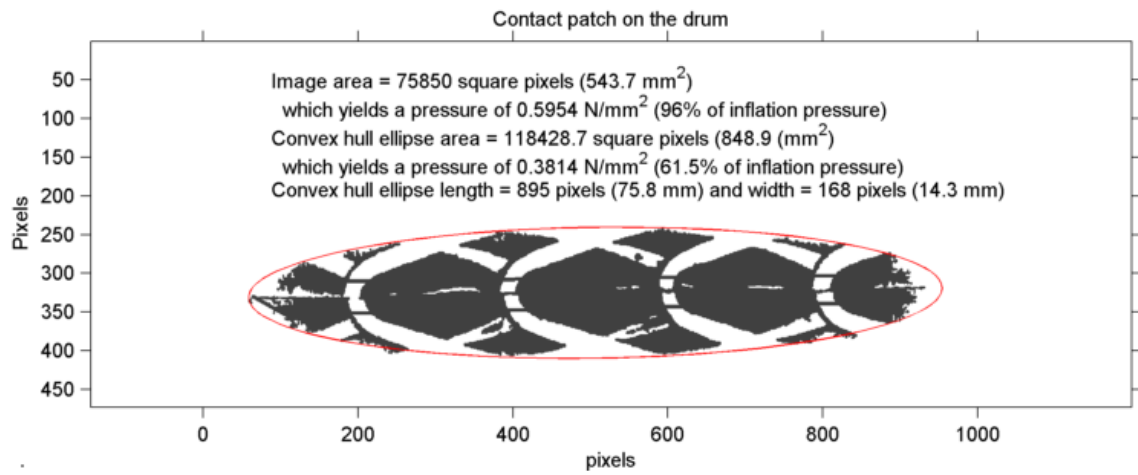
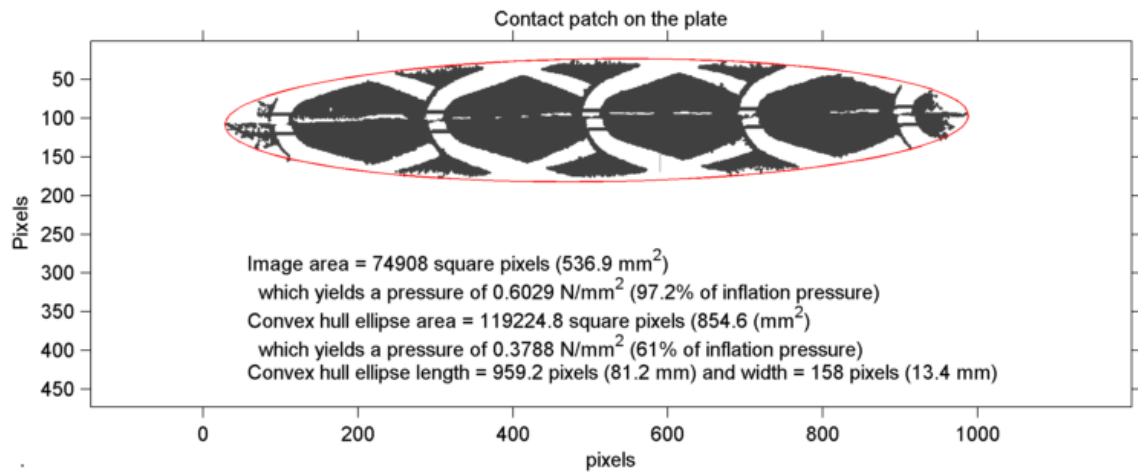
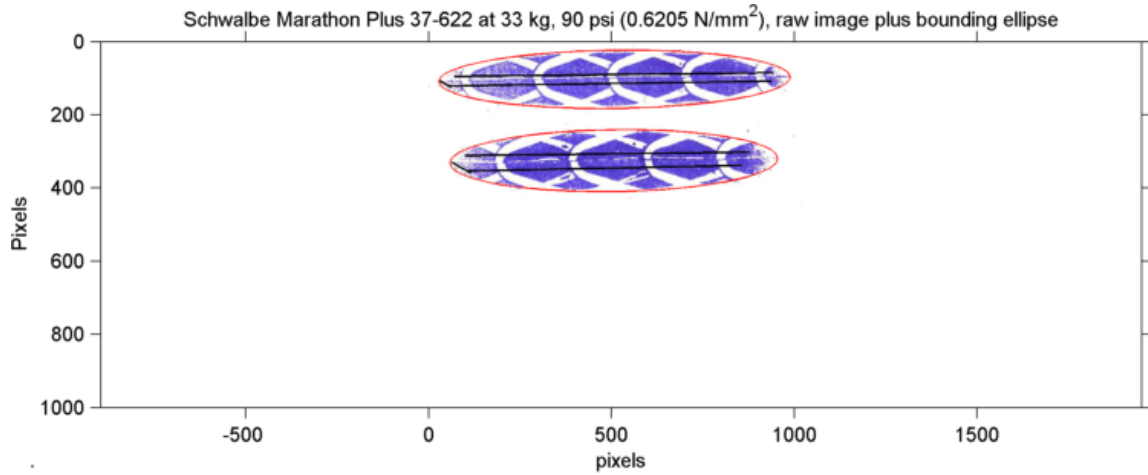


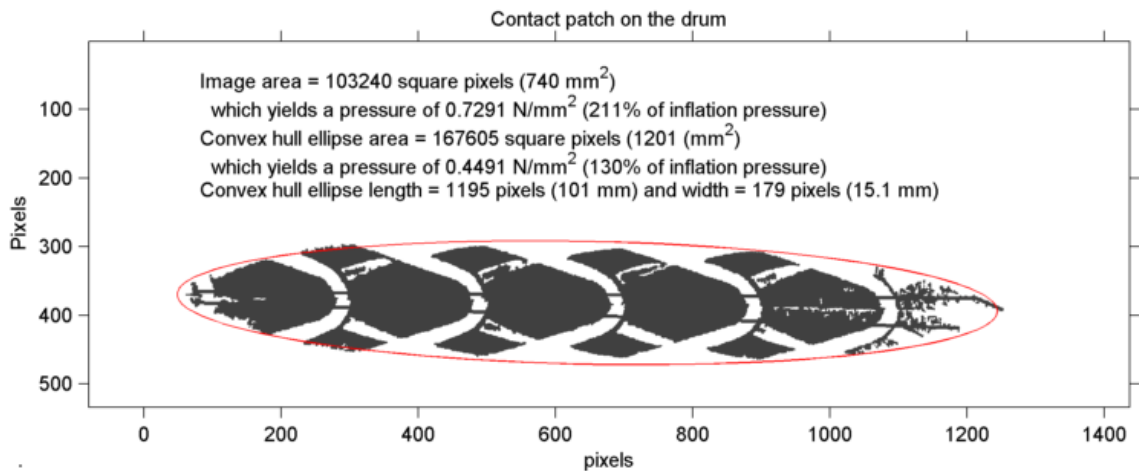
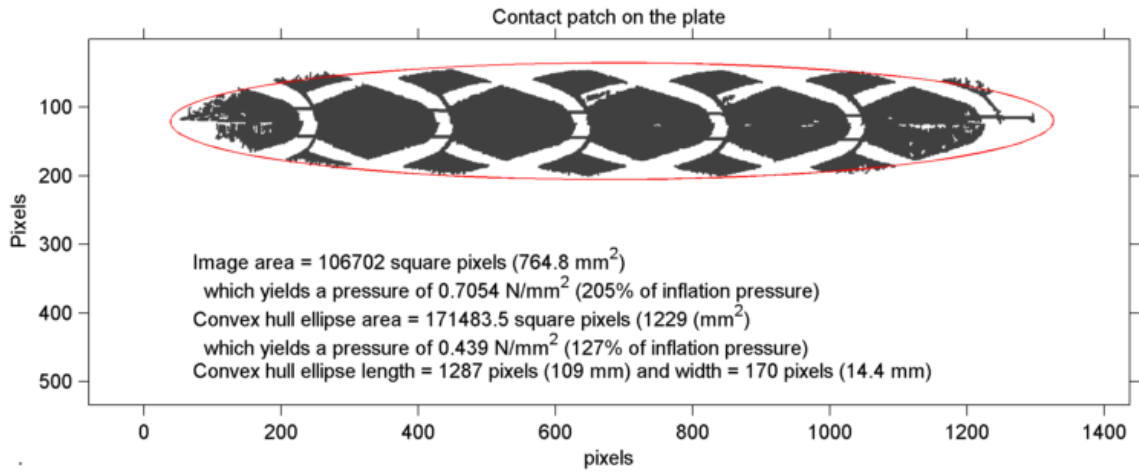
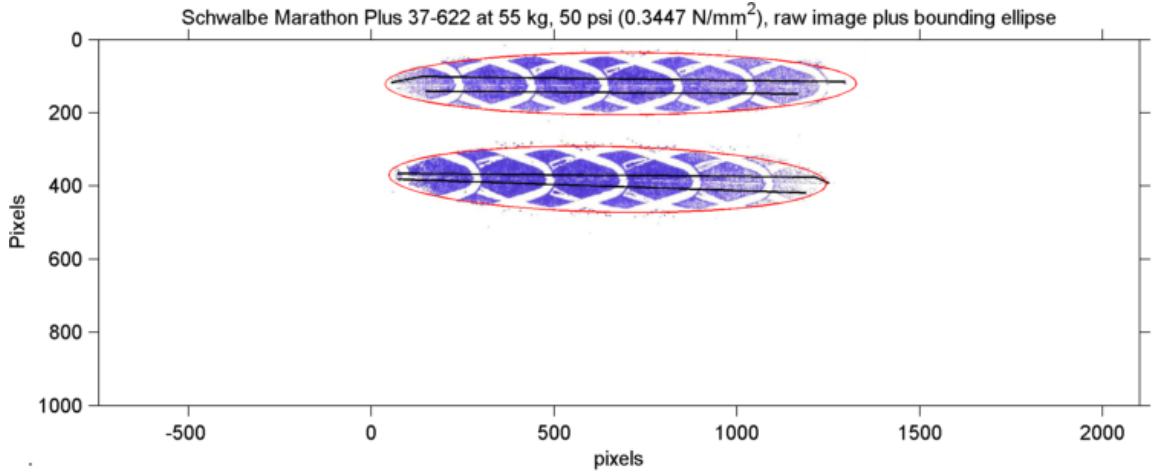


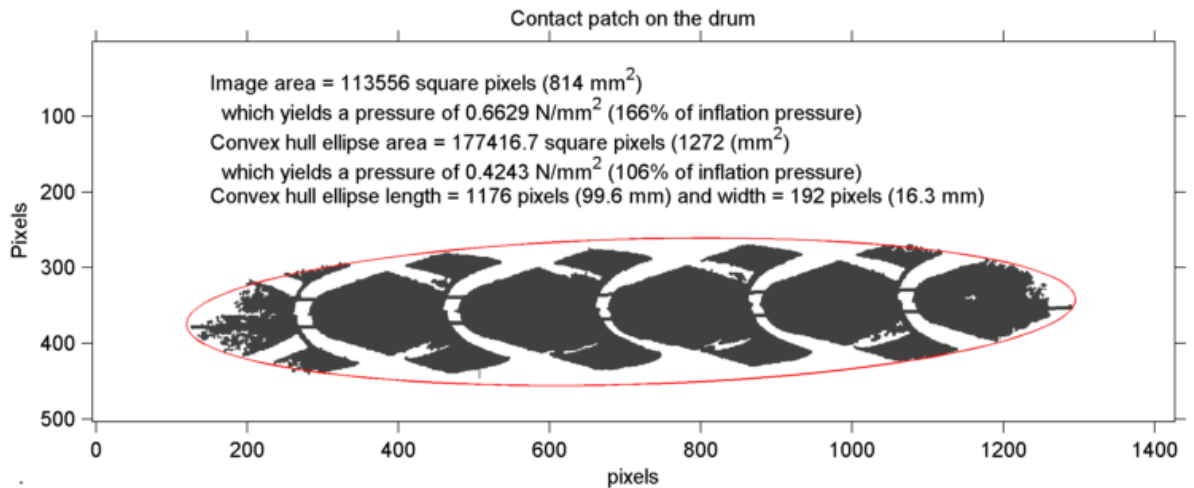
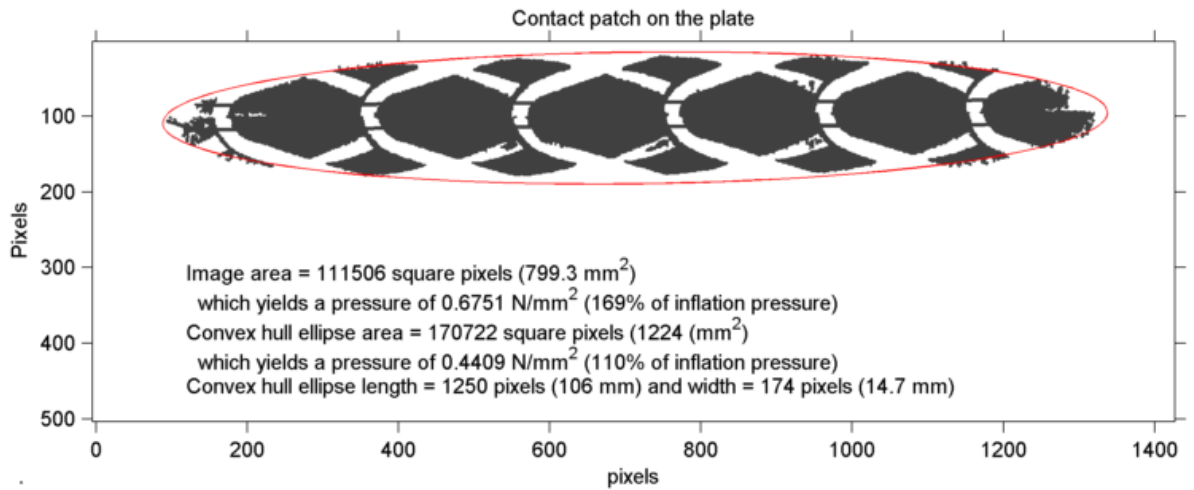
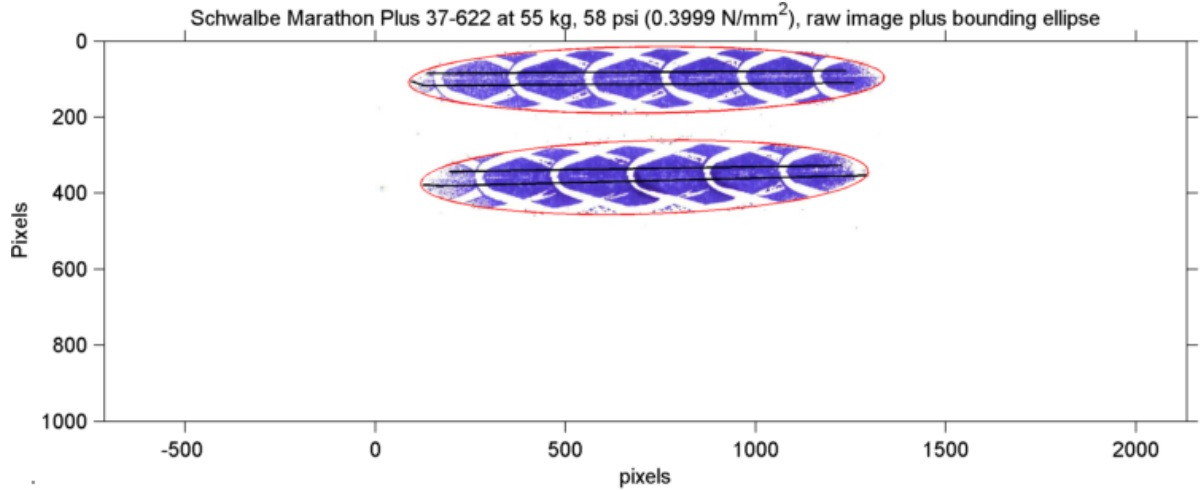


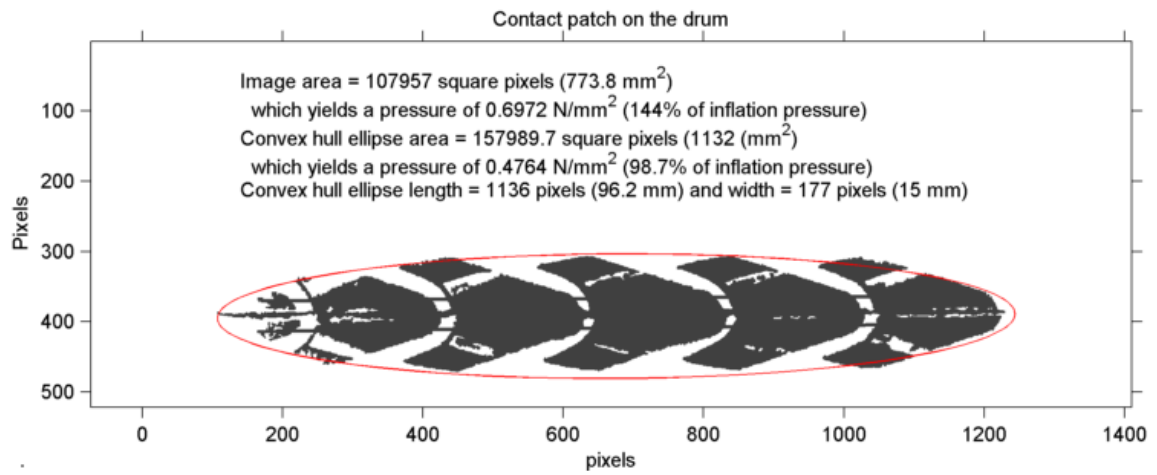
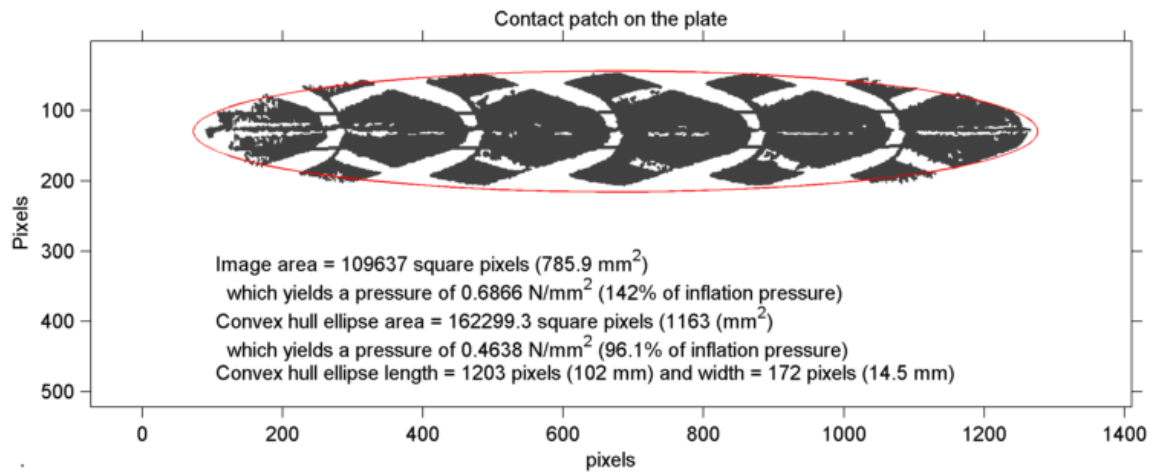
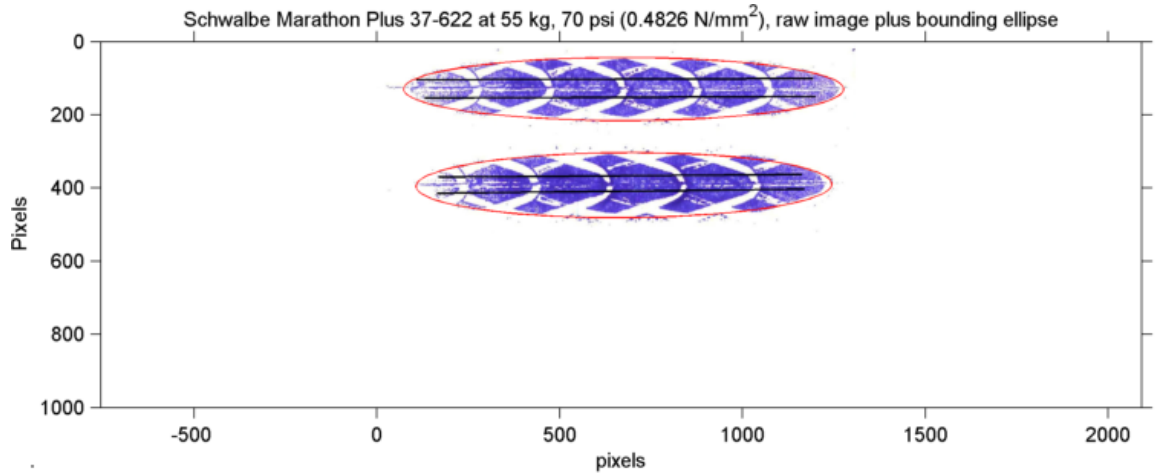


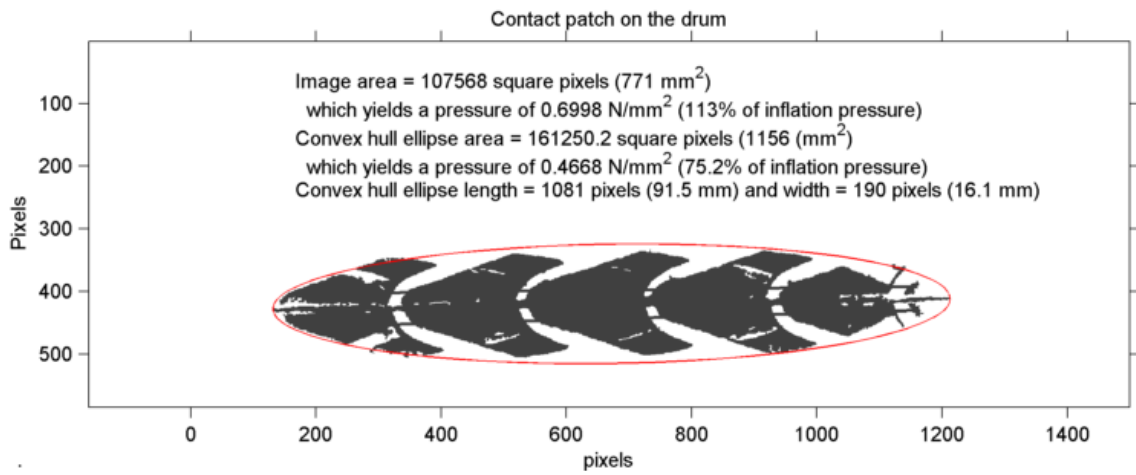
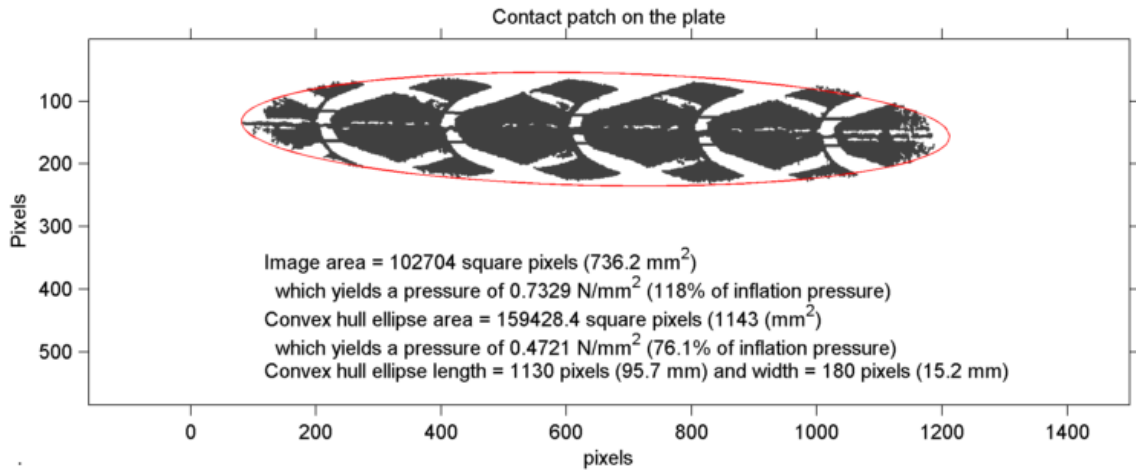
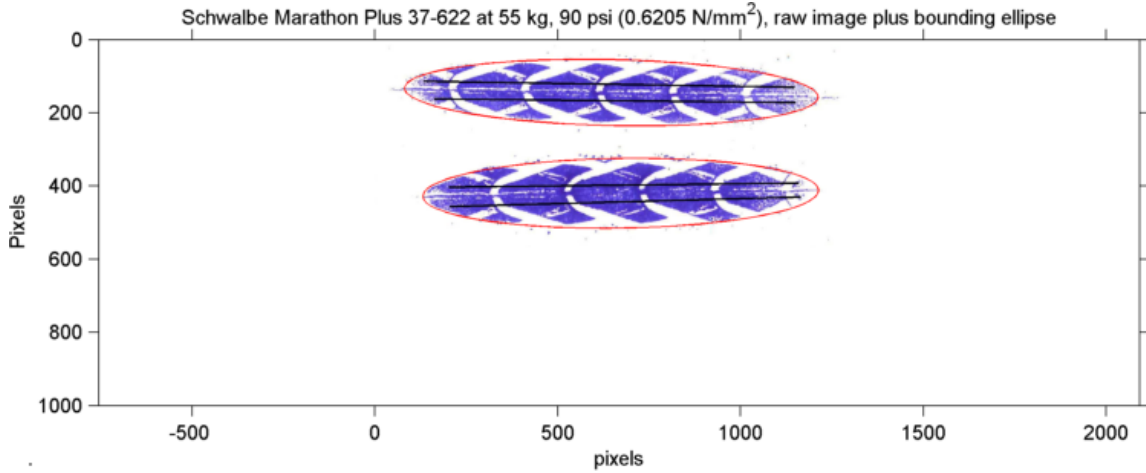


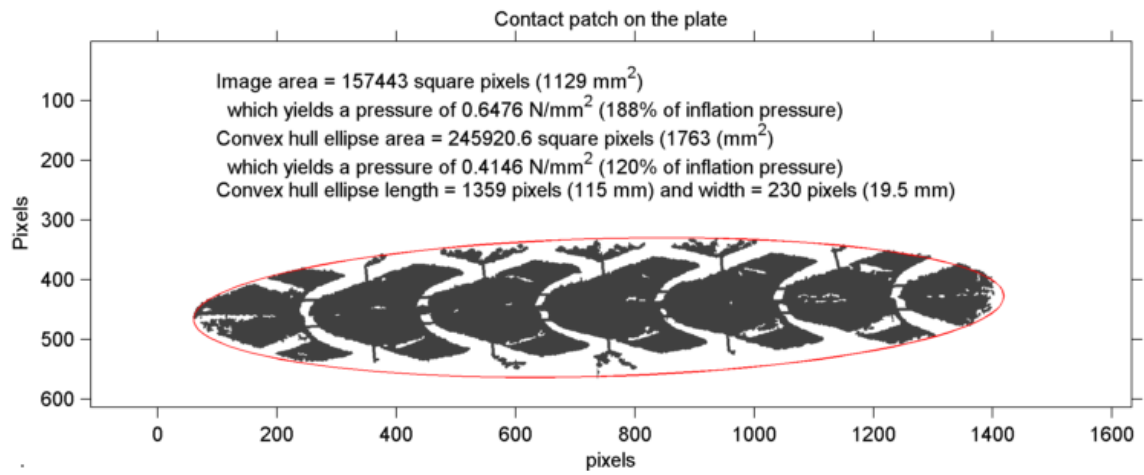
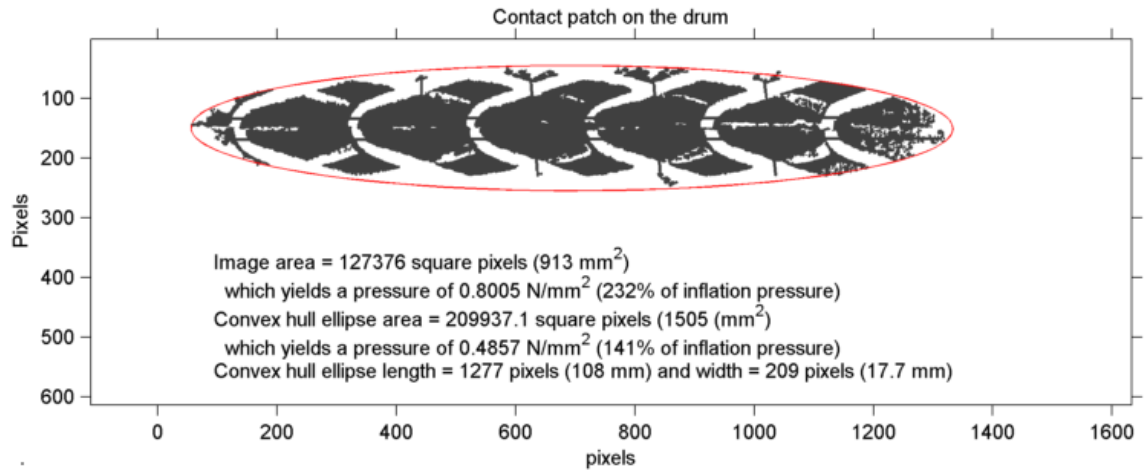
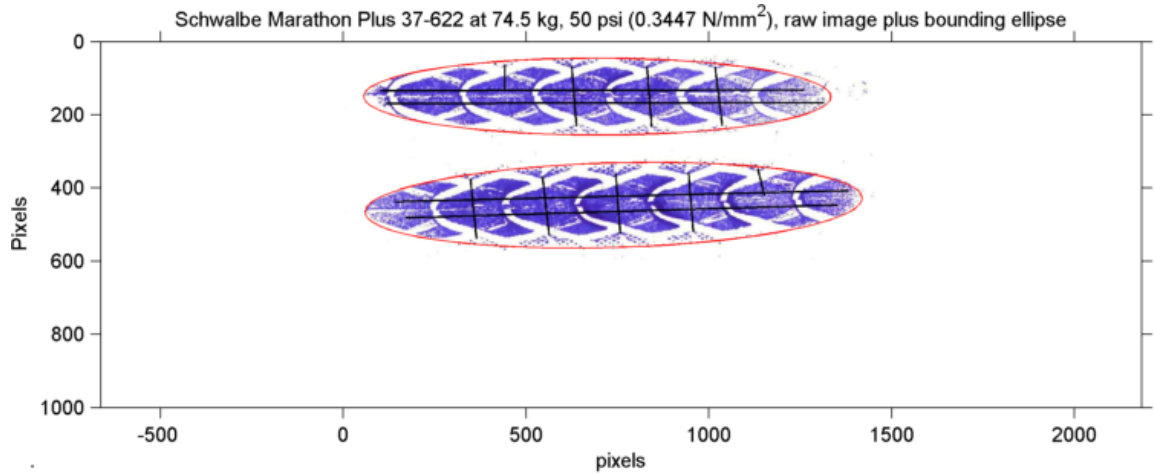


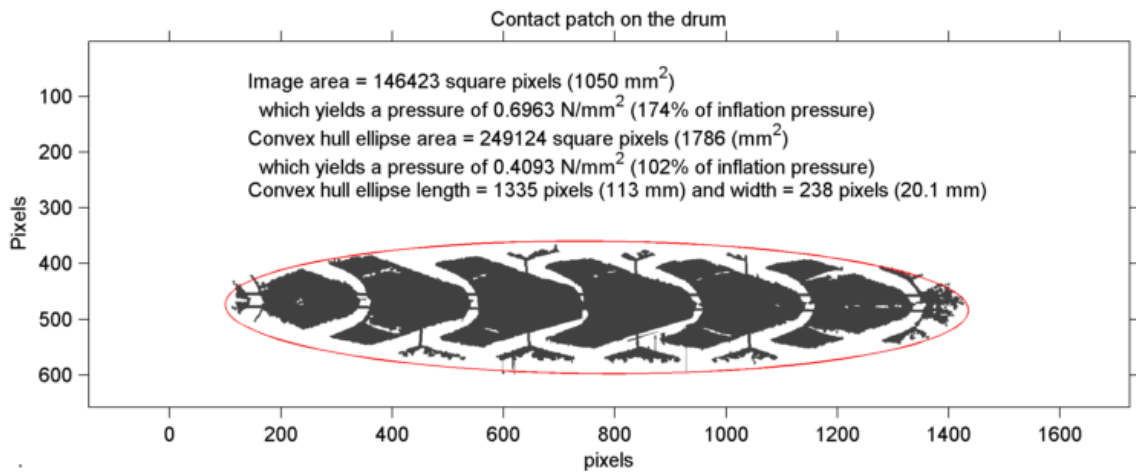
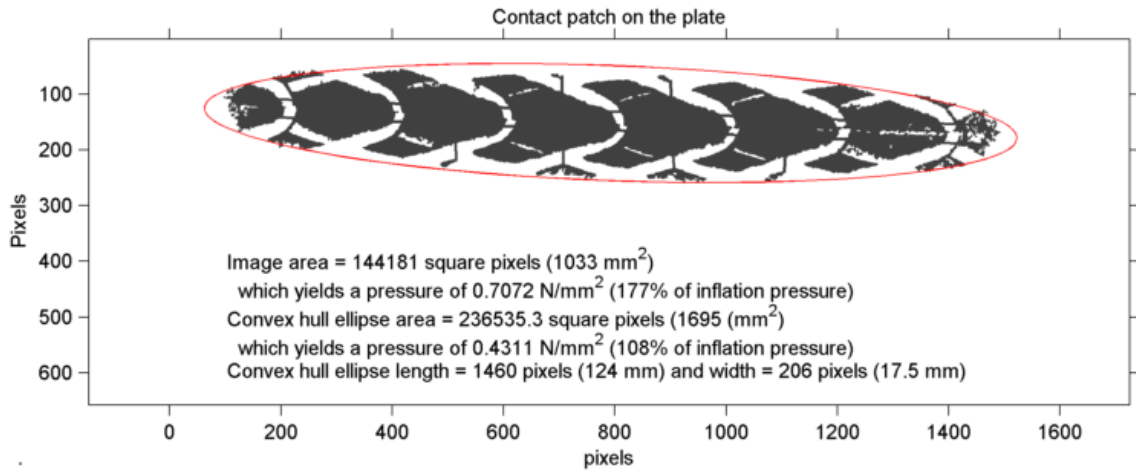
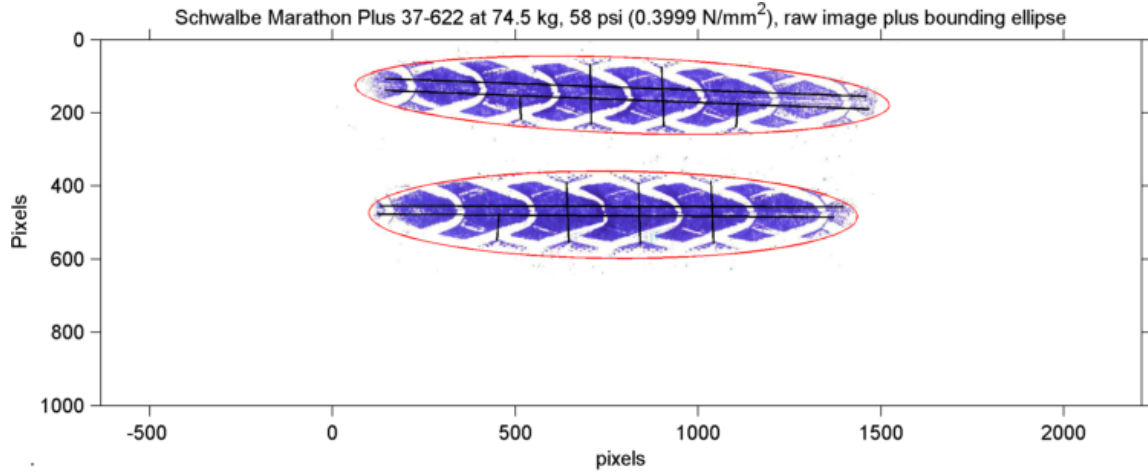


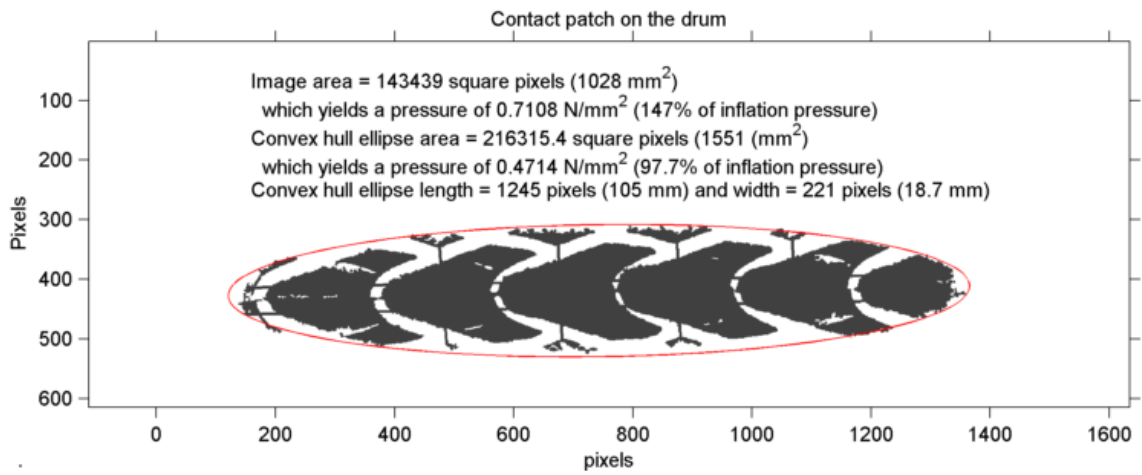
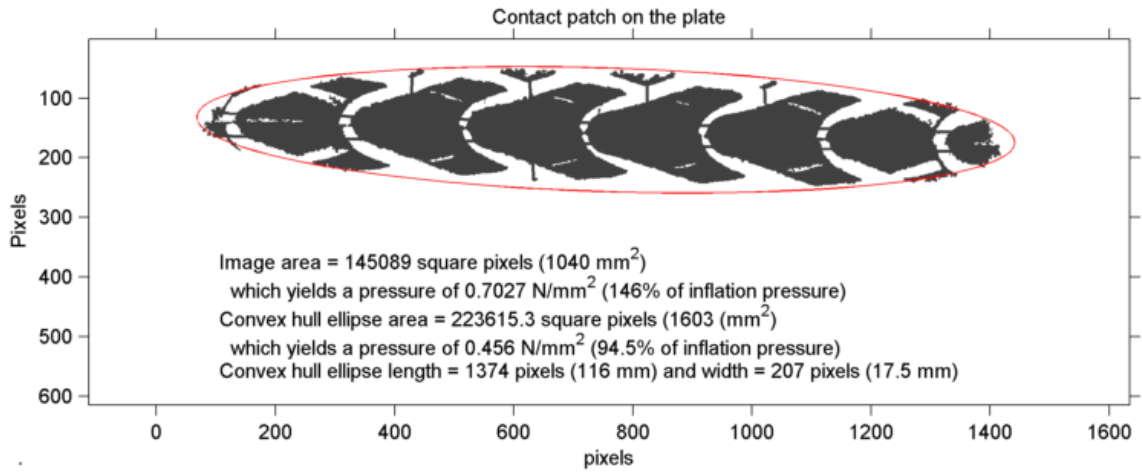
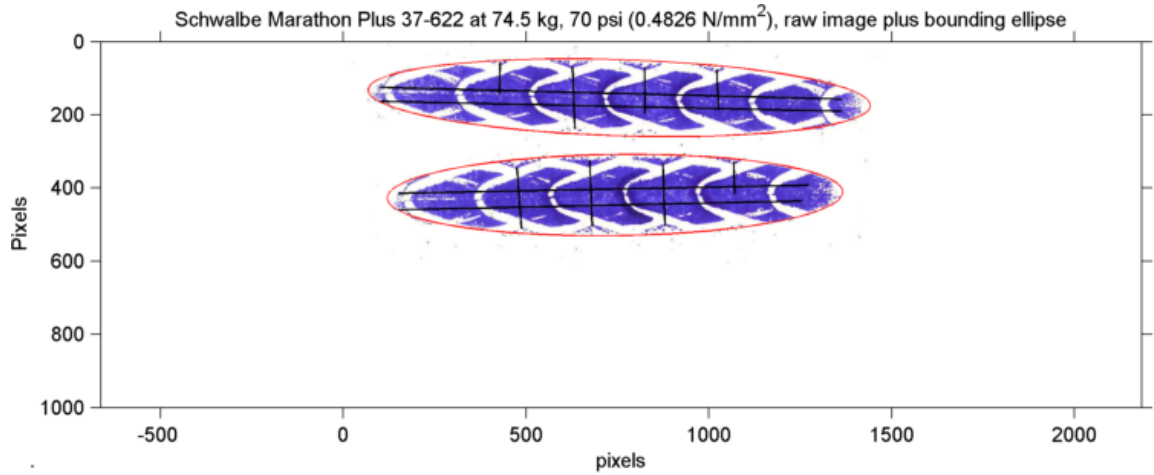


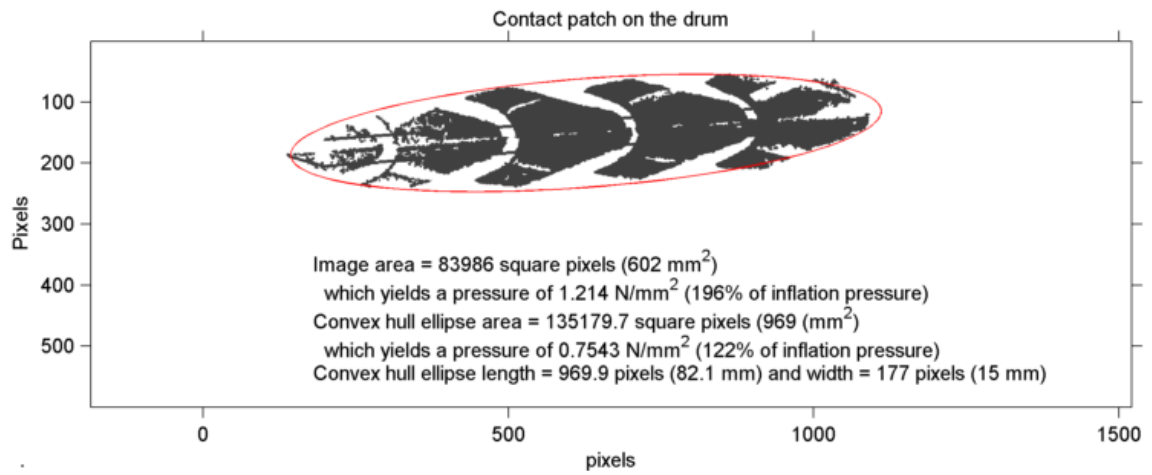
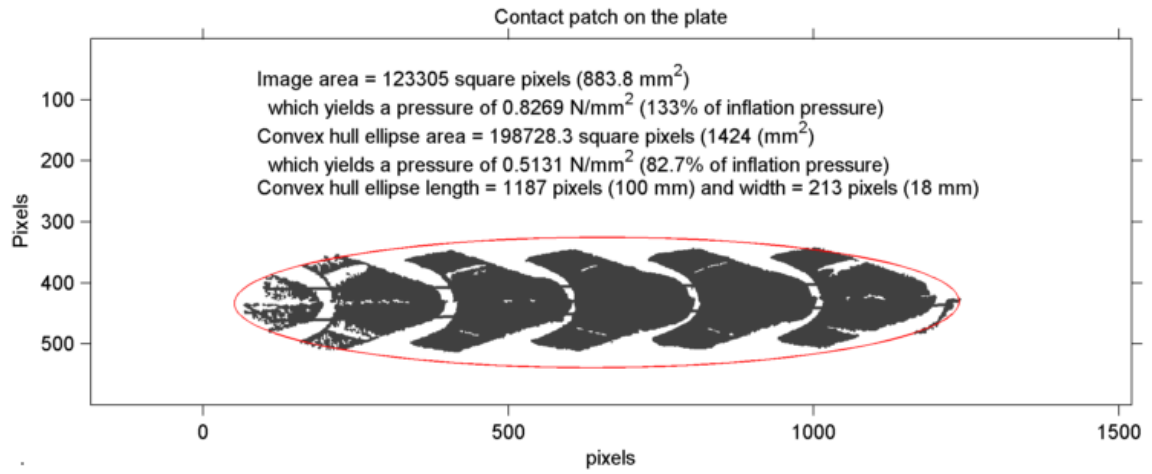
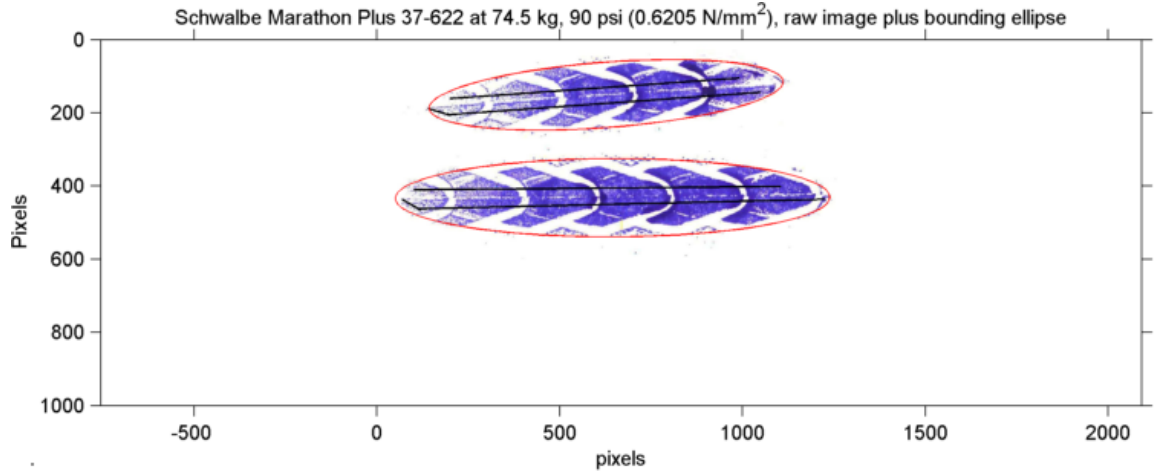


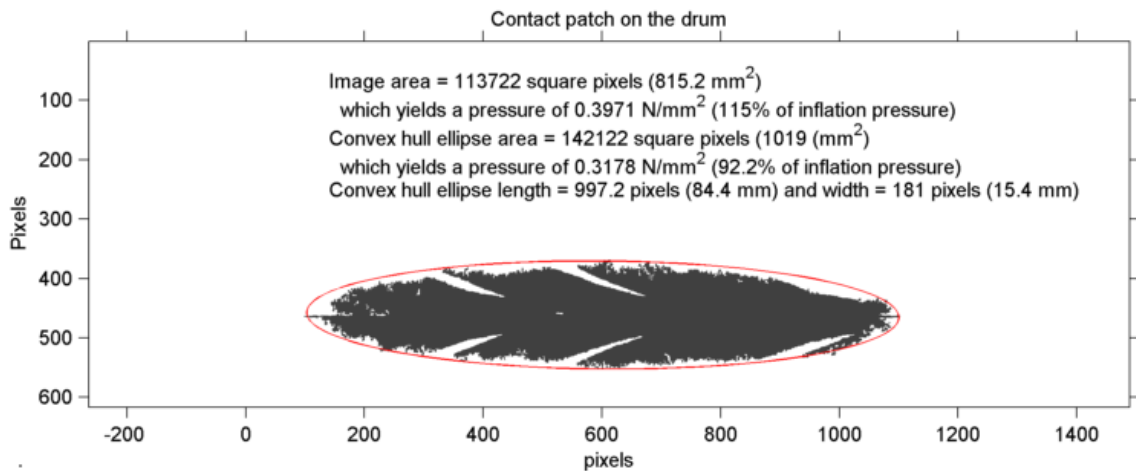
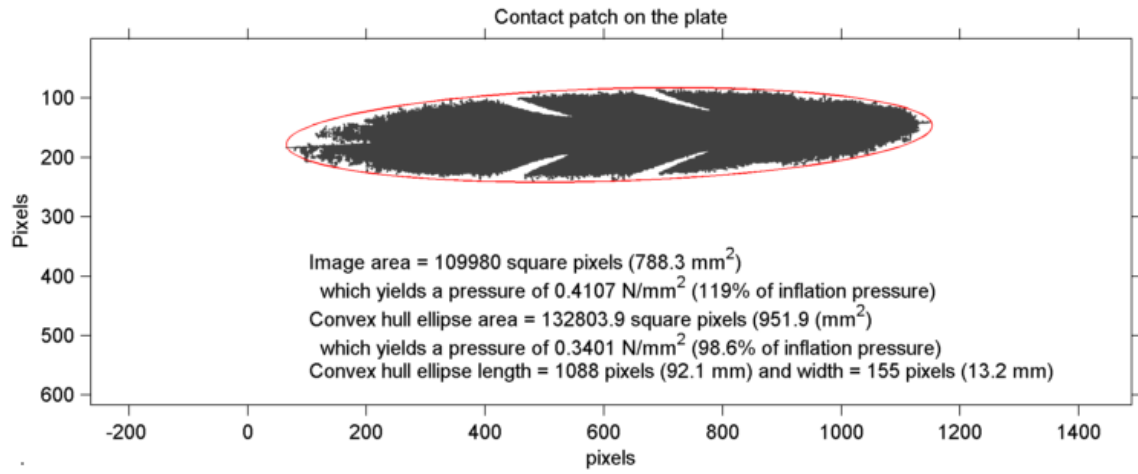
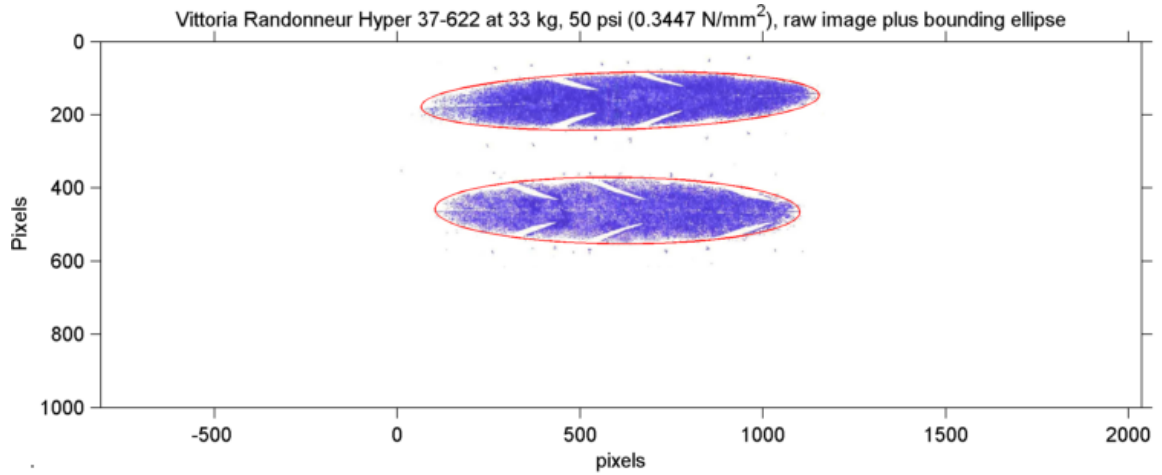


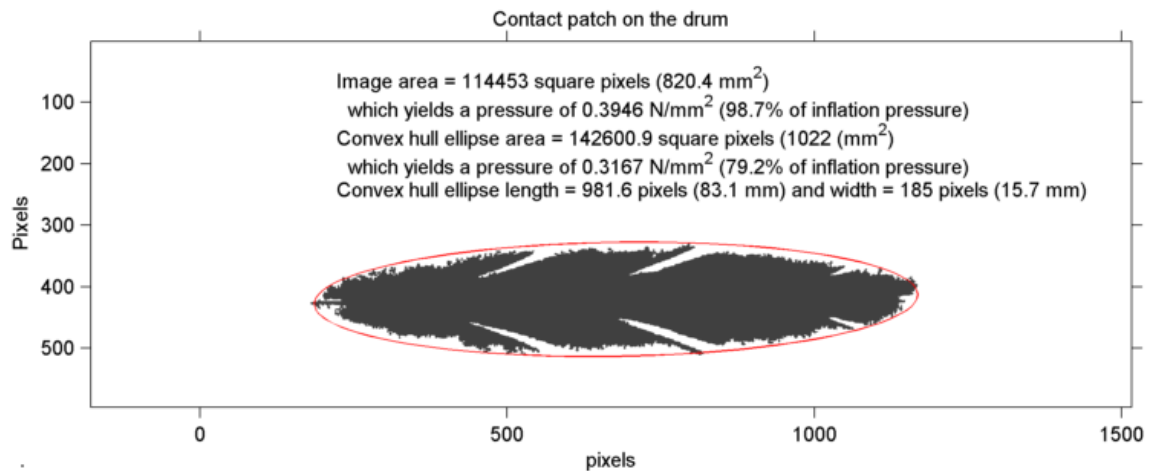
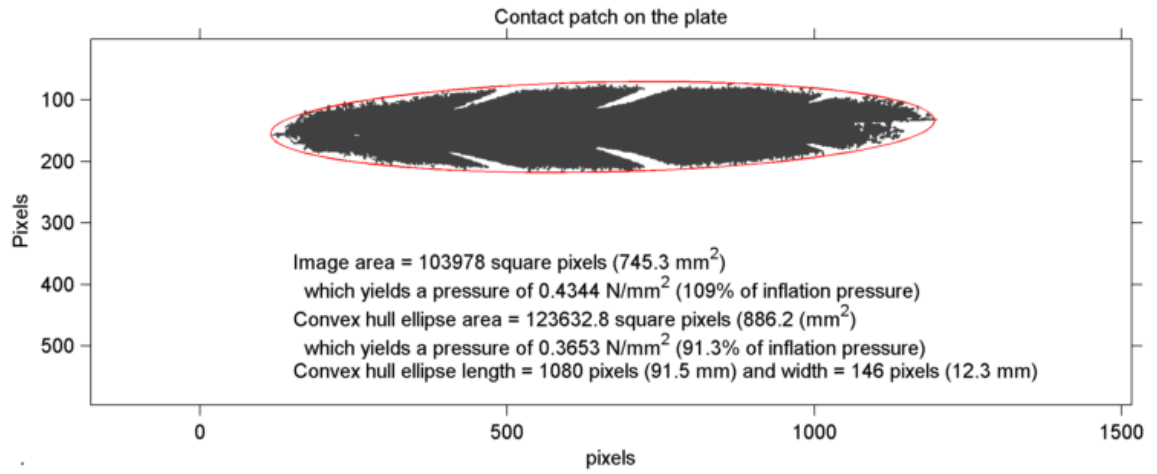
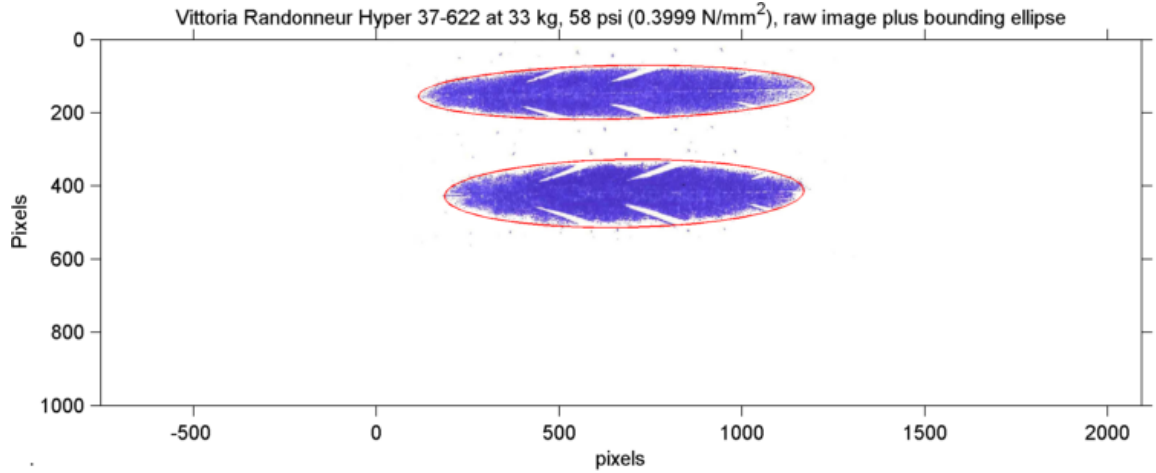


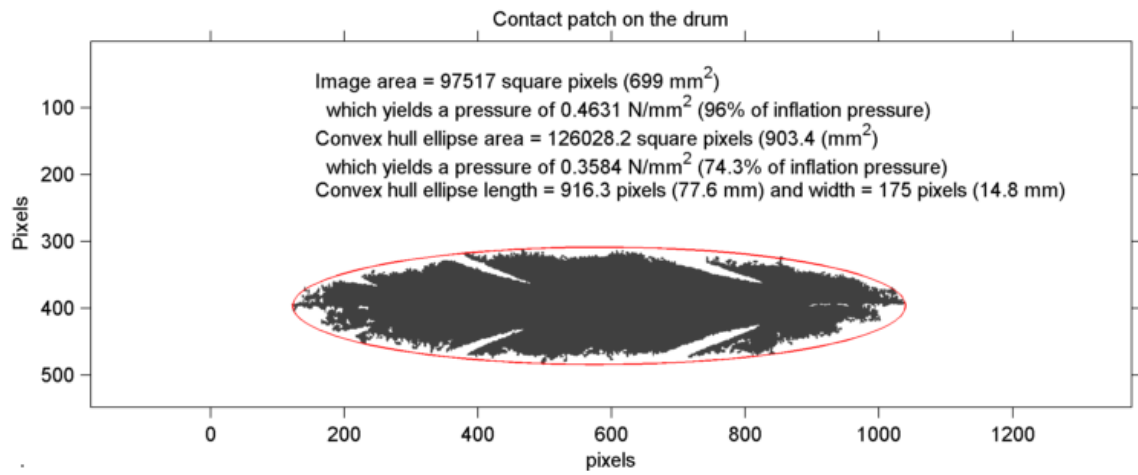
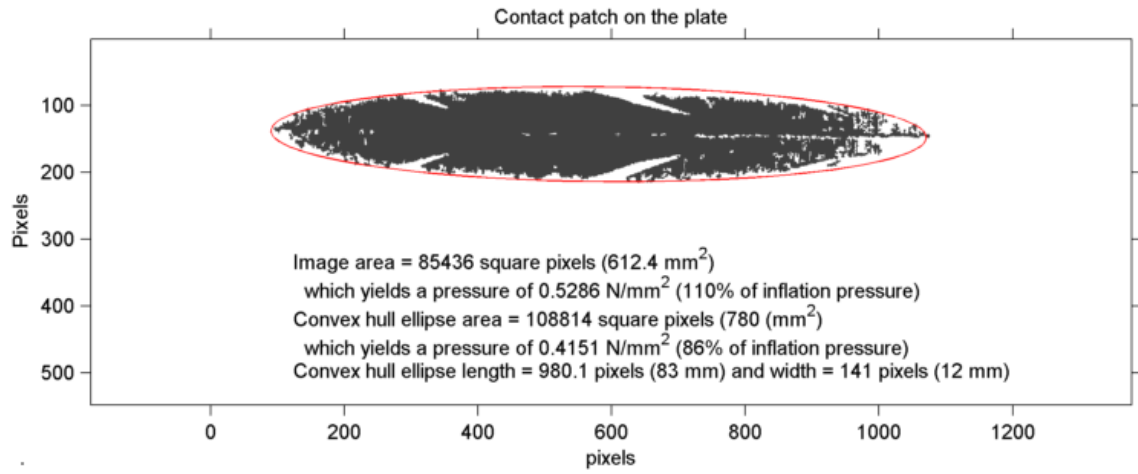
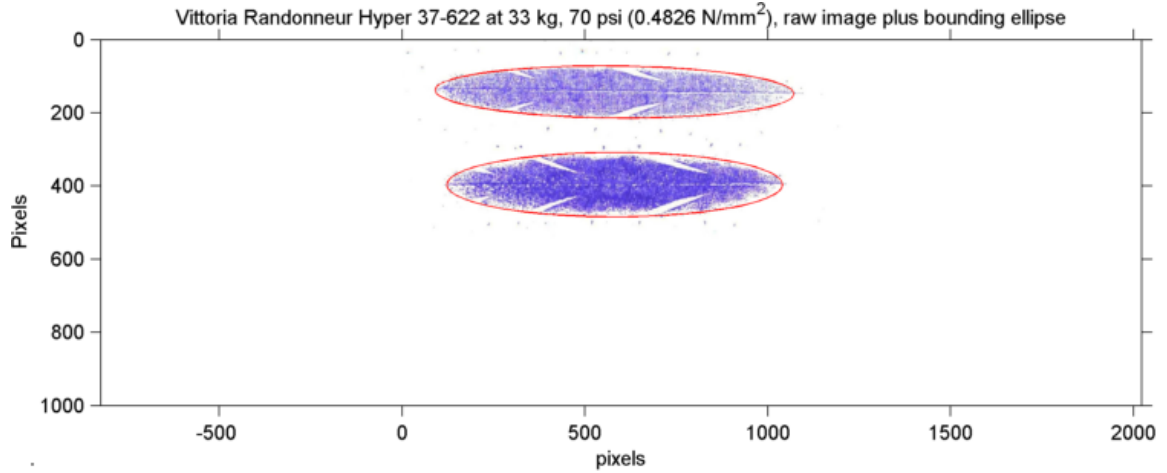


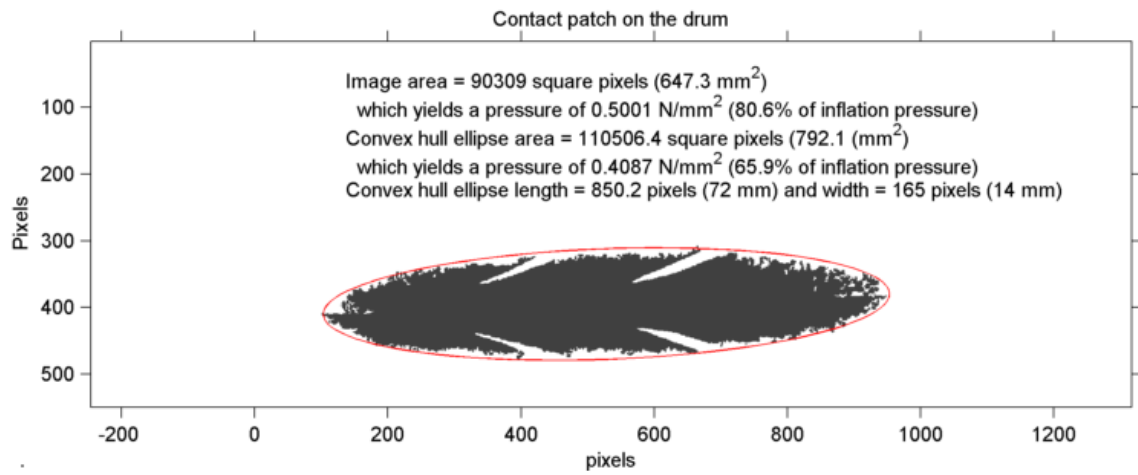
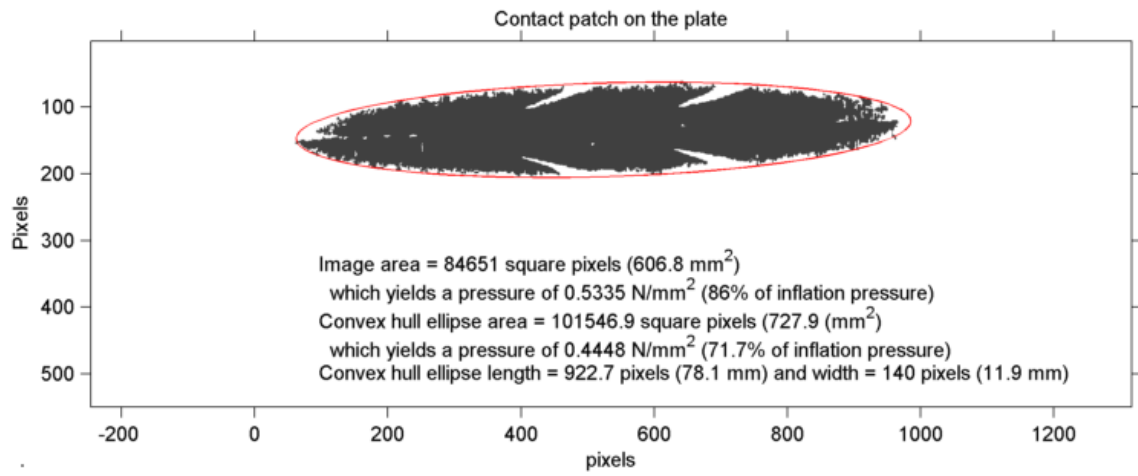
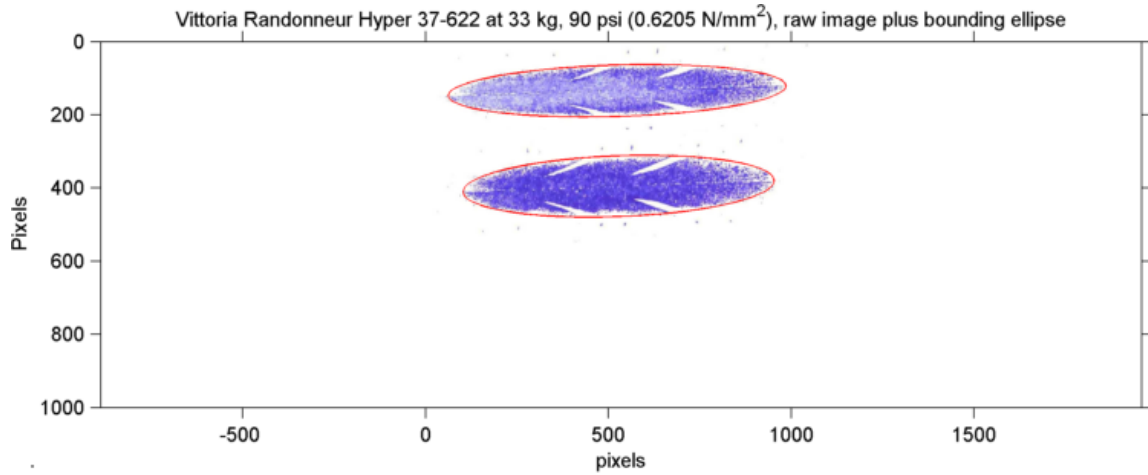


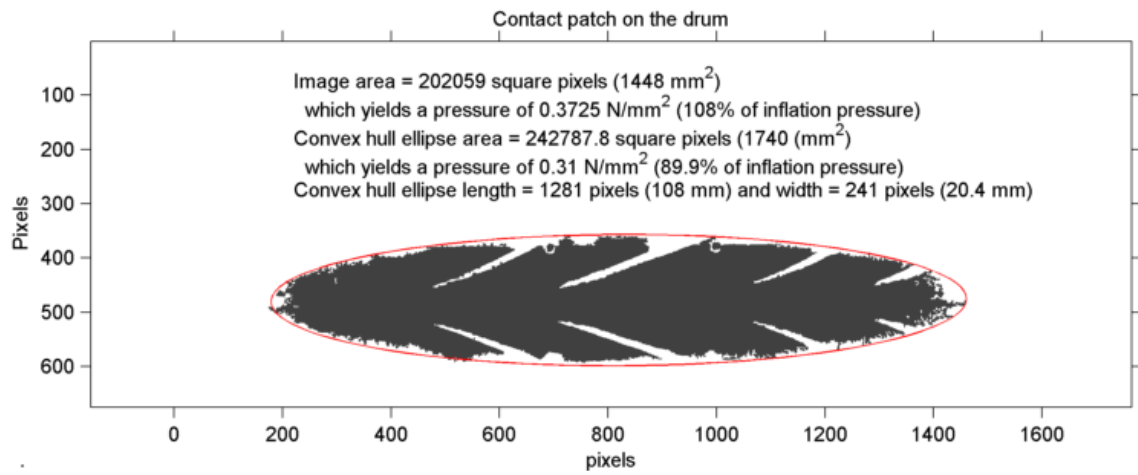
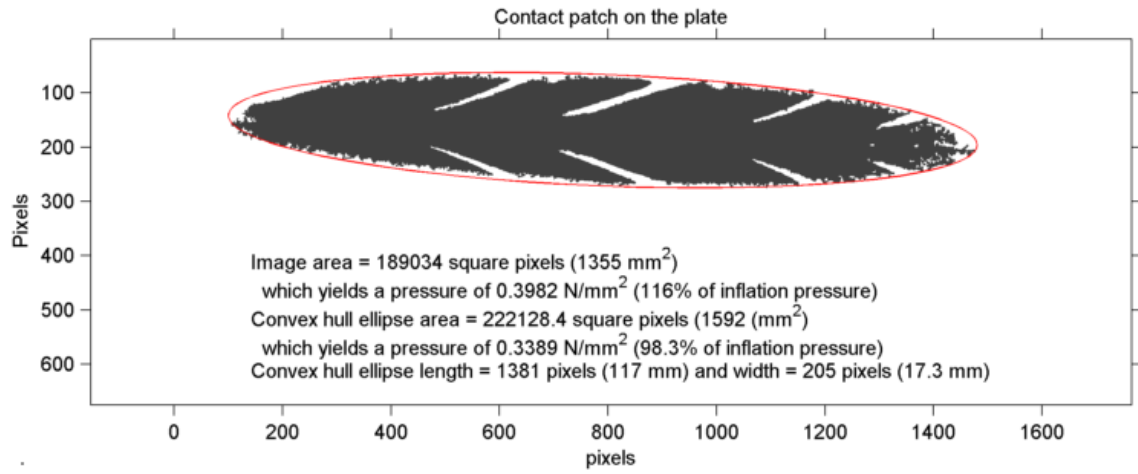
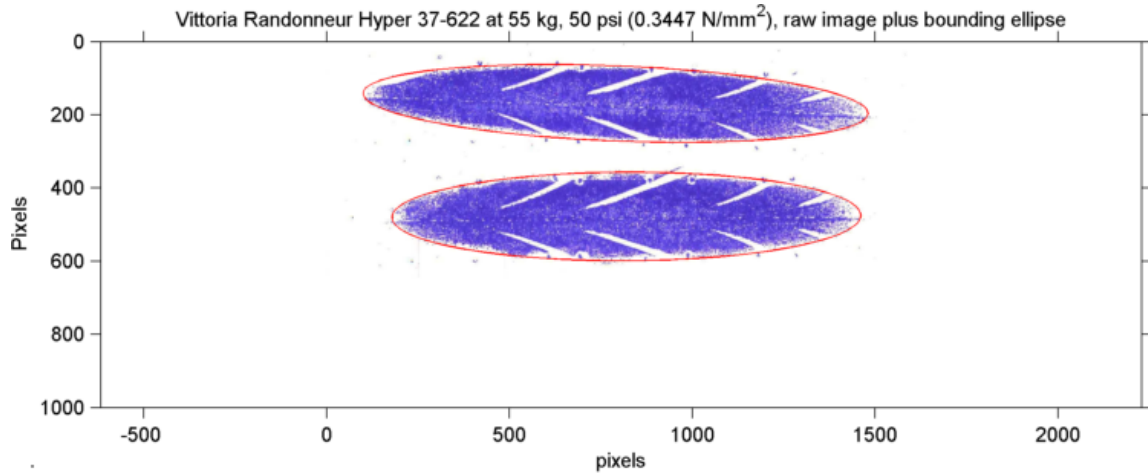


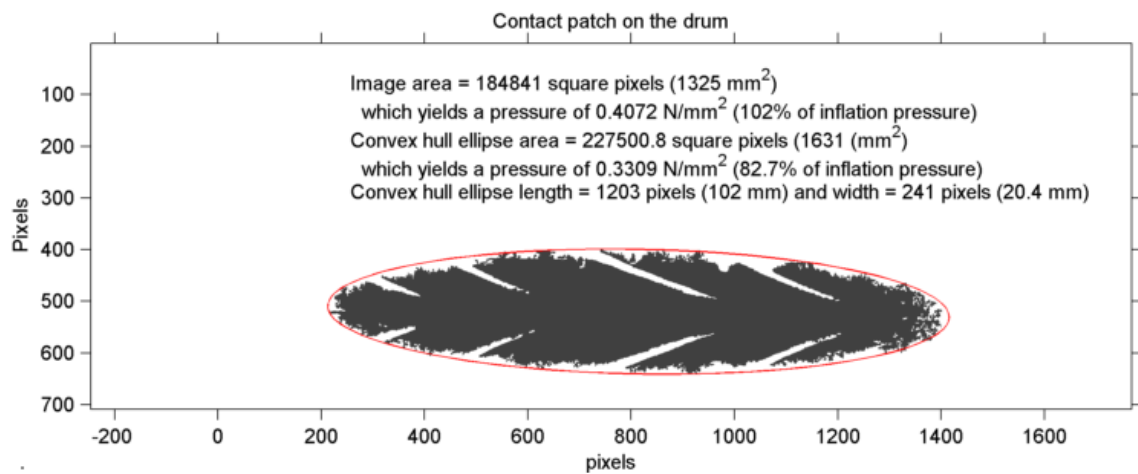
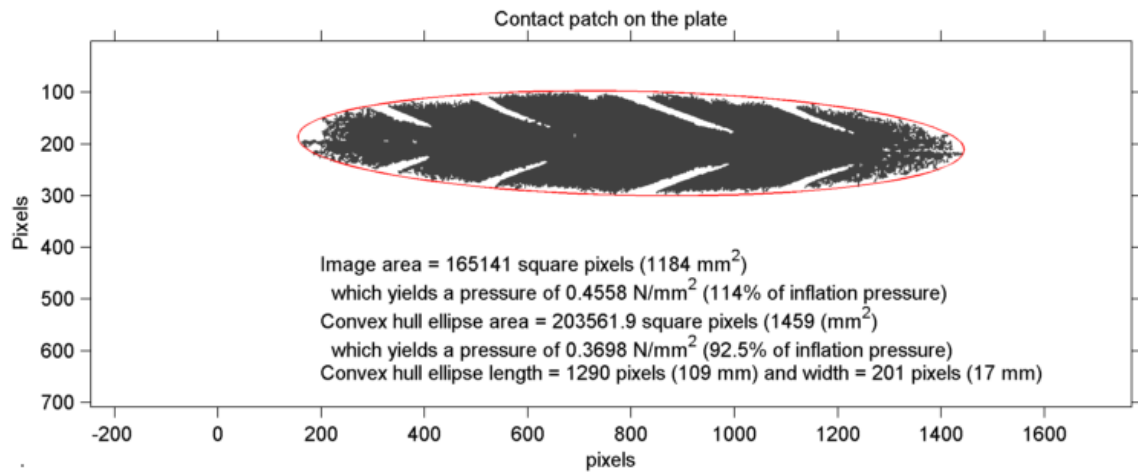
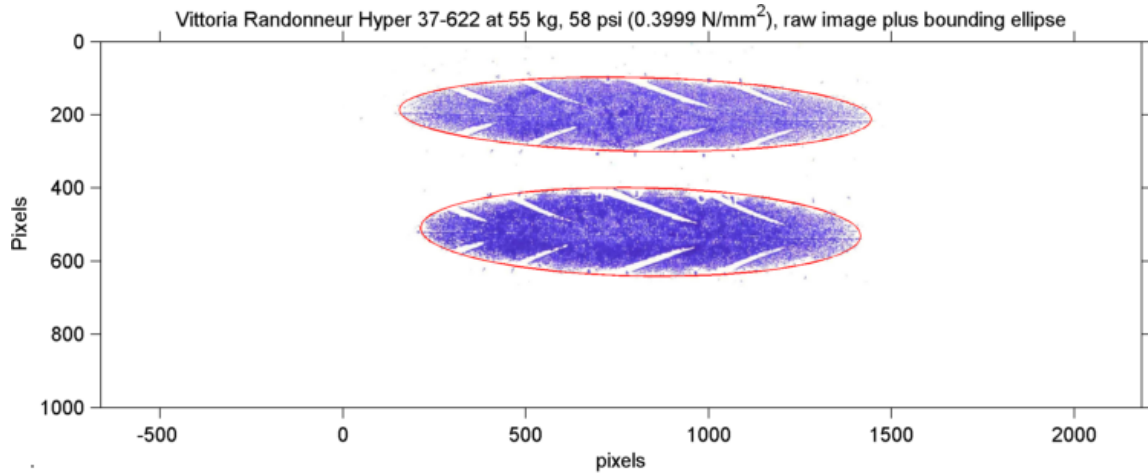


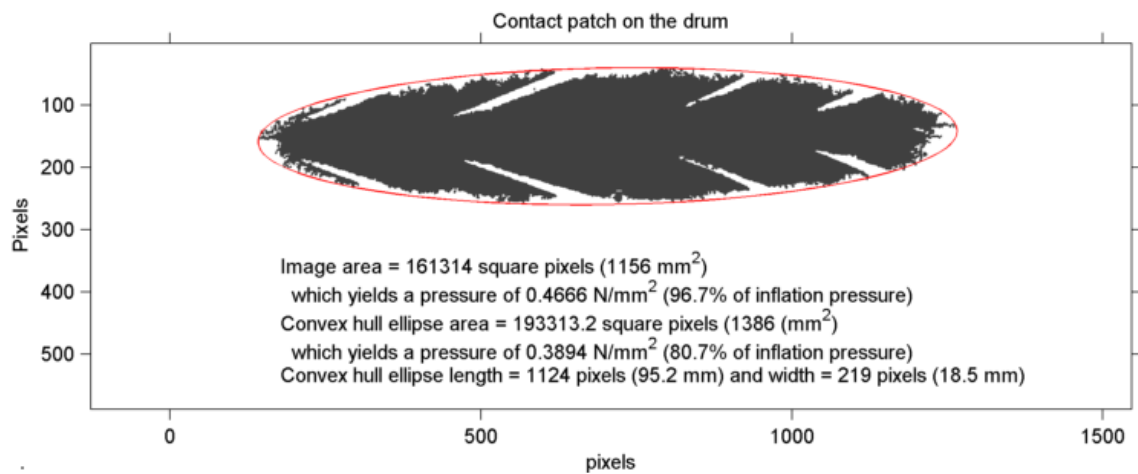
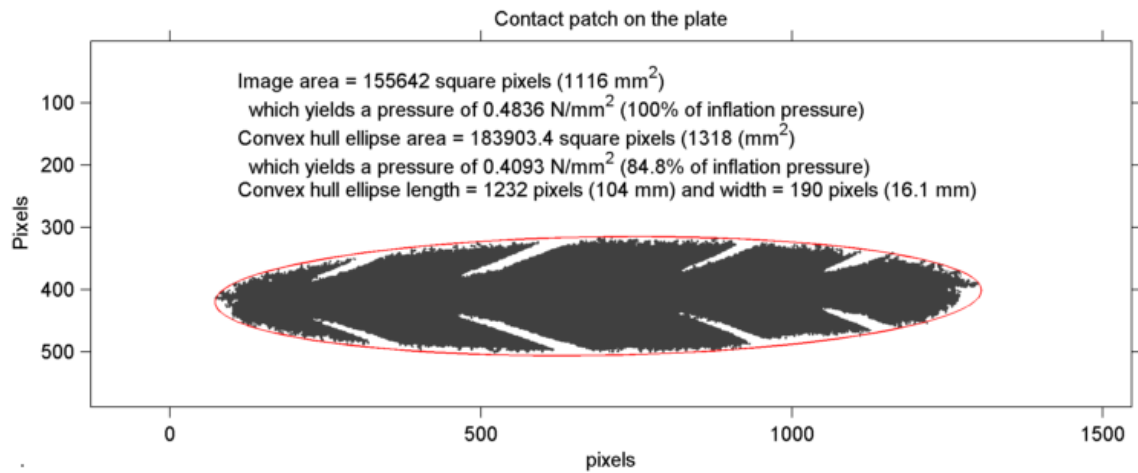
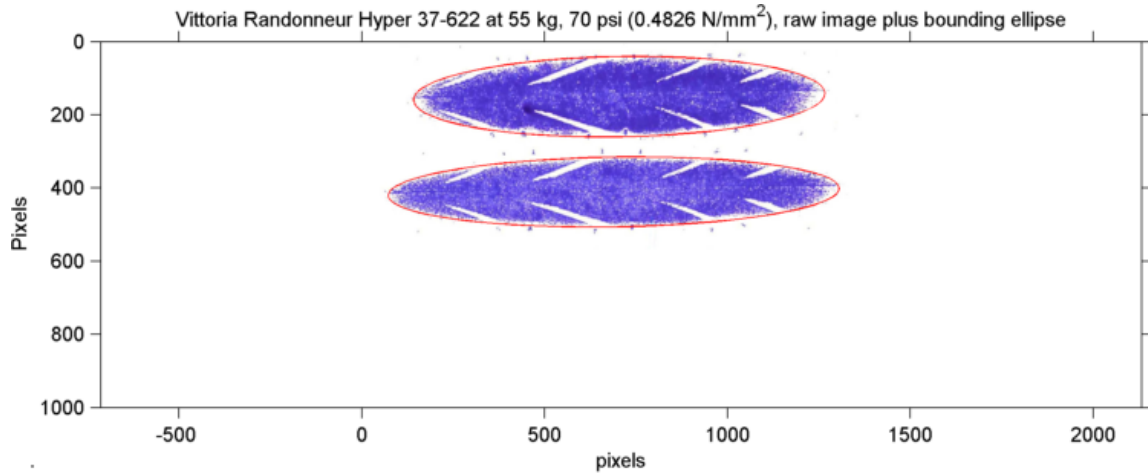


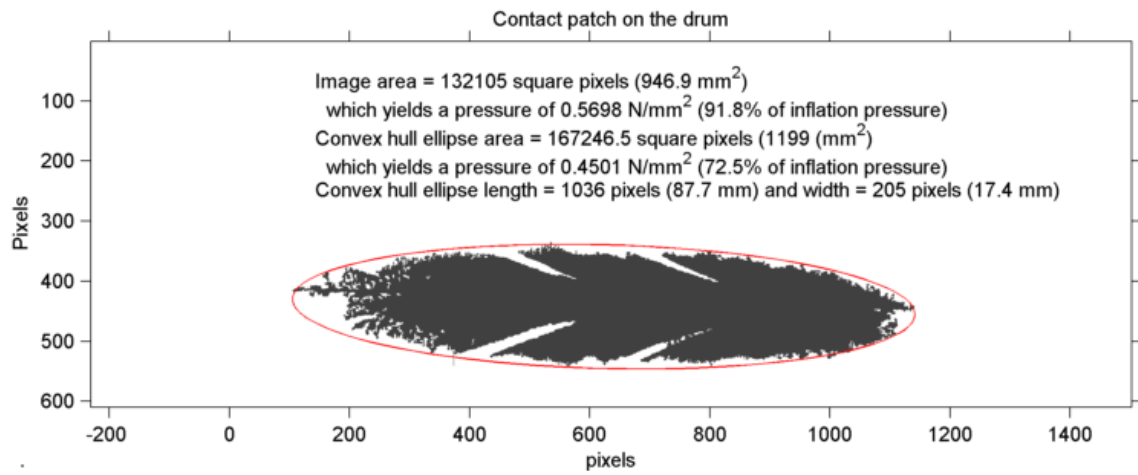
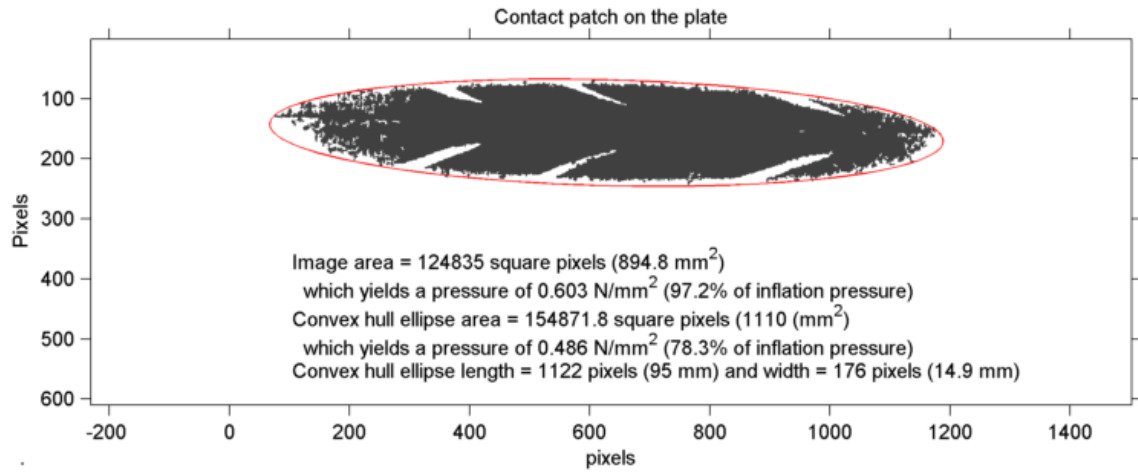
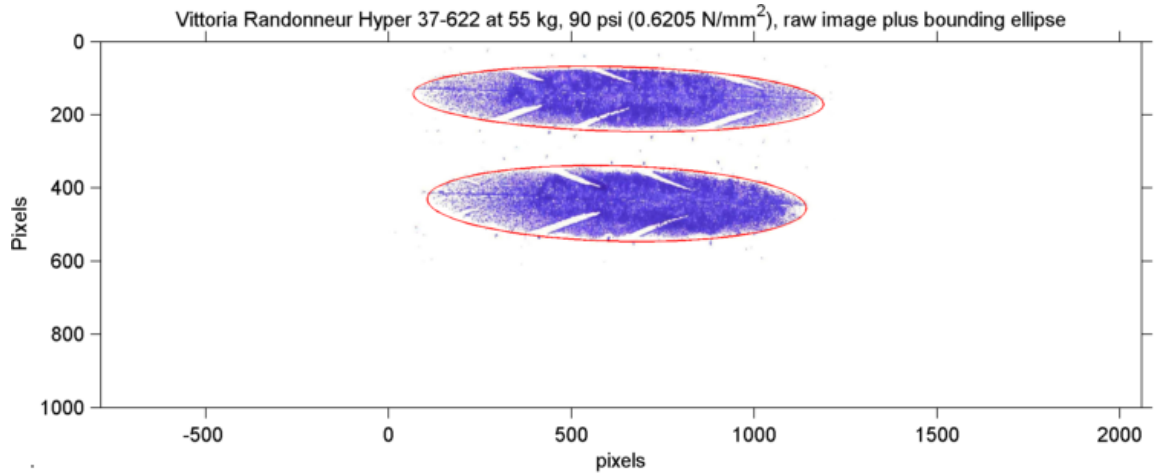


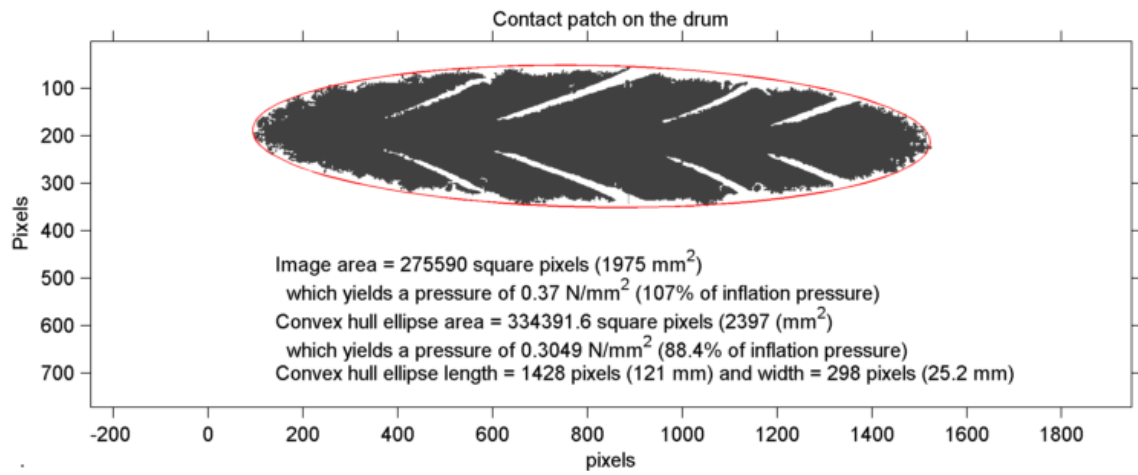
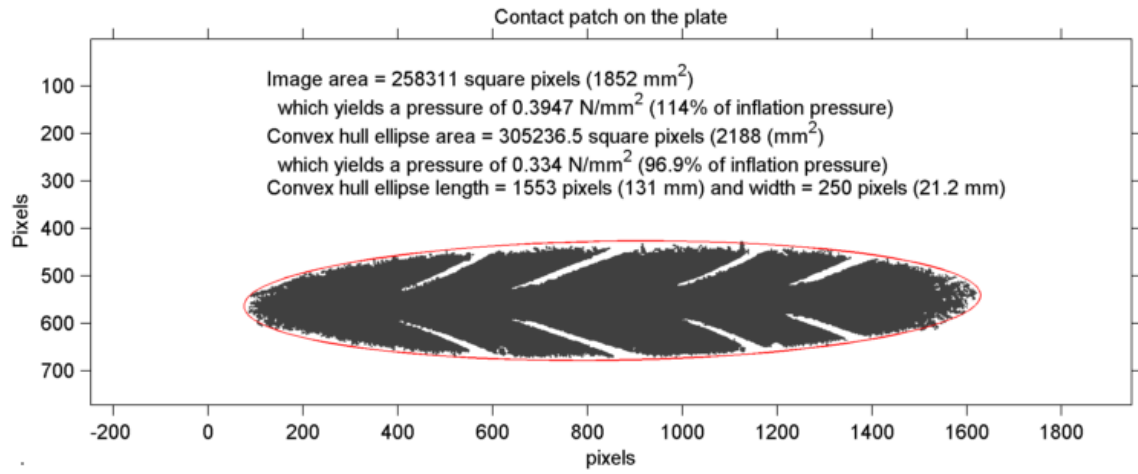
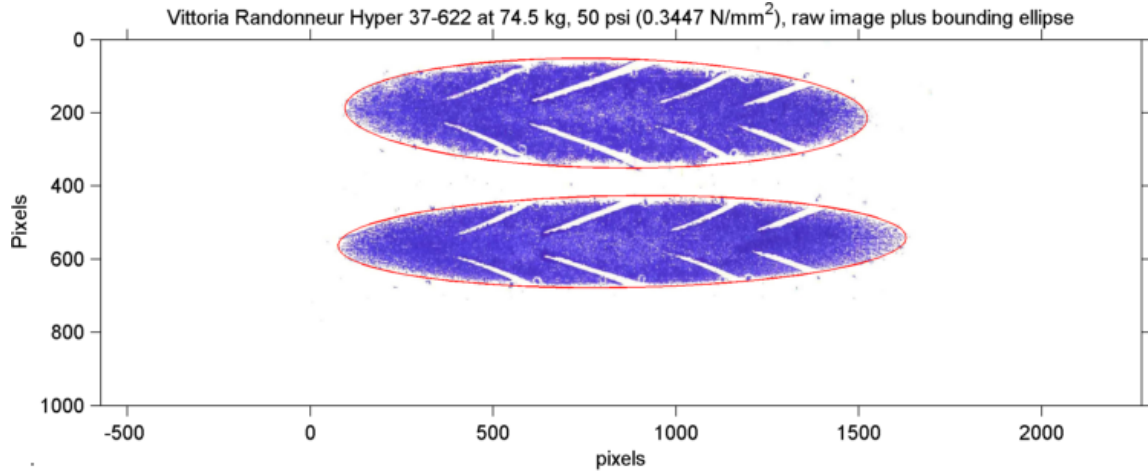


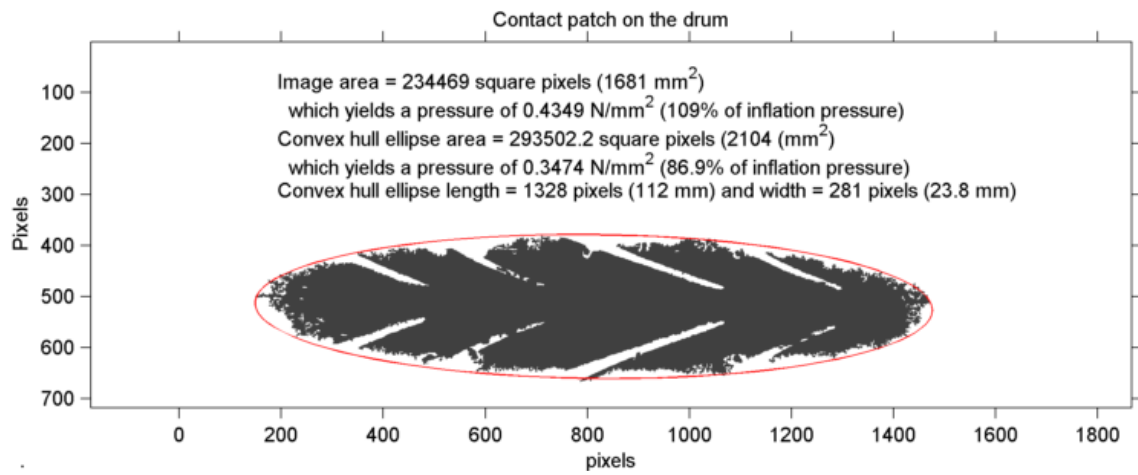
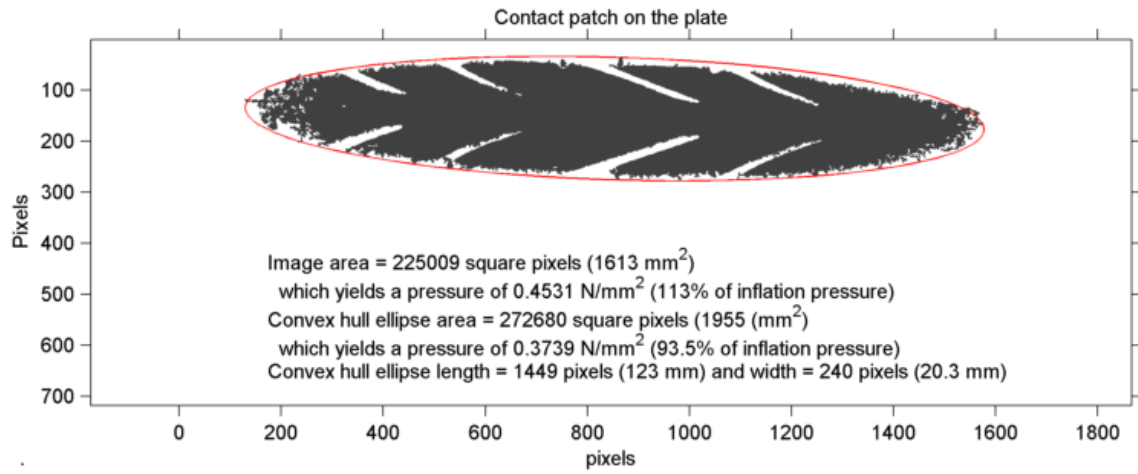
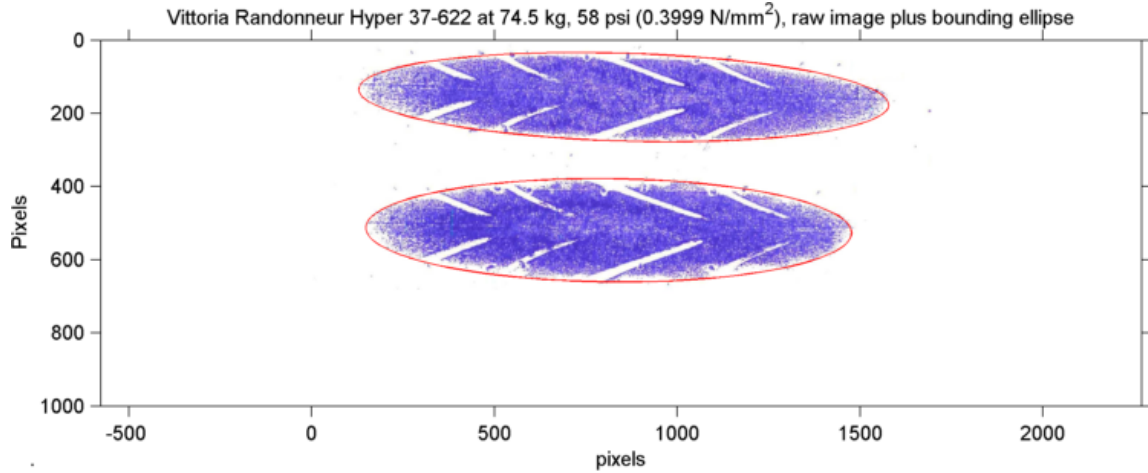


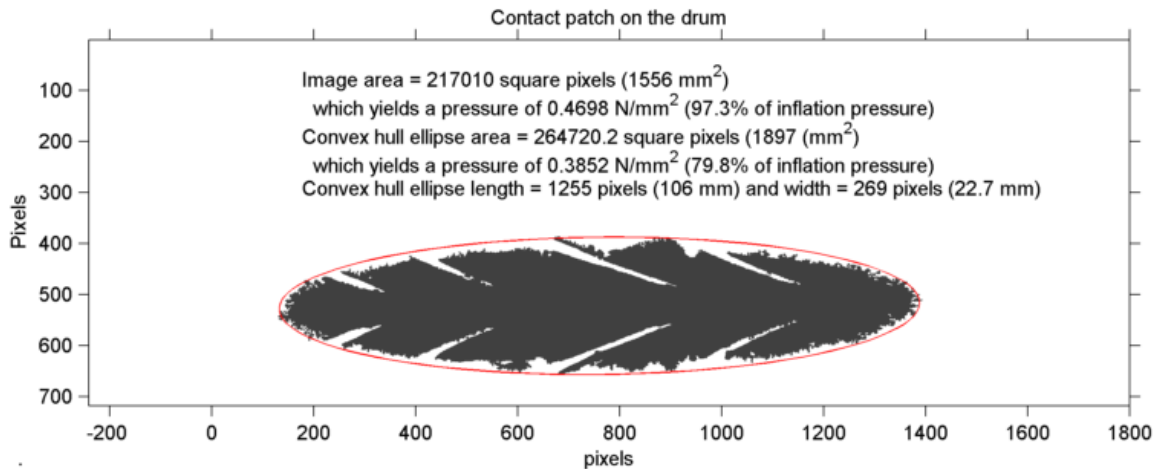
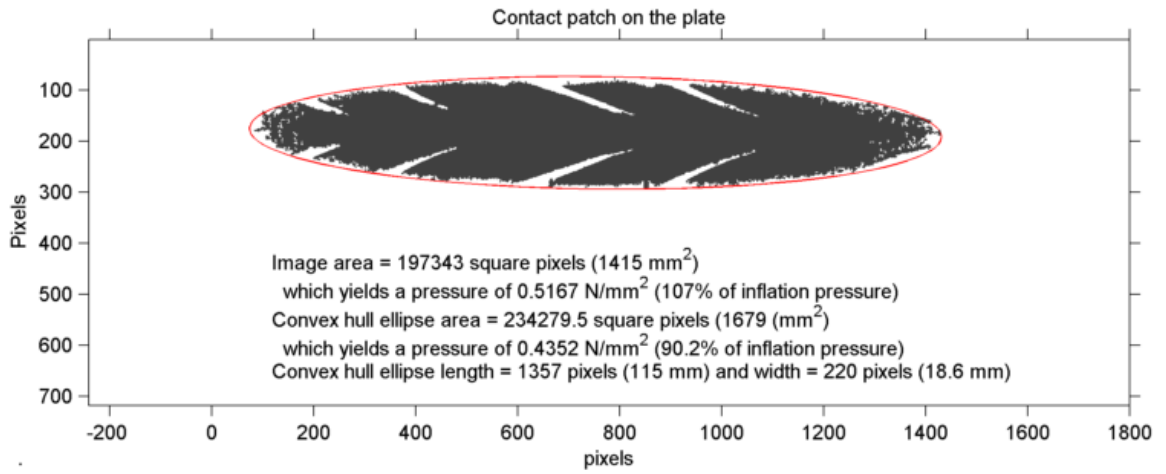
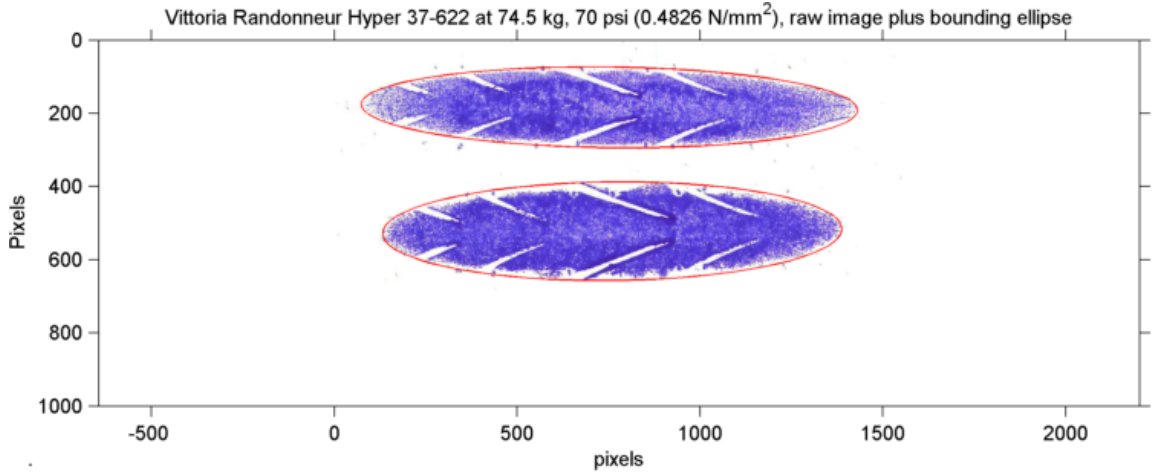


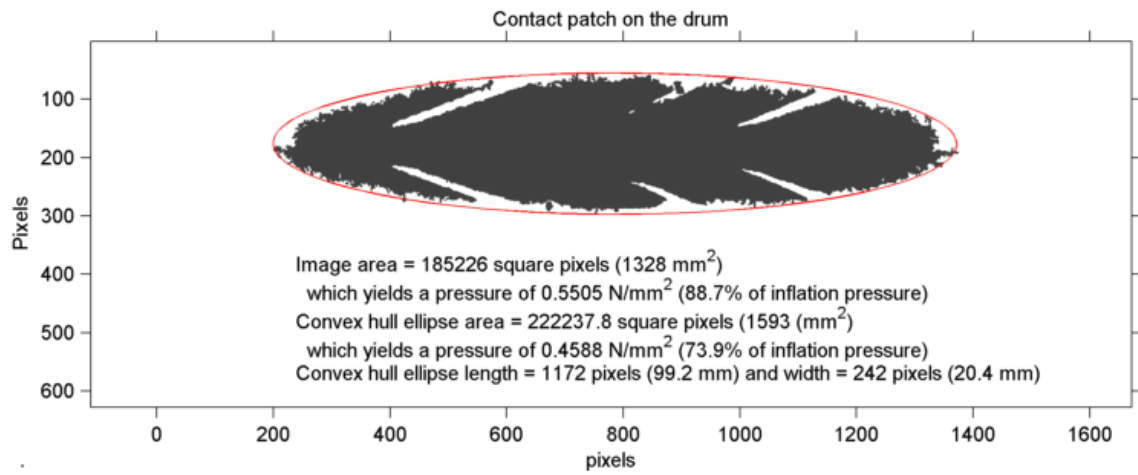
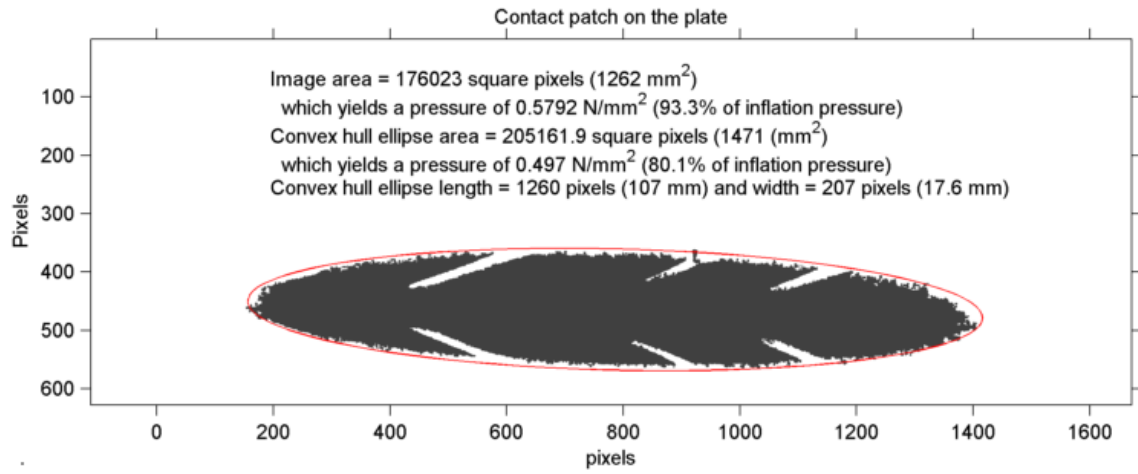
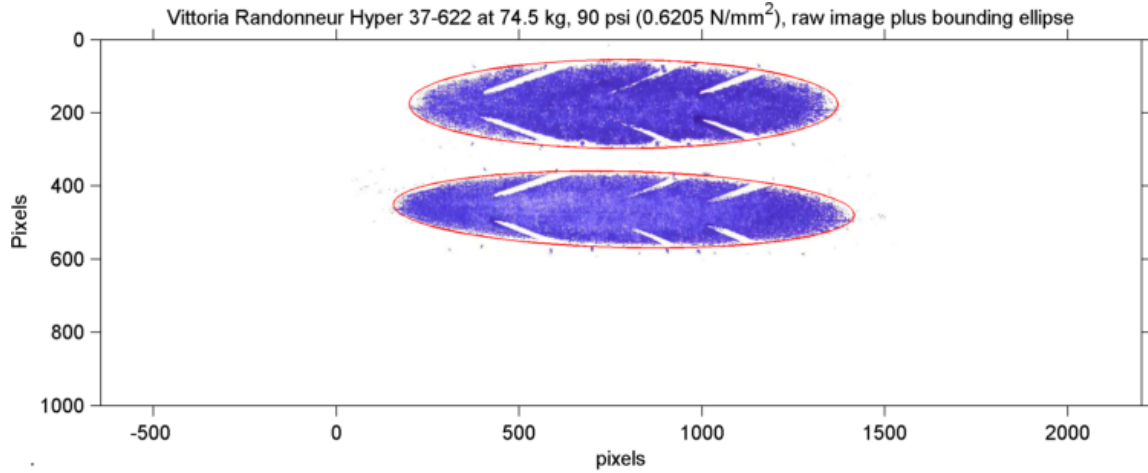


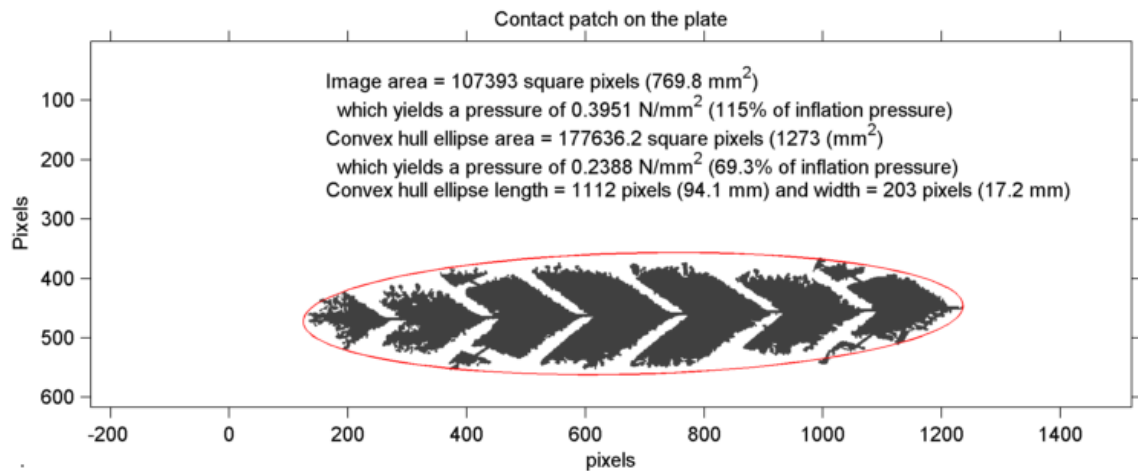
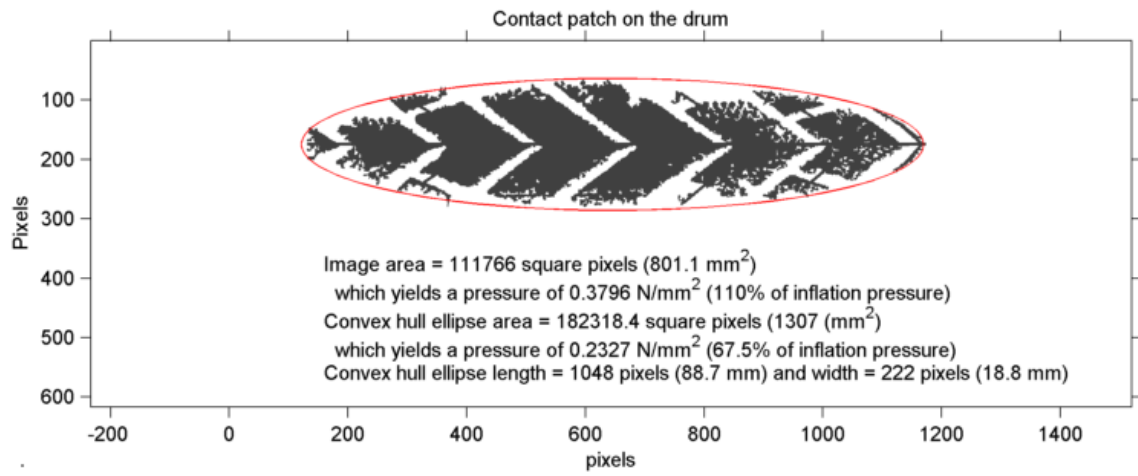
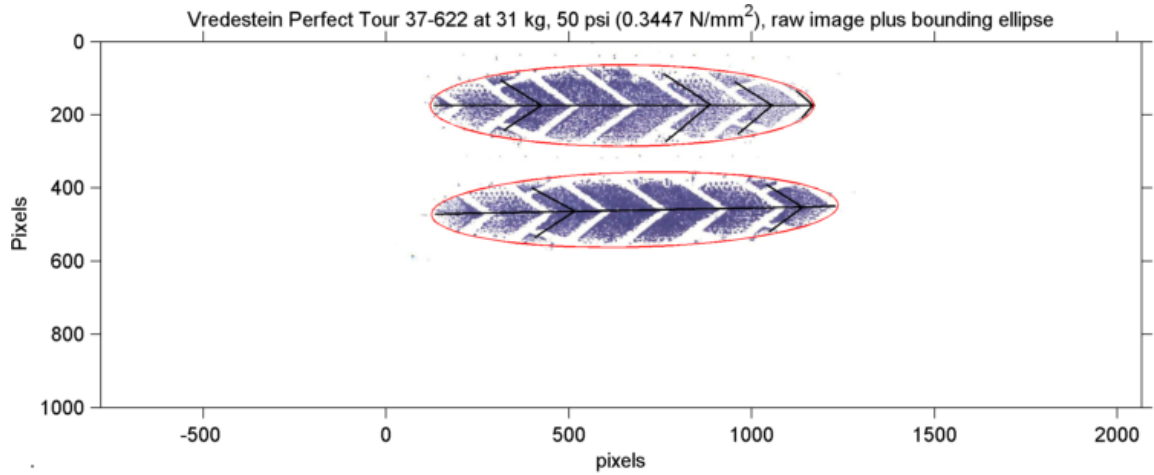


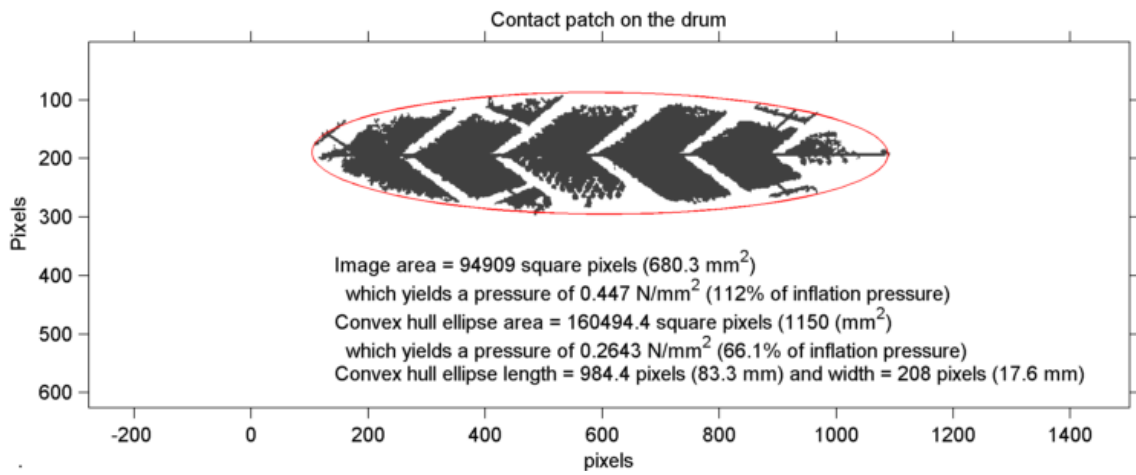
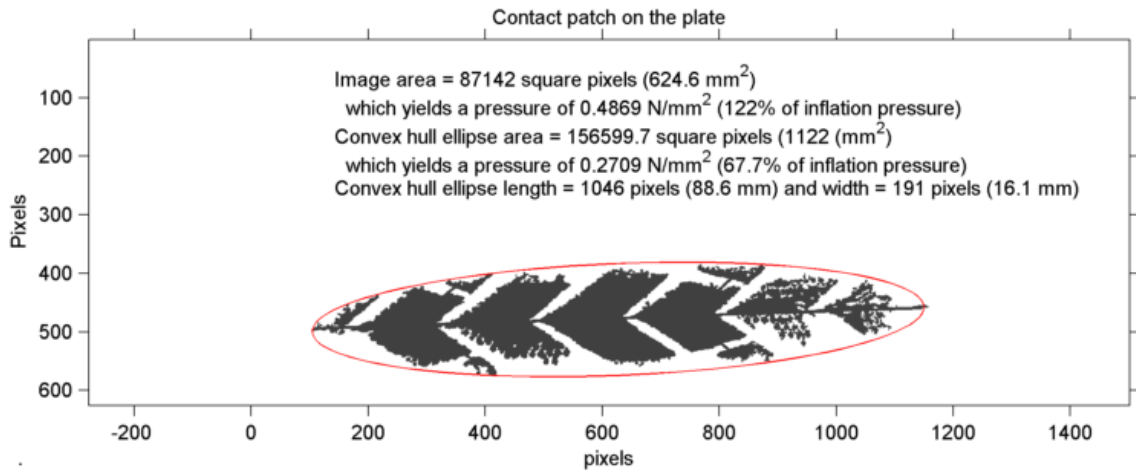
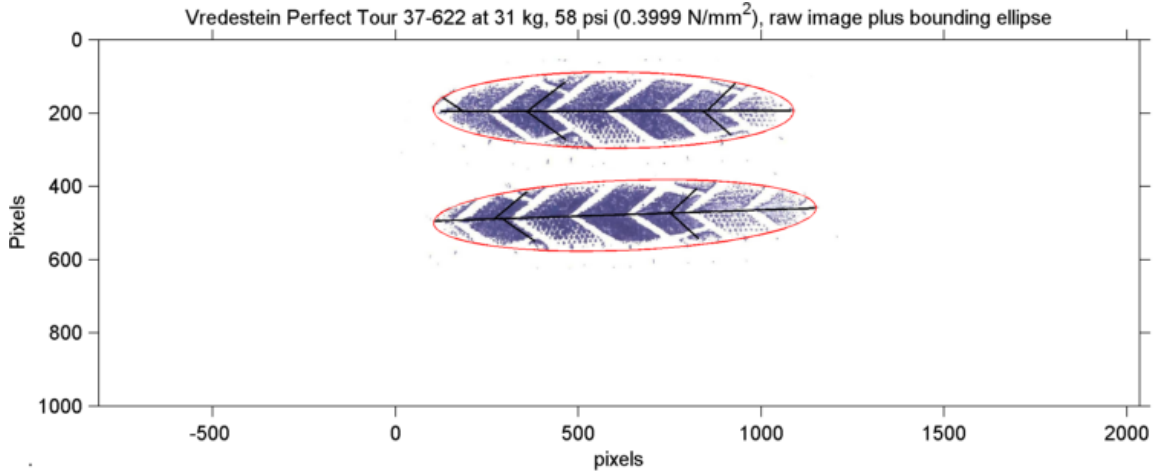


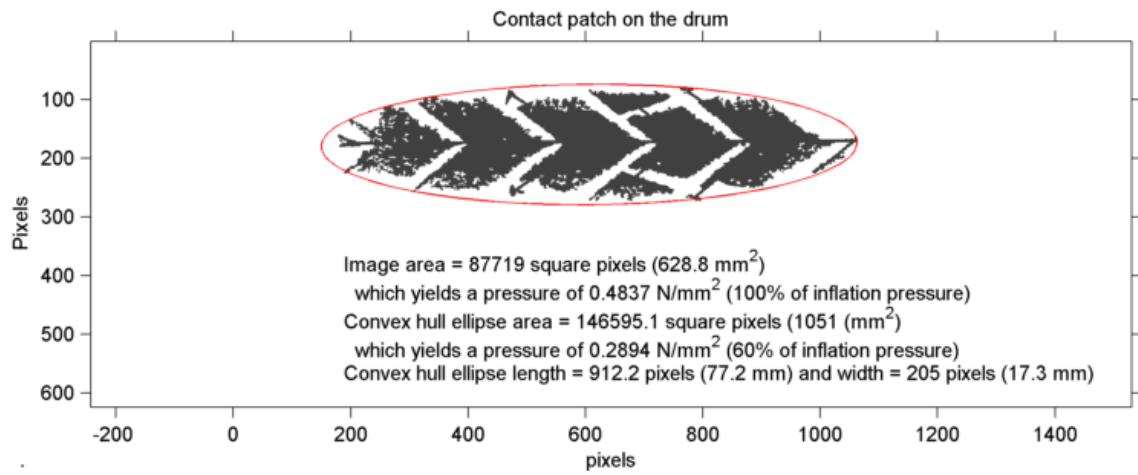
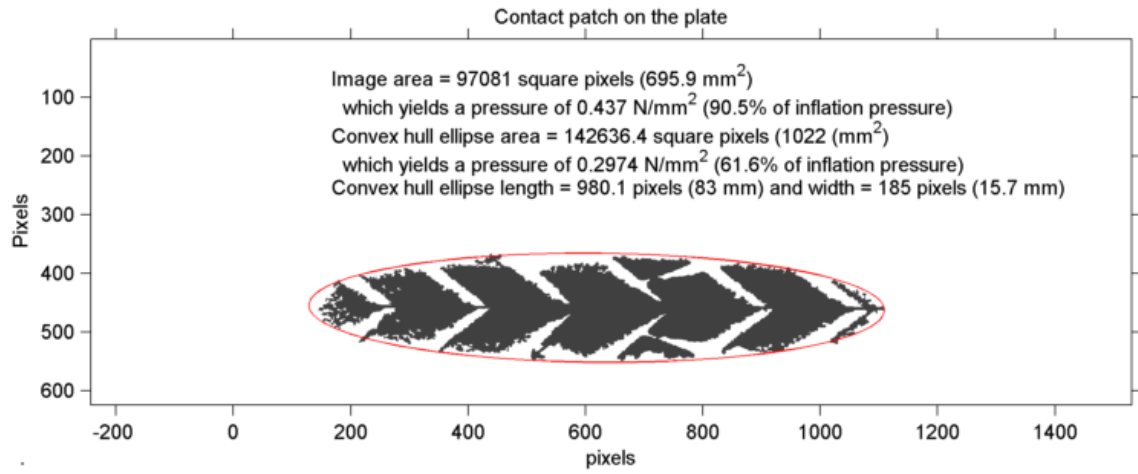
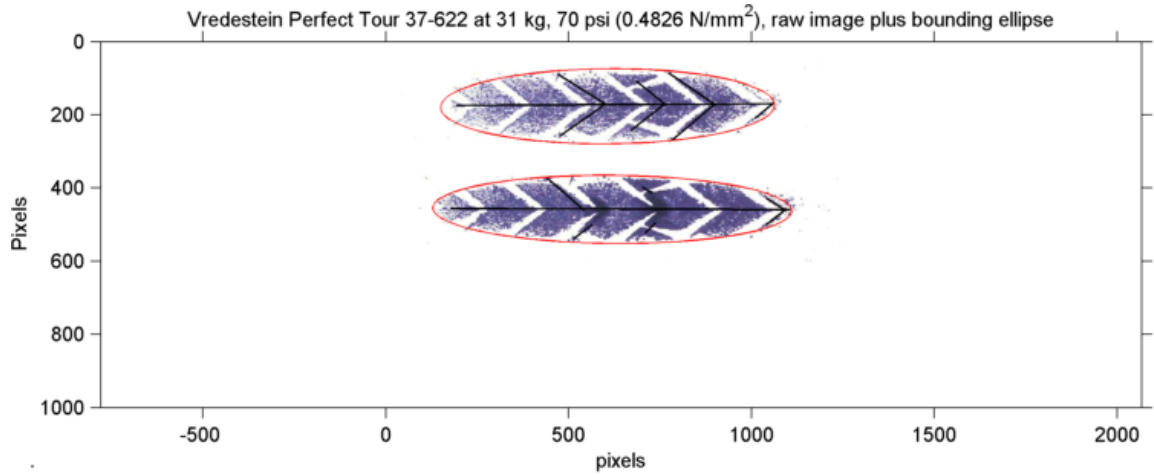


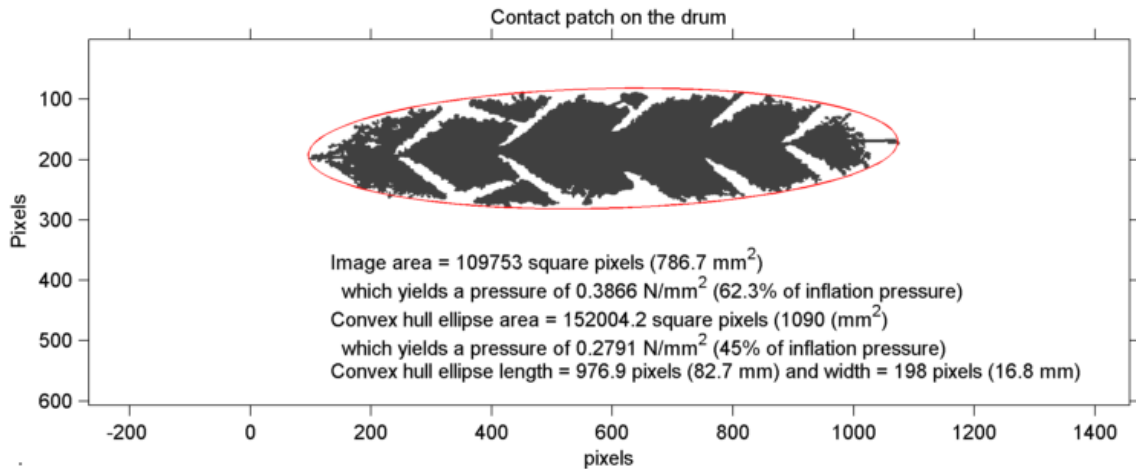
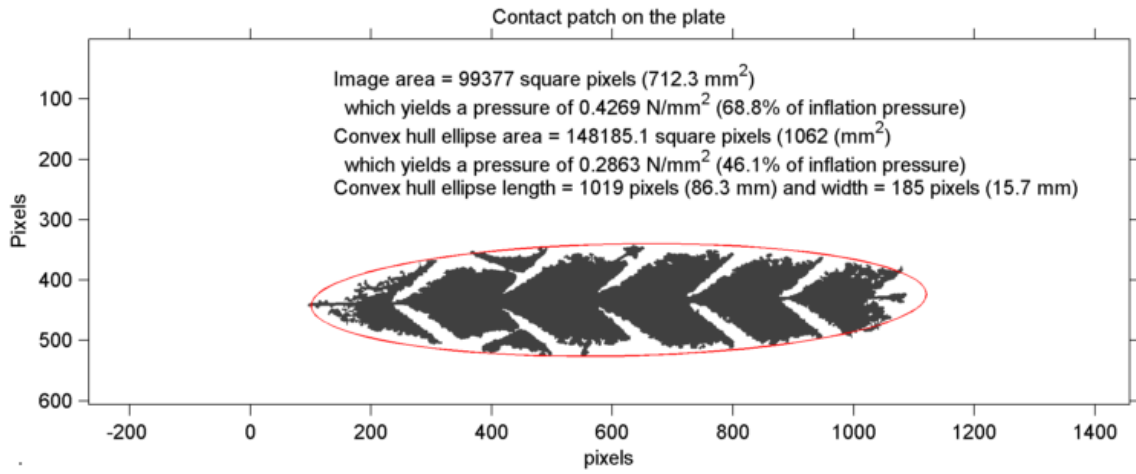
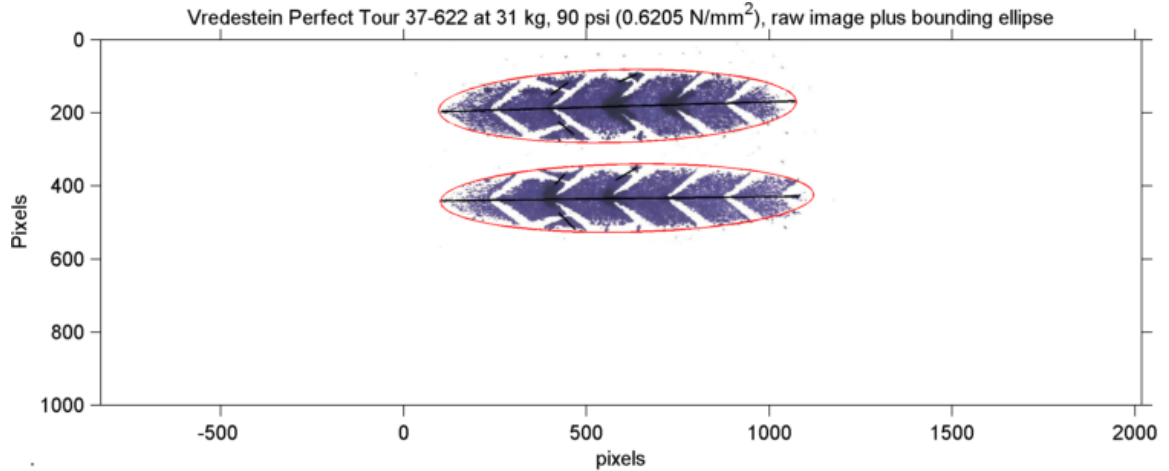


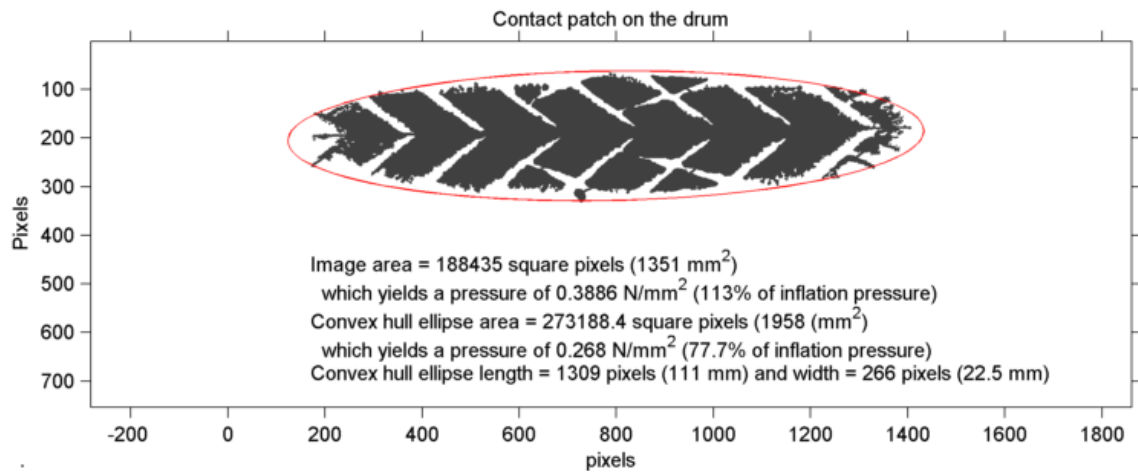
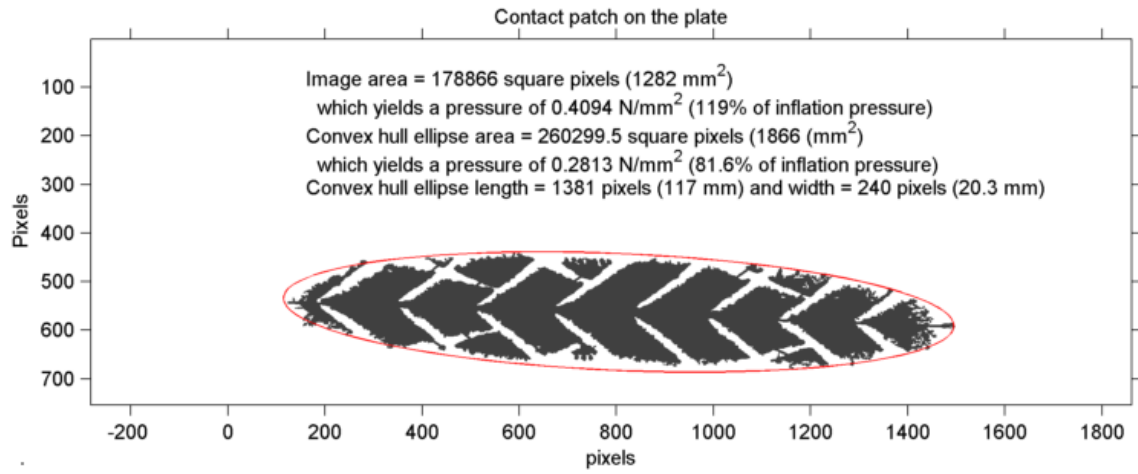
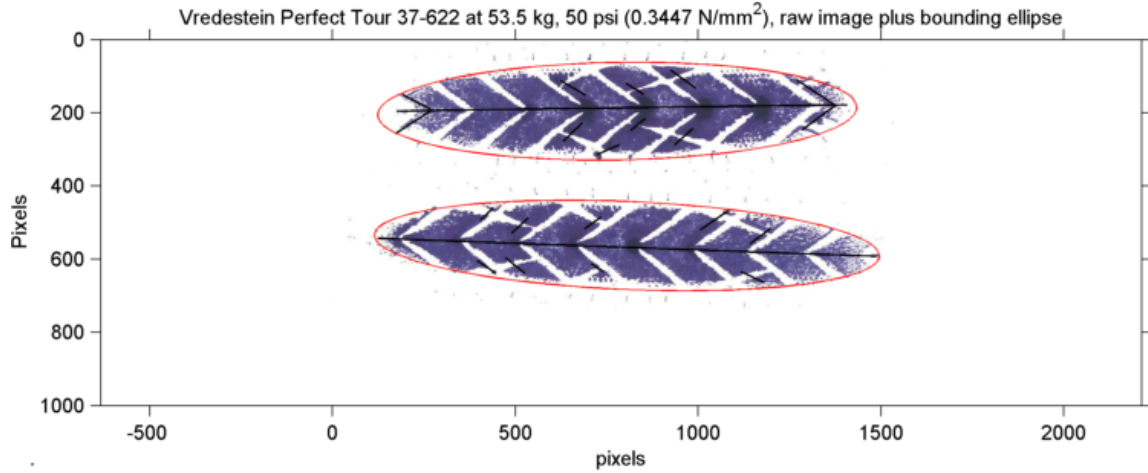


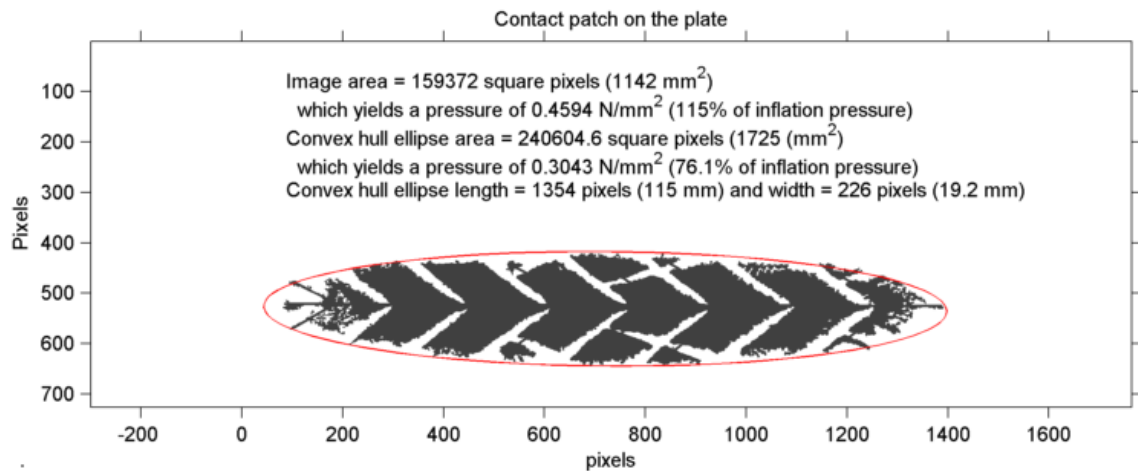
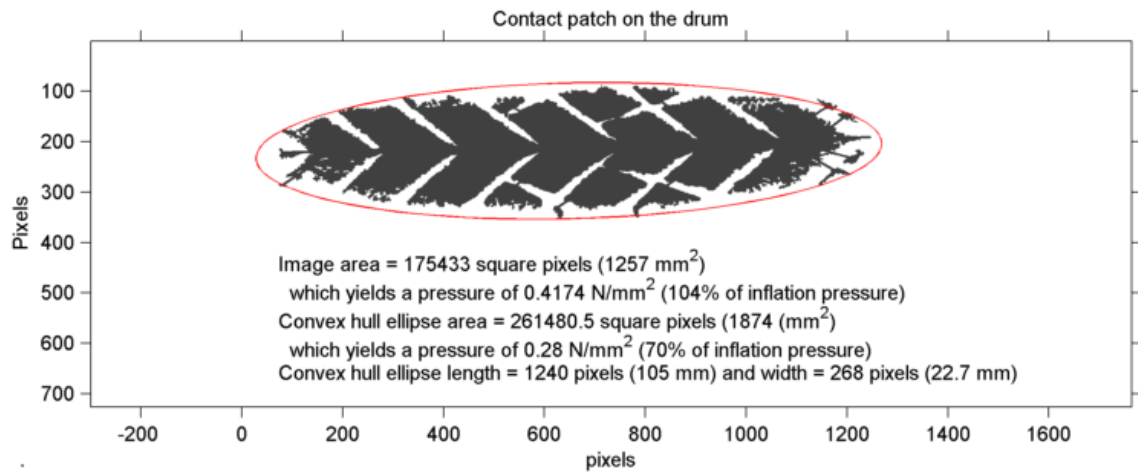
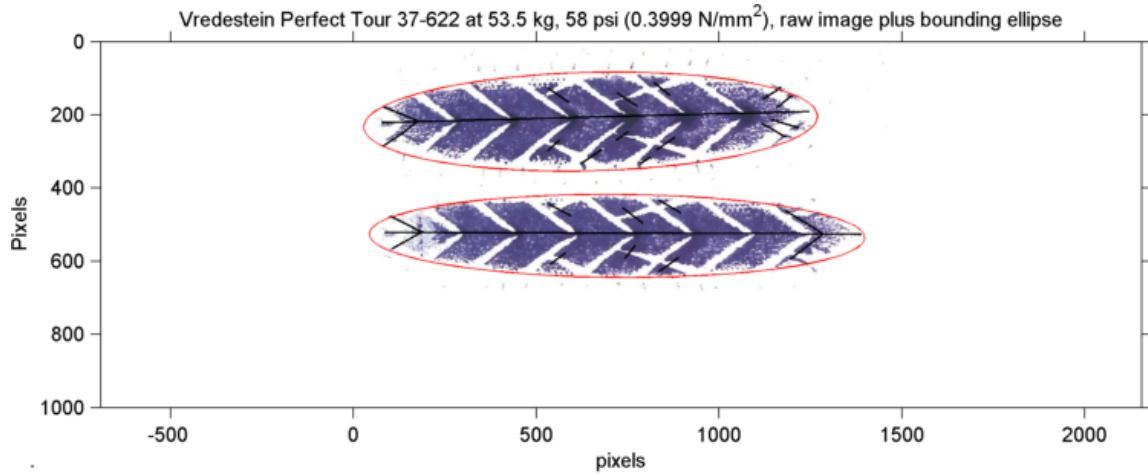


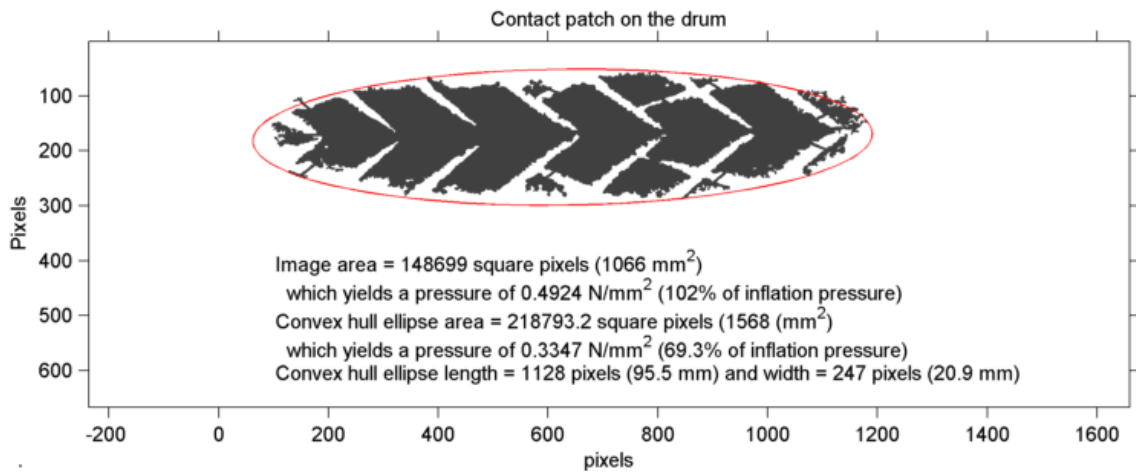
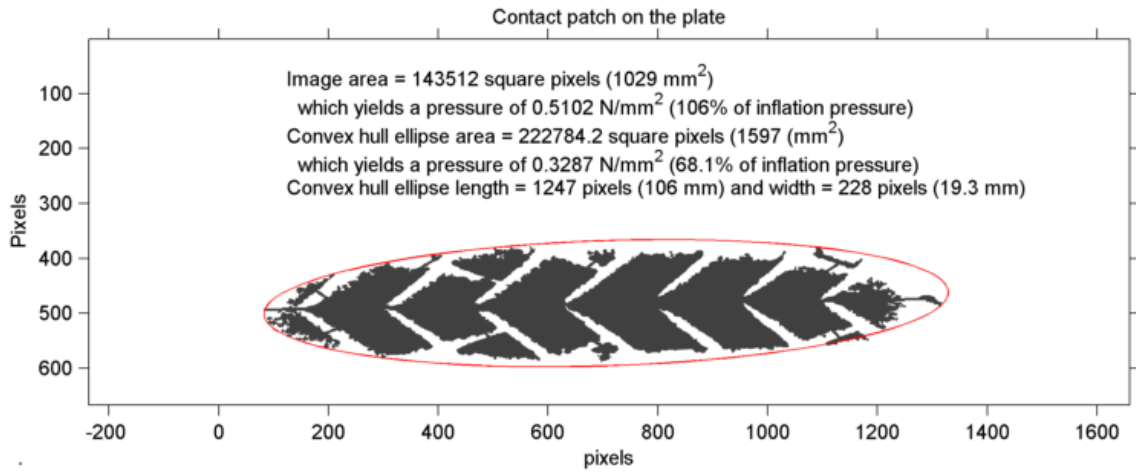
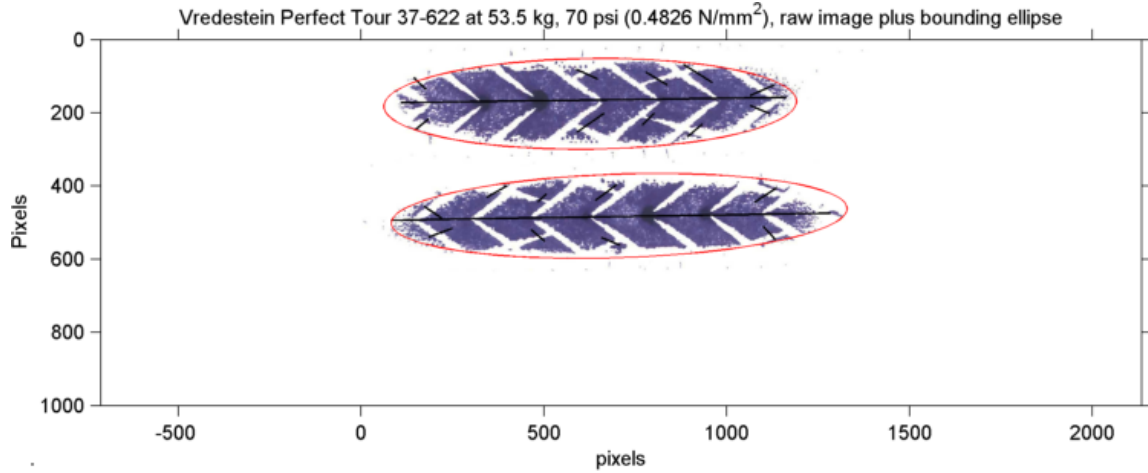


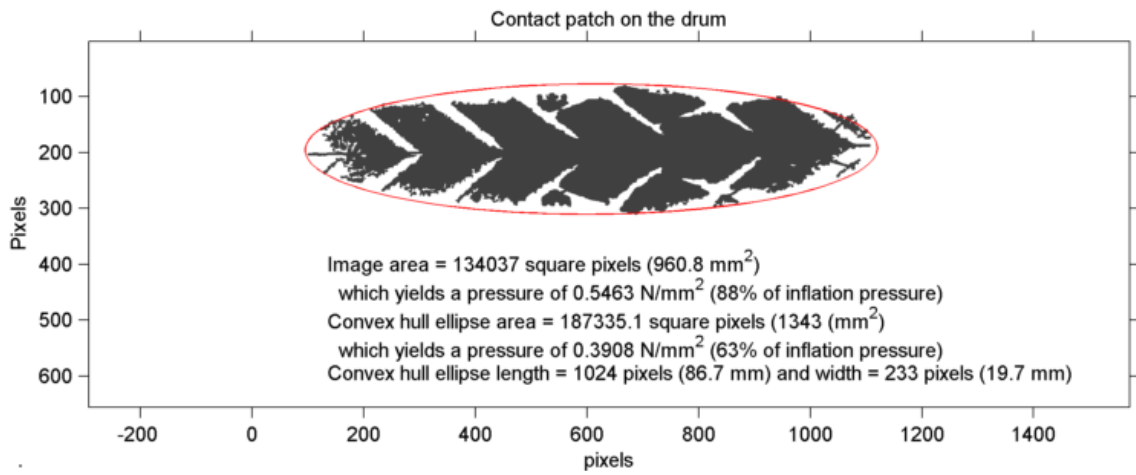
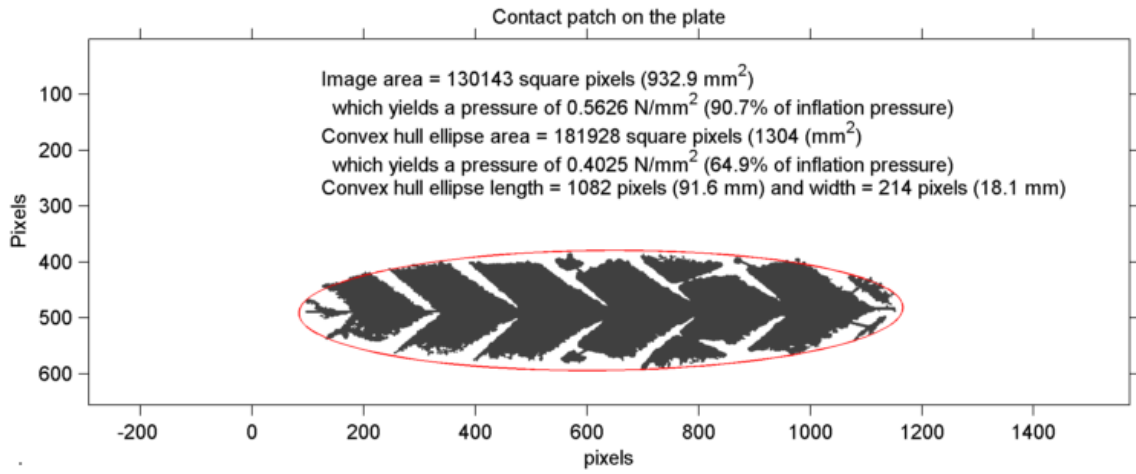
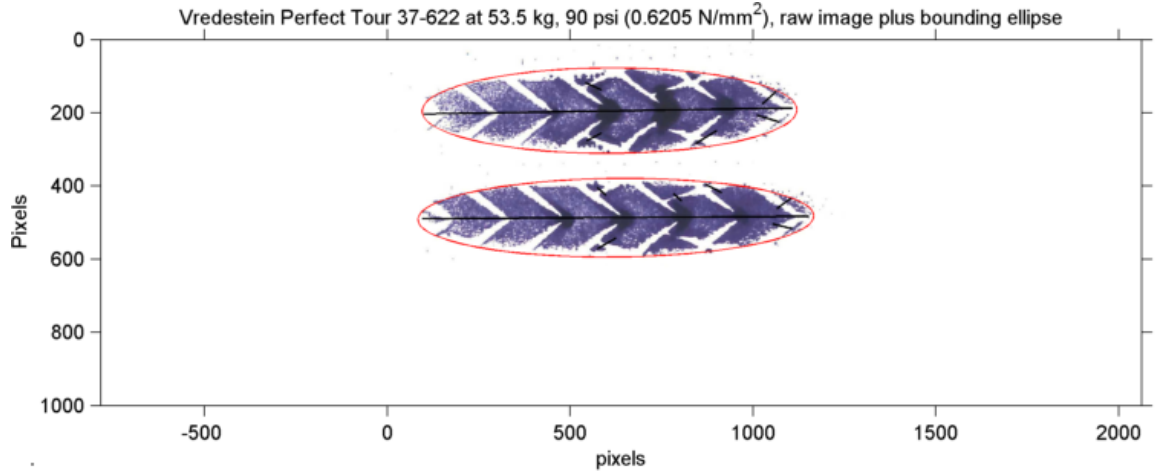


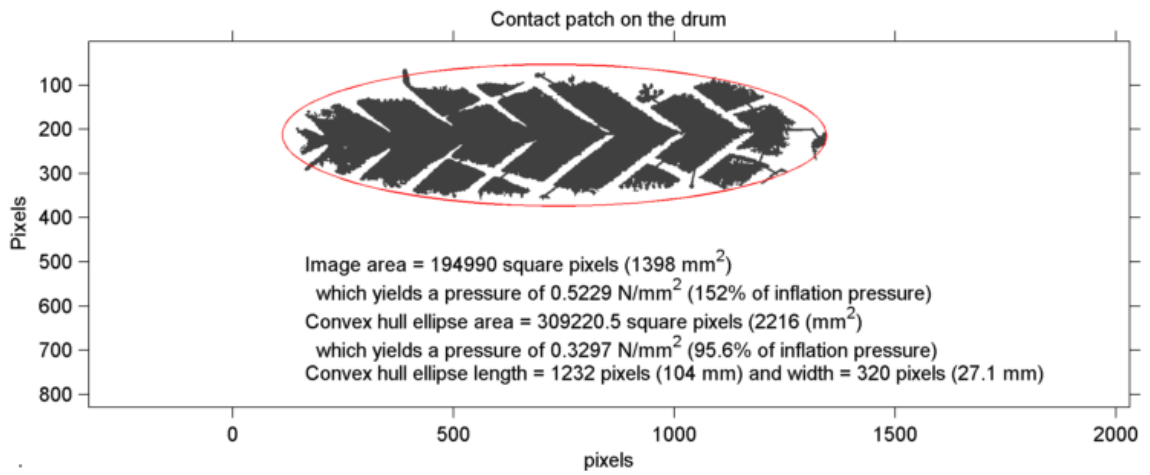
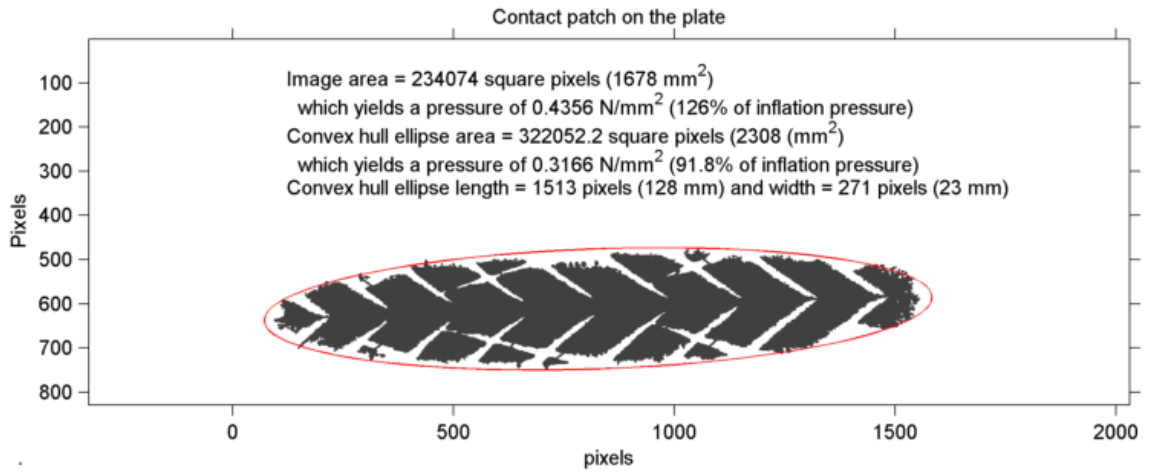
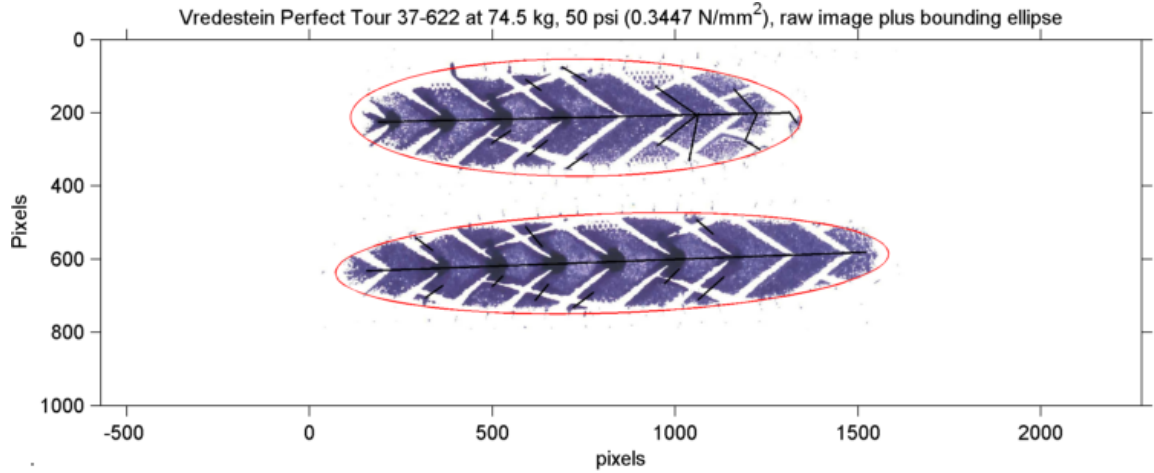


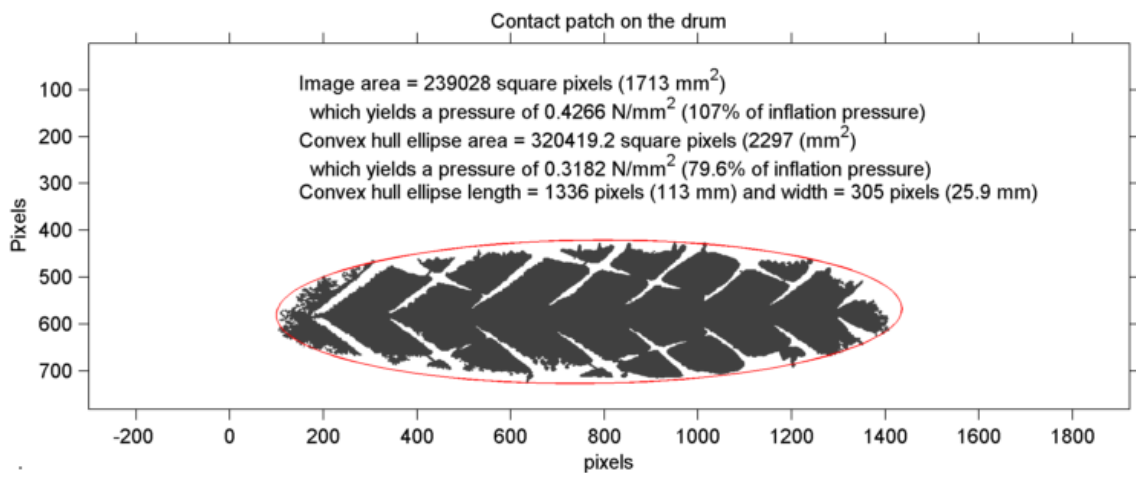
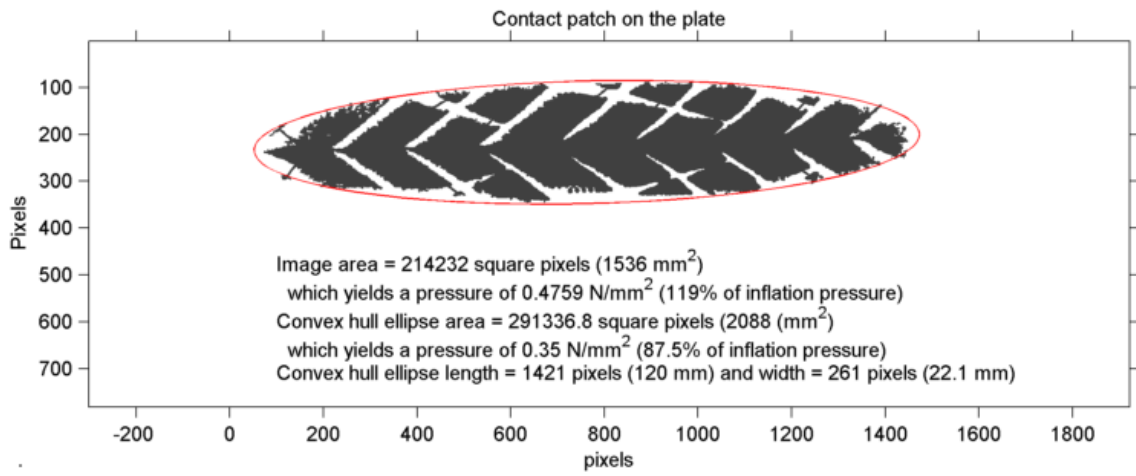
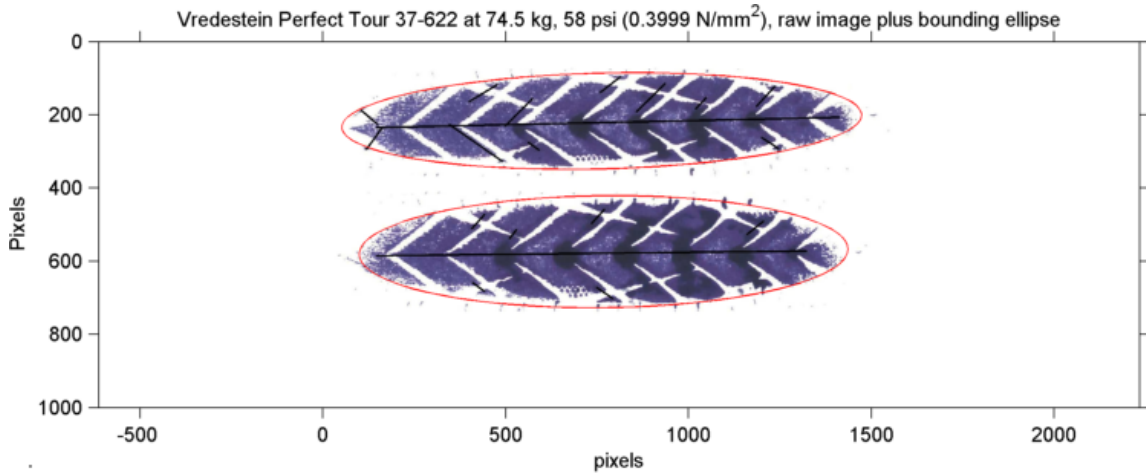


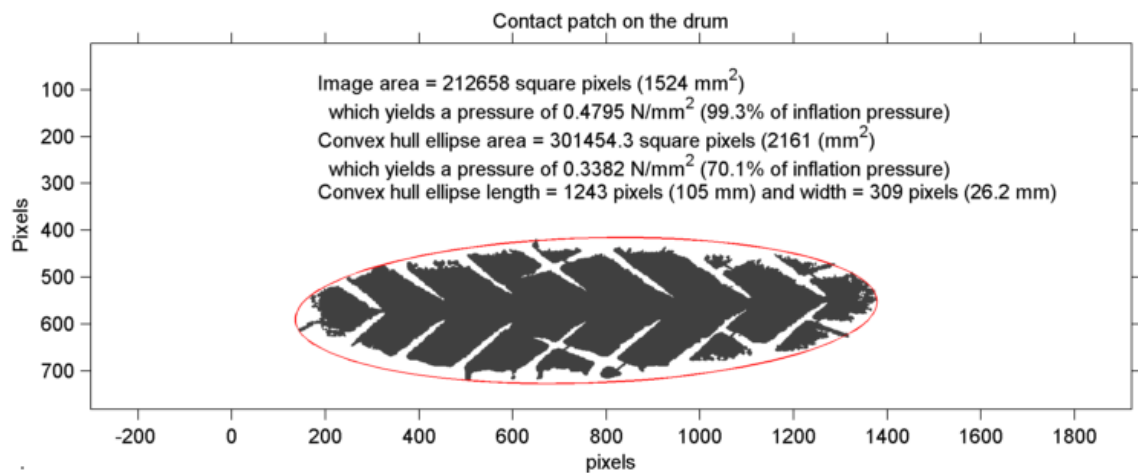
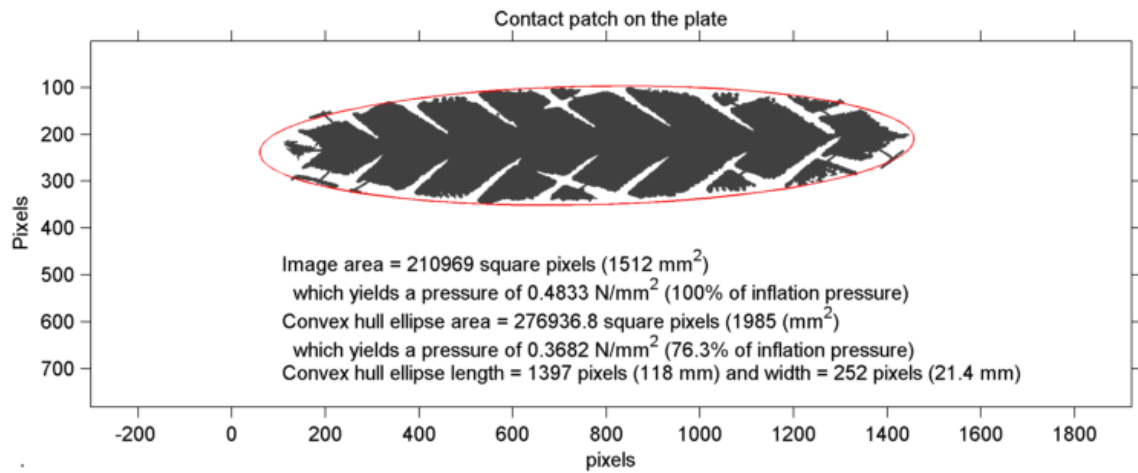
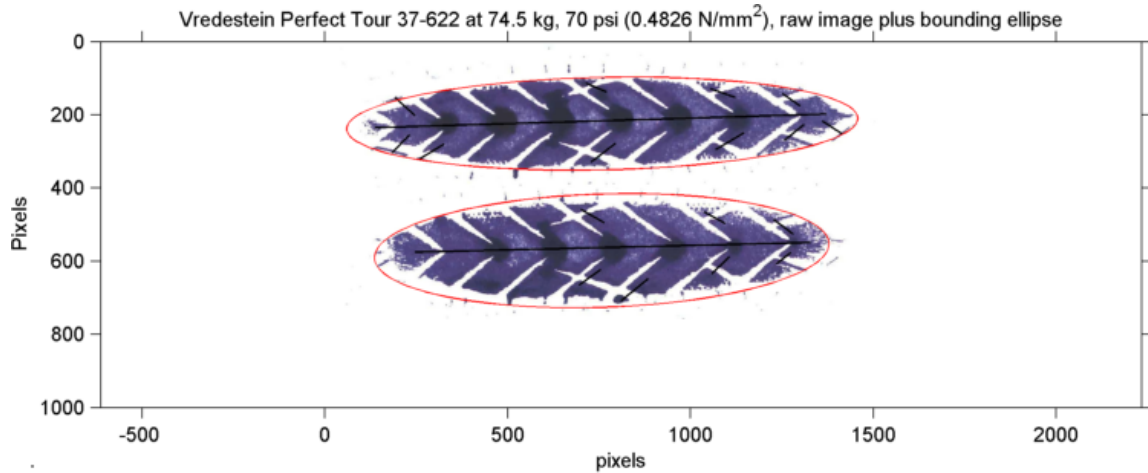


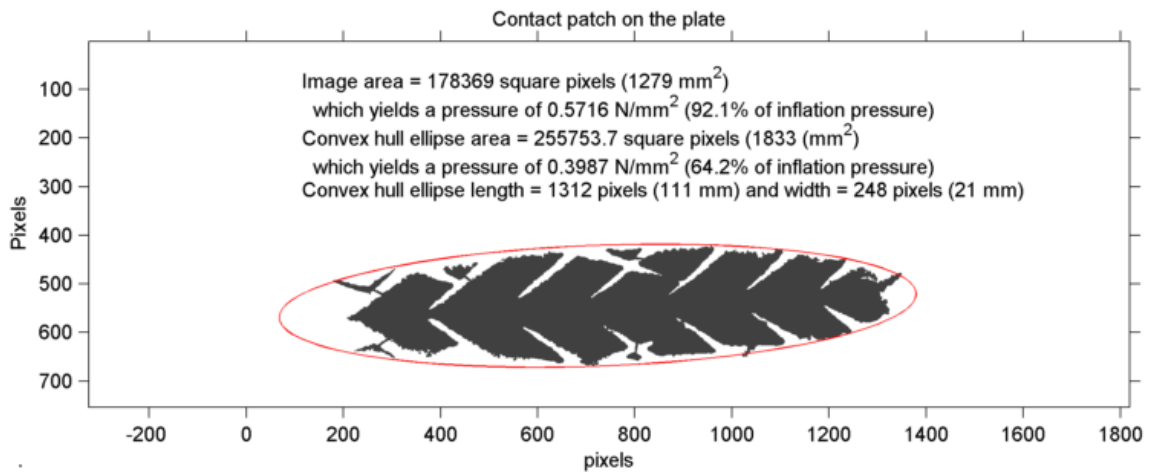
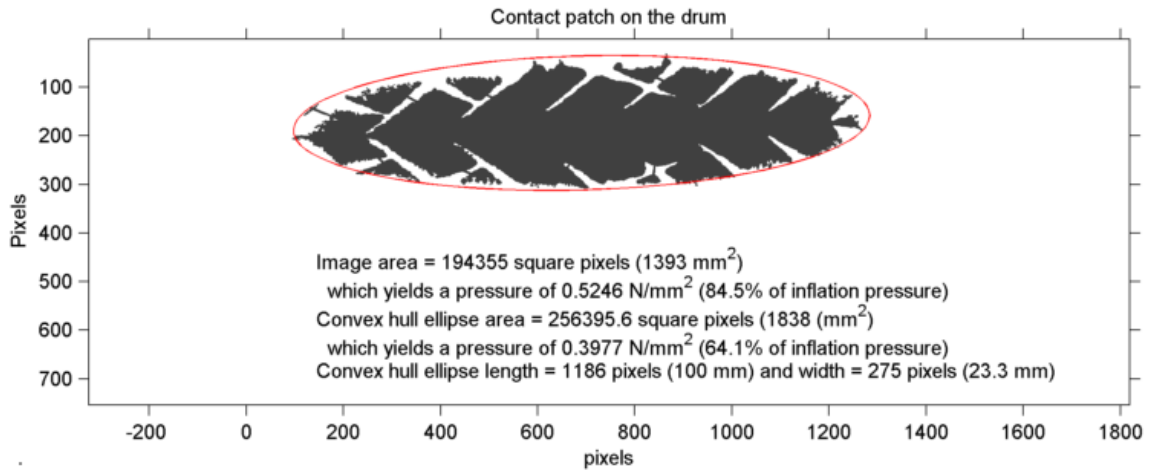
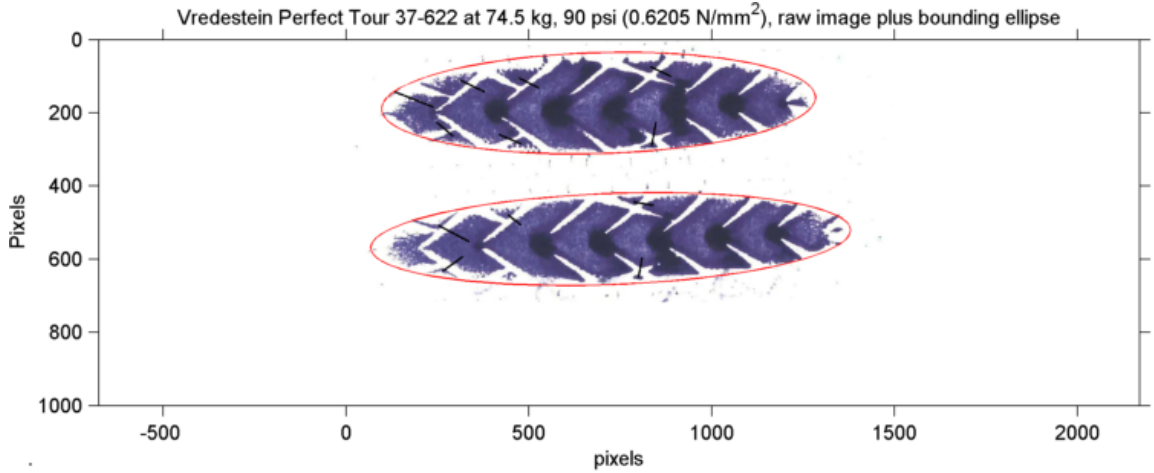


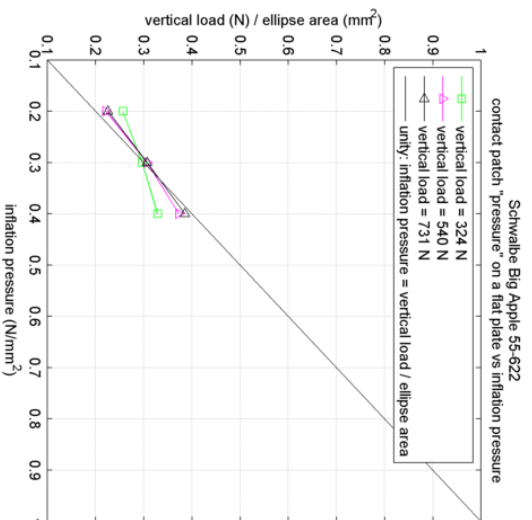
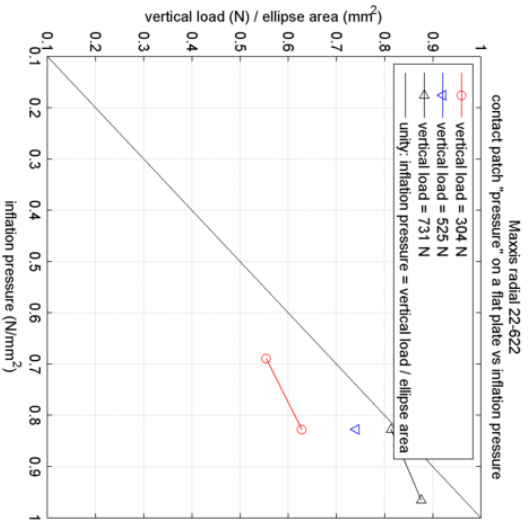
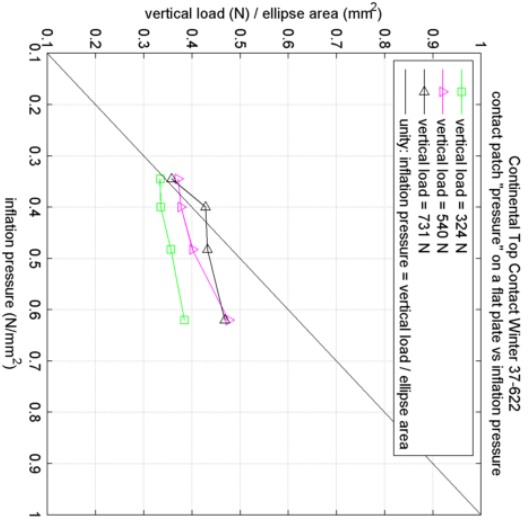
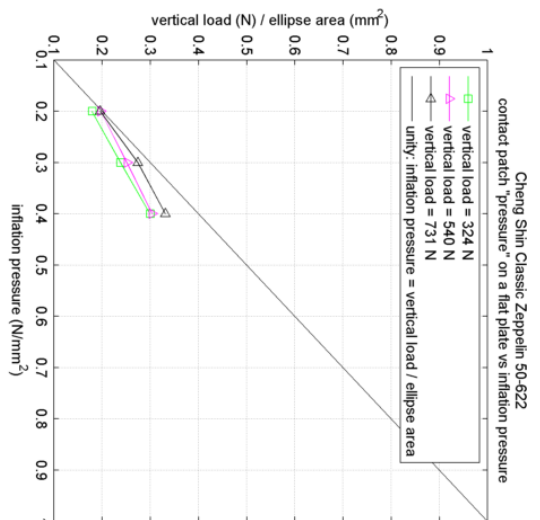
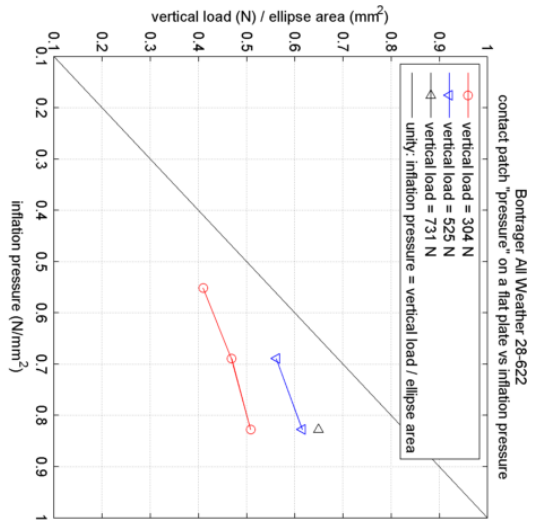
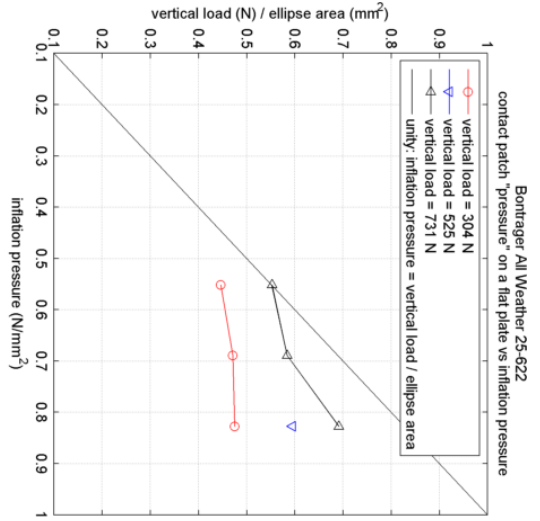


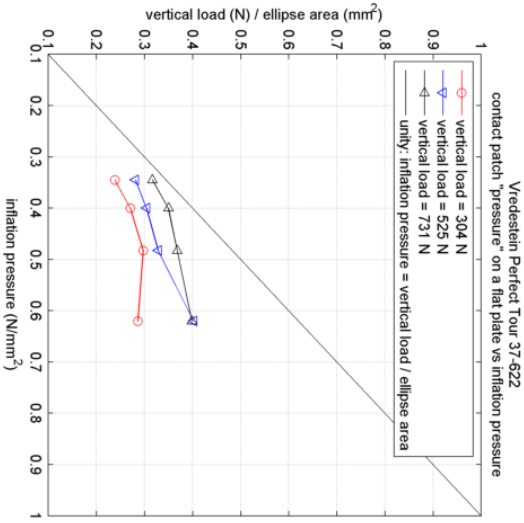
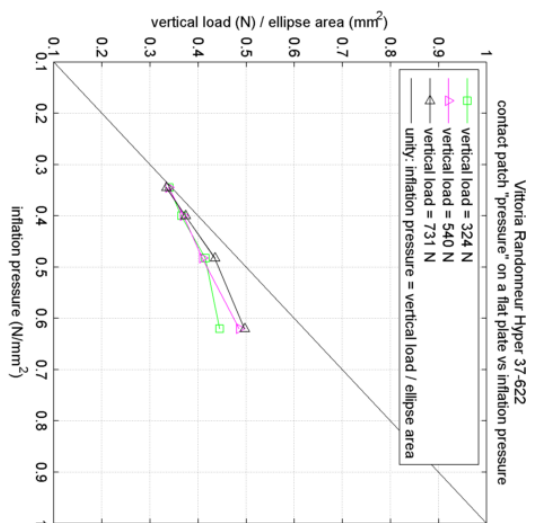
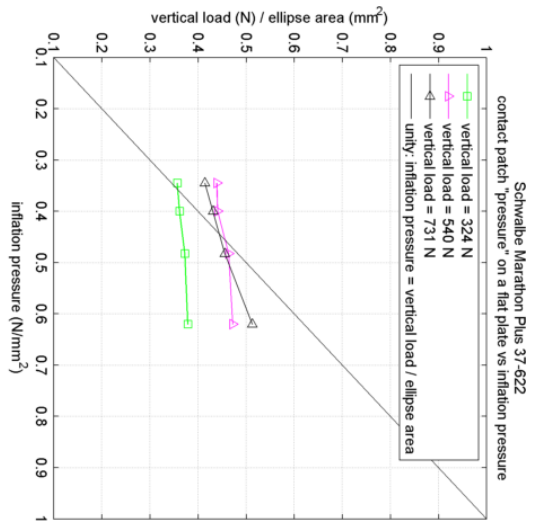
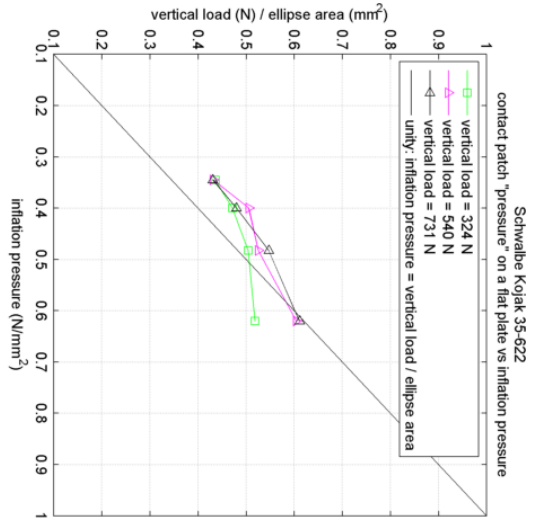


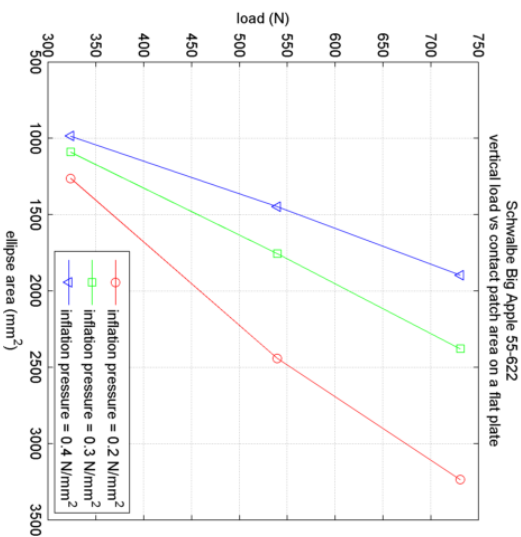
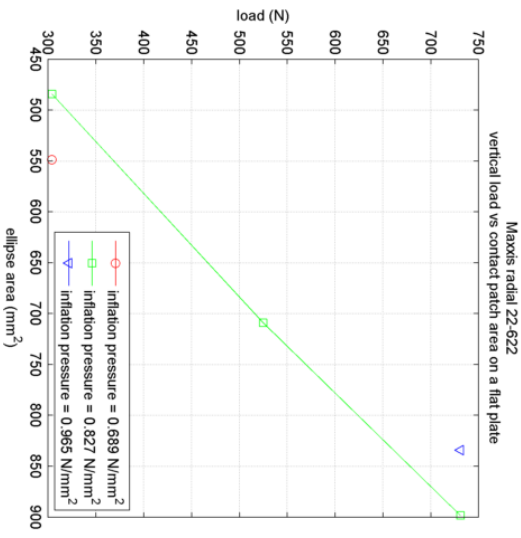
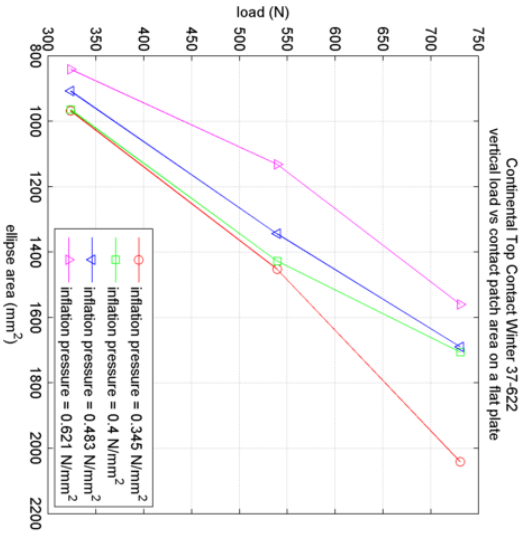
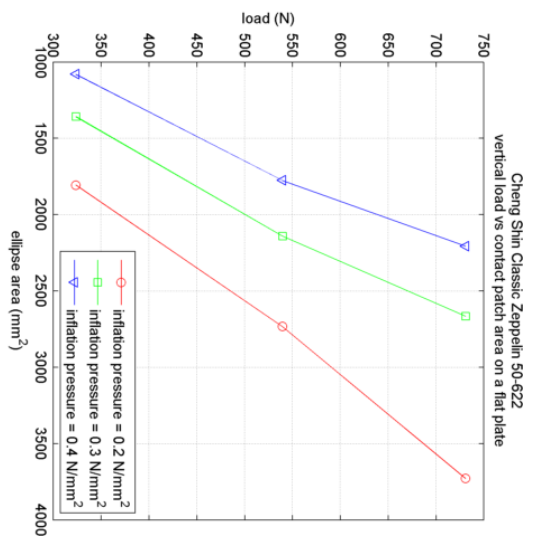
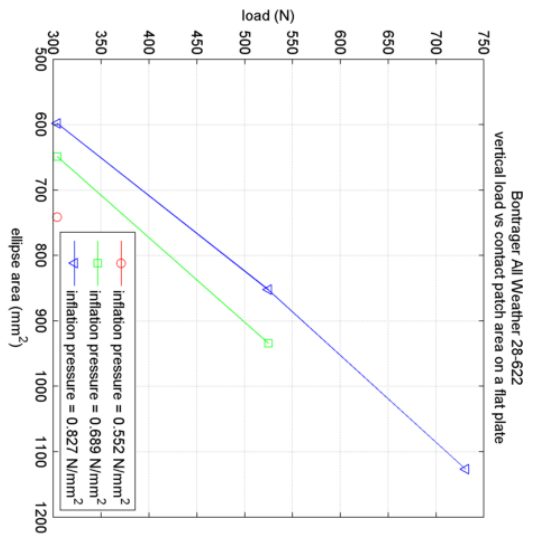
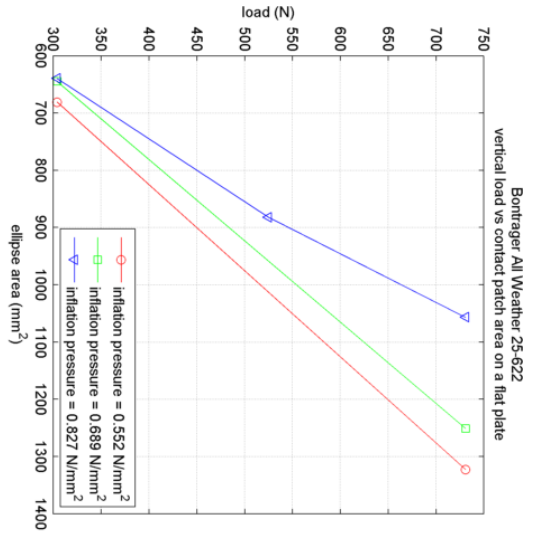


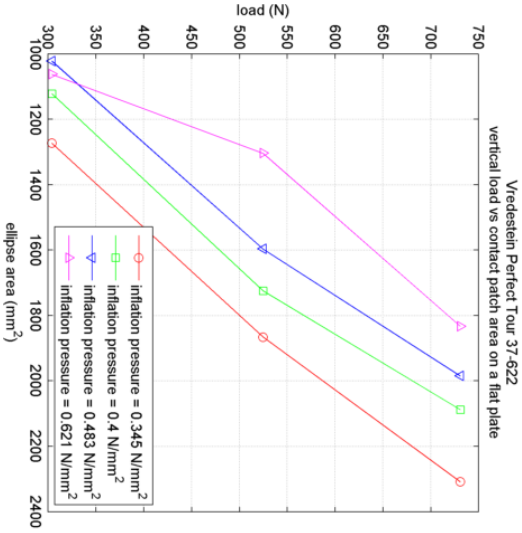
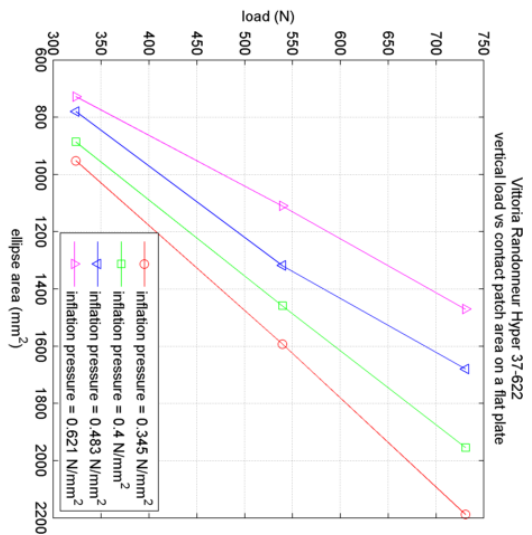
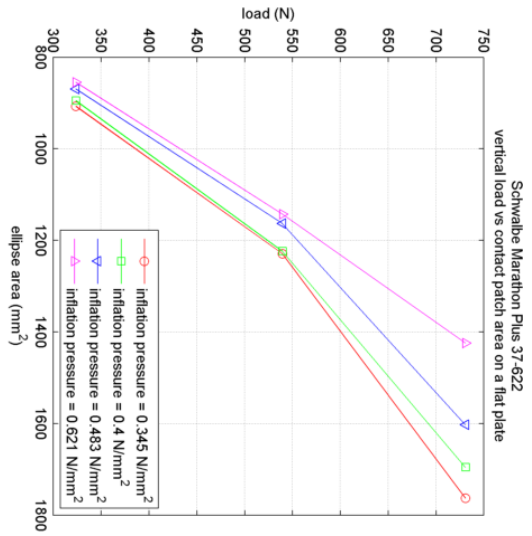
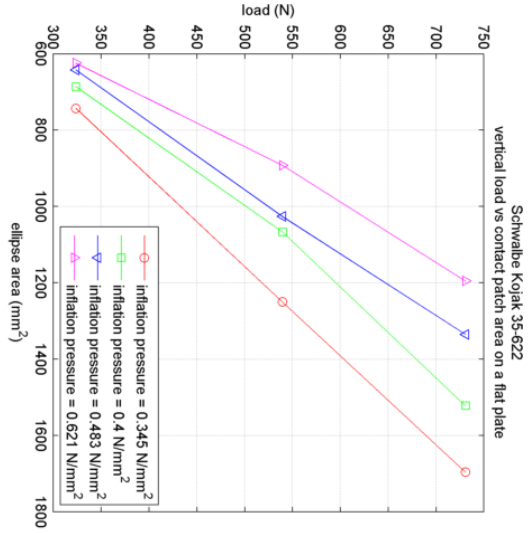


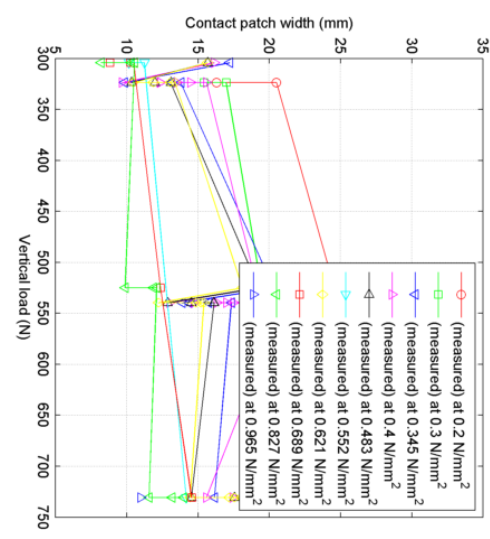
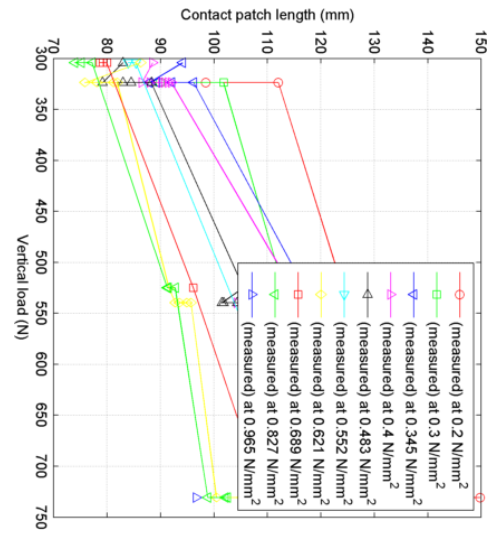
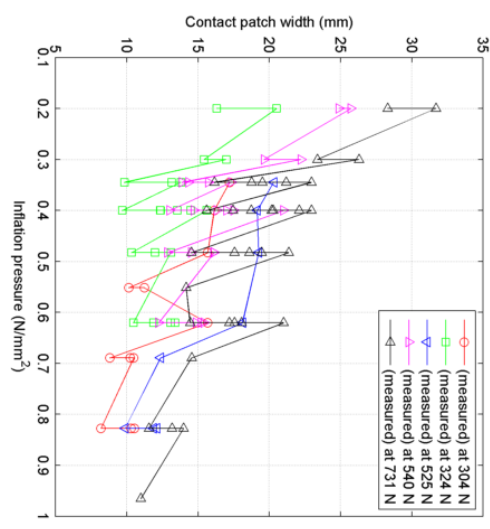
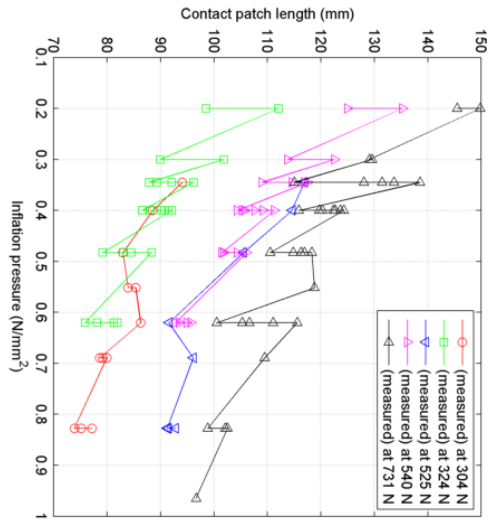
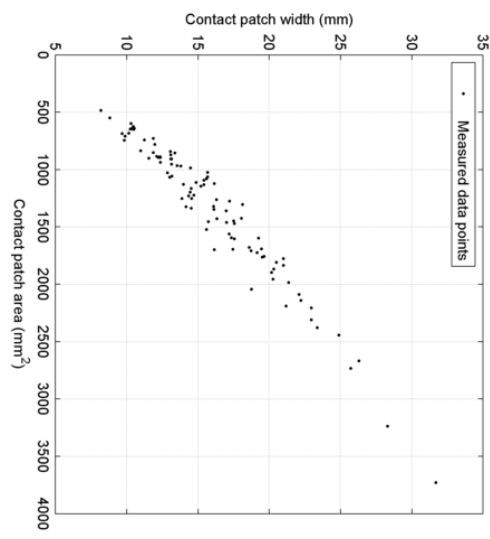
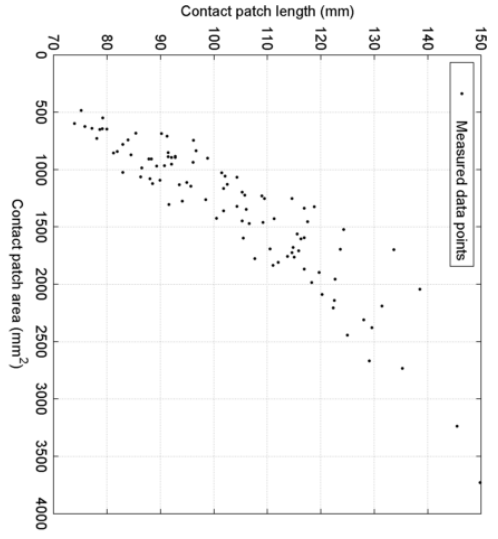


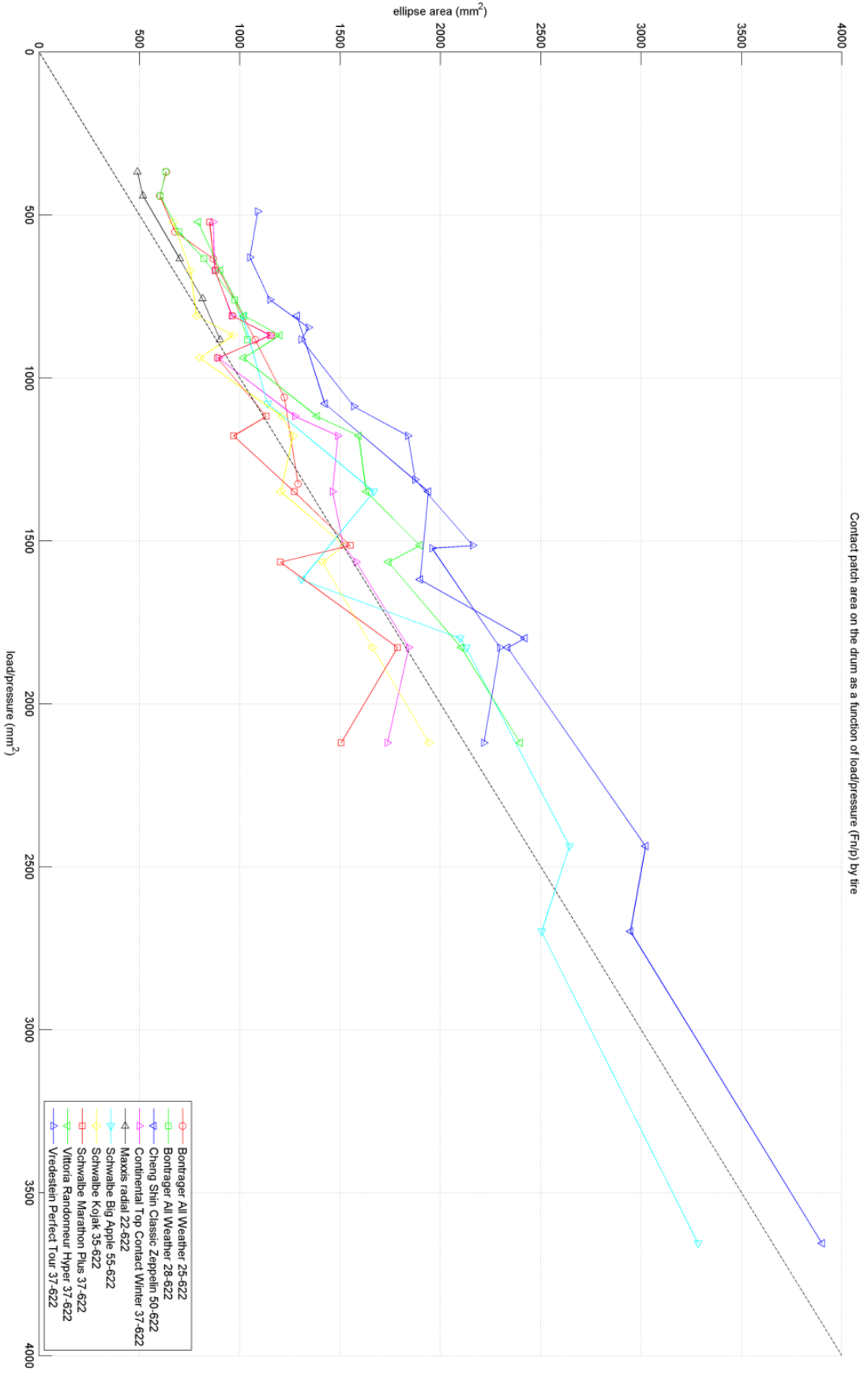


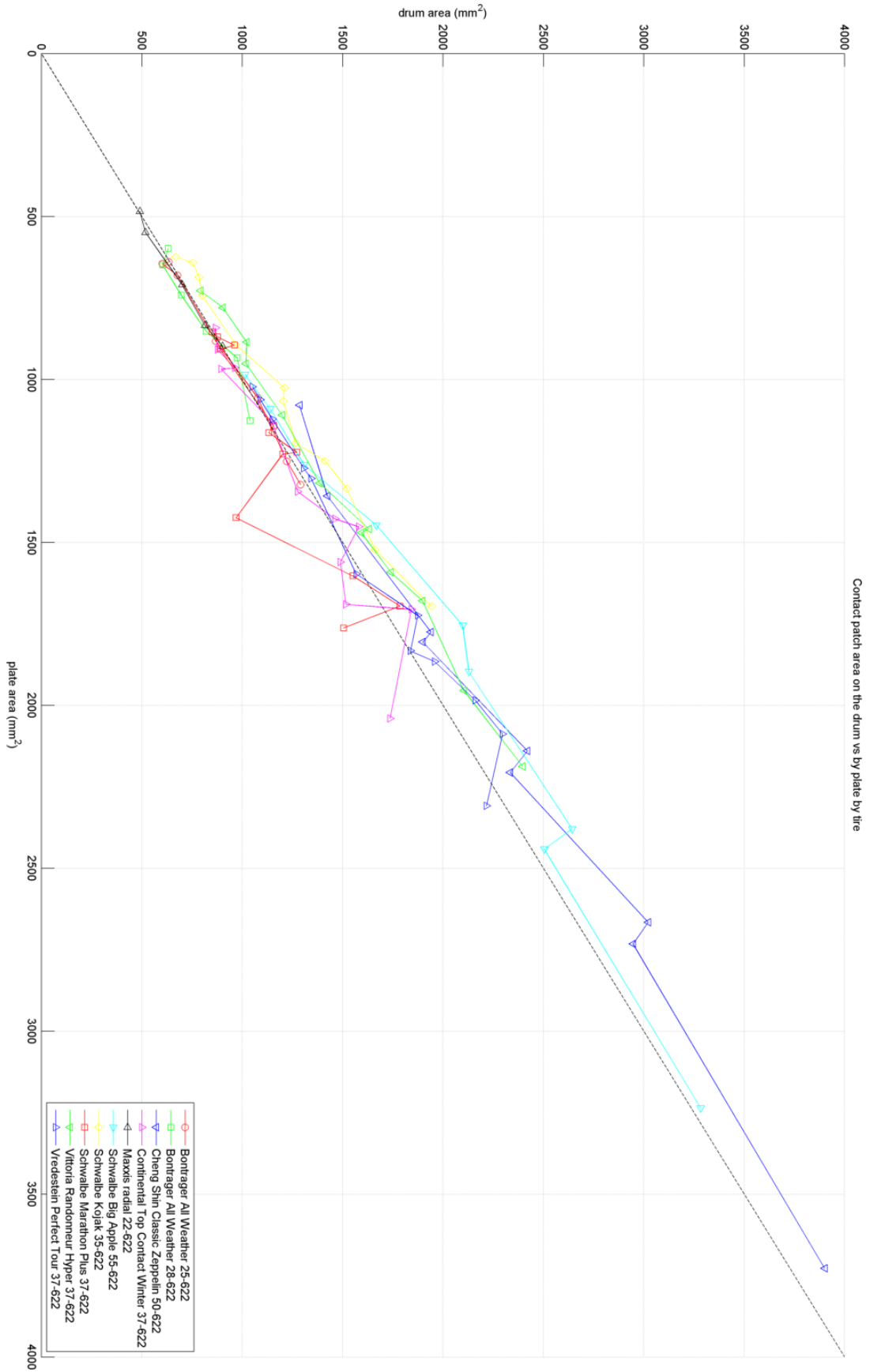


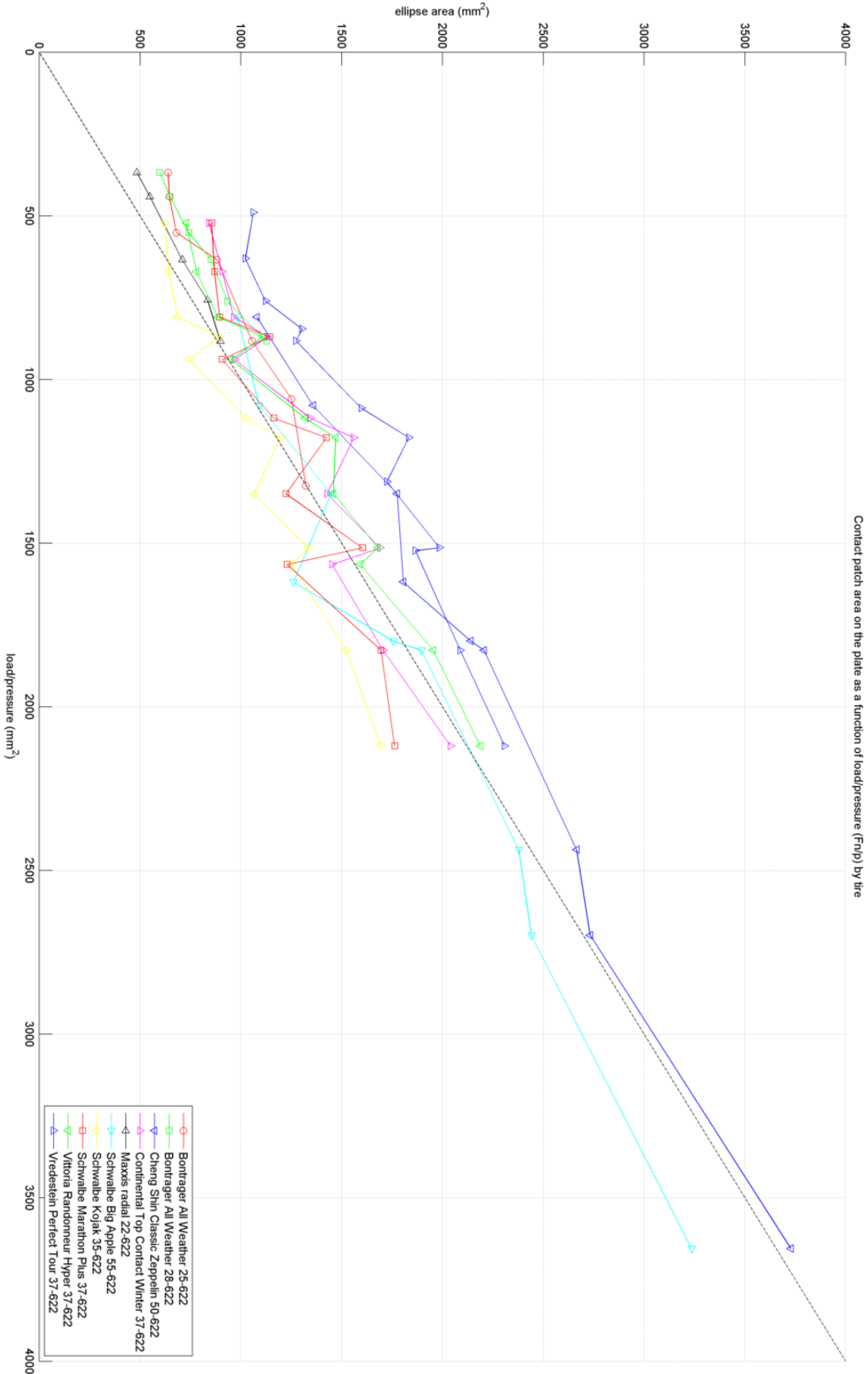


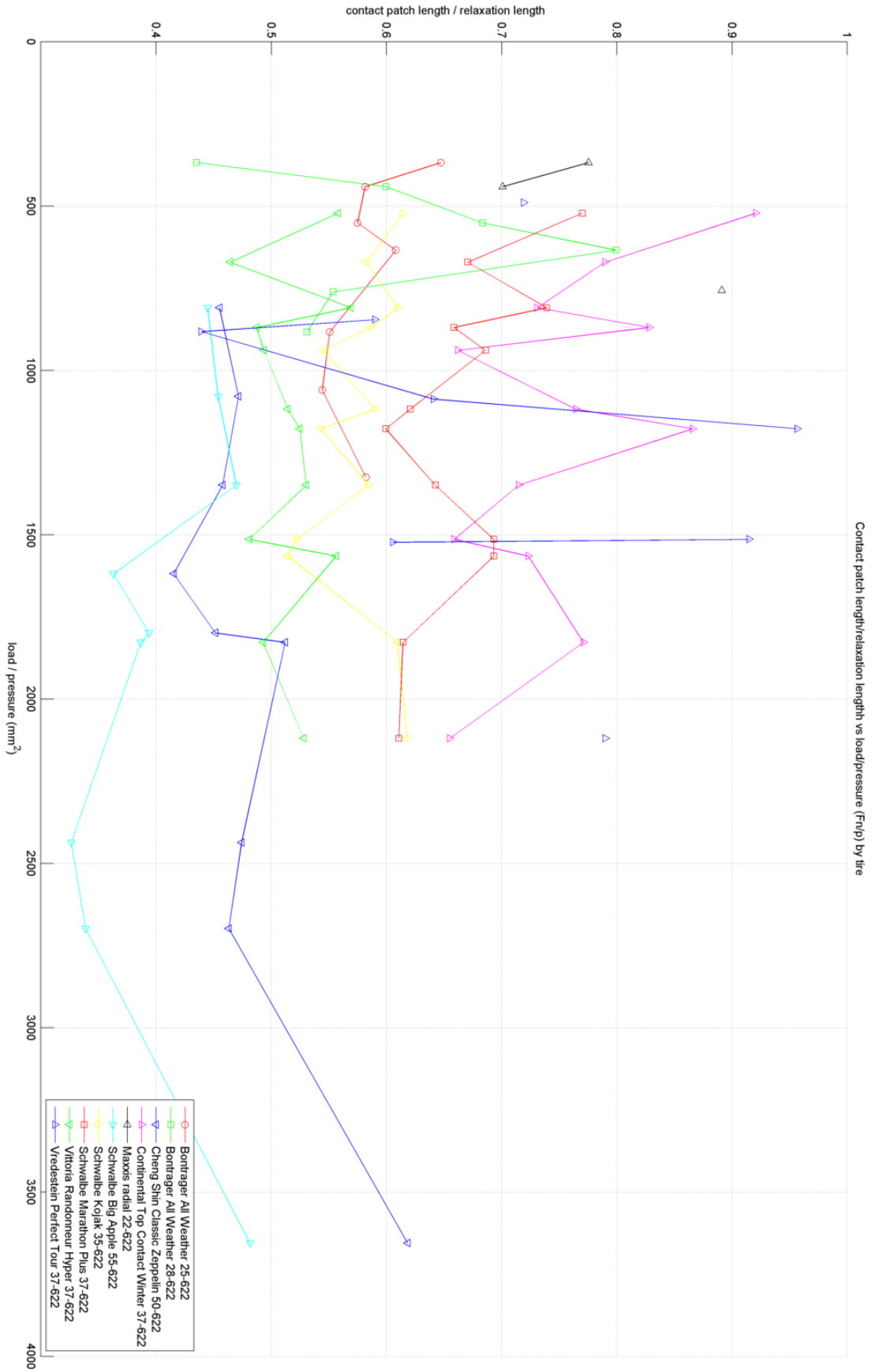


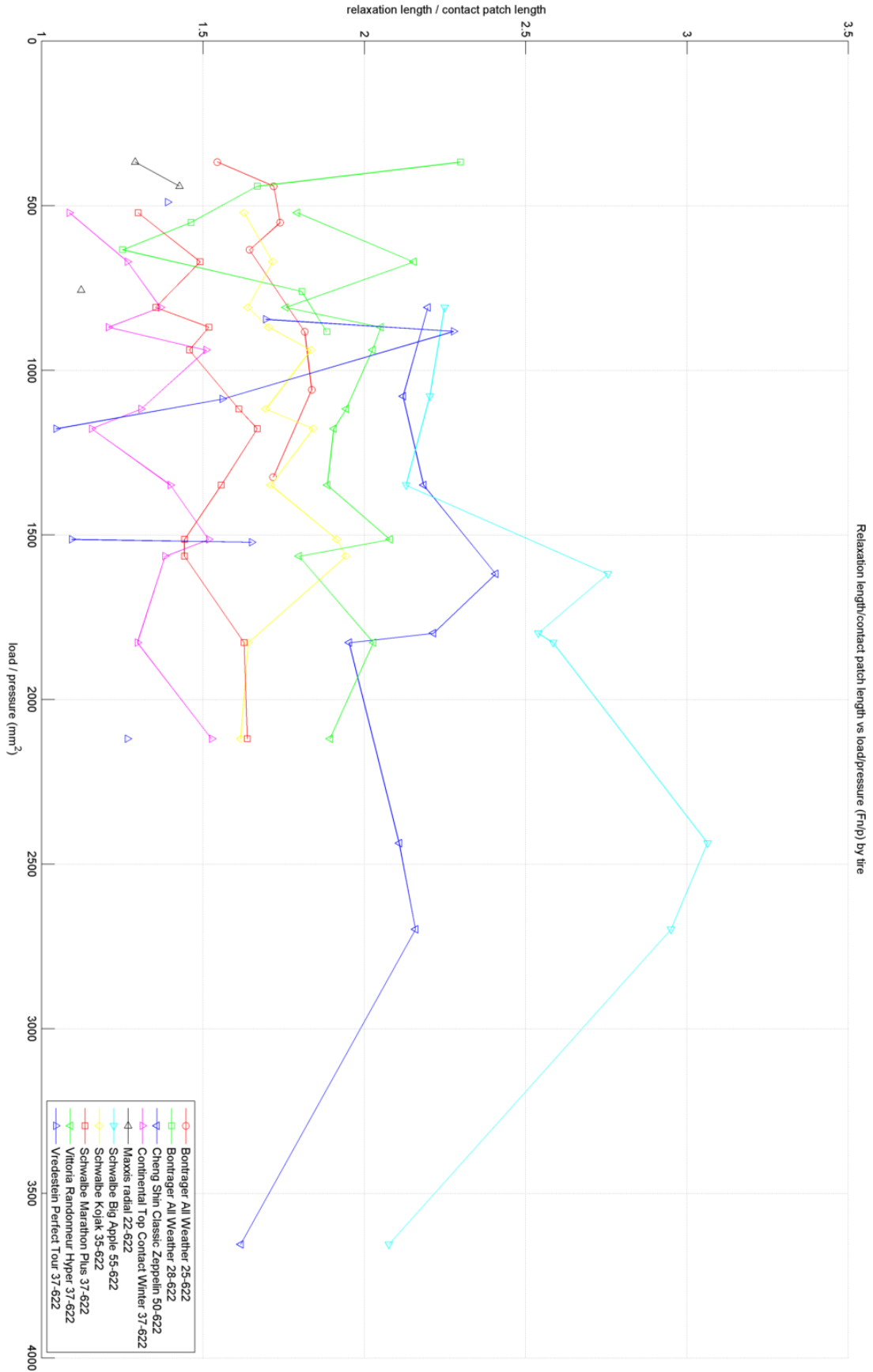










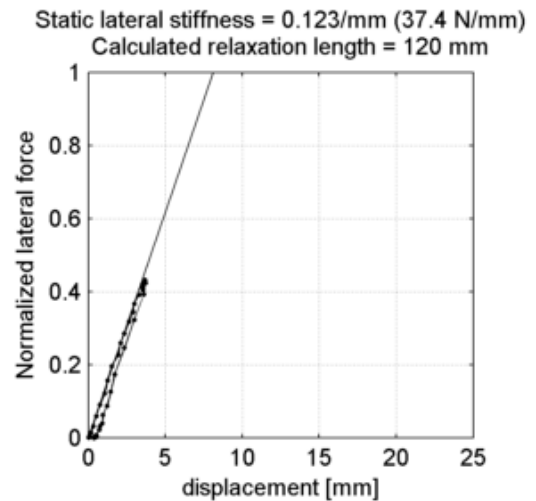
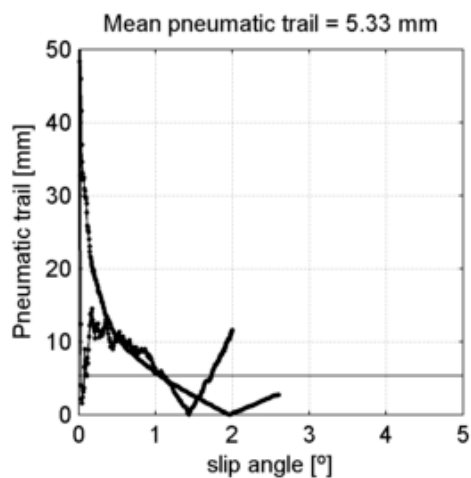
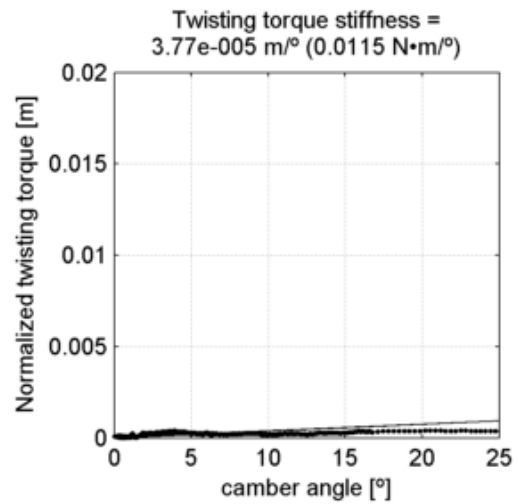
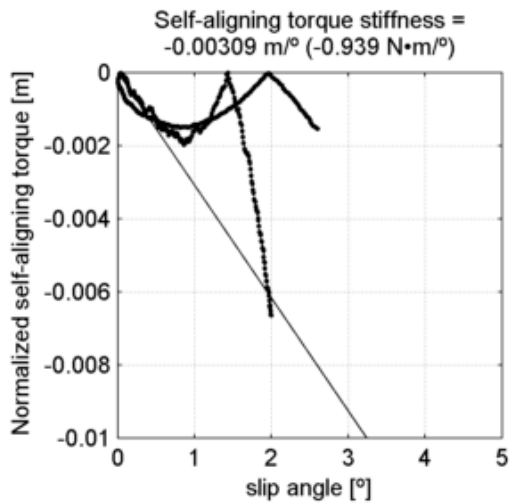
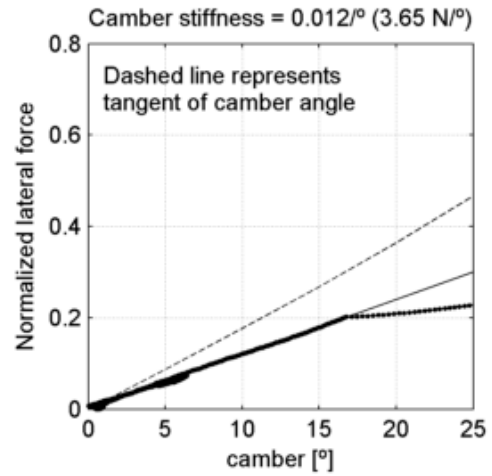
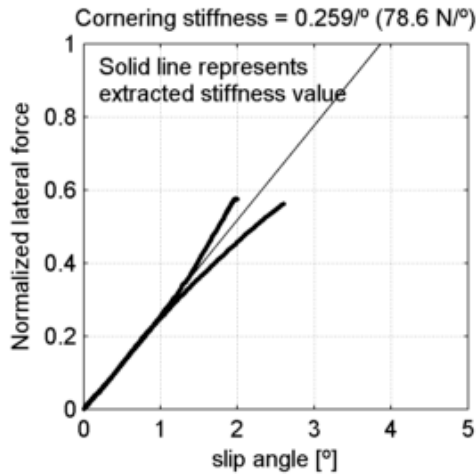


APPENDIX B

INDIVIDUAL TIRE TEST RESULTS

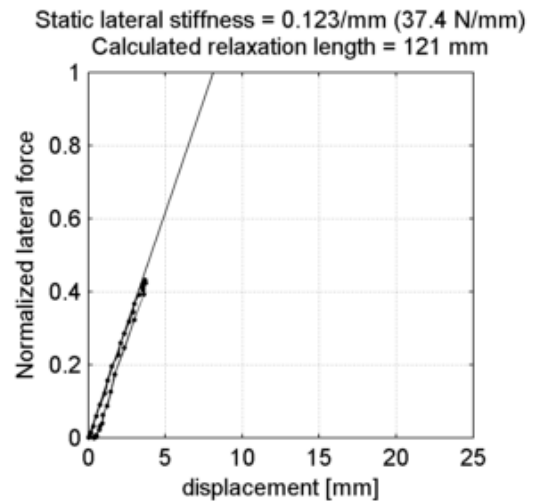
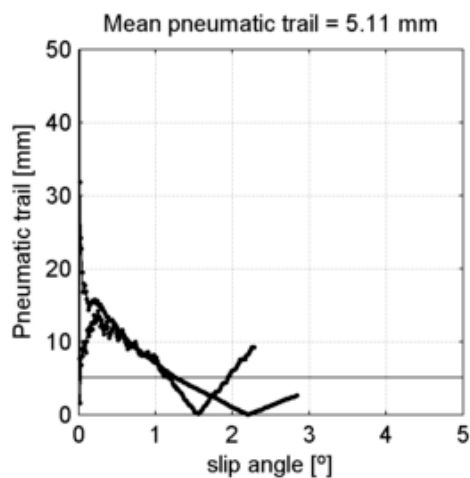
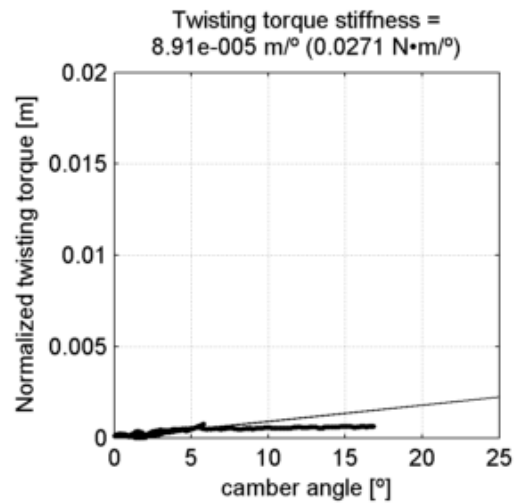
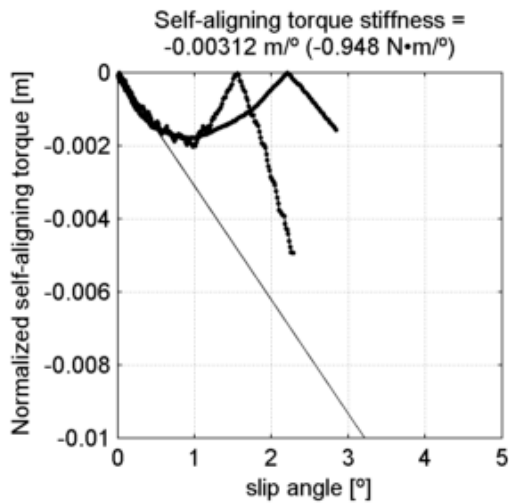
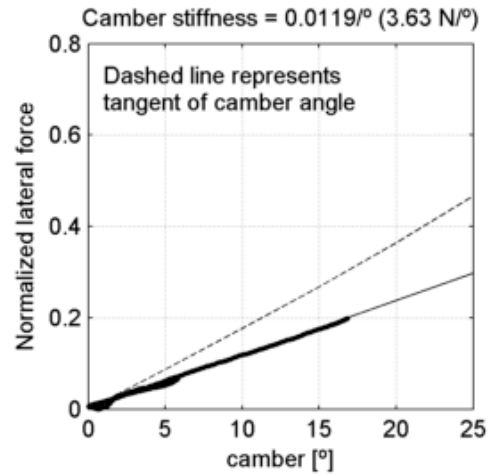
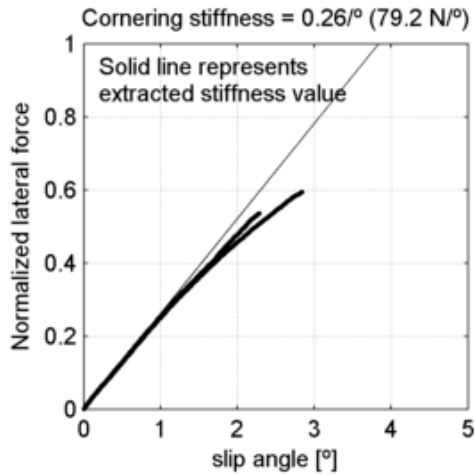
Bontrager All Weather 23-622
 tire radius = 11.5 mm, rim width = 13.4 mm

at 5.52 bar (80 psi) and
 under 304 N (31 kg, 68.3 lb)



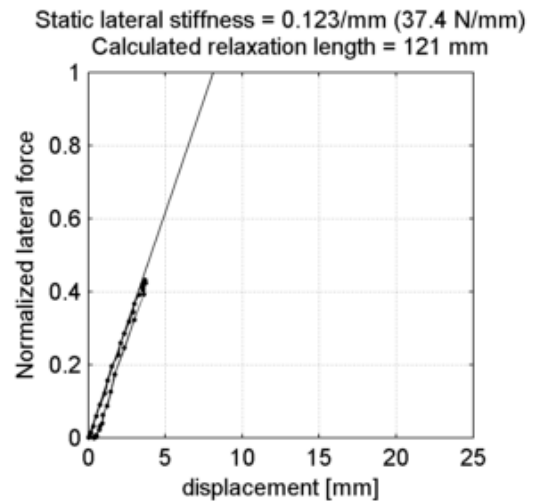
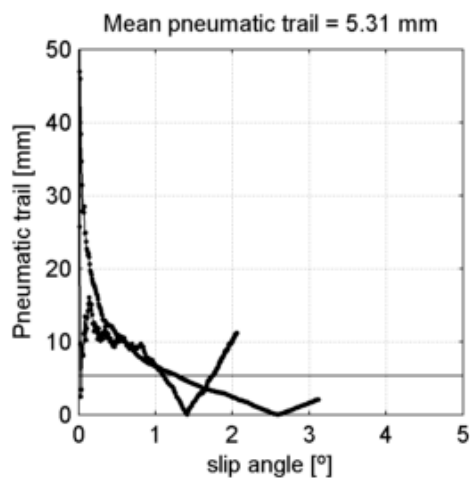
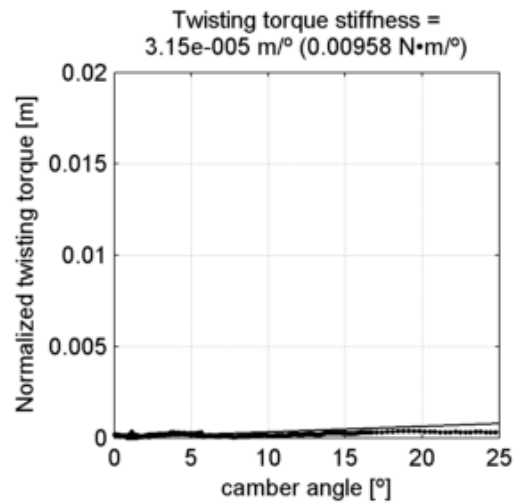
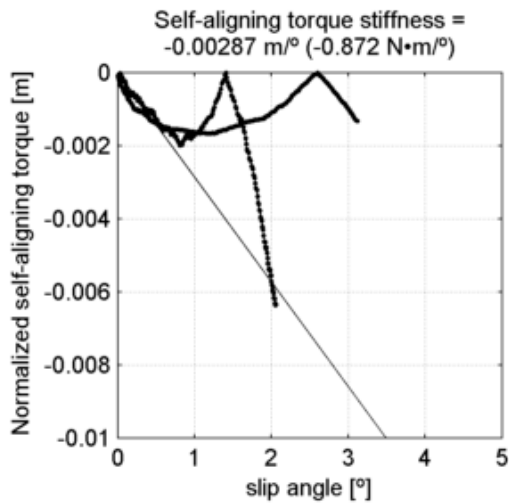
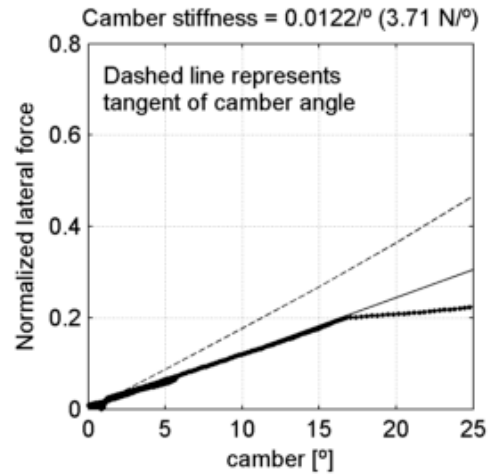
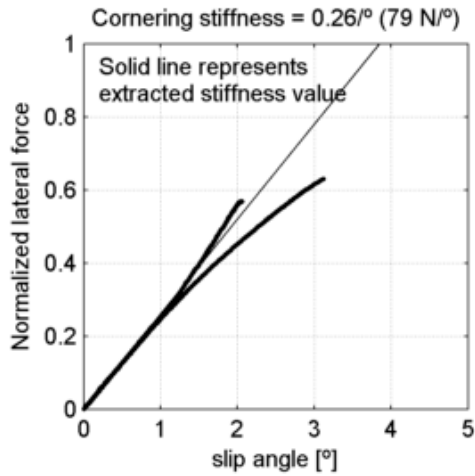
Bontrager All Weather 23-622
 tire radius = 11.5 mm, rim width = 13.4 mm

at 5.52 bar (80 psi) and
 under 304 N (31 kg, 68.3 lb)



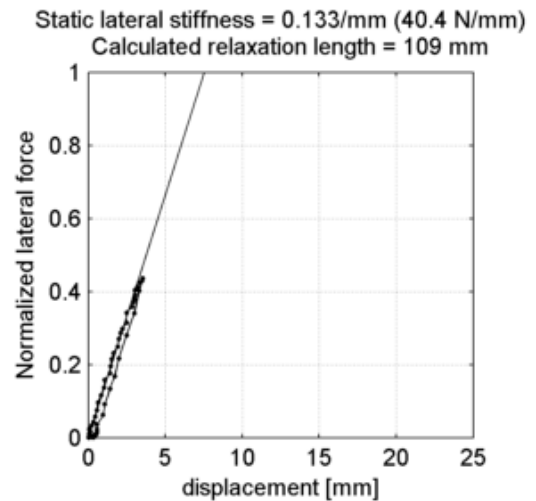
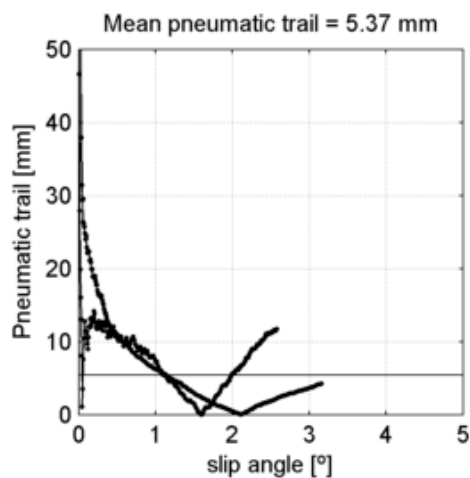
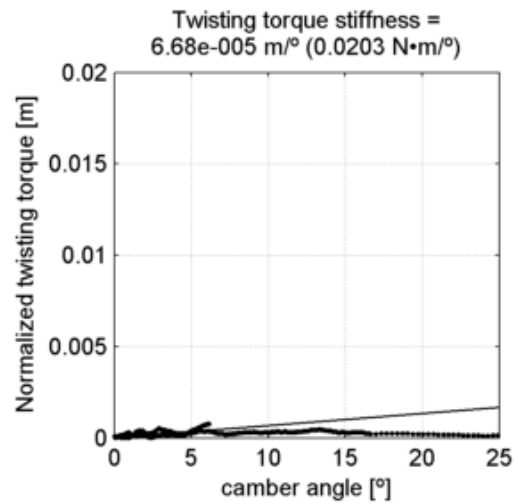
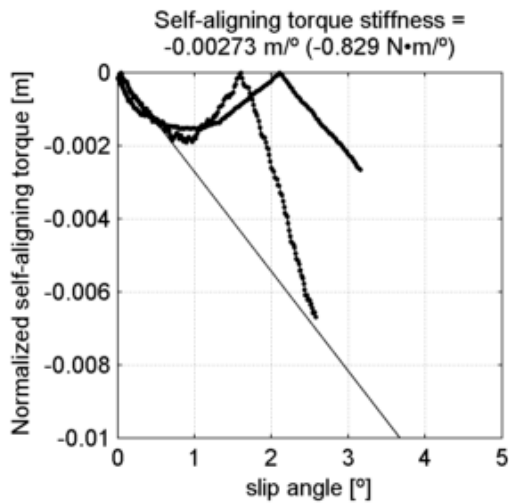
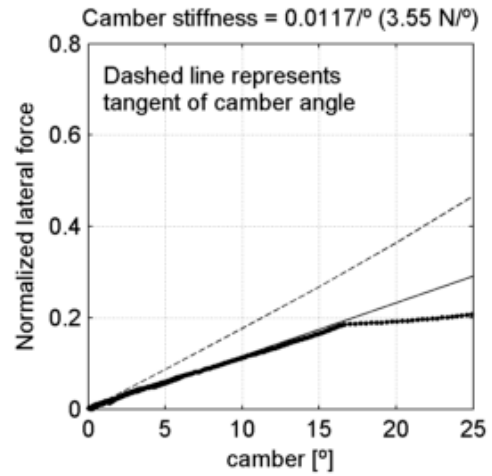
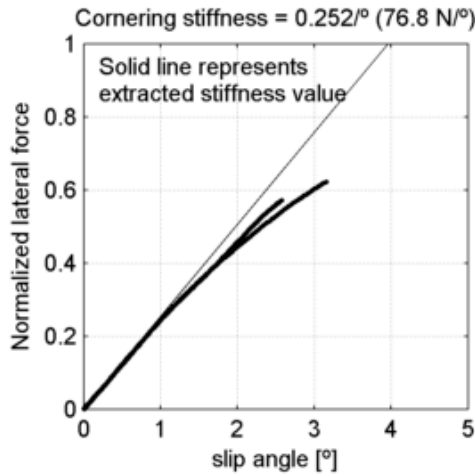
Bontrager All Weather 23-622
 tire radius = 11.5 mm, rim width = 13.4 mm

at 5.52 bar (80 psi) and
 under 304 N (31 kg, 68.3 lb)



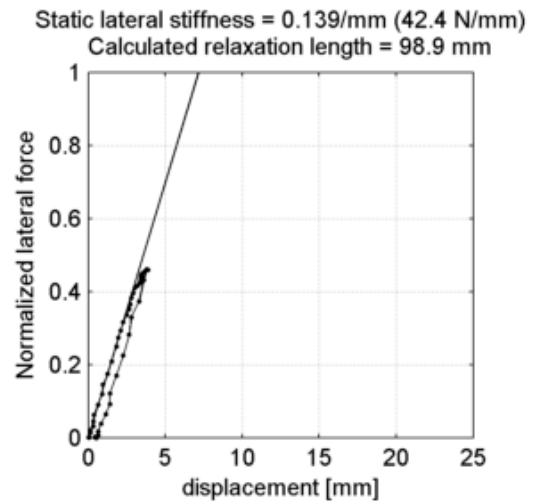
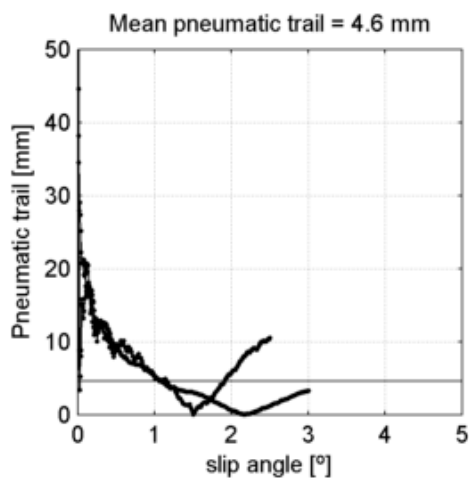
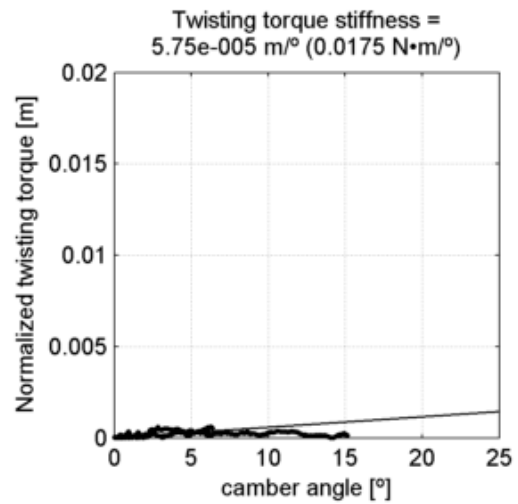
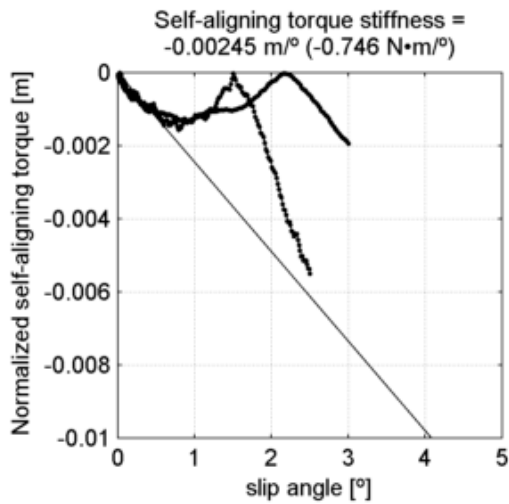
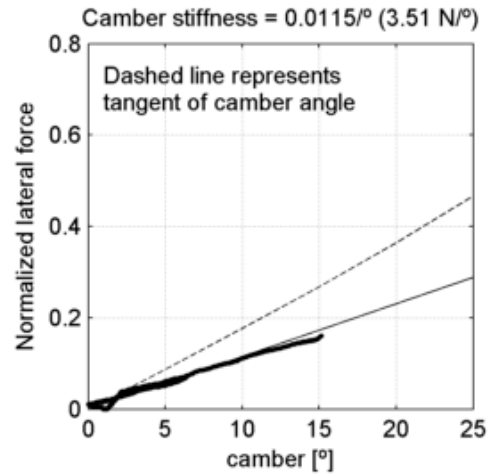
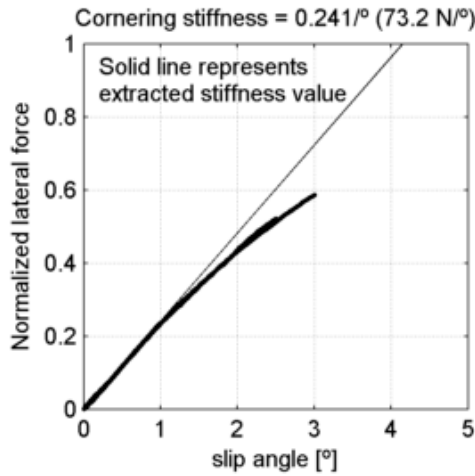
Bontrager All Weather 23-622
 tire radius = 11.5 mm, rim width = 13.4 mm

at 6.89 bar (100 psi) and
 under 304 N (31 kg, 68.3 lb)



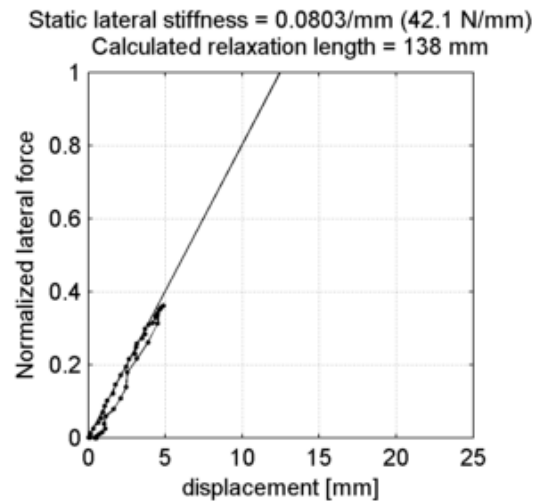
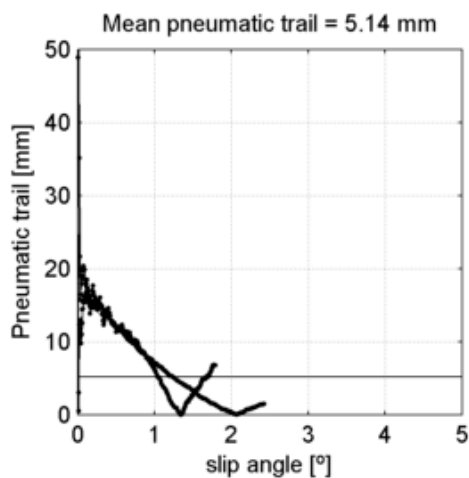
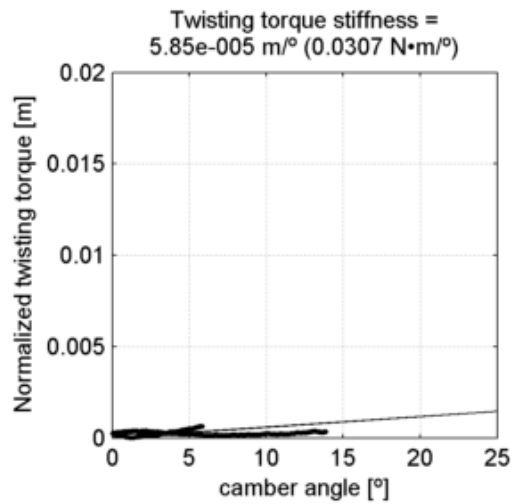
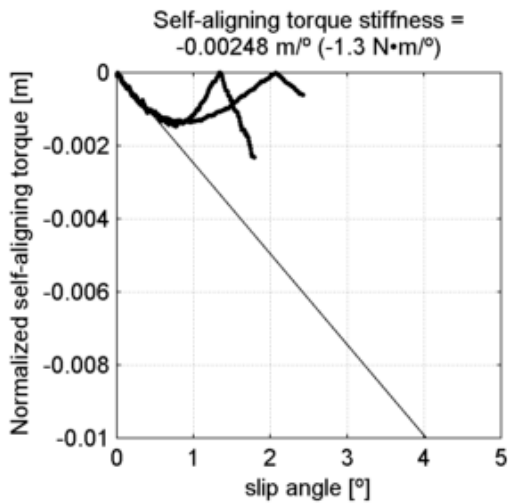
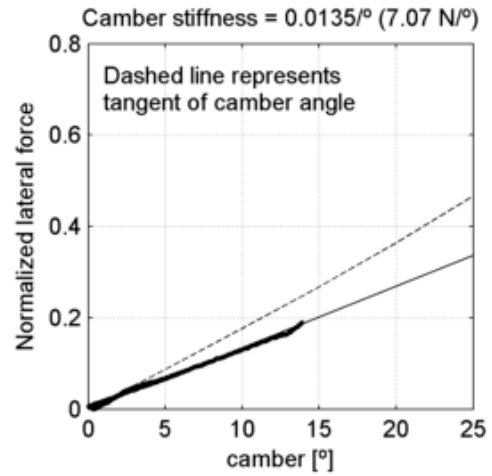
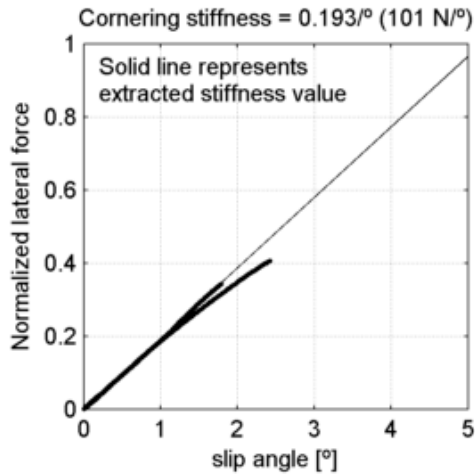
Bontrager All Weather 23-622
 tire radius = 11.5 mm, rim width = 13.4 mm

at 8.27 bar (120 psi) and
 under 304 N (31 kg, 68.3 lb)



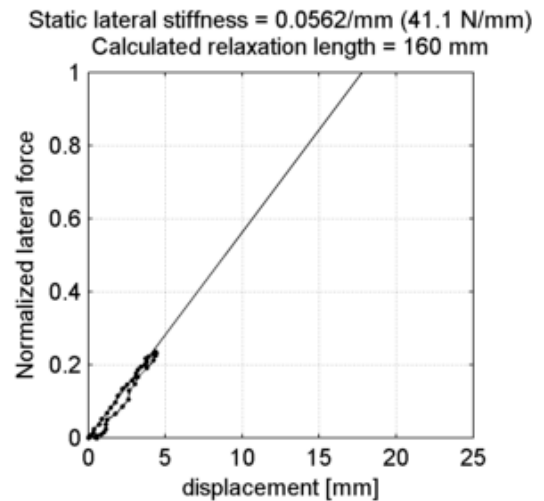
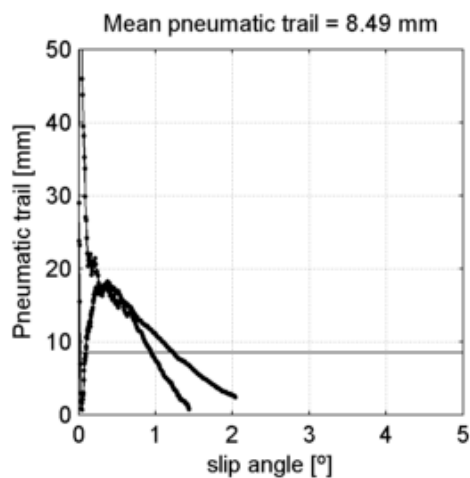
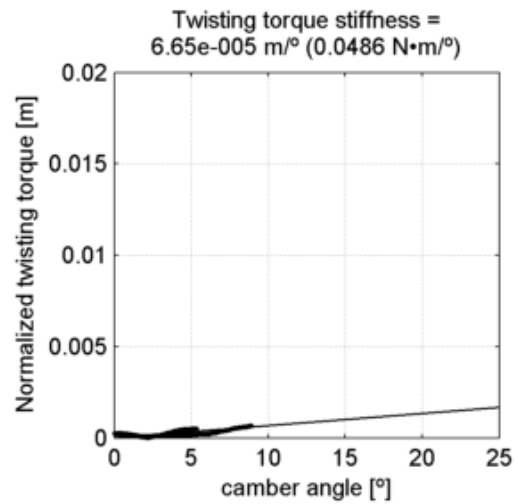
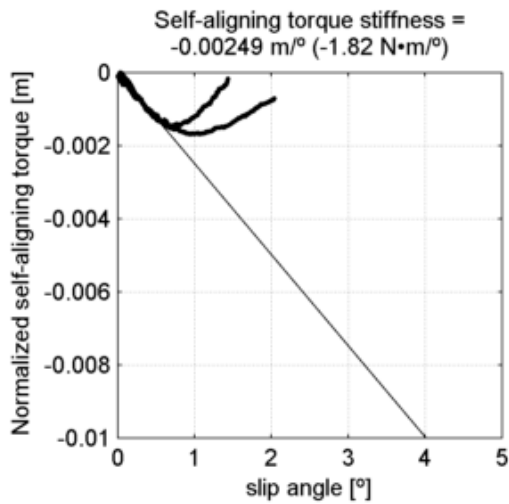
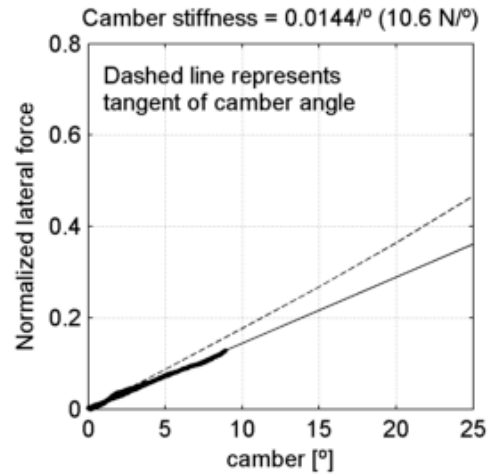
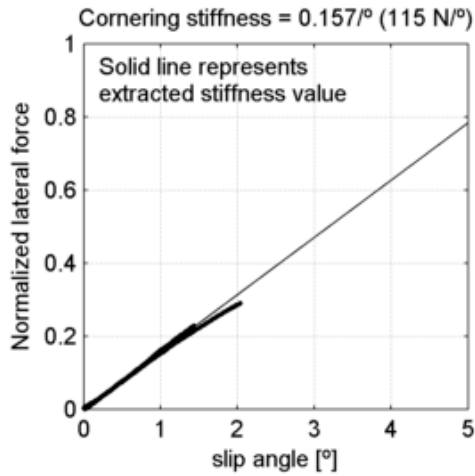
Bontrager All Weather 23-622
 tire radius = 11.5 mm, rim width = 13.4 mm

at 8.27 bar (120 psi) and
 under 525 N (53.5 kg, 118 lb)



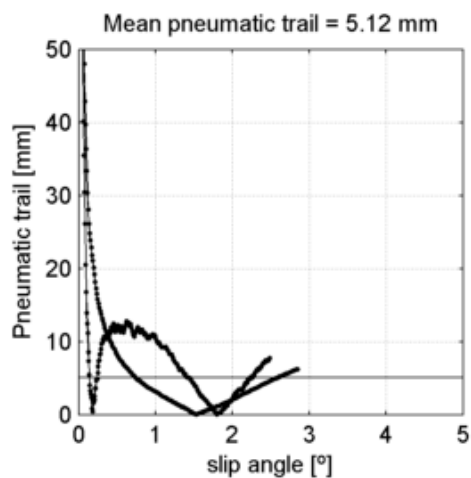
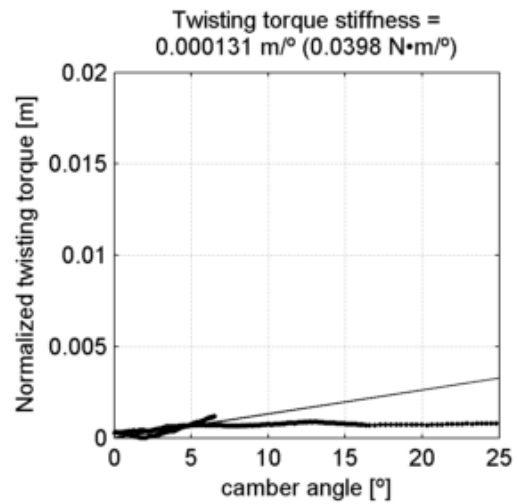
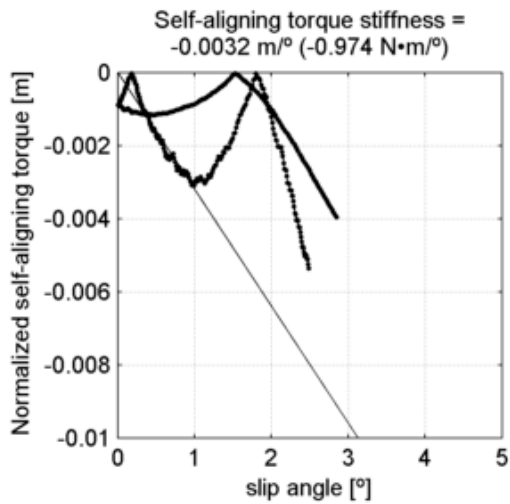
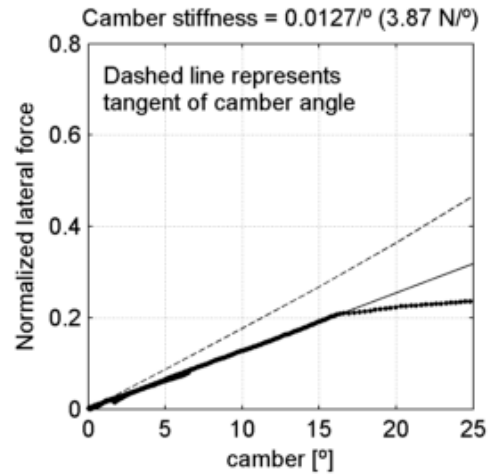
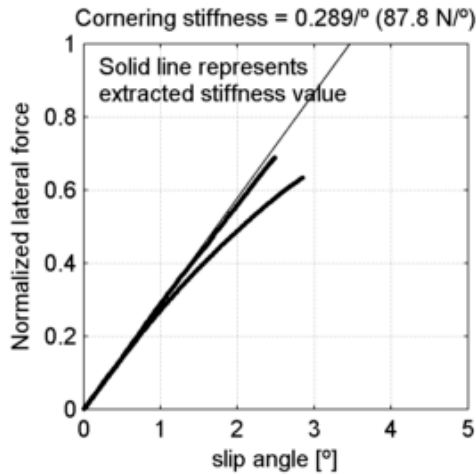
Bontrager All Weather 23-622
 tire radius = 11.5 mm, rim width = 13.4 mm

at 8.27 bar (120 psi) and
 under 731 N (74.5 kg, 164 lb)



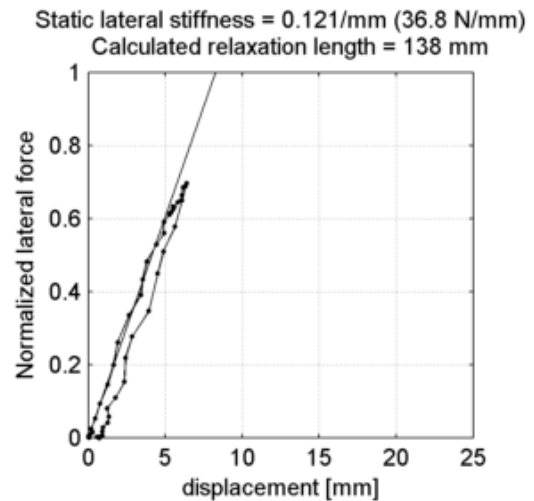
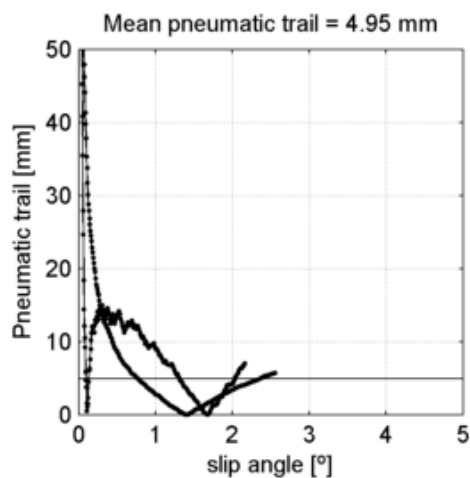
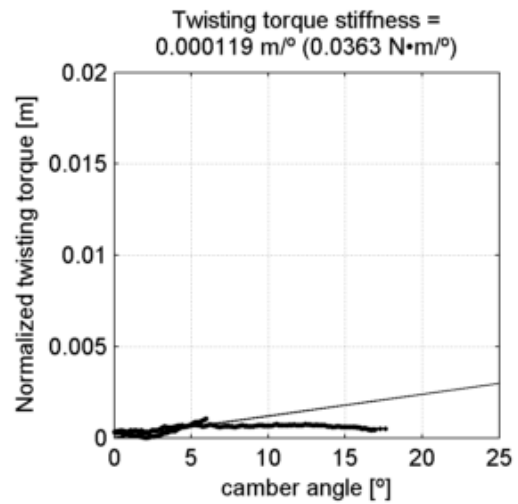
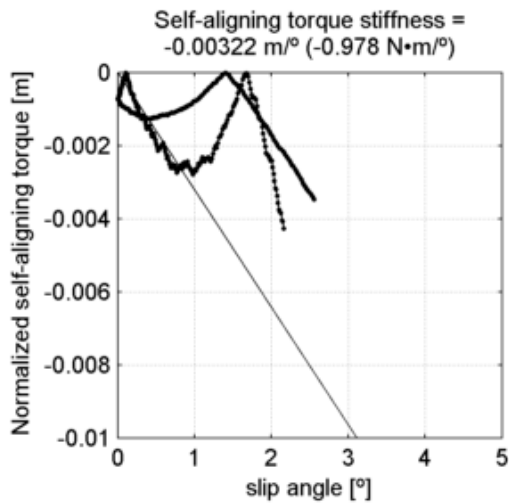
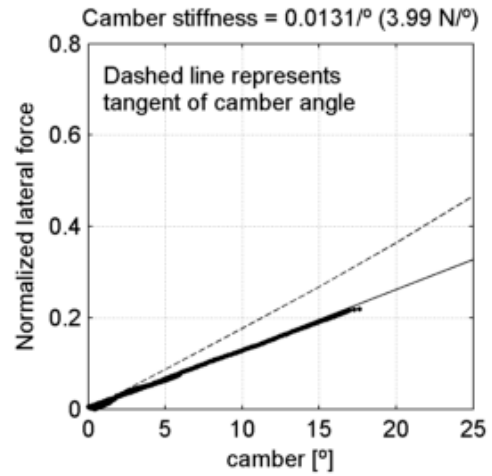
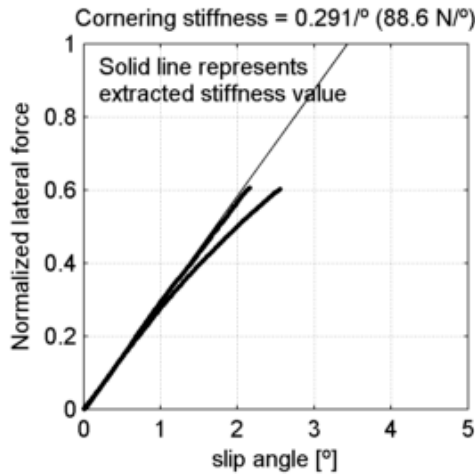
Bontrager All Weather 25-622
 tire radius = 12.5 mm, rim width = 13.4 mm

at 5.17 bar (75 psi) and
 under 304 N (31 kg, 68.3 lb)



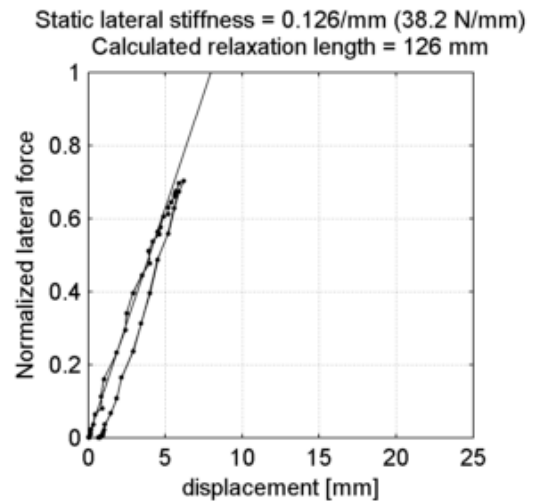
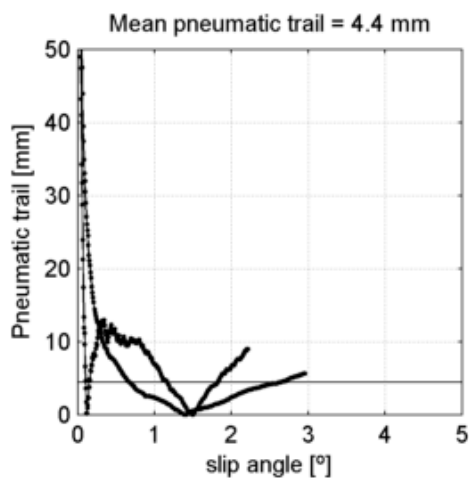
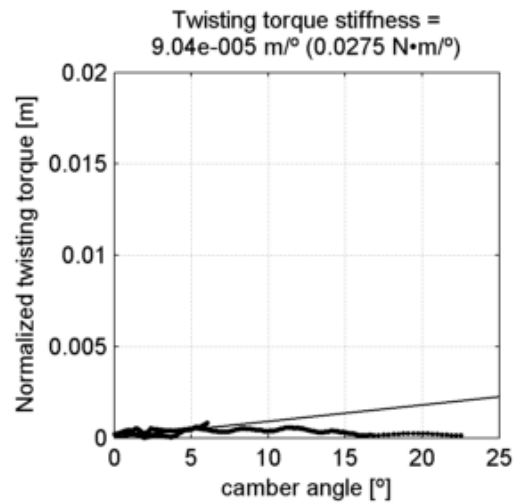
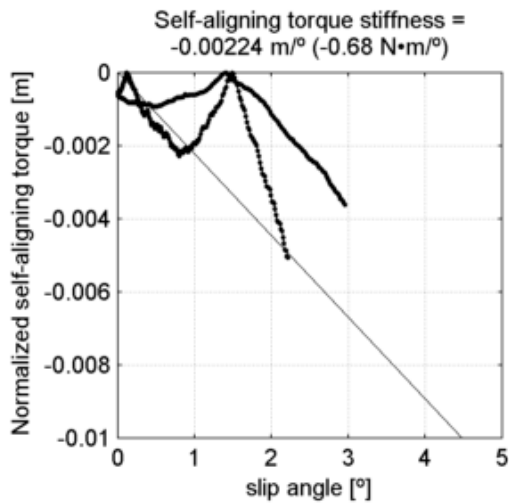
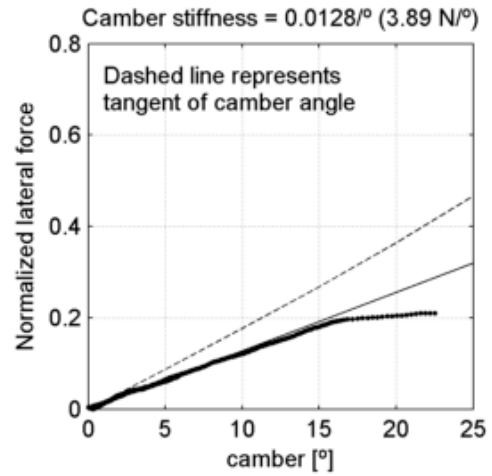
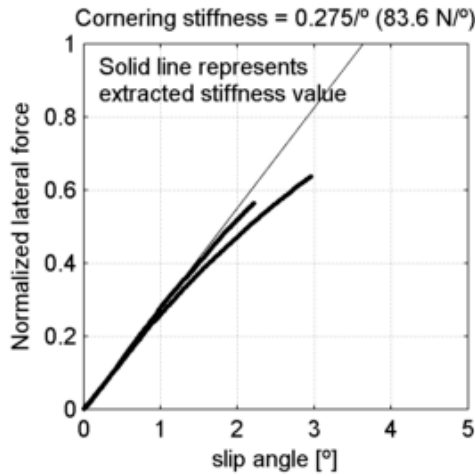
Bontrager All Weather 25-622
 tire radius = 12.5 mm, rim width = 13.4 mm

at 5.52 bar (80 psi) and
 under 304 N (31 kg, 68.3 lb)



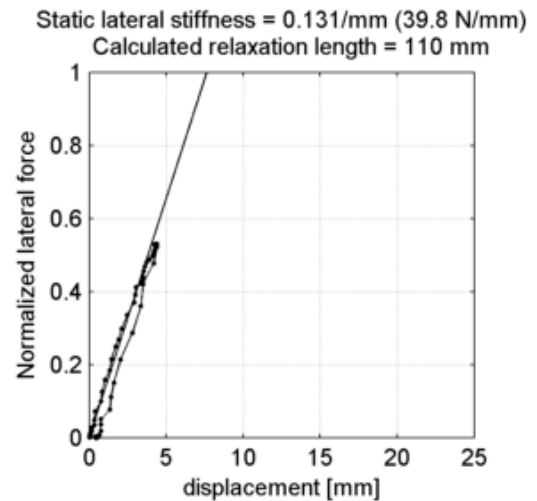
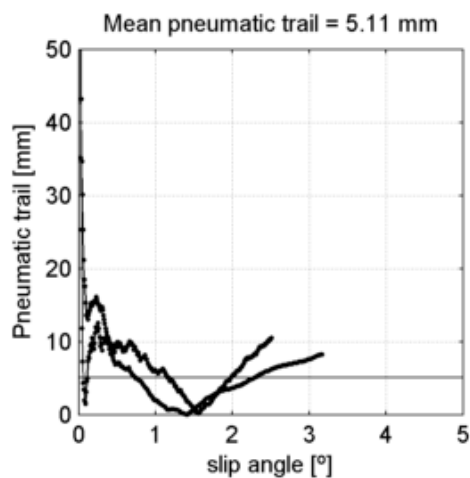
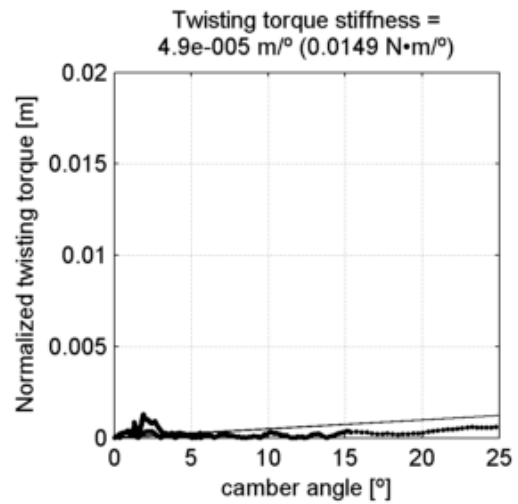
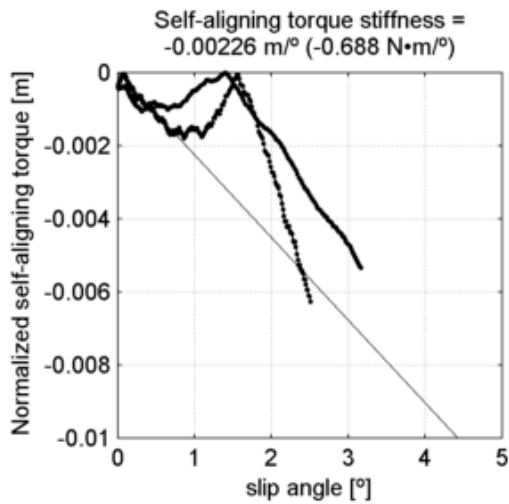
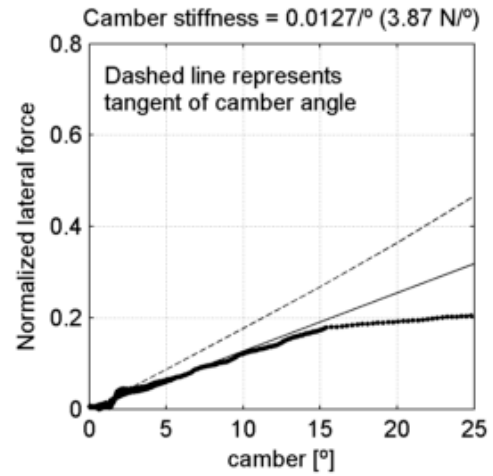
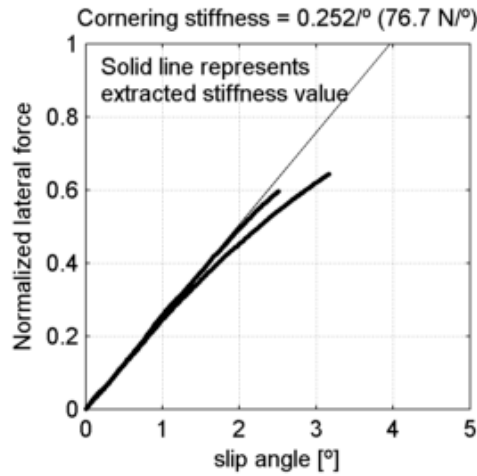
Bontrager All Weather 25-622
 tire radius = 12.5 mm, rim width = 13.4 mm

at 6.89 bar (100 psi) and
 under 304 N (31 kg, 68.3 lb)



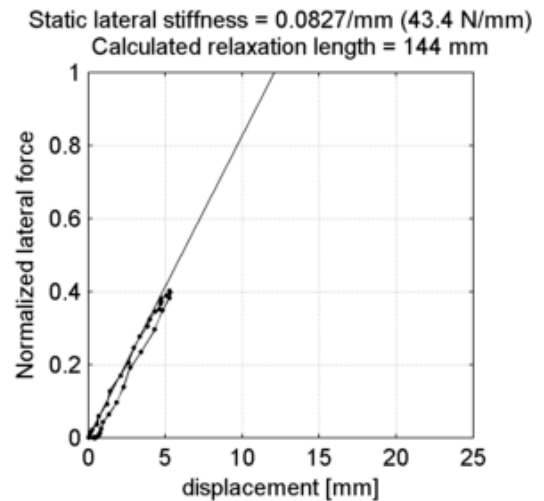
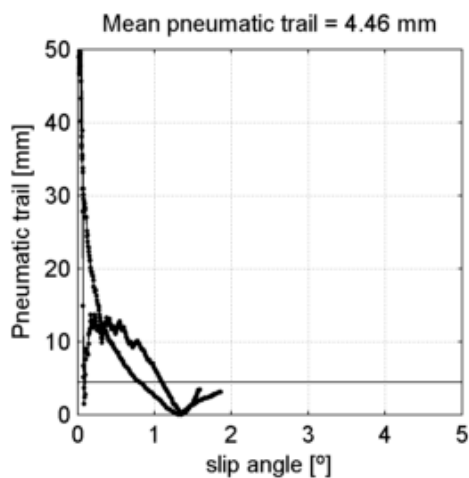
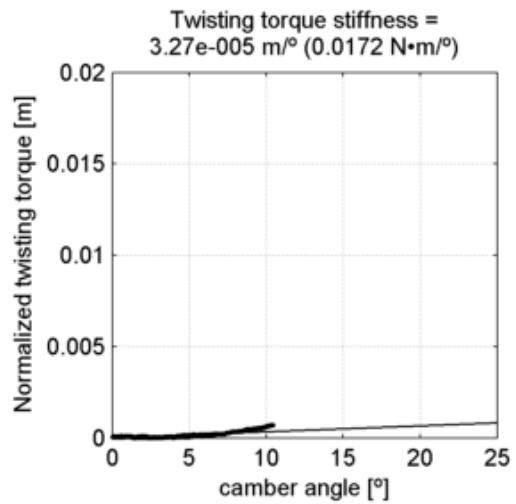
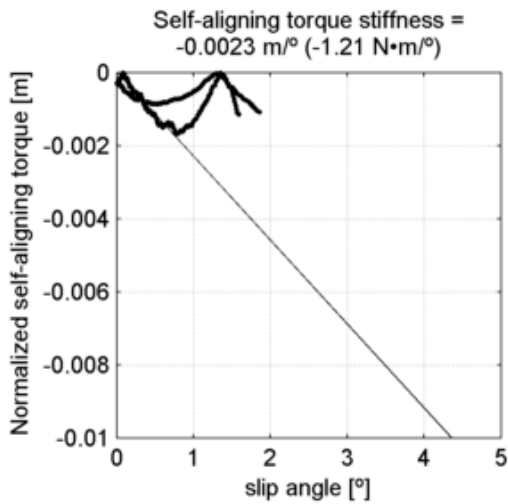
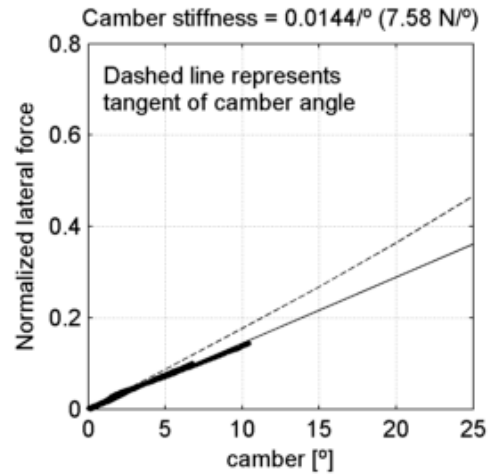
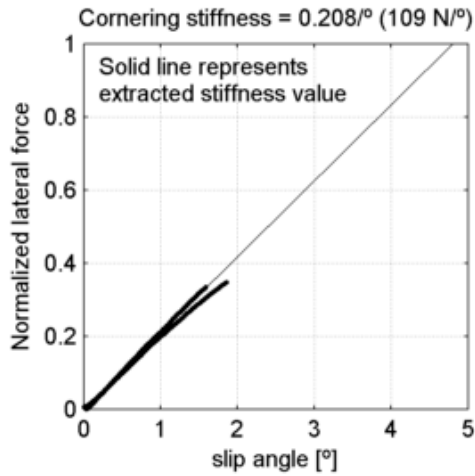
Bontrager All Weather 25-622
 tire radius = 12.5 mm, rim width = 13.4 mm

at 8.27 bar (120 psi) and
 under 304 N (31 kg, 68.3 lb)



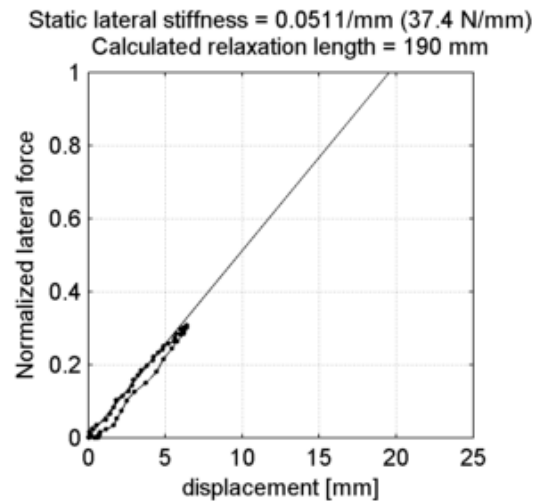
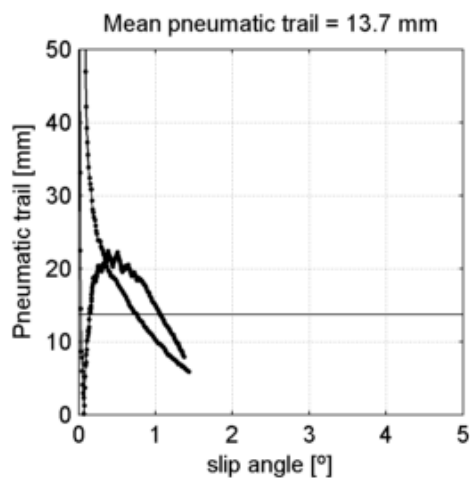
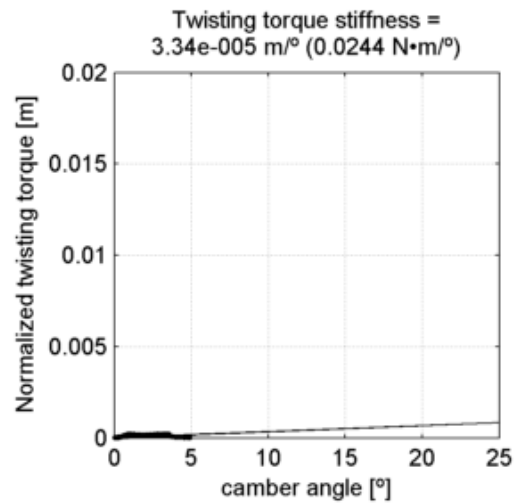
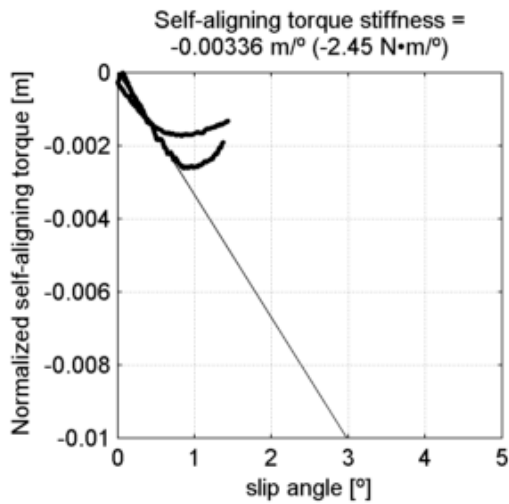
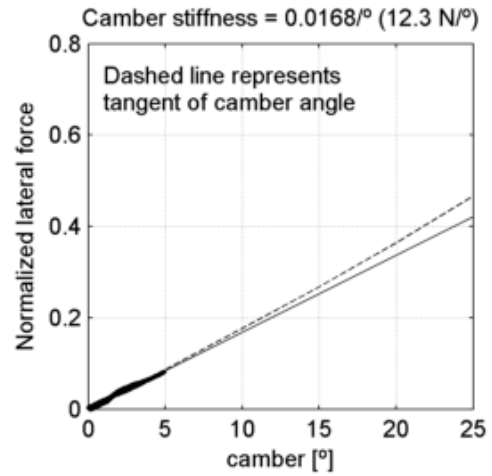
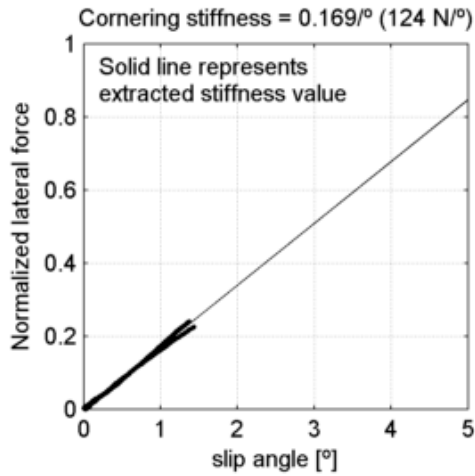
Bontrager All Weather 25-622
 tire radius = 12.5 mm, rim width = 13.4 mm

at 8.27 bar (120 psi) and
 under 525 N (53.5 kg, 118 lb)



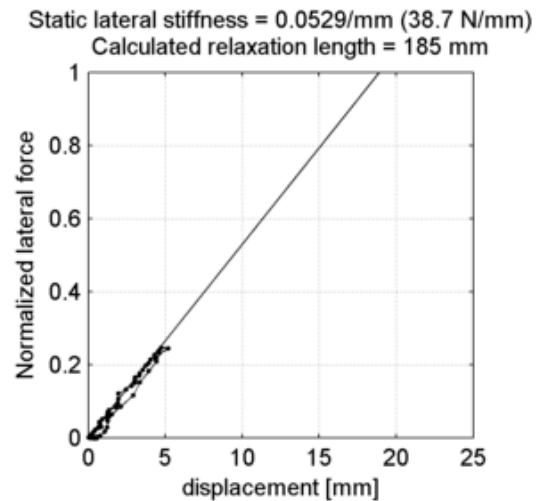
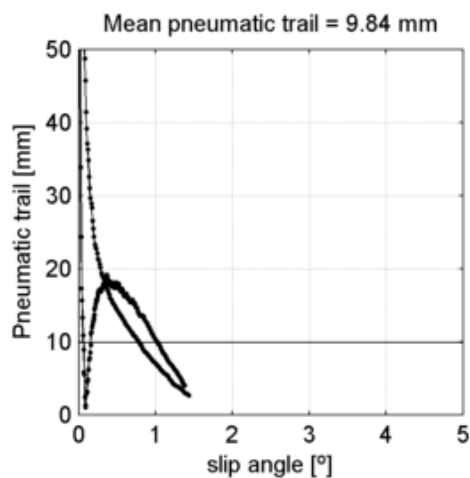
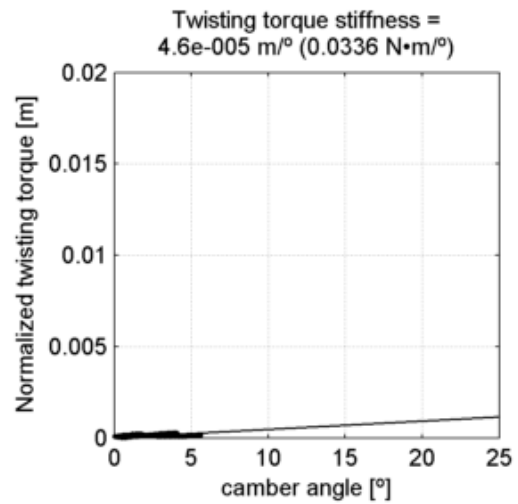
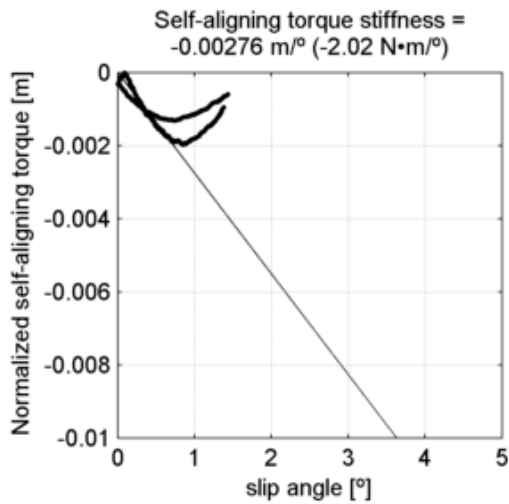
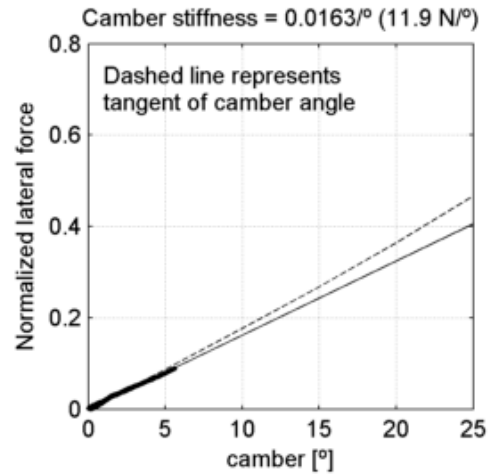
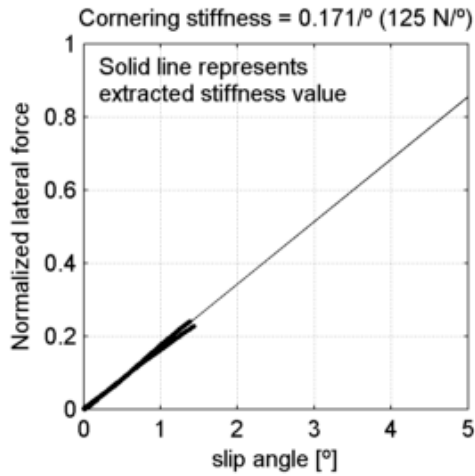
Bontrager All Weather 25-622
 tire radius = 12.5 mm, rim width = 13.4 mm

at 5.52 bar (80 psi) and
 under 731 N (74.5 kg, 164 lb)



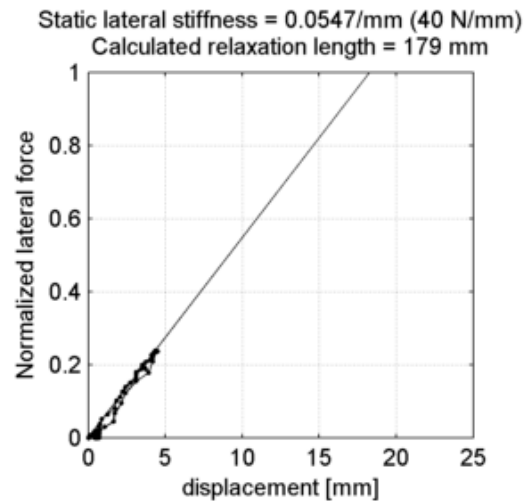
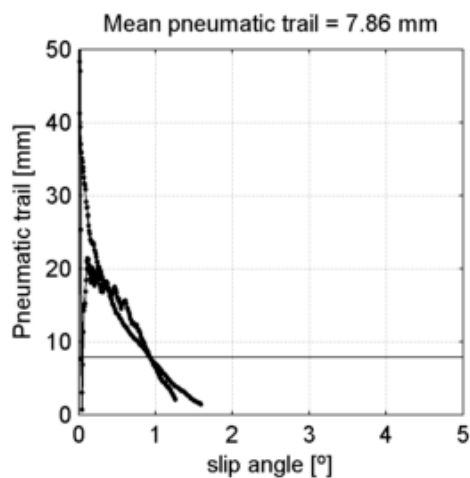
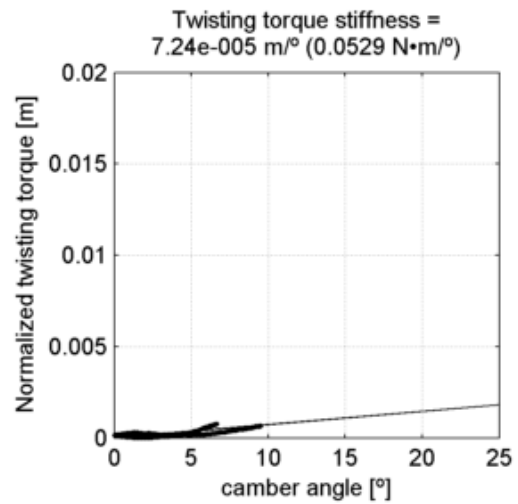
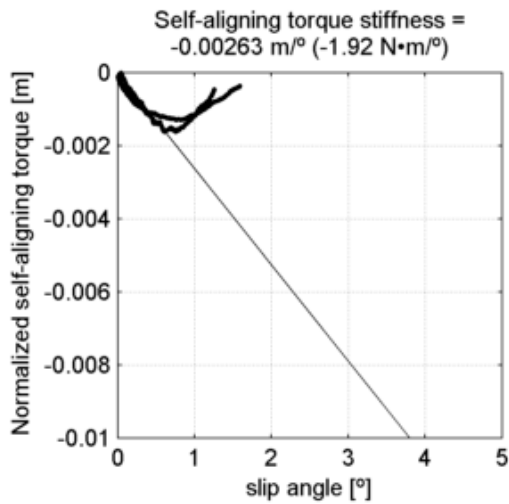
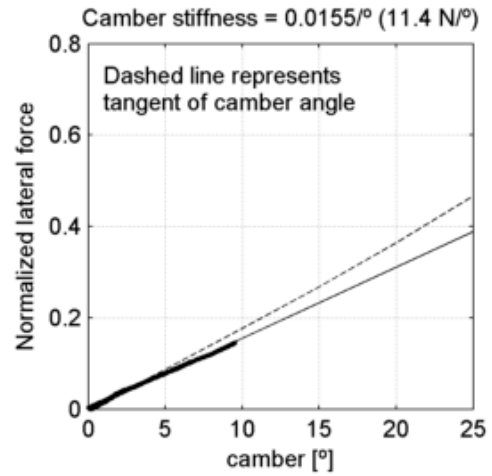
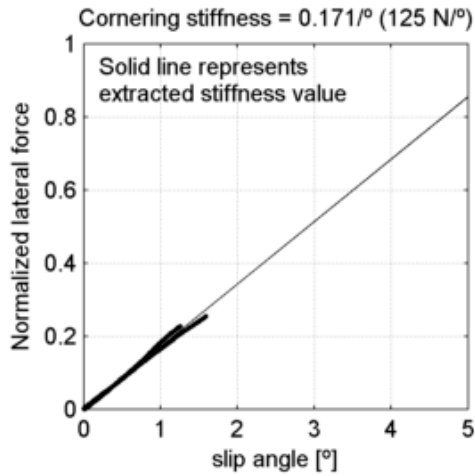
Bontrager All Weather 25-622
 tire radius = 12.5 mm, rim width = 13.4 mm

at 6.89 bar (100 psi) and
 under 731 N (74.5 kg, 164 lb)



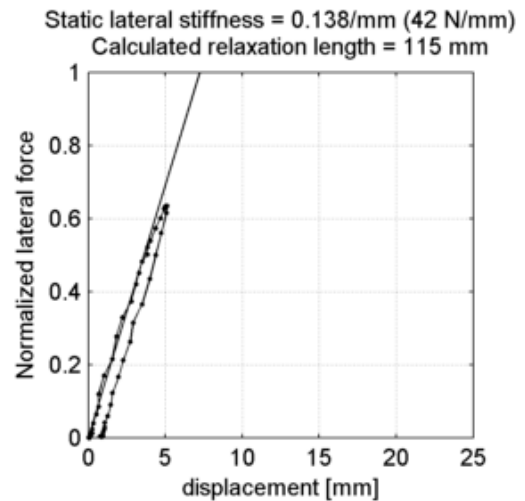
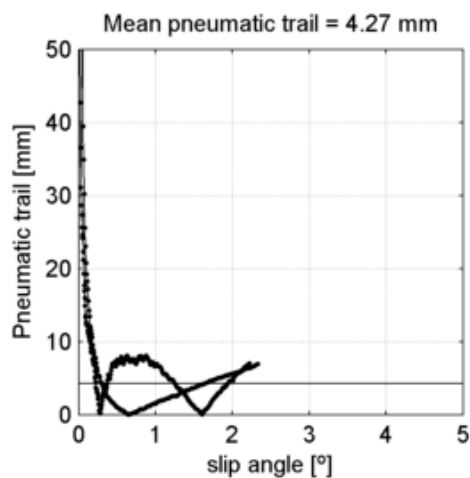
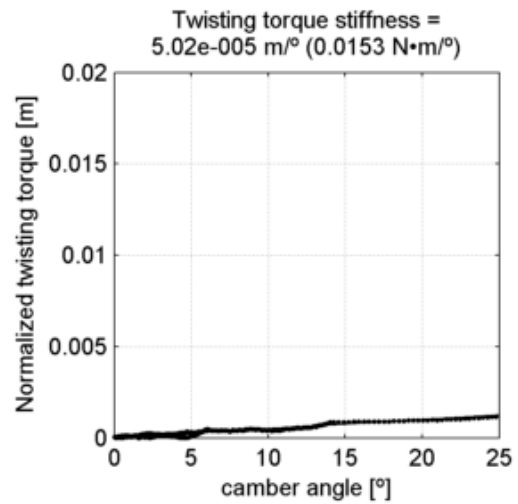
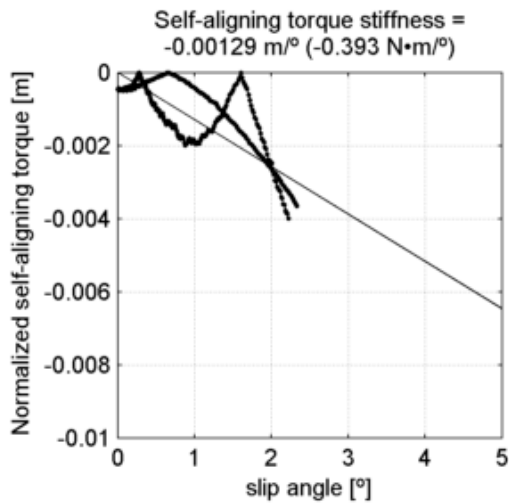
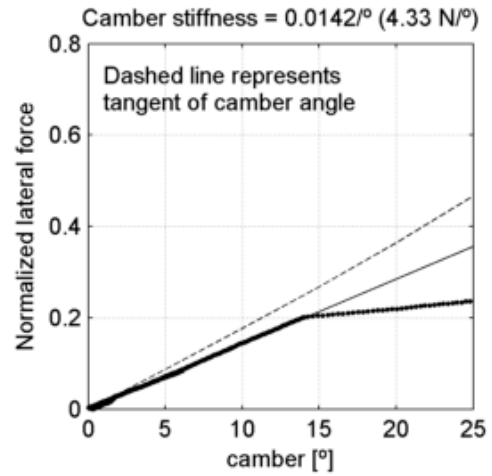
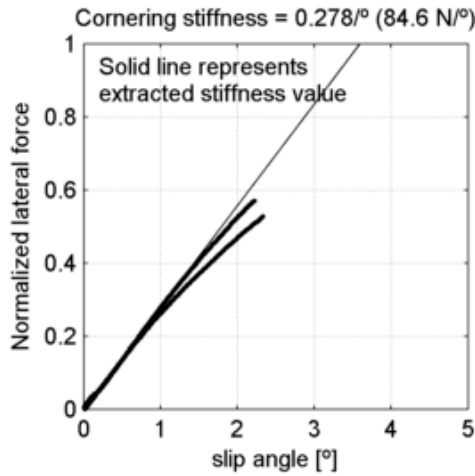
Bontrager All Weather 25-622
 tire radius = 12.5 mm, rim width = 13.4 mm

at 8.27 bar (120 psi) and
 under 731 N (74.5 kg, 164 lb)



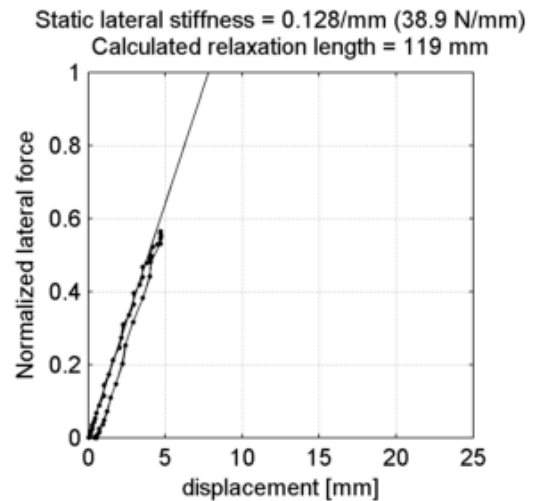
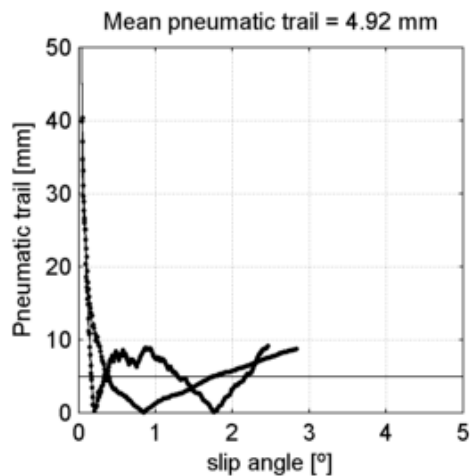
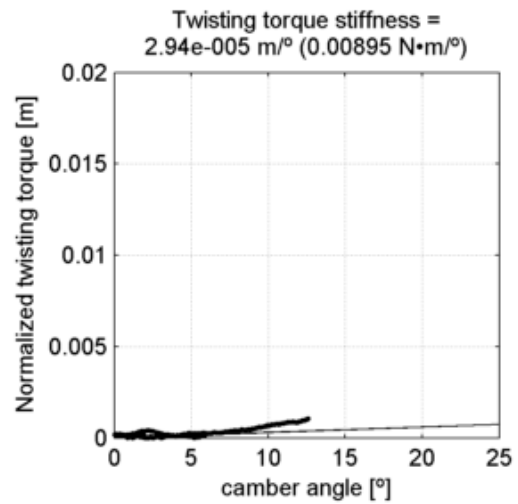
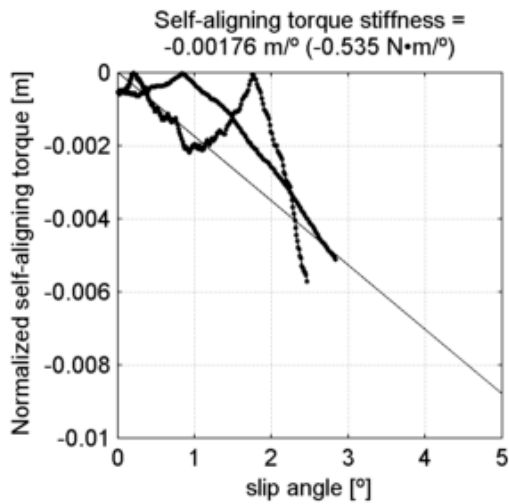
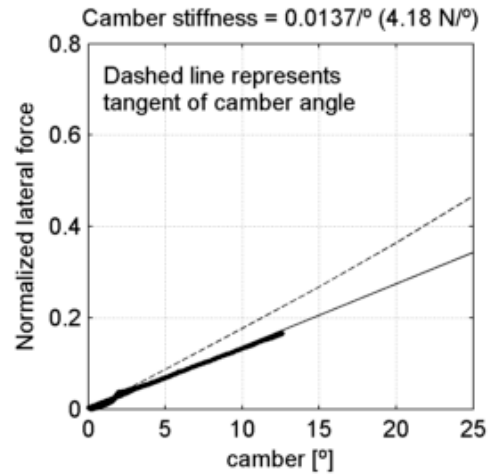
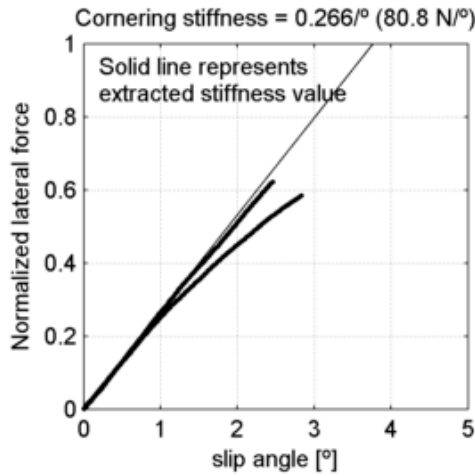
Bontrager All Weather 28-622
 tire radius = 14 mm, rim width = 13.4 mm

at 5.52 bar (80 psi) and
 under 304 N (31 kg, 68.3 lb)



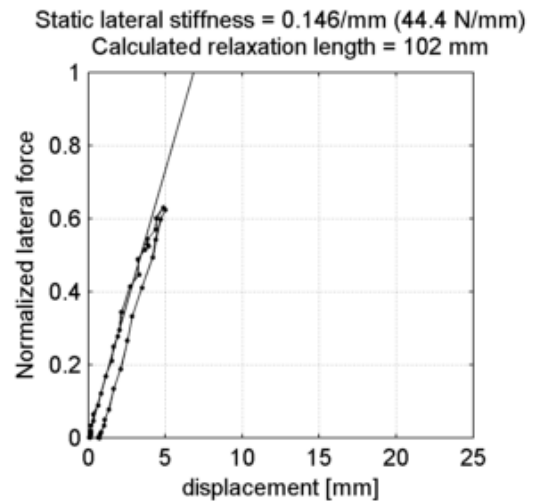
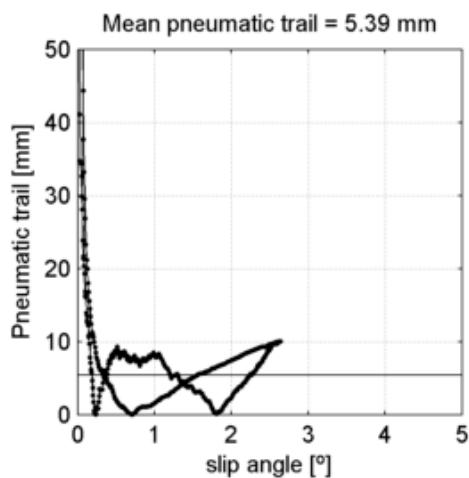
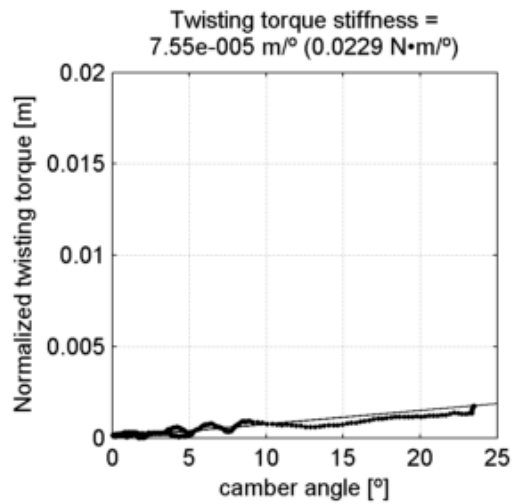
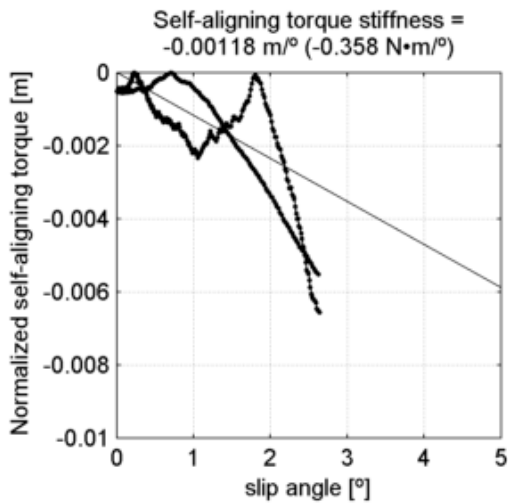
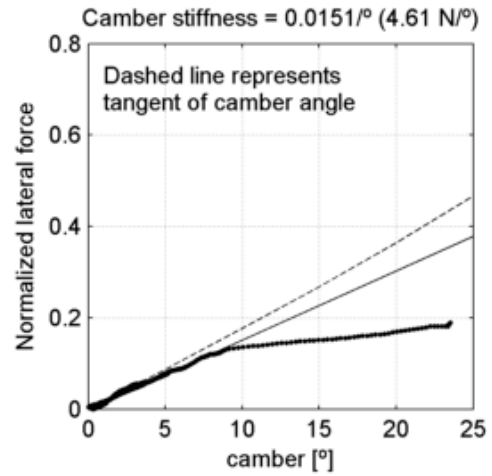
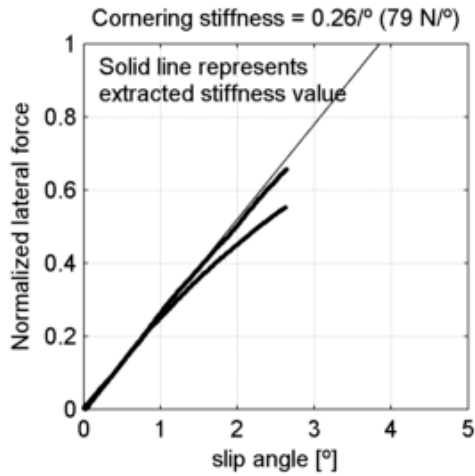
Bontrager All Weather 28-622
 tire radius = 14 mm, rim width = 13.4 mm

at 6.89 bar (100 psi) and
 under 304 N (31 kg, 68.3 lb)



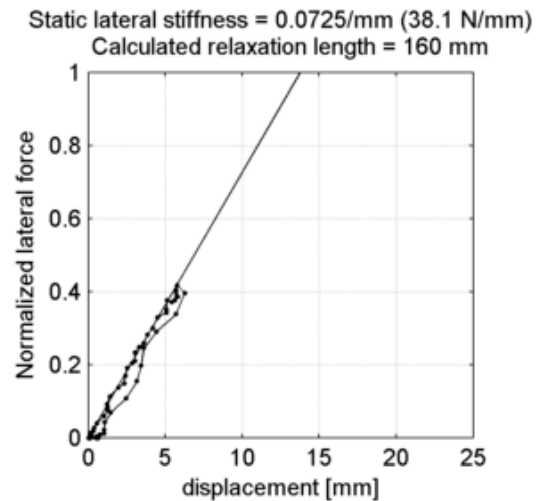
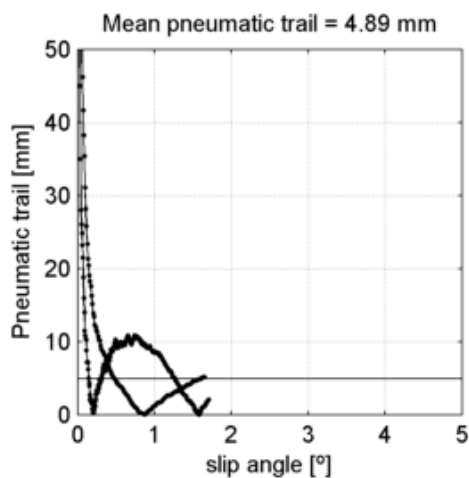
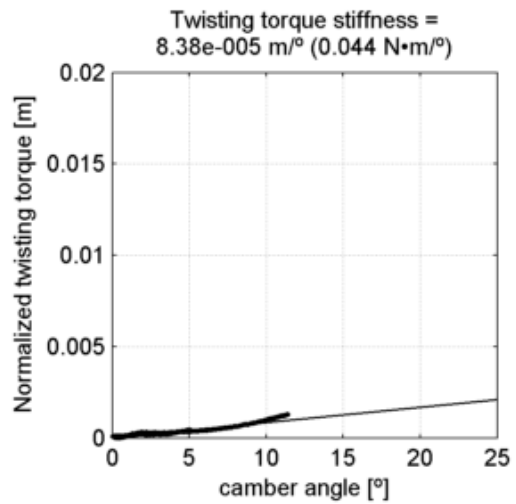
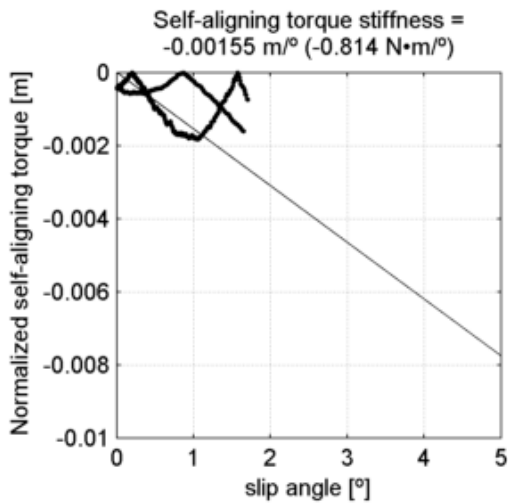
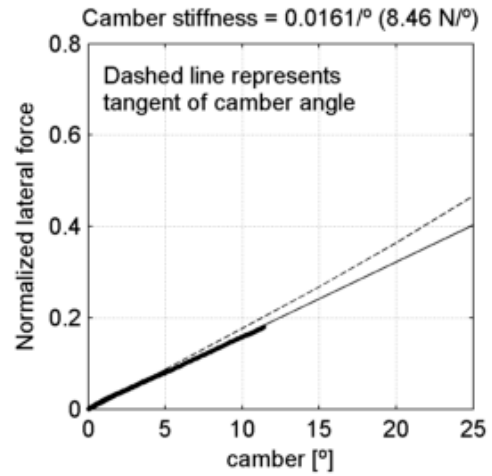
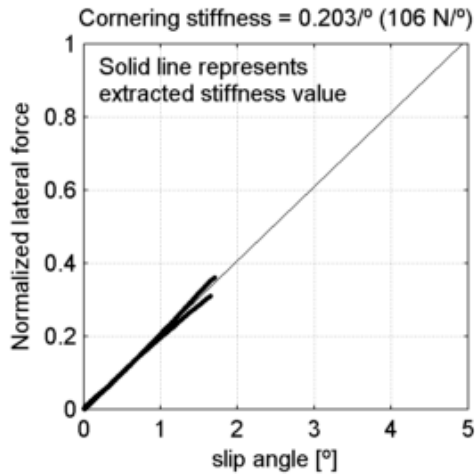
Bontrager All Weather 28-622
 tire radius = 14 mm, rim width = 13.4 mm

at 8.27 bar (120 psi) and
 under 304 N (31 kg, 68.3 lb)



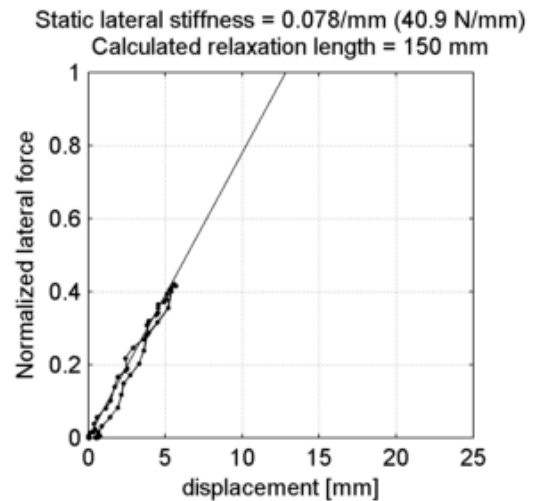
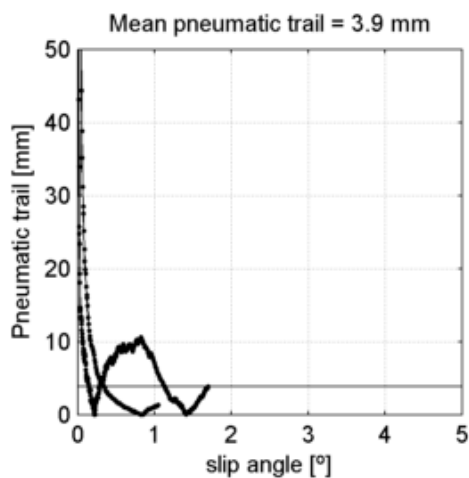
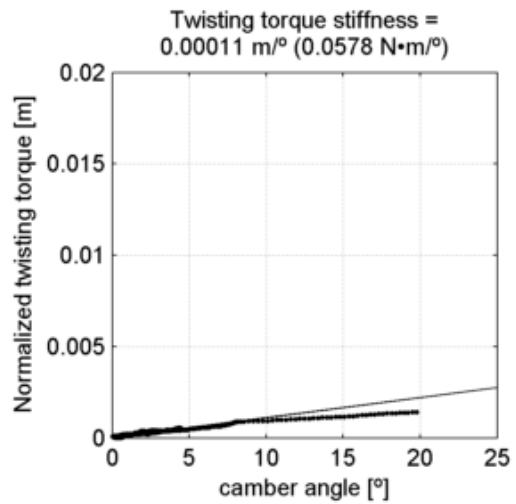
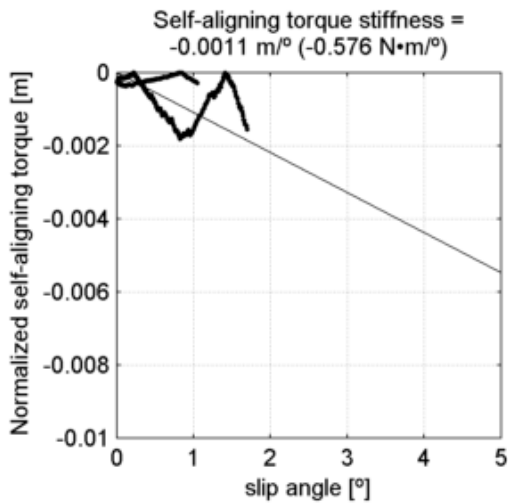
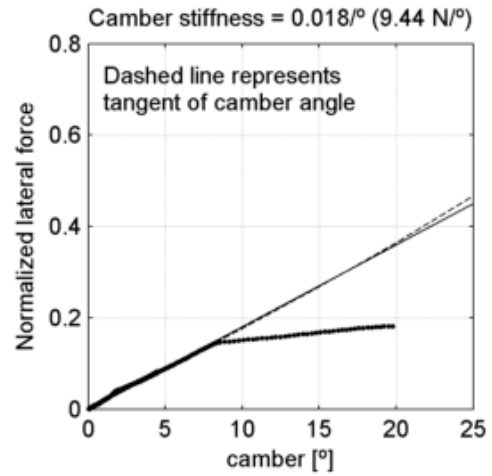
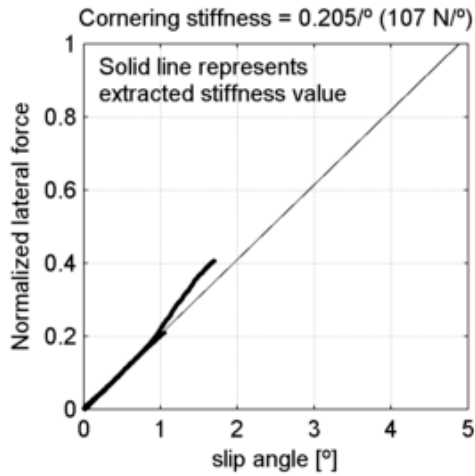
Bontrager All Weather 28-622
 tire radius = 14 mm, rim width = 13.4 mm

at 6.89 bar (100 psi) and
 under 525 N (53.5 kg, 118 lb)



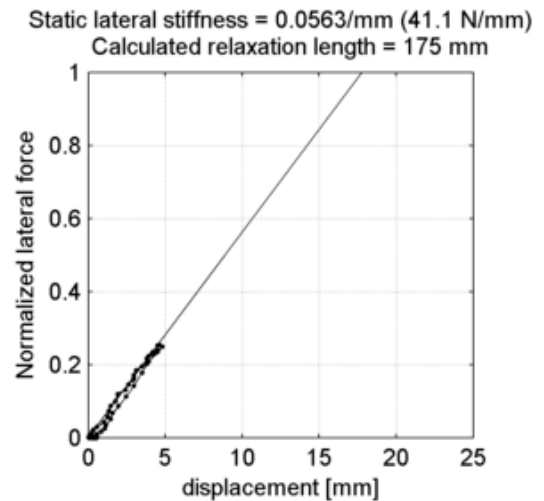
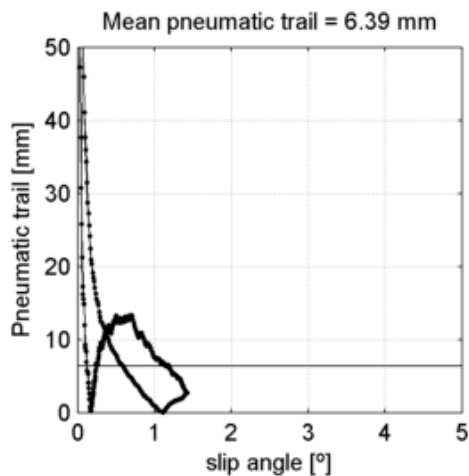
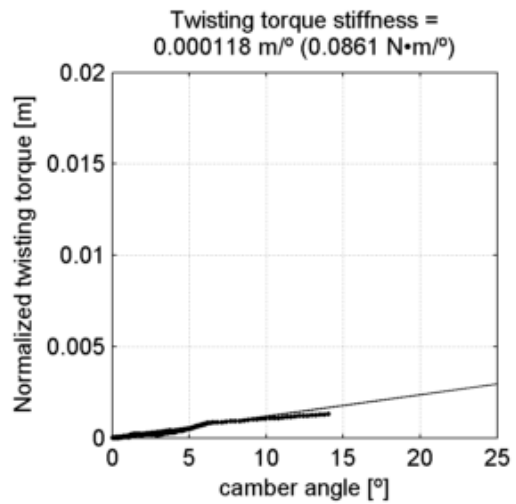
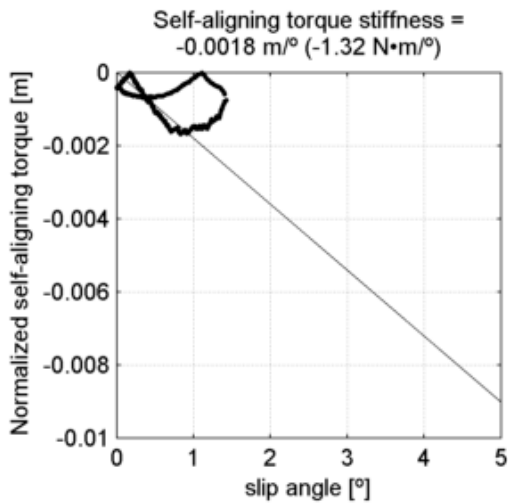
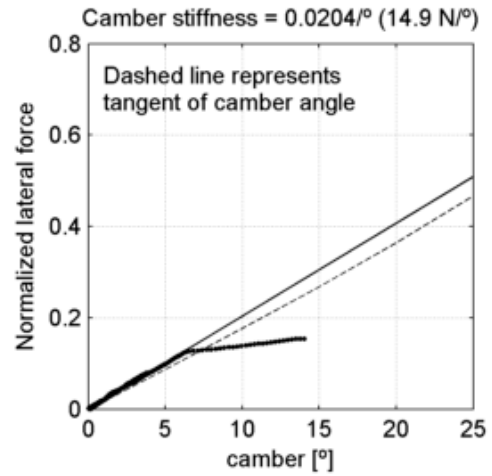
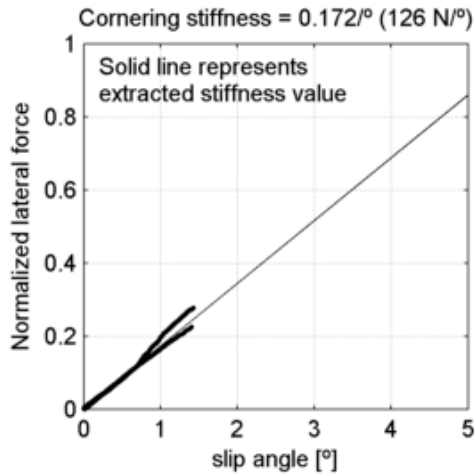
Bontrager All Weather 28-622
 tire radius = 14 mm, rim width = 13.4 mm

at 8.27 bar (120 psi) and
 under 525 N (53.5 kg, 118 lb)



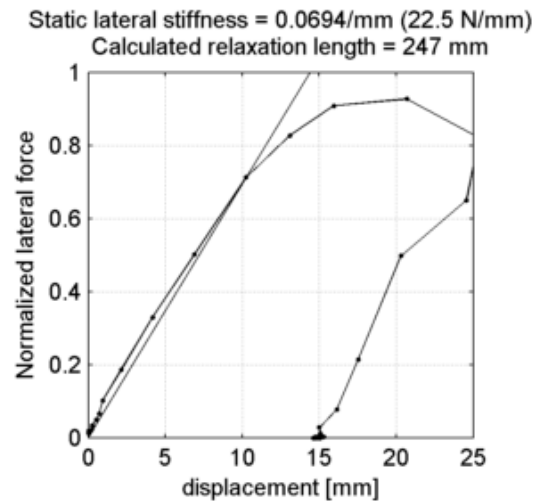
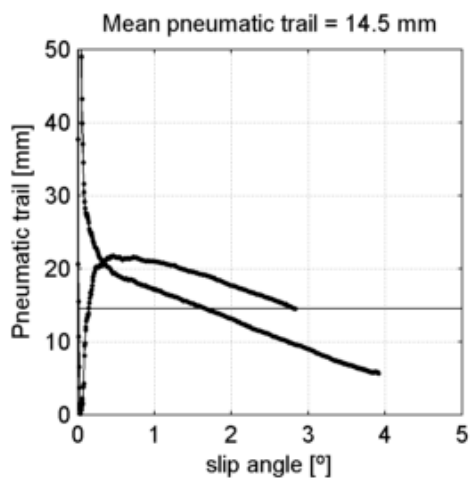
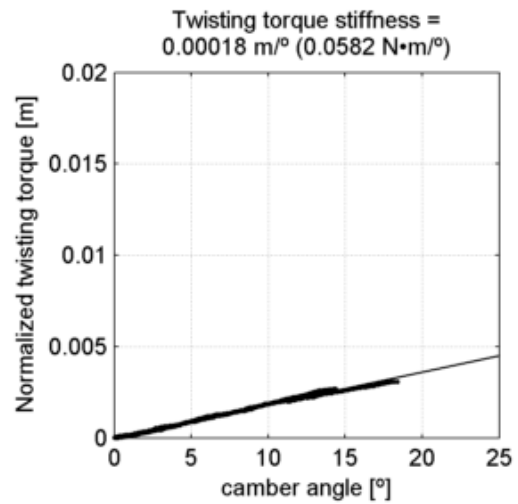
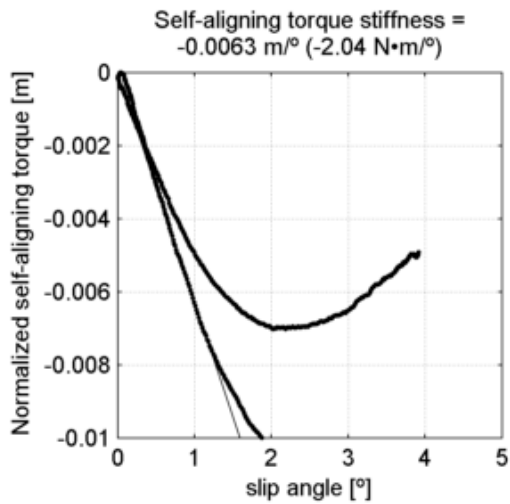
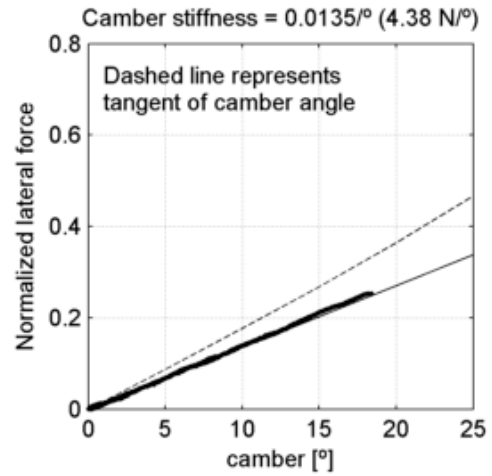
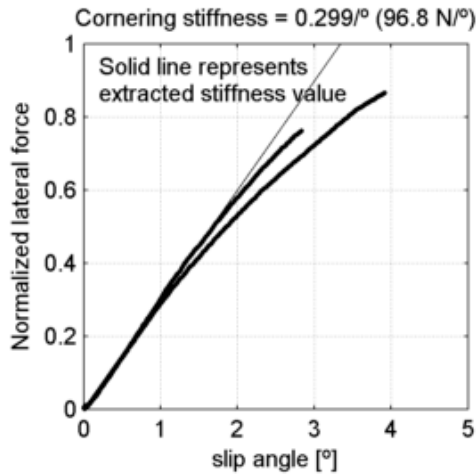
Bontrager All Weather 28-622
 tire radius = 14 mm, rim width = 13.4 mm

at 8.27 bar (120 psi) and
 under 731 N (74.5 kg, 164 lb)



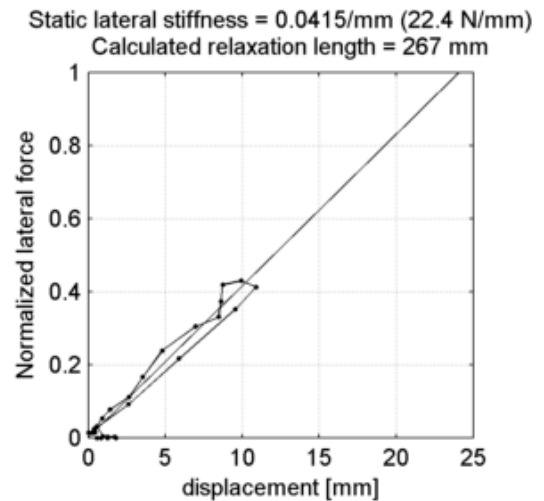
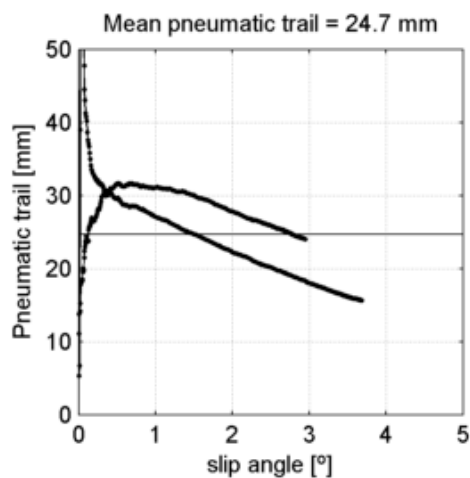
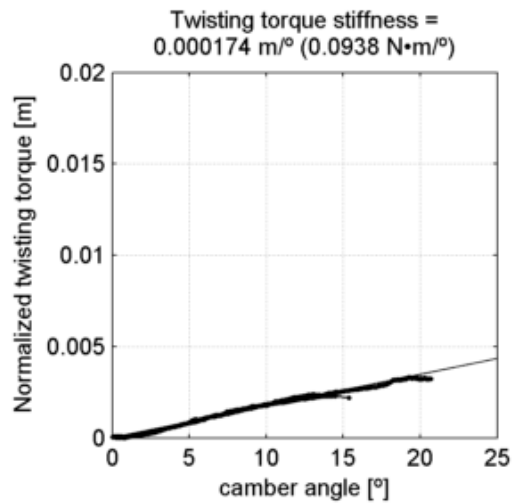
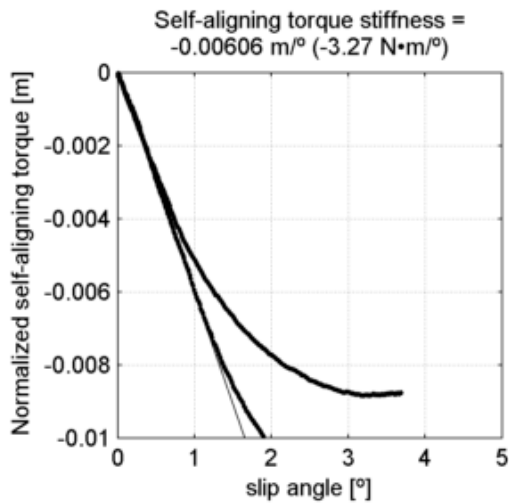
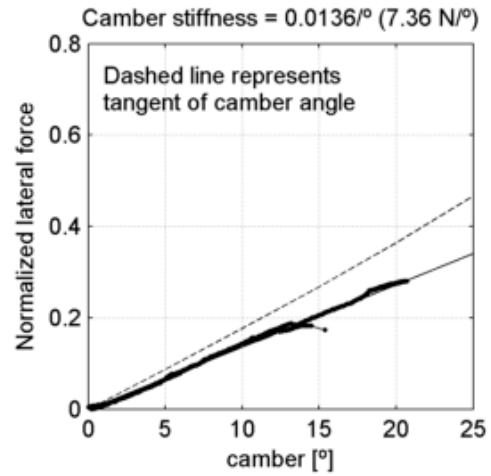
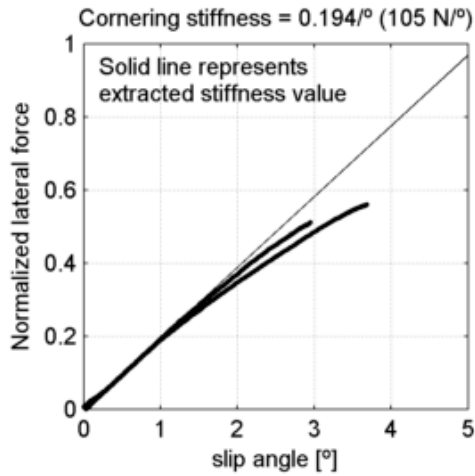
Cheng Shin Classic Zeppelin 50-622
 tire radius = 22.1 mm, rim width = 18.7 mm

at 2 bar (29 psi) and
 under 324 N (33 kg, 72.8 lb)



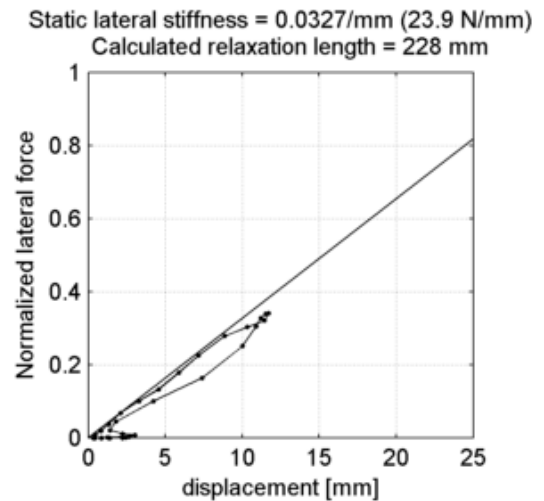
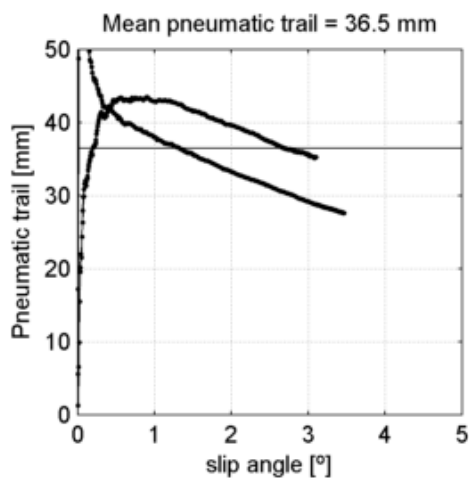
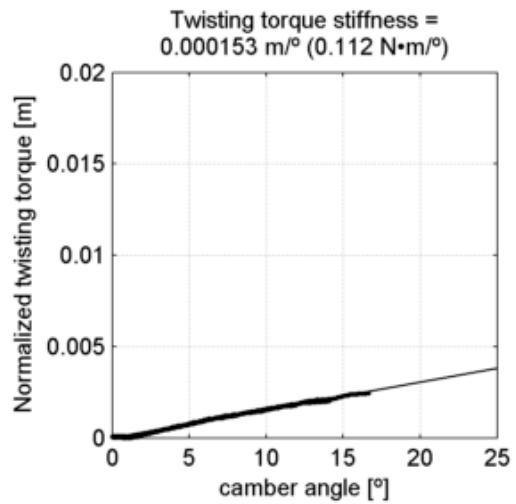
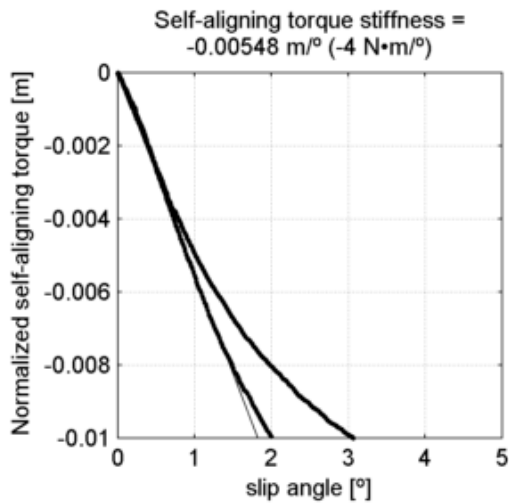
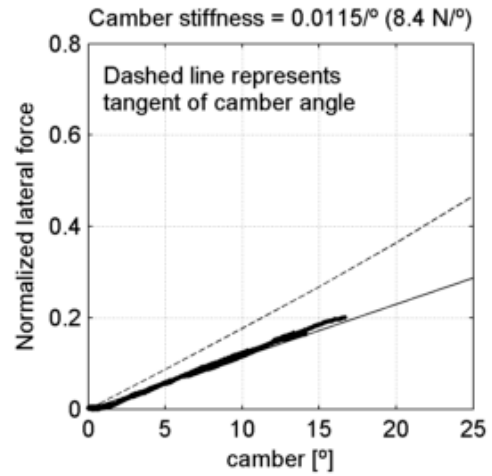
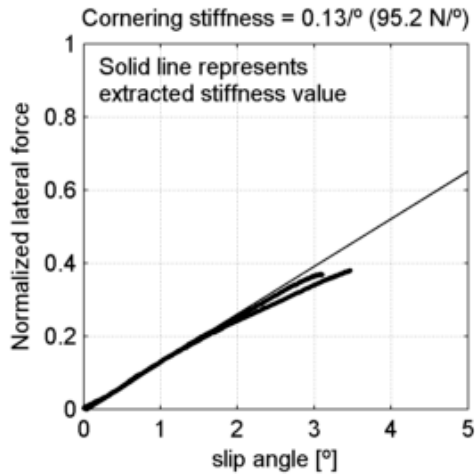
Cheng Shin Classic Zeppelin 50-622
 tire radius = 22.1 mm, rim width = 18.7 mm

at 2 bar (29 psi) and
 under 540 N (55 kg, 121 lb)



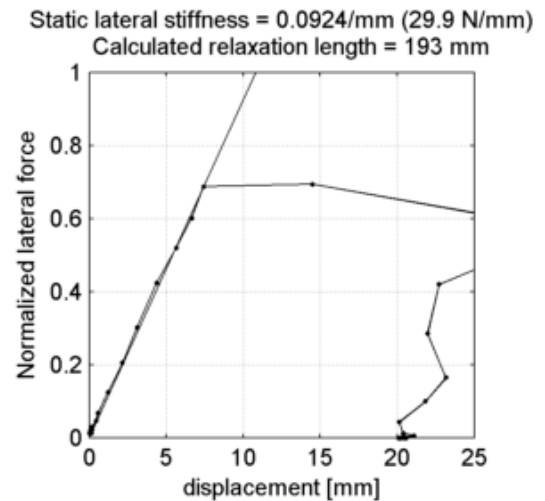
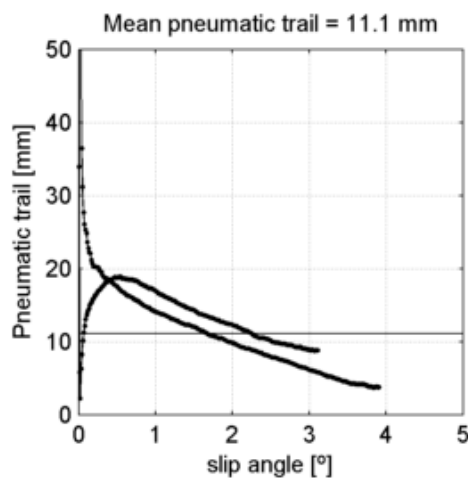
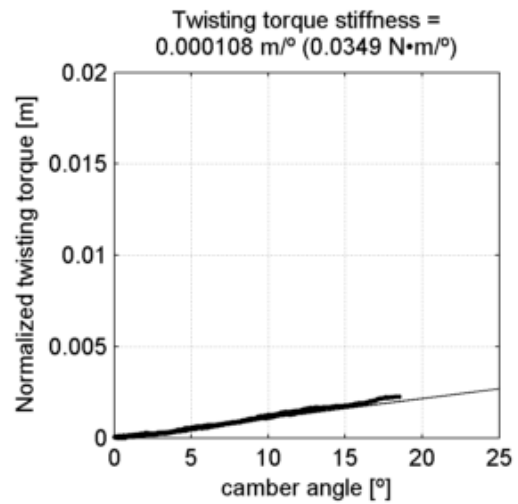
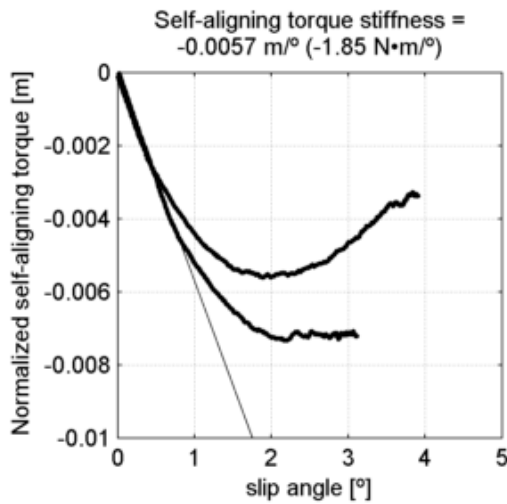
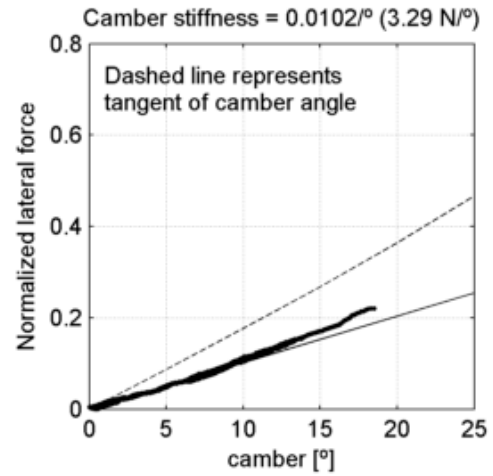
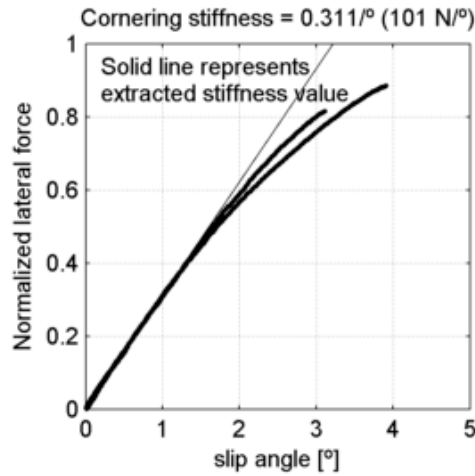
Cheng Shin Classic Zeppelin 50-622
 tire radius = 22.1 mm, rim width = 18.7 mm

at 2 bar (29 psi) and
 under 731 N (74.5 kg, 164 lb)



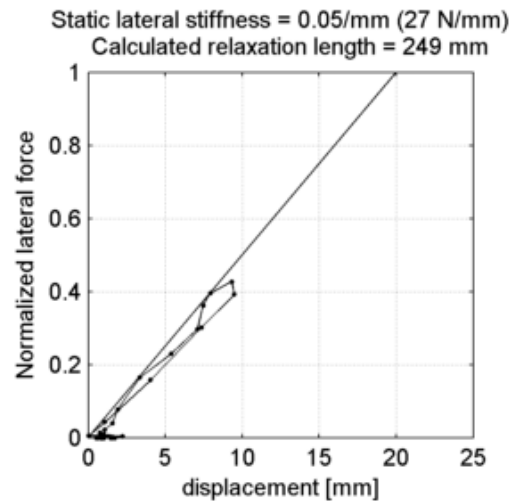
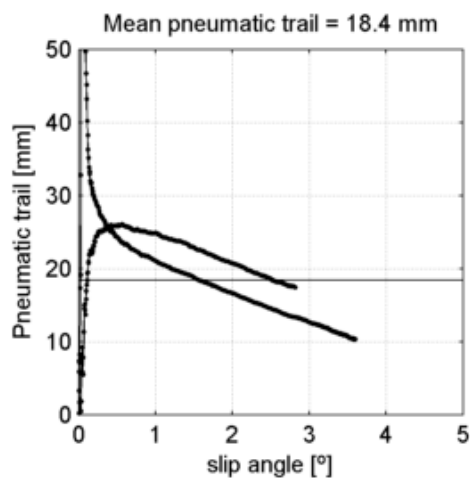
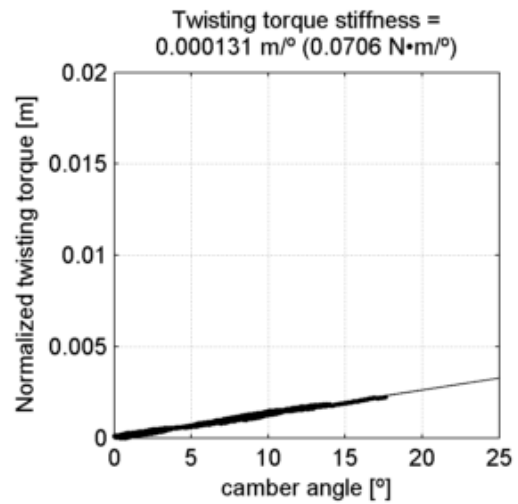
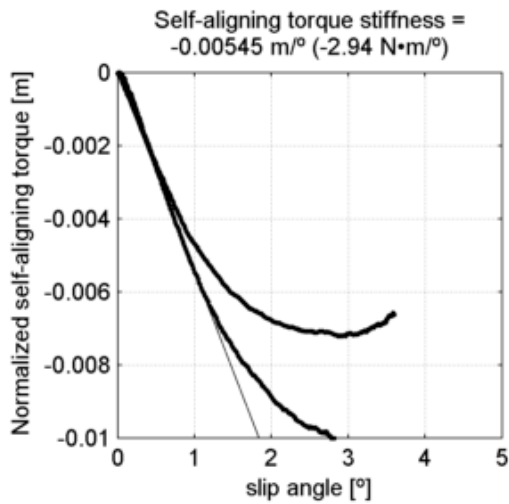
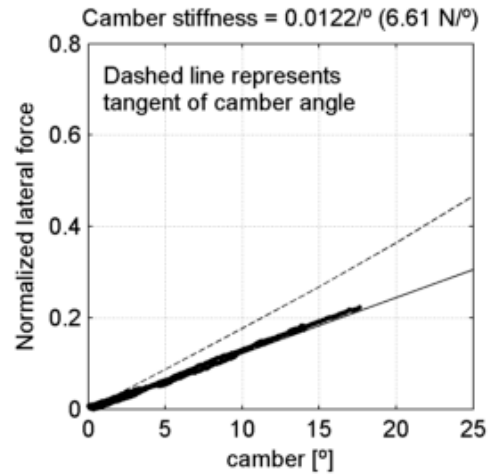
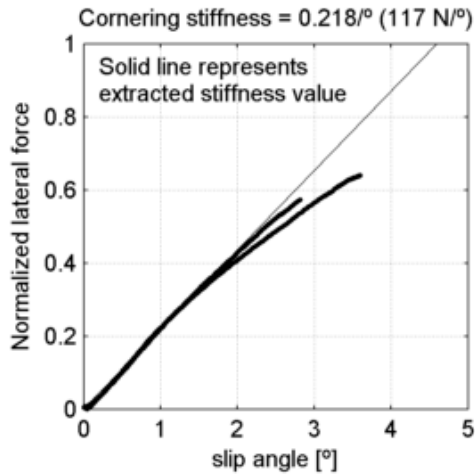
Cheng Shin Classic Zeppelin 50-622
 tire radius = 22.1 mm, rim width = 18.7 mm

at 3.03 bar (44 psi) and
 under 324 N (33 kg, 72.8 lb)



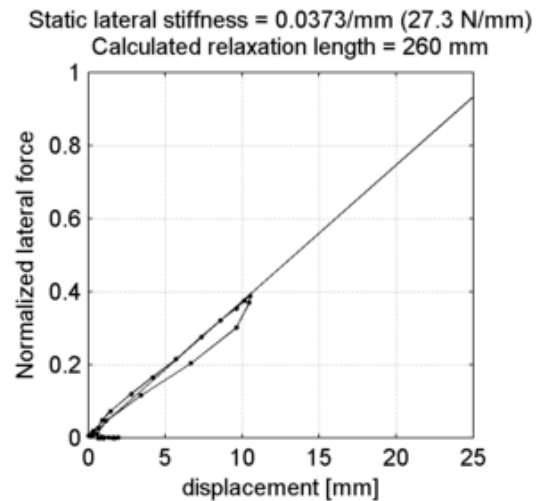
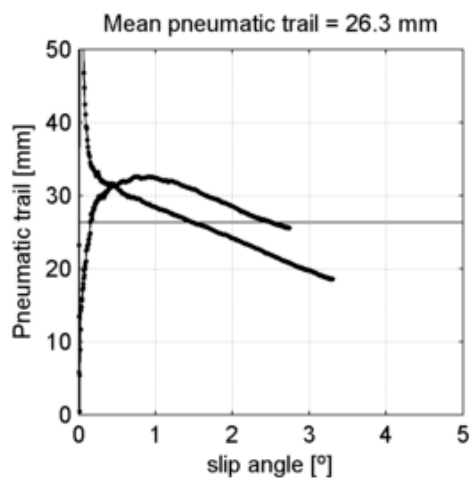
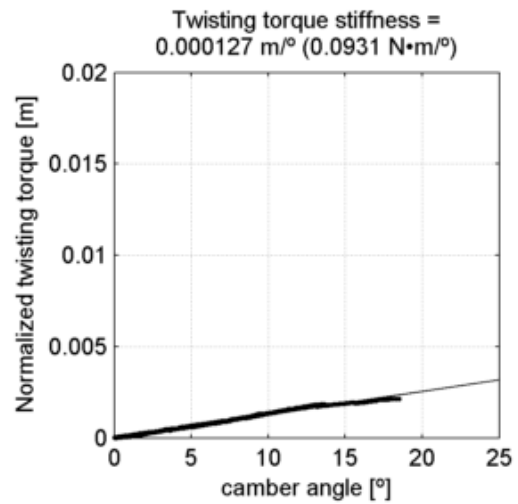
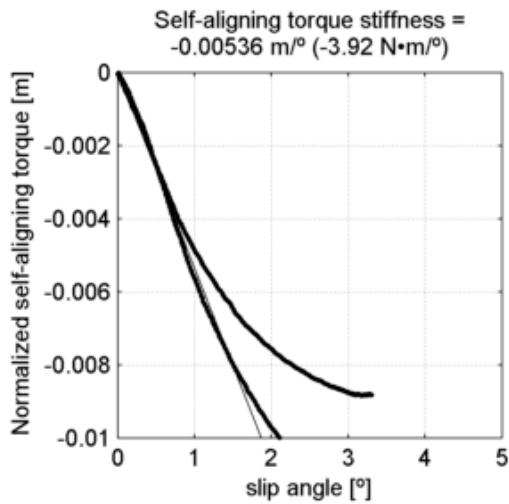
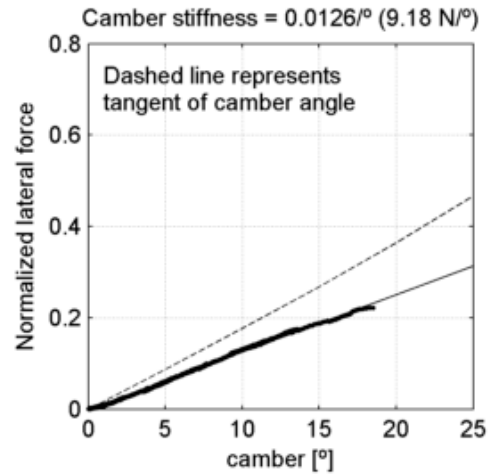
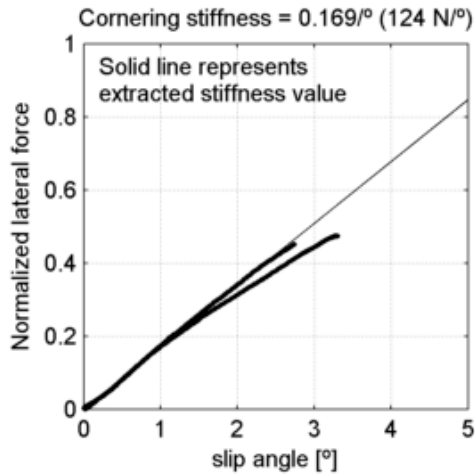
Cheng Shin Classic Zeppelin 50-622
 tire radius = 22.1 mm, rim width = 18.7 mm

at 3.03 bar (44 psi) and
 under 540 N (55 kg, 121 lb)



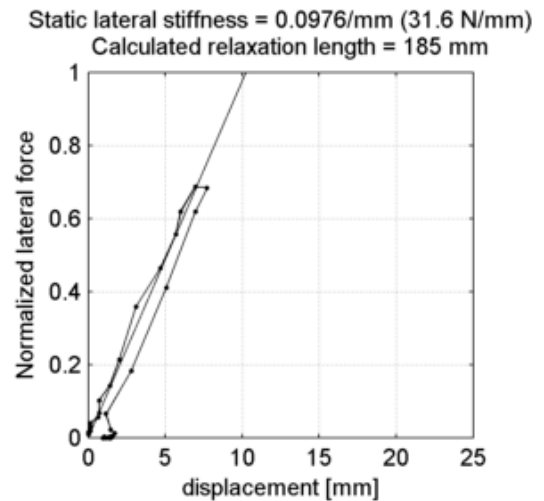
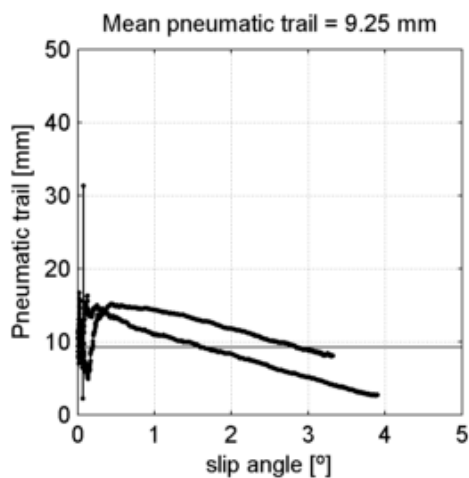
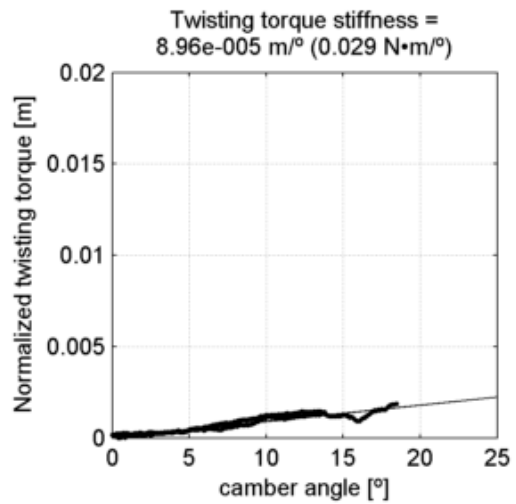
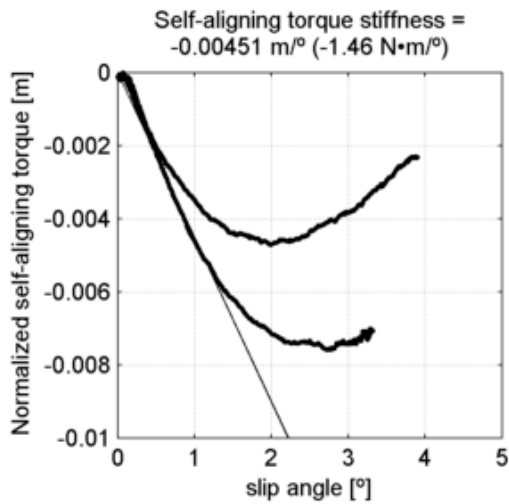
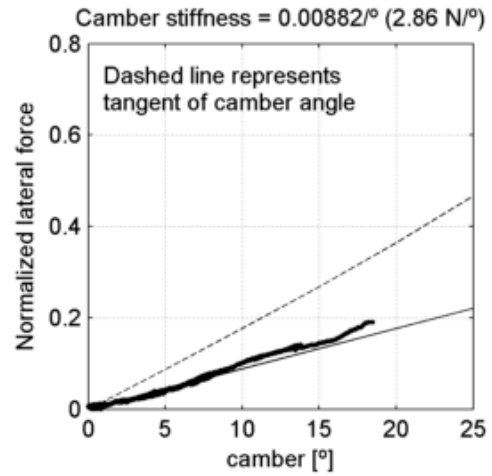
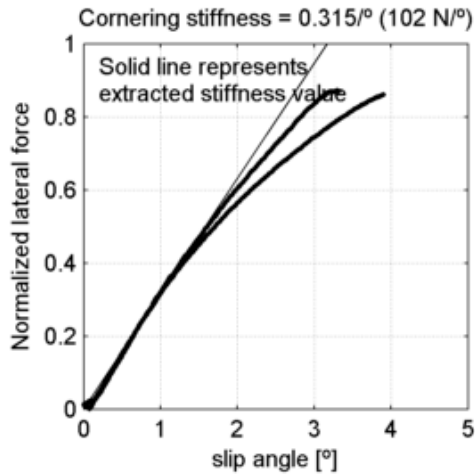
Cheng Shin Classic Zeppelin 50-622
 tire radius = 22.1 mm, rim width = 18.7 mm

at 3.03 bar (44 psi) and
 under 731 N (74.5 kg, 164 lb)



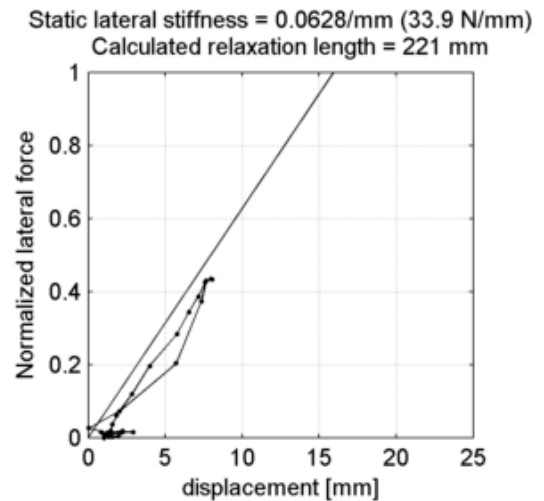
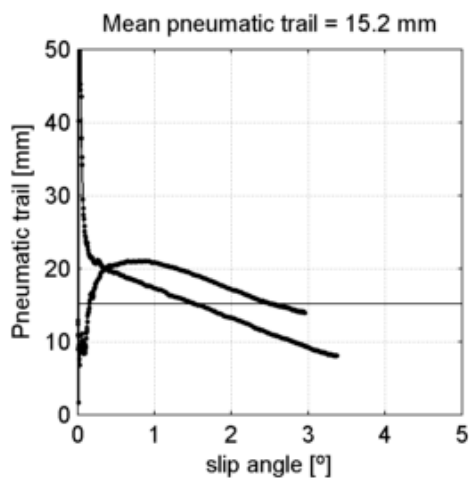
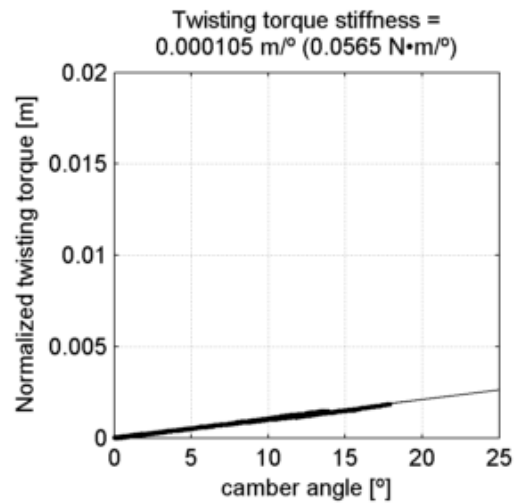
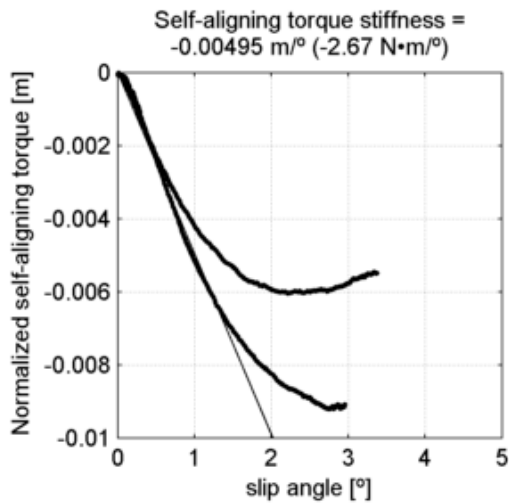
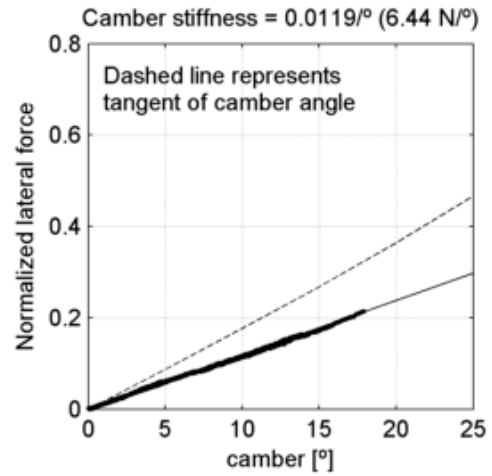
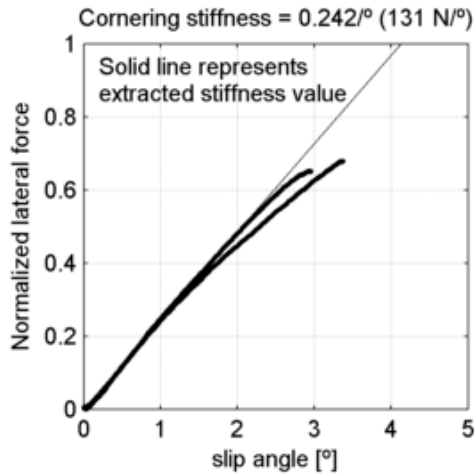
Cheng Shin Classic Zeppelin 50-622
 tire radius = 22.1 mm, rim width = 18.7 mm

at 4 bar (58 psi) and
 under 324 N (33 kg, 72.8 lb)



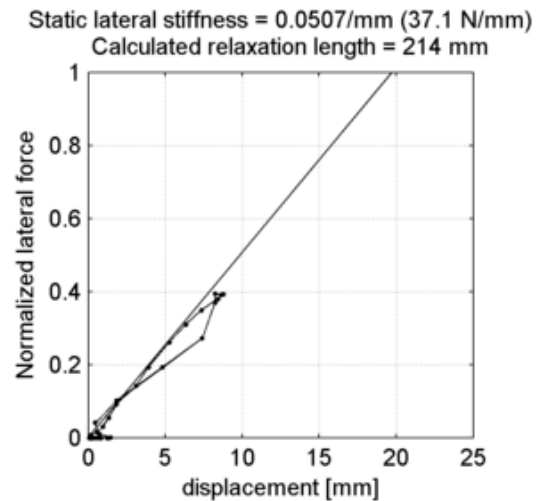
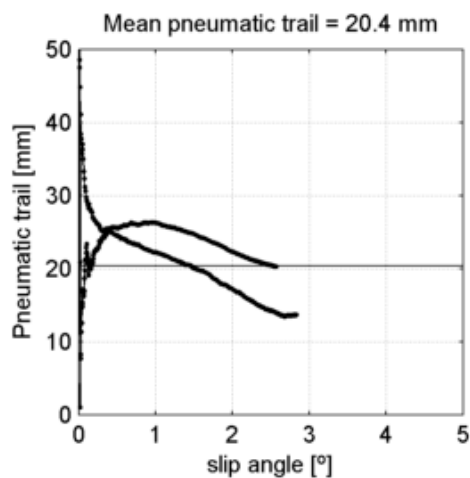
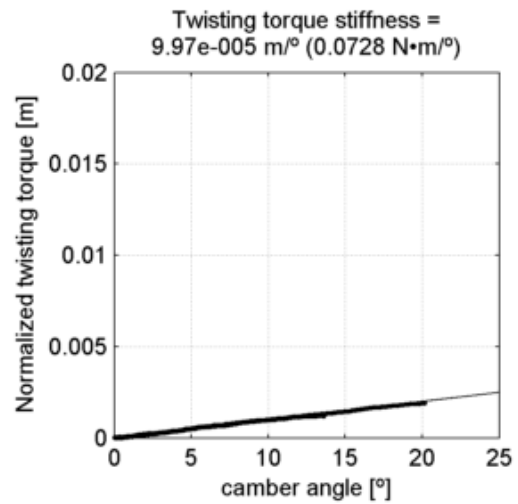
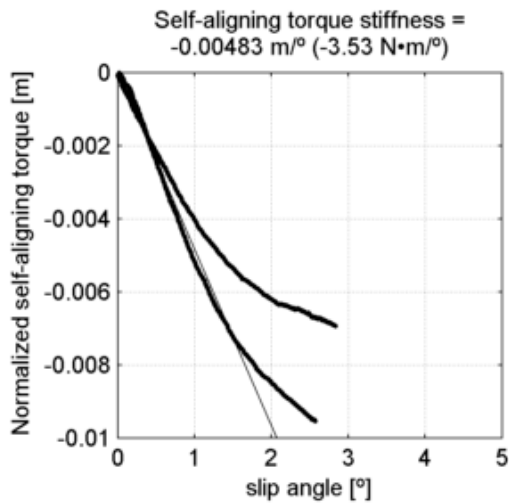
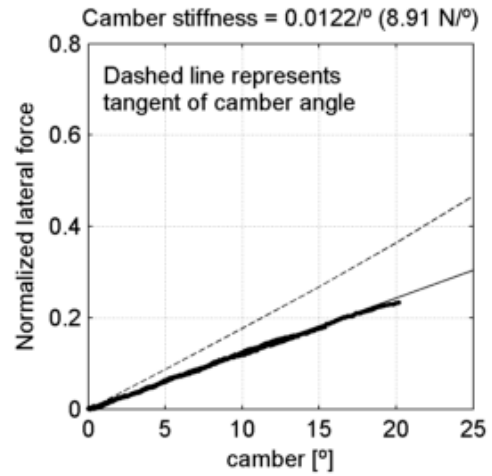
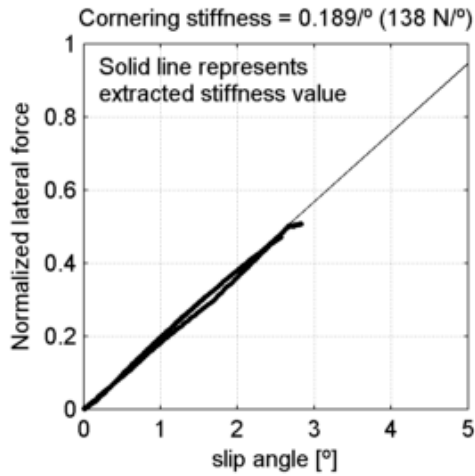
Cheng Shin Classic Zeppelin 50-622
 tire radius = 22.1 mm, rim width = 18.7 mm

at 4 bar (58 psi) and
 under 540 N (55 kg, 121 lb)



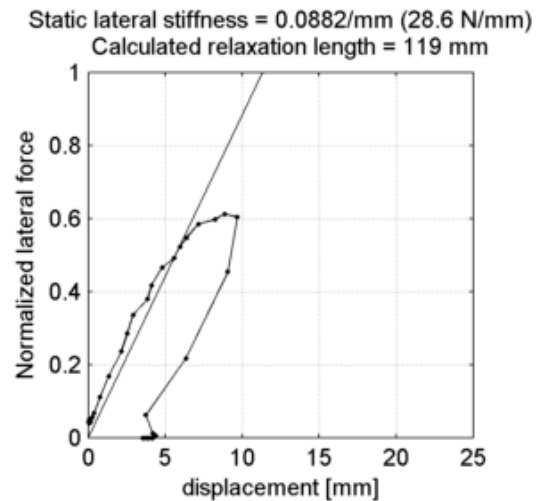
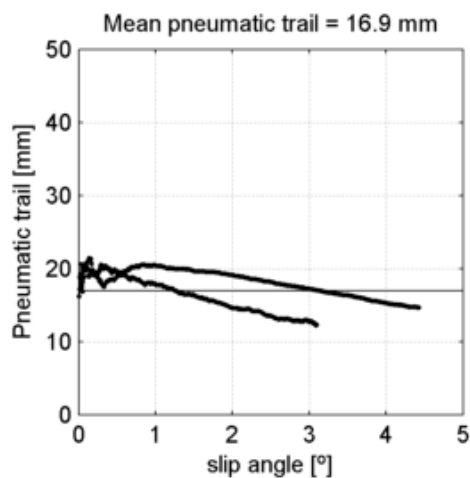
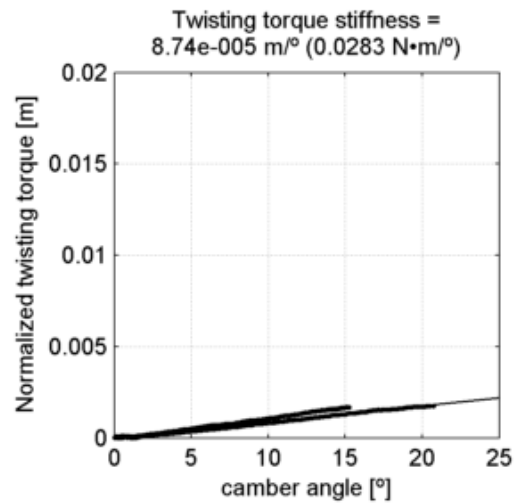
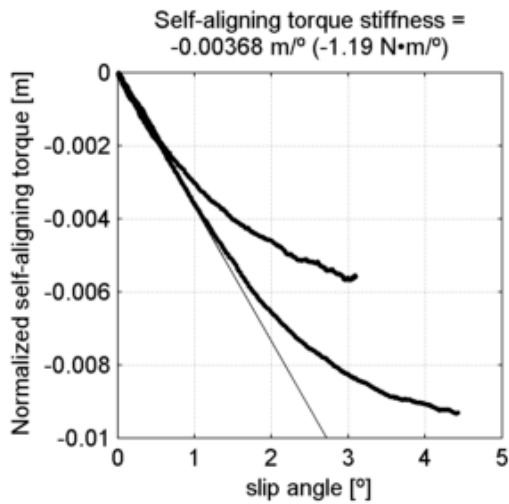
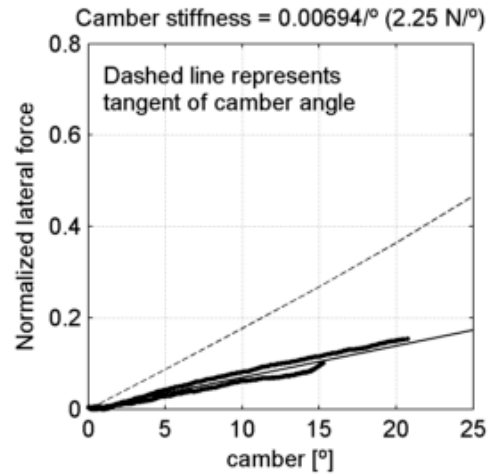
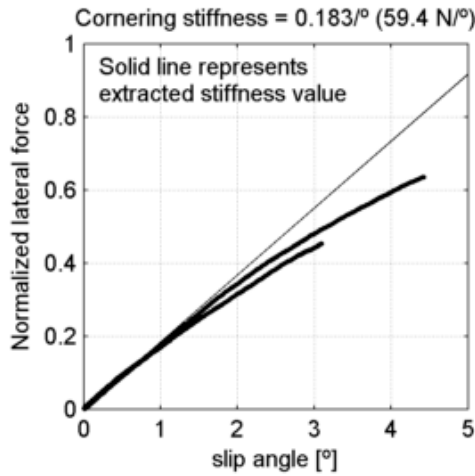
Cheng Shin Classic Zeppelin 50-622
 tire radius = 22.1 mm, rim width = 18.7 mm

at 4 bar (58 psi) and
 under 731 N (74.5 kg, 164 lb)



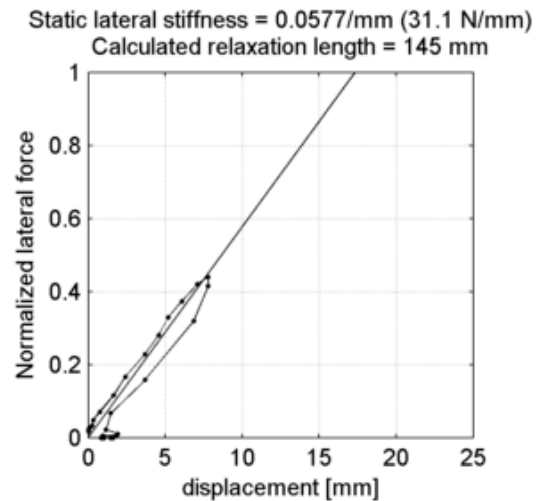
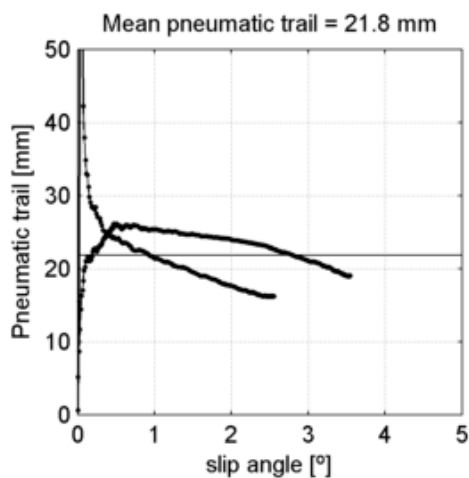
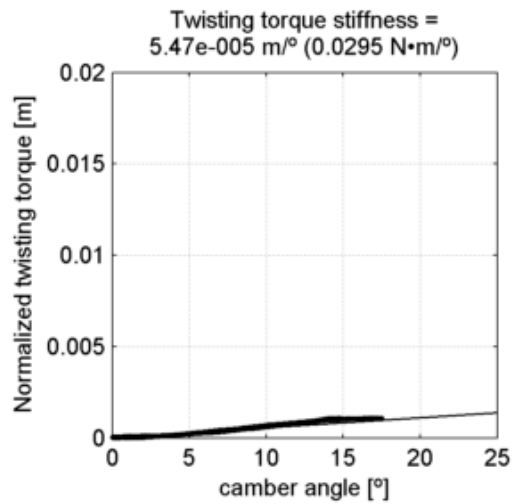
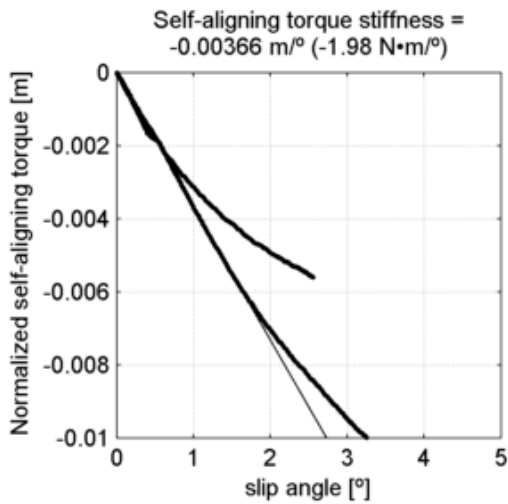
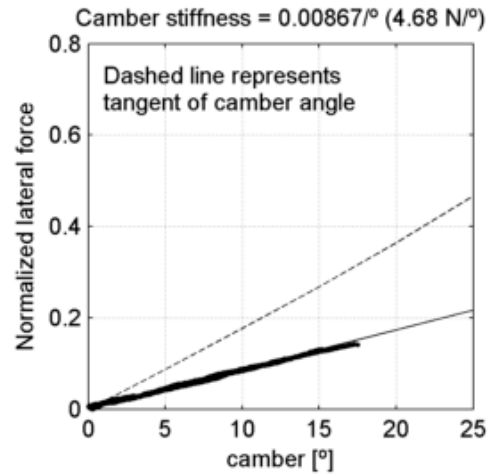
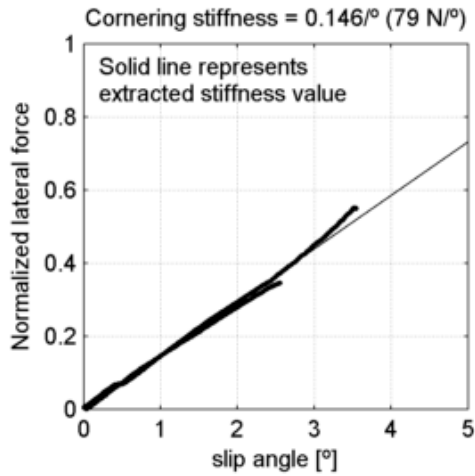
Continental Top Contact Winter 37-622
 tire radius = 15.6 mm, rim width = 18.7 mm

at 4 bar (58 psi) and
 under 324 N (33 kg, 72.8 lb)



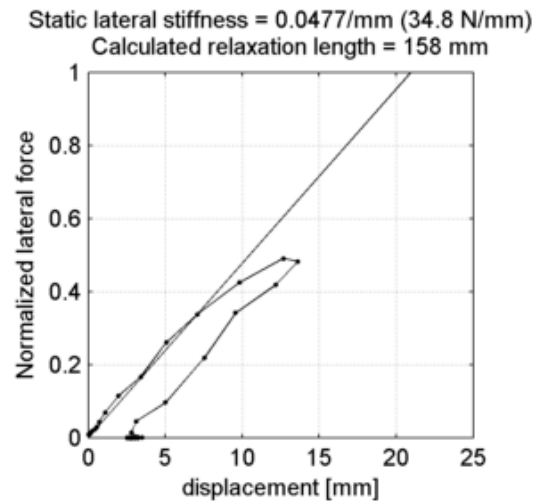
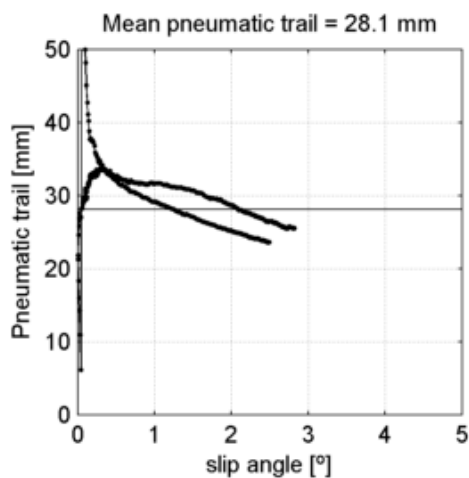
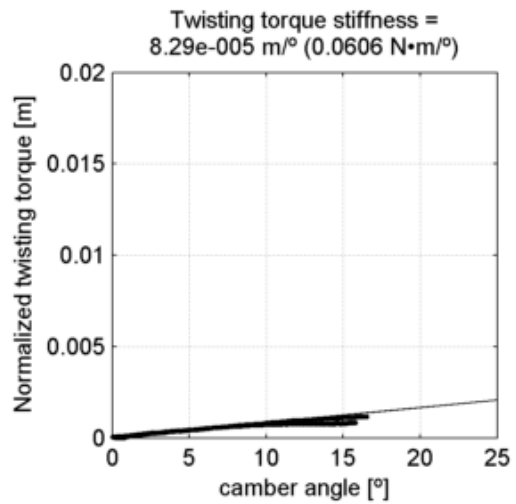
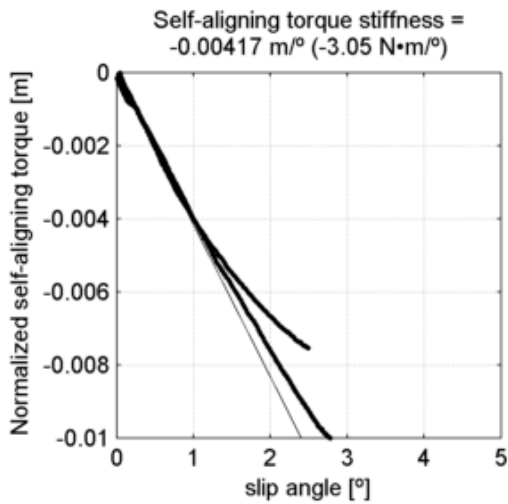
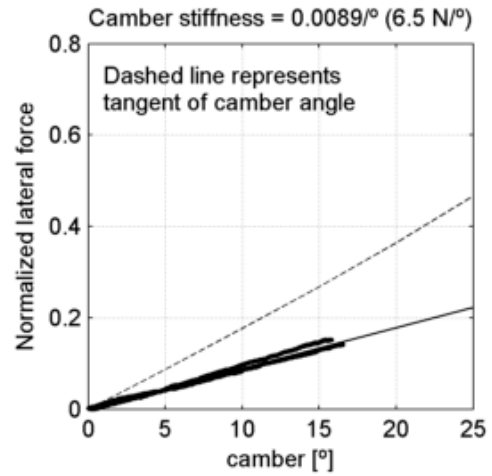
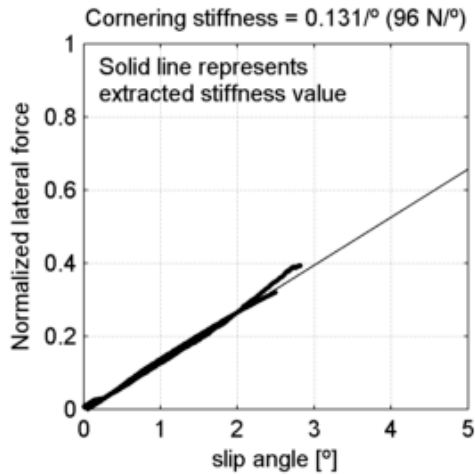
Continental Top Contact Winter 37-622
 tire radius = 15.6 mm, rim width = 18.7 mm

at 4 bar (58 psi) and
 under 540 N (55 kg, 121 lb)



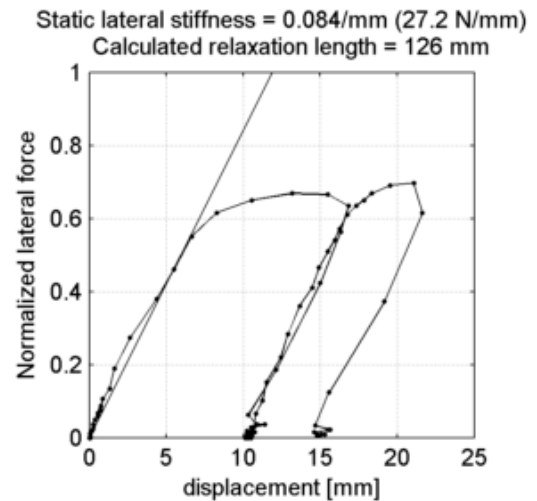
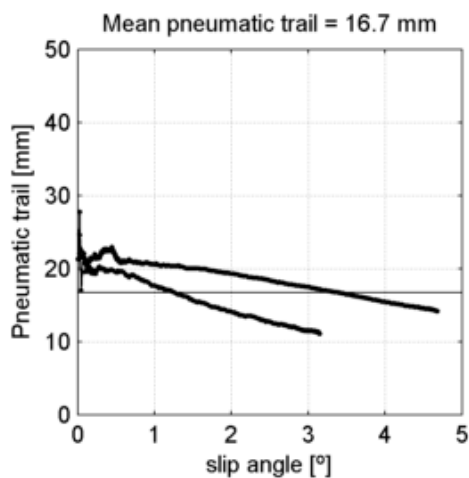
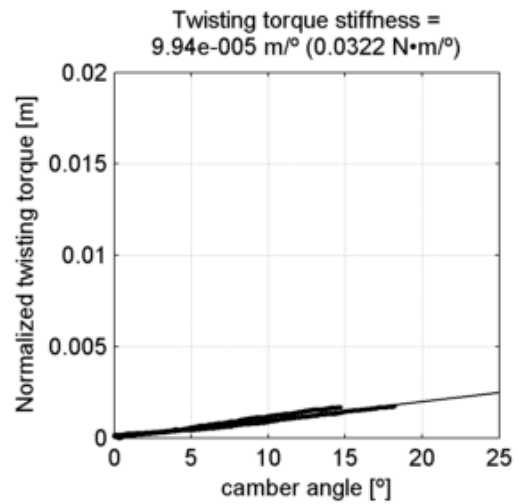
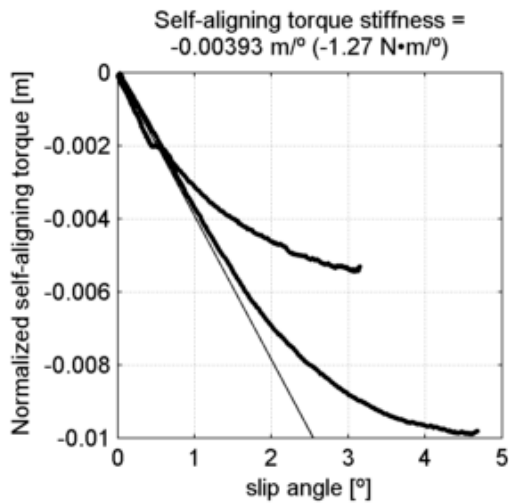
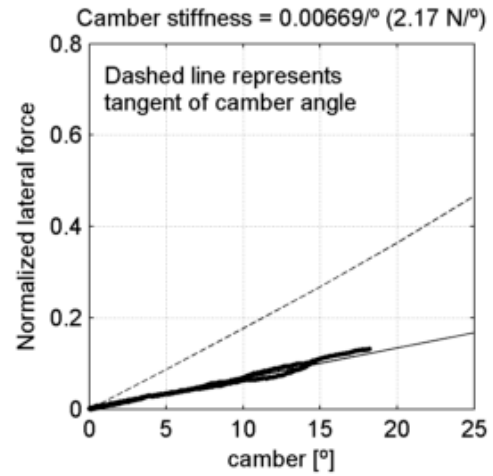
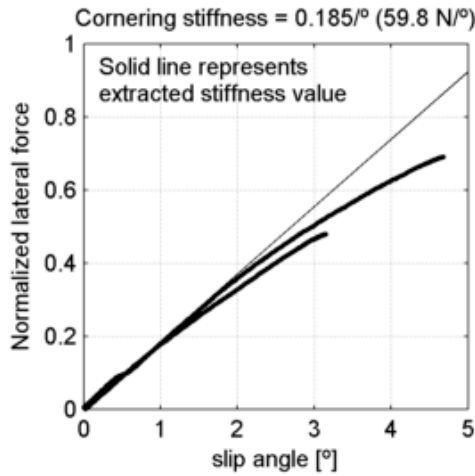
Continental Top Contact Winter 37-622
 tire radius = 15.6 mm, rim width = 18.7 mm

at 4 bar (58 psi) and
 under 731 N (74.5 kg, 164 lb)



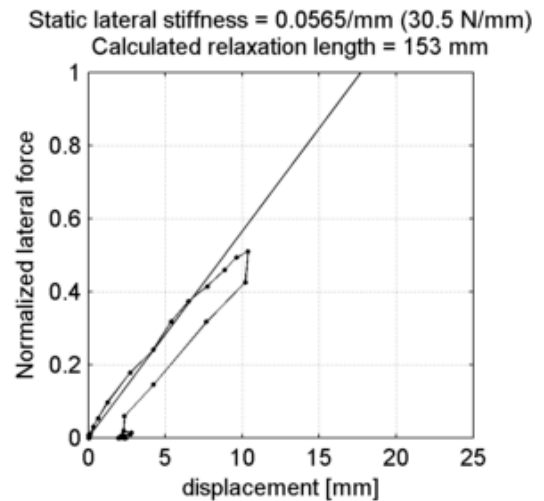
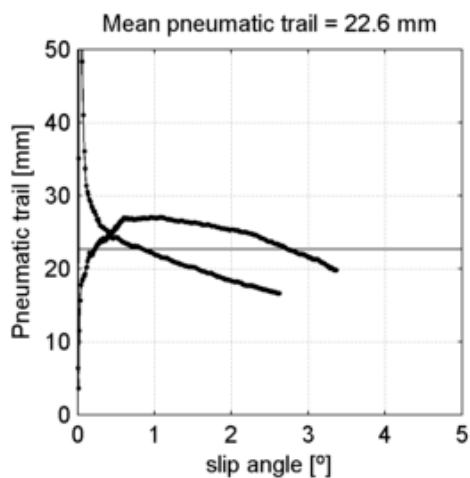
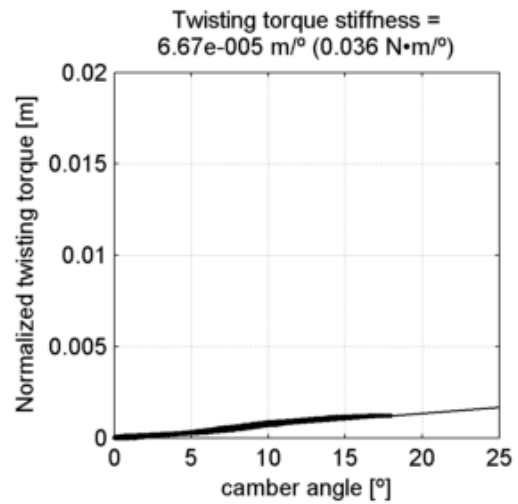
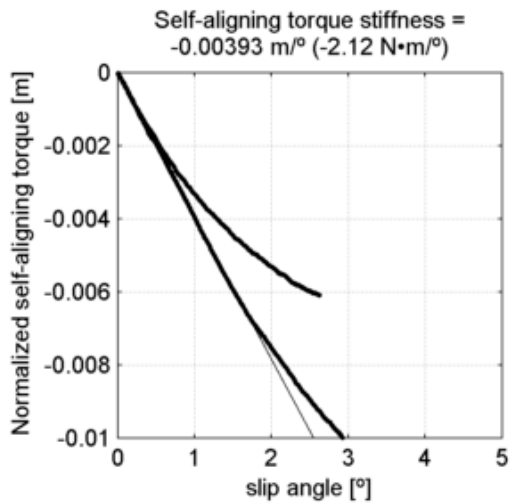
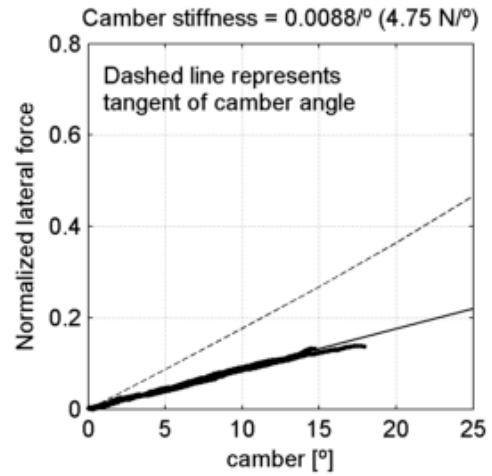
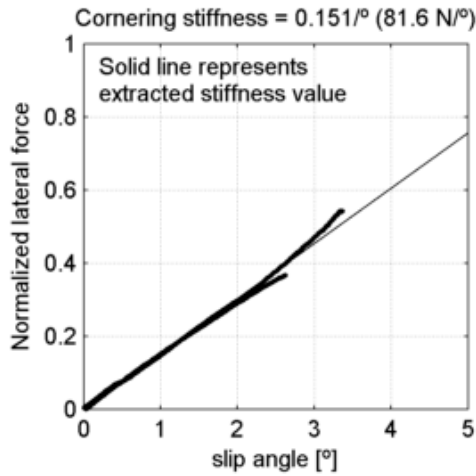
Continental Top Contact Winter 37-622
 tire radius = 15.6 mm, rim width = 18.7 mm

at 3.45 bar (50 psi) and
 under 324 N (33 kg, 72.8 lb)



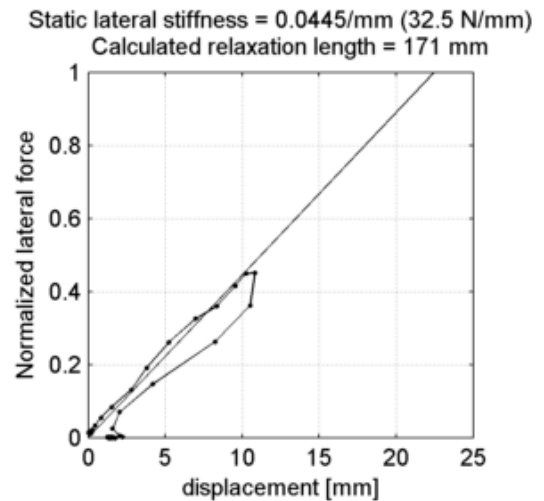
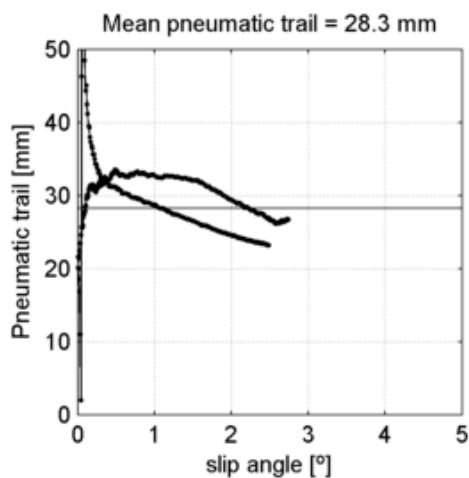
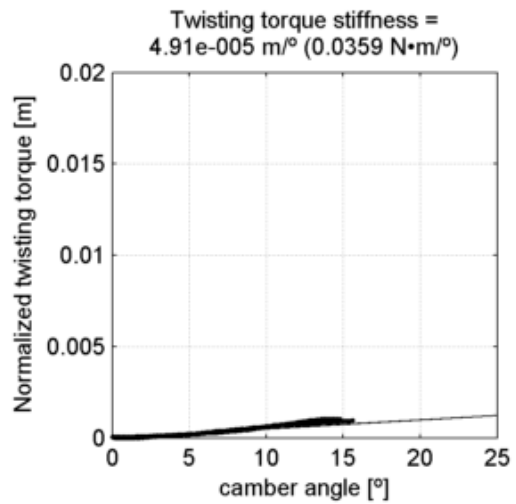
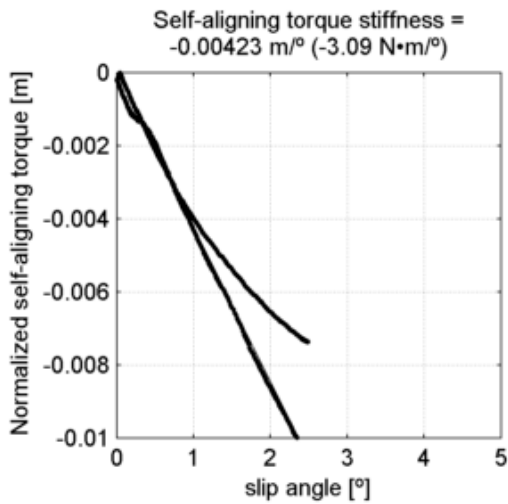
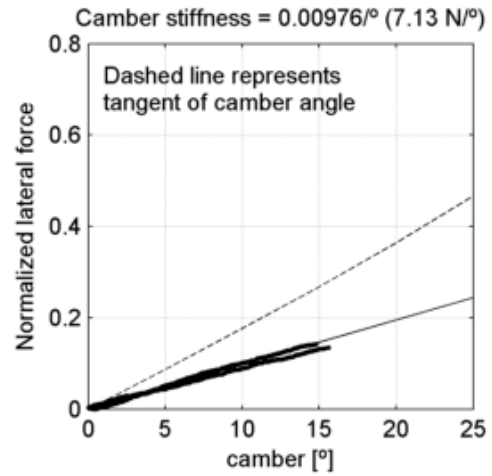
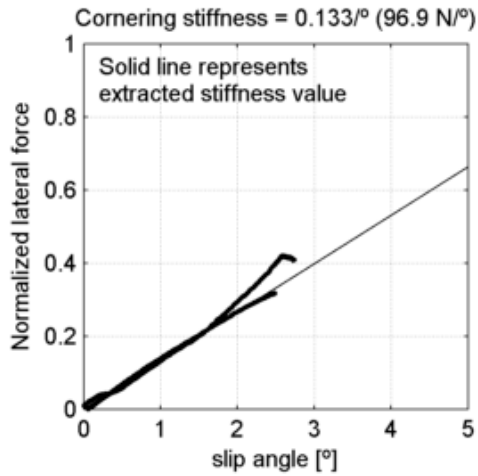
Continental Top Contact Winter 37-622
 tire radius = 15.6 mm, rim width = 18.7 mm

at 3.45 bar (50 psi) and
 under 540 N (55 kg, 121 lb)



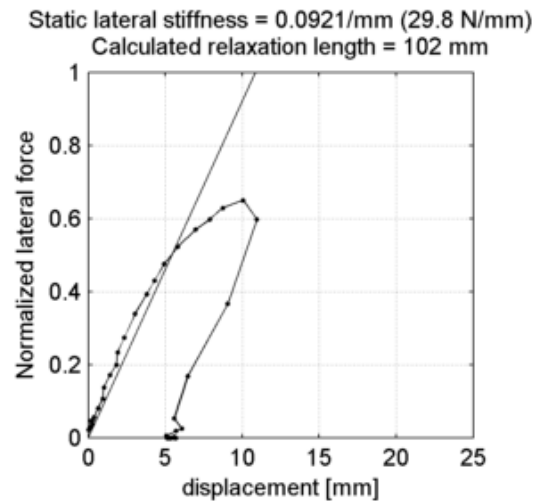
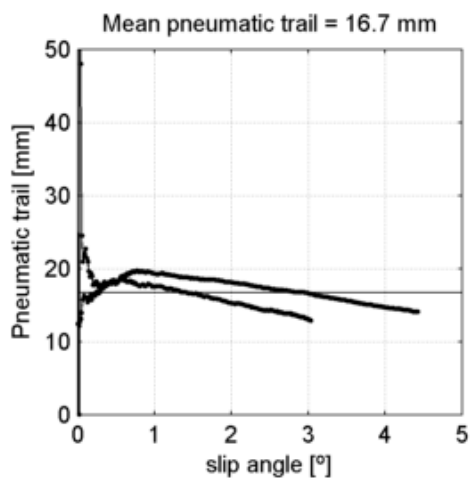
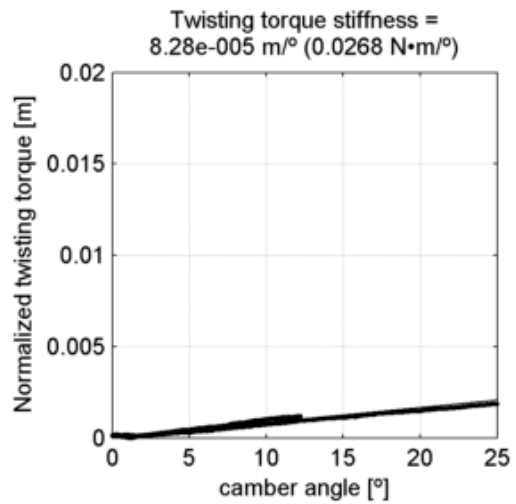
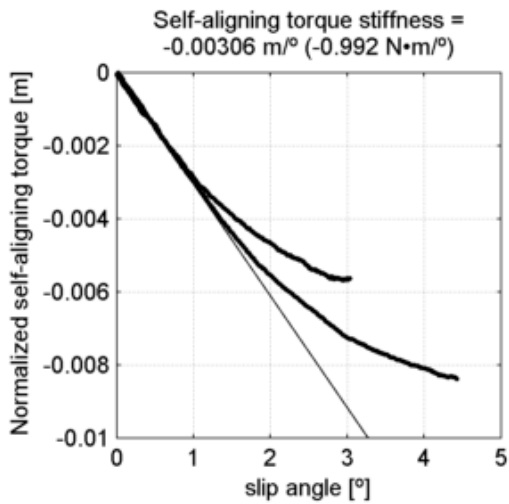
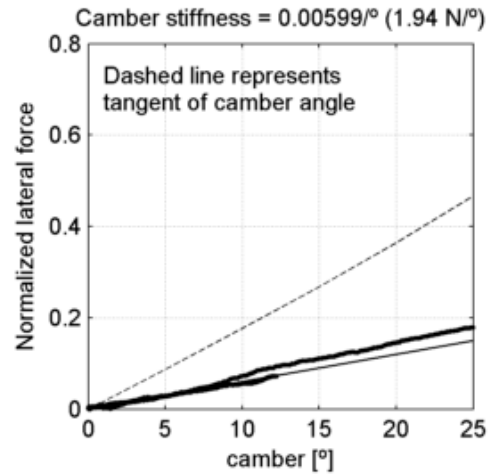
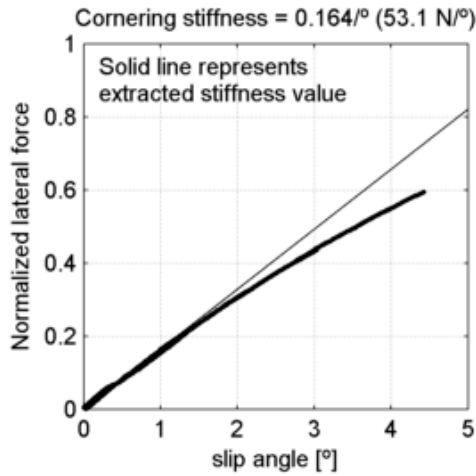
Continental Top Contact Winter 37-622
 tire radius = 15.6 mm, rim width = 18.7 mm

at 3.45 bar (50 psi) and
 under 731 N (74.5 kg, 164 lb)



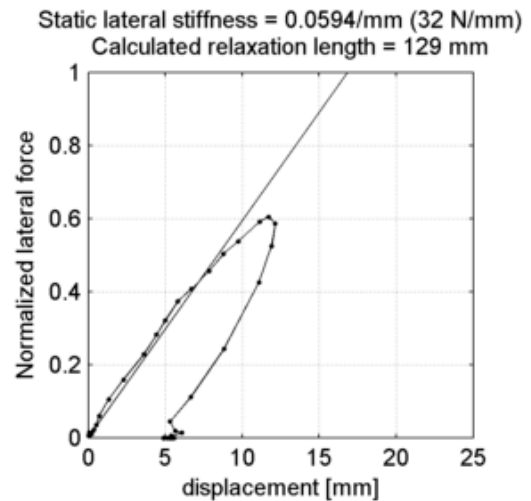
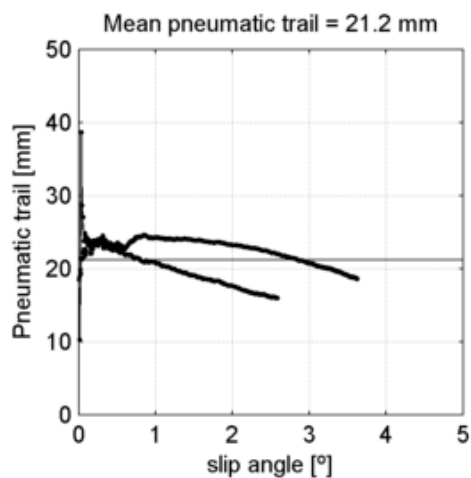
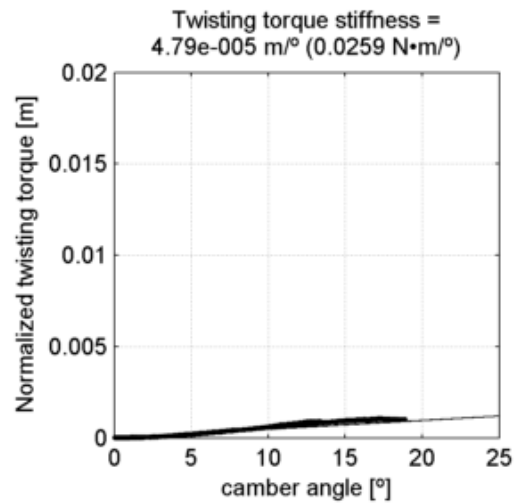
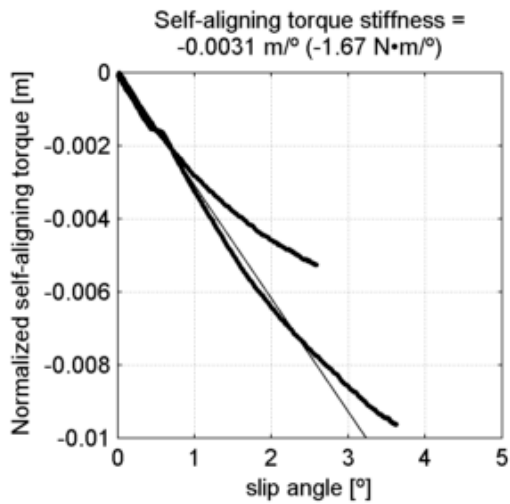
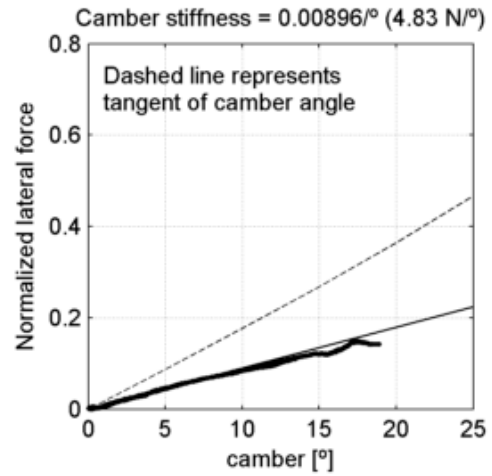
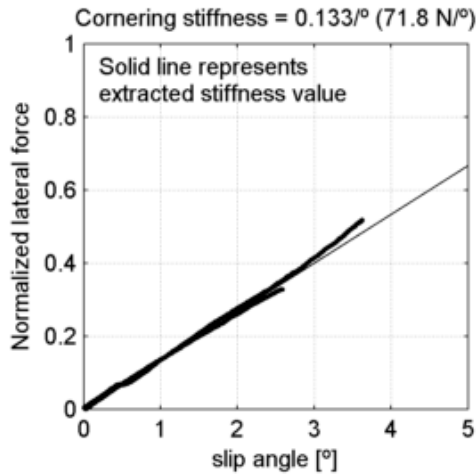
Continental Top Contact Winter 37-622
 tire radius = 15.6 mm, rim width = 18.7 mm

at 4.83 bar (70 psi) and
 under 324 N (33 kg, 72.8 lb)



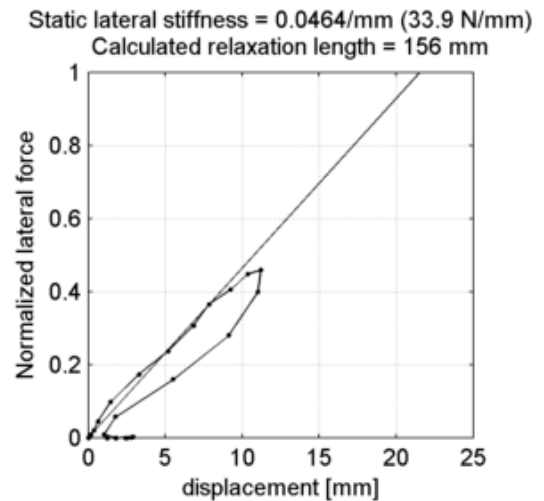
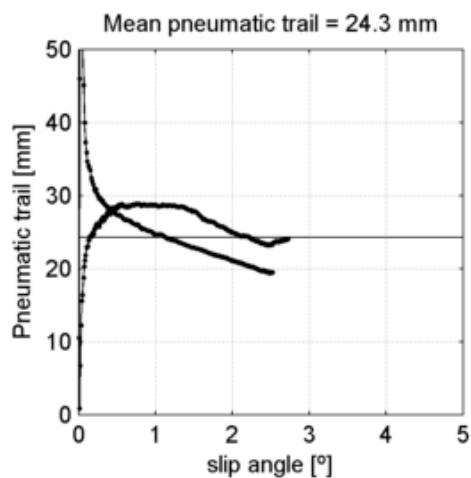
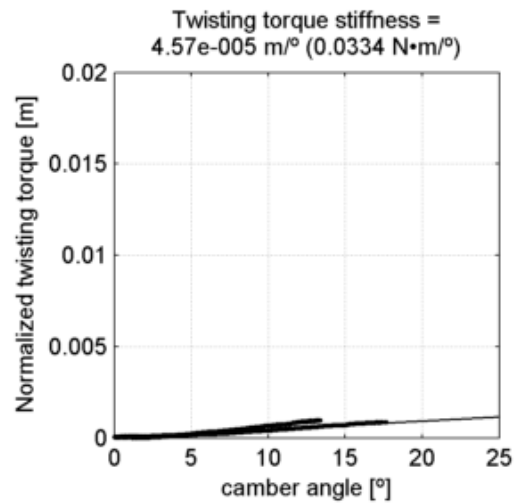
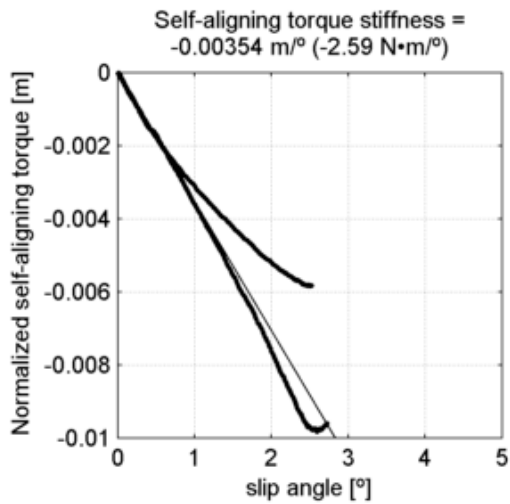
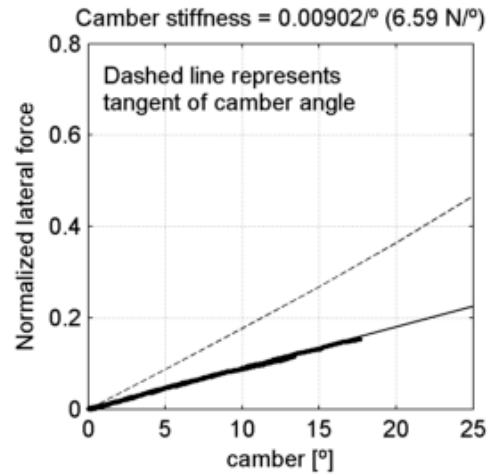
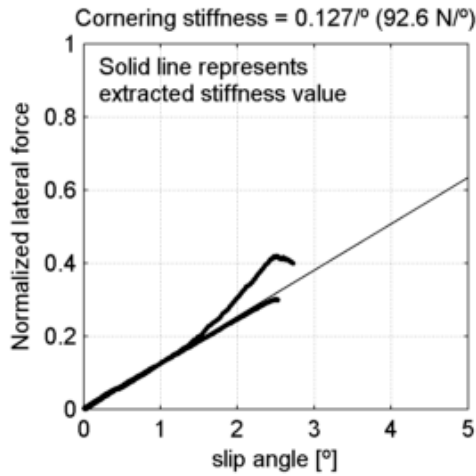
Continental Top Contact Winter 37-622
 tire radius = 15.6 mm, rim width = 18.7 mm

at 4.83 bar (70 psi) and
 under 540 N (55 kg, 121 lb)



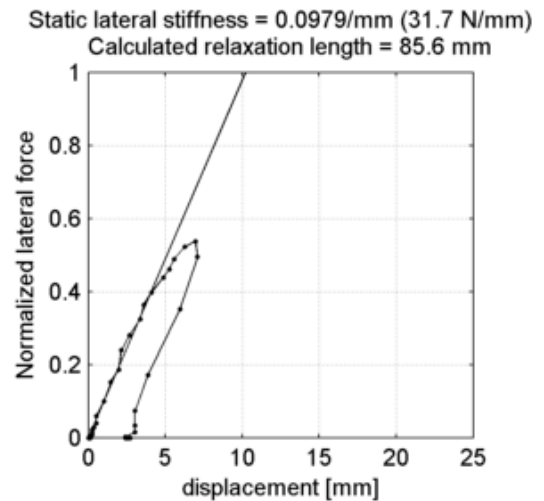
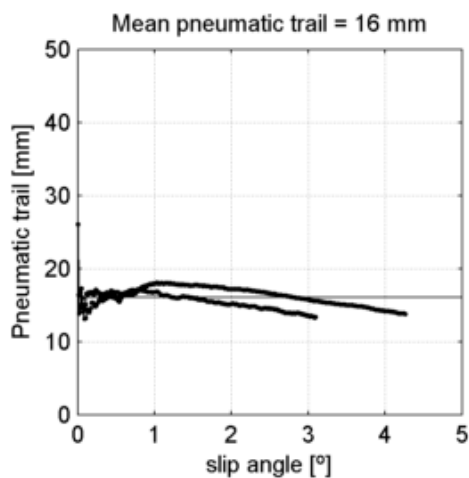
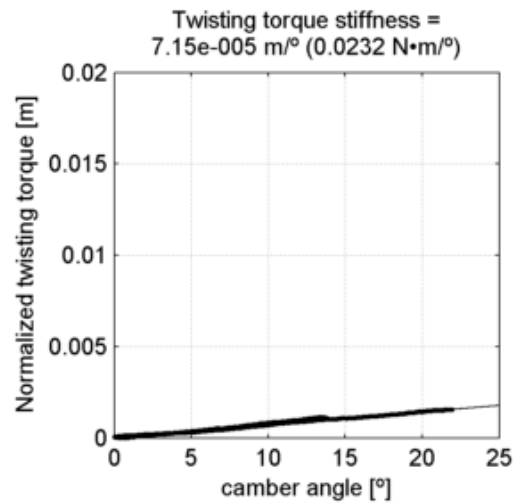
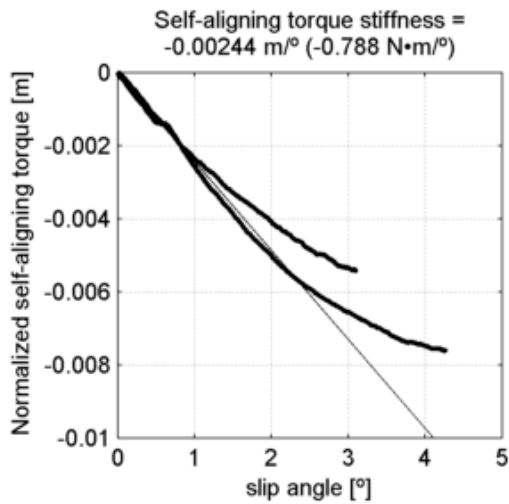
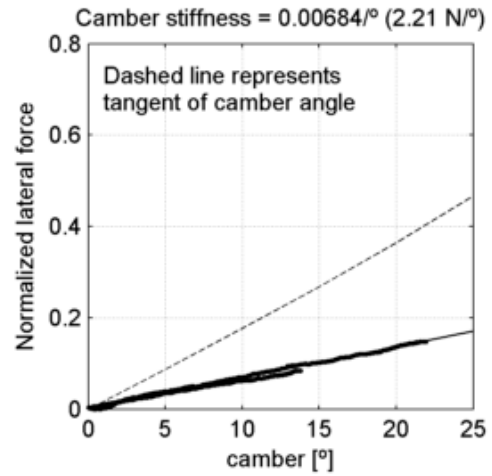
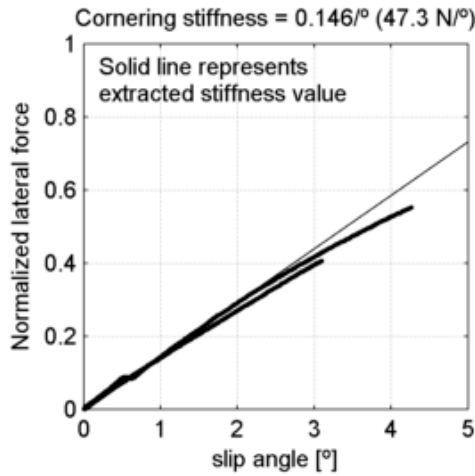
Continental Top Contact Winter 37-622
 tire radius = 15.6 mm, rim width = 18.7 mm

at 4.83 bar (70 psi) and
 under 731 N (74.5 kg, 164 lb)



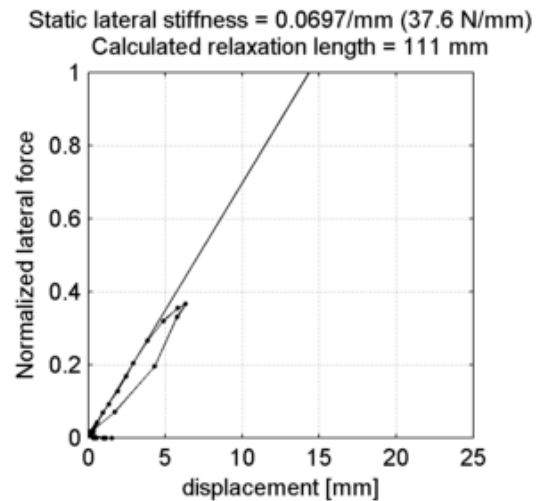
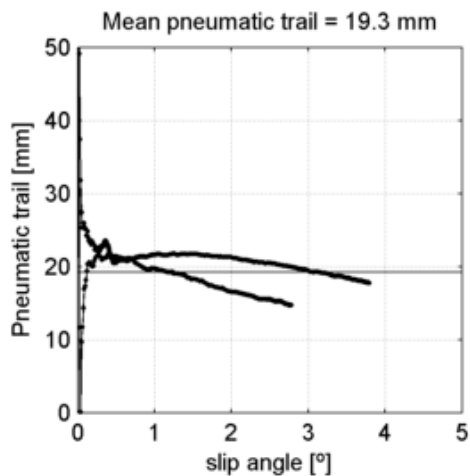
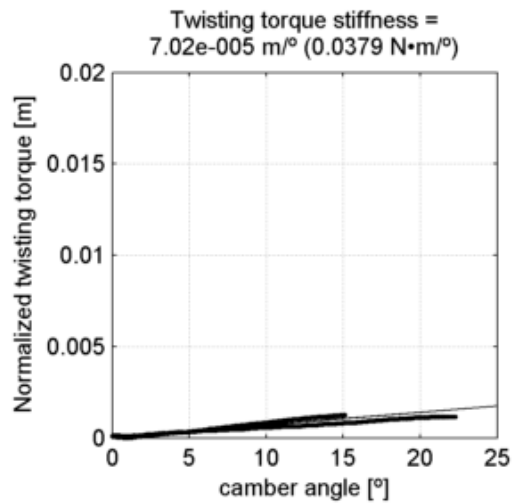
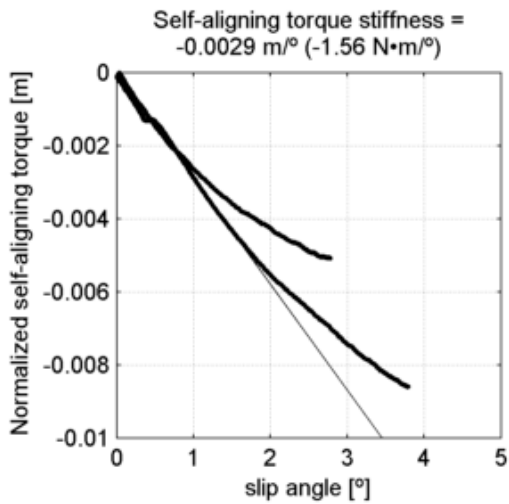
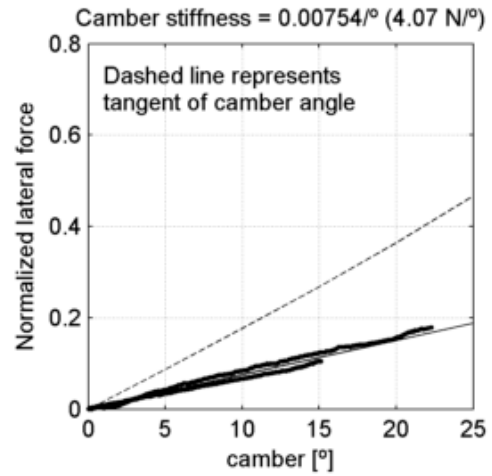
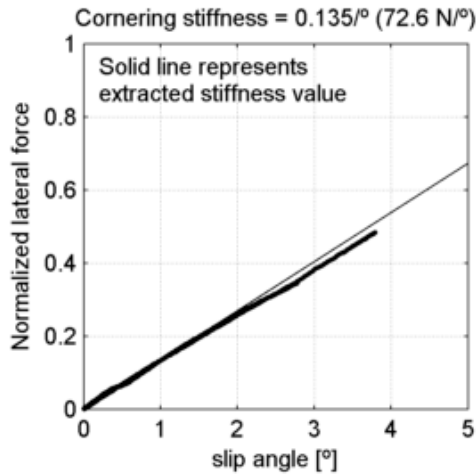
Continental Top Contact Winter 37-622
 tire radius = 15.6 mm, rim width = 18.7 mm

at 6.21 bar (90 psi) and
 under 324 N (33 kg, 72.8 lb)



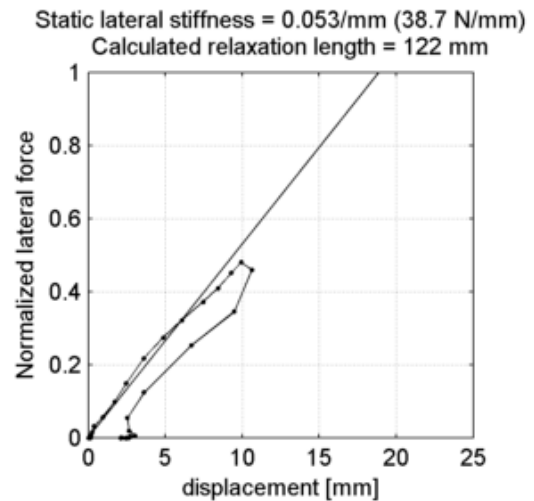
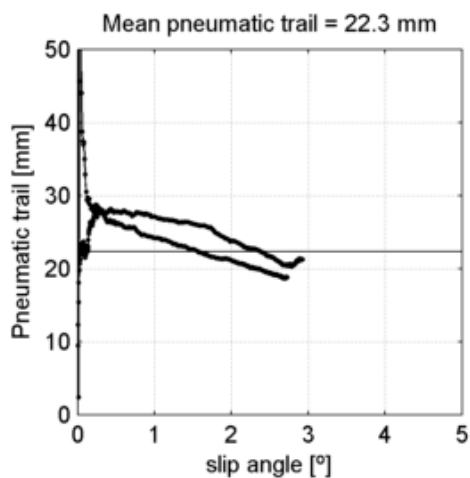
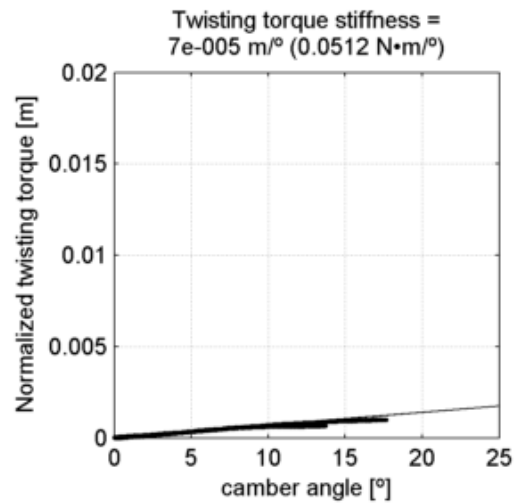
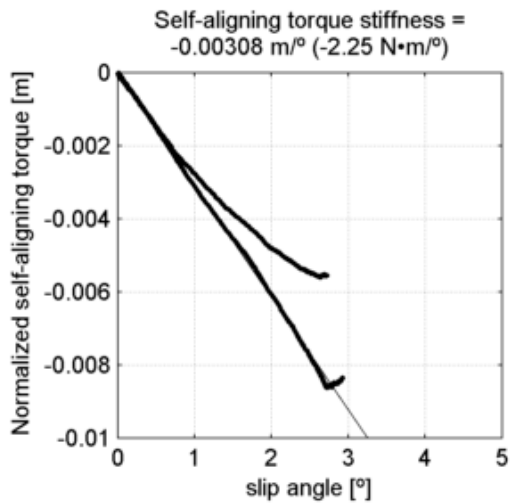
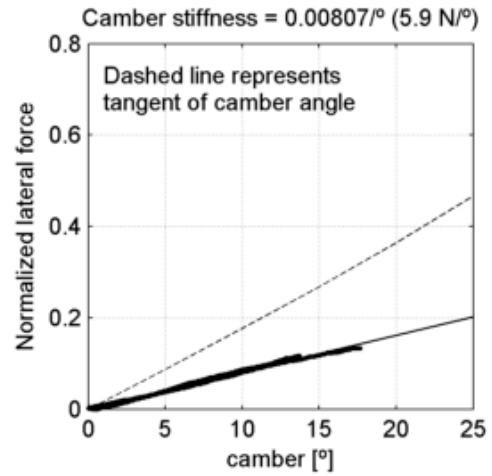
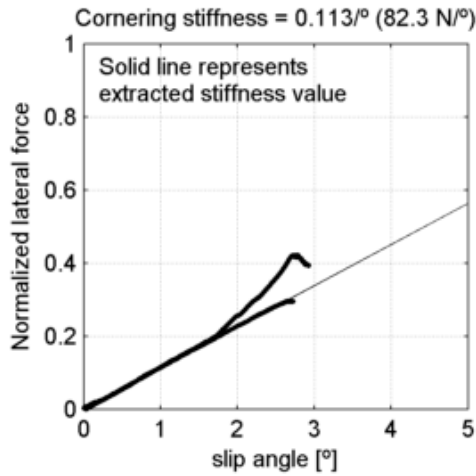
Continental Top Contact Winter 37-622
 tire radius = 15.6 mm, rim width = 18.7 mm

at 6.21 bar (90 psi) and
 under 540 N (55 kg, 121 lb)



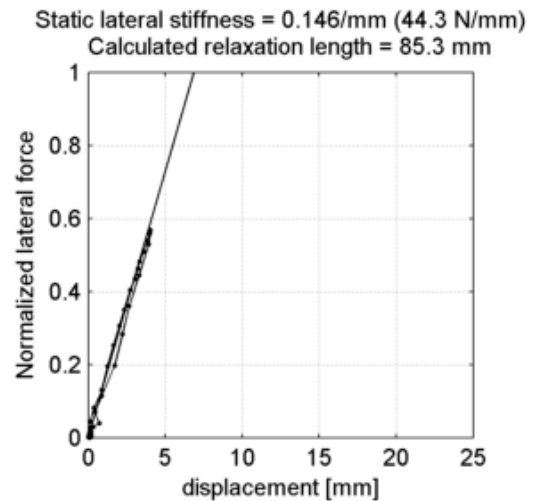
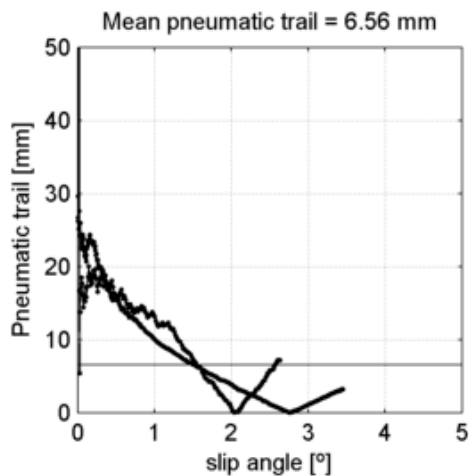
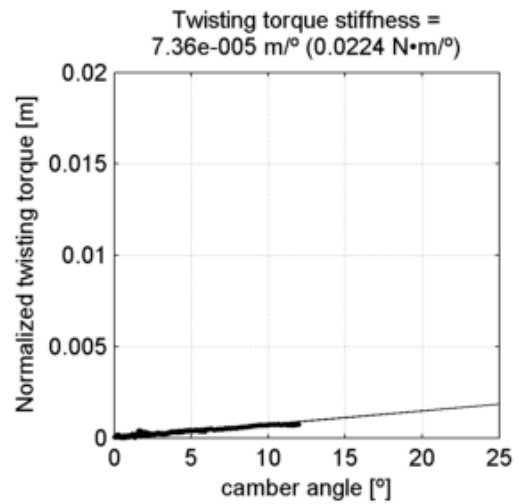
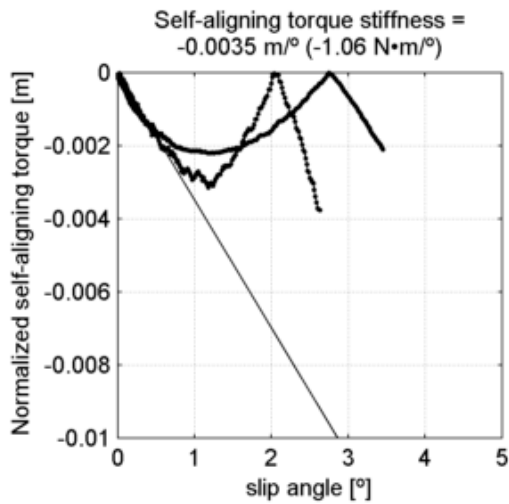
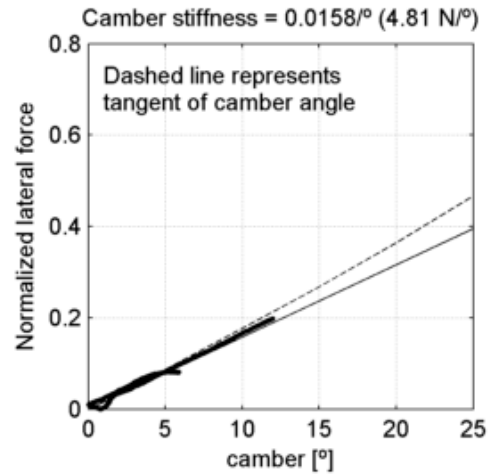
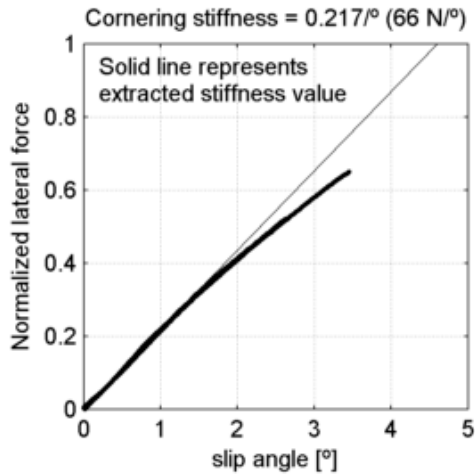
Continental Top Contact Winter 37-622
 tire radius = 15.6 mm, rim width = 18.7 mm

at 6.21 bar (90 psi) and
 under 731 N (74.5 kg, 164 lb)



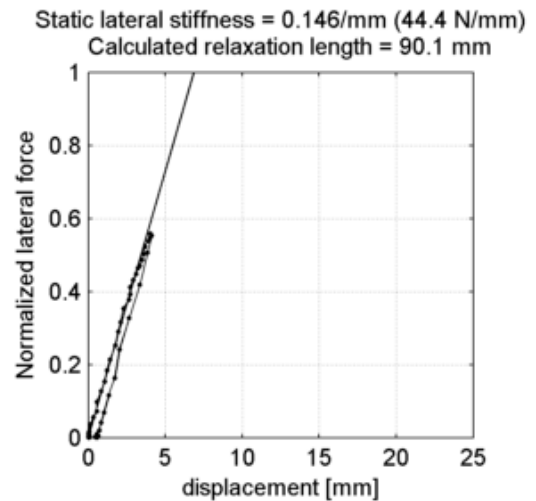
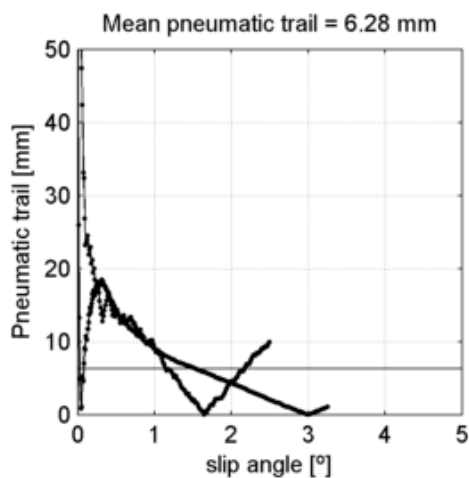
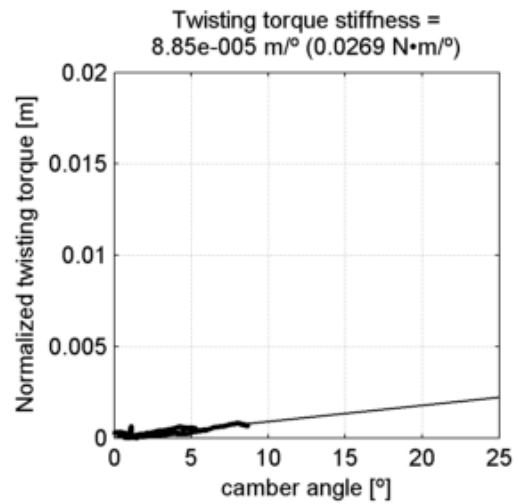
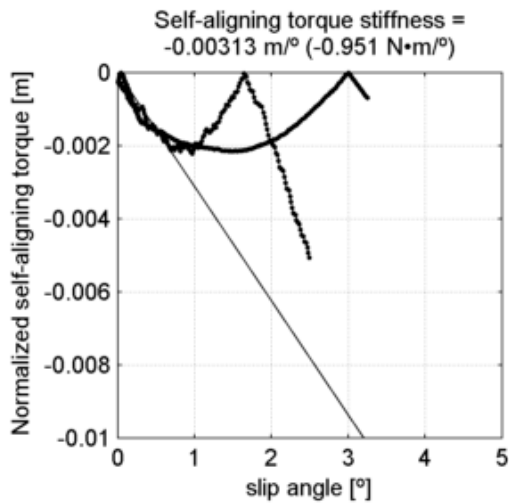
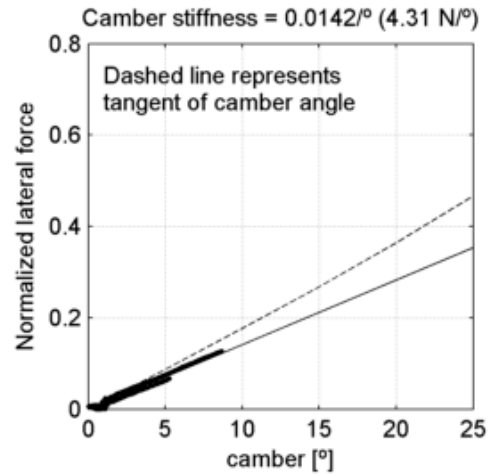
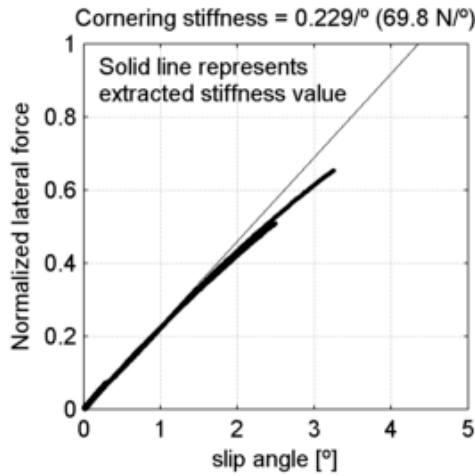
Maxis Radial 22-622
 tire radius = 11 mm, rim width = 13.4 mm

at 6.89 bar (100 psi) and
 under 304 N (31 kg, 68.3 lb)



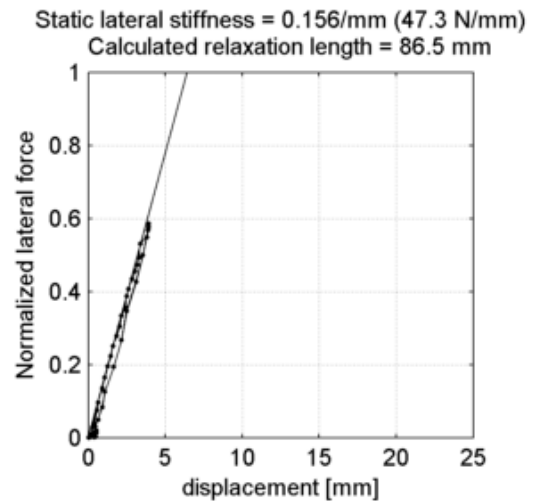
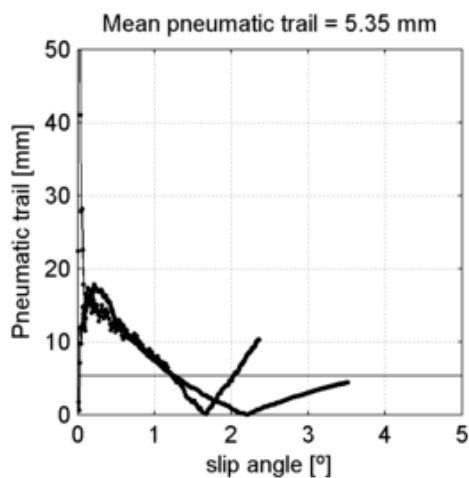
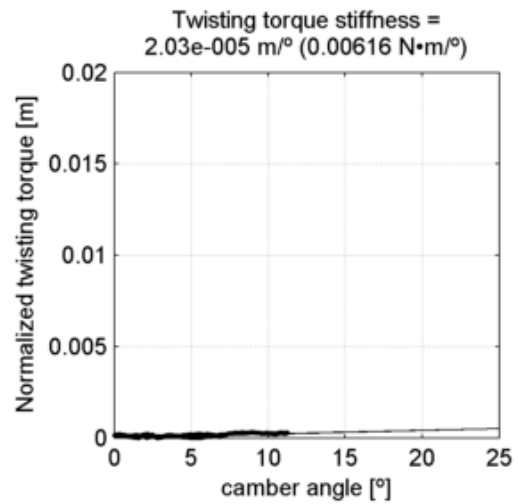
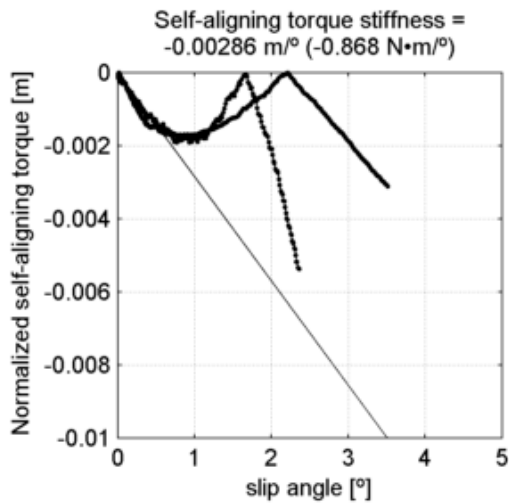
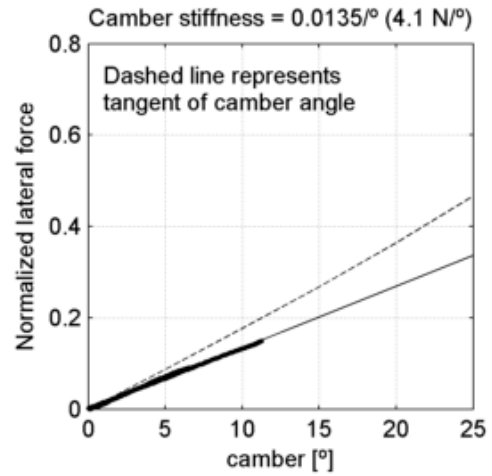
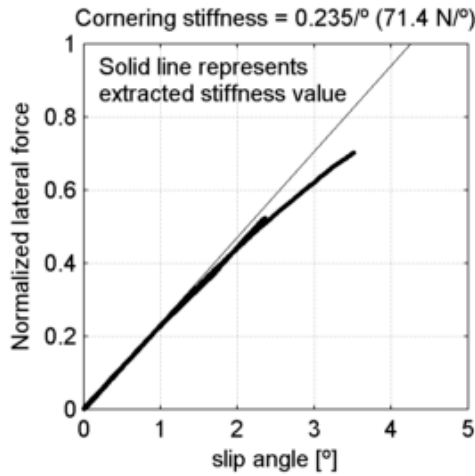
Maxis Radial 22-622
 tire radius = 11 mm, rim width = 13.4 mm

at 8.27 bar (120 psi) and
 under 304 N (31 kg, 68.3 lb)



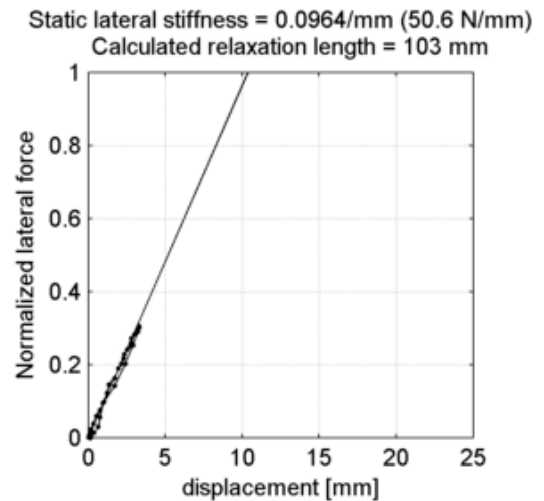
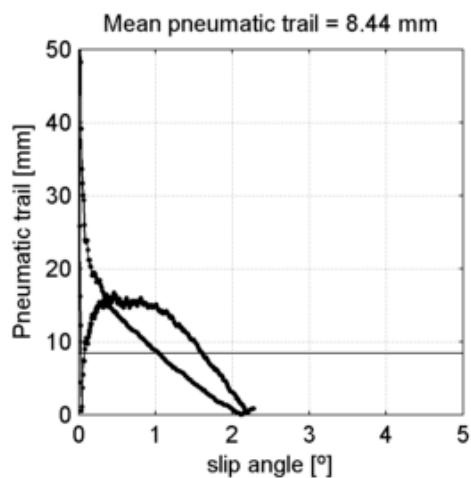
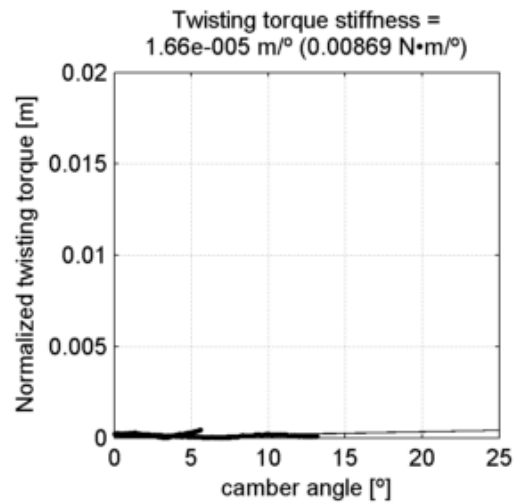
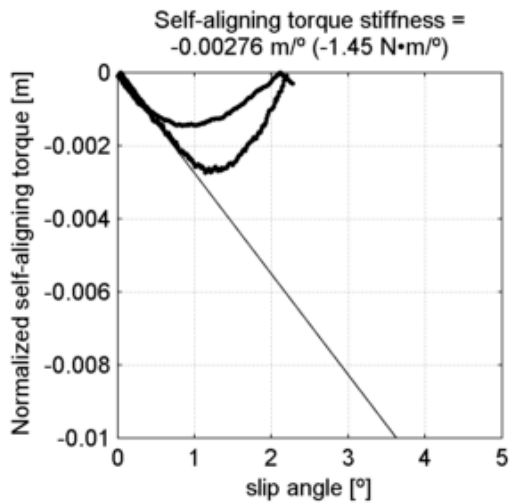
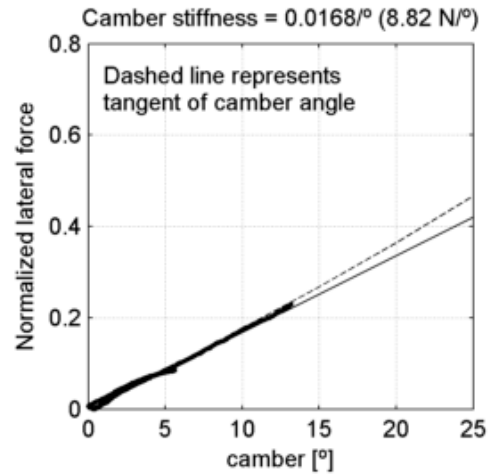
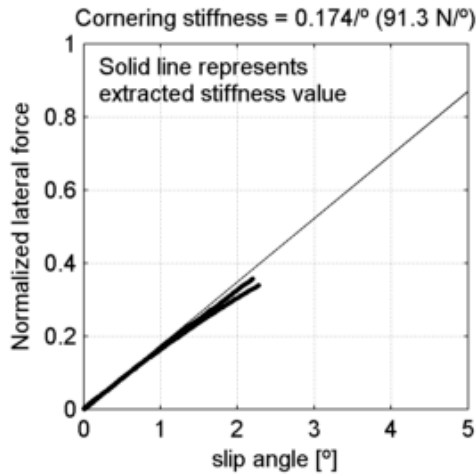
Maxis Radial 22-622
 tire radius = 11 mm, rim width = 13.4 mm

at 9.65 bar (140 psi) and
 under 304 N (31 kg, 68.3 lb)



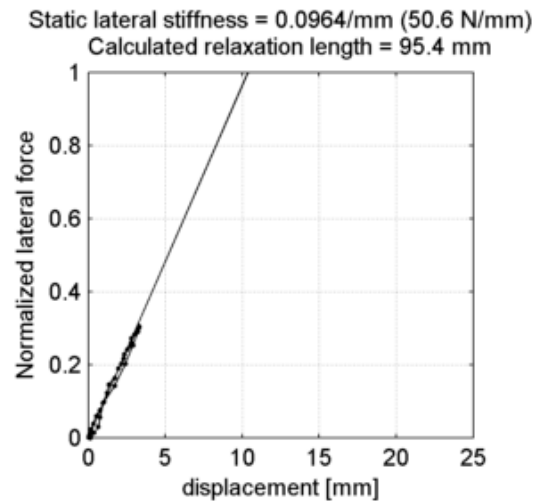
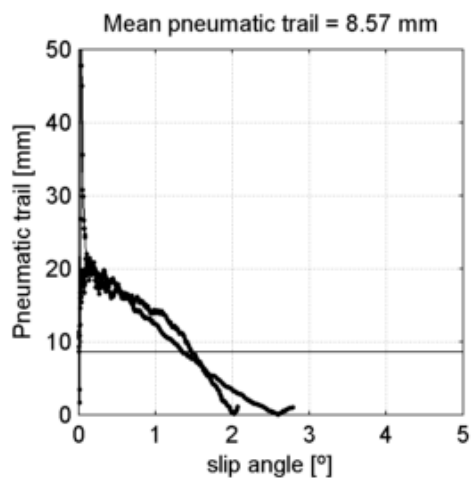
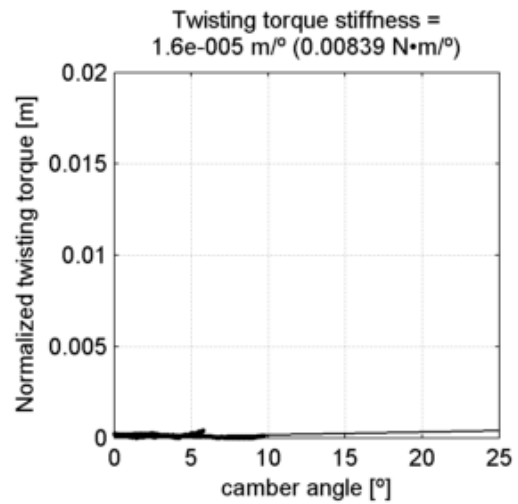
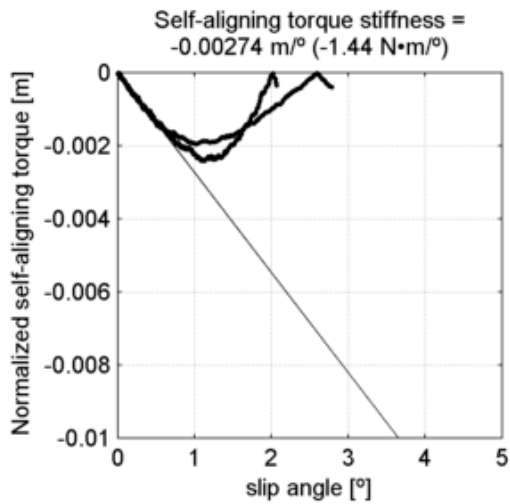
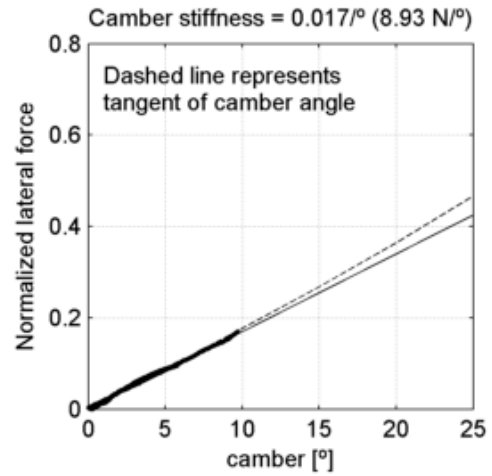
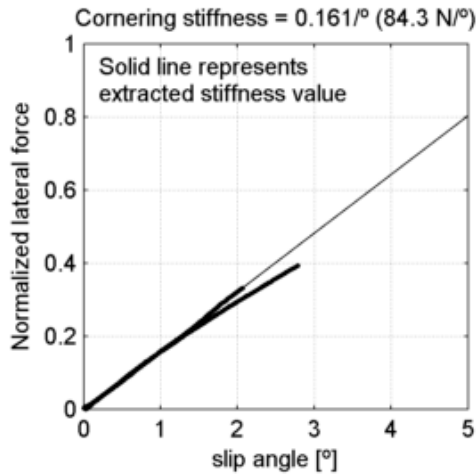
Maxis Radial 22-622
 tire radius = 11 mm, rim width = 13.4 mm

at 9.65 bar (140 psi) and
 under 525 N (53.5 kg, 118 lb)



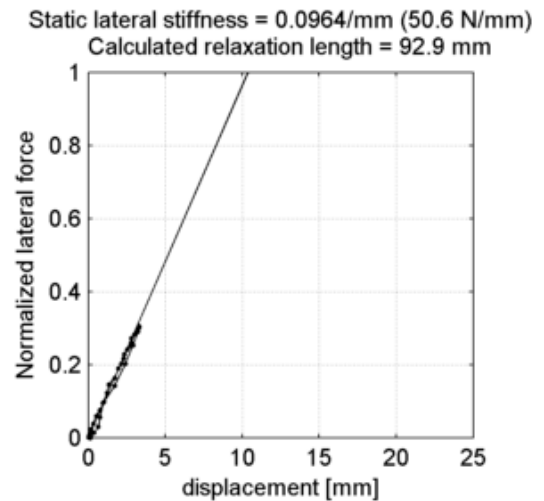
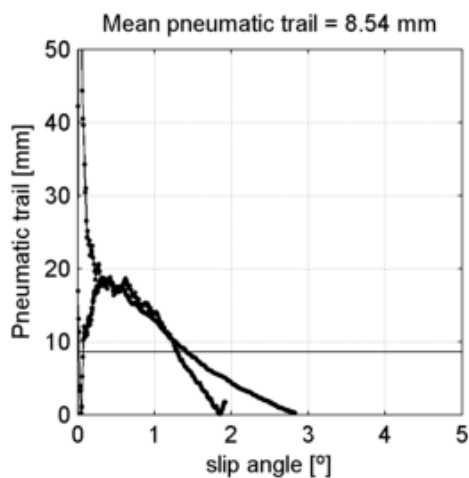
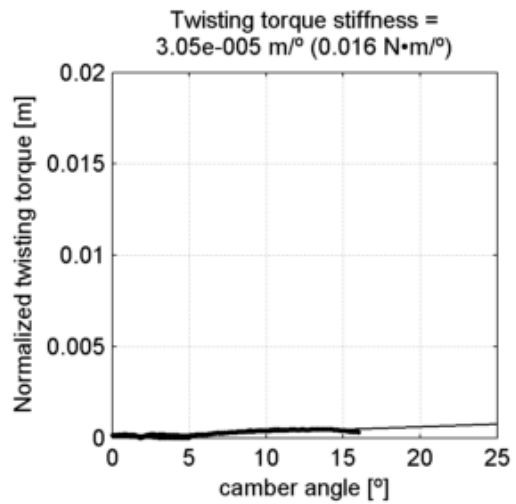
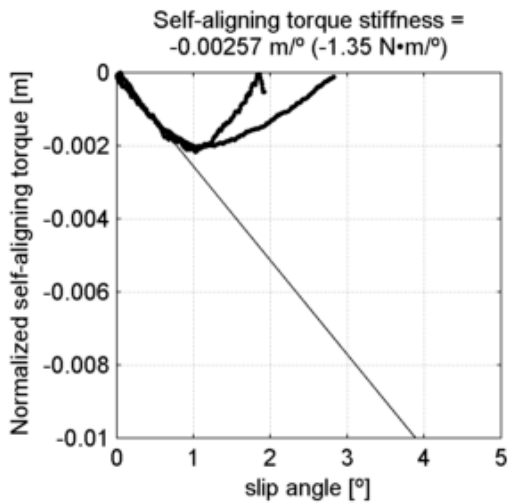
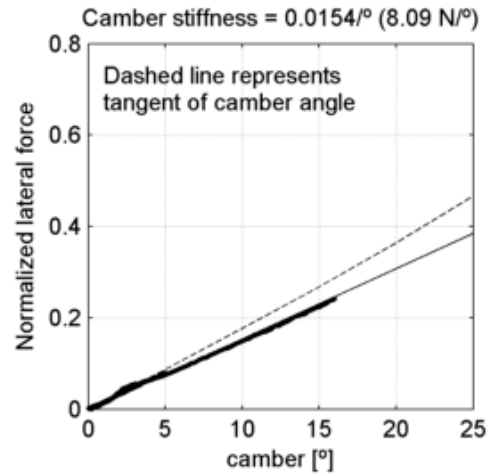
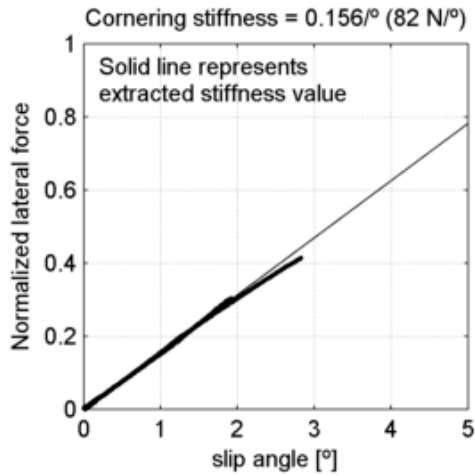
Maxis Radial 22-622
 tire radius = 11 mm, rim width = 13.4 mm

at 9.65 bar (140 psi) and
 under 525 N (53.5 kg, 118 lb)



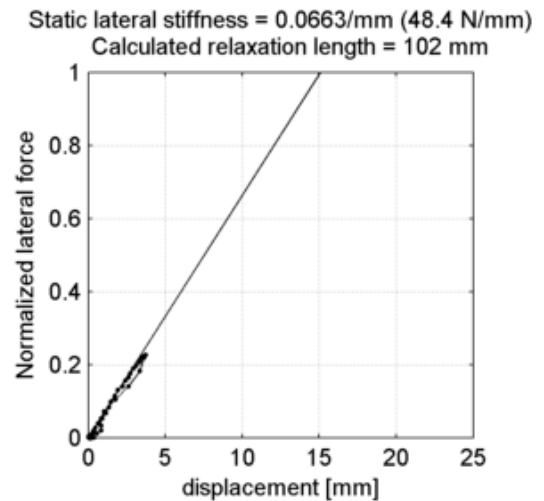
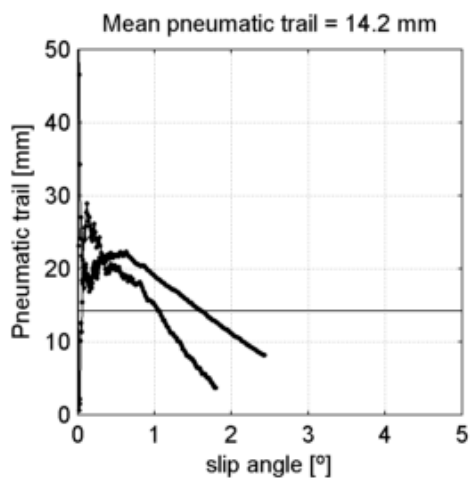
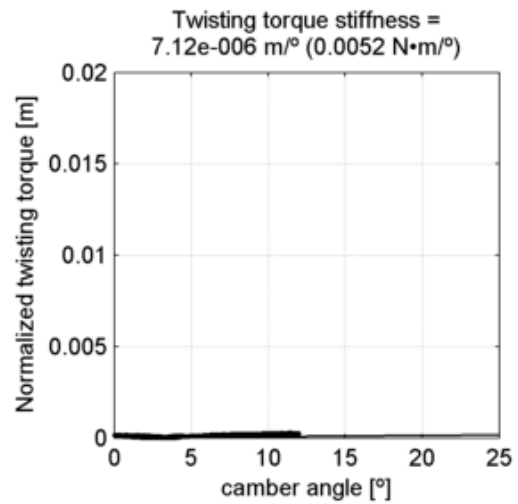
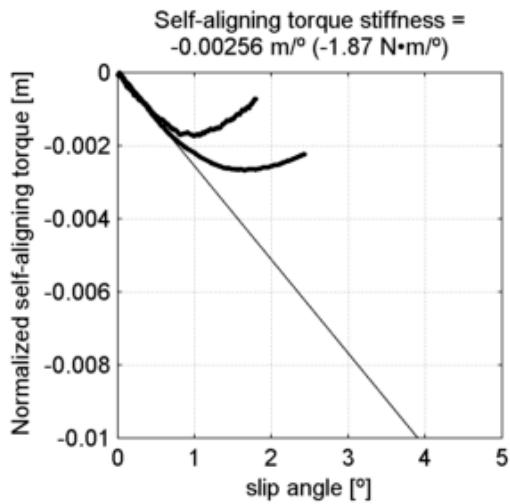
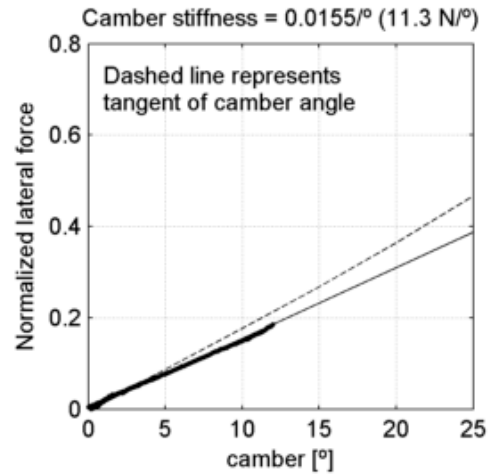
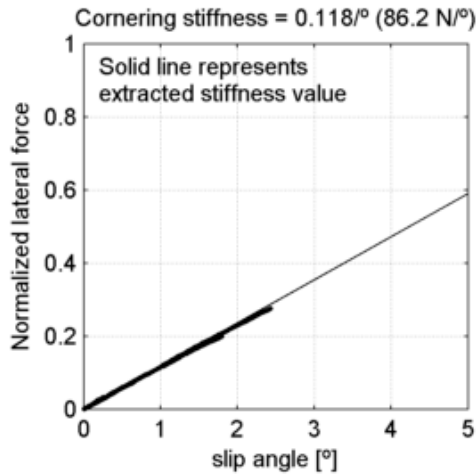
Maxis Radial 22-622
 tire radius = 11 mm, rim width = 13.4 mm

at 9.65 bar (140 psi) and
 under 525 N (53.5 kg, 118 lb)



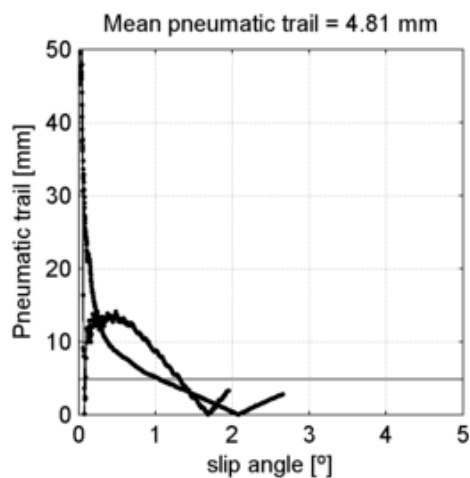
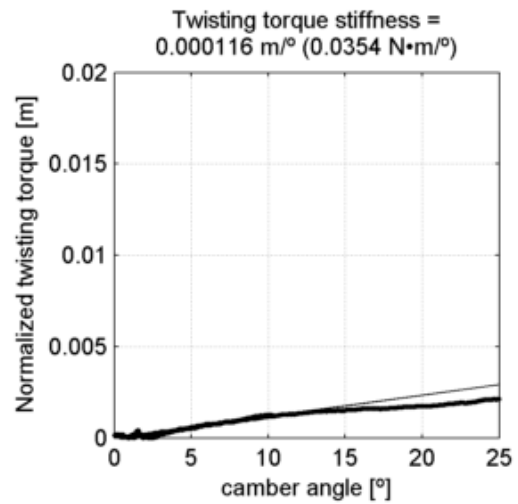
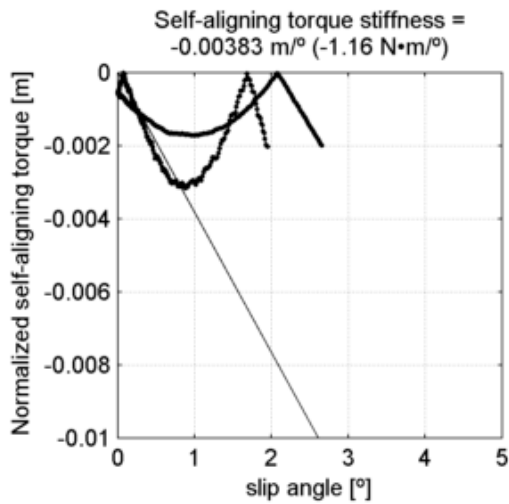
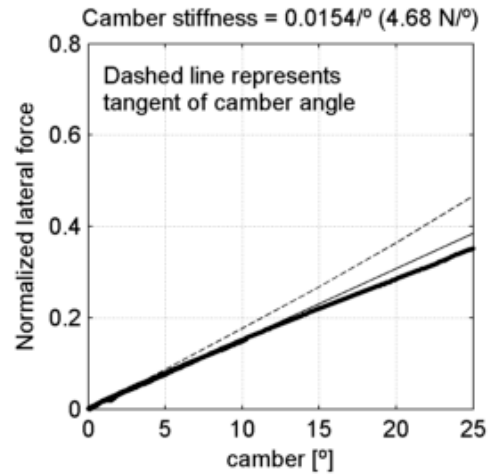
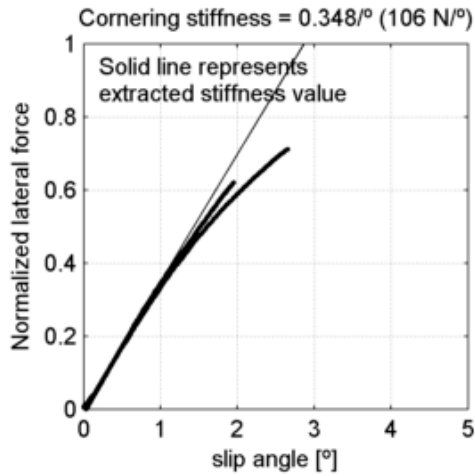
Maxis Radial 22-622
 tire radius = 11 mm, rim width = 13.4 mm

at 9.65 bar (140 psi) and
 under 731 N (74.5 kg, 164 lb)



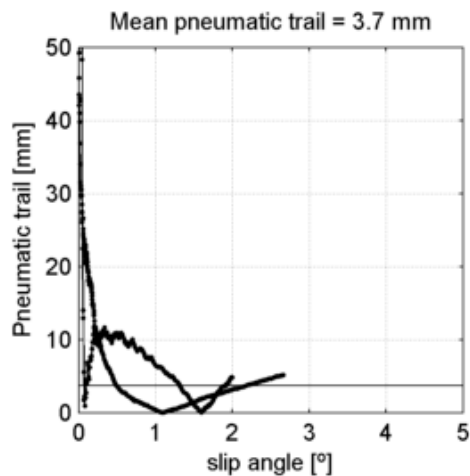
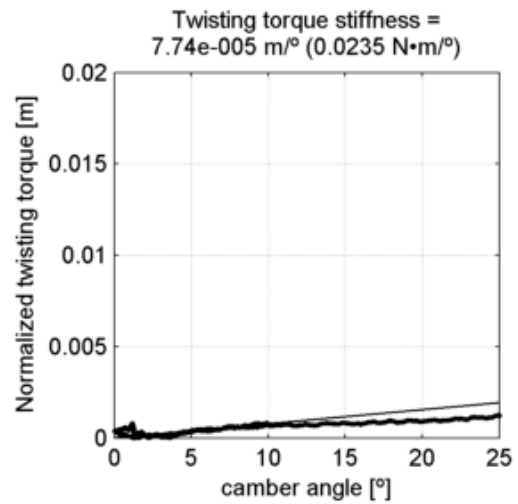
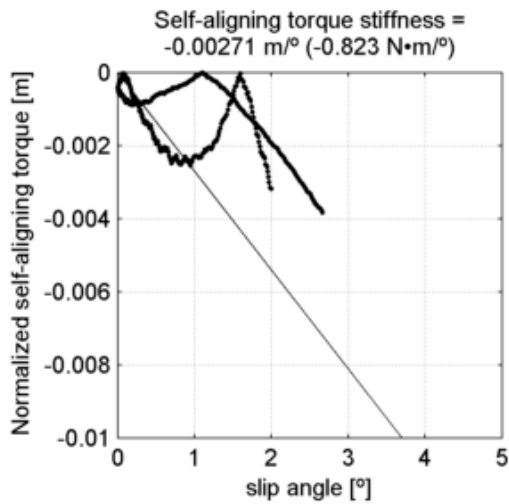
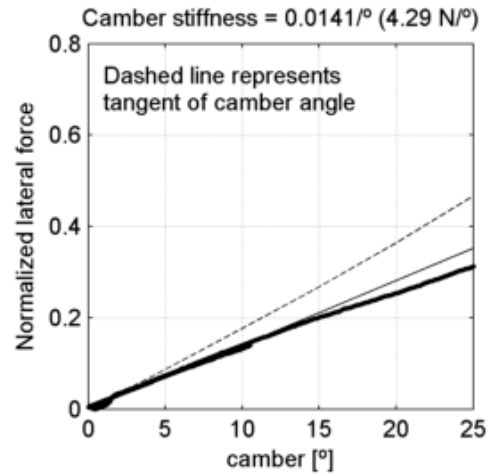
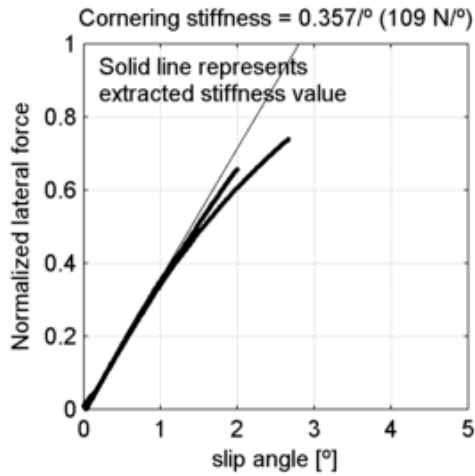
Michelin Dynamic xx-622
 tire radius = 12.5 mm, rim width = 13.4 mm

at 4.14 bar (60 psi) and
 under 304 N (31 kg, 68.3 lb)



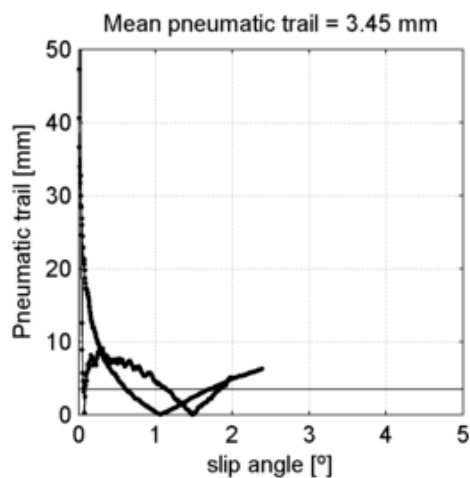
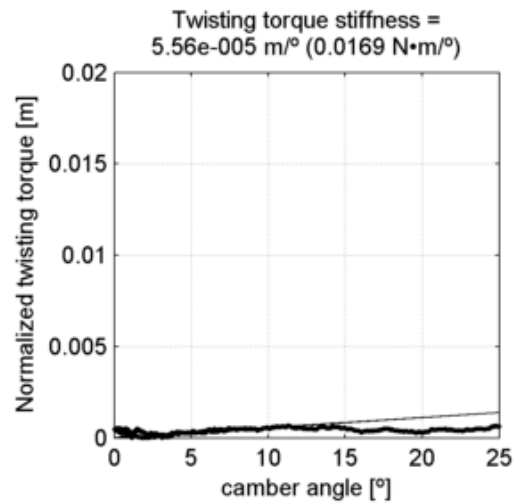
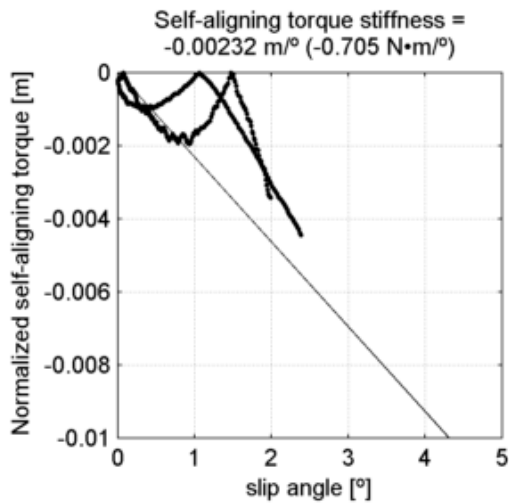
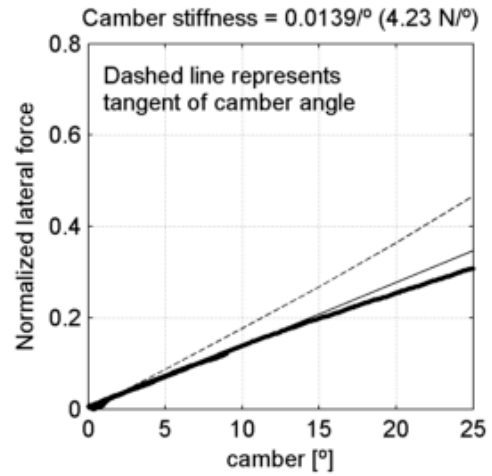
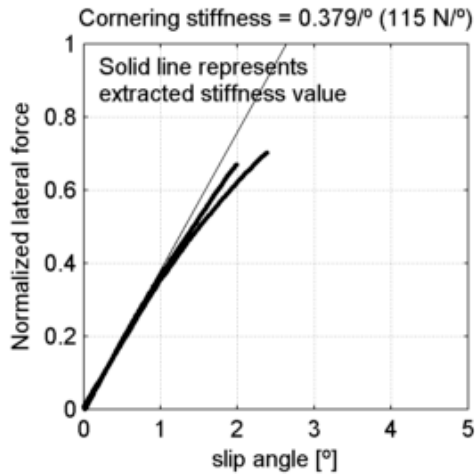
Michelin Dynamic xx-622
 tire radius = 12.5 mm, rim width = 13.4 mm

at 6.21 bar (90 psi) and
 under 304 N (31 kg, 68.3 lb)



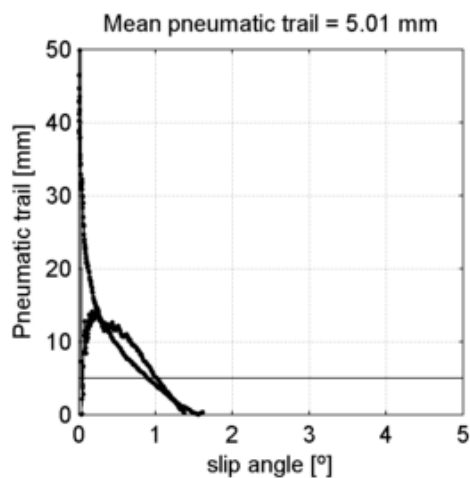
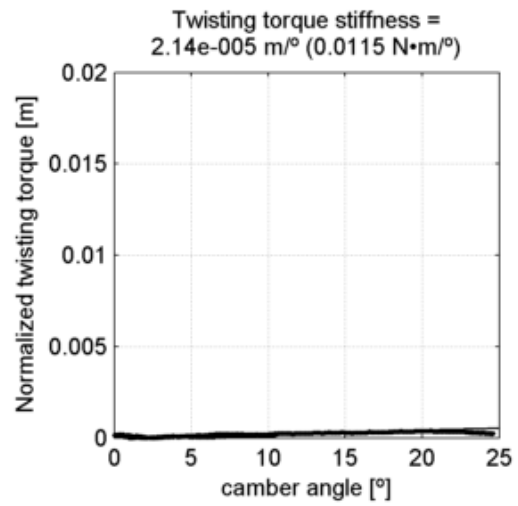
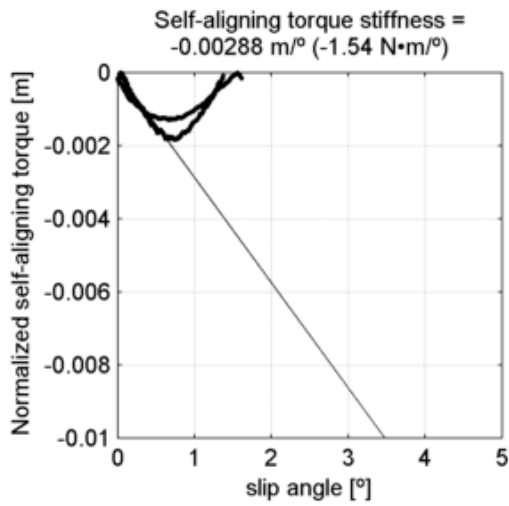
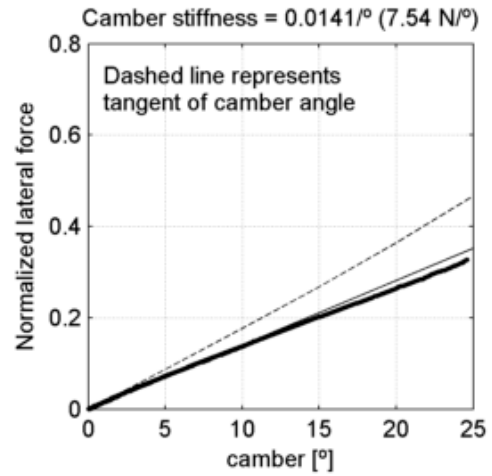
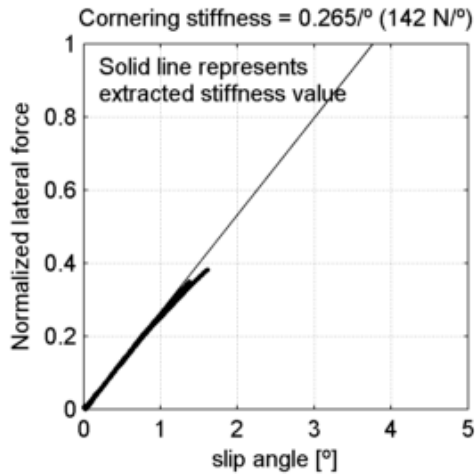
Michelin Dynamic xx-622
 tire radius = 12.5 mm, rim width = 13.4 mm

at 8.27 bar (120 psi) and
 under 304 N (31 kg, 68.3 lb)



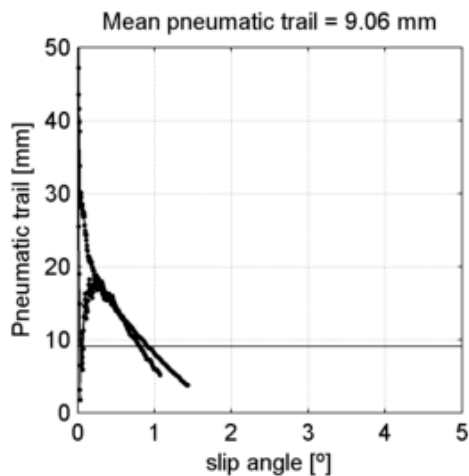
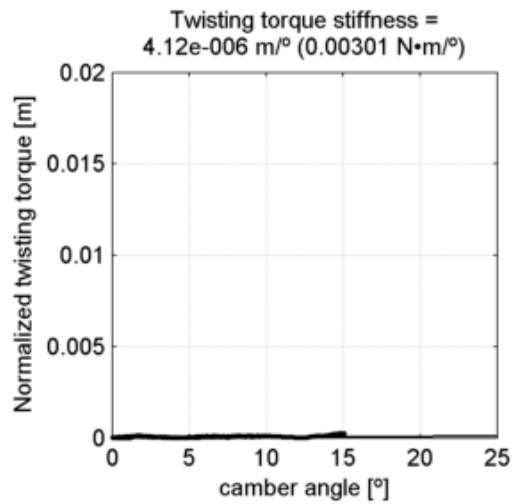
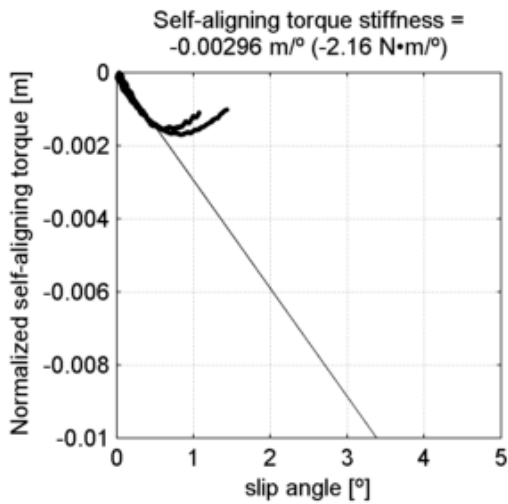
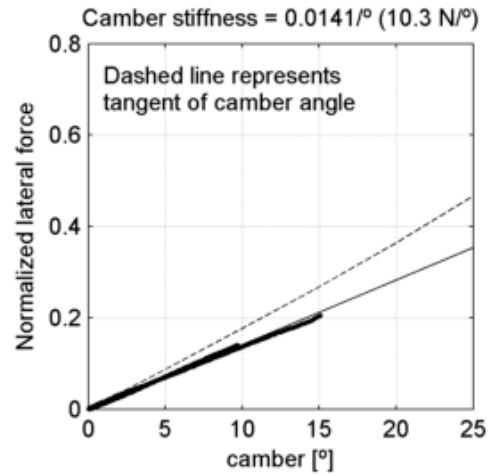
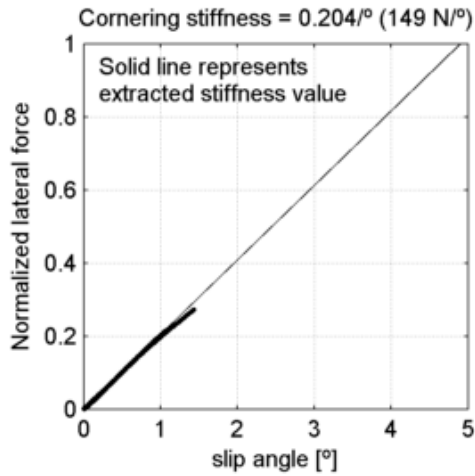
Michelin Dynamic xx-622
 tire radius = 12.5 mm, rim width = 13.4 mm

at 8.27 bar (120 psi) and
 under 535 N (54.5 kg, 120 lb)



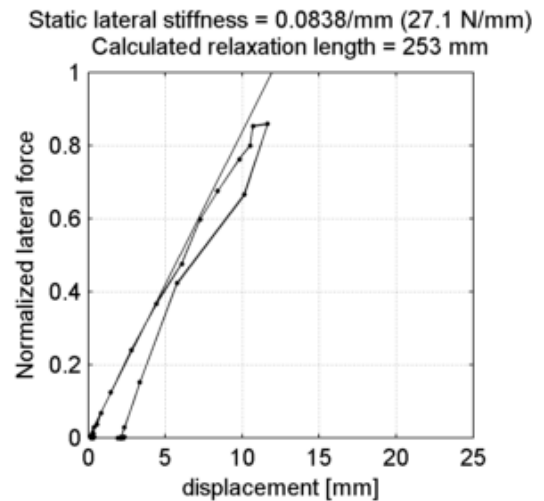
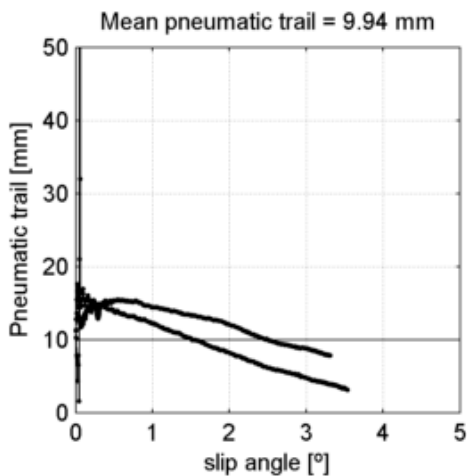
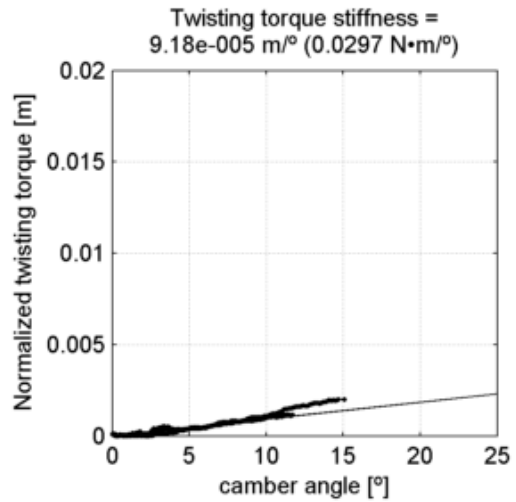
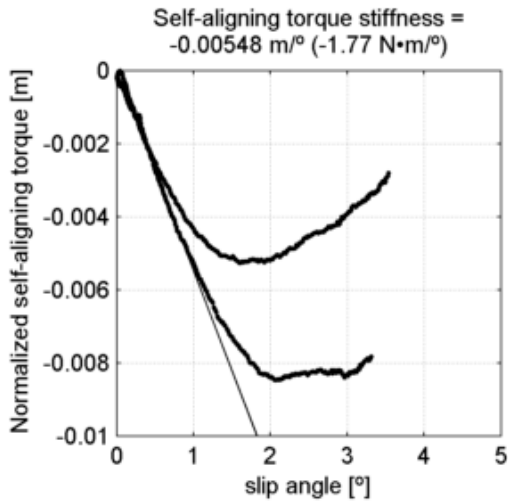
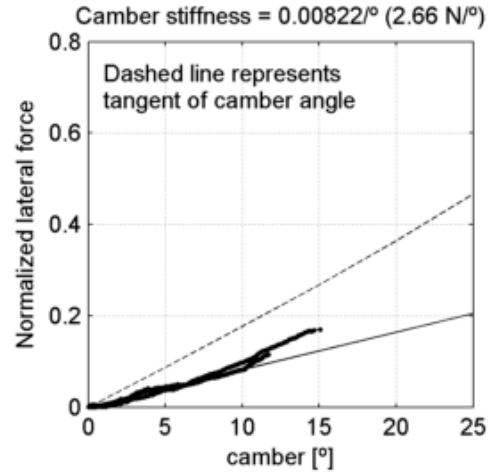
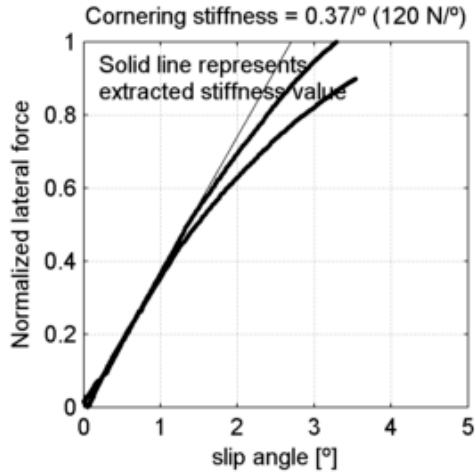
Michelin Dynamic xx-622
 tire radius = 12.5 mm, rim width = 13.4 mm

at 8.27 bar (120 psi) and
 under 731 N (74.5 kg, 164 lb)



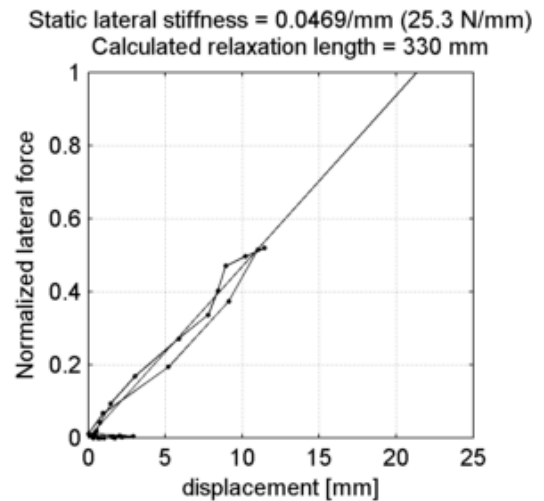
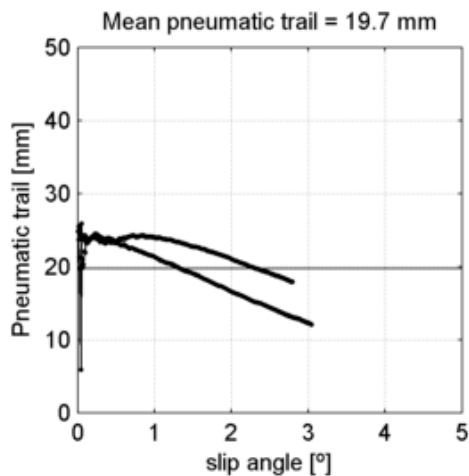
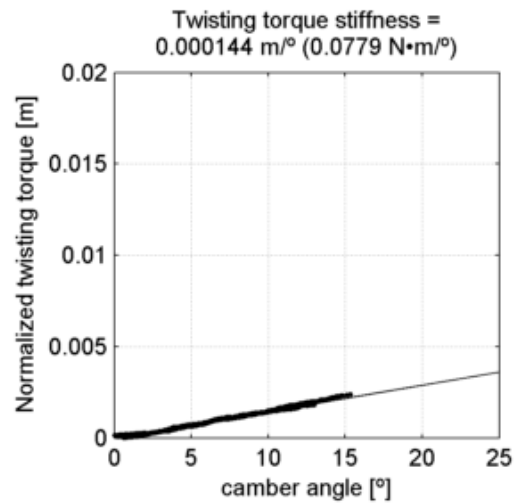
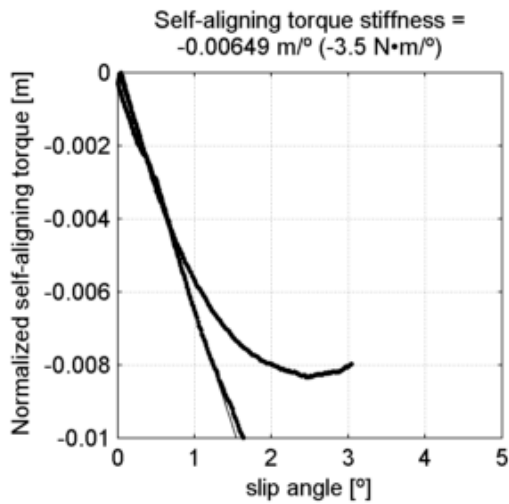
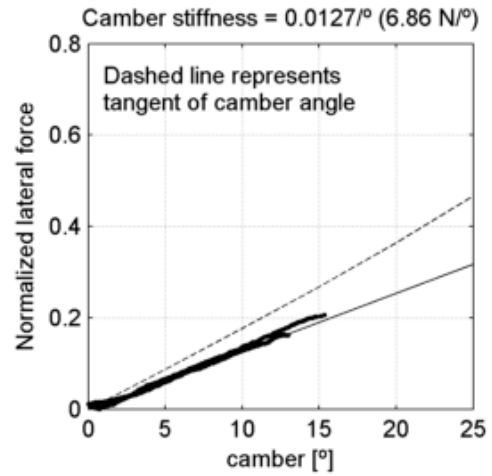
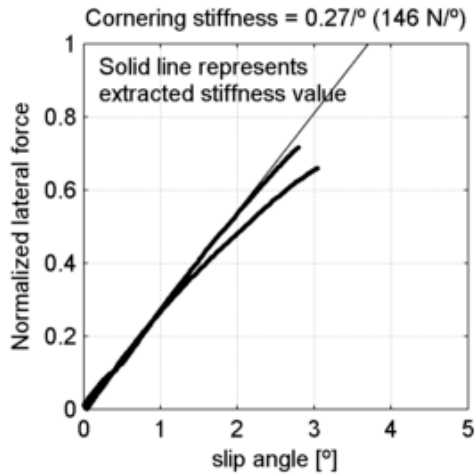
Schwalbe Big Apple 55-622
 tire radius = 23.5 mm, rim width = 18.7 mm

at 2 bar (29 psi) and
 under 324 N (33 kg, 72.8 lb)



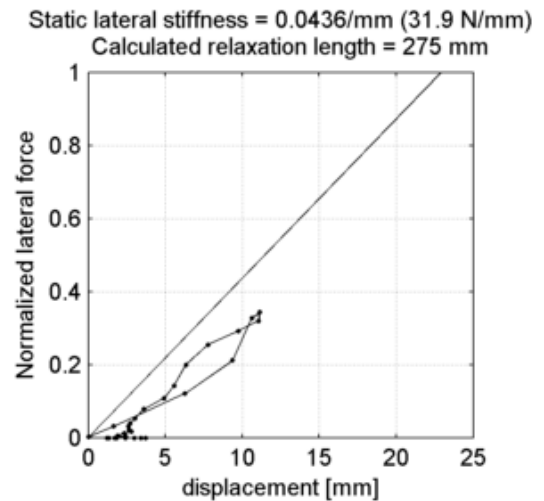
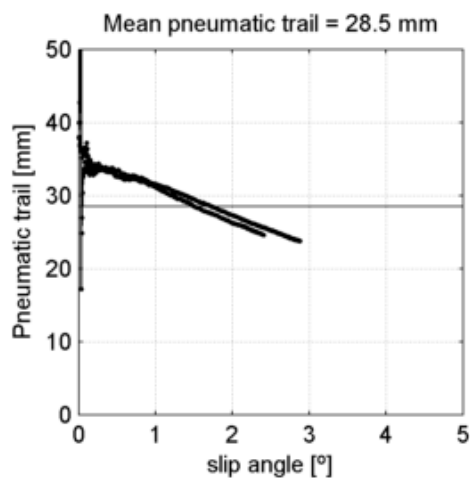
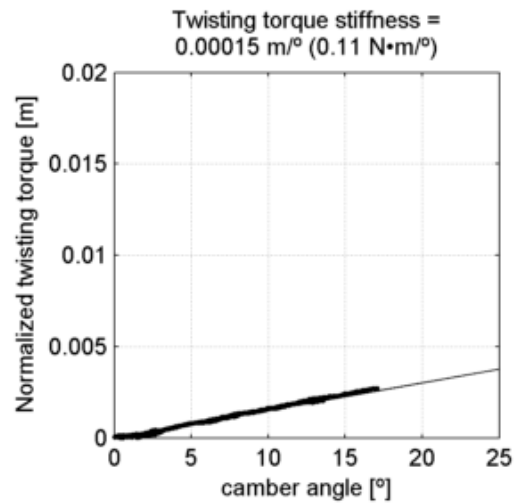
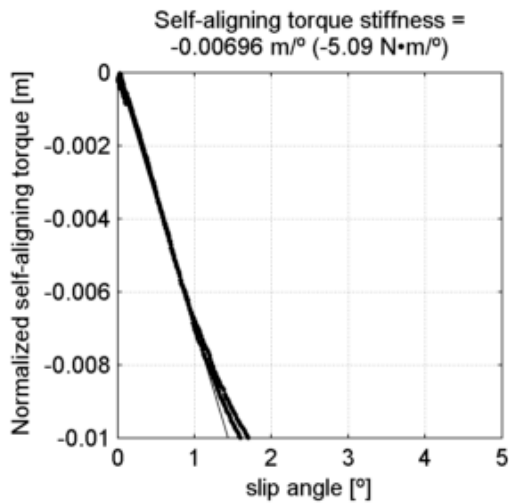
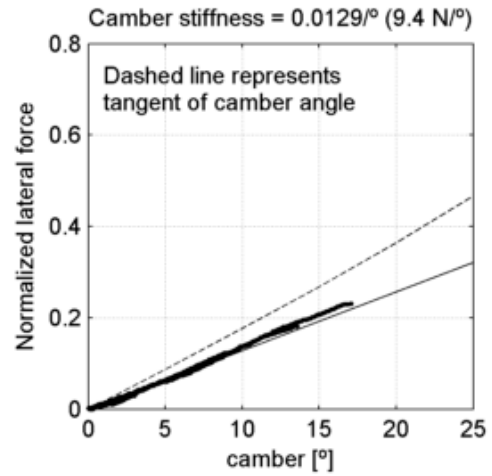
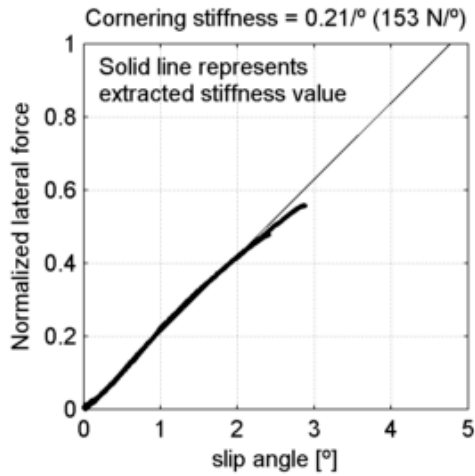
Schwalbe Big Apple 55-622
 tire radius = 23.5 mm, rim width = 18.7 mm

at 2 bar (29 psi) and
 under 540 N (55 kg, 121 lb)



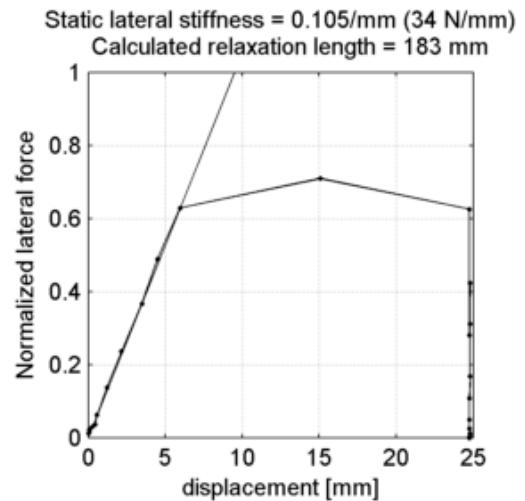
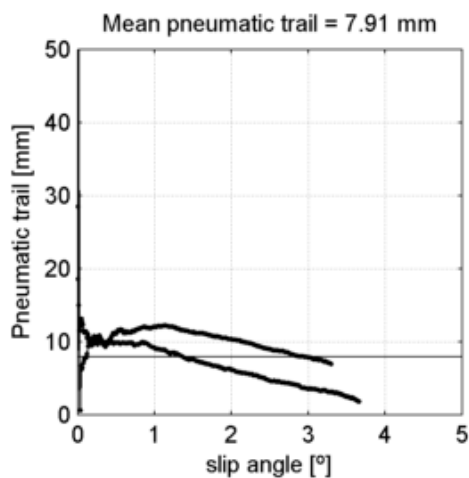
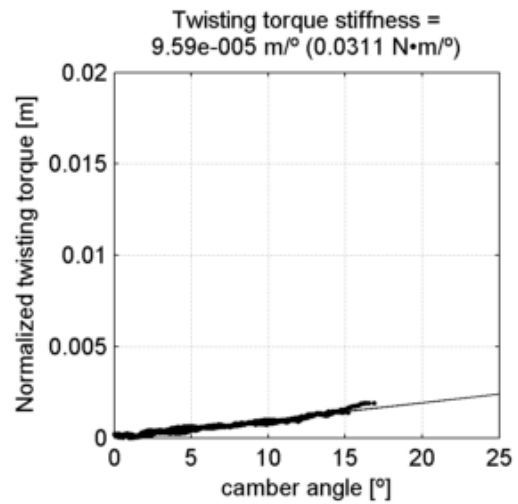
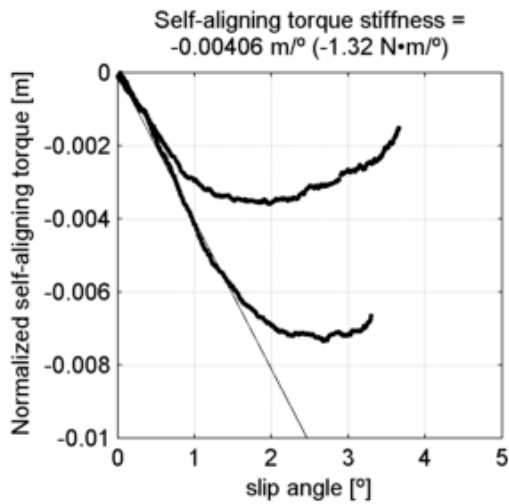
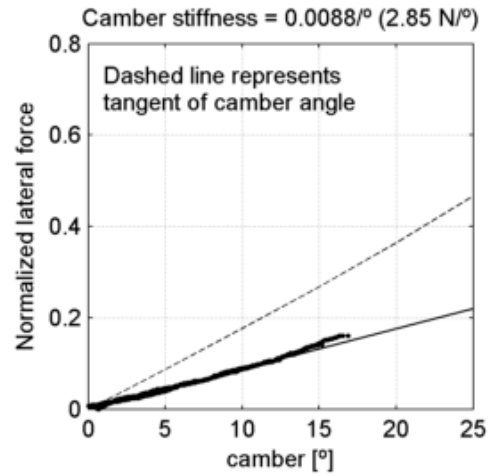
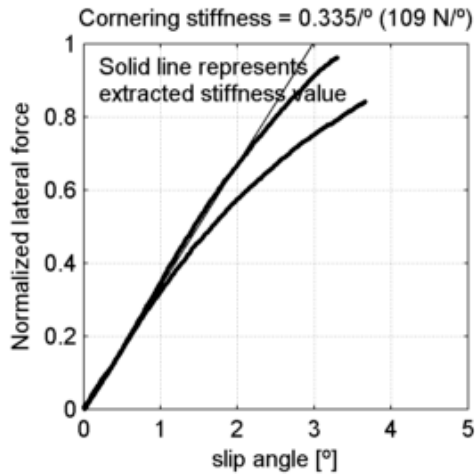
Schwalbe Big Apple 55-622
 tire radius = 23.5 mm, rim width = 18.7 mm

at 2 bar (29 psi) and
 under 731 N (74.5 kg, 164 lb)



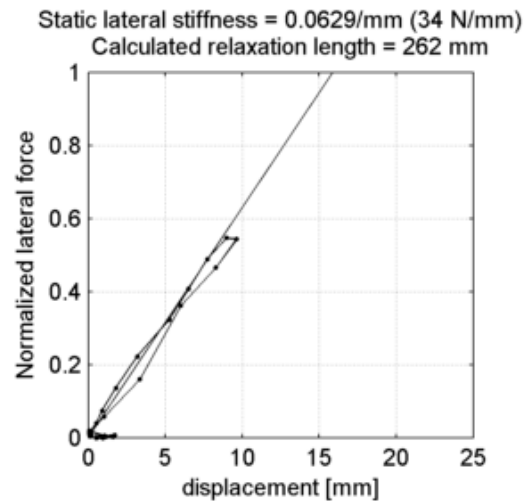
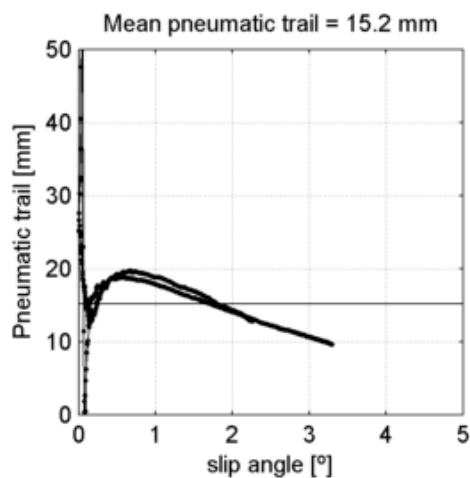
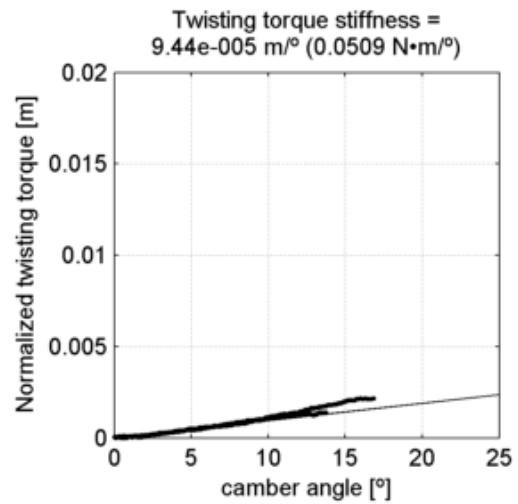
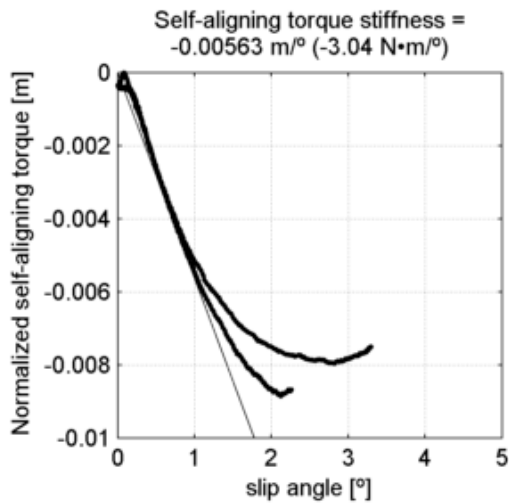
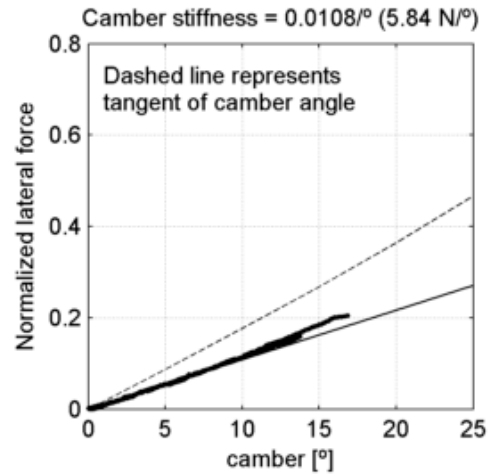
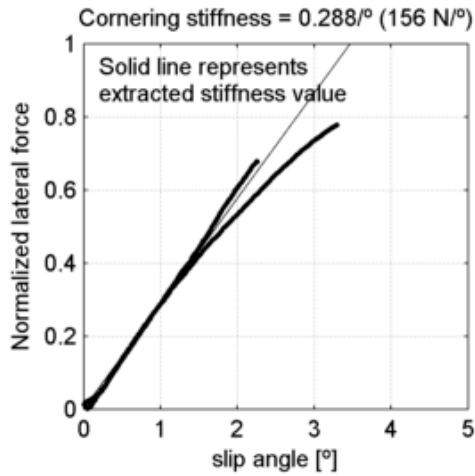
Schwalbe Big Apple 55-622
 tire radius = 23.5 mm, rim width = 18.7 mm

at 3.03 bar (44 psi) and
 under 324 N (33 kg, 72.8 lb)



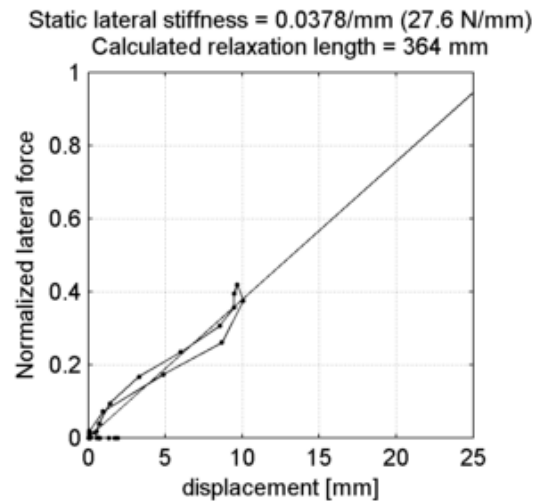
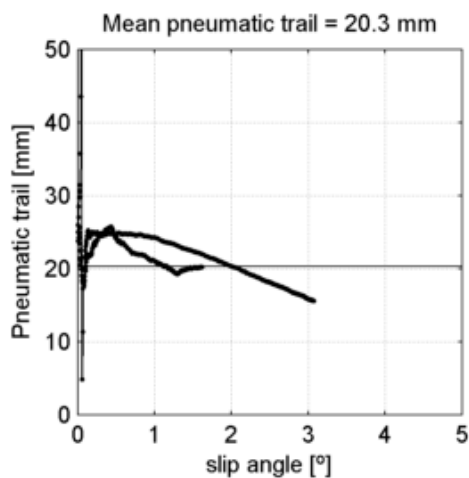
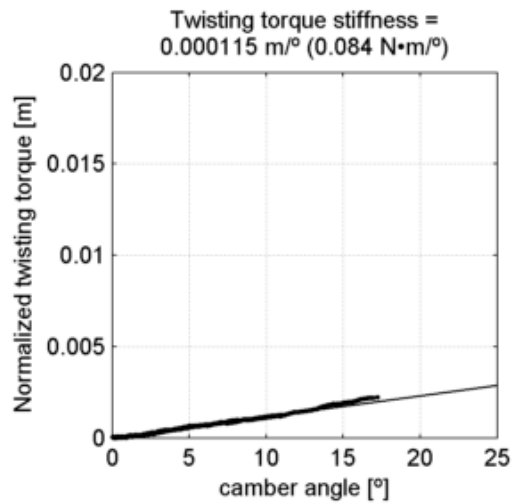
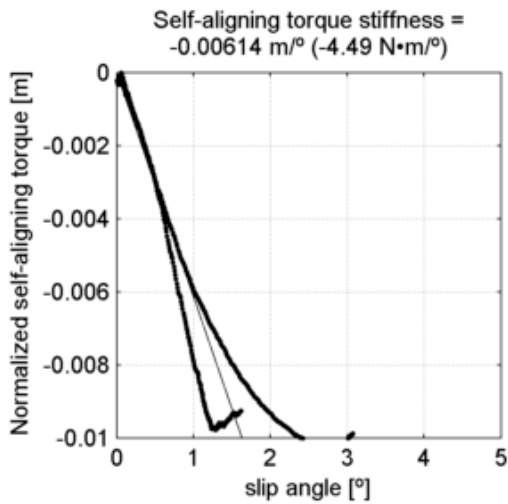
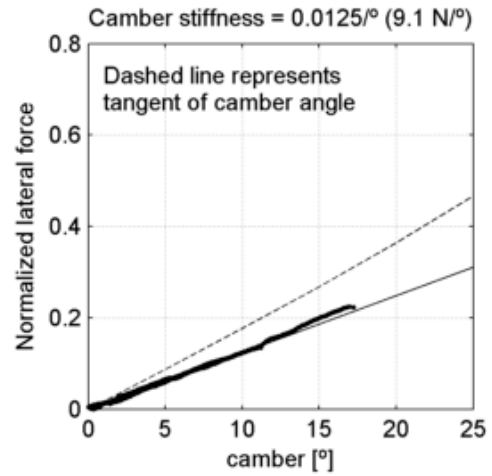
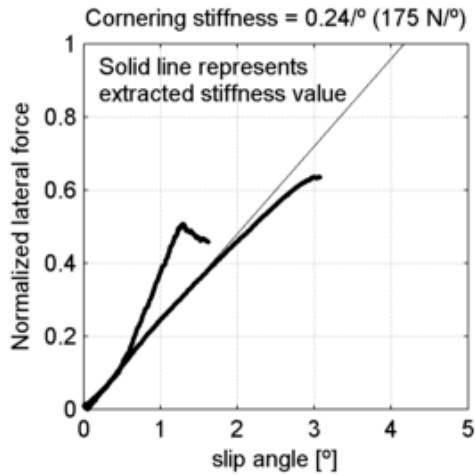
Schwalbe Big Apple 55-622
 tire radius = 23.5 mm, rim width = 18.7 mm

at 3.03 bar (44 psi) and
 under 540 N (55 kg, 121 lb)



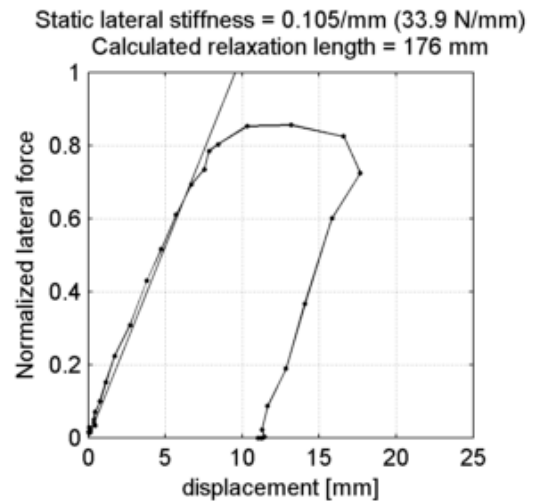
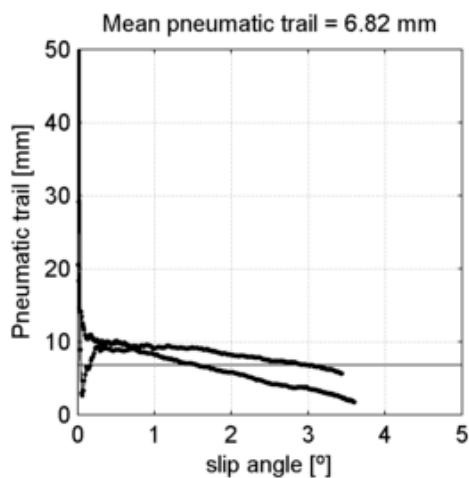
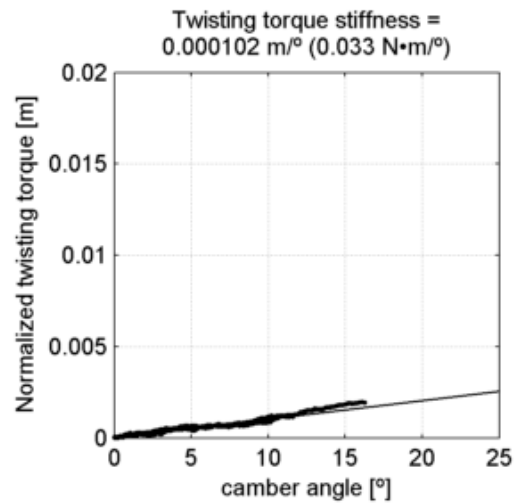
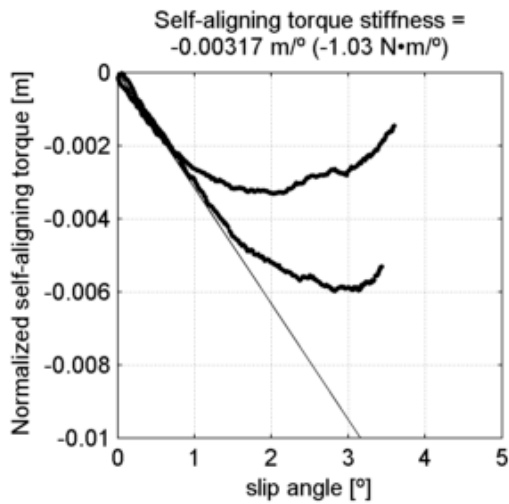
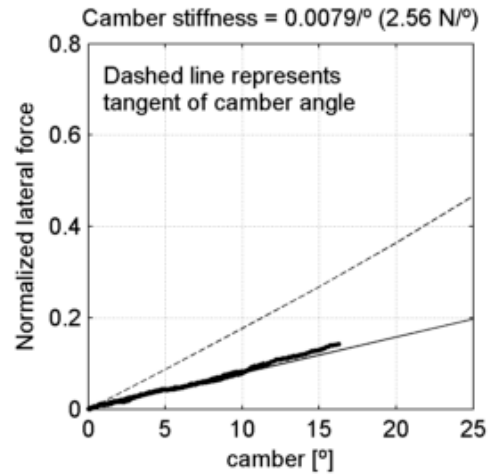
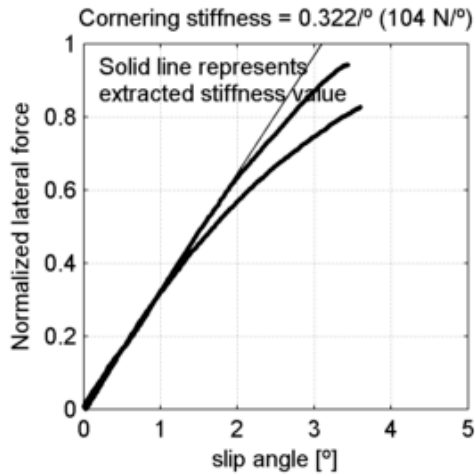
Schwalbe Big Apple 55-622
 tire radius = 23.5 mm, rim width = 18.7 mm

at 3.03 bar (44 psi) and
 under 731 N (74.5 kg, 164 lb)



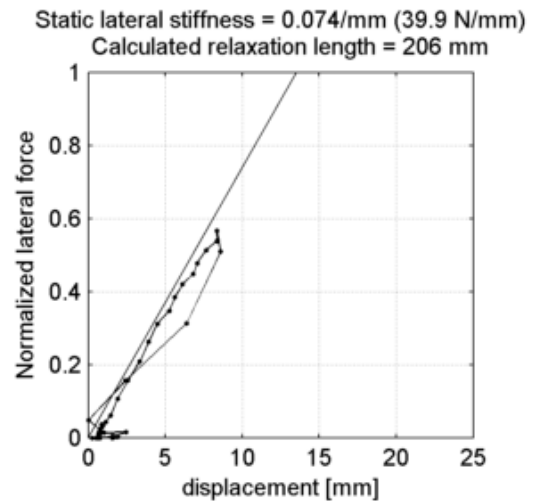
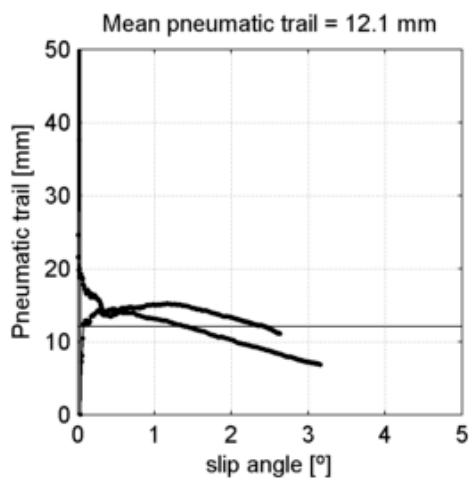
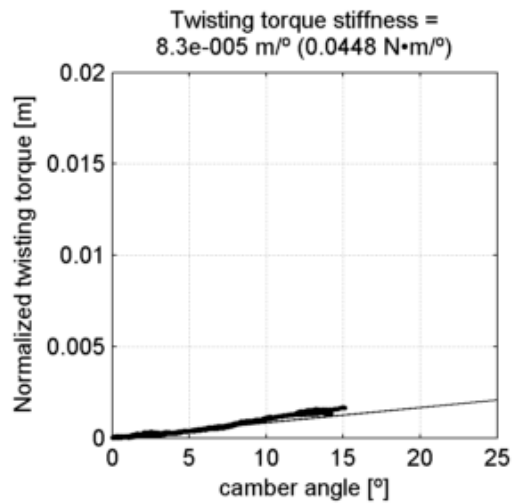
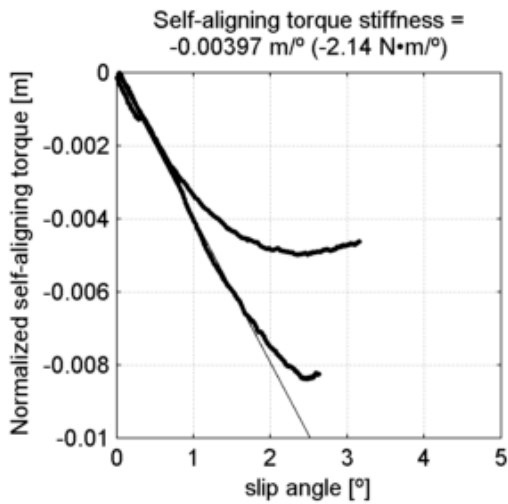
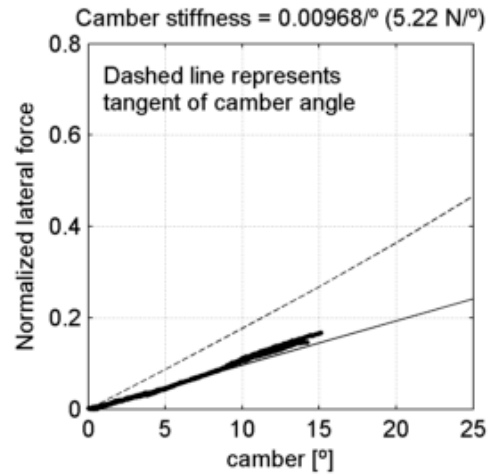
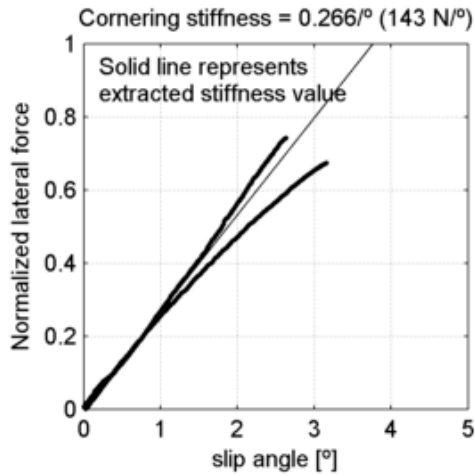
Schwalbe Big Apple 55-622
 tire radius = 23.5 mm, rim width = 18.7 mm

at 4 bar (58 psi) and
 under 324 N (33 kg, 72.8 lb)



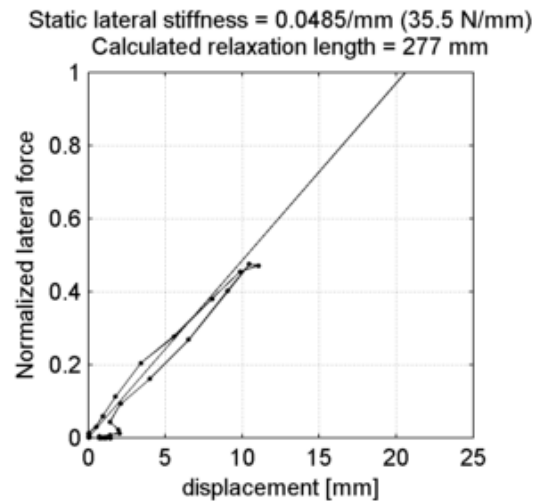
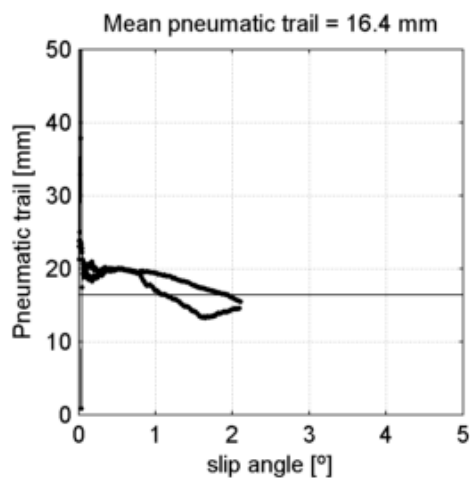
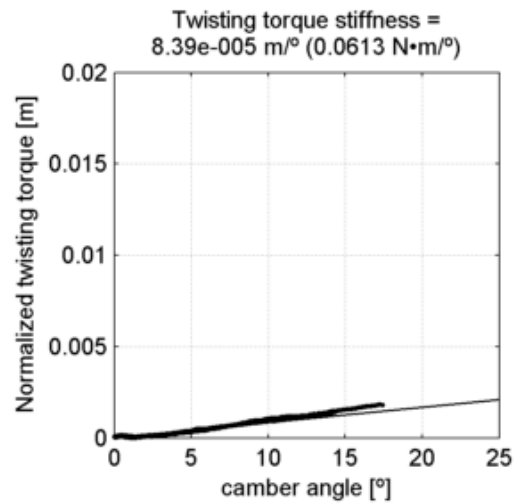
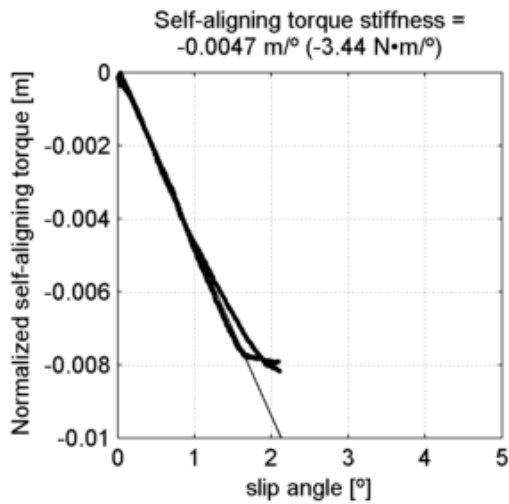
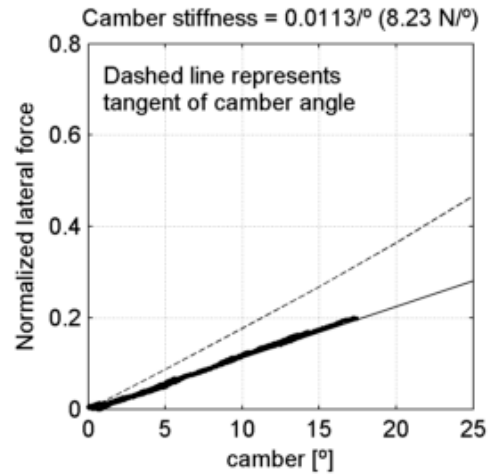
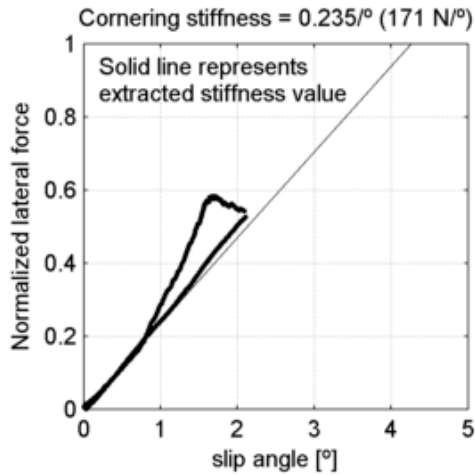
Schwalbe Big Apple 55-622
 tire radius = 23.5 mm, rim width = 18.7 mm

at 4 bar (58 psi) and
 under 540 N (55 kg, 121 lb)



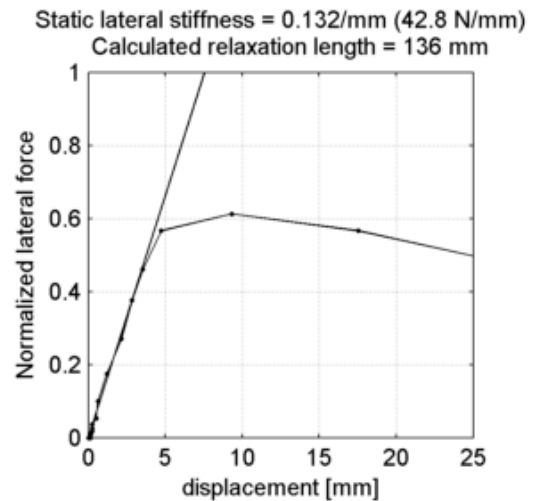
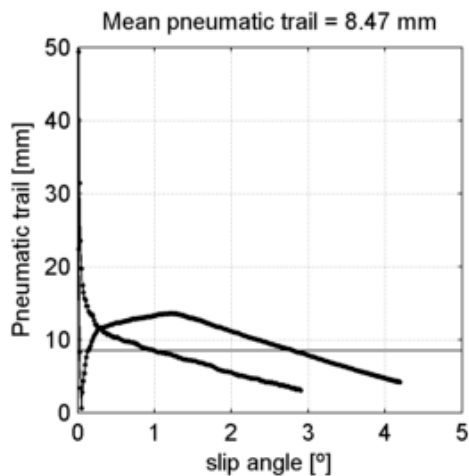
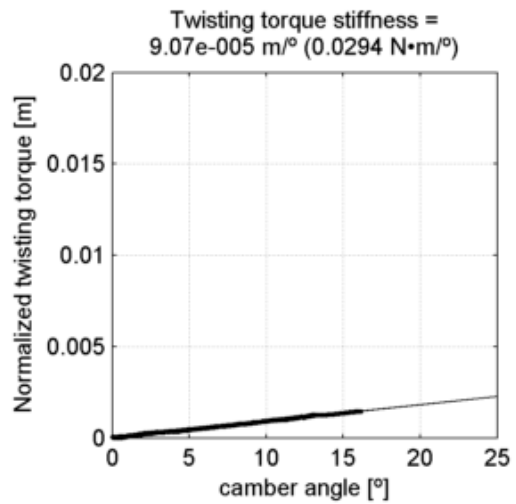
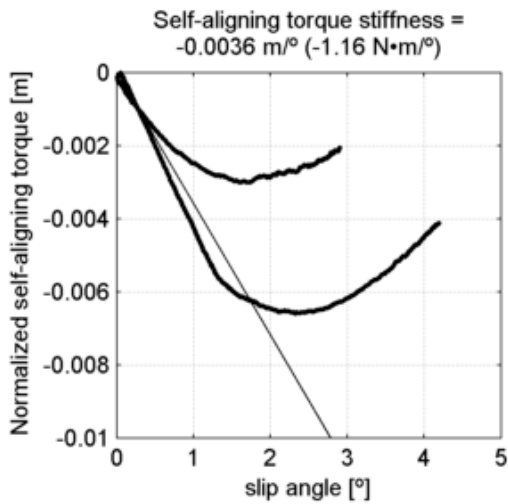
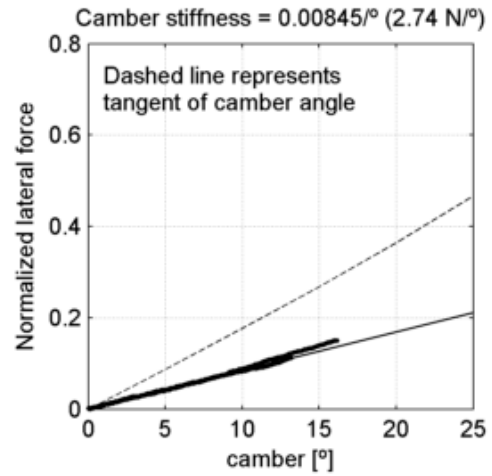
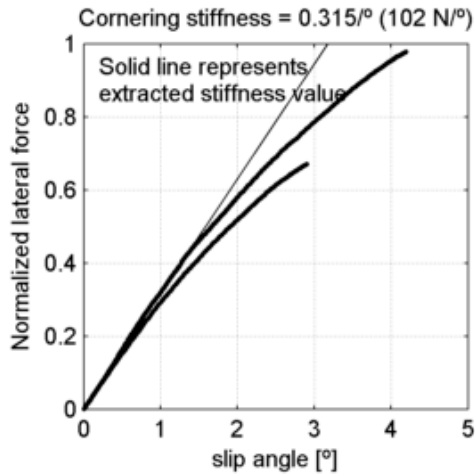
Schwalbe Big Apple 55-622
 tire radius = 23.5 mm, rim width = 18.7 mm

at 4 bar (58 psi) and
 under 731 N (74.5 kg, 164 lb)



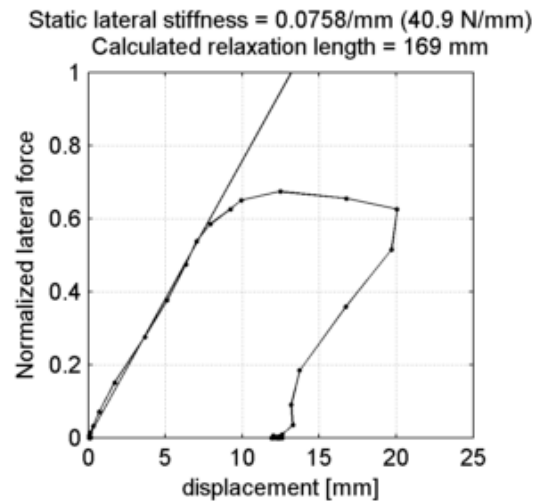
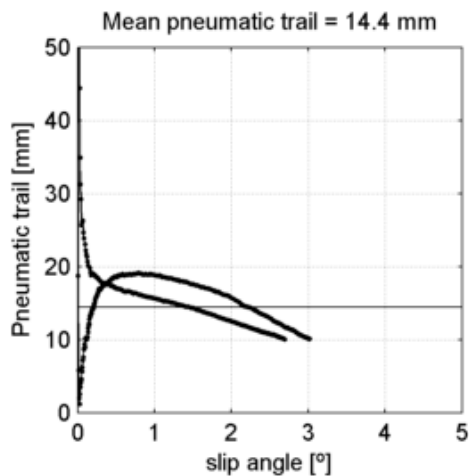
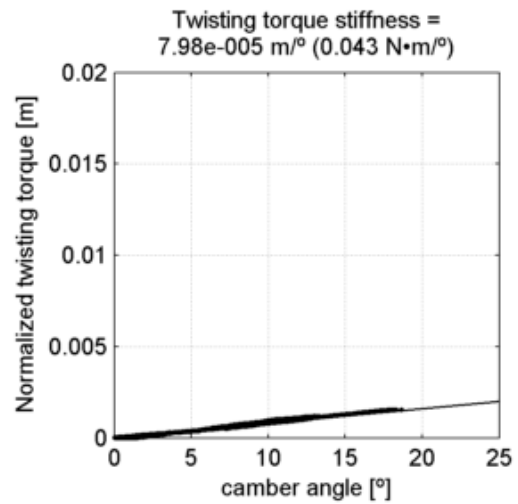
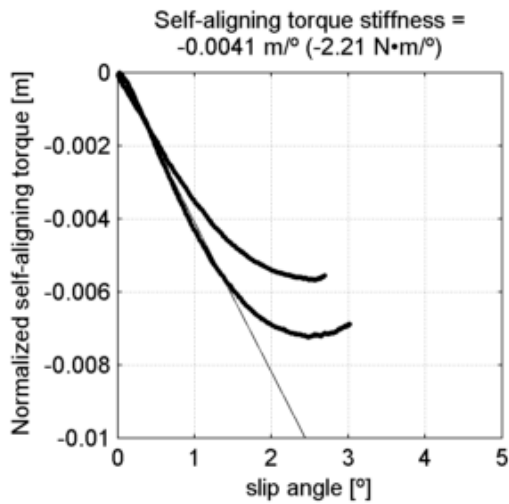
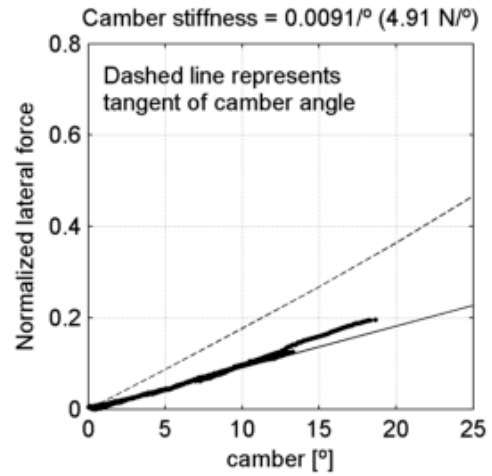
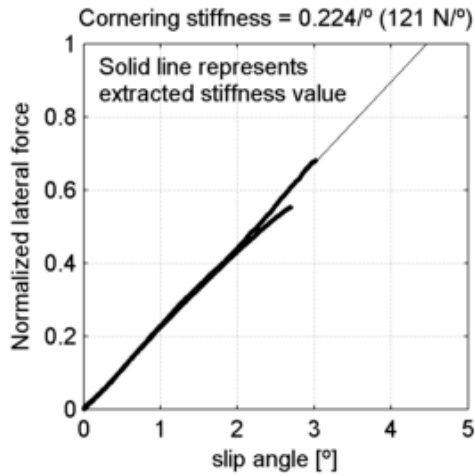
Schwalbe Kojak 35-622
 tire radius = 15.7 mm, rim width = 18.7 mm

at 4 bar (58 psi) and
 under 324 N (33 kg, 72.8 lb)



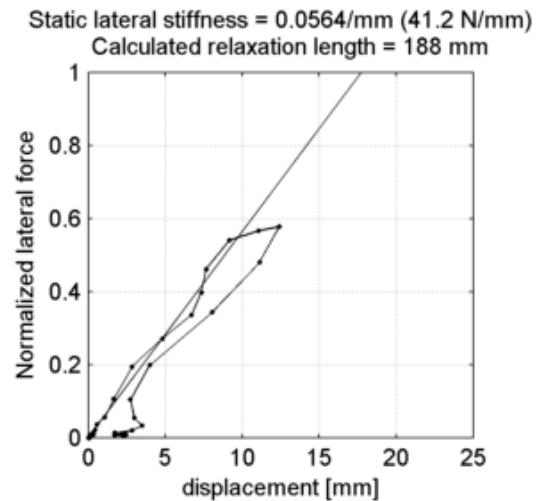
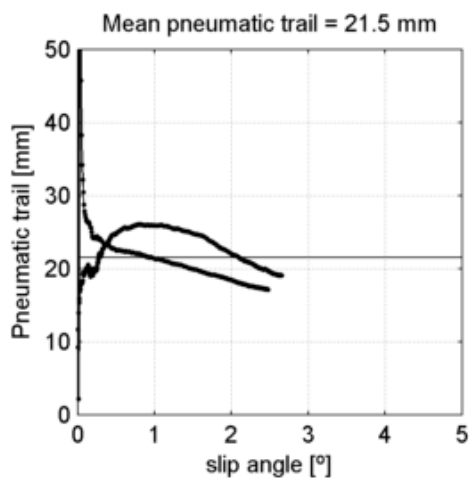
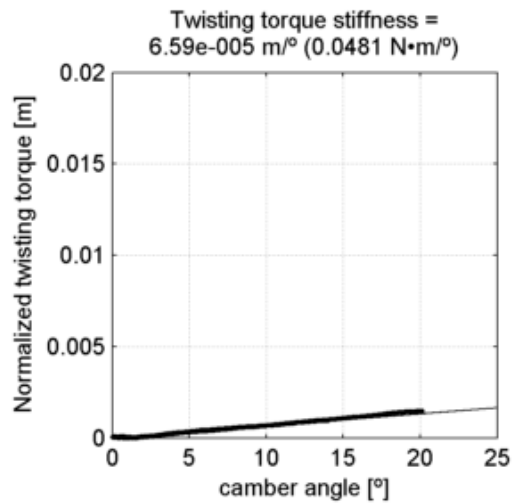
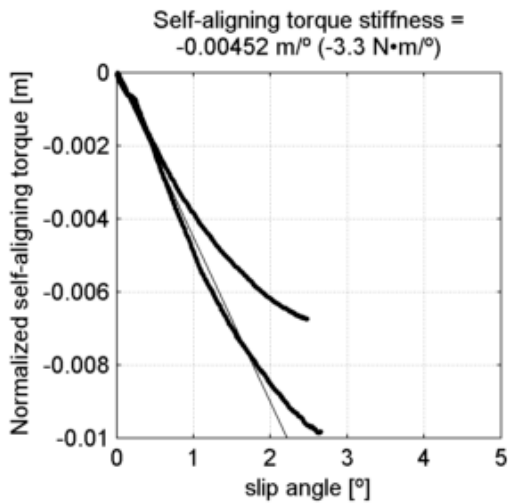
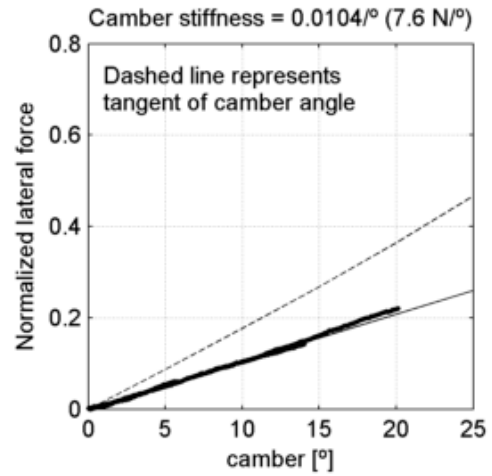
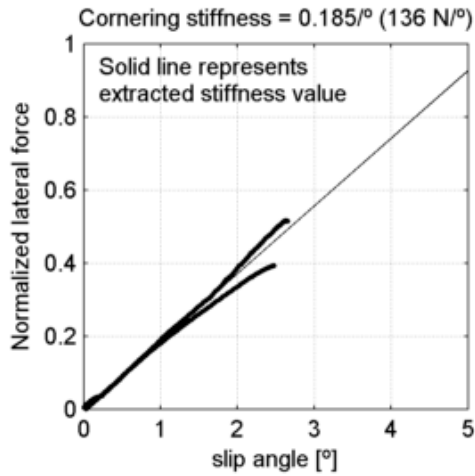
Schwalbe Kojak 35-622
 tire radius = 15.7 mm, rim width = 18.7 mm

at 4 bar (58 psi) and
 under 540 N (55 kg, 121 lb)



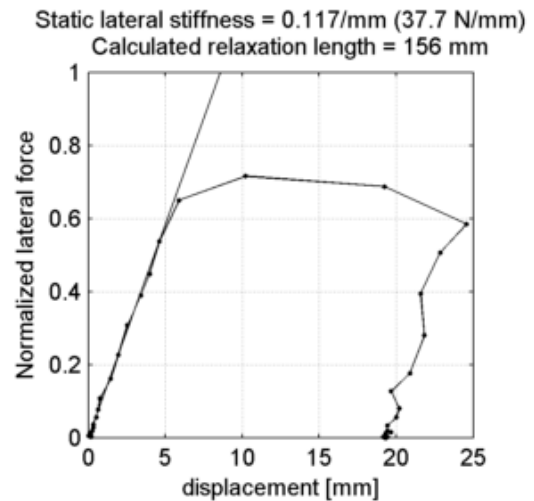
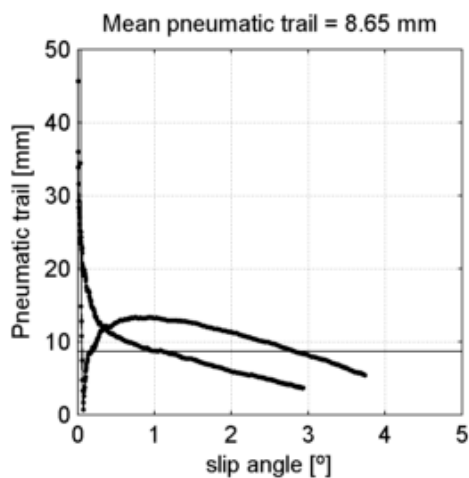
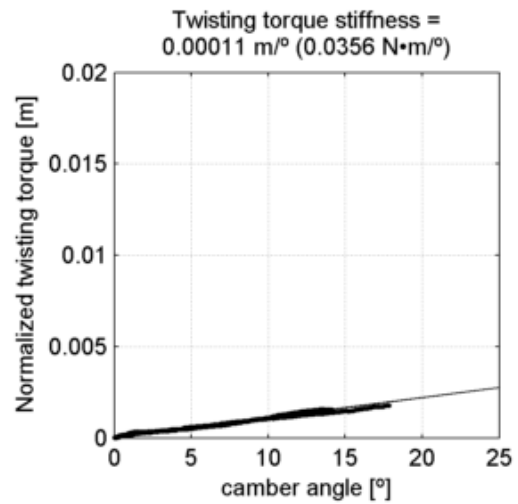
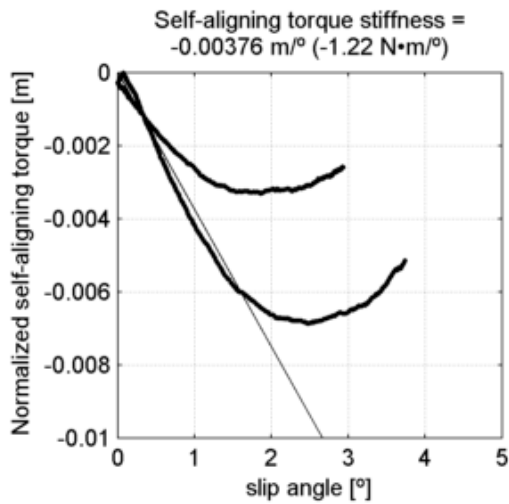
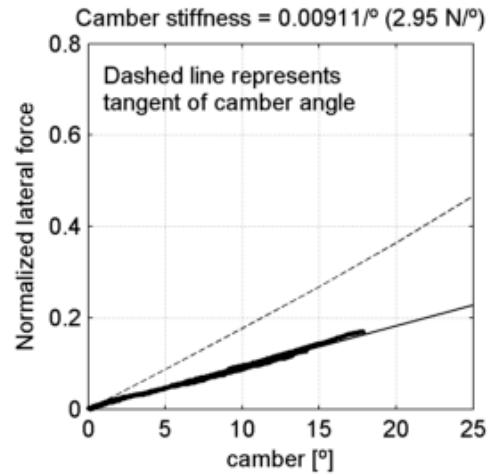
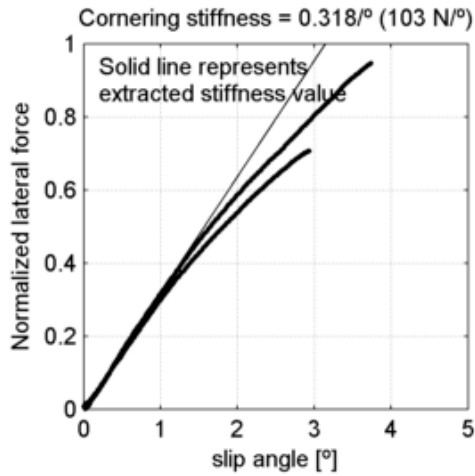
Schwalbe Kojak 35-622
 tire radius = 15.7 mm, rim width = 18.7 mm

at 4 bar (58 psi) and
 under 731 N (74.5 kg, 164 lb)



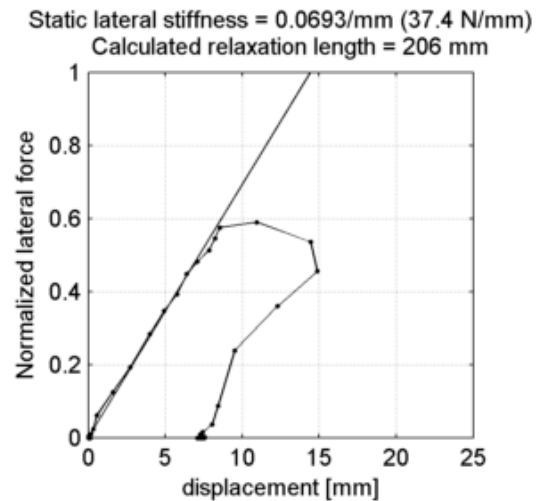
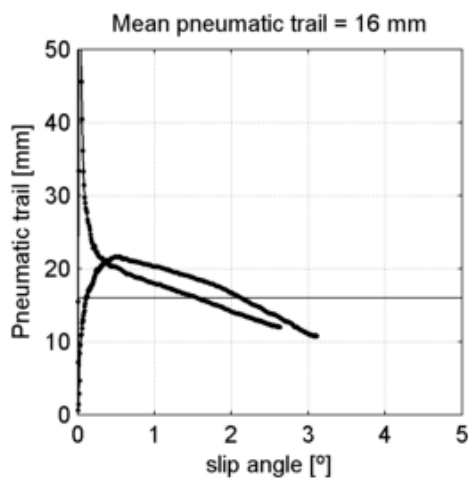
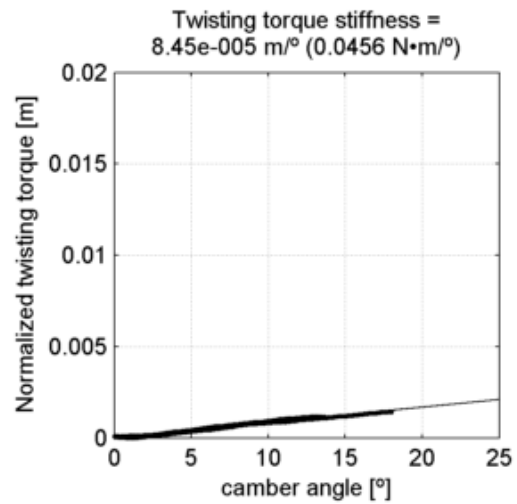
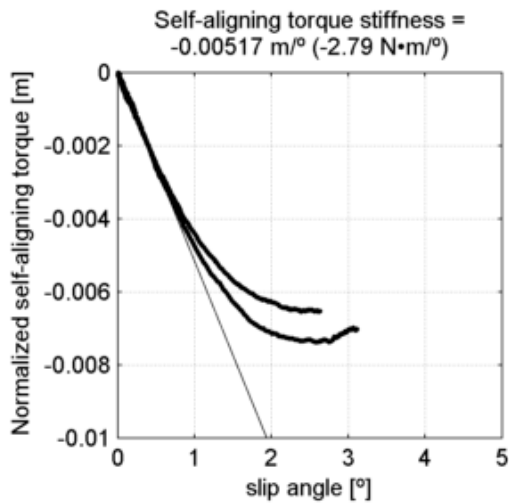
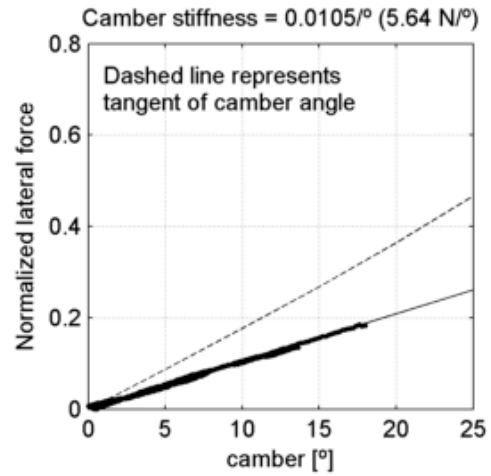
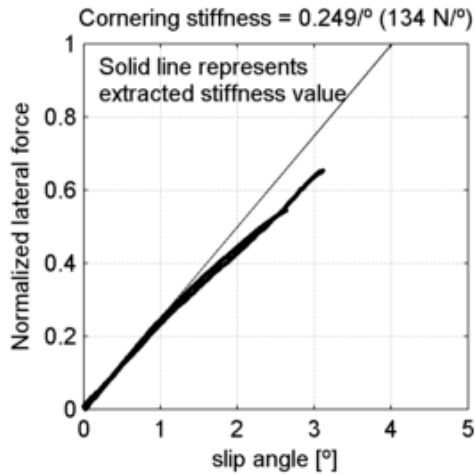
Schwalbe Kojak 35-622
 tire radius = 15.7 mm, rim width = 18.7 mm

at 3.45 bar (50 psi) and
 under 324 N (33 kg, 72.8 lb)



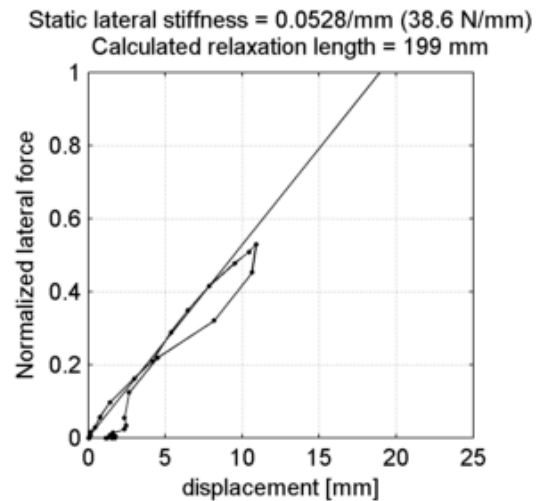
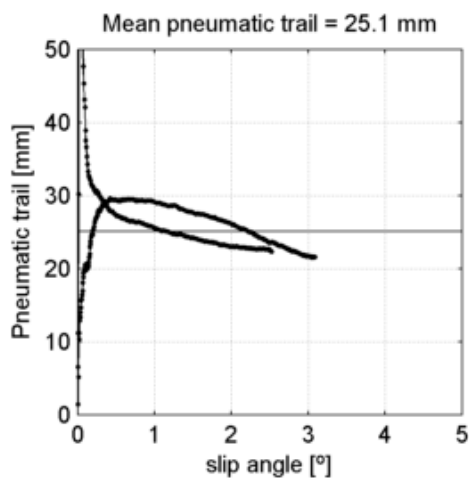
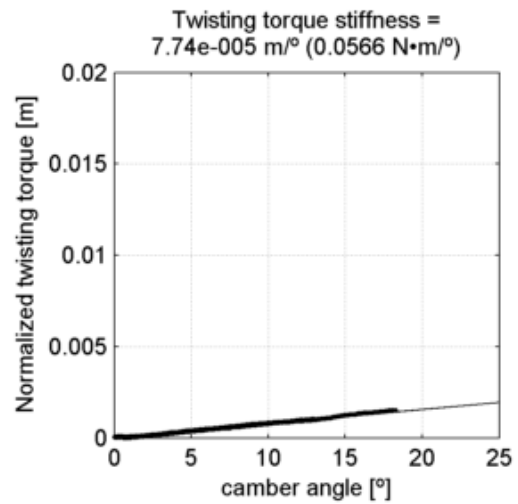
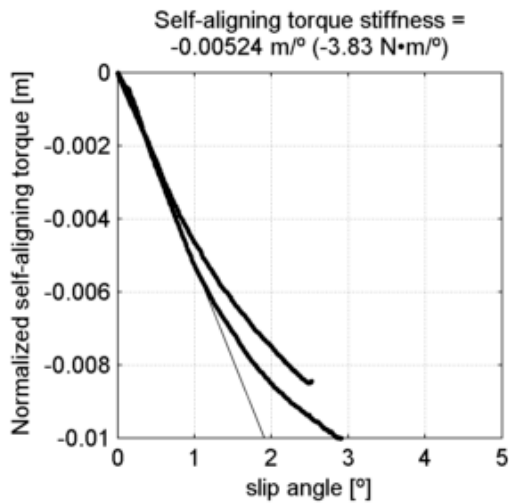
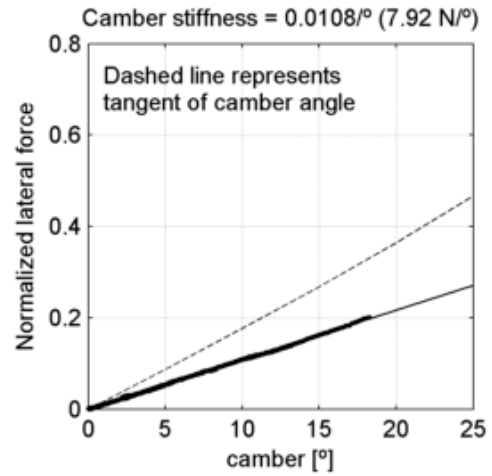
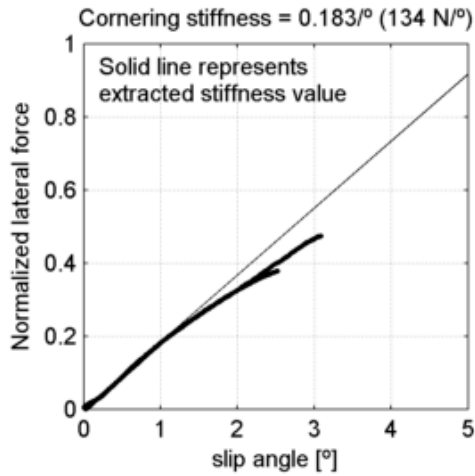
Schwalbe Kojak 35-622
 tire radius = 15.7 mm, rim width = 18.7 mm

at 3.45 bar (50 psi) and
 under 540 N (55 kg, 121 lb)



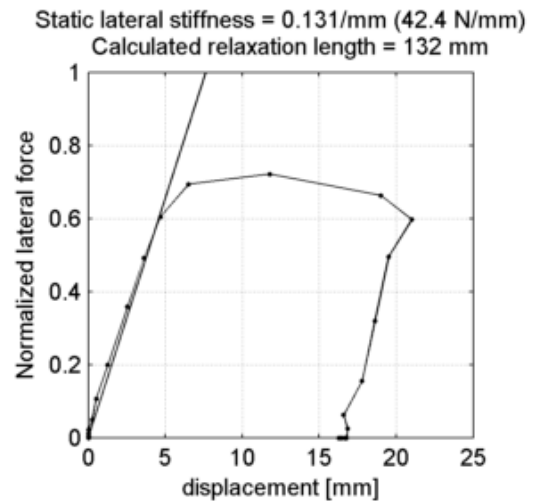
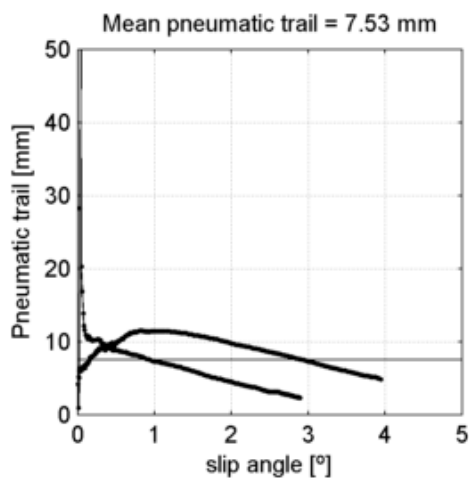
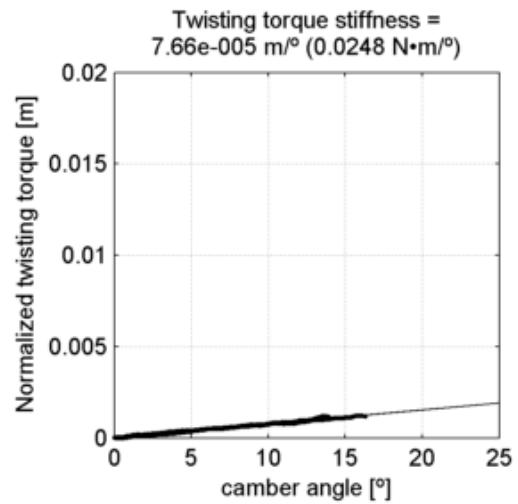
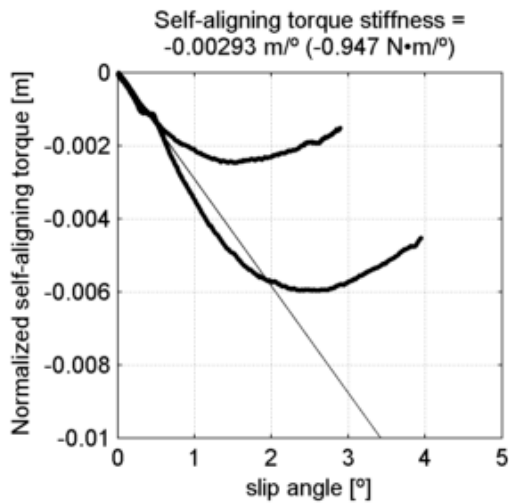
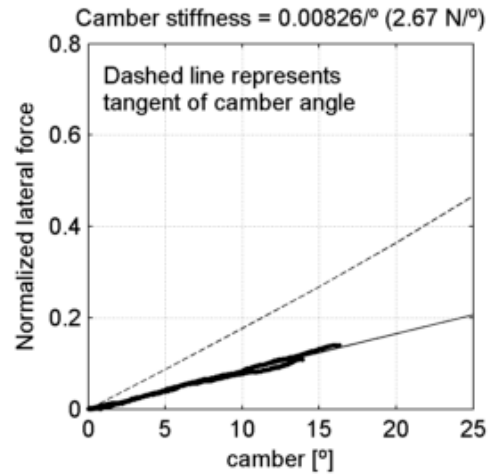
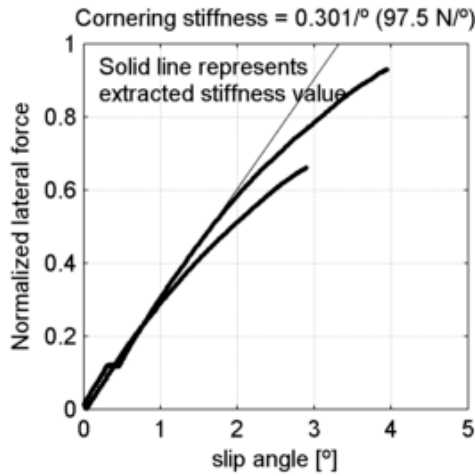
Schwalbe Kojak 35-622
 tire radius = 15.7 mm, rim width = 18.7 mm

at 3.45 bar (50 psi) and
 under 731 N (74.5 kg, 164 lb)



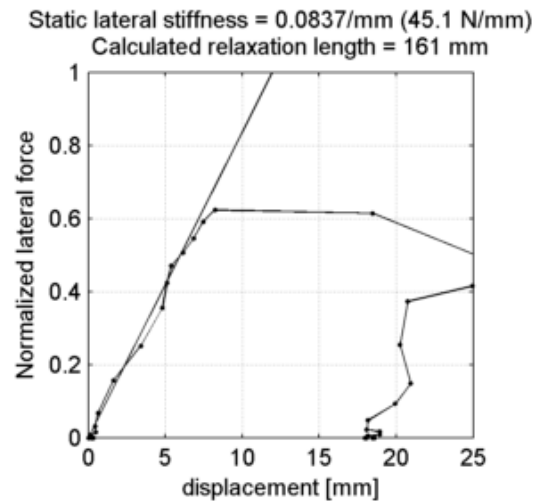
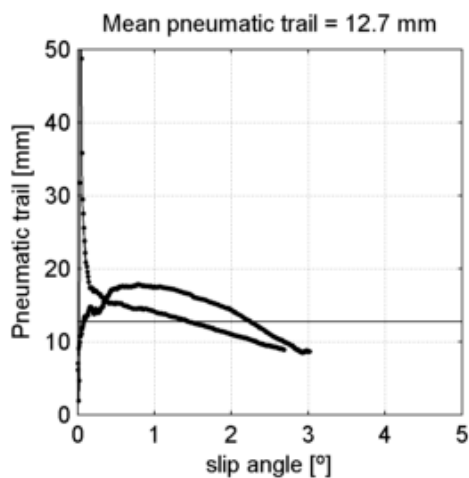
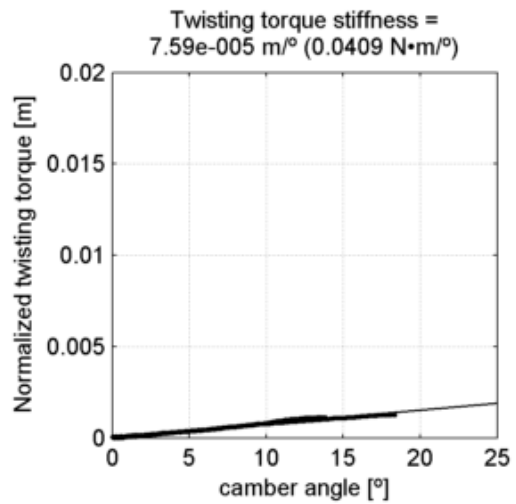
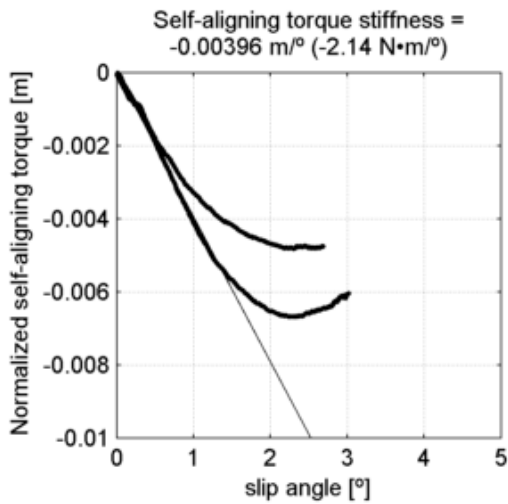
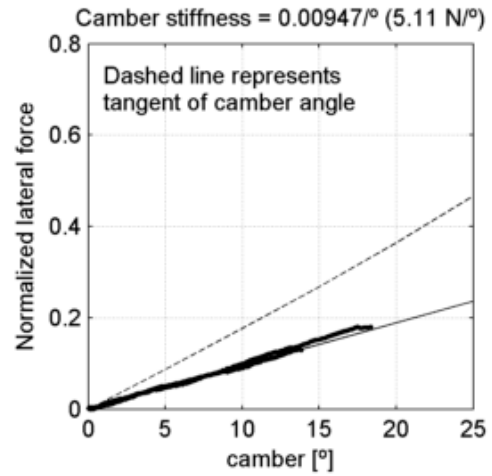
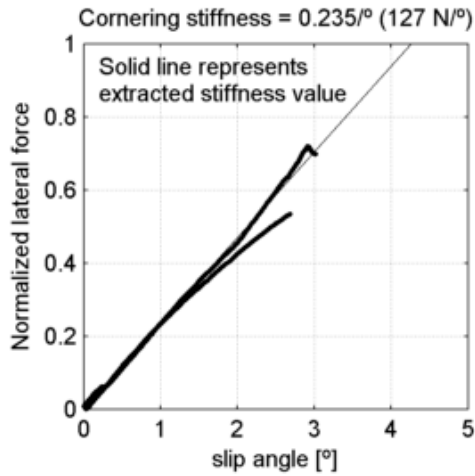
Schwalbe Kojak 35-622
 tire radius = 15.7 mm, rim width = 18.7 mm

at 4.83 bar (70 psi) and
 under 324 N (33 kg, 72.8 lb)



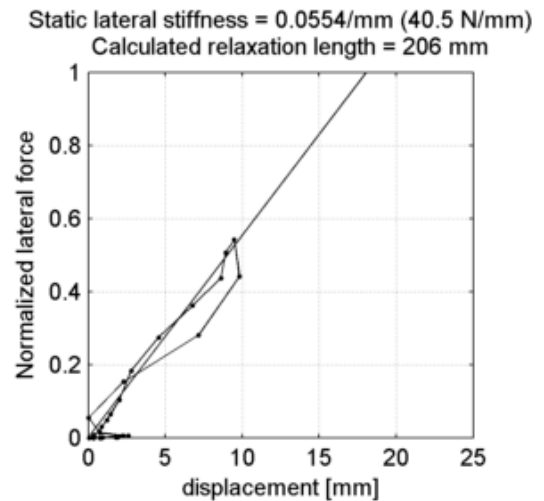
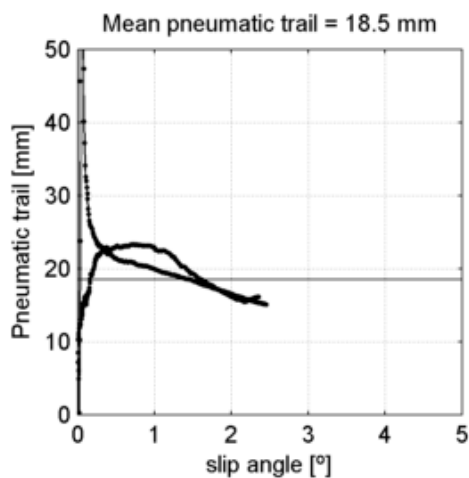
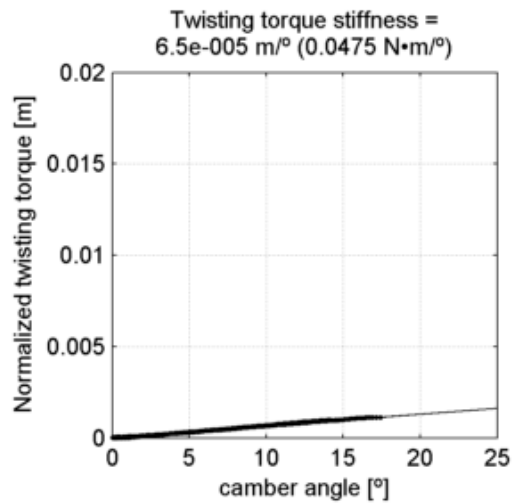
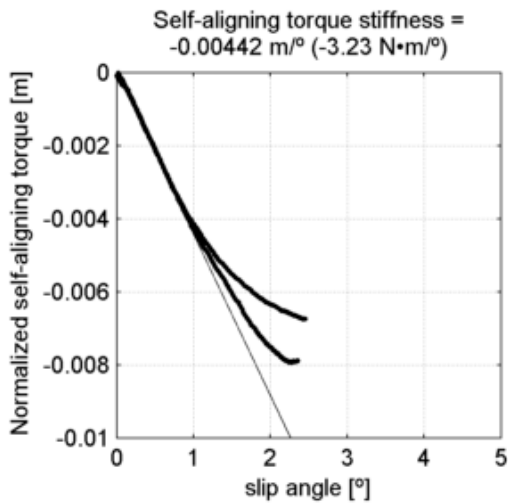
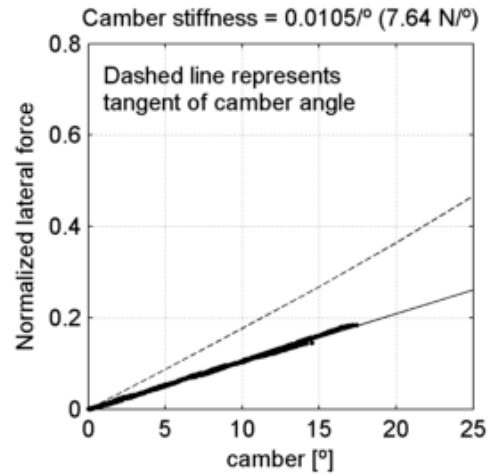
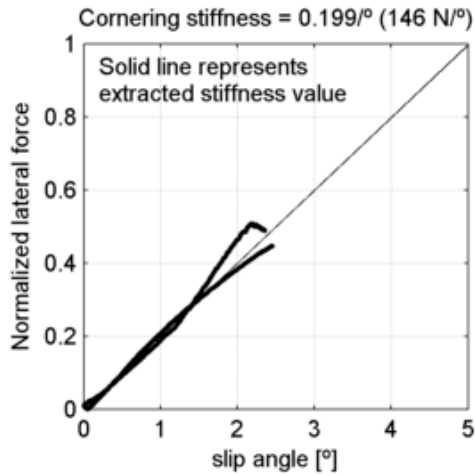
Schwalbe Kojak 35-622
 tire radius = 15.7 mm, rim width = 18.7 mm

at 4.83 bar (70 psi) and
 under 540 N (55 kg, 121 lb)



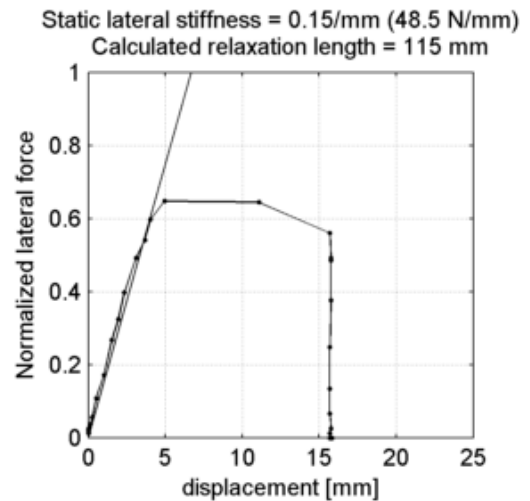
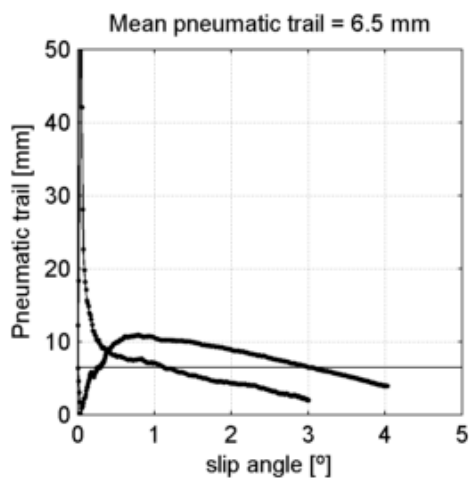
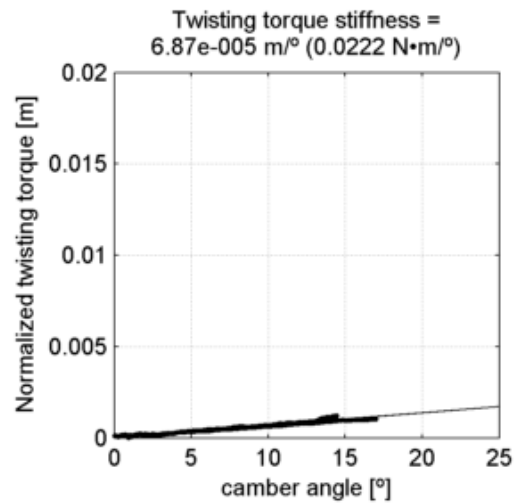
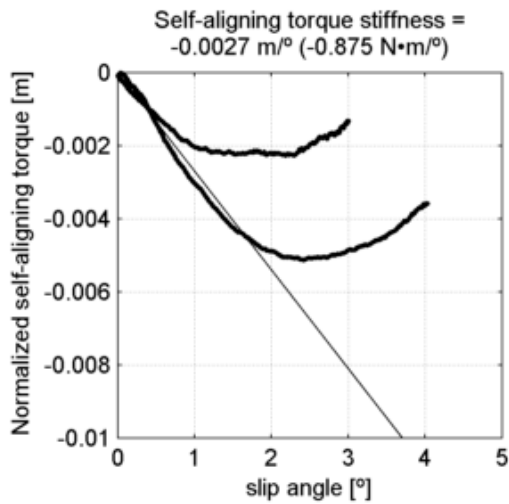
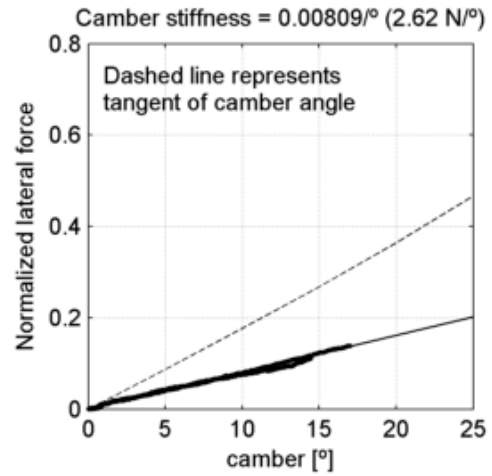
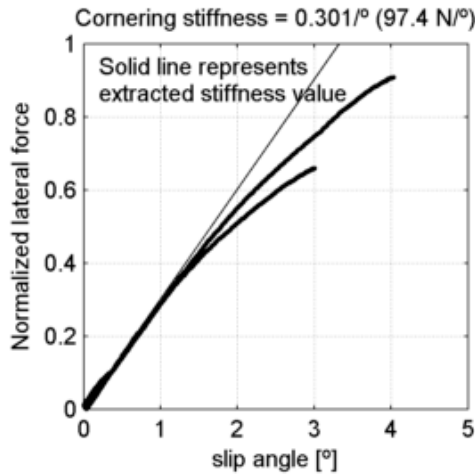
Schwalbe Kojak 35-622
 tire radius = 15.7 mm, rim width = 18.7 mm

at 4.83 bar (70 psi) and
 under 731 N (74.5 kg, 164 lb)



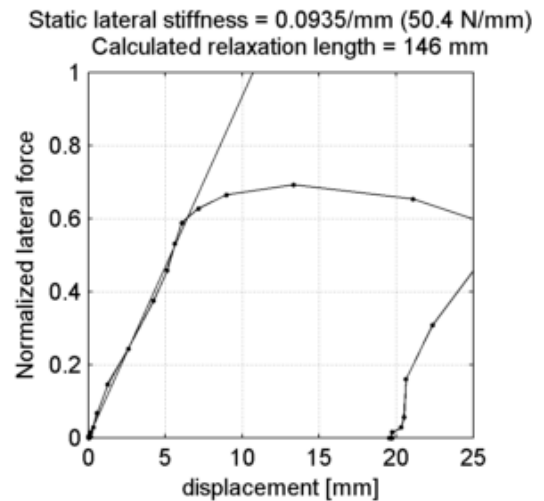
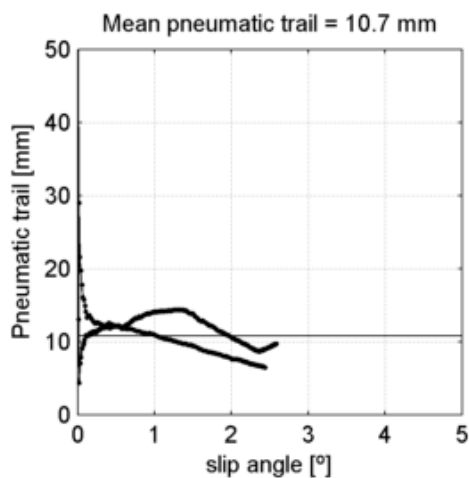
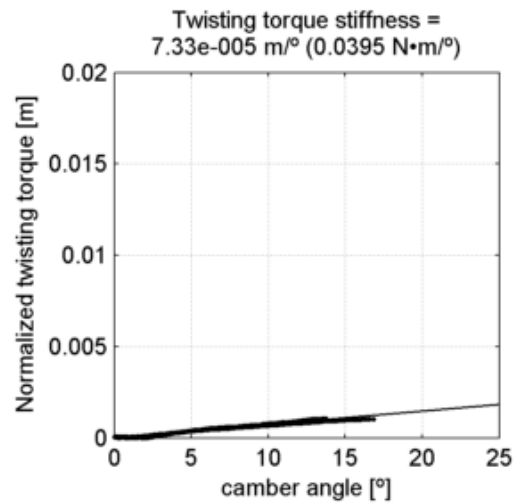
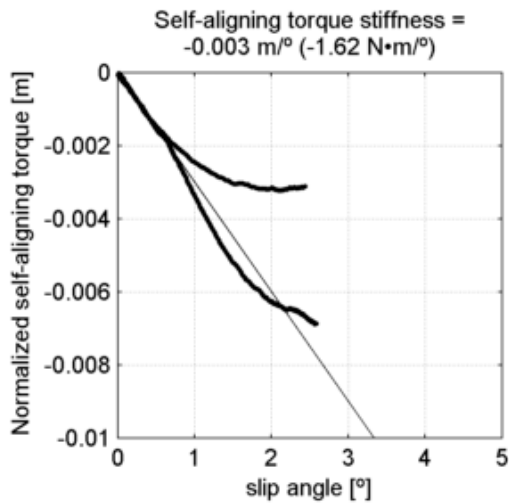
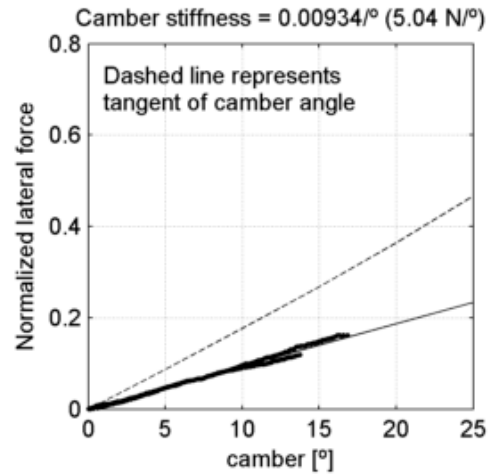
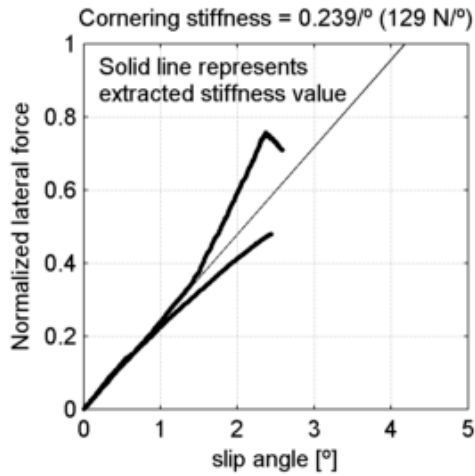
Schwalbe Kojak 35-622
 tire radius = 15.7 mm, rim width = 18.7 mm

at 6.21 bar (90 psi) and
 under 324 N (33 kg, 72.8 lb)



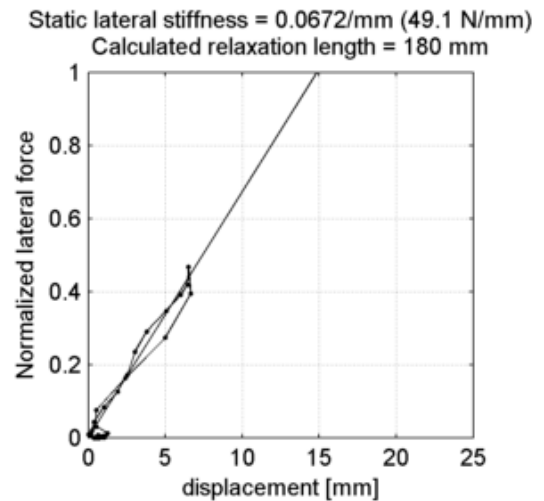
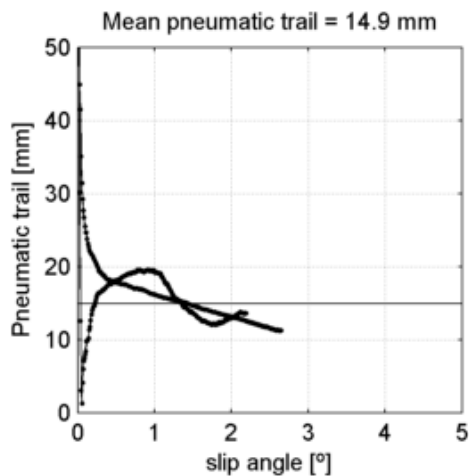
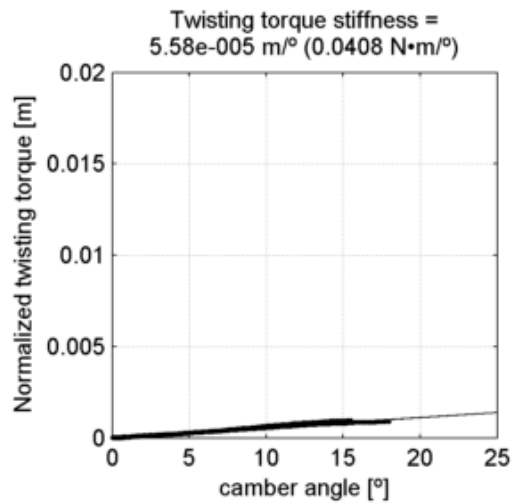
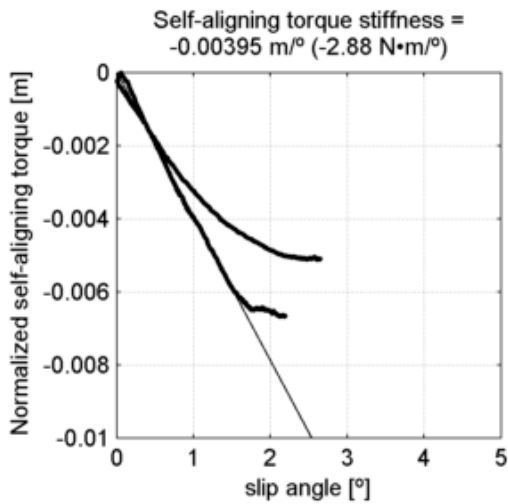
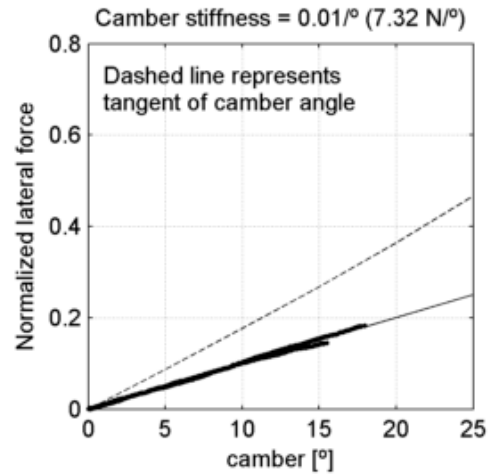
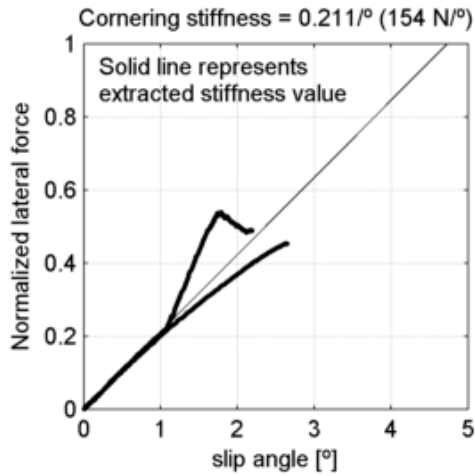
Schwalbe Kojak 35-622
 tire radius = 15.7 mm, rim width = 18.7 mm

at 6.21 bar (90 psi) and
 under 540 N (55 kg, 121 lb)



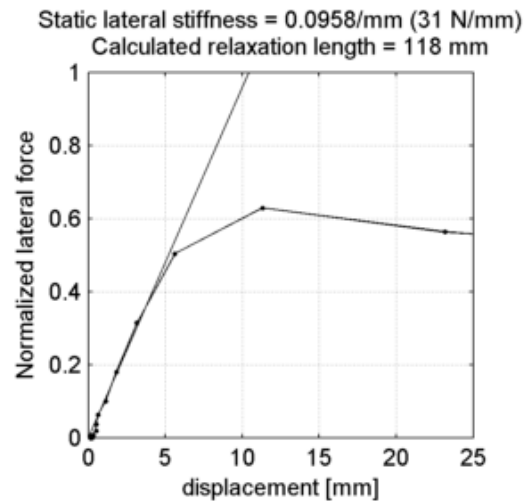
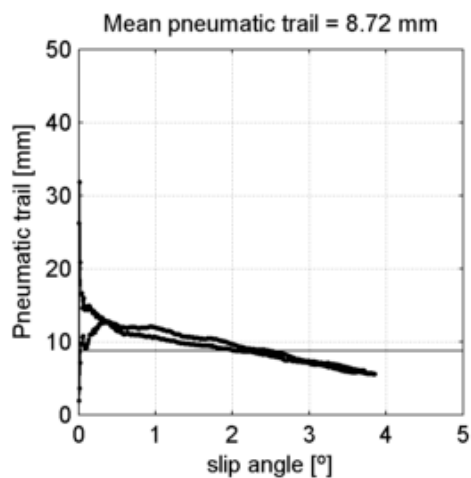
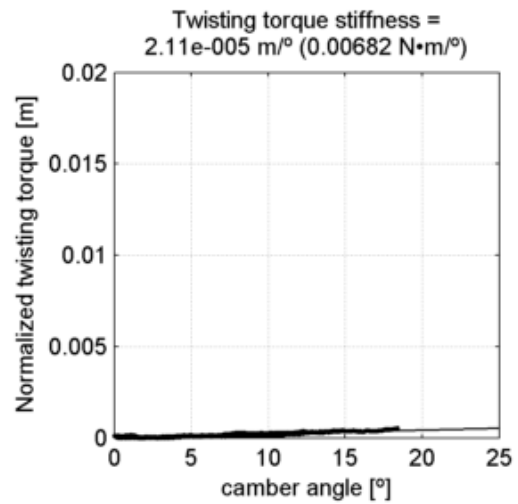
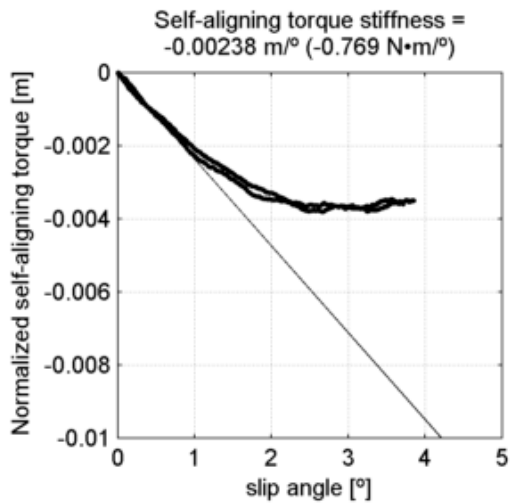
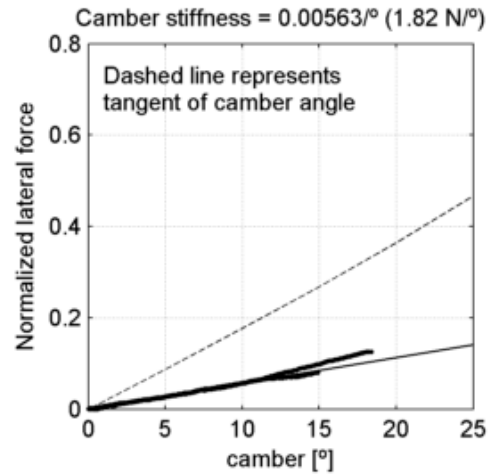
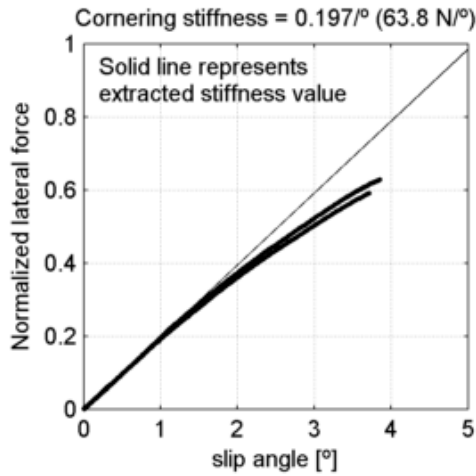
Schwalbe Kojak 35-622
 tire radius = 15.7 mm, rim width = 18.7 mm

at 6.21 bar (90 psi) and
 under 731 N (74.5 kg, 164 lb)



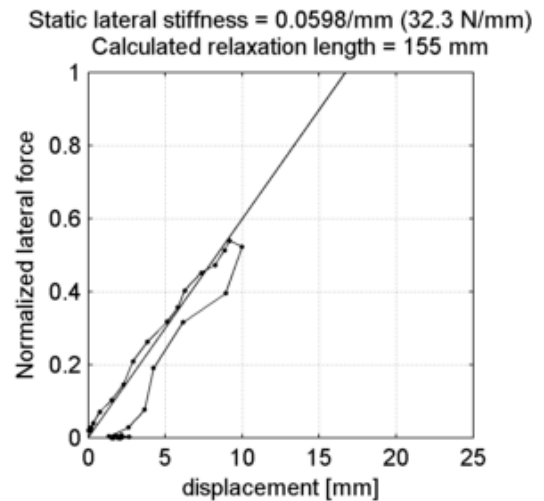
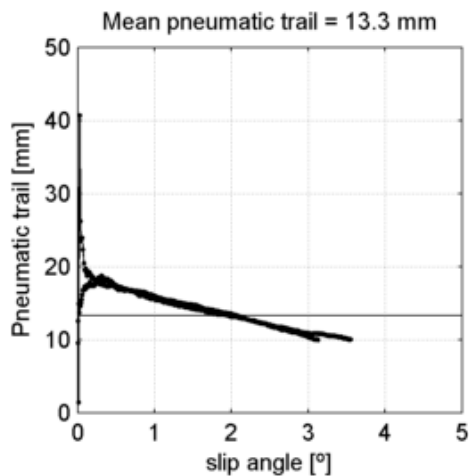
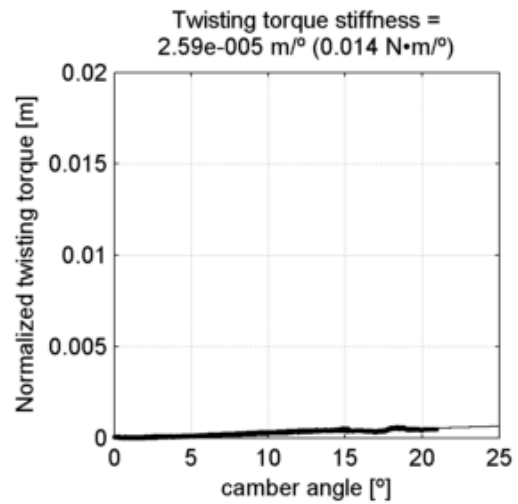
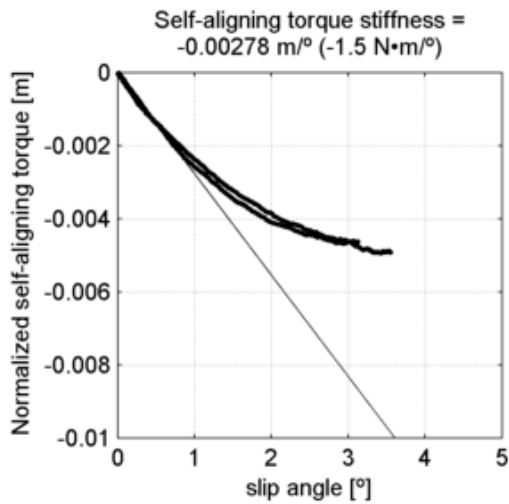
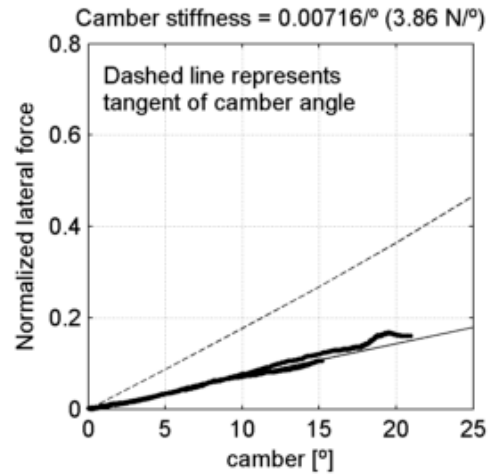
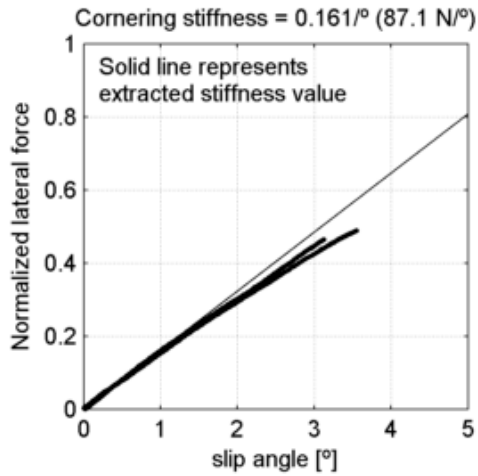
Schwalbe Marathon Plus 37-622
 tire radius = 14.9 mm, rim width = 18.7 mm

at 4 bar (58 psi) and
 under 324 N (33 kg, 72.8 lb)



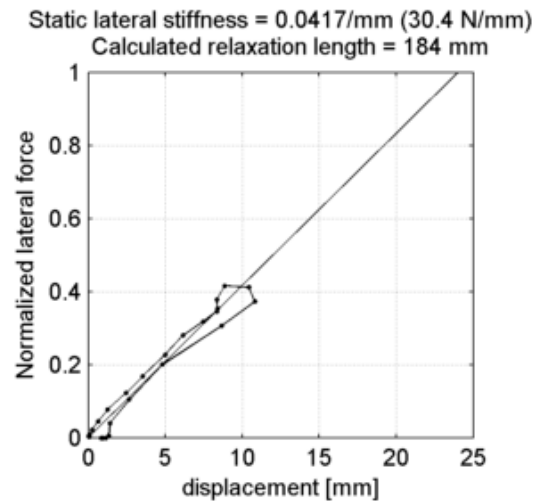
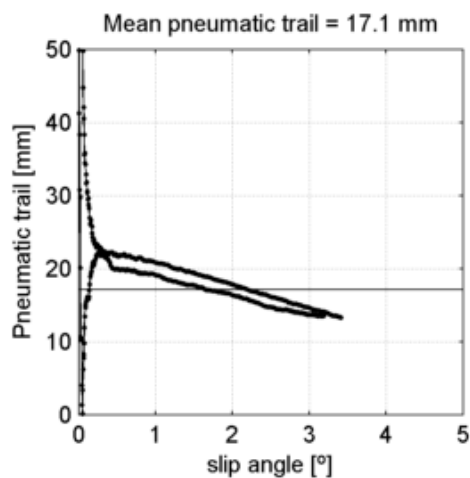
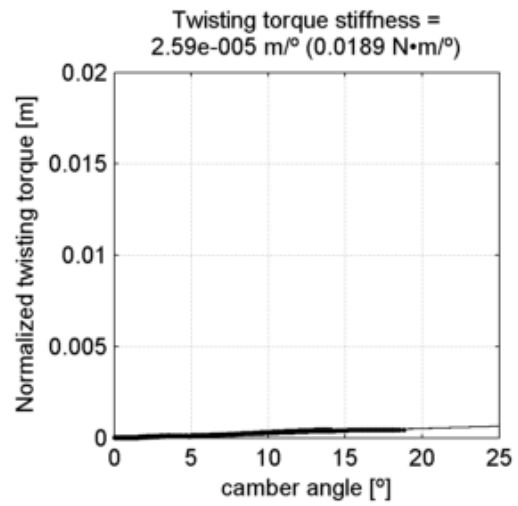
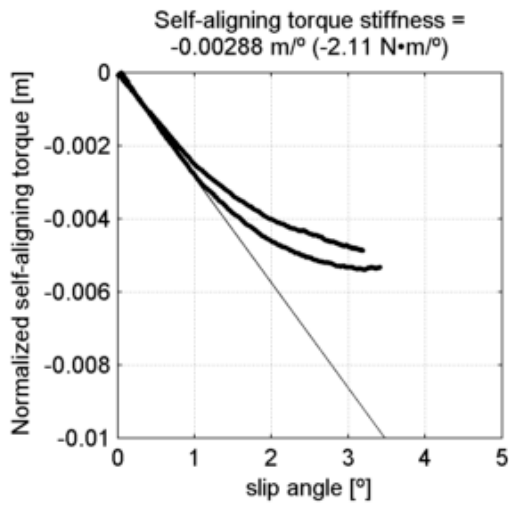
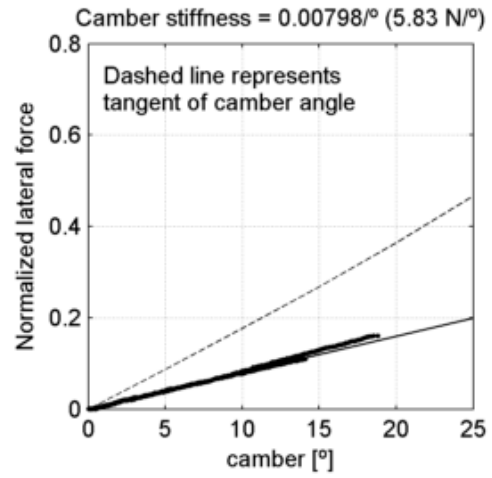
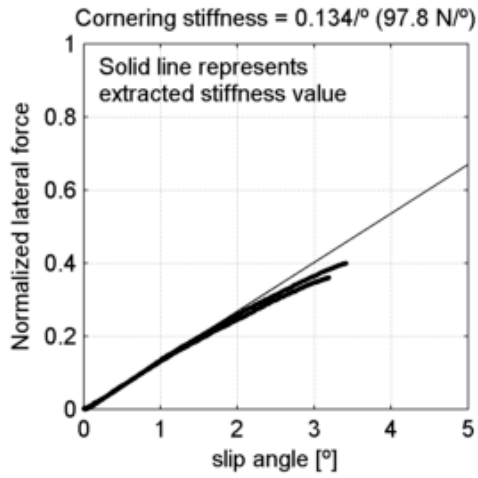
Schwalbe Marathon Plus 37-622
 tire radius = 14.9 mm, rim width = 18.7 mm

at 4 bar (58 psi) and
 under 540 N (55 kg, 121 lb)



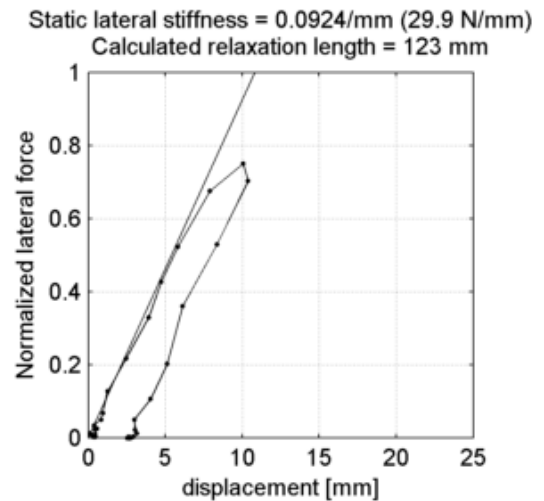
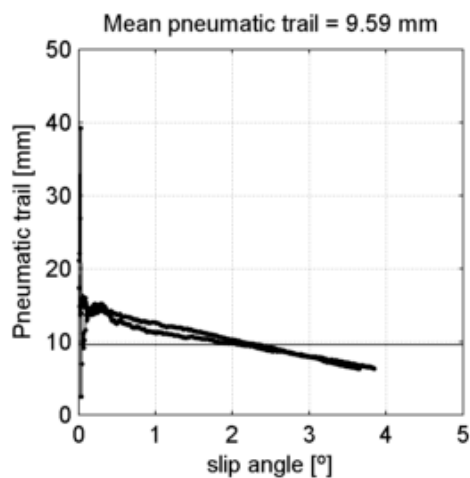
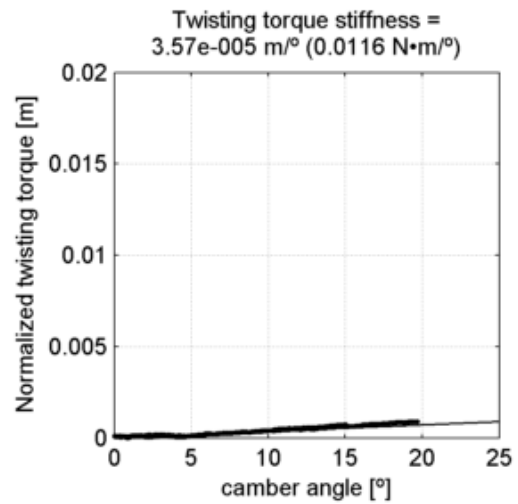
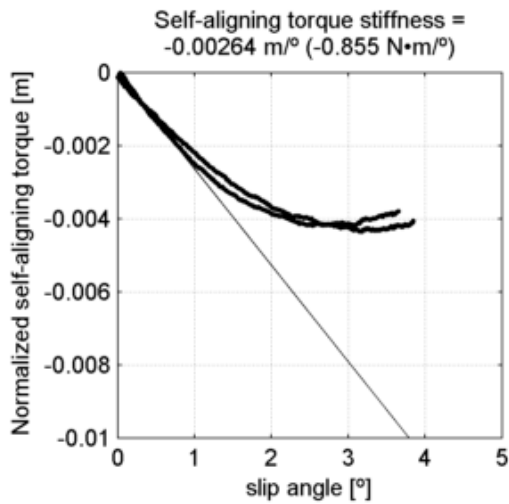
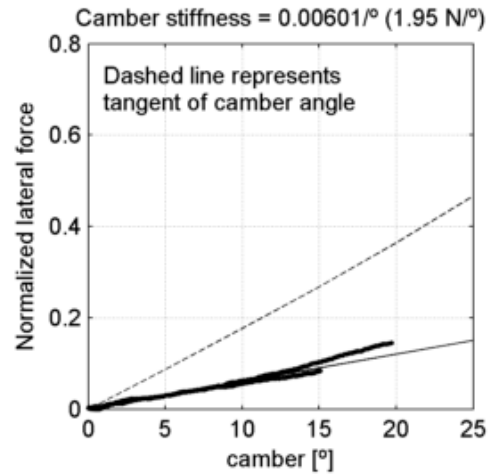
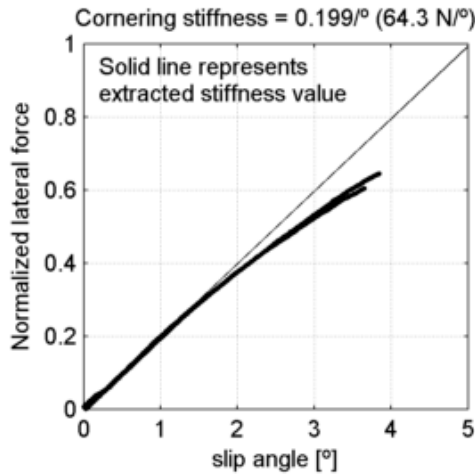
Schwalbe Marathon Plus 37-622
 tire radius = 14.9 mm, rim width = 18.7 mm

at 4 bar (58 psi) and
 under 731 N (74.5 kg, 164 lb)



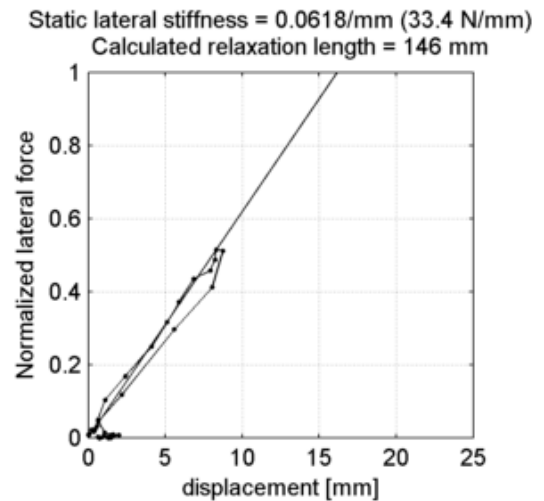
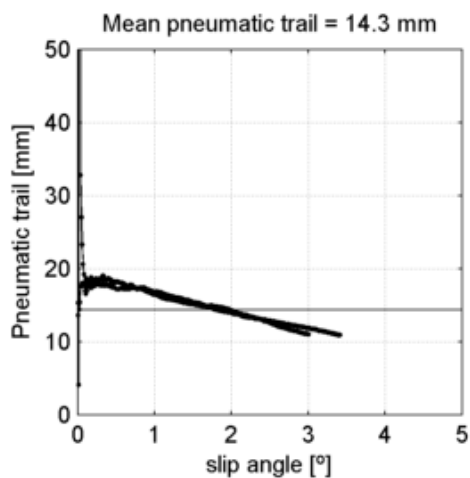
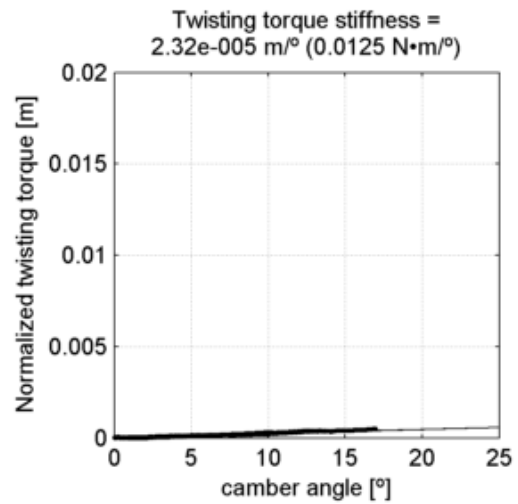
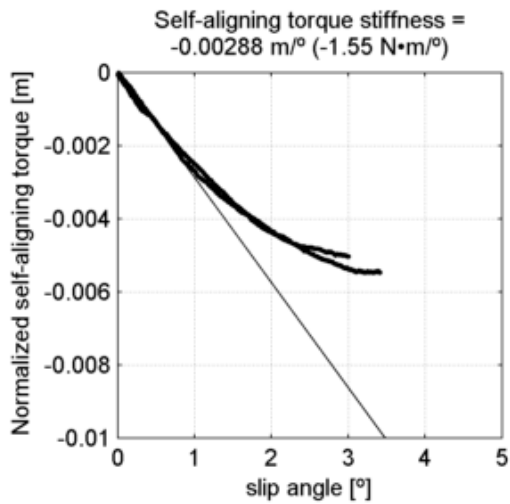
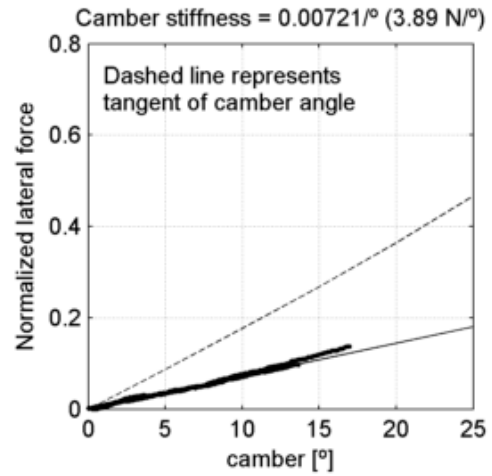
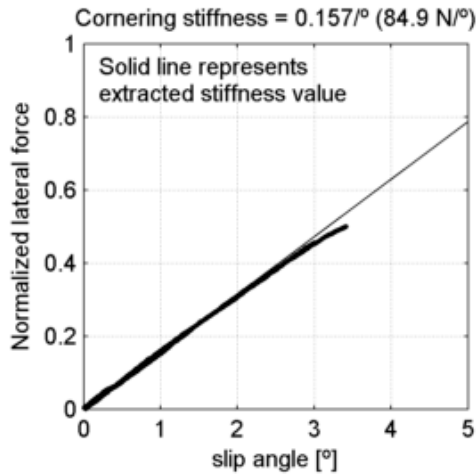
Schwalbe Marathon Plus 37-622
 tire radius = 14.9 mm, rim width = 18.7 mm

at 3.45 bar (50 psi) and
 under 324 N (33 kg, 72.8 lb)



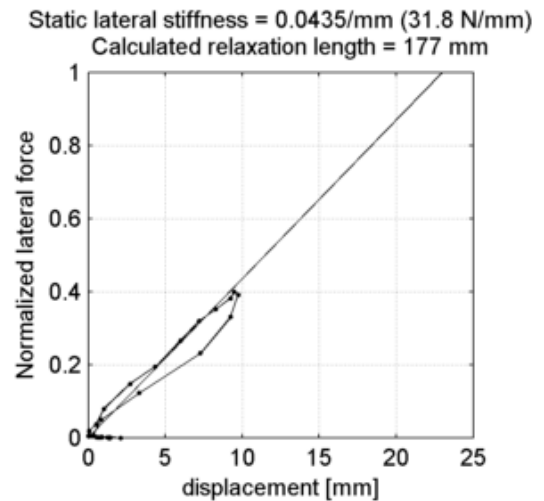
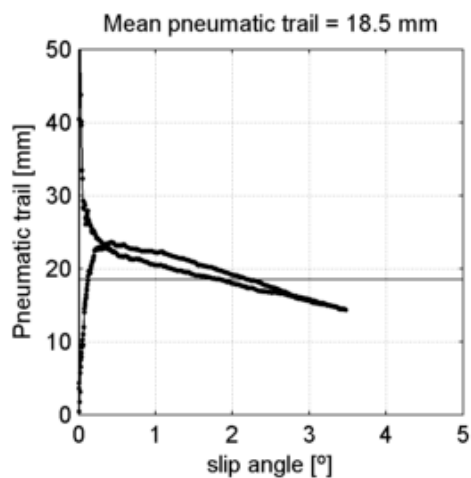
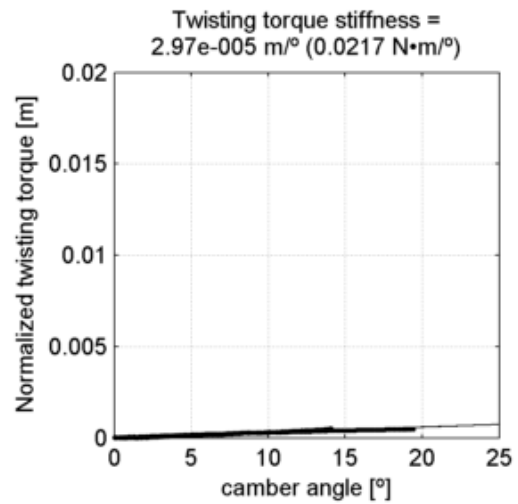
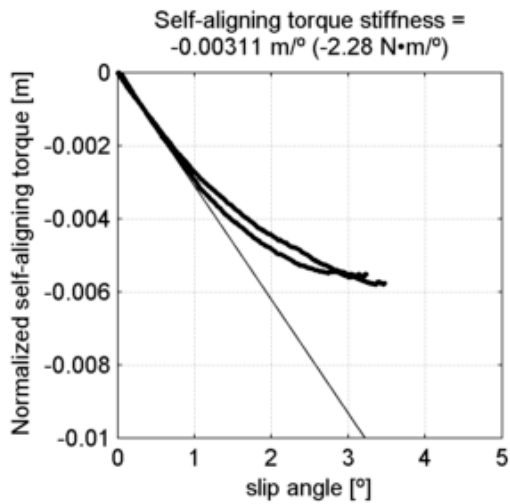
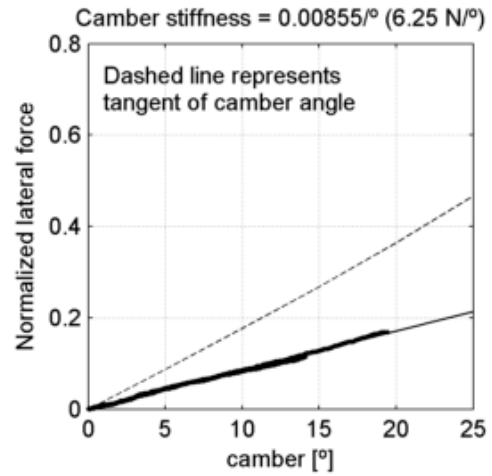
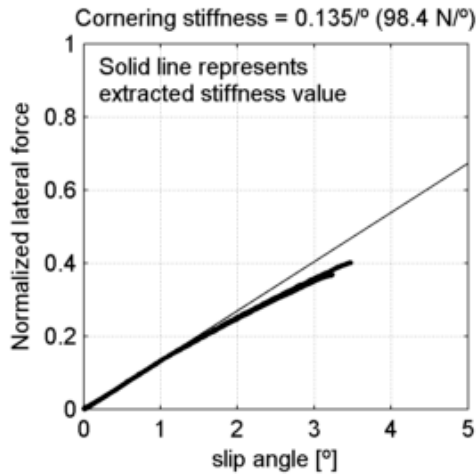
Schwalbe Marathon Plus 37-622
 tire radius = 14.9 mm, rim width = 18.7 mm

at 3.45 bar (50 psi) and
 under 540 N (55 kg, 121 lb)



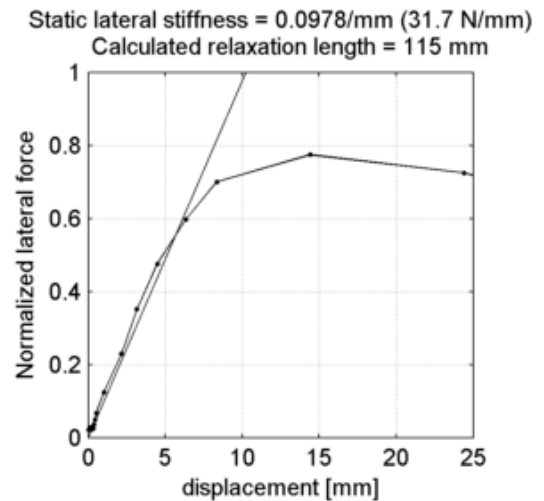
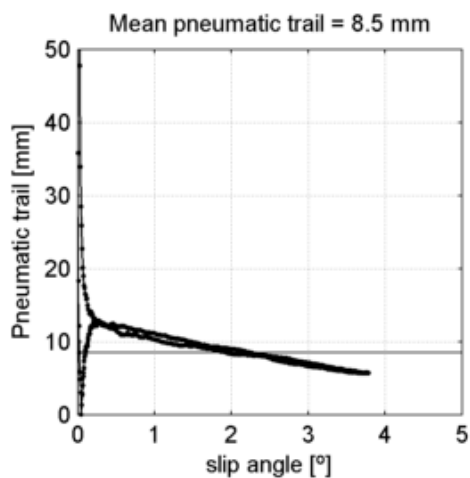
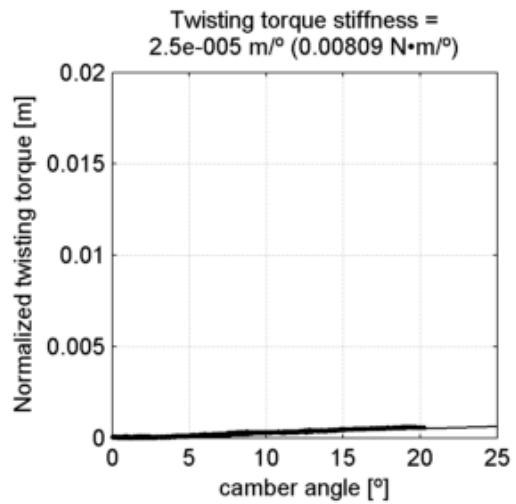
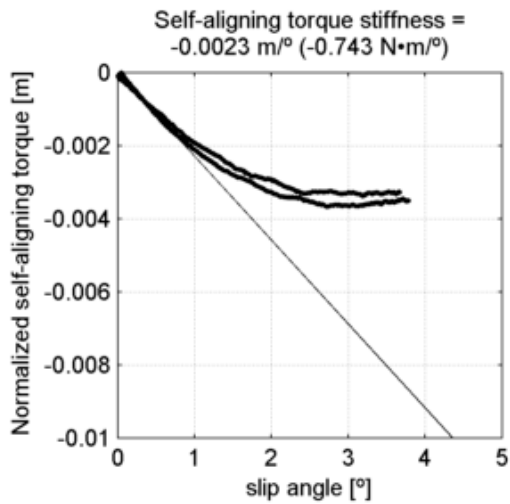
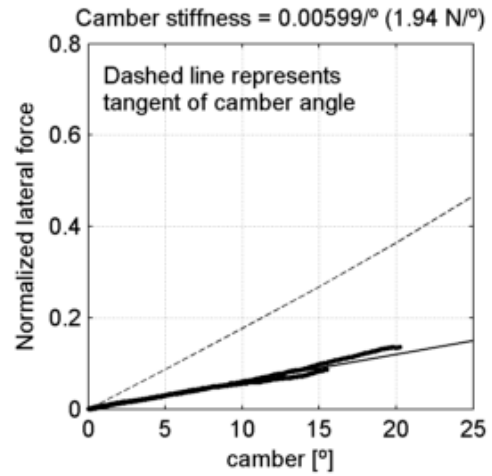
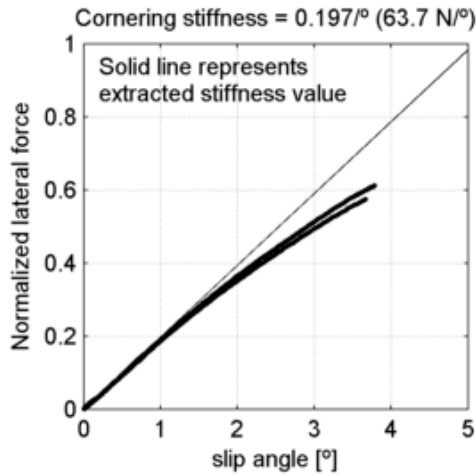
Schwalbe Marathon Plus 37-622
 tire radius = 14.9 mm, rim width = 18.7 mm

at 3.45 bar (50 psi) and
 under 731 N (74.5 kg, 164 lb)



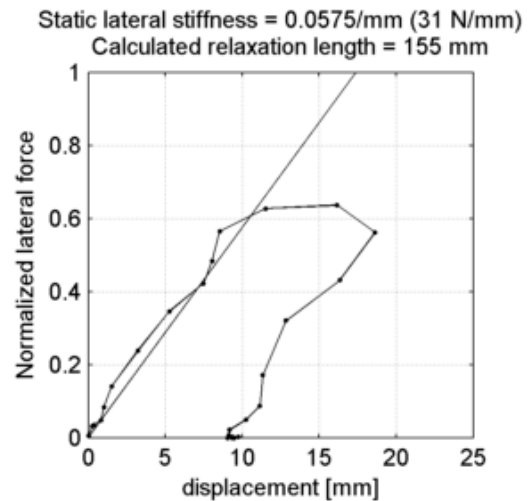
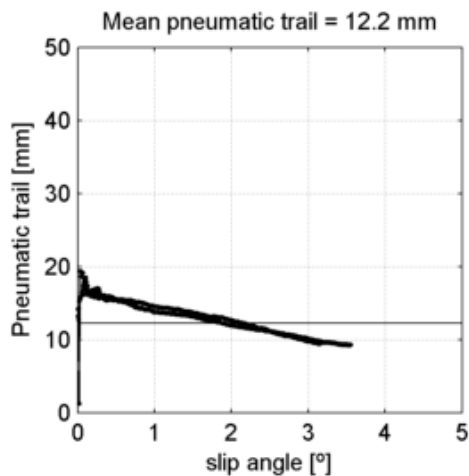
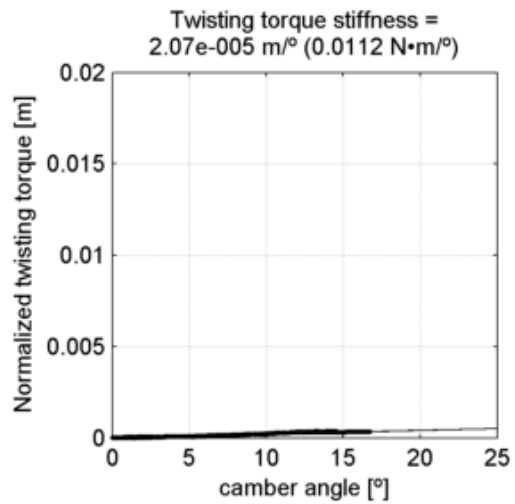
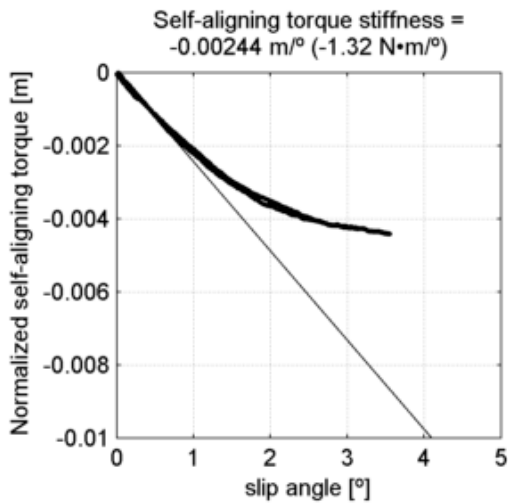
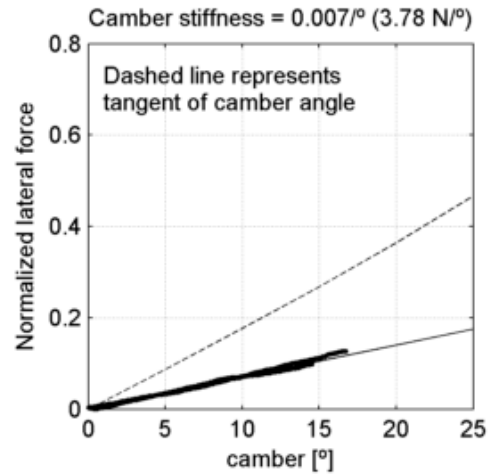
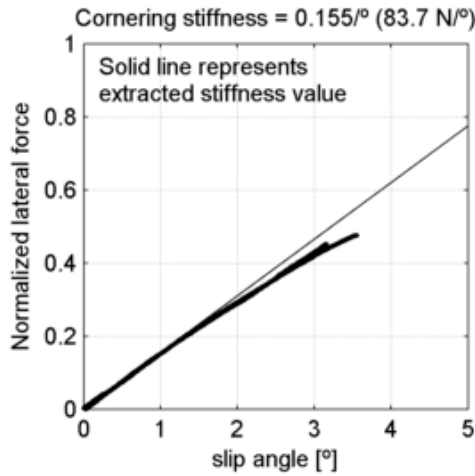
Schwalbe Marathon Plus 37-622
 tire radius = 14.9 mm, rim width = 18.7 mm

at 4.83 bar (70 psi) and
 under 324 N (33 kg, 72.8 lb)



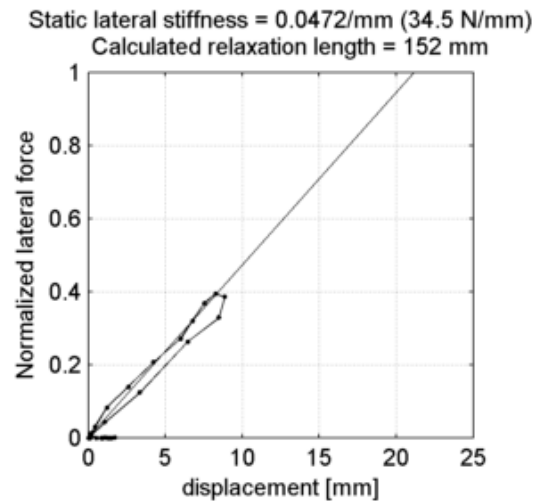
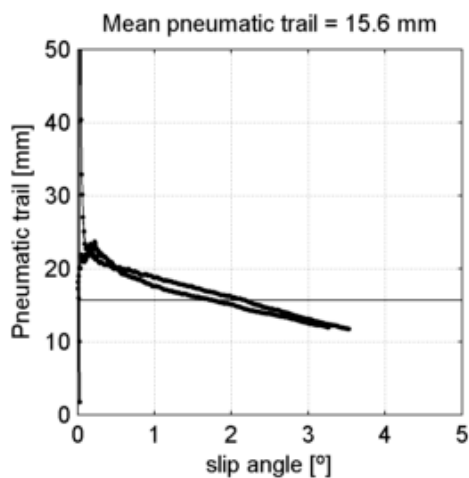
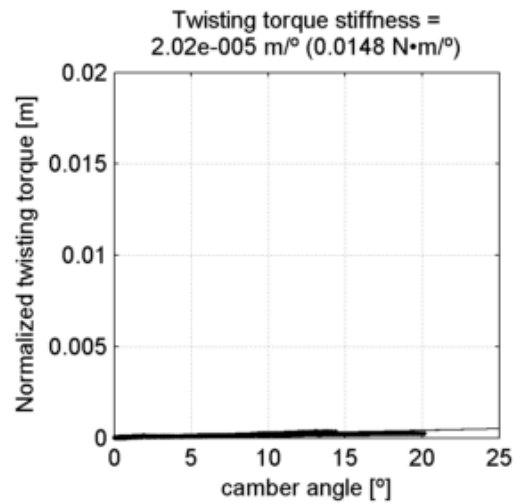
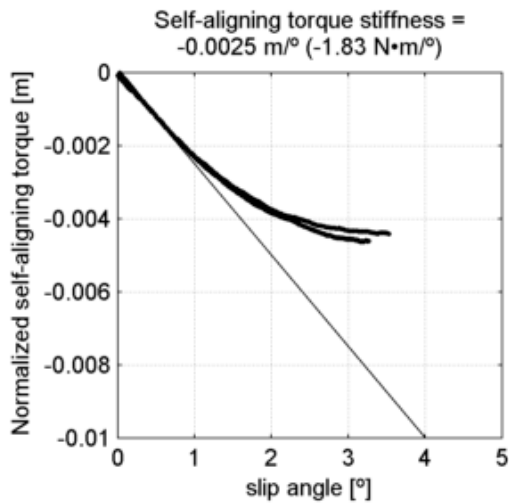
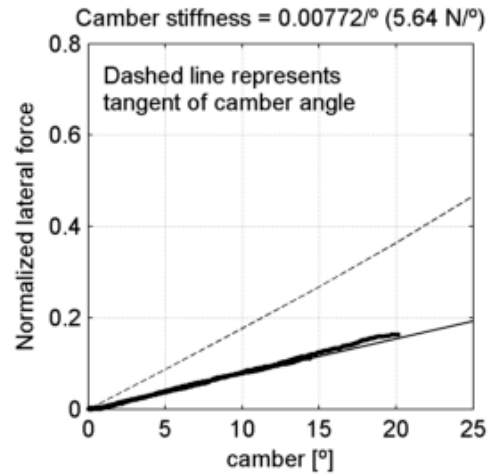
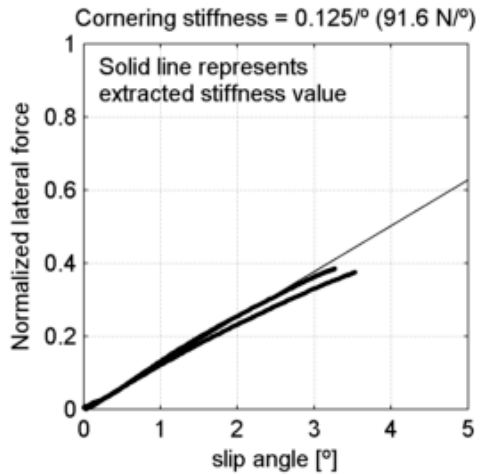
Schwalbe Marathon Plus 37-622
 tire radius = 14.9 mm, rim width = 18.7 mm

at 4.83 bar (70 psi) and
 under 540 N (55 kg, 121 lb)



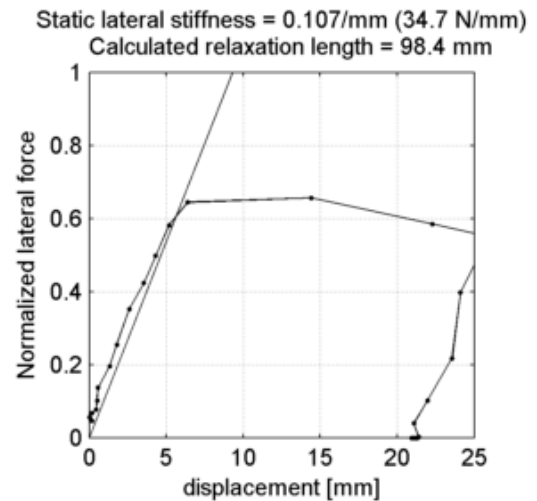
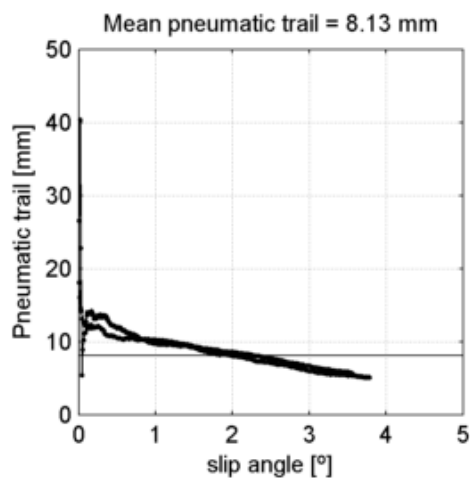
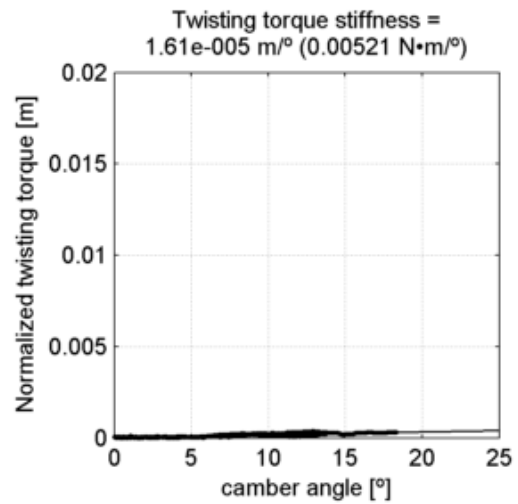
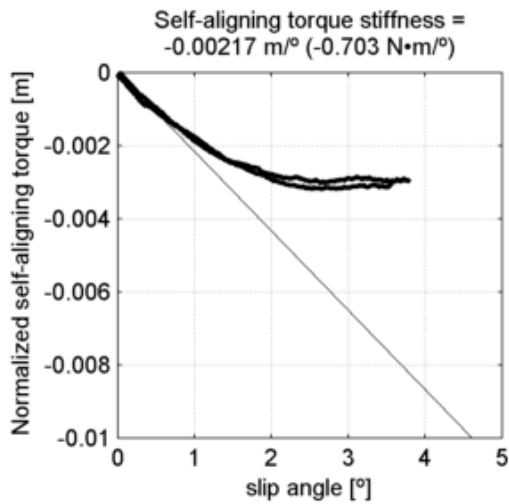
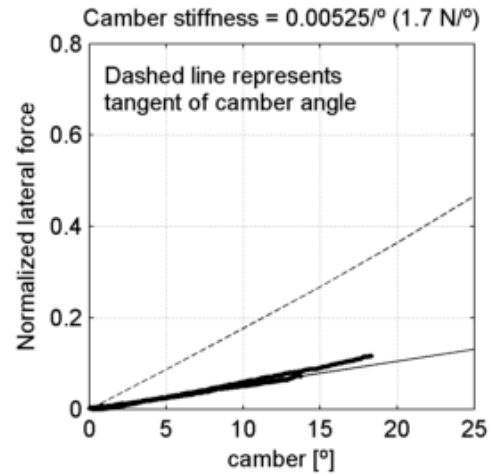
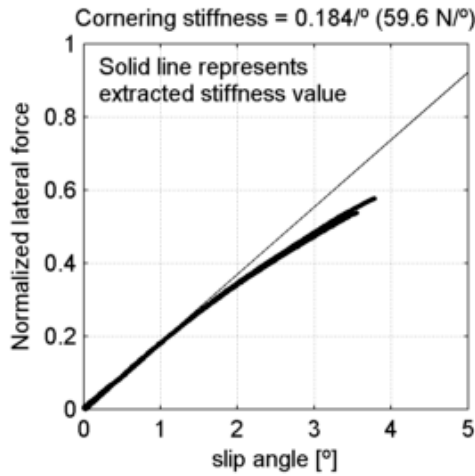
Schwalbe Marathon Plus 37-622
 tire radius = 14.9 mm, rim width = 18.7 mm

at 4.83 bar (70 psi) and
 under 731 N (74.5 kg, 164 lb)



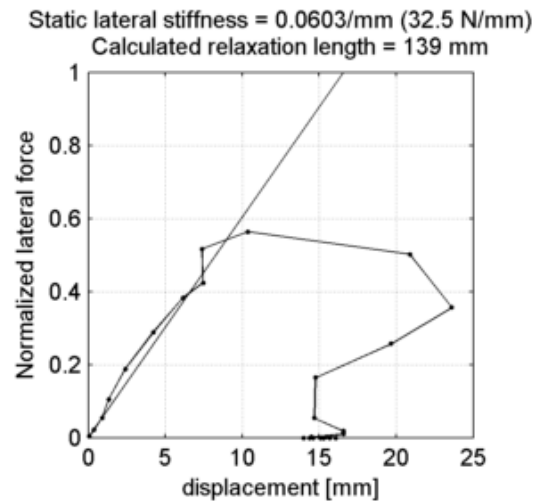
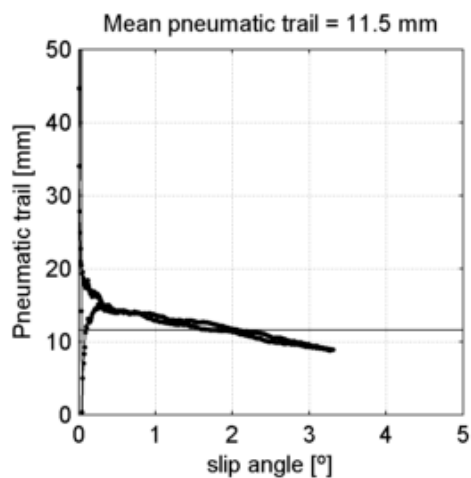
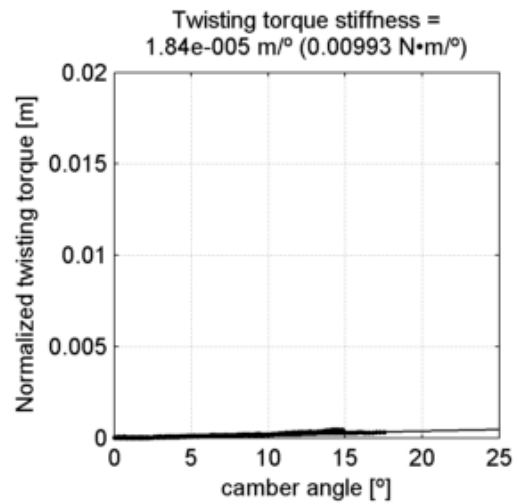
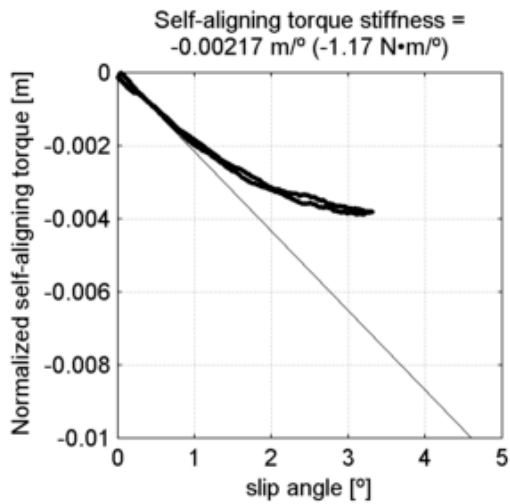
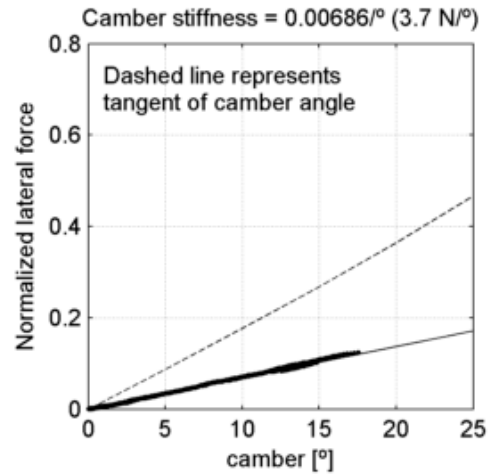
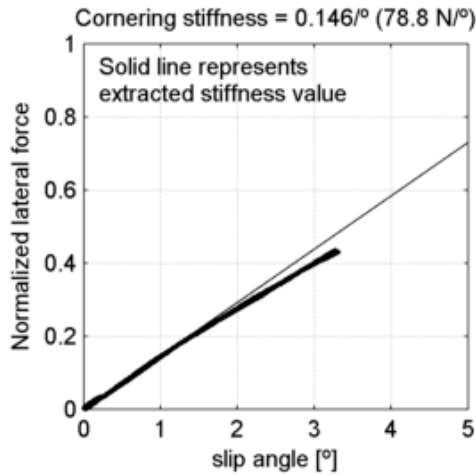
Schwalbe Marathon Plus 37-622
 tire radius = 14.9 mm, rim width = 18.7 mm

at 6.21 bar (90 psi) and
 under 324 N (33 kg, 72.8 lb)



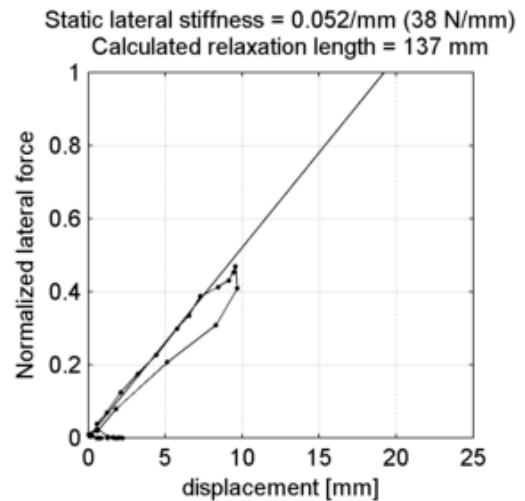
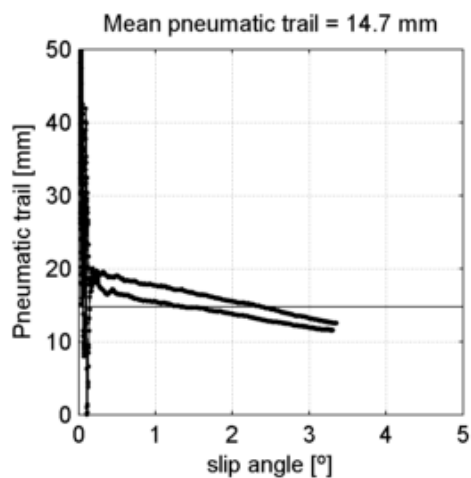
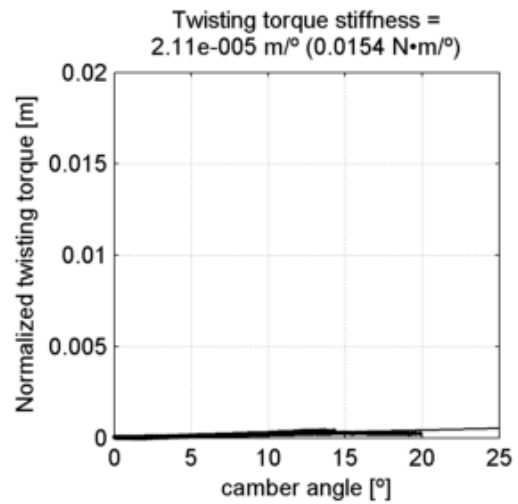
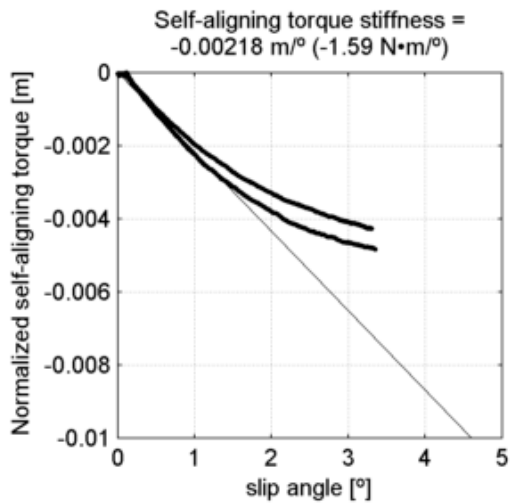
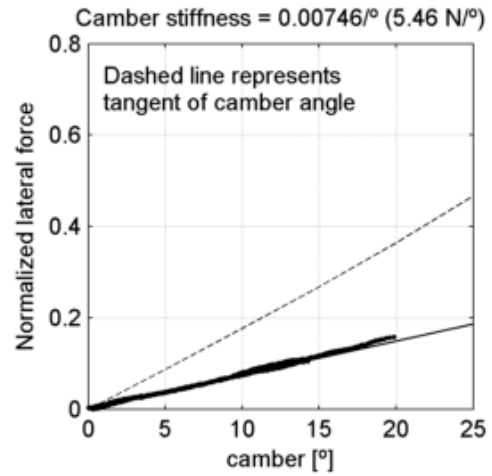
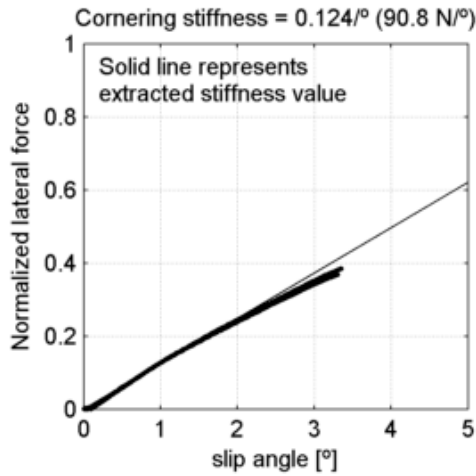
Schwalbe Marathon Plus 37-622
 tire radius = 14.9 mm, rim width = 18.7 mm

at 6.21 bar (90 psi) and
 under 540 N (55 kg, 121 lb)



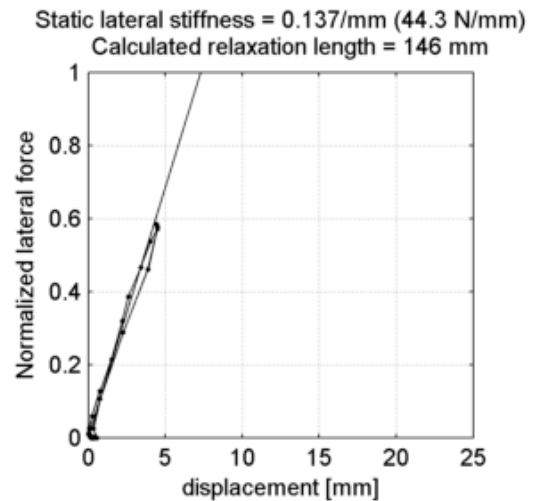
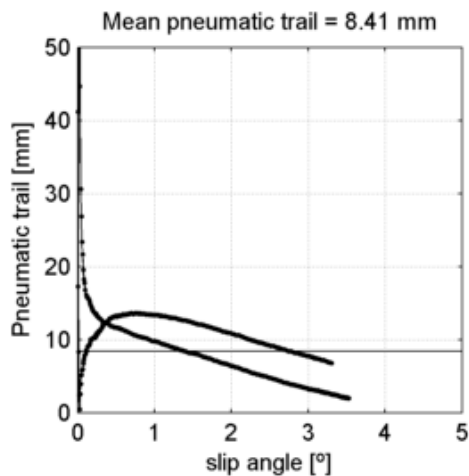
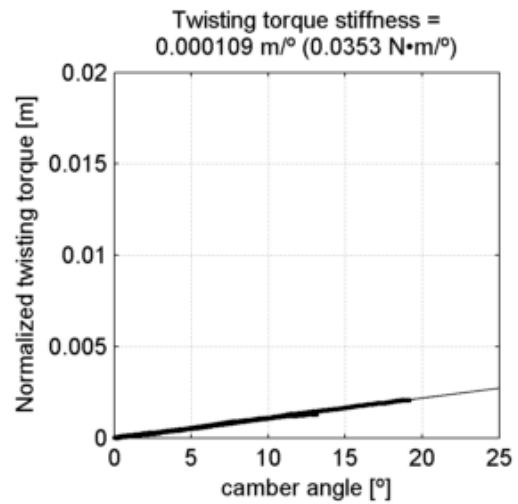
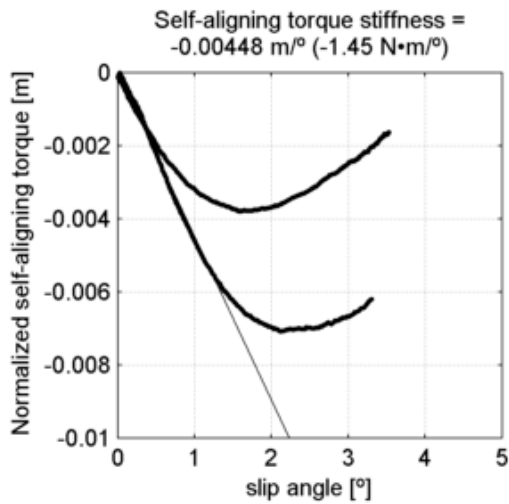
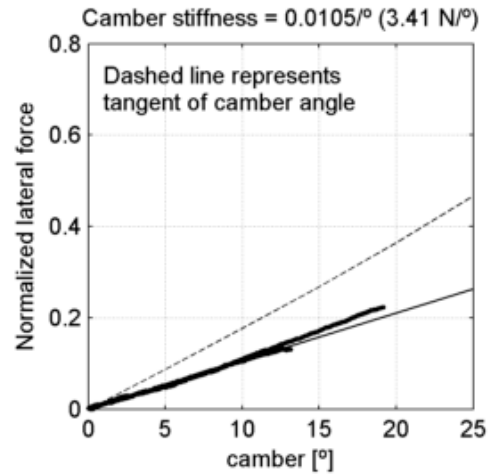
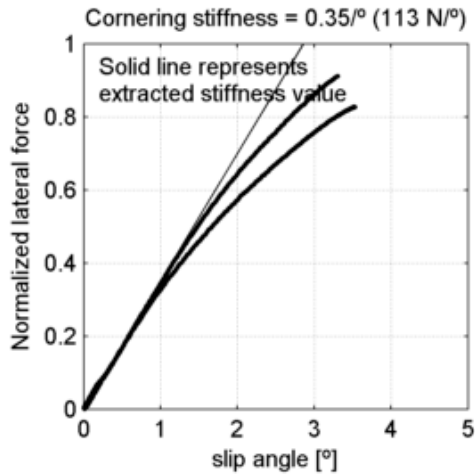
Schwalbe Marathon Plus 37-622
 tire radius = 14.9 mm, rim width = 18.7 mm

at 6.21 bar (90 psi) and
 under 731 N (74.5 kg, 164 lb)



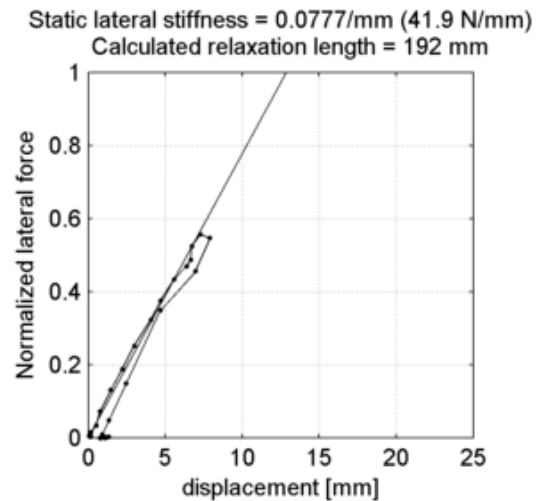
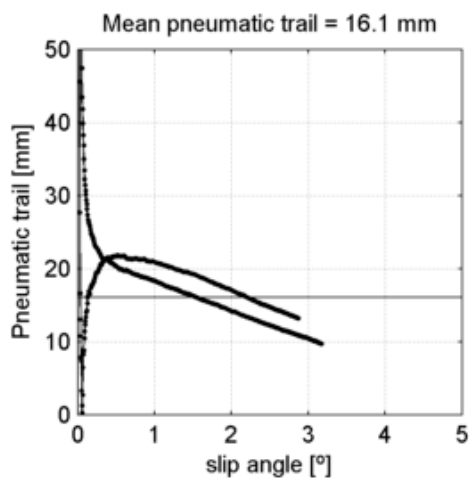
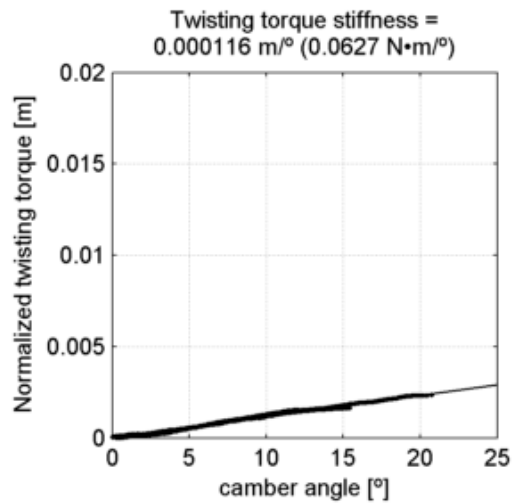
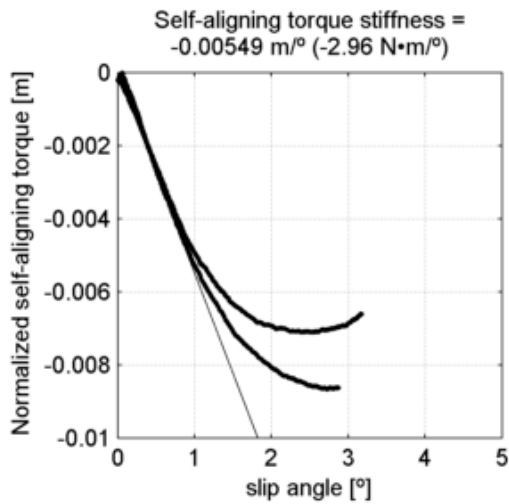
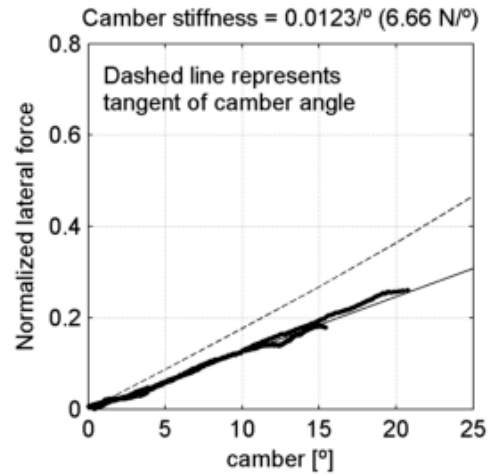
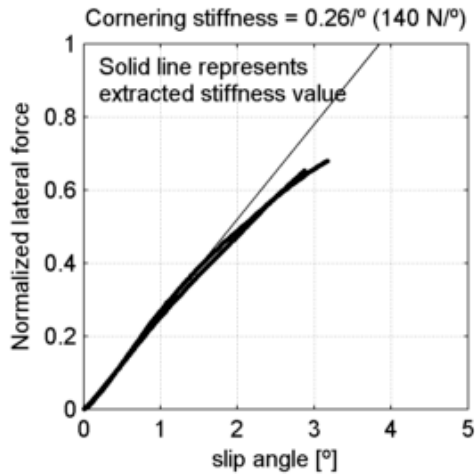
Vittoria Randonneur Hyper 37-622
 tire radius = 17.5 mm, rim width = 18.7 mm

at 4 bar (58 psi) and
 under 324 N (33 kg, 72.8 lb)



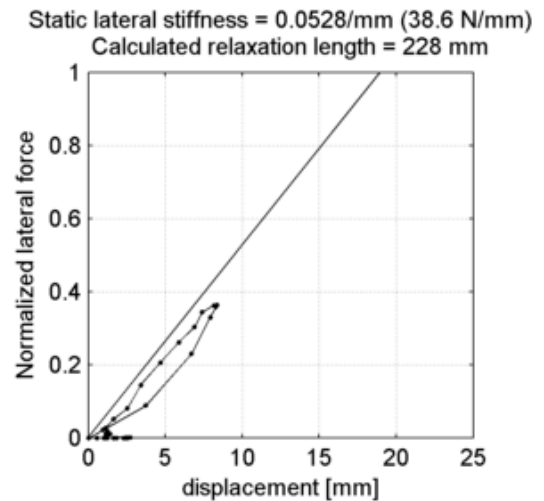
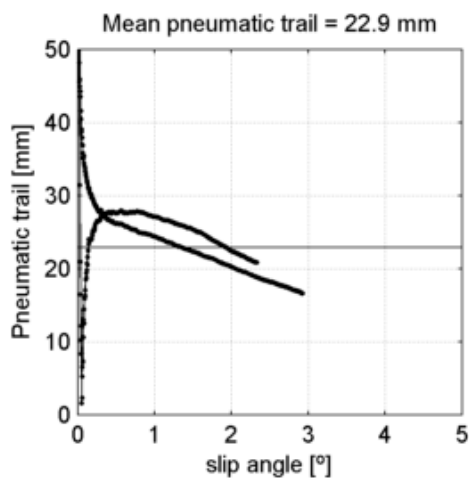
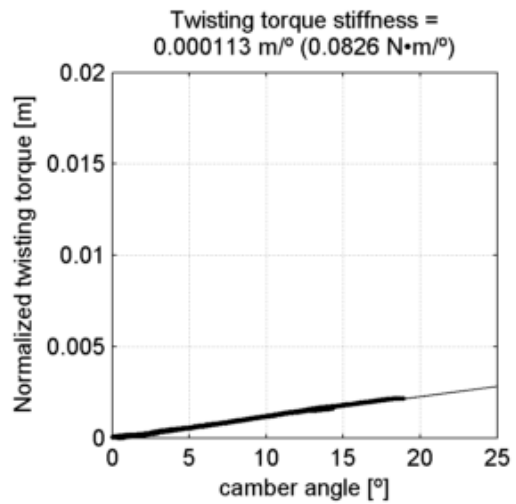
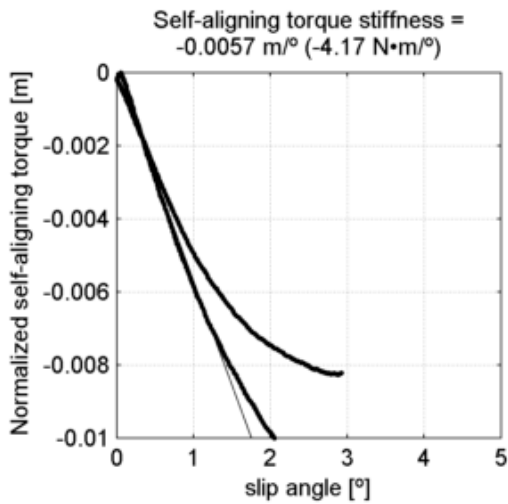
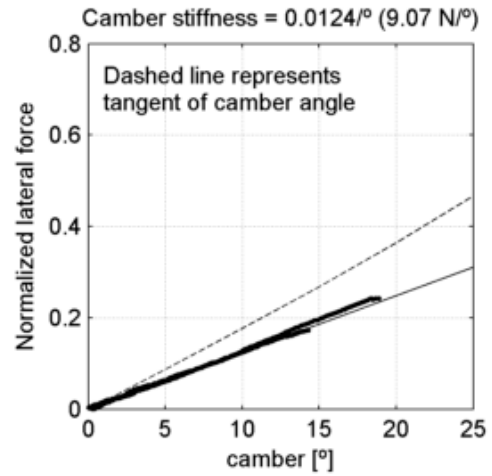
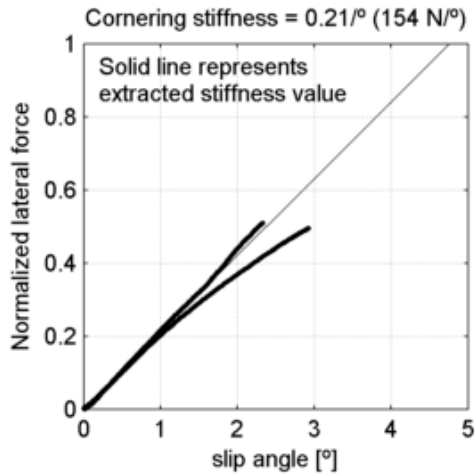
Vittoria Randonneur Hyper 37-622
 tire radius = 17.5 mm, rim width = 18.7 mm

at 4 bar (58 psi) and
 under 540 N (55 kg, 121 lb)



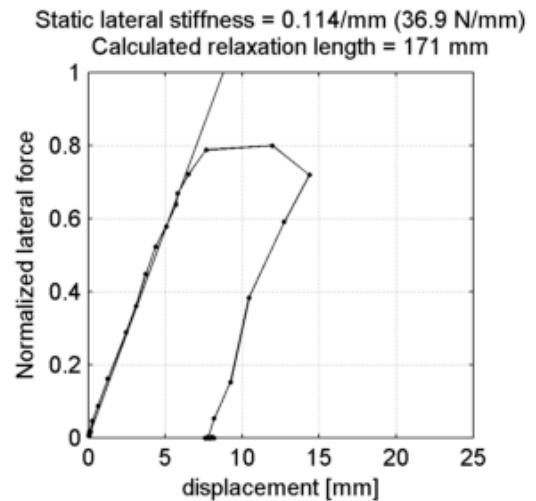
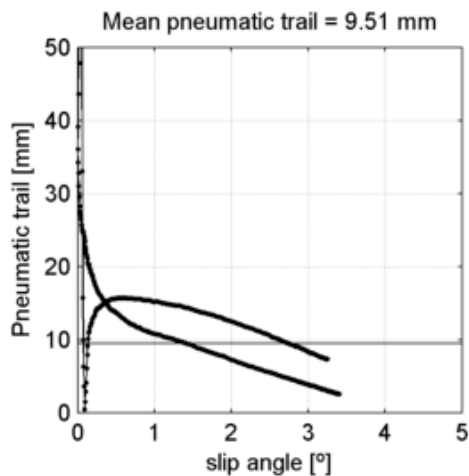
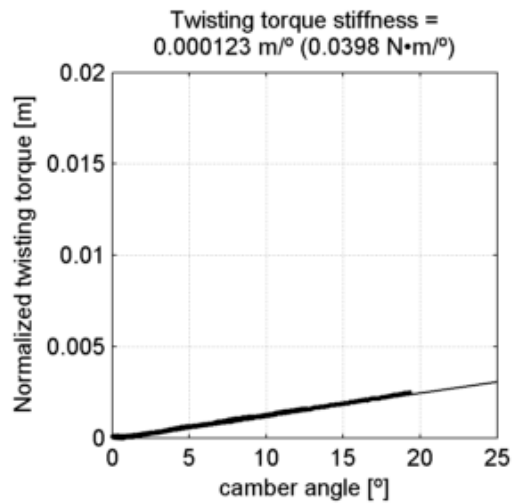
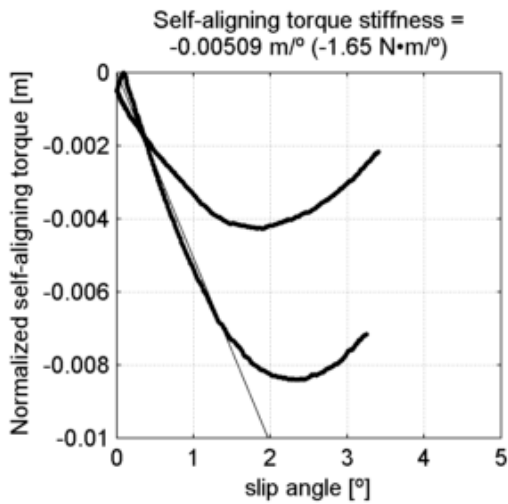
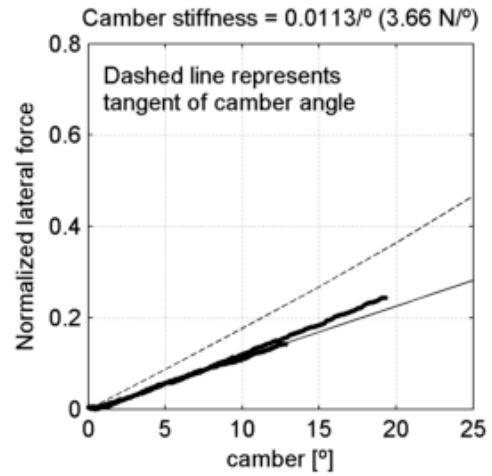
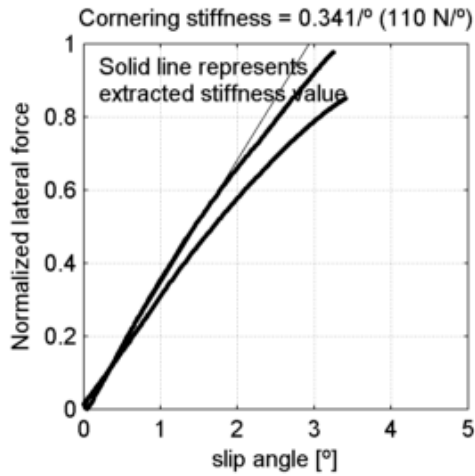
Vittoria Randonneur Hyper 37-622
 tire radius = 17.5 mm, rim width = 18.7 mm

at 4 bar (58 psi) and
 under 731 N (74.5 kg, 164 lb)



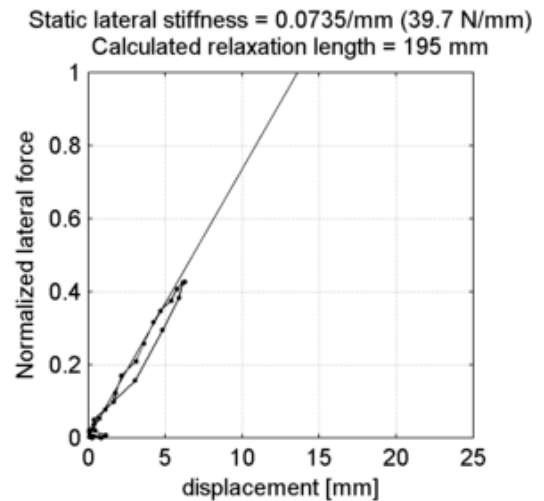
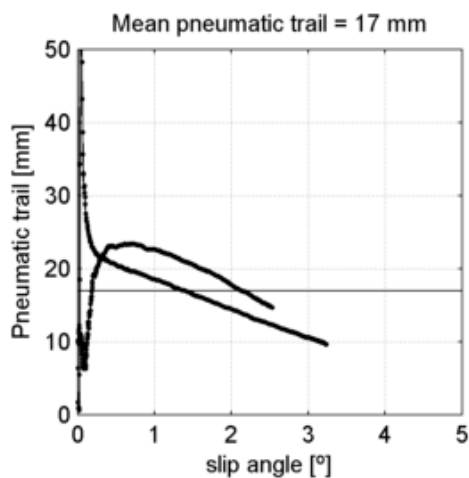
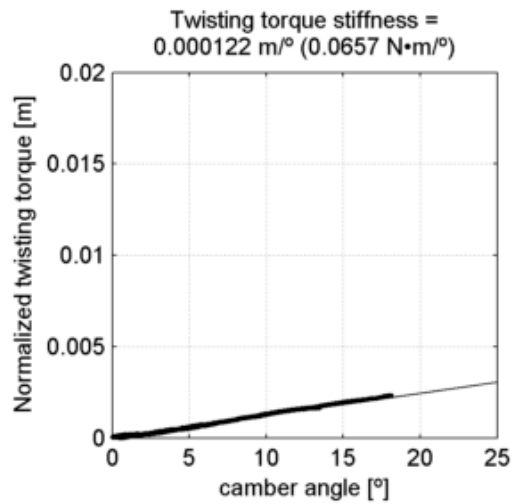
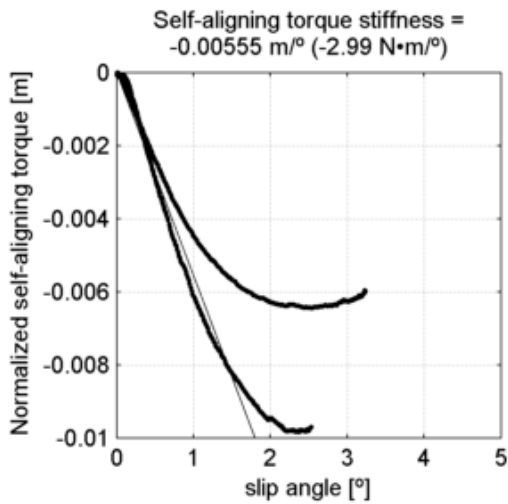
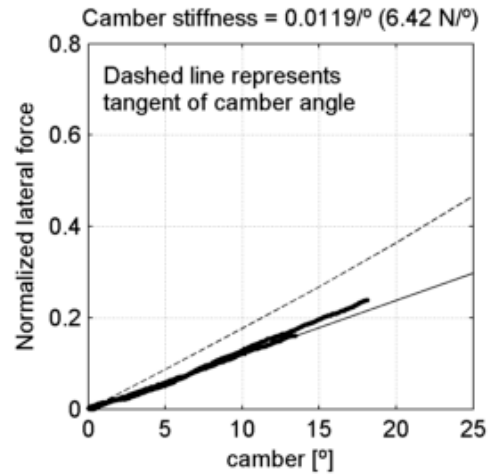
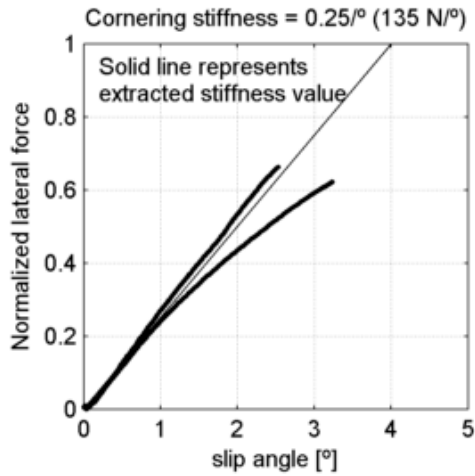
Vittoria Randonneur Hyper 37-622
 tire radius = 17.5 mm, rim width = 18.7 mm

at 3.45 bar (50 psi) and
 under 324 N (33 kg, 72.8 lb)



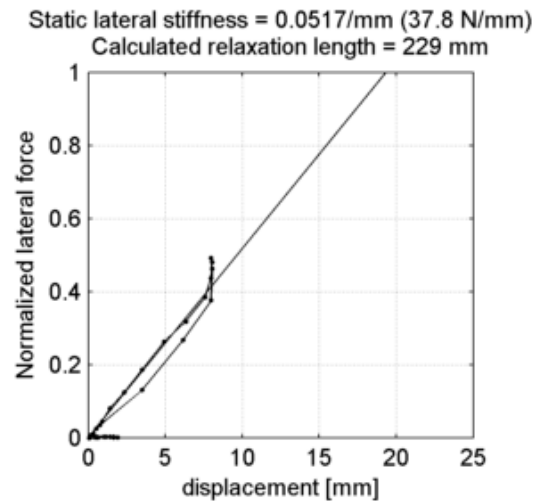
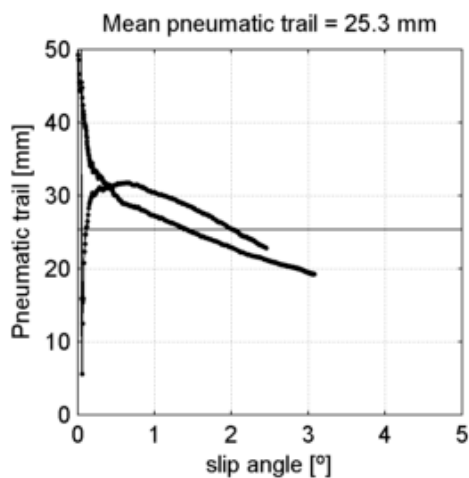
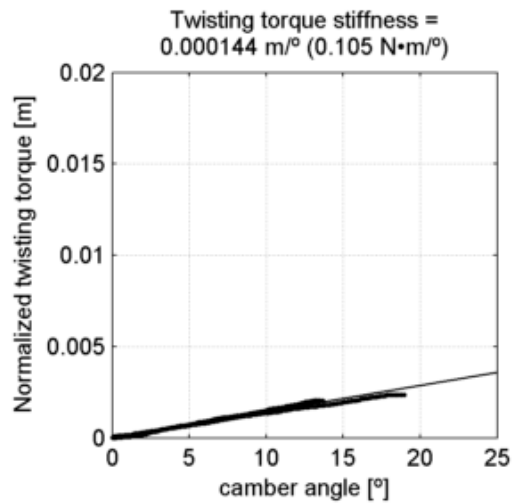
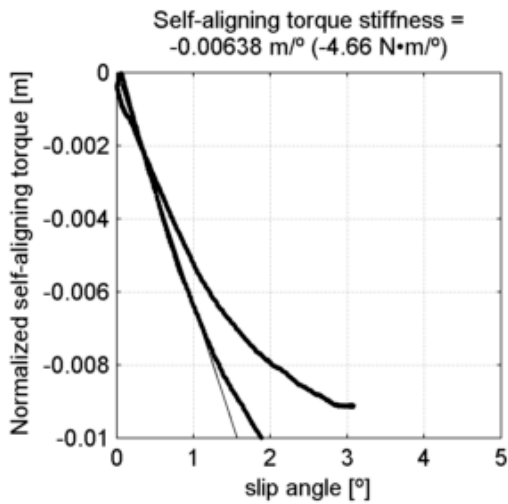
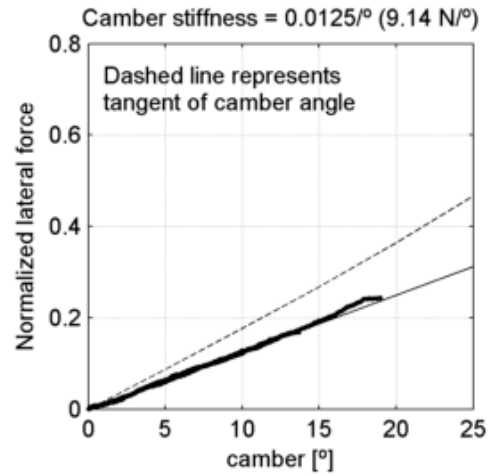
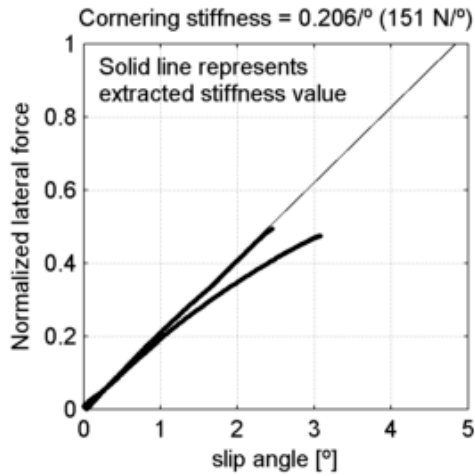
Vittoria Randonneur Hyper 37-622
 tire radius = 17.5 mm, rim width = 18.7 mm

at 3.45 bar (50 psi) and
 under 540 N (55 kg, 121 lb)



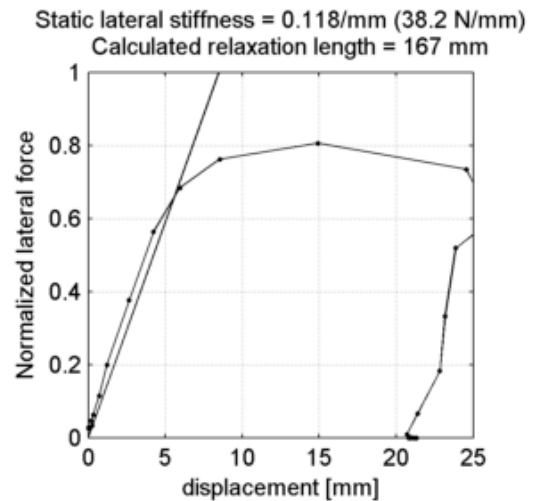
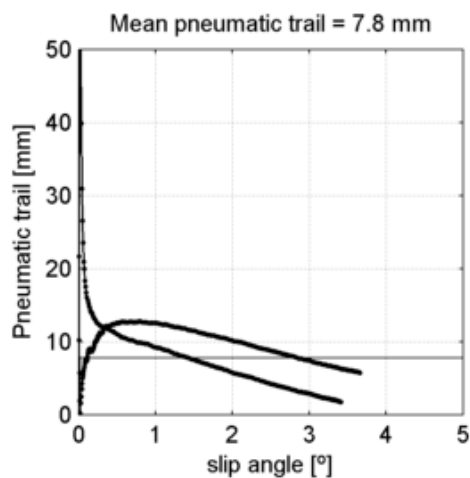
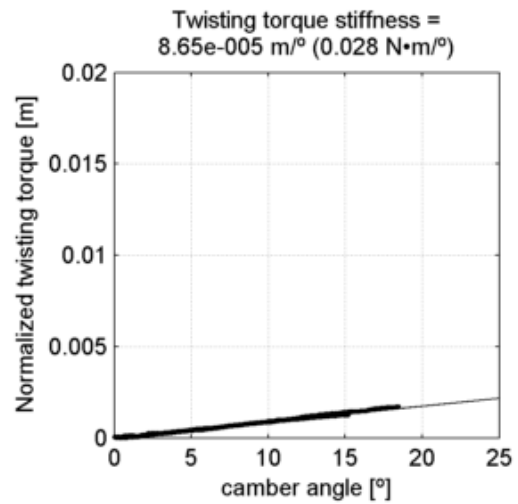
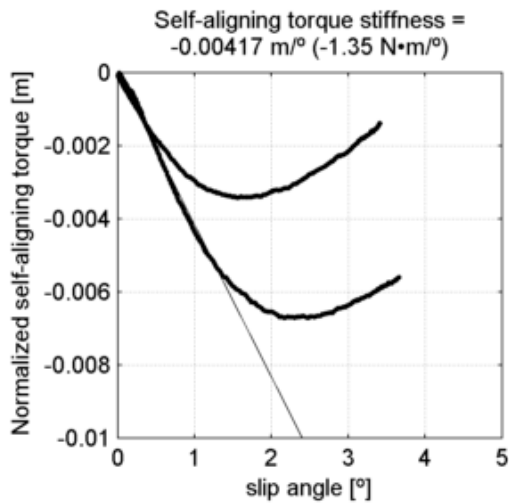
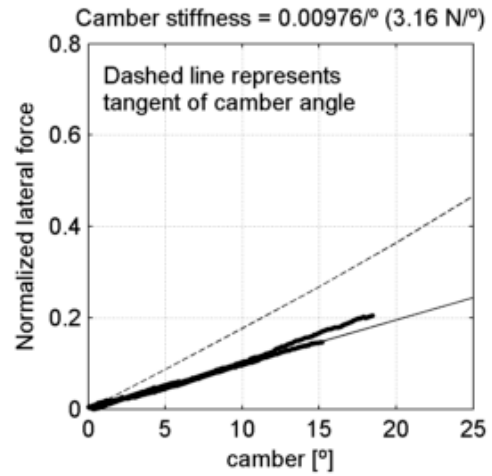
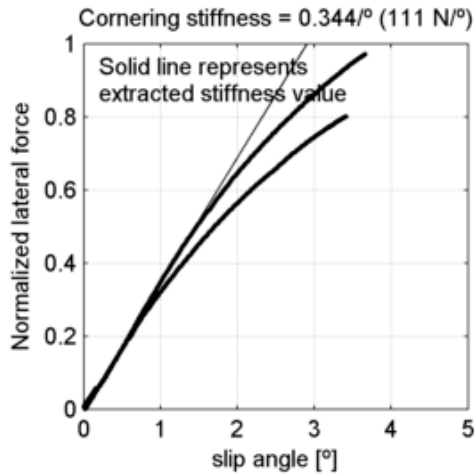
Vittoria Randonneur Hyper 37-622
 tire radius = 17.5 mm, rim width = 18.7 mm

at 3.45 bar (50 psi) and
 under 731 N (74.5 kg, 164 lb)



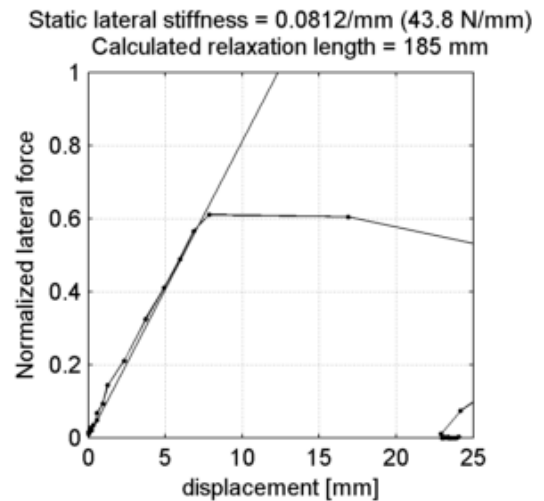
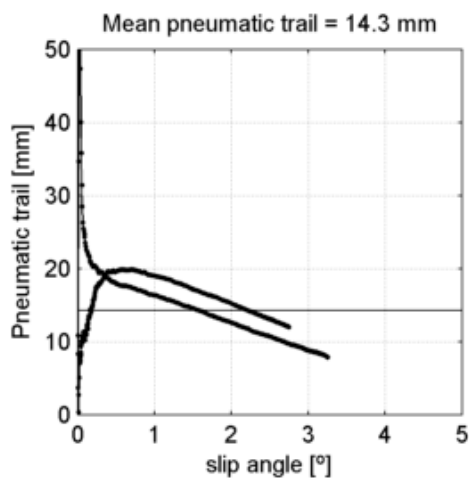
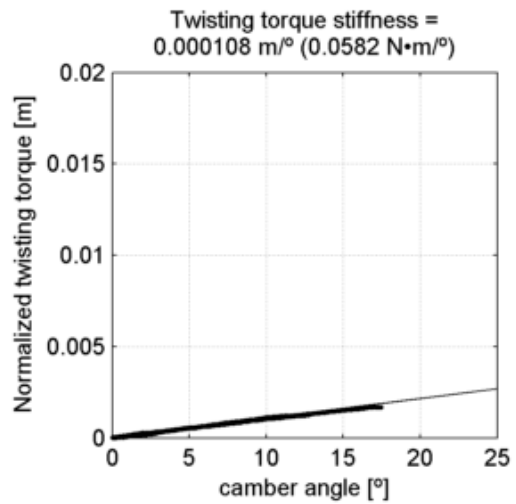
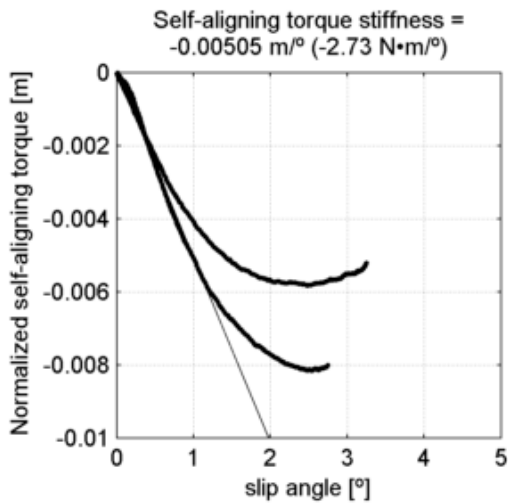
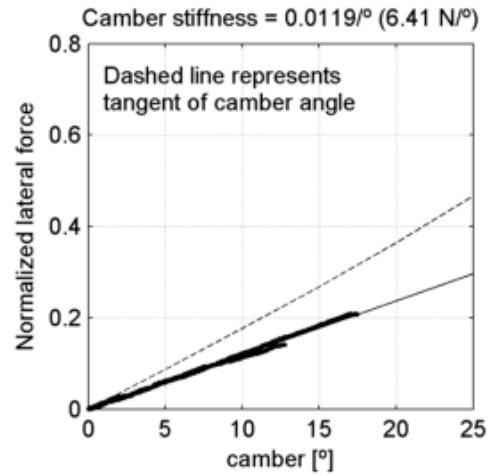
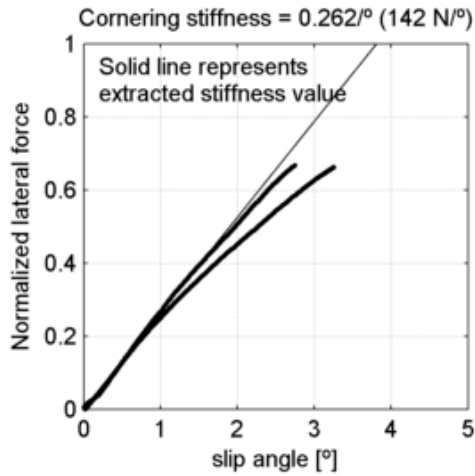
Vittoria Randonneur Hyper 37-622
 tire radius = 17.5 mm, rim width = 18.7 mm

at 4.83 bar (70 psi) and
 under 324 N (33 kg, 72.8 lb)



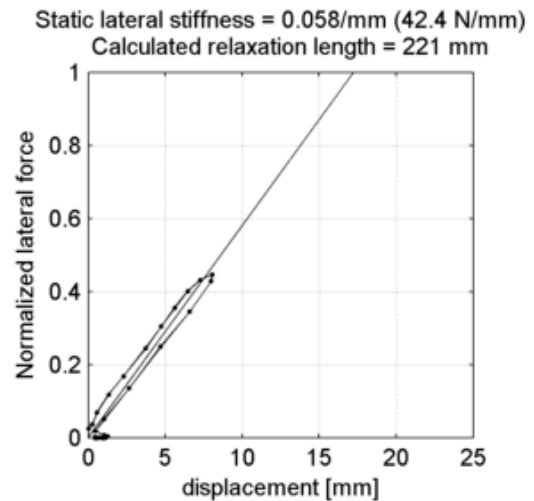
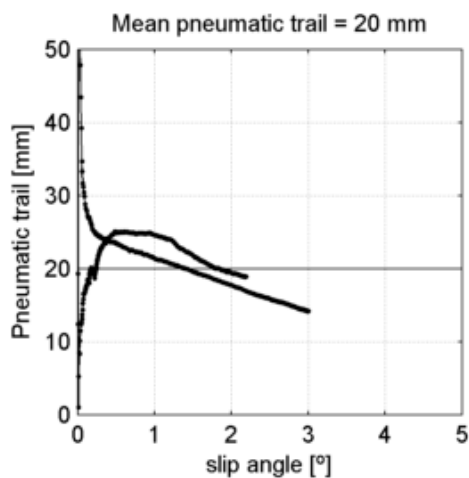
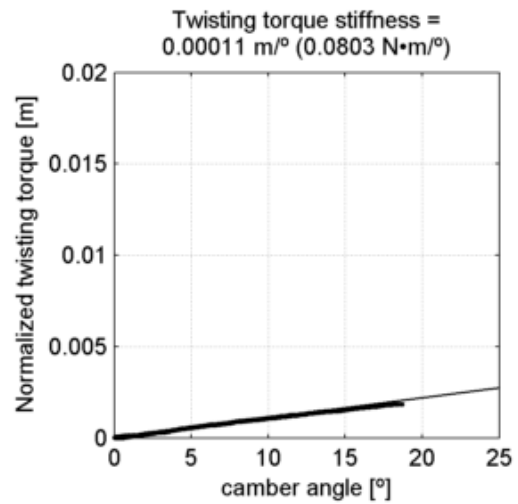
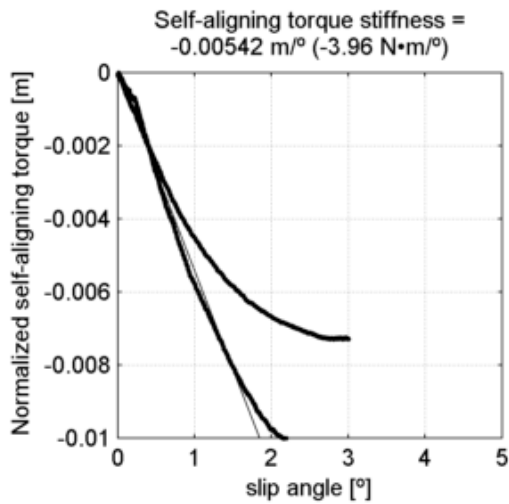
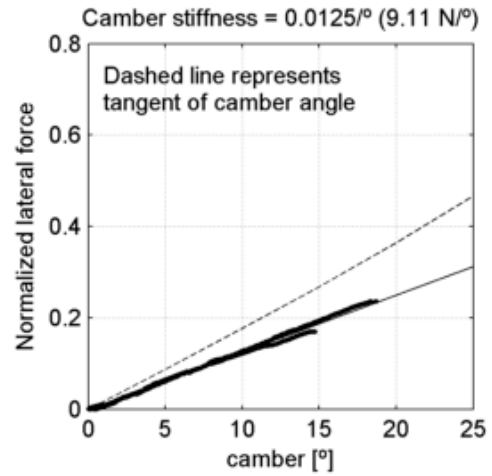
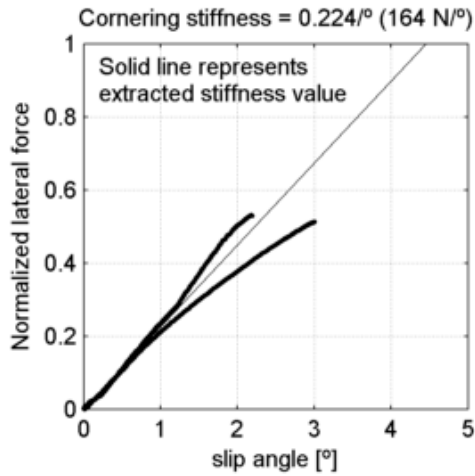
Vittoria Randonneur Hyper 37-622
 tire radius = 17.5 mm, rim width = 18.7 mm

at 4.83 bar (70 psi) and
 under 540 N (55 kg, 121 lb)



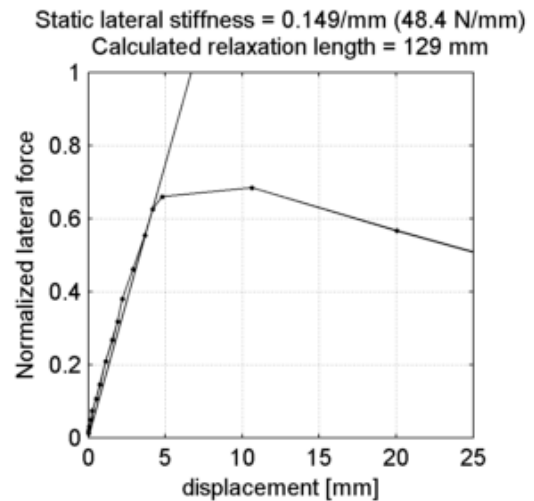
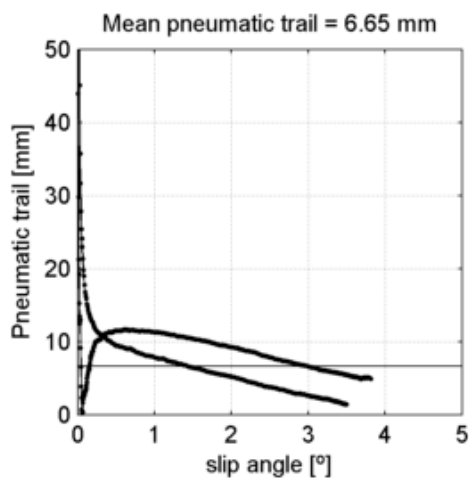
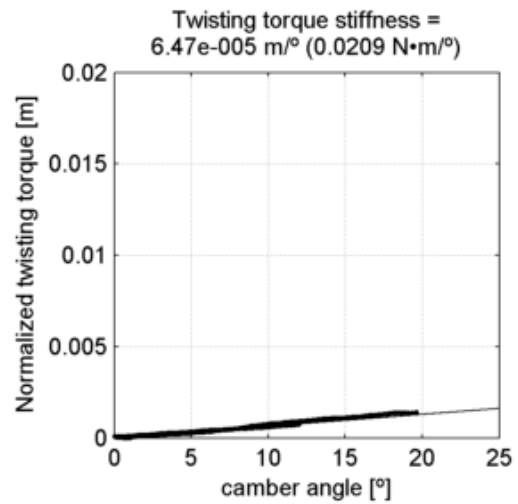
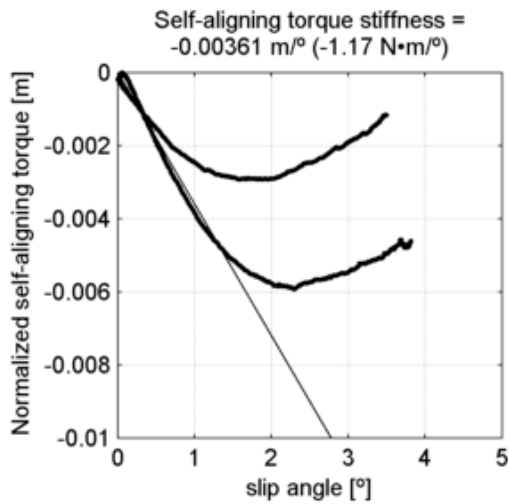
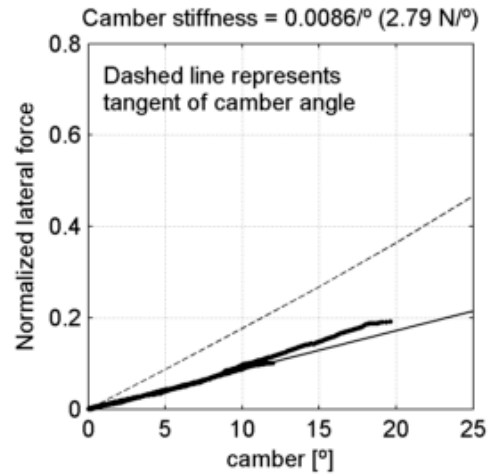
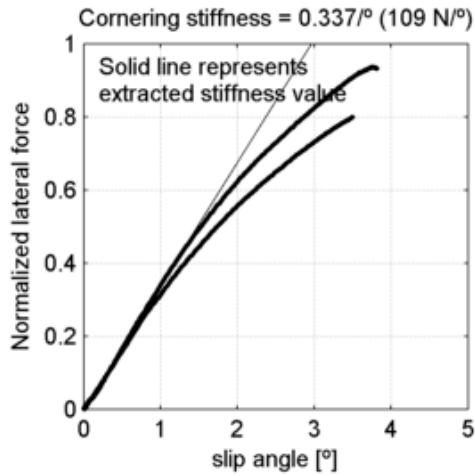
Vittoria Randonneur Hyper 37-622
 tire radius = 17.5 mm, rim width = 18.7 mm

at 4.83 bar (70 psi) and
 under 731 N (74.5 kg, 164 lb)



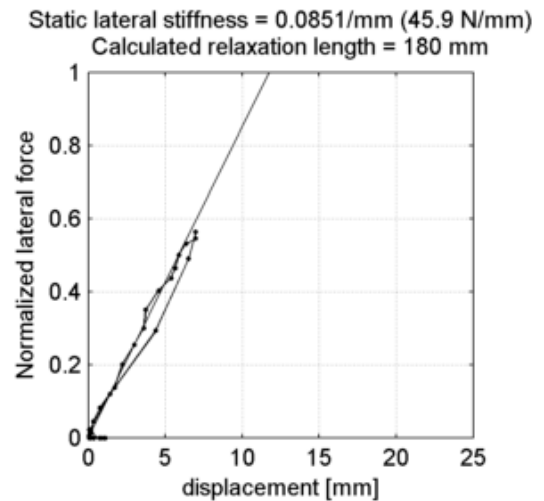
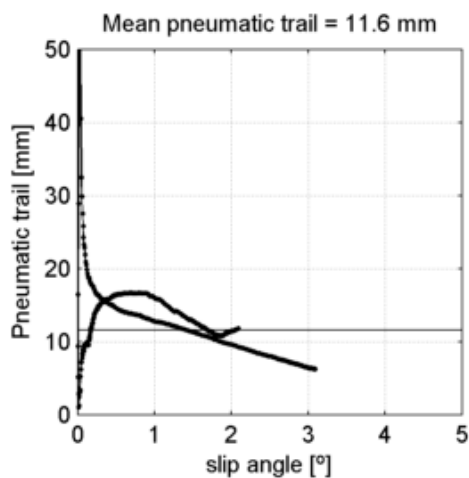
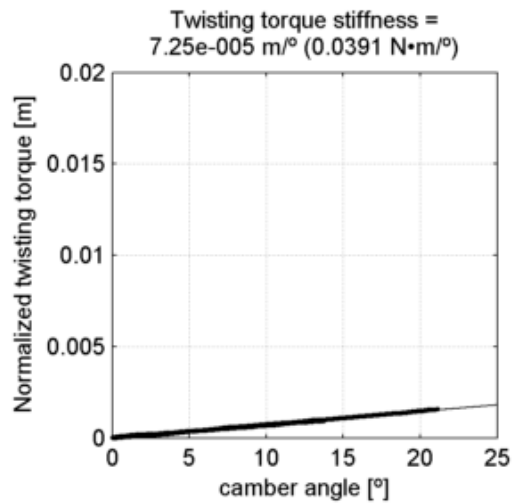
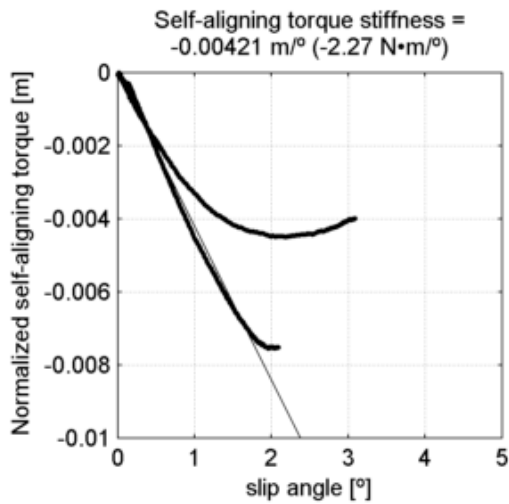
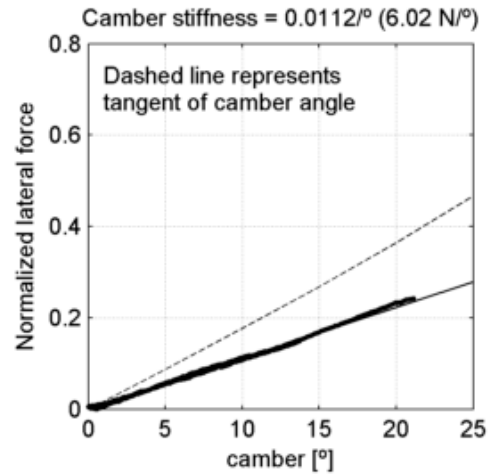
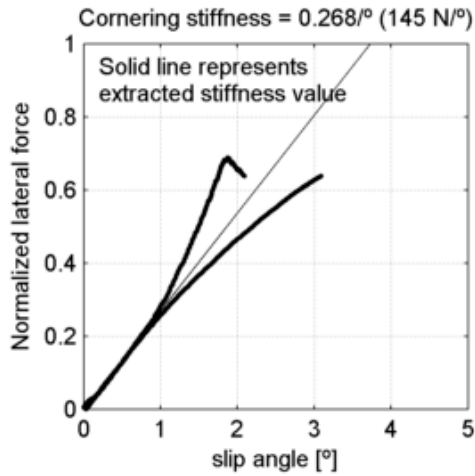
Vittoria Randonneur Hyper 37-622
 tire radius = 17.5 mm, rim width = 18.7 mm

at 6.21 bar (90 psi) and
 under 324 N (33 kg, 72.8 lb)



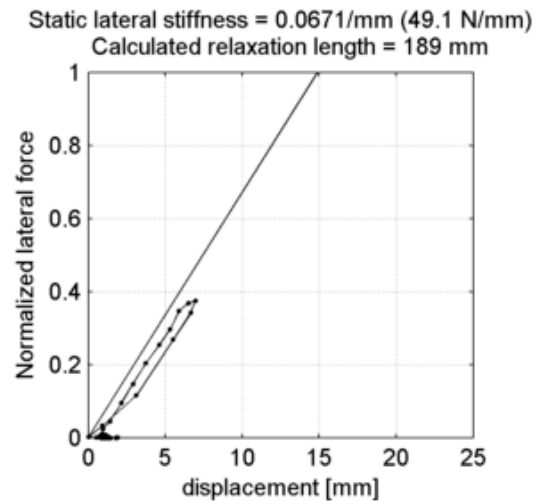
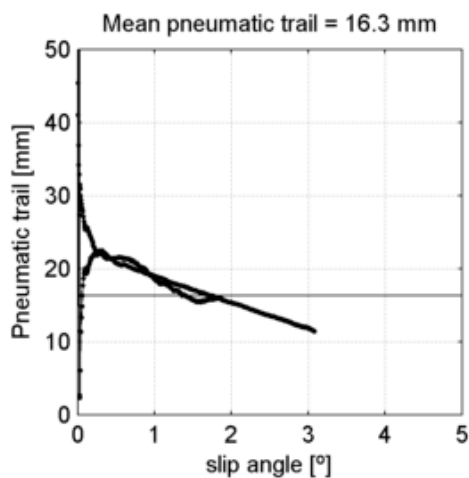
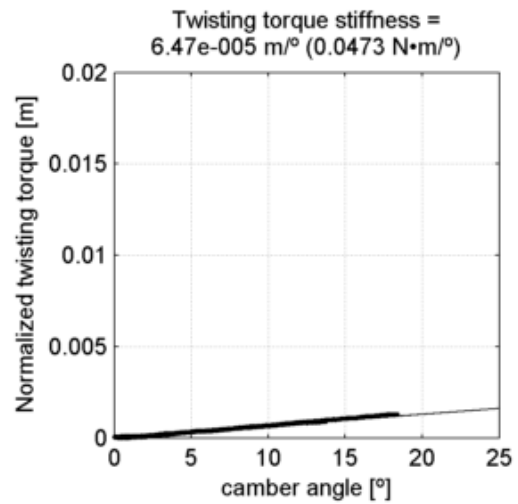
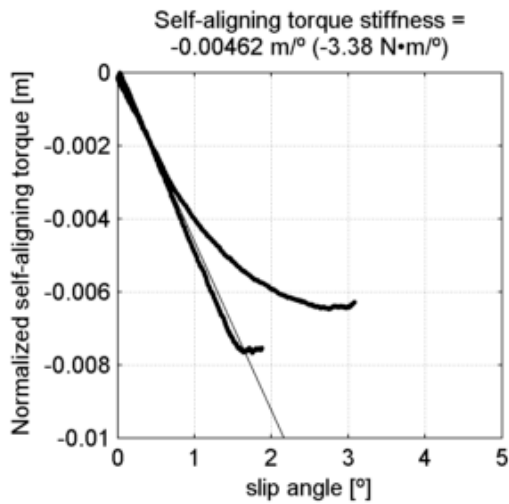
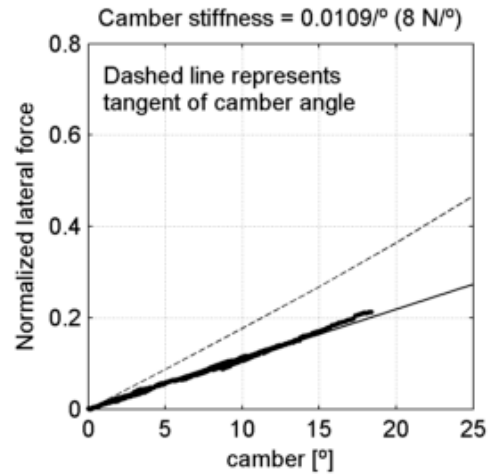
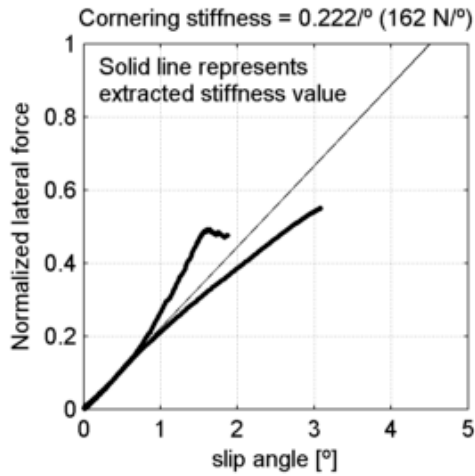
Vittoria Randonneur Hyper 37-622
 tire radius = 17.5 mm, rim width = 18.7 mm

at 6.21 bar (90 psi) and
 under 540 N (55 kg, 121 lb)



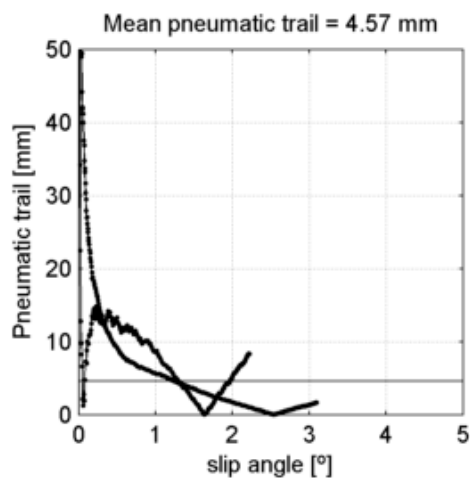
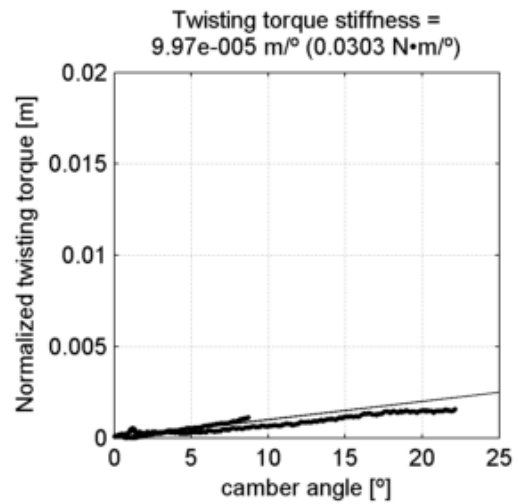
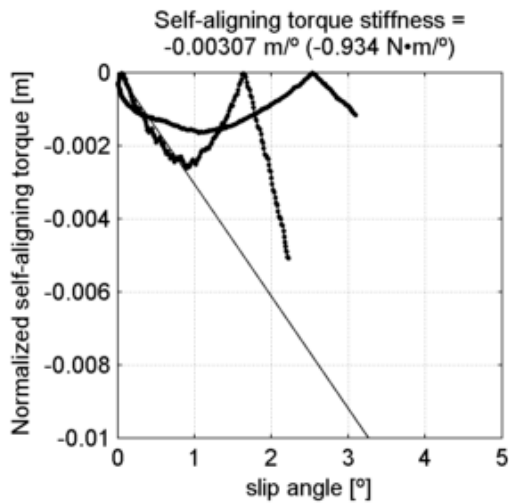
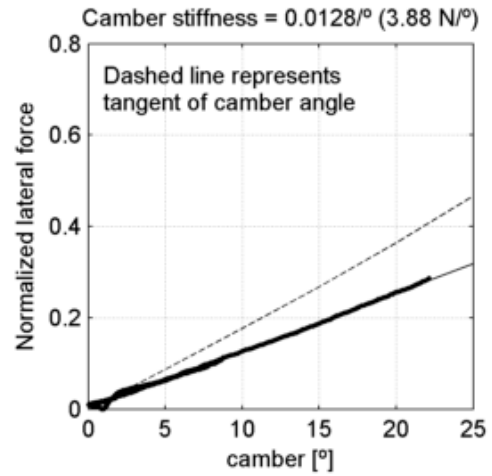
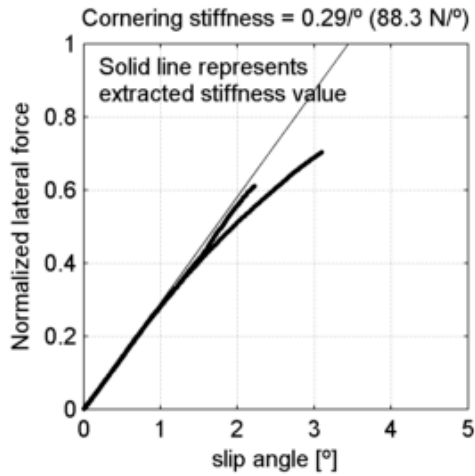
Vittoria Randonneur Hyper 37-622
 tire radius = 17.5 mm, rim width = 18.7 mm

at 6.21 bar (90 psi) and
 under 731 N (74.5 kg, 164 lb)



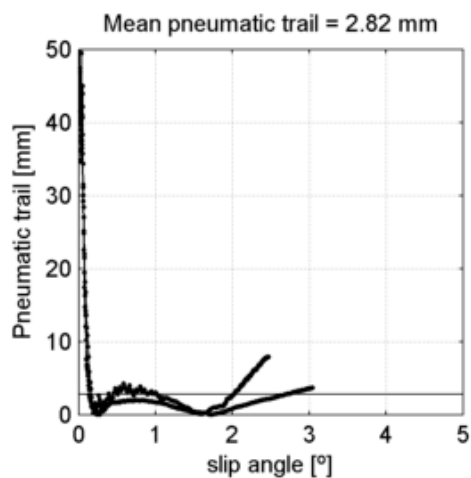
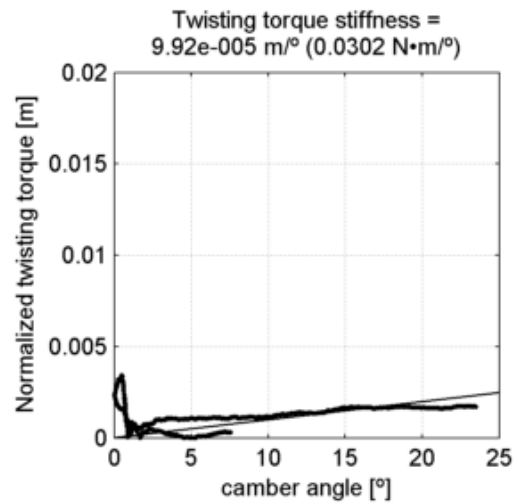
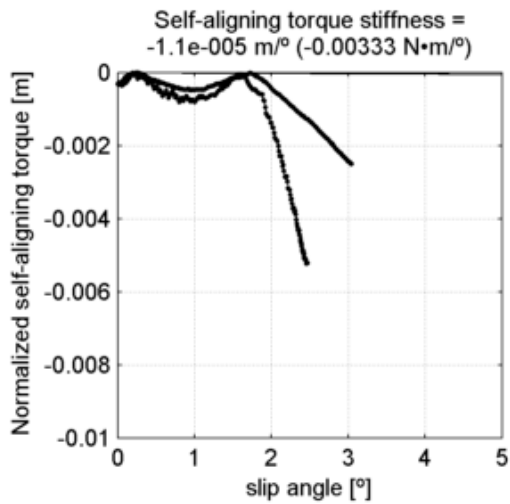
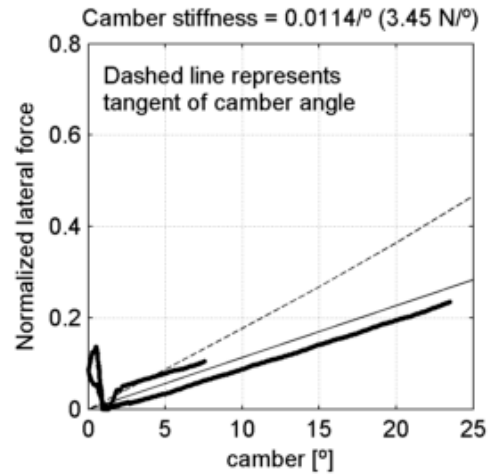
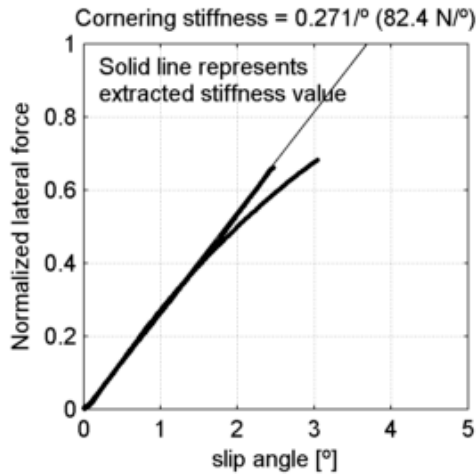
Vredestein Fortezza DuoComp 23-622
 tire radius = 11.5 mm, rim width = 13.4 mm

at 5.52 bar (80 psi) and
 under 304 N (31 kg, 68.3 lb)



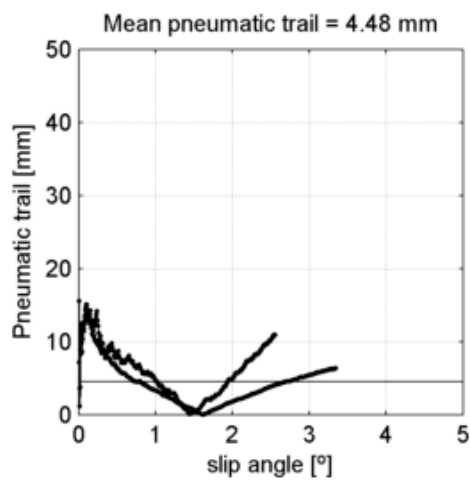
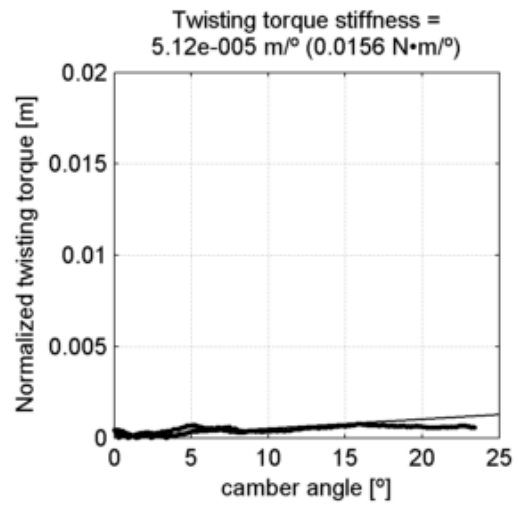
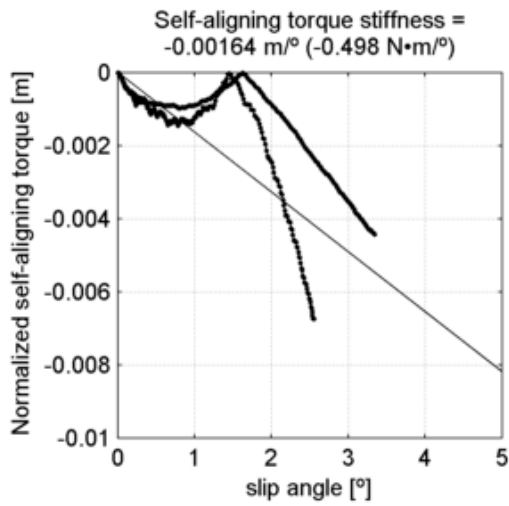
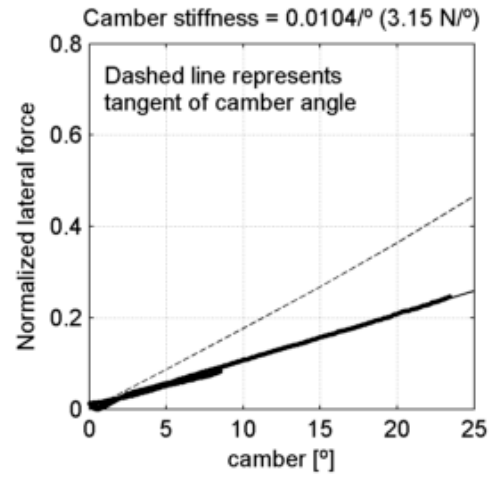
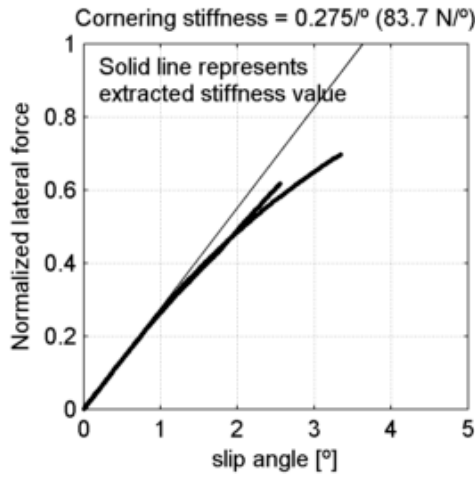
Vredestein Fortezza DuoComp 23-622
 tire radius = 11.5 mm, rim width = 13.4 mm

at 8.27 bar (120 psi) and
 under 304 N (31 kg, 68.3 lb)



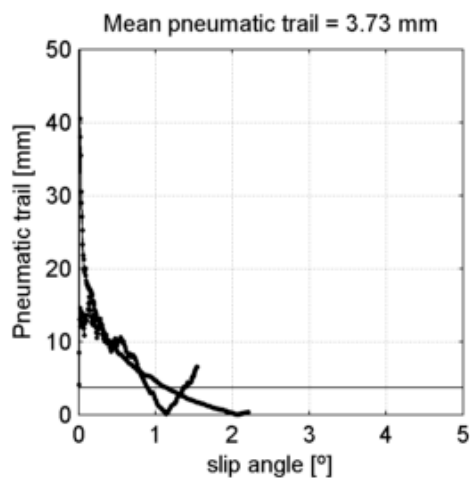
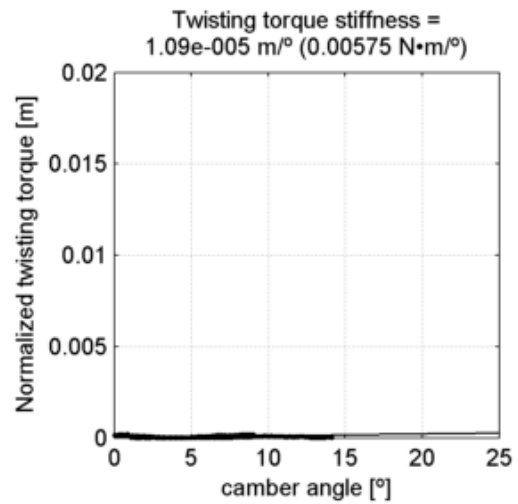
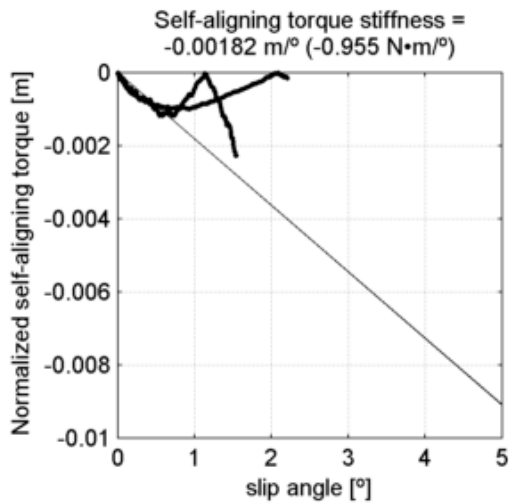
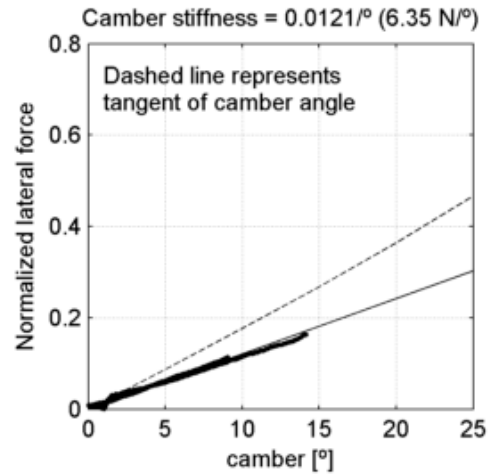
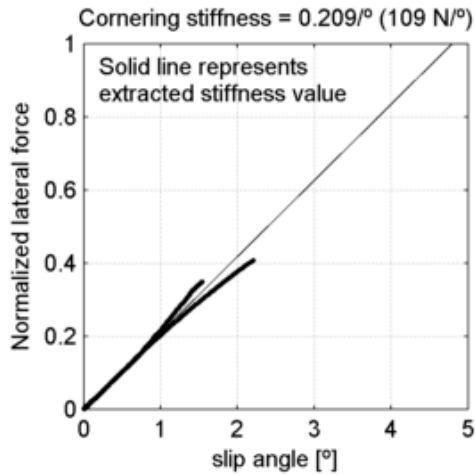
Vredestein Fortezza DuoComp 23-622
 tire radius = 11.5 mm, rim width = 13.4 mm

at 11 bar (160 psi) and
 under 304 N (31 kg, 68.3 lb)



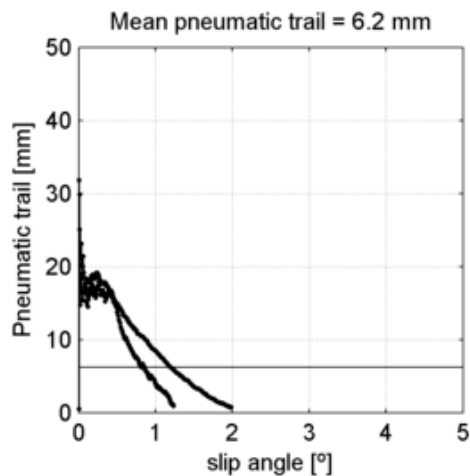
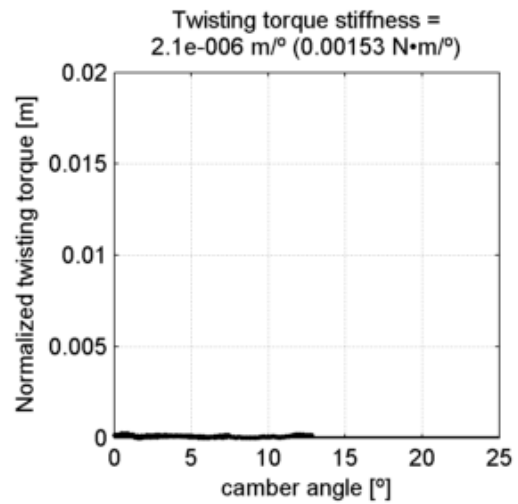
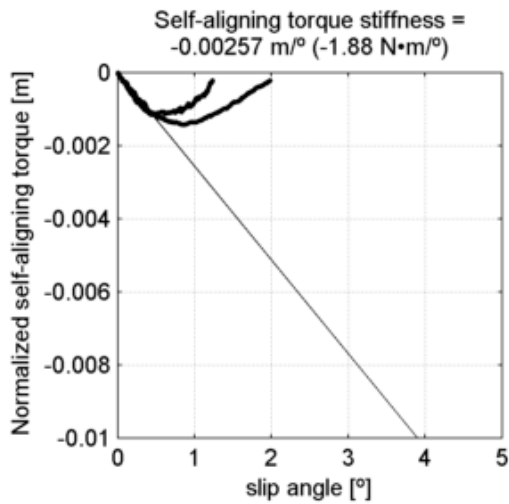
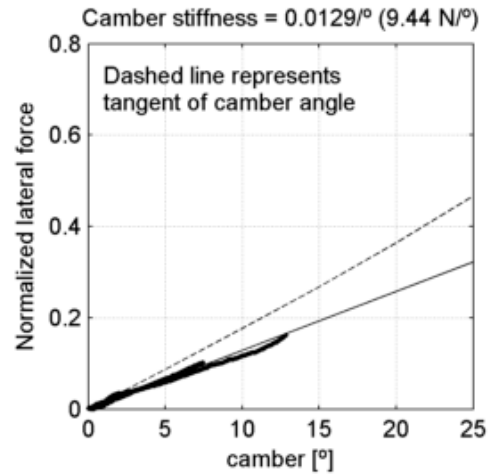
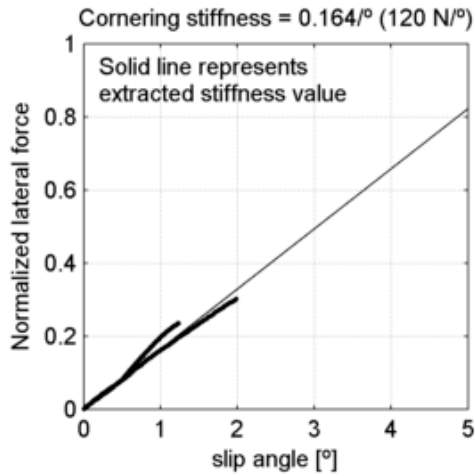
Vredestein Fortezza DuoComp 23-622
 tire radius = 11.5 mm, rim width = 13.4 mm

at 11 bar (160 psi) and
 under 525 N (53.5 kg, 118 lb)



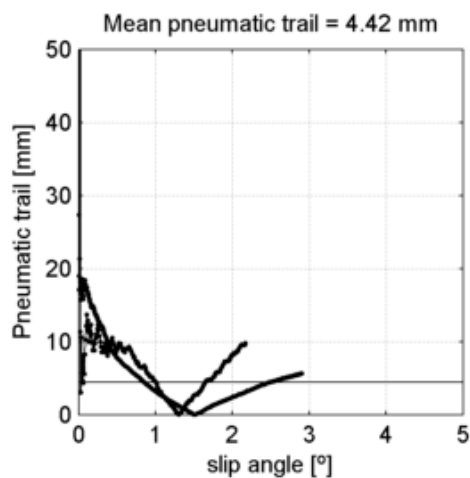
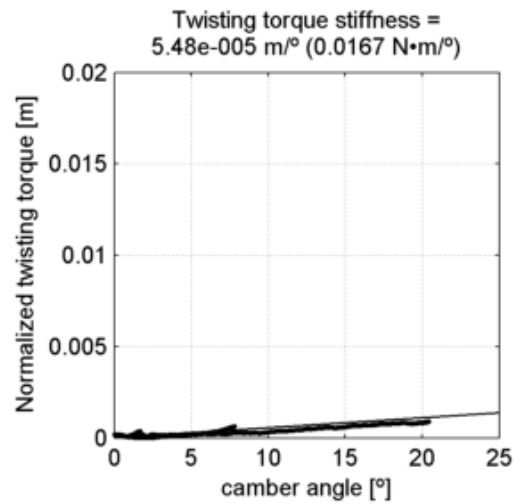
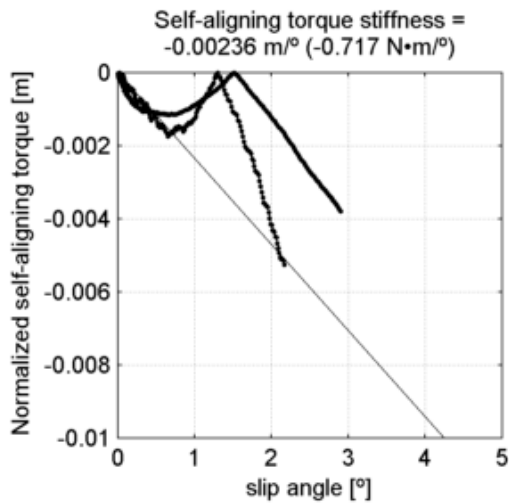
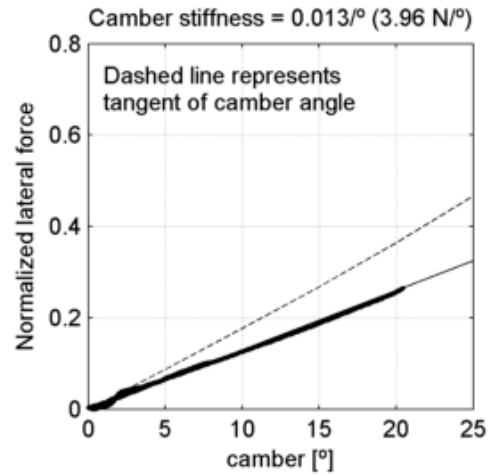
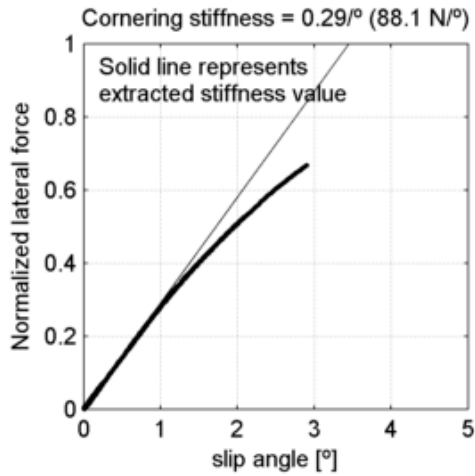
Vredestein Fortezza DuoComp 23-622
 tire radius = 11.5 mm, rim width = 13.4 mm

at 11 bar (160 psi) and
 under 731 N (74.5 kg, 164 lb)



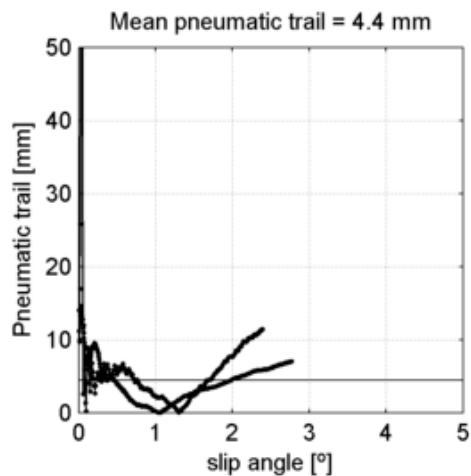
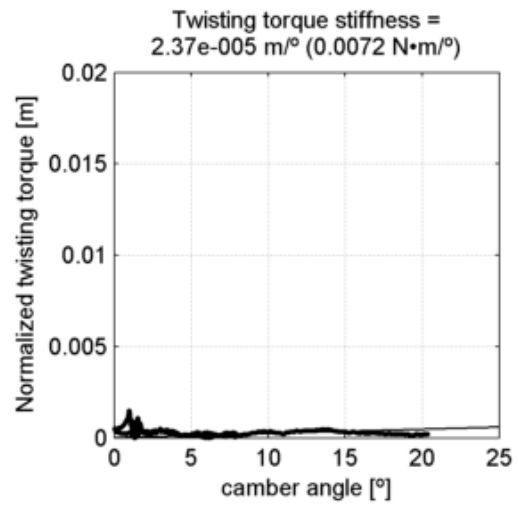
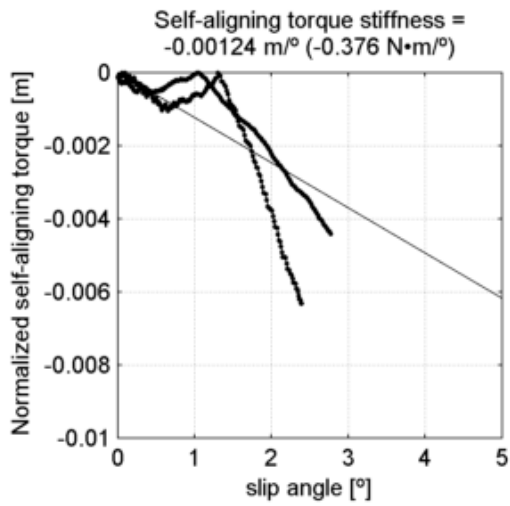
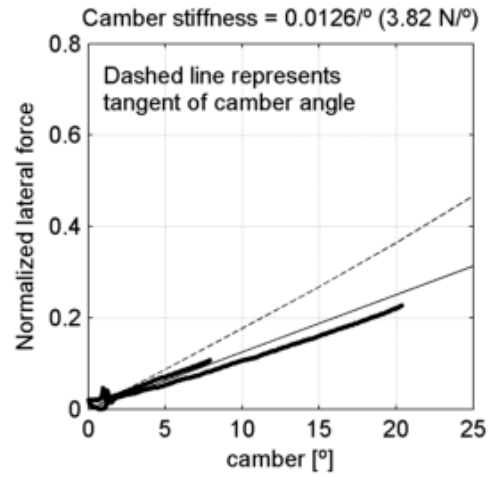
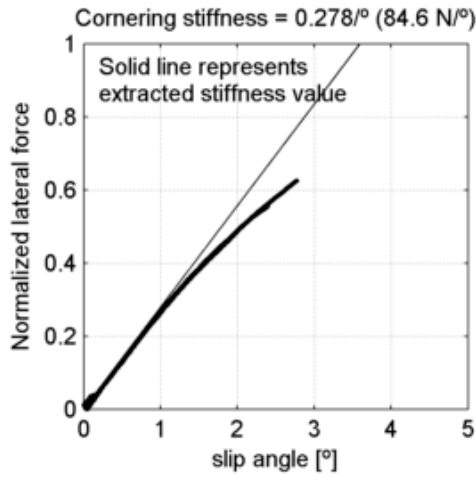
Vredestein Fortezza TriComp 23-622
 tire radius = 11.5 mm, rim width = 13.4 mm

at 5.52 bar (80 psi) and
 under 304 N (31 kg, 68.3 lb)



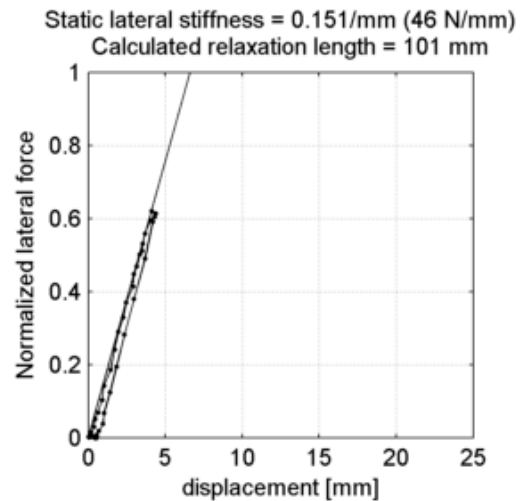
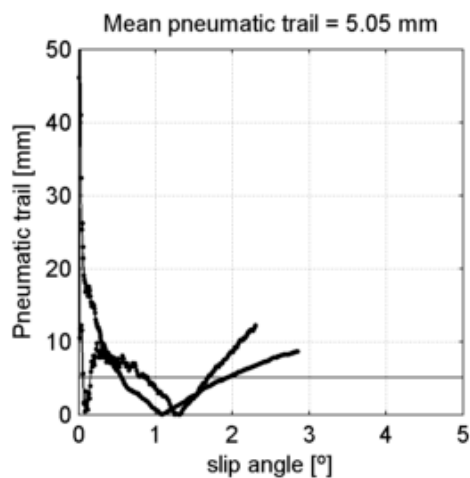
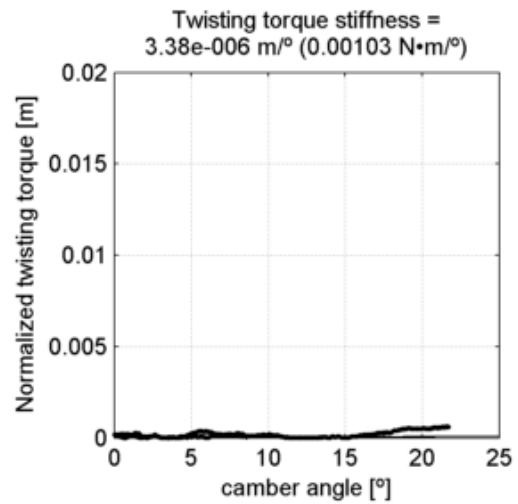
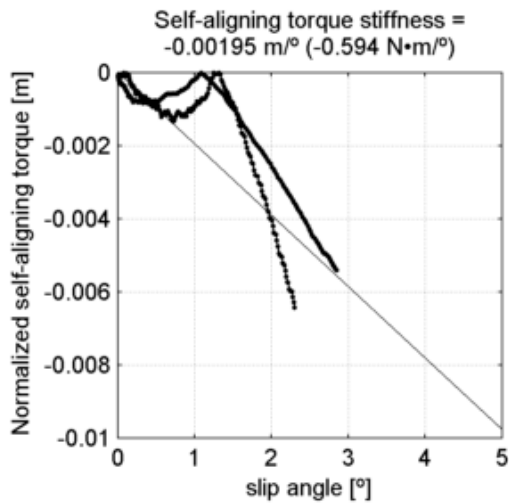
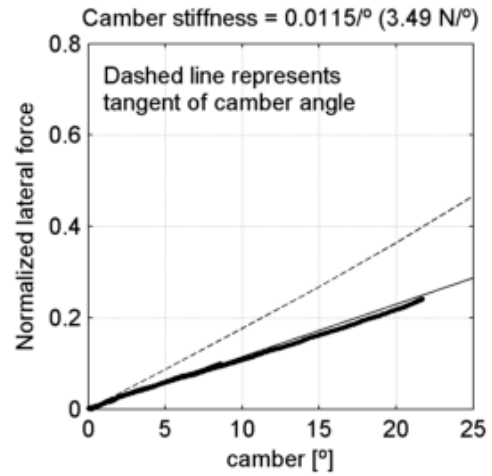
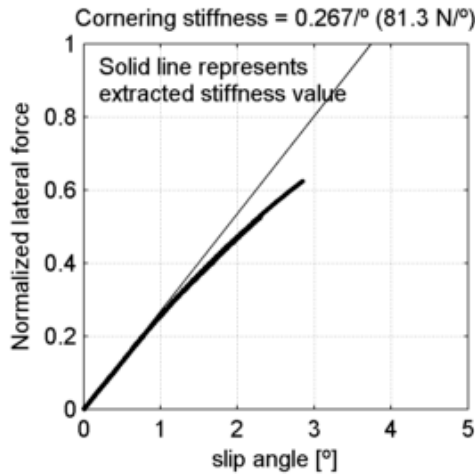
Vredestein Fortezza TriComp 23-622
 tire radius = 11.5 mm, rim width = 13.4 mm

at 8.27 bar (120 psi) and
 under 304 N (31 kg, 68.3 lb)



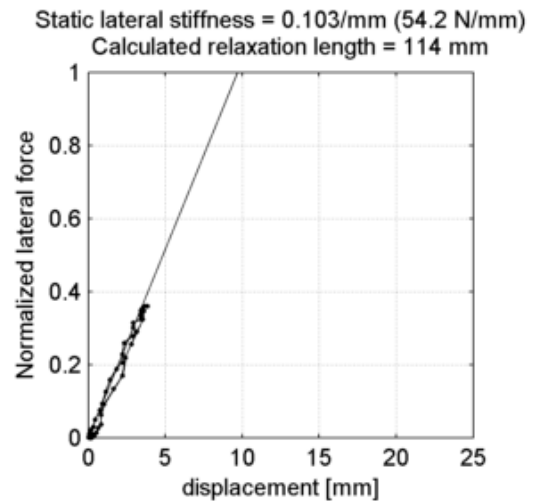
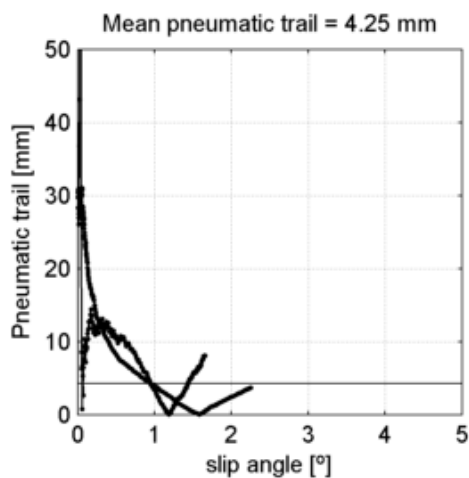
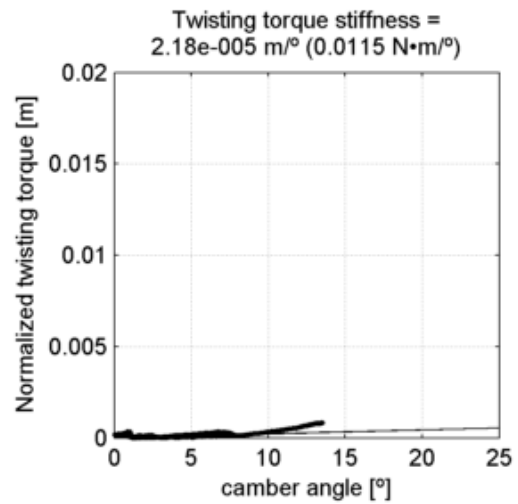
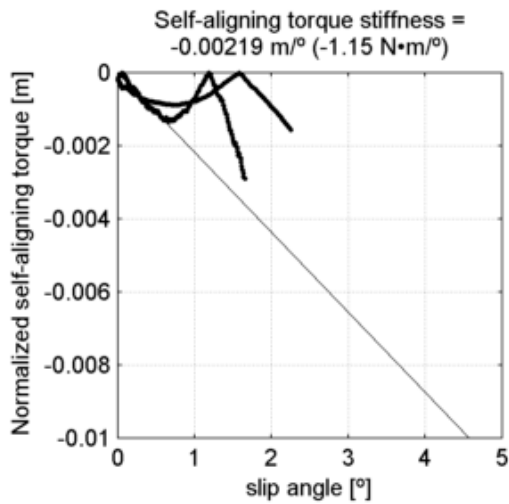
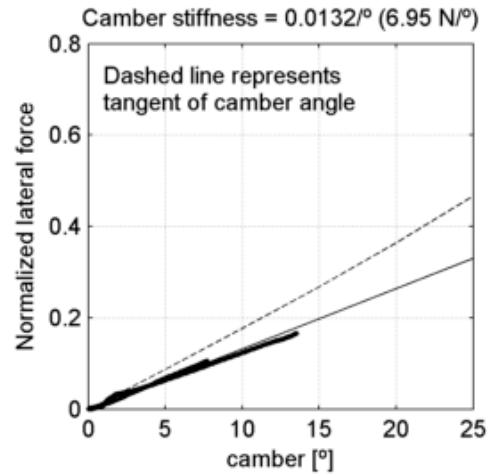
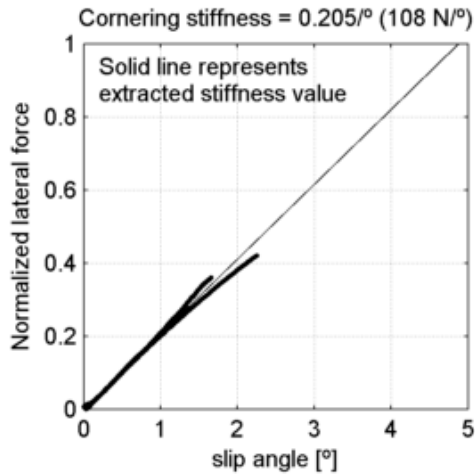
Vredestein Fortezza TriComp 23-622
 tire radius = 11.5 mm, rim width = 13.4 mm

at 11 bar (160 psi) and
 under 304 N (31 kg, 68.3 lb)



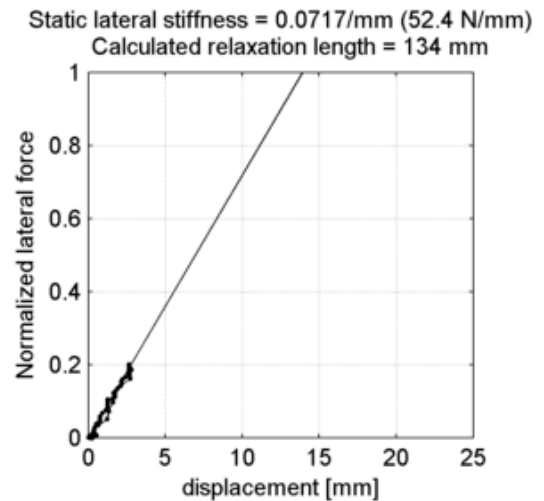
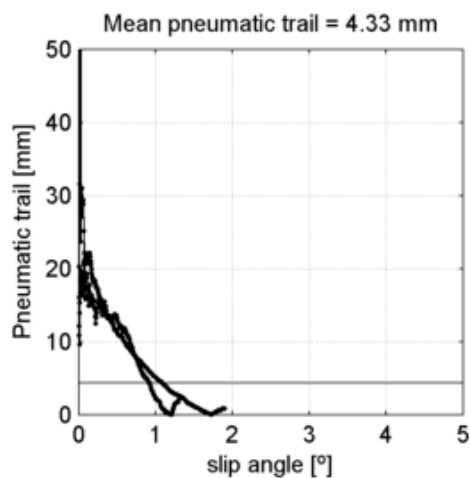
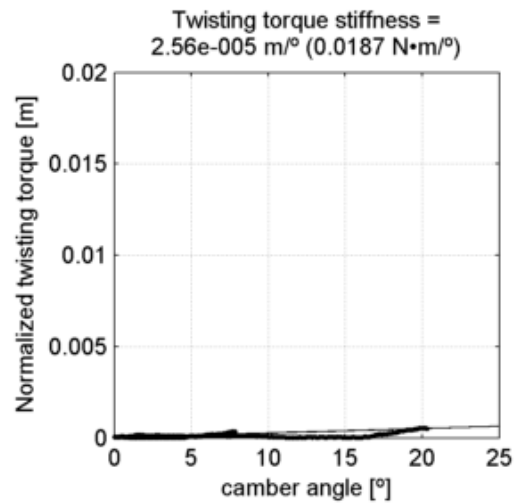
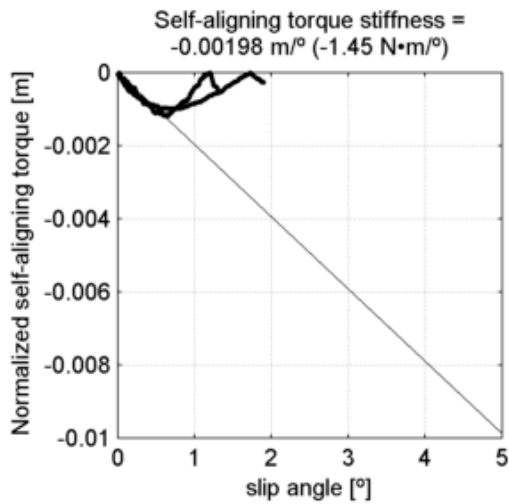
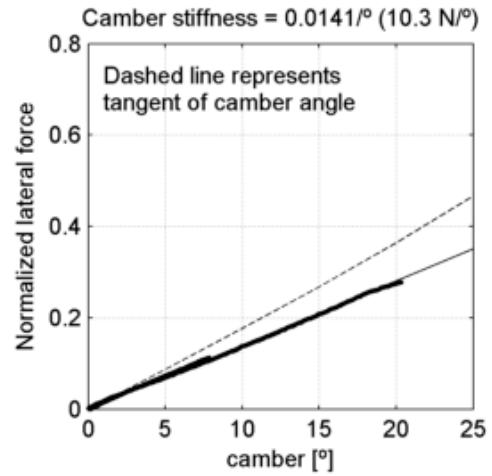
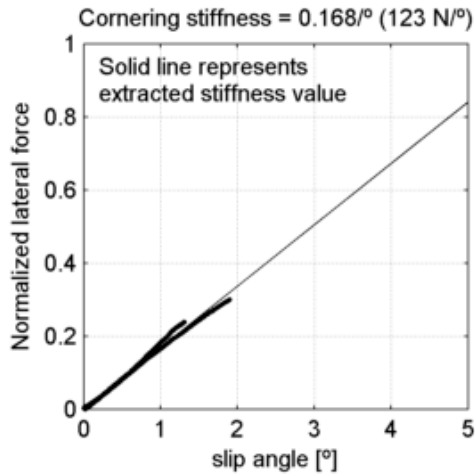
Vredestein Fortezza TriComp 23-622
 tire radius = 11.5 mm, rim width = 13.4 mm

at 11 bar (160 psi) and
 under 525 N (53.5 kg, 118 lb)



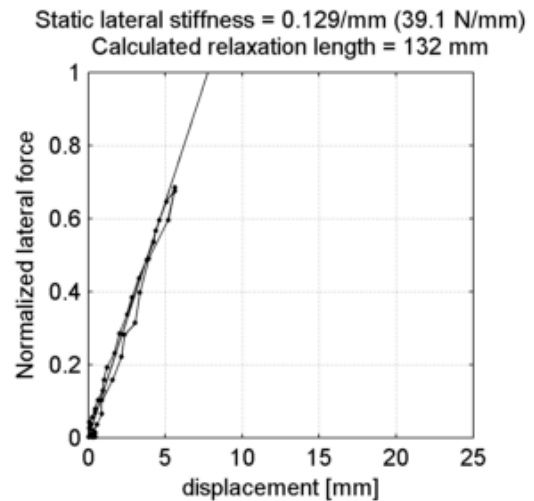
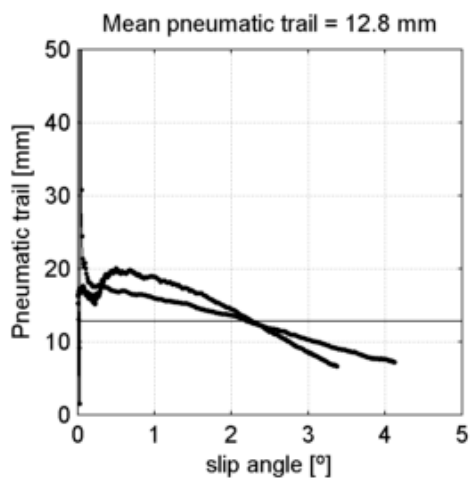
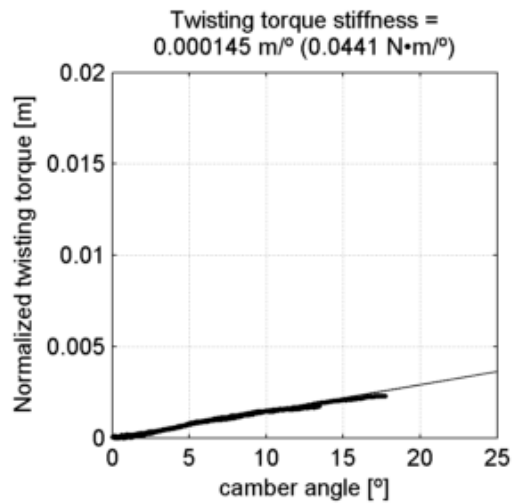
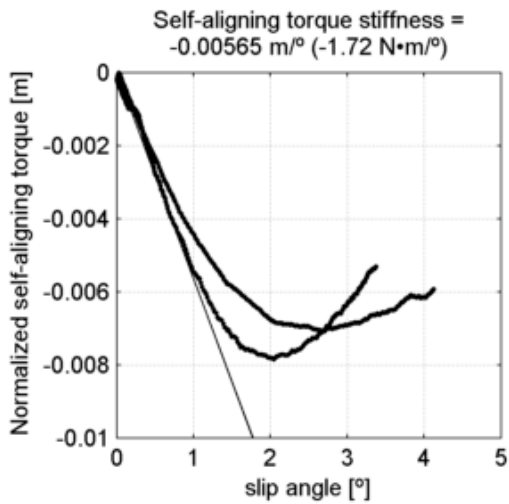
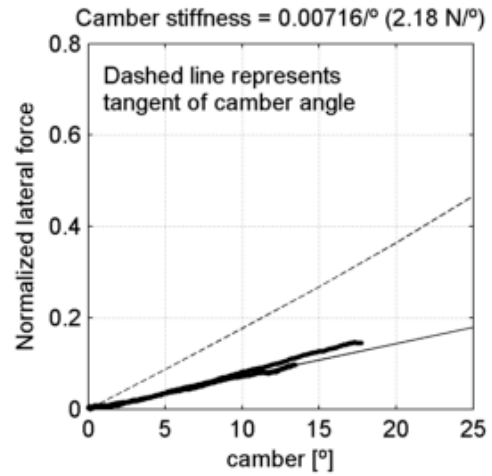
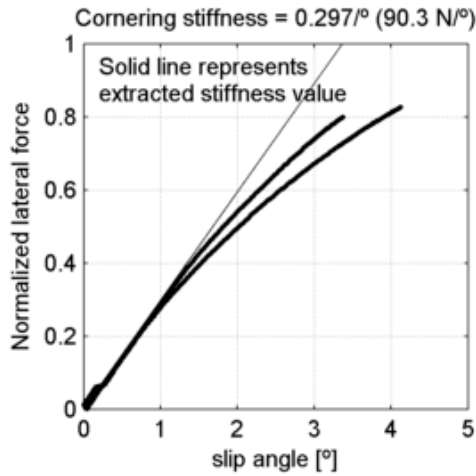
Vredestein Fortezza TriComp 23-622
 tire radius = 11.5 mm, rim width = 13.4 mm

at 11 bar (160 psi) and
 under 731 N (74.5 kg, 164 lb)



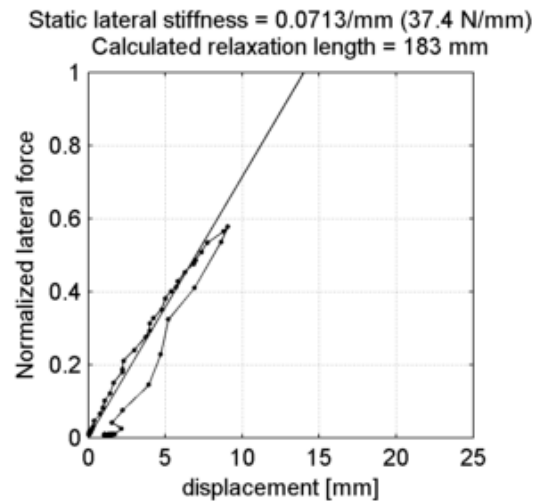
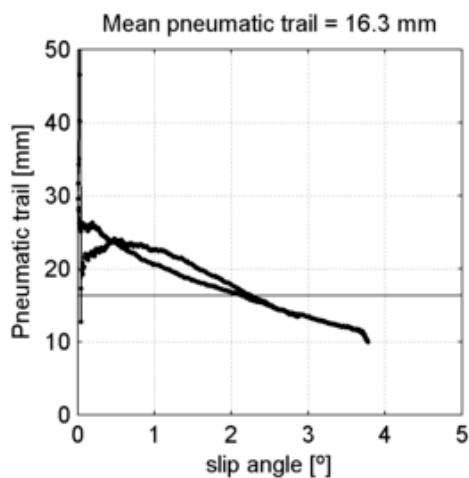
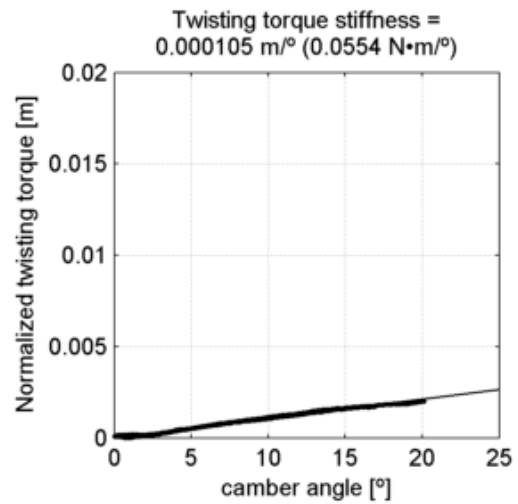
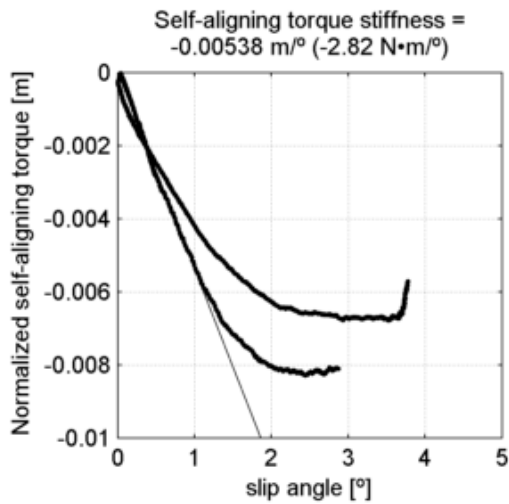
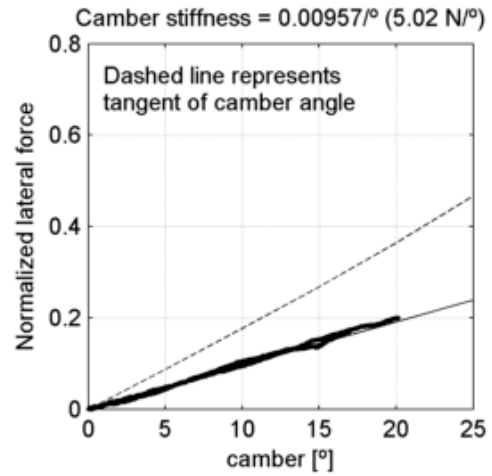
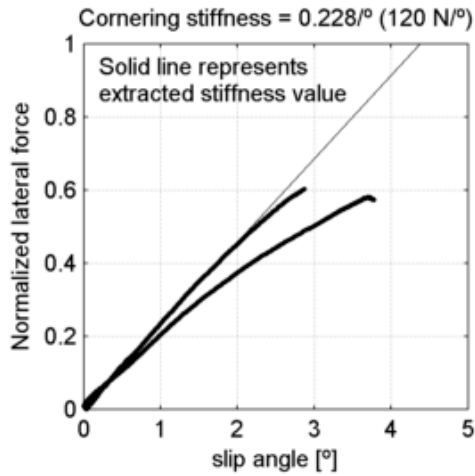
Vredestein Perfect Tour 37-622
 tire radius = 16.8 mm, rim width = 18.7 mm

at 3.45 bar (50 psi) and
 under 304 N (31 kg, 68.3 lb)



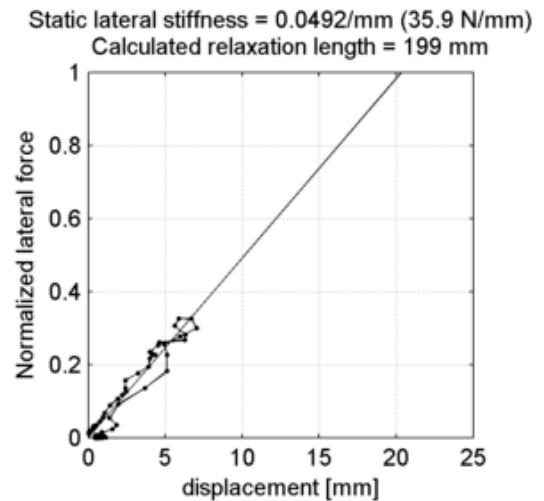
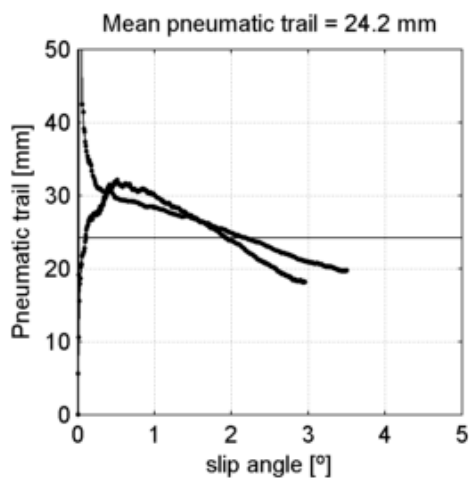
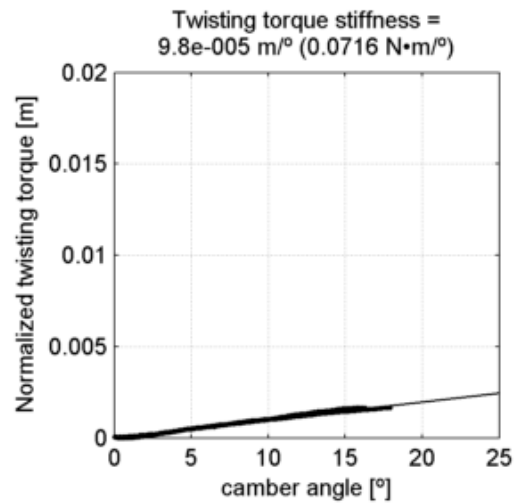
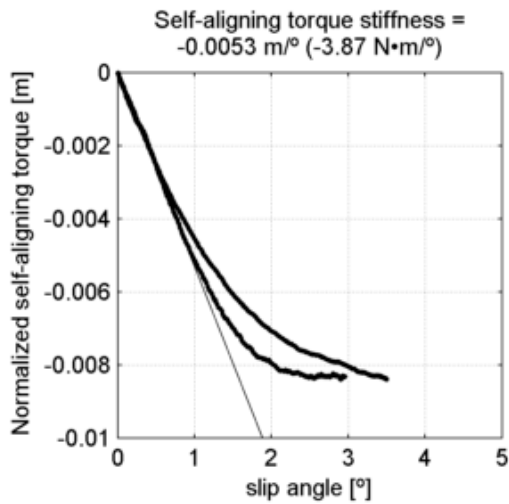
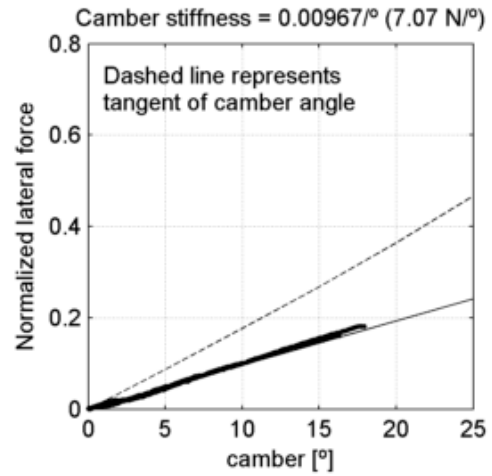
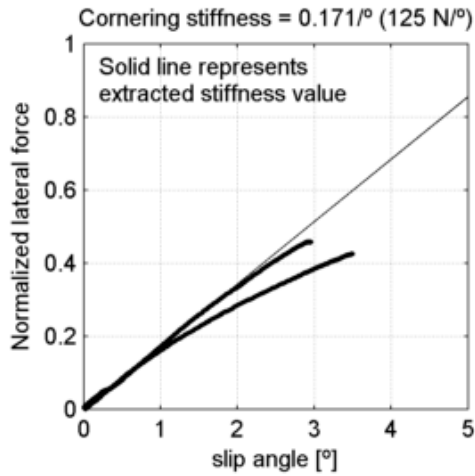
Vredestein Perfect Tour 37-622
 tire radius = 16.8 mm, rim width = 18.7 mm

at 3.45 bar (50 psi) and
 under 525 N (53.5 kg, 118 lb)



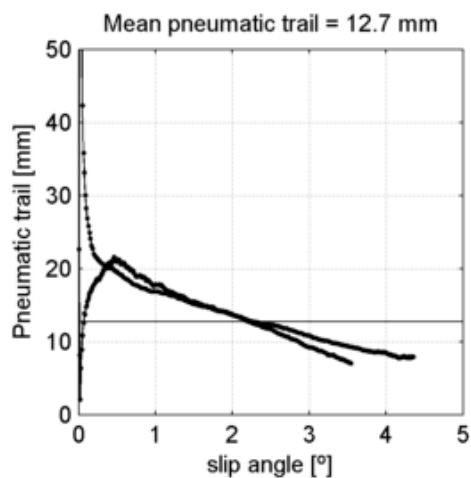
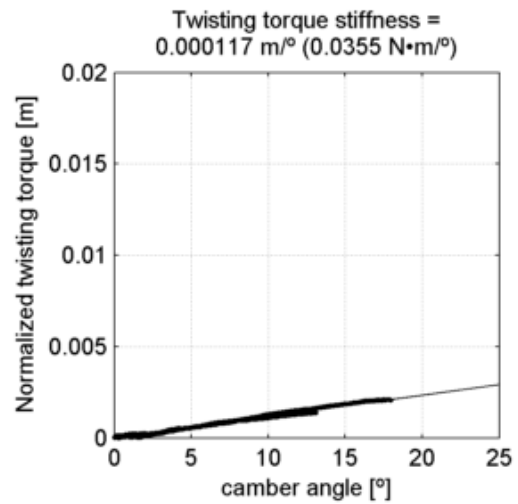
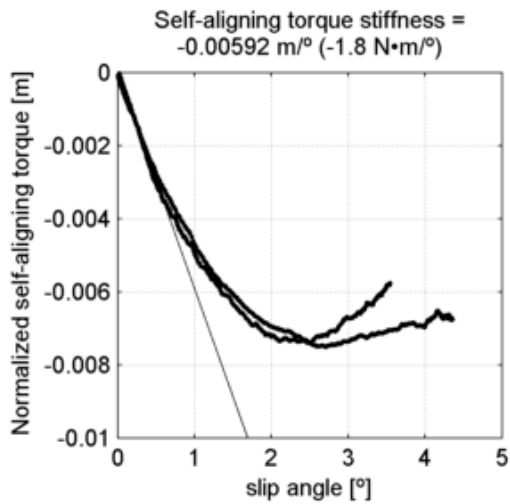
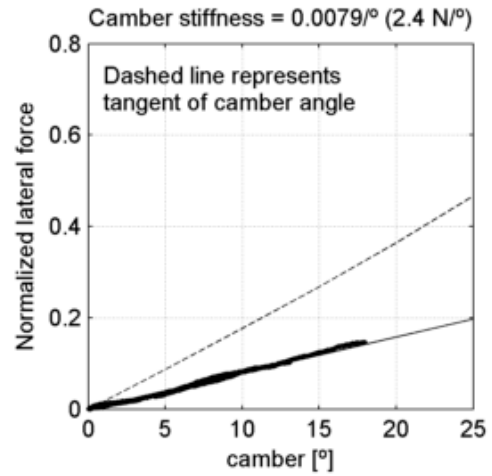
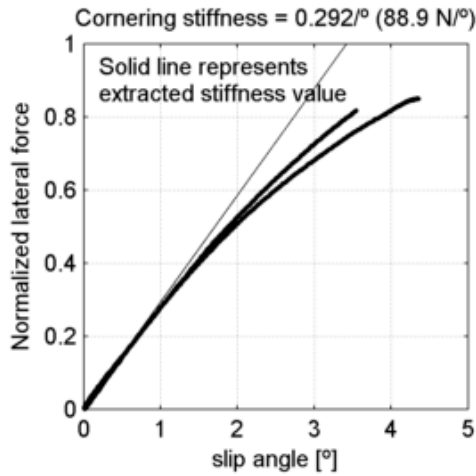
Vredestein Perfect Tour 37-622
 tire radius = 16.8 mm, rim width = 18.7 mm

at 3.45 bar (50 psi) and
 under 731 N (74.5 kg, 164 lb)



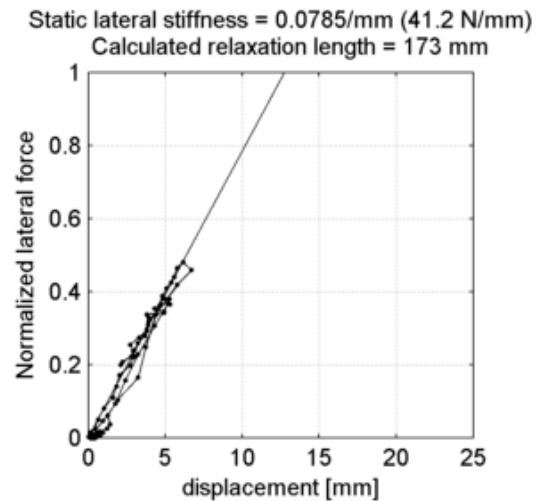
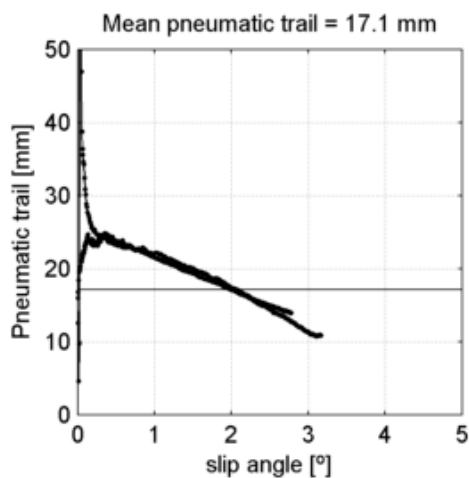
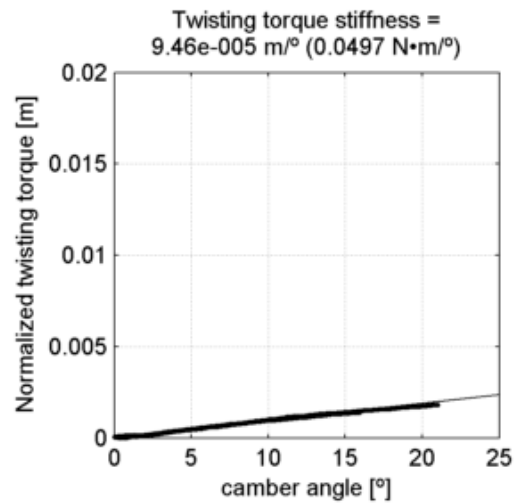
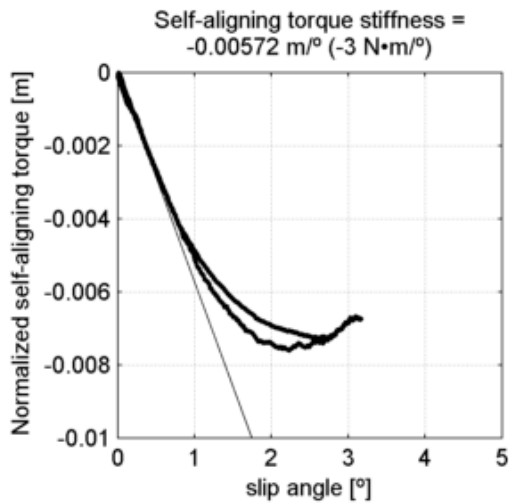
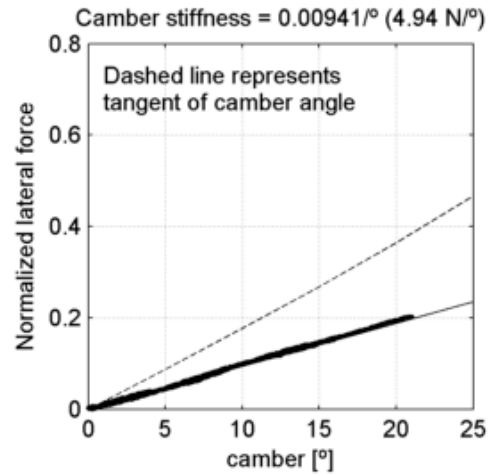
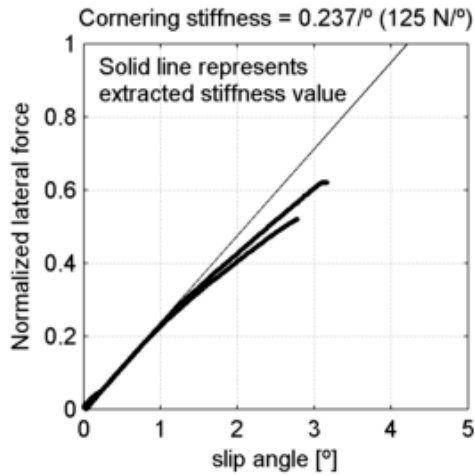
Vredestein Perfect Tour 37-622
 tire radius = 16.8 mm, rim width = 18.7 mm

at 4.14 bar (60 psi) and
 under 304 N (31 kg, 68.3 lb)



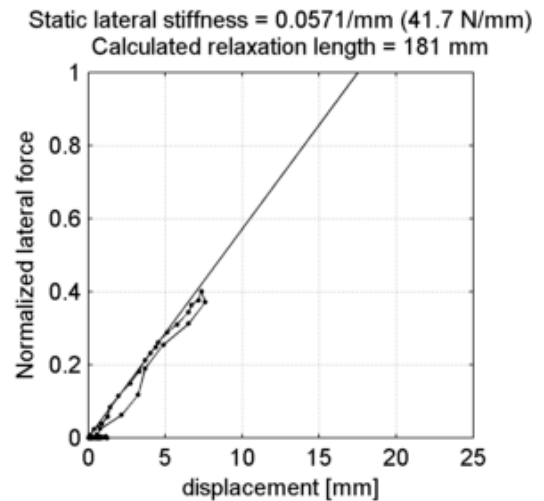
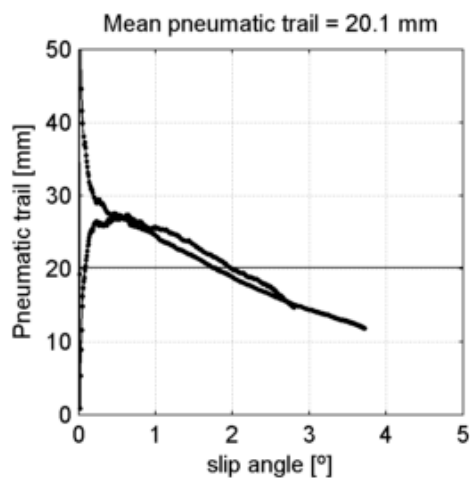
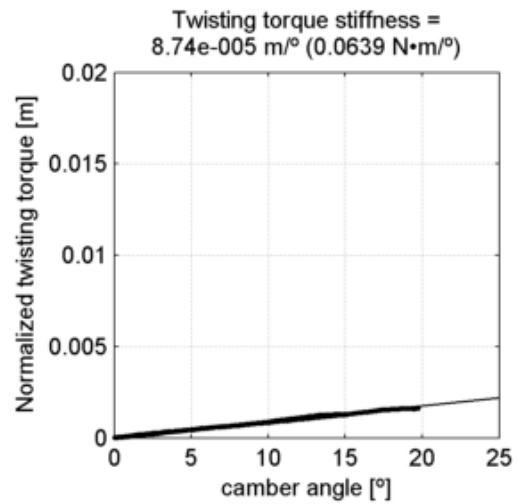
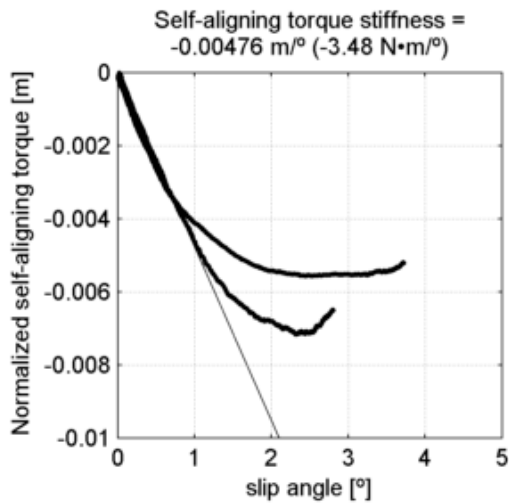
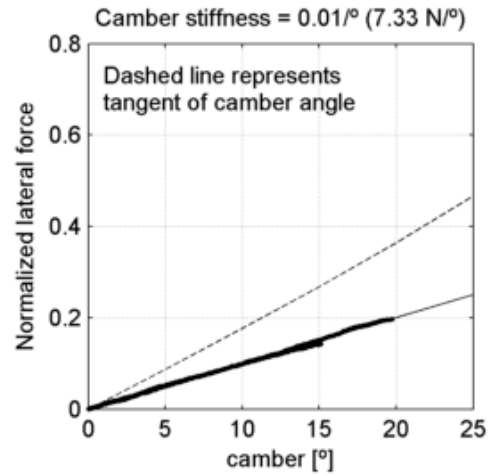
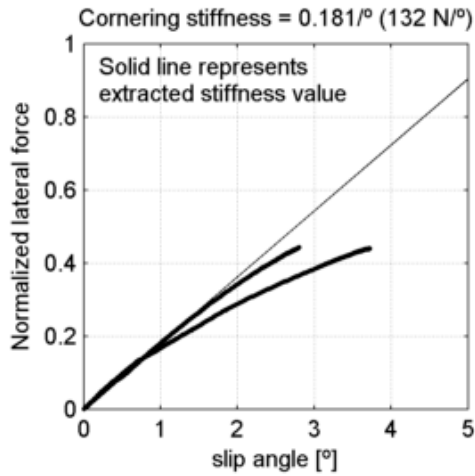
Vredestein Perfect Tour 37-622
 tire radius = 16.8 mm, rim width = 18.7 mm

at 4.14 bar (60 psi) and
 under 525 N (53.5 kg, 118 lb)



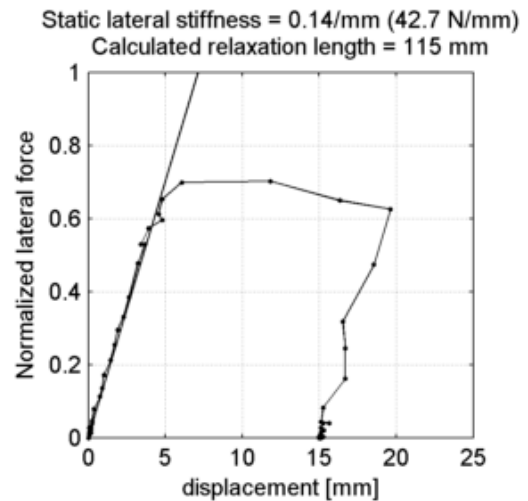
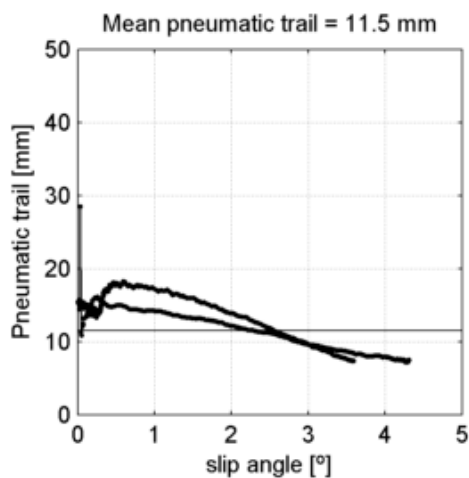
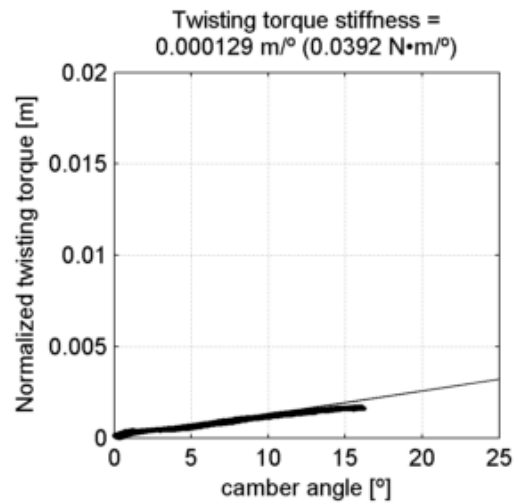
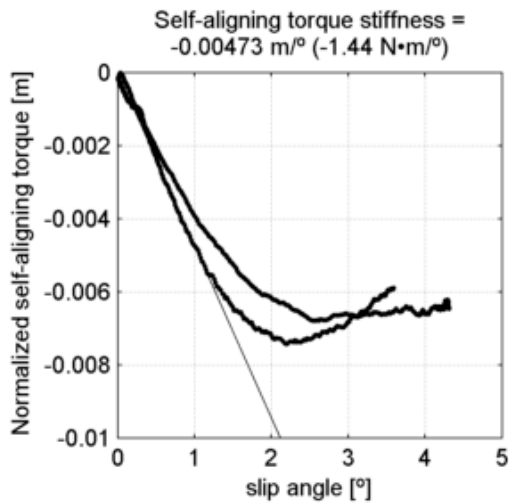
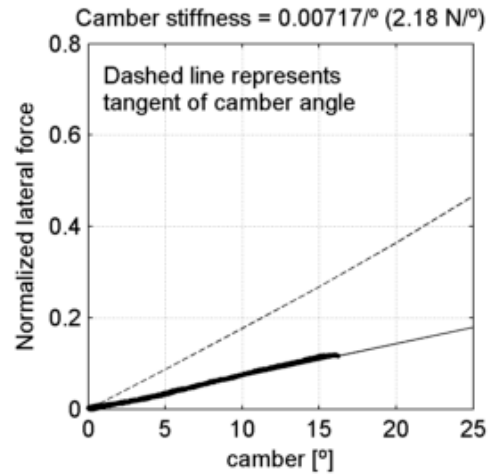
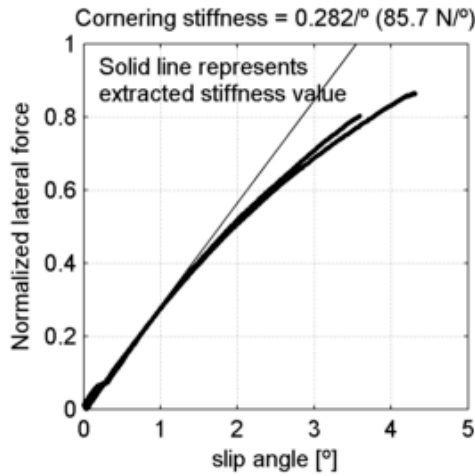
Vredestein Perfect Tour 37-622
 tire radius = 16.8 mm, rim width = 18.7 mm

at 4.14 bar (60 psi) and
 under 731 N (74.5 kg, 164 lb)



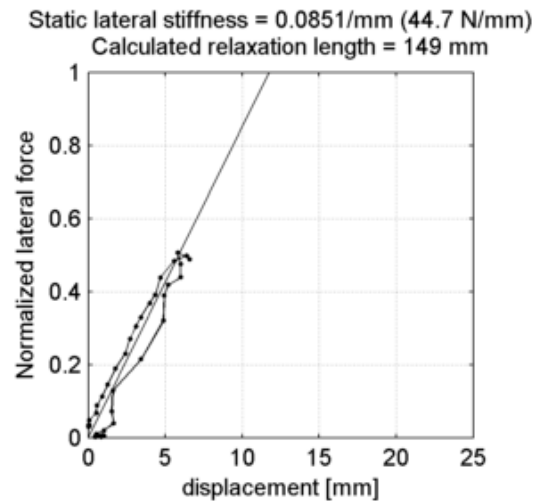
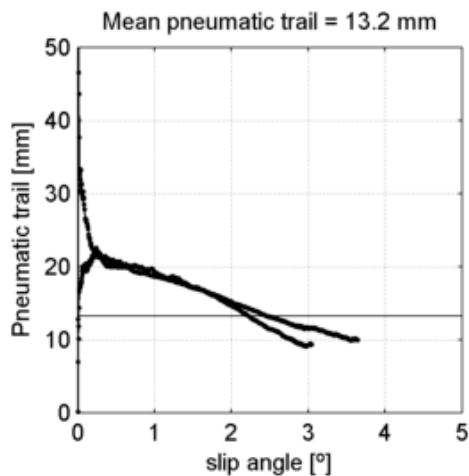
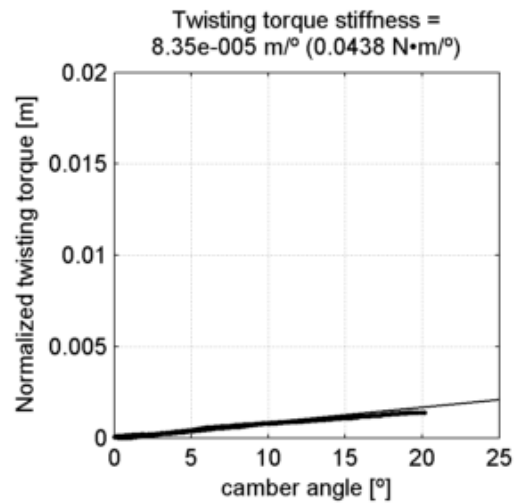
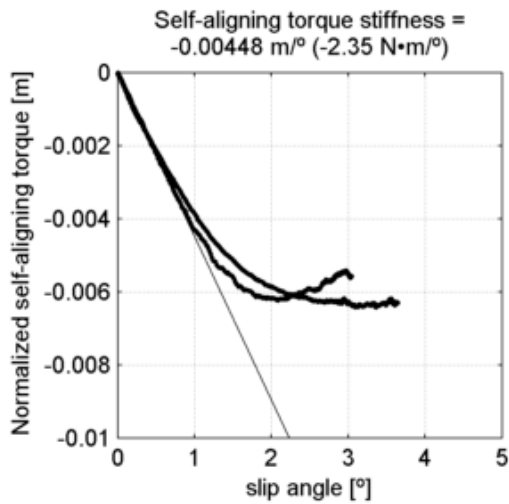
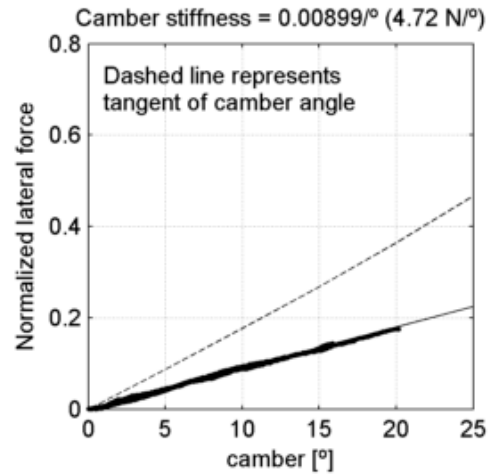
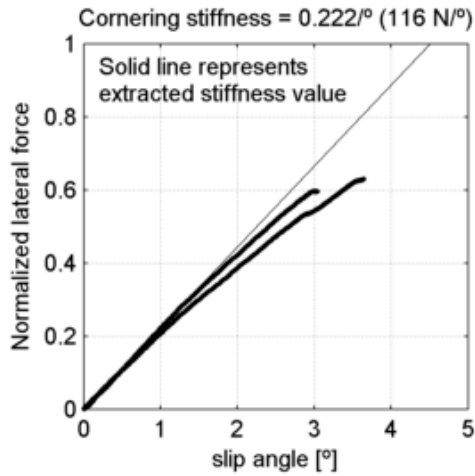
Vredestein Perfect Tour 37-622
 tire radius = 16.8 mm, rim width = 18.7 mm

at 4.83 bar (70 psi) and
 under 304 N (31 kg, 68.3 lb)



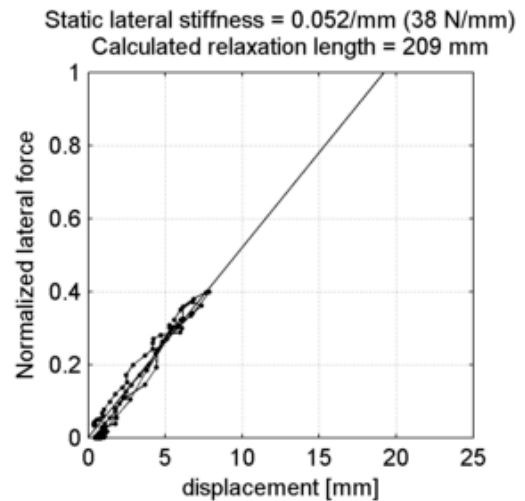
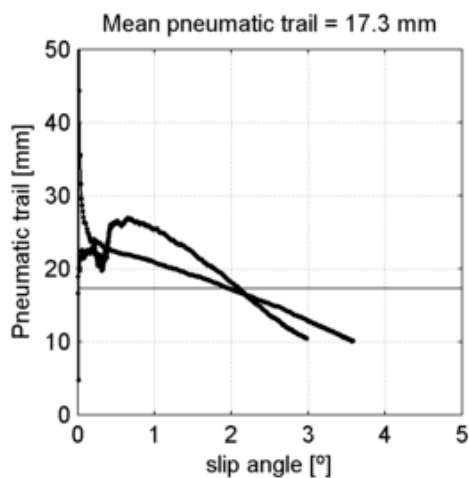
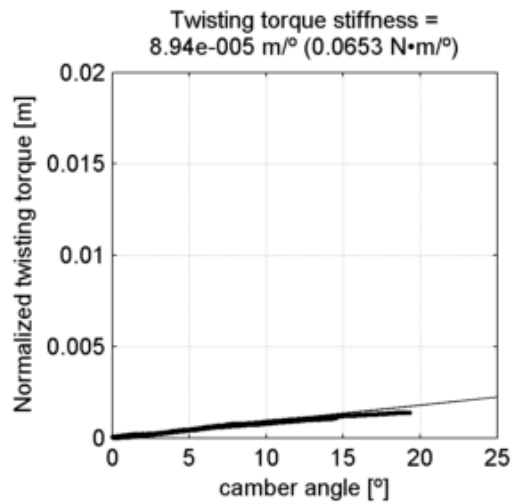
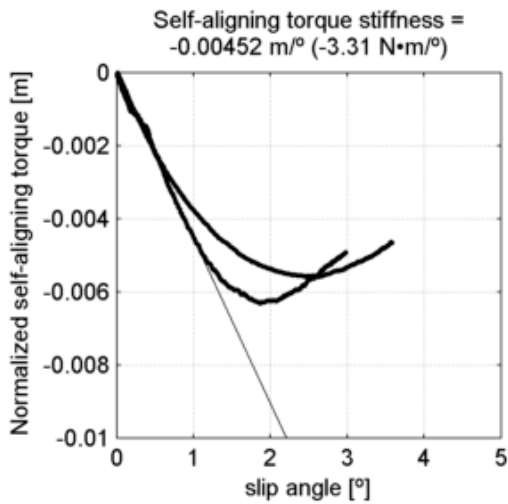
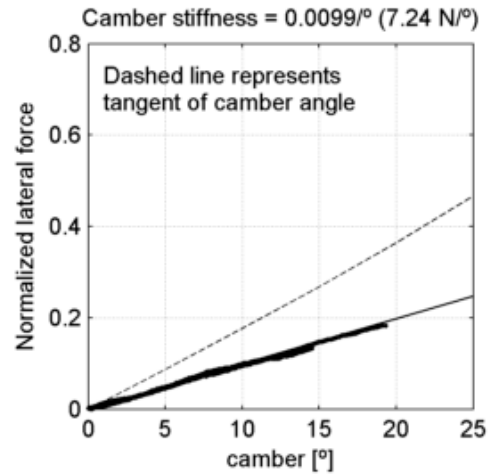
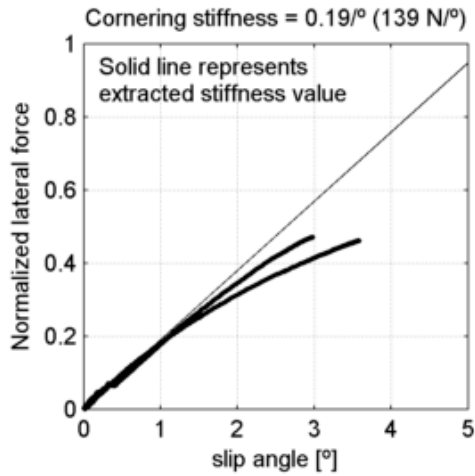
Vredestein Perfect Tour 37-622
 tire radius = 16.8 mm, rim width = 18.7 mm

at 4.83 bar (70 psi) and
 under 525 N (53.5 kg, 118 lb)



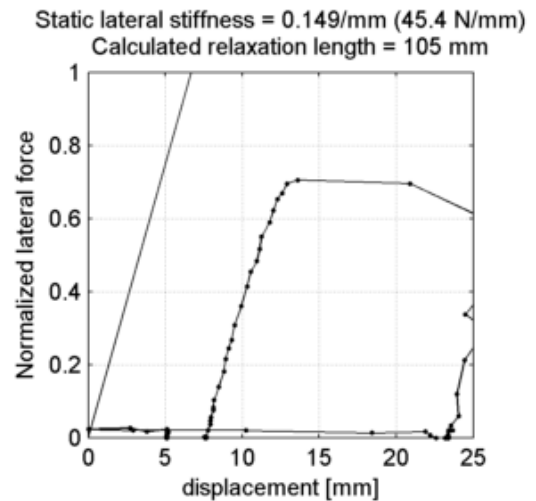
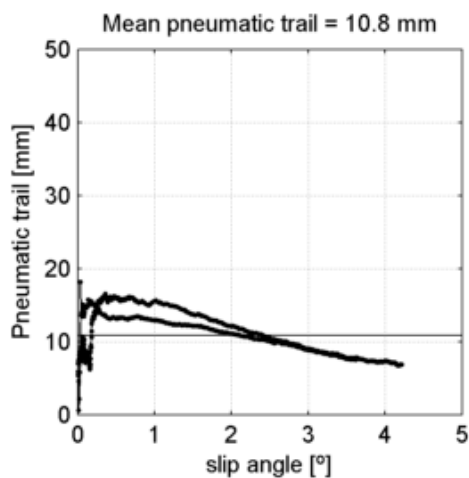
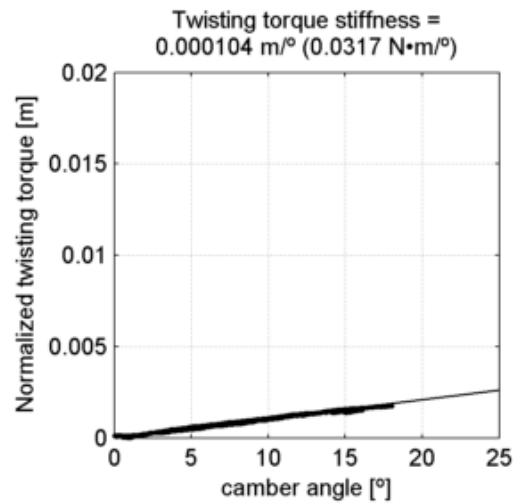
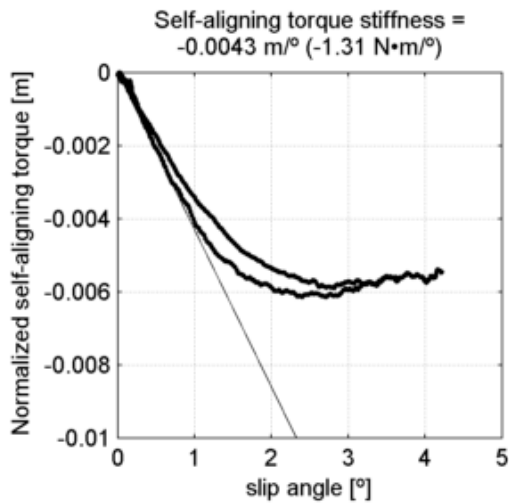
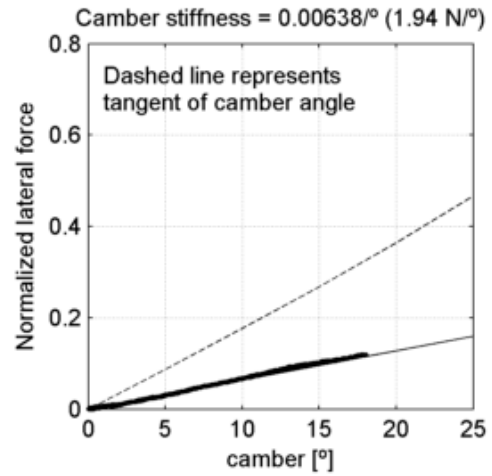
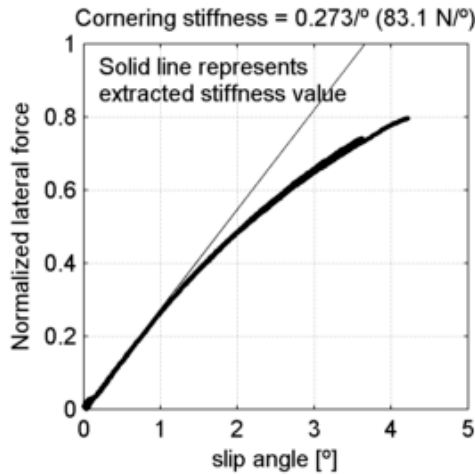
Vredestein Perfect Tour 37-622
 tire radius = 16.8 mm, rim width = 18.7 mm

at 4.83 bar (70 psi) and
 under 731 N (74.5 kg, 164 lb)



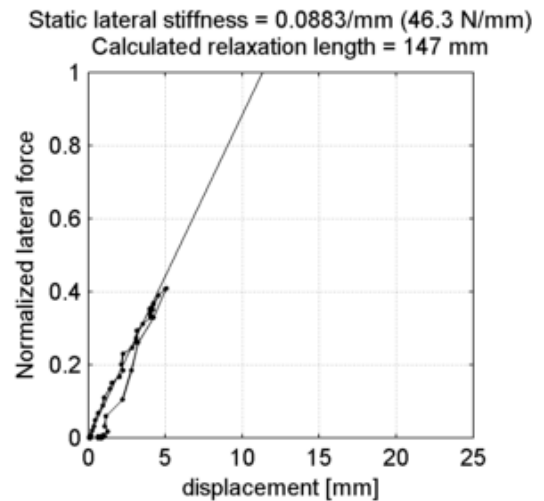
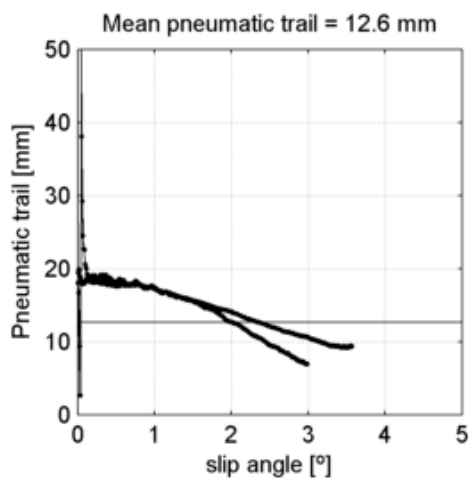
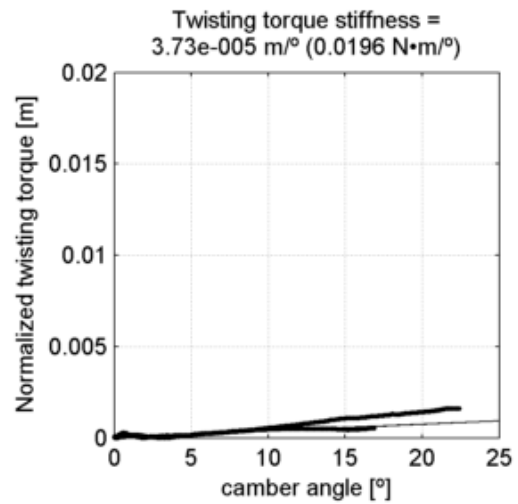
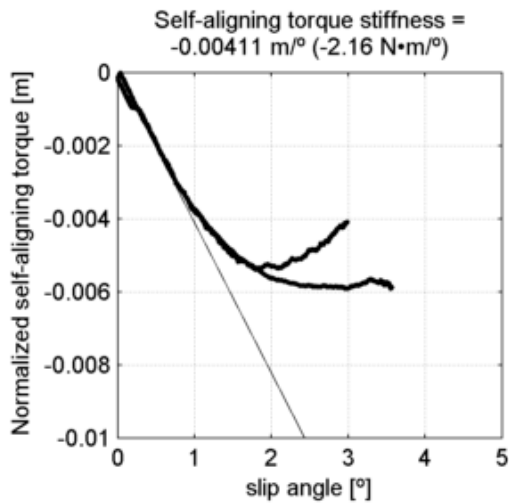
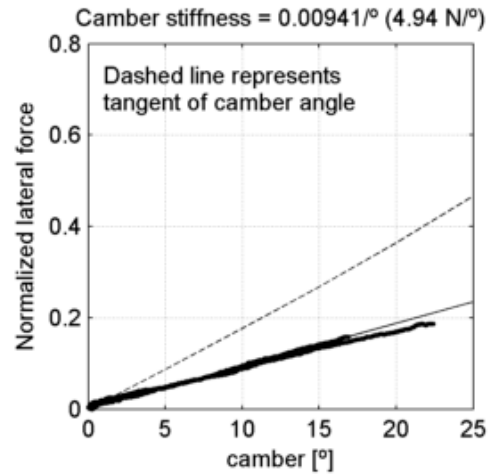
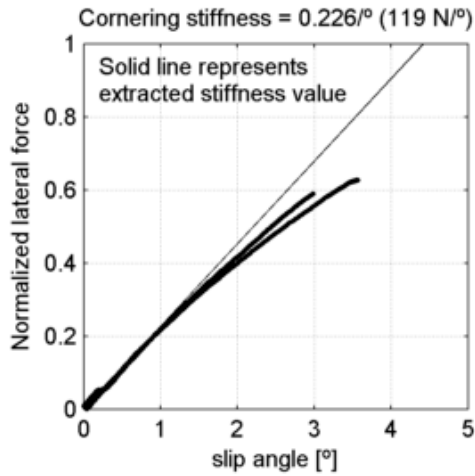
Vredestein Perfect Tour 37-622
 tire radius = 16.8 mm, rim width = 18.7 mm

at 6.21 bar (90 psi) and
 under 304 N (31 kg, 68.3 lb)



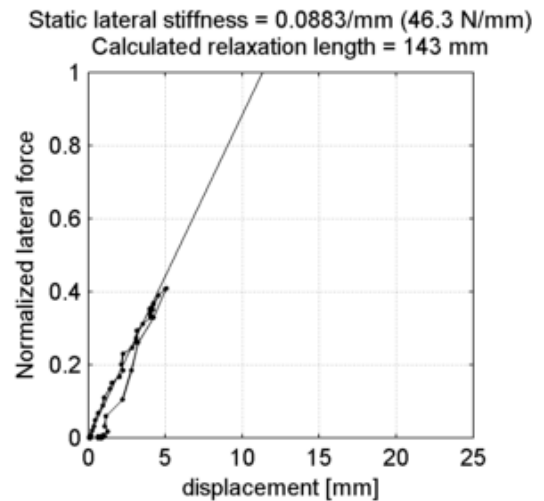
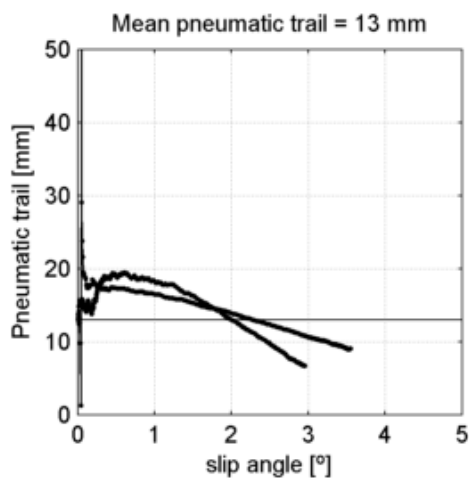
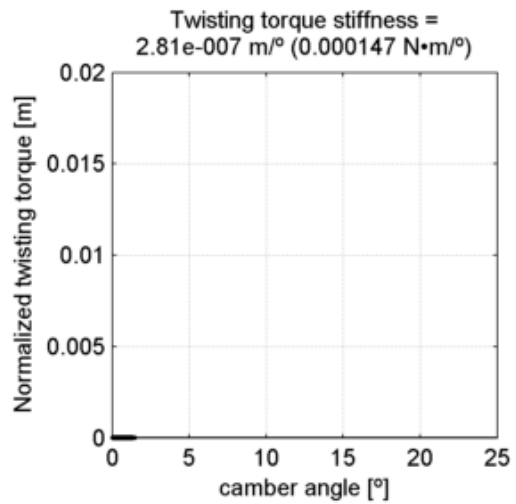
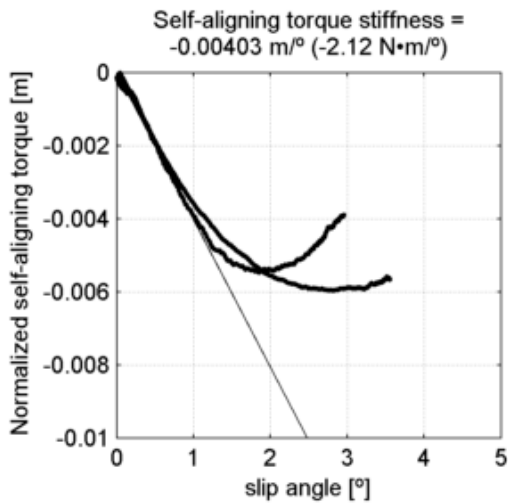
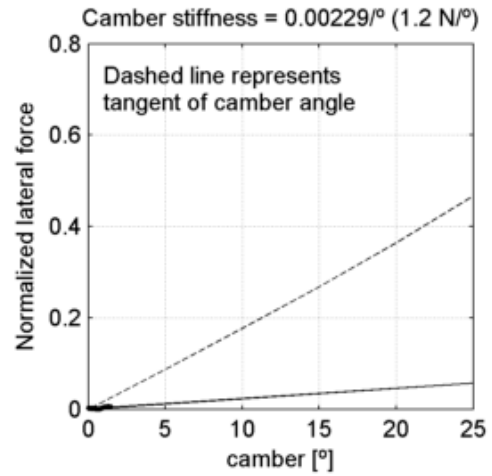
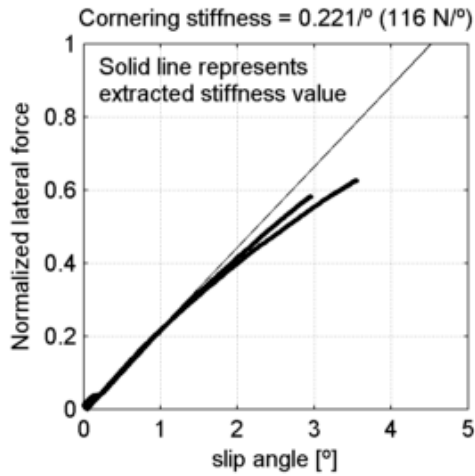
Vredestein Perfect Tour 37-622
 tire radius = 16.8 mm, rim width = 18.7 mm

at 6.21 bar (90 psi) and
 under 525 N (53.5 kg, 118 lb)



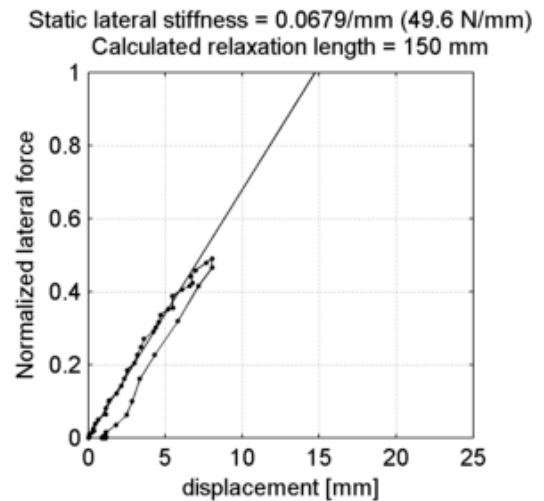
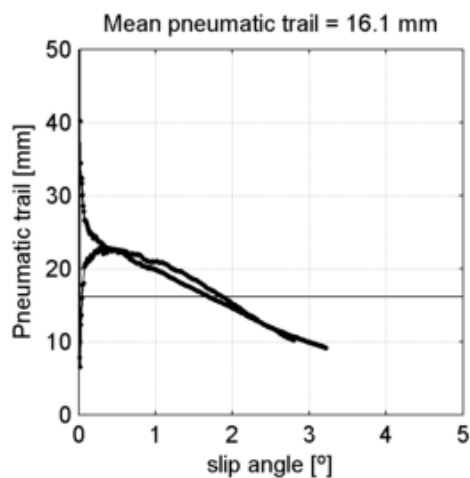
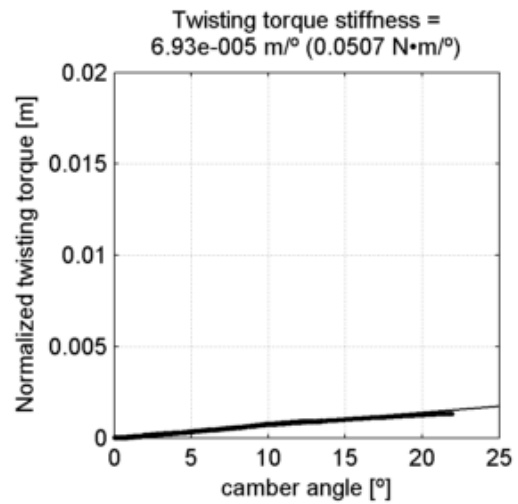
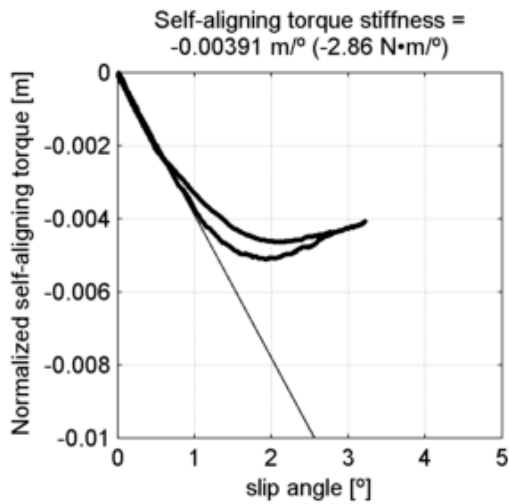
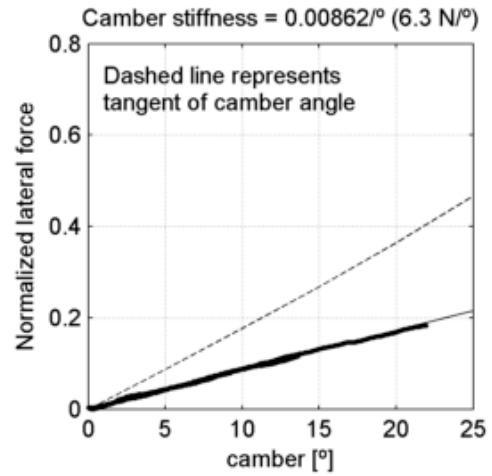
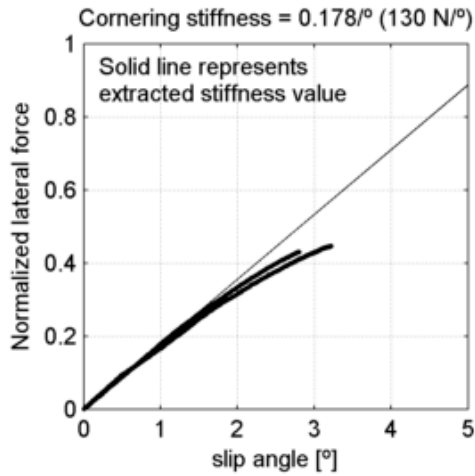
Vredestein Perfect Tour 37-622
 tire radius = 16.8 mm, rim width = 18.7 mm

at 6.21 bar (90 psi) and
 under 525 N (53.5 kg, 118 lb)



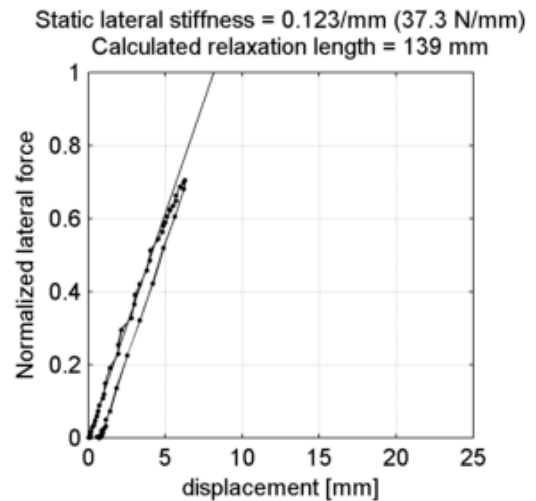
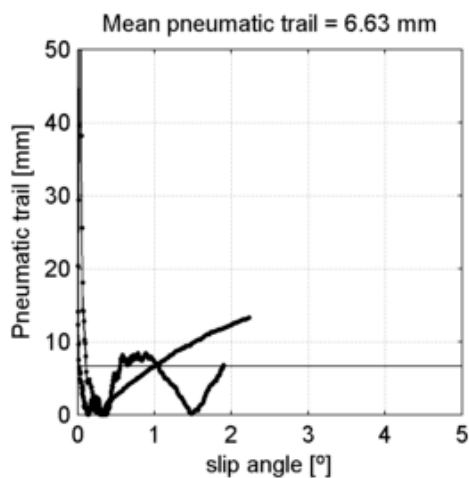
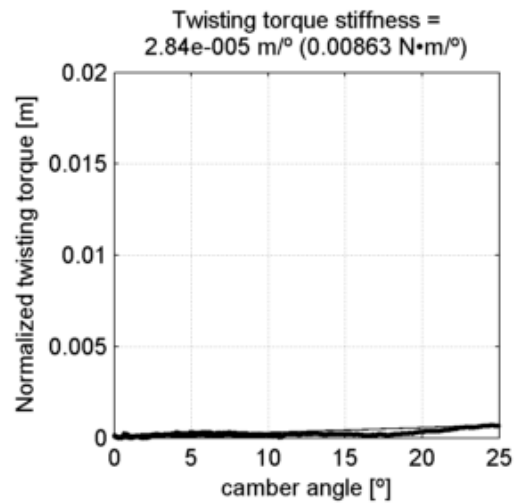
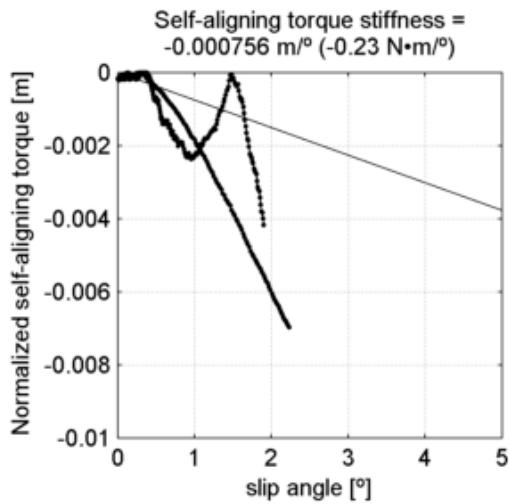
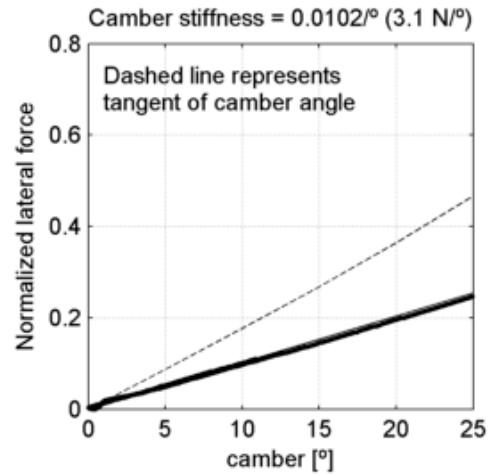
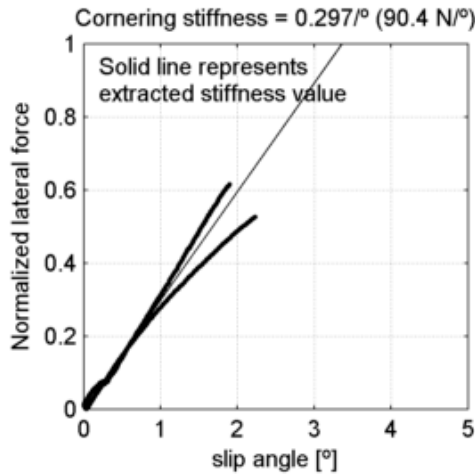
Vredestein Perfect Tour 37-622
 tire radius = 16.8 mm, rim width = 18.7 mm

at 6.21 bar (90 psi) and
 under 731 N (74.5 kg, 164 lb)



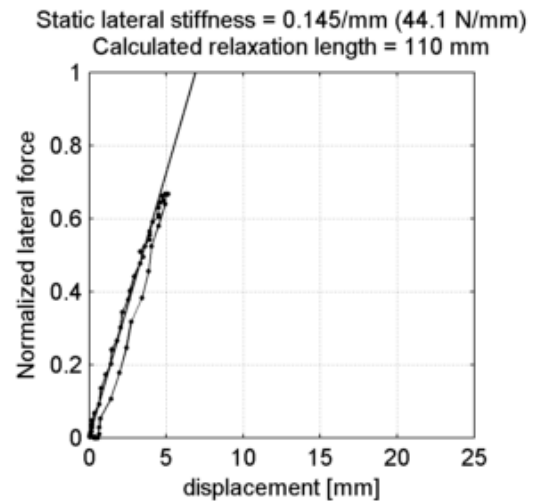
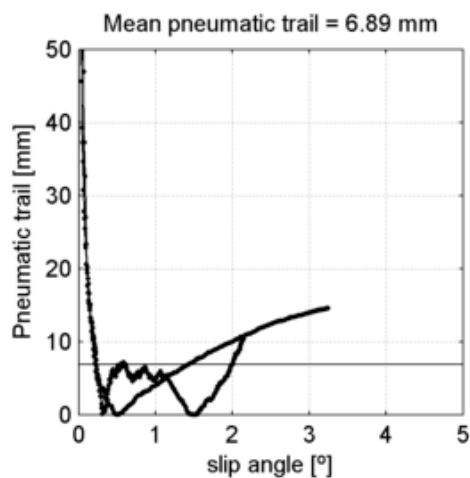
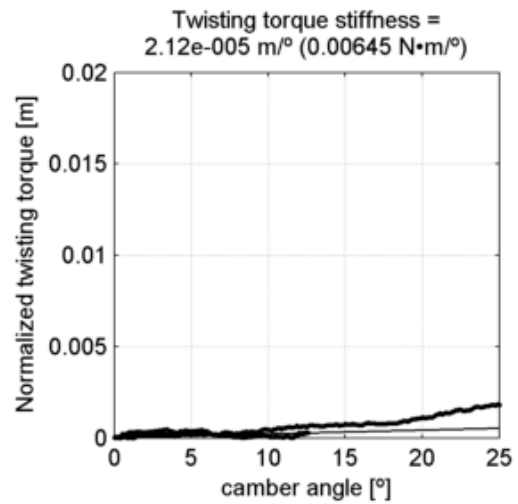
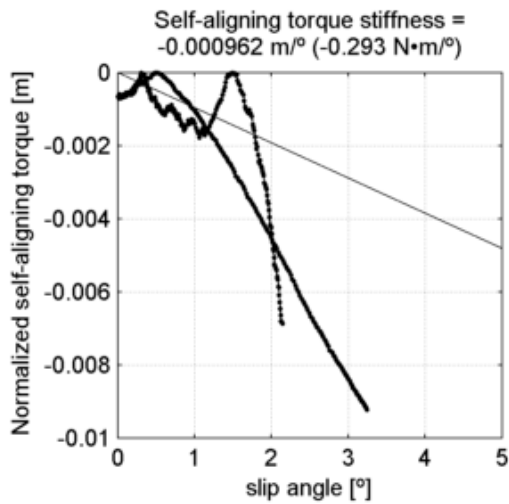
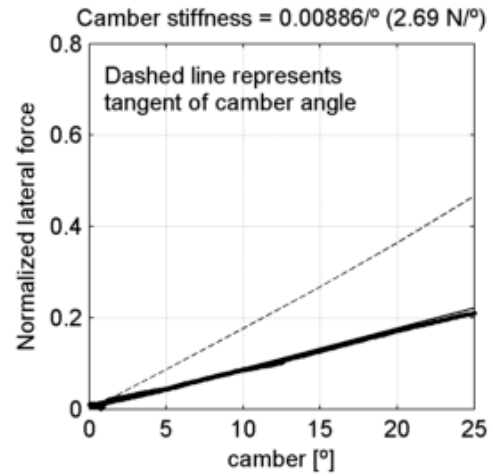
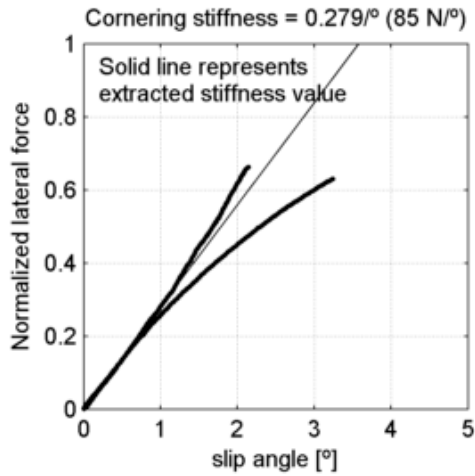
Vredestein Perfect Tour 37-622
 tire radius = 16.8 mm, rim width = 18.7 mm

at 3.45 bar (50 psi) and
 under 304 N (31 kg, 68.3 lb)



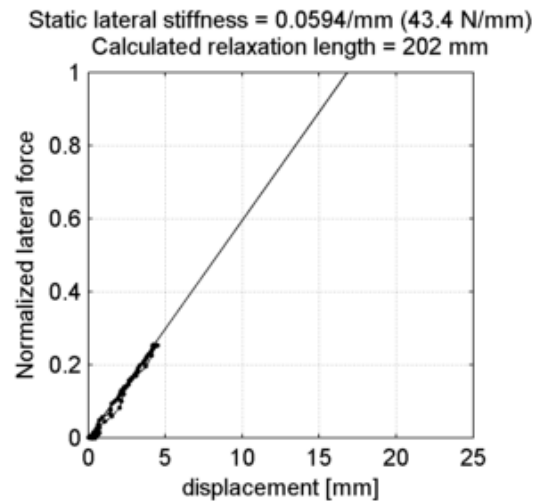
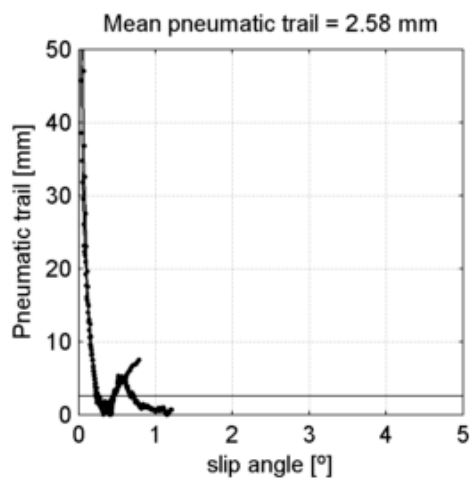
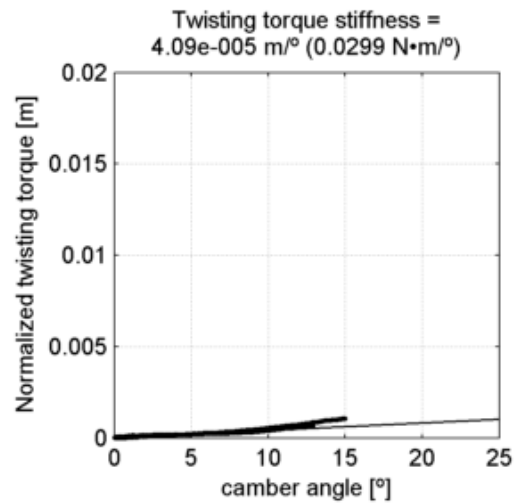
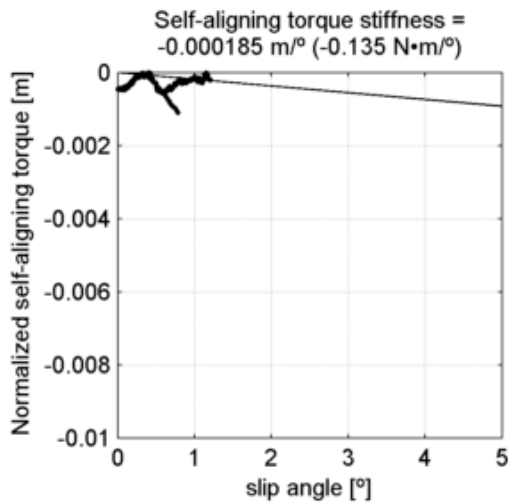
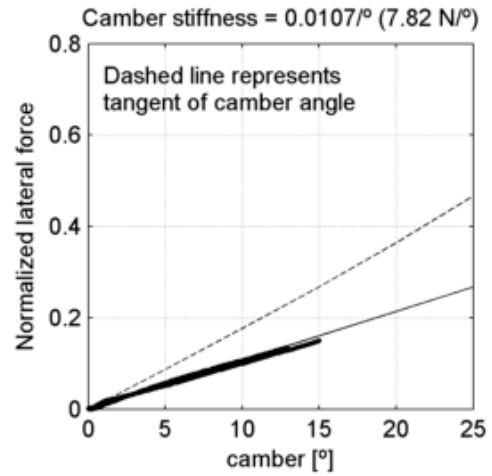
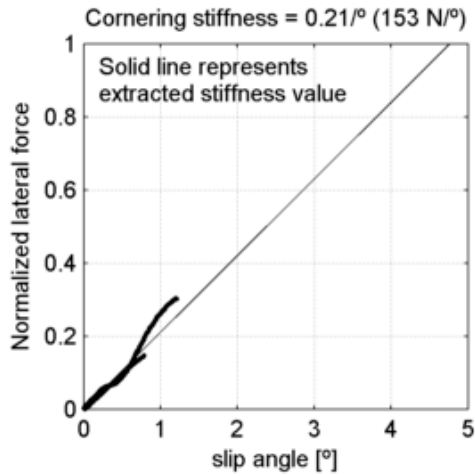
Vredestein Perfect Tour 37-622
 tire radius = 16.8 mm, rim width = 18.7 mm

at 6.21 bar (90 psi) and
 under 304 N (31 kg, 68.3 lb)



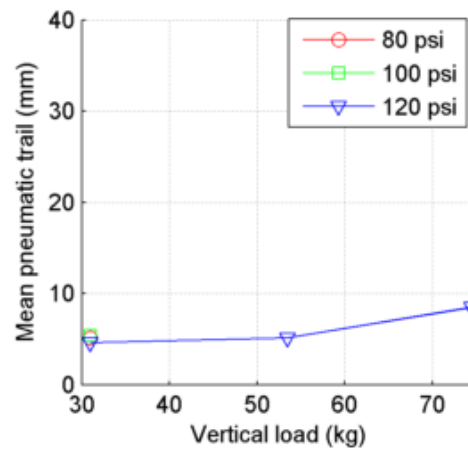
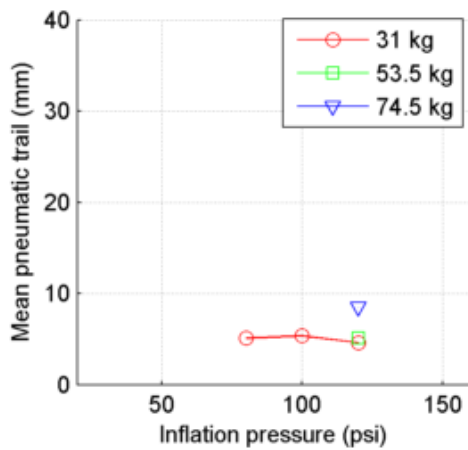
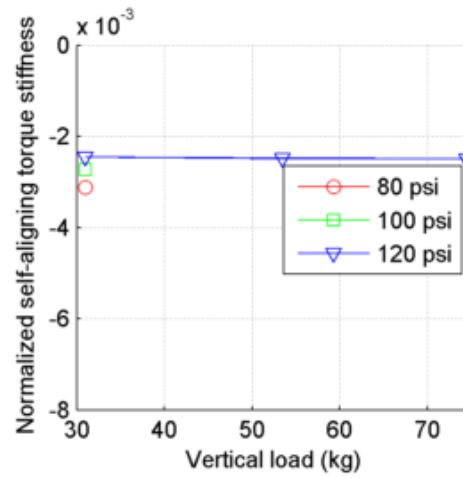
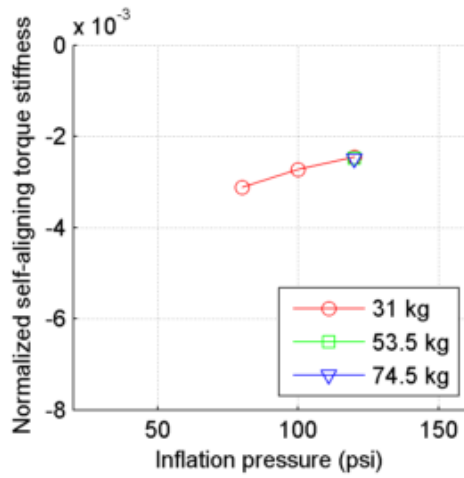
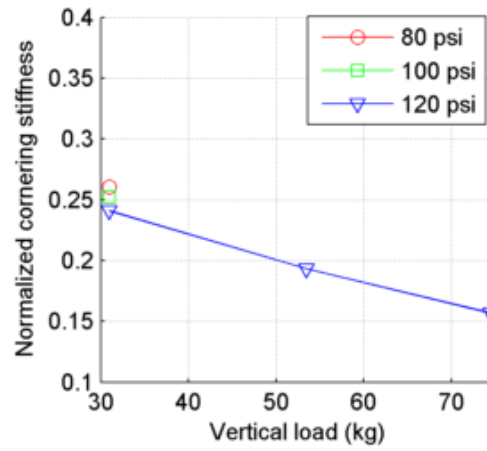
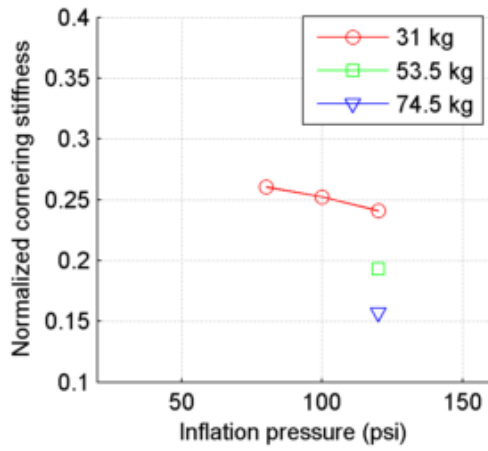
Vredestein Perfect Tour 37-622
 tire radius = 16.8 mm, rim width = 18.7 mm

at 6.21 bar (90 psi) and
 under 731 N (74.5 kg, 164 lb)



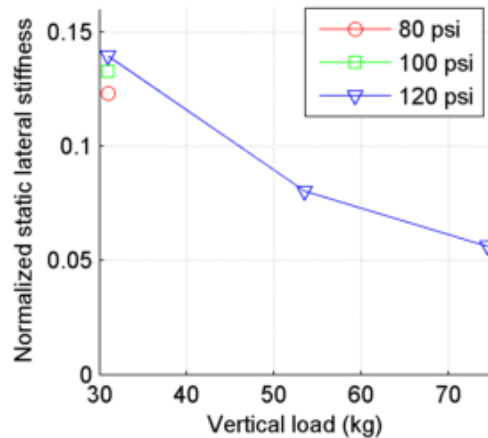
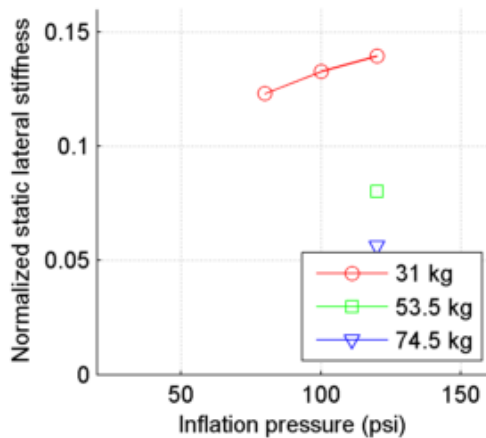
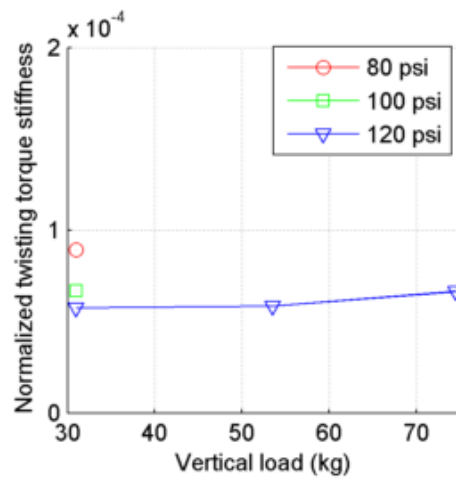
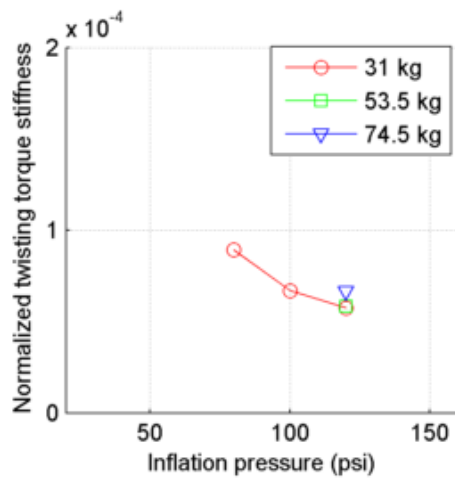
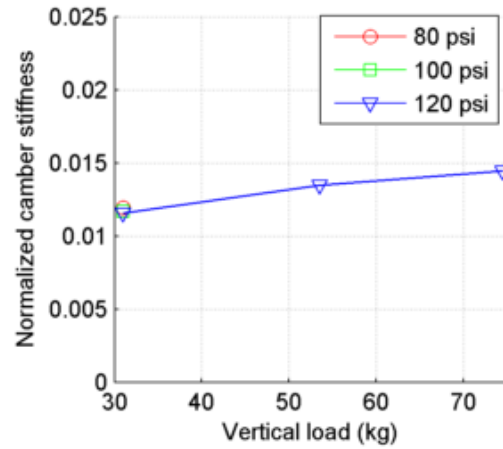
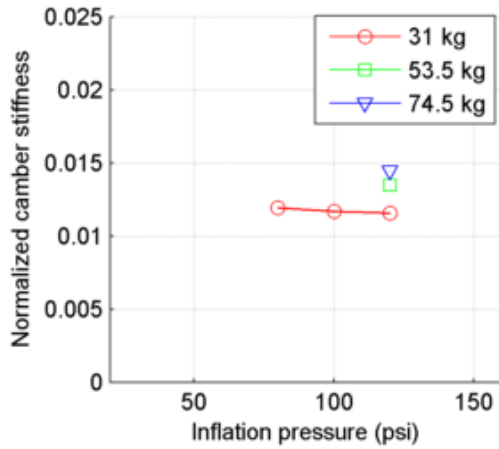
Bontrager All Weather 23-622
 tire radius = 11.5 mm, rim width = 13.4 mm

summary
 part 1 of 2



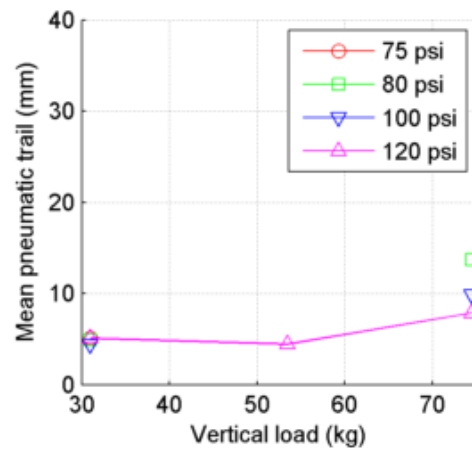
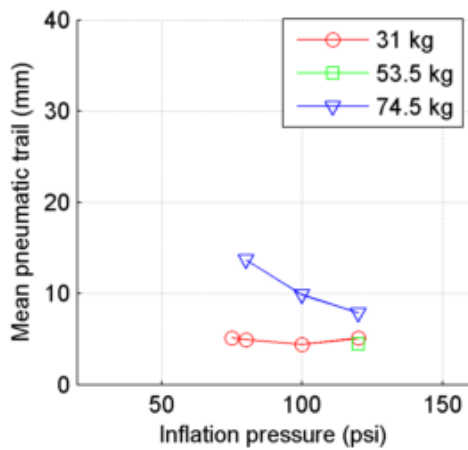
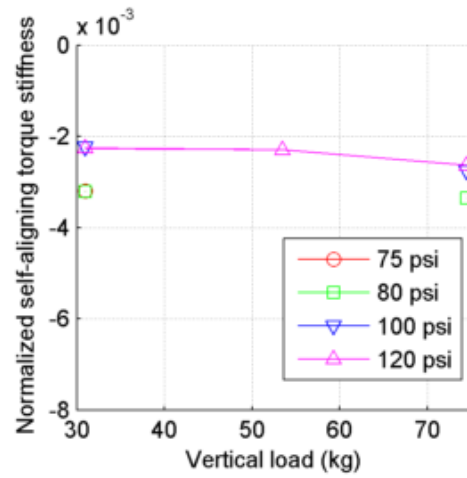
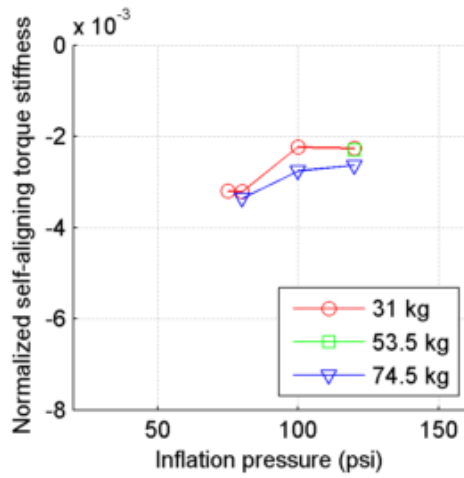
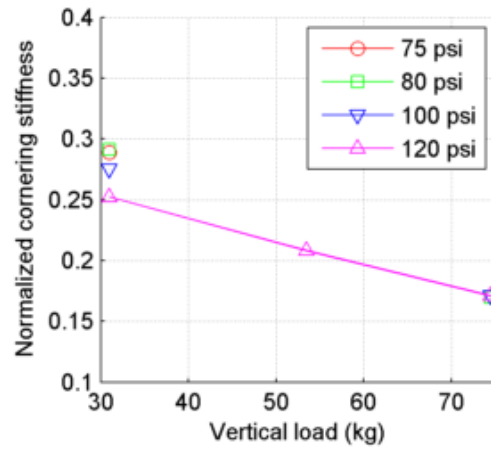
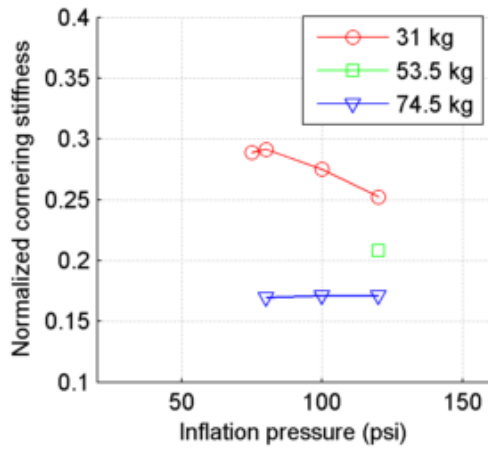
Bontrager All Weather 23-622
 tire radius = 11.5 mm, rim width = 13.4 mm

summary
 part 2 of 2



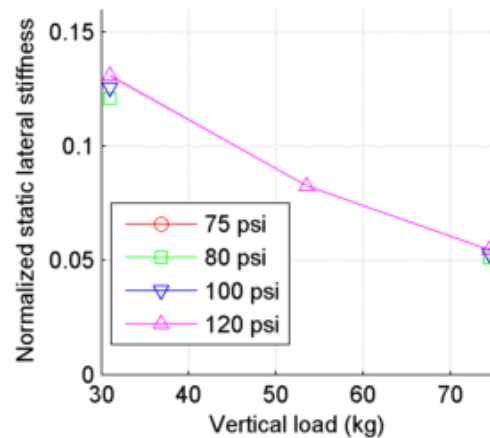
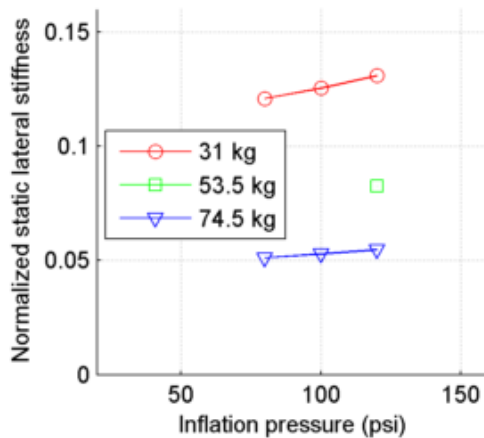
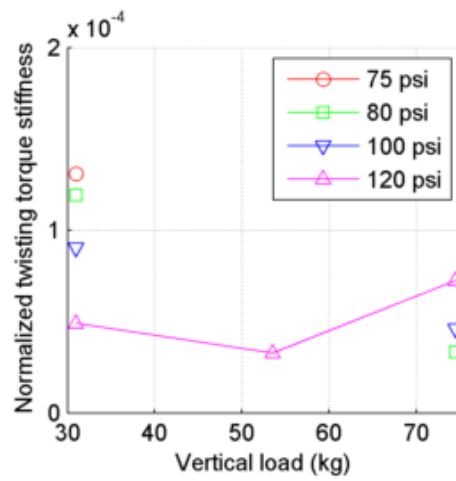
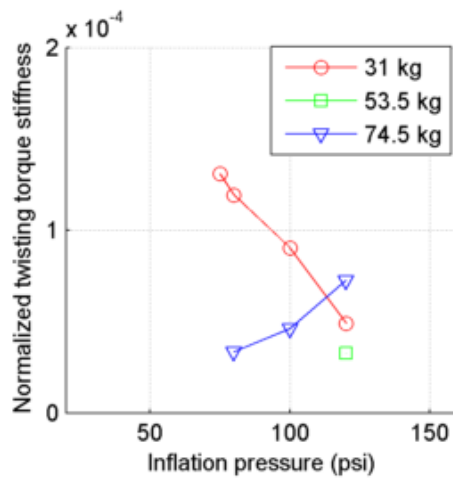
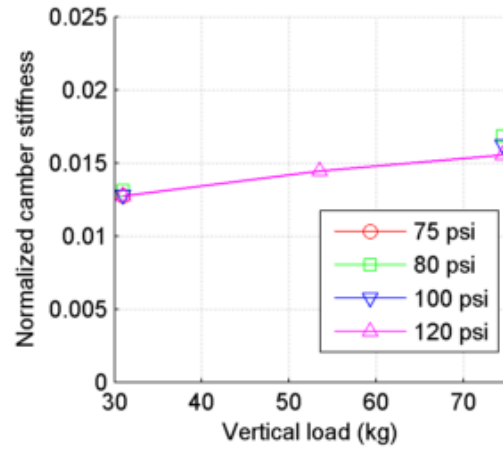
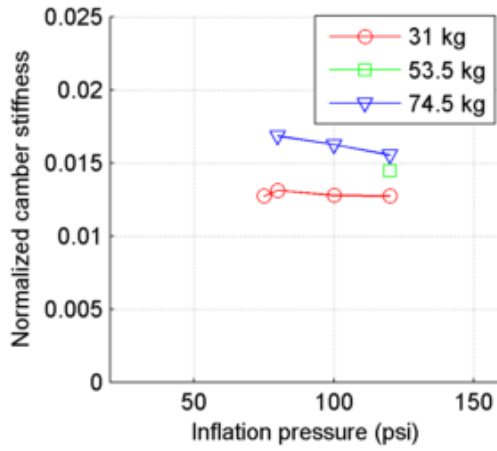
Bontrager All Weather 25-622
 tire radius = 12.5 mm, rim width = 13.4 mm

summary
 part 1 of 2



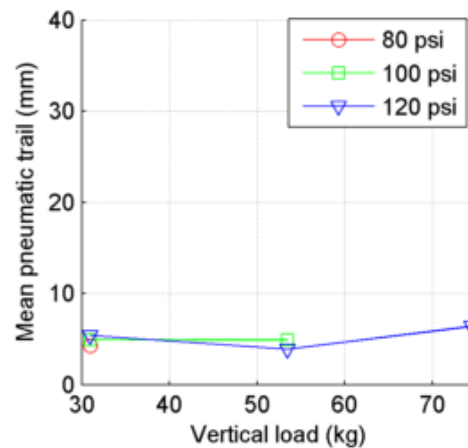
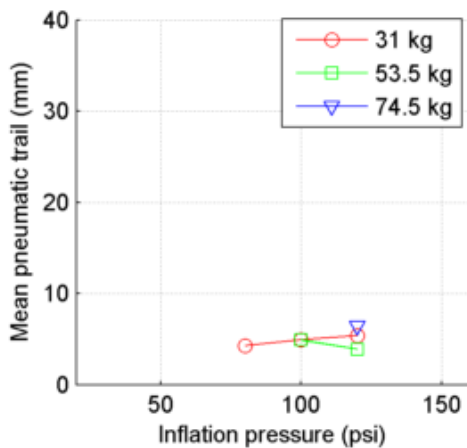
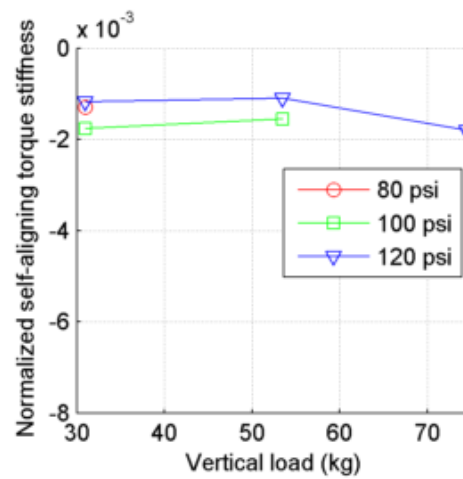
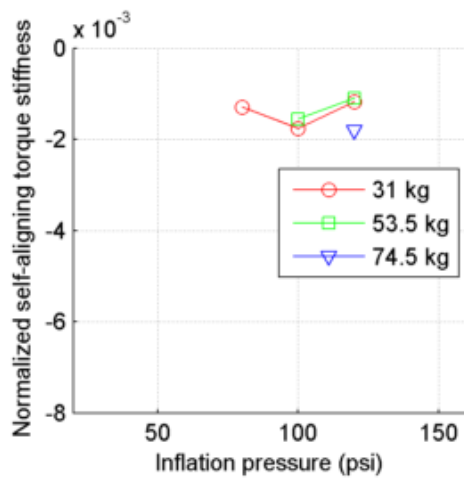
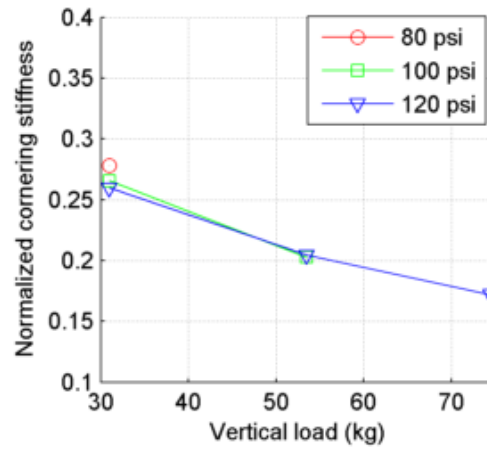
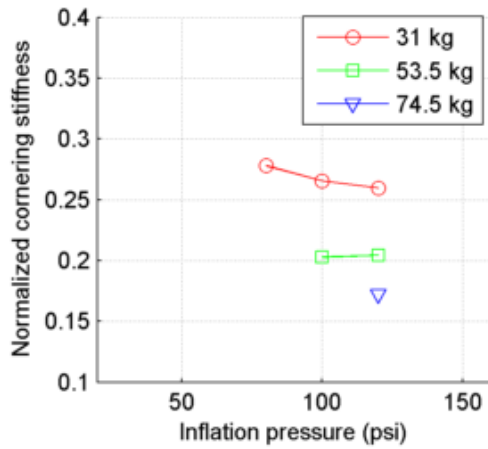
Bontrager All Weather 25-622
 tire radius = 12.5 mm, rim width = 13.4 mm

summary
 part 2 of 2



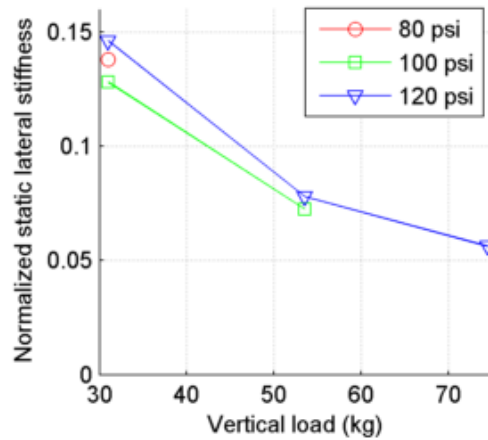
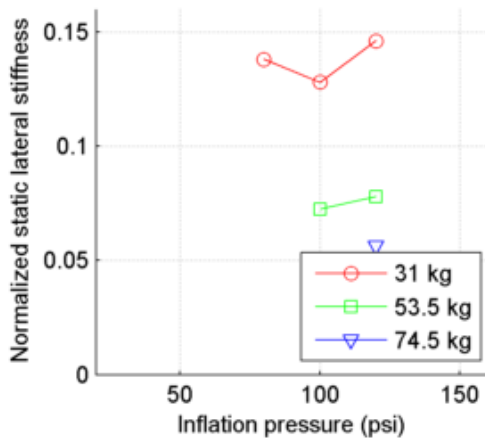
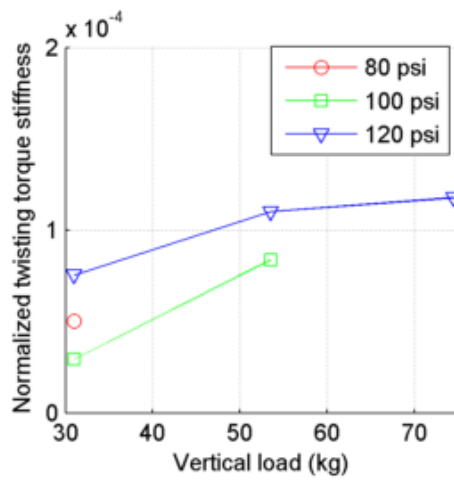
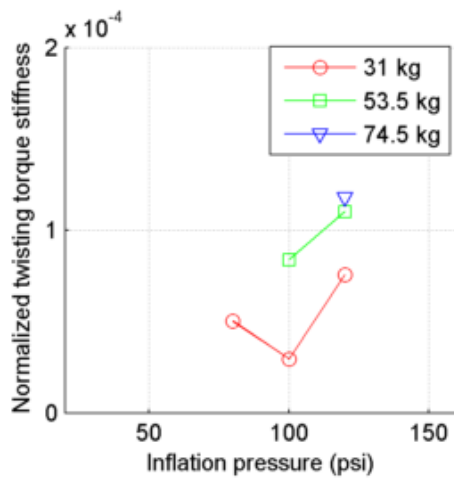
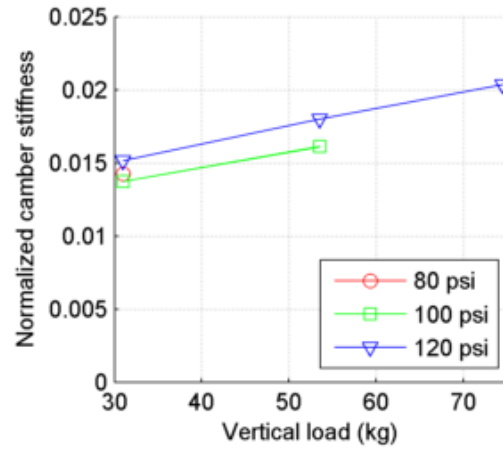
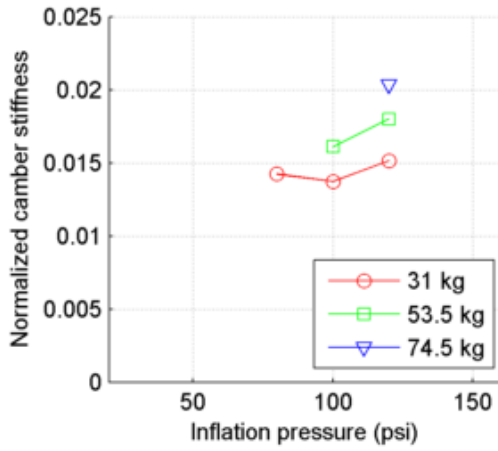
Bontrager All Weather 28-622
 tire radius = 14 mm, rim width = 13.4 mm

summary
 part 1 of 2



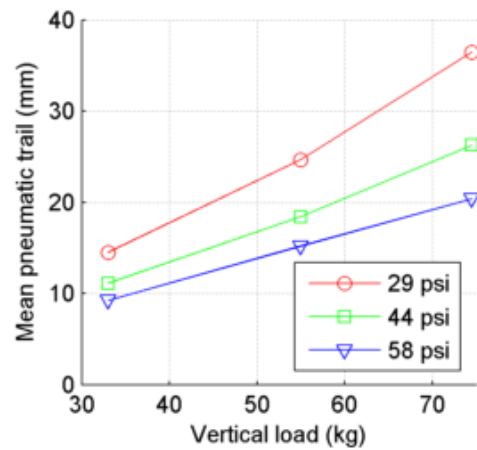
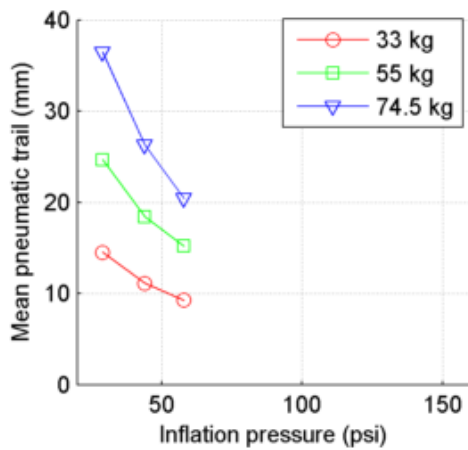
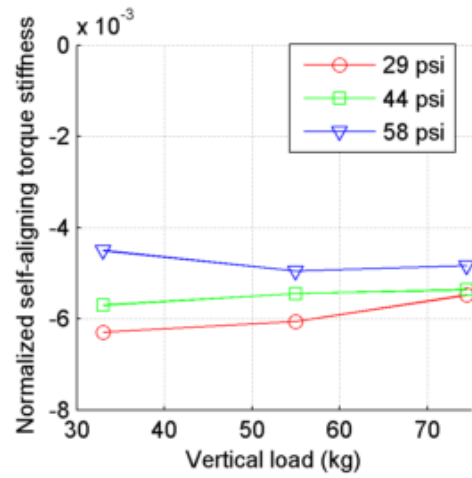
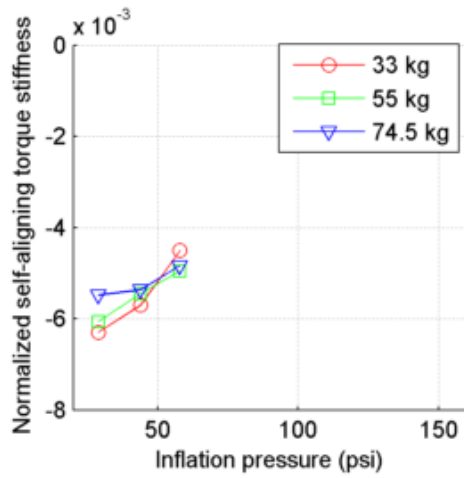
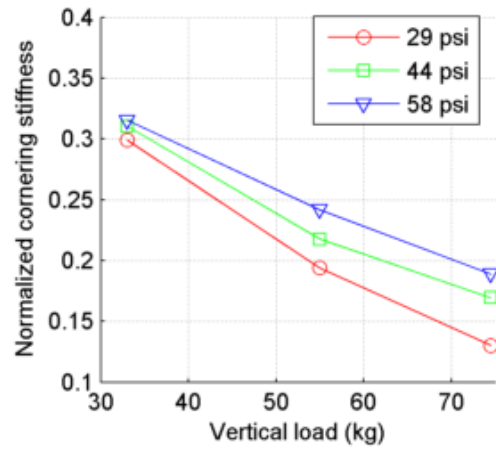
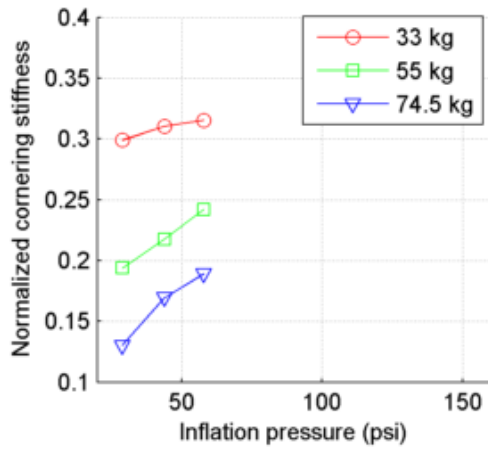
Bontrager All Weather 28-622
 tire radius = 14 mm, rim width = 13.4 mm

summary
 part 2 of 2



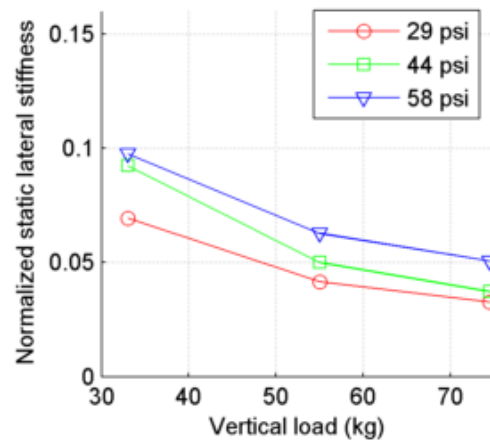
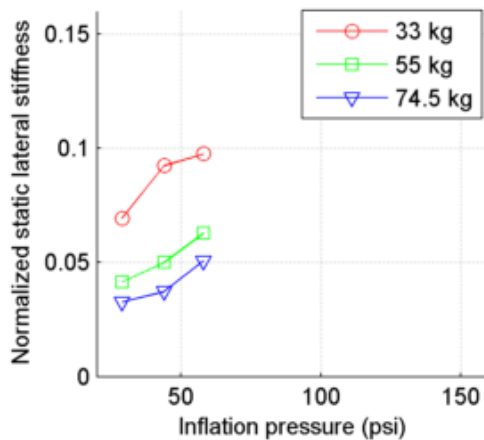
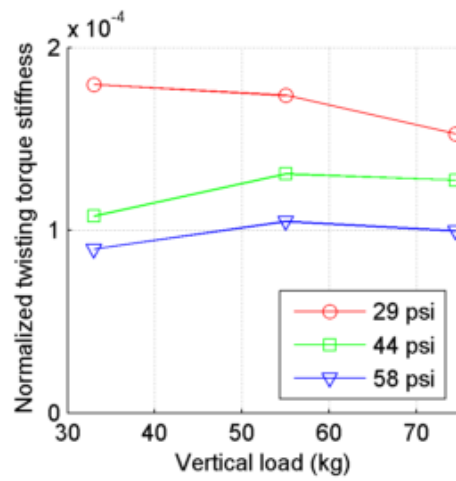
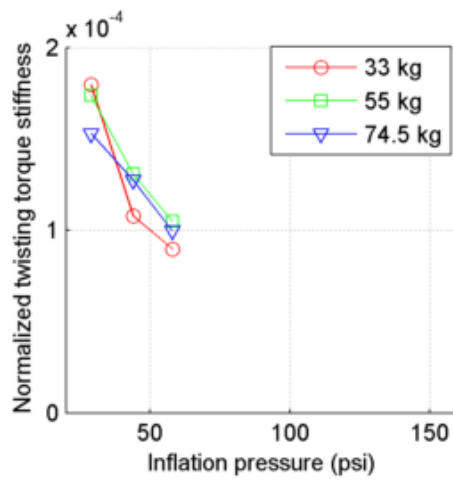
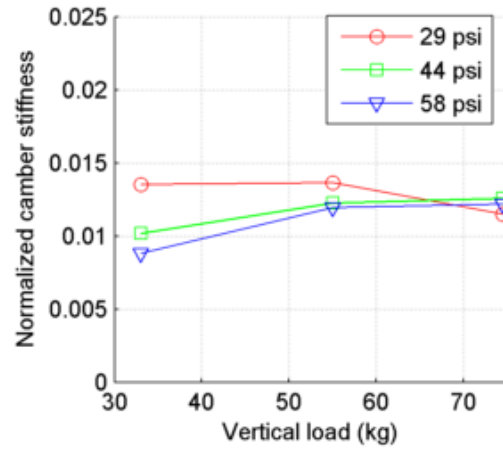
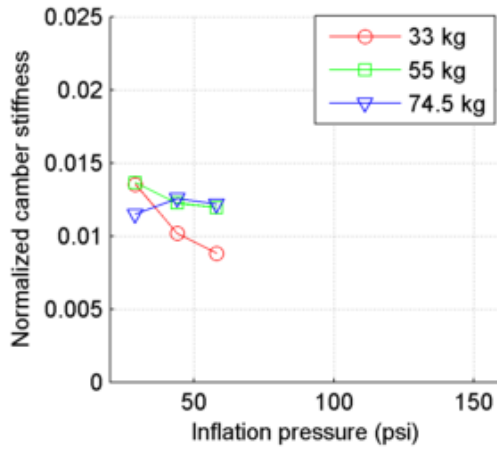
Cheng Shin Classic Zeppelin 50-622
 tire radius = 22.1 mm, rim width = 18.7 mm

summary
 part 1 of 2



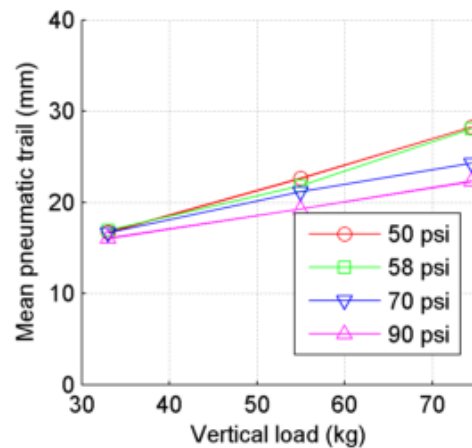
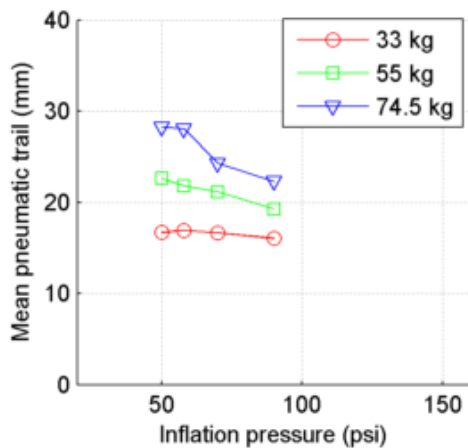
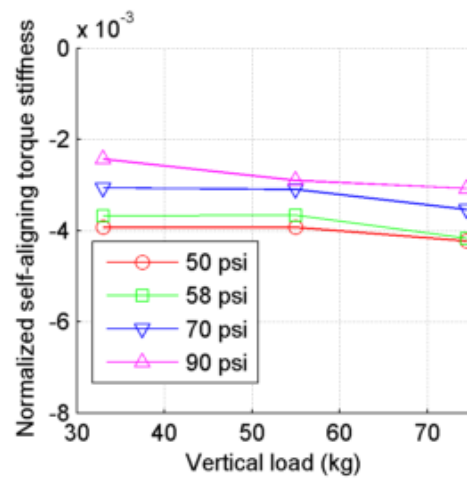
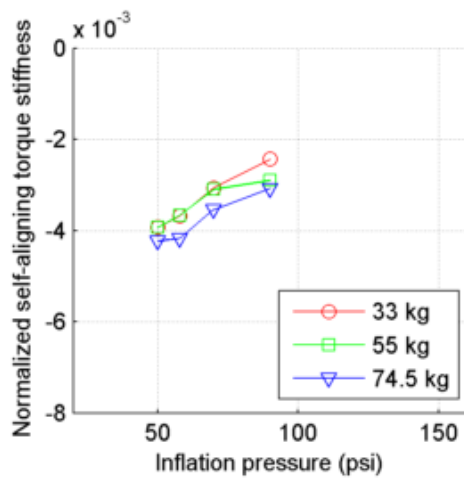
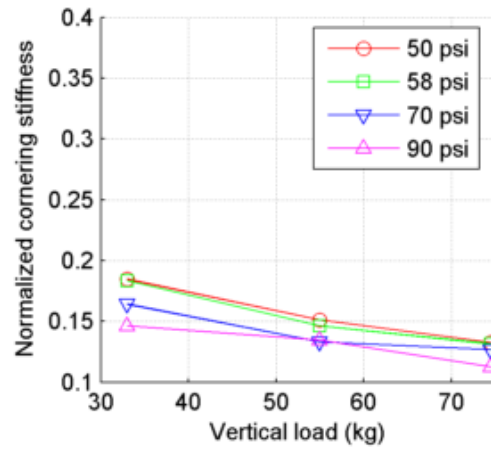
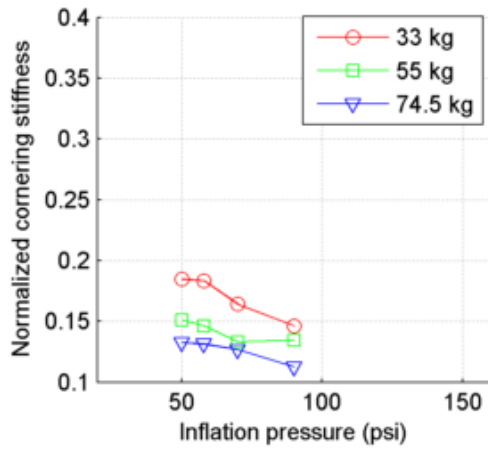
Cheng Shin Classic Zeppelin 50-622
 tire radius = 22.1 mm, rim width = 18.7 mm

summary
 part 2 of 2



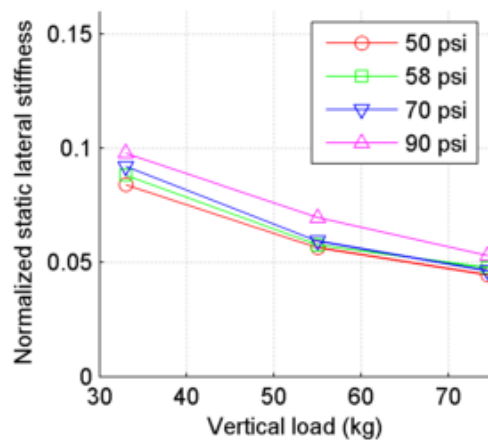
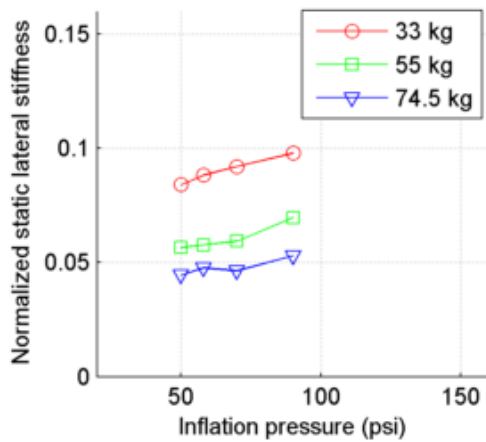
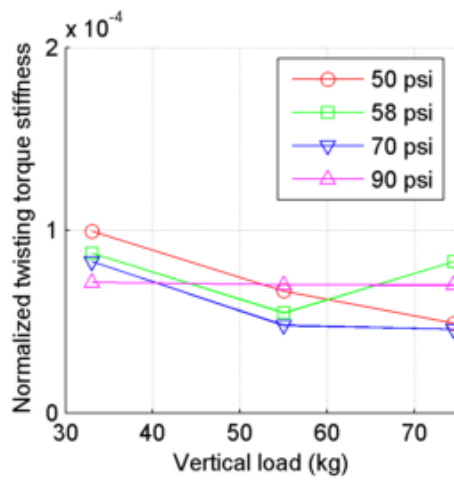
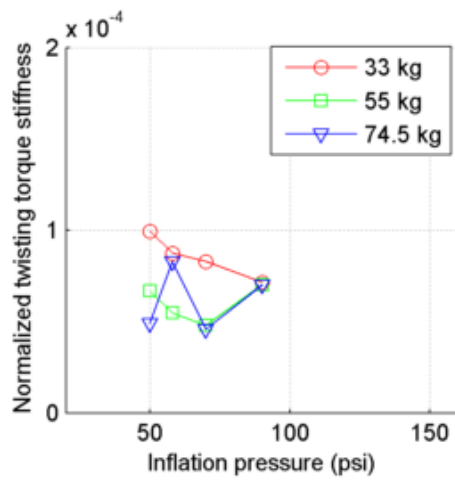
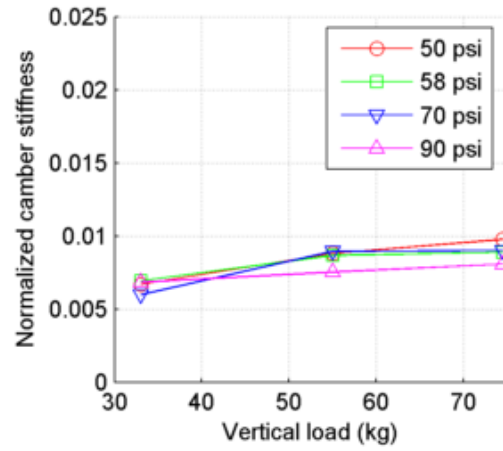
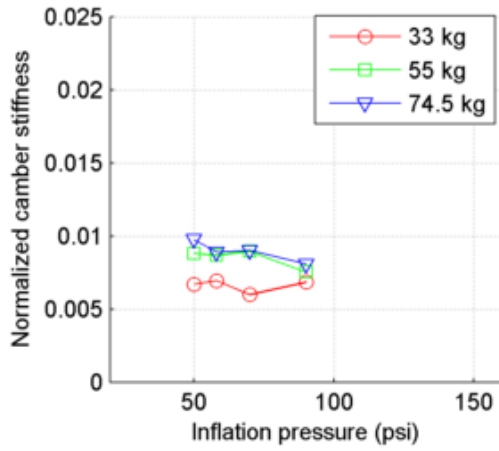
Continental Top Contact Winter 37-622
 tire radius = 15.6 mm, rim width = 18.7 mm

summary
 part 1 of 2



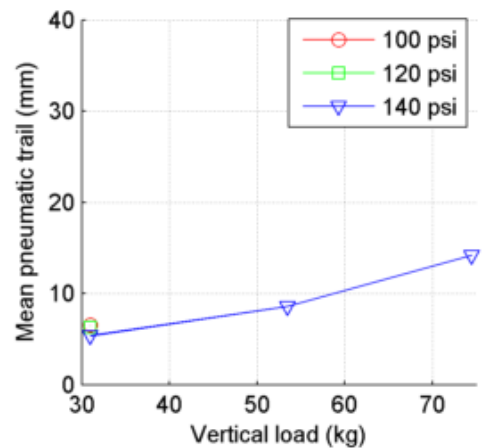
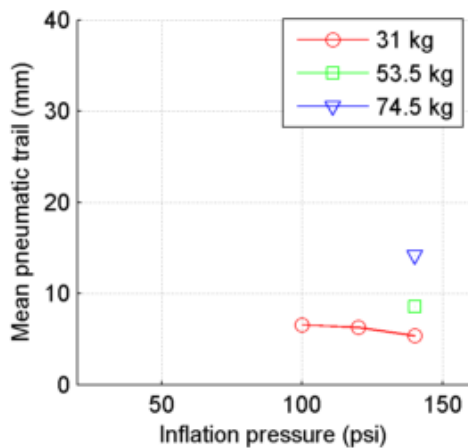
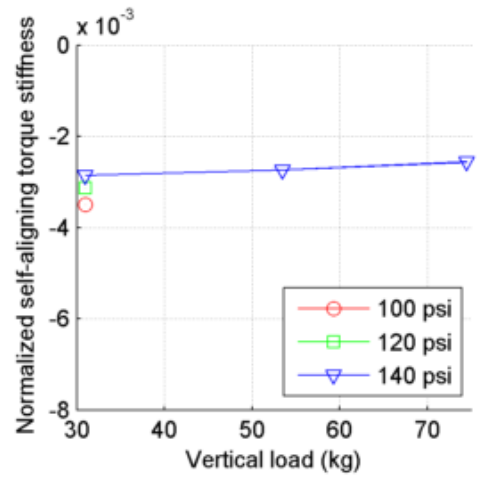
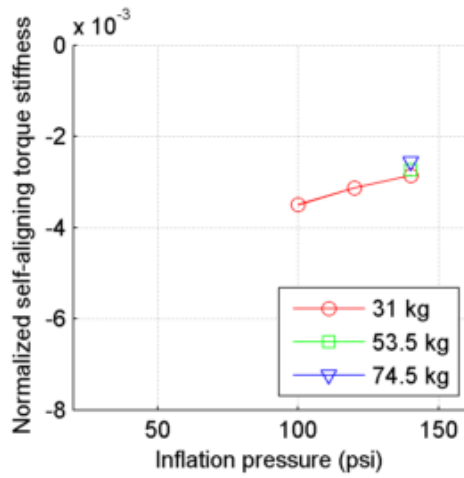
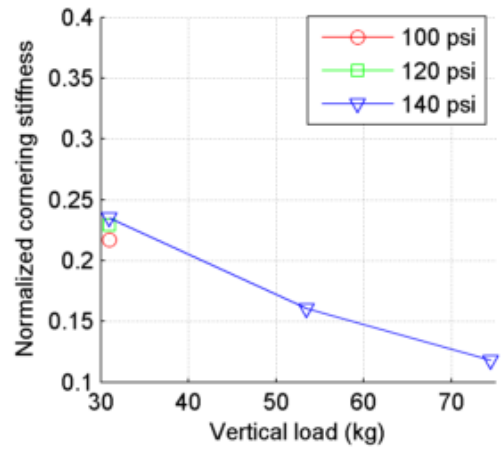
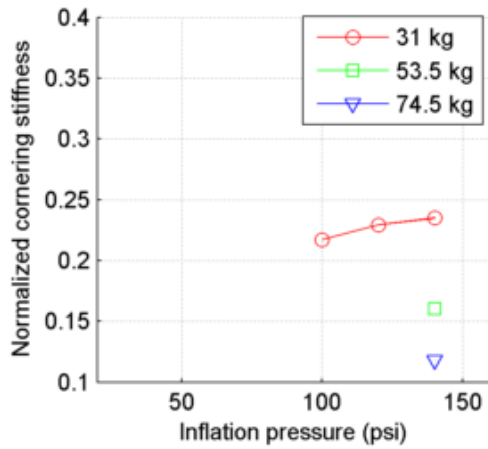
Continental Top Contact Winter 37-622
 tire radius = 15.6 mm, rim width = 18.7 mm

summary
 part 2 of 2



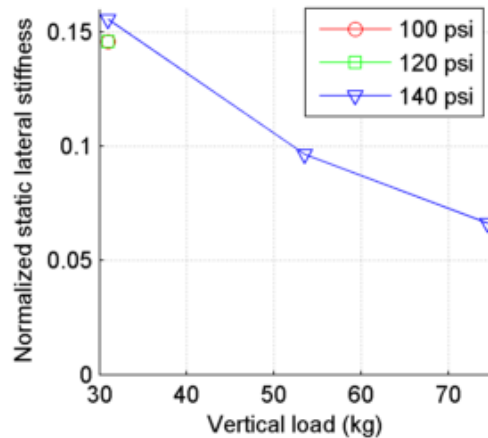
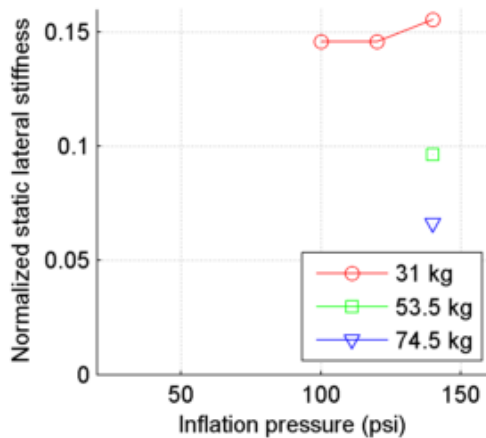
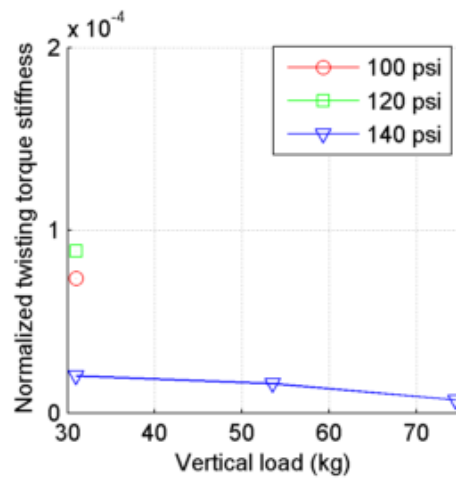
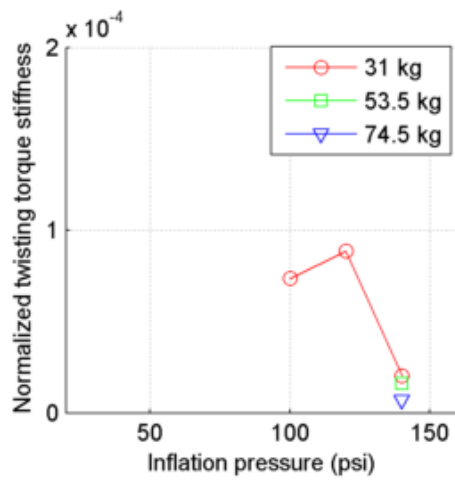
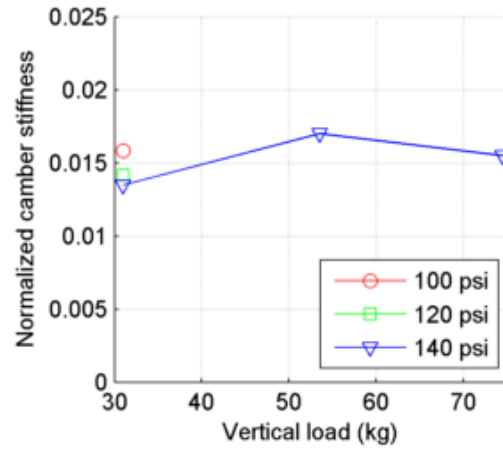
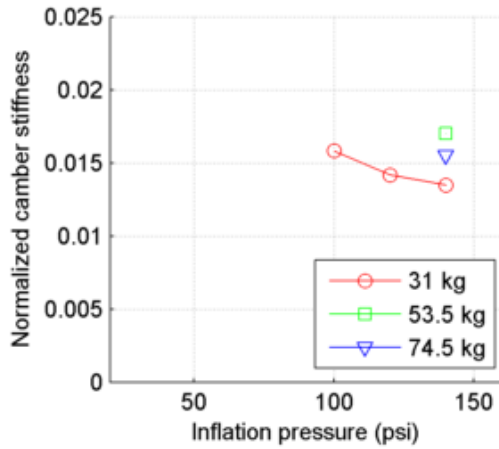
Maxis Radial 22-622
 tire radius = 11 mm, rim width = 13.4 mm

summary
 part 1 of 2



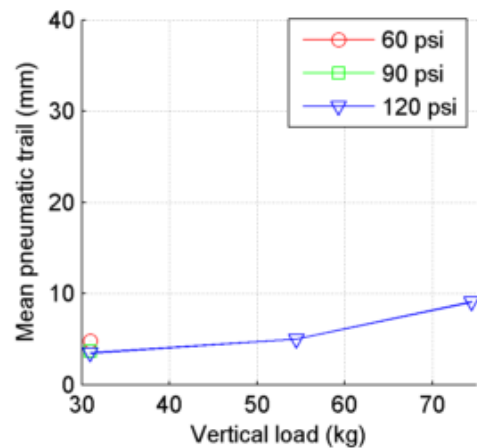
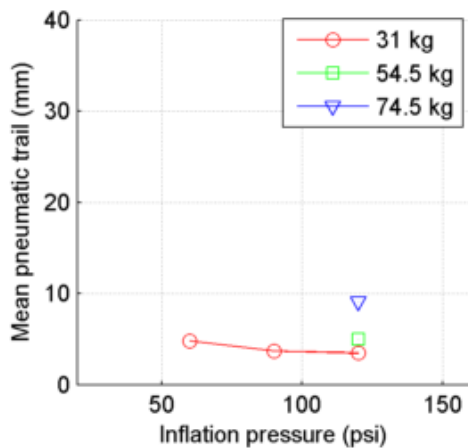
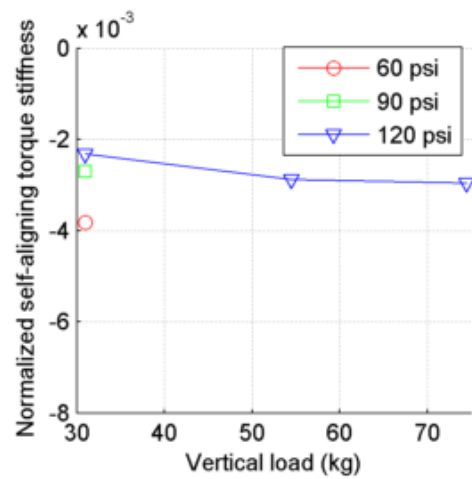
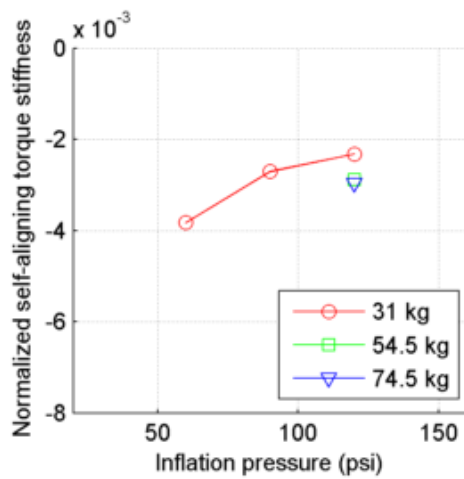
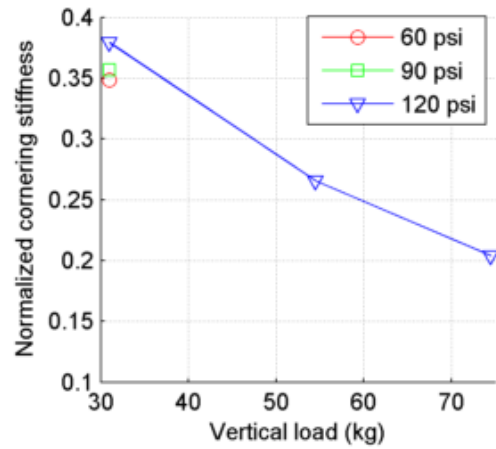
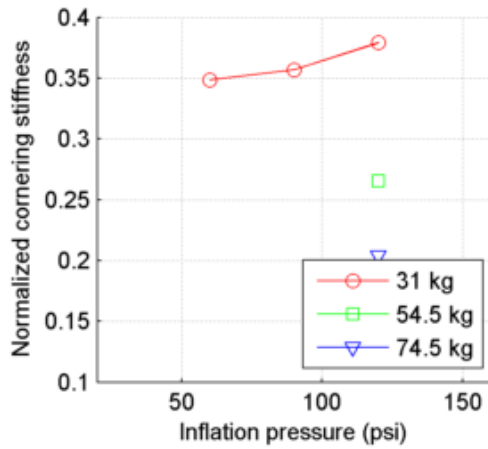
Maxis Radial 22-622
 tire radius = 11 mm, rim width = 13.4 mm

summary
 part 2 of 2



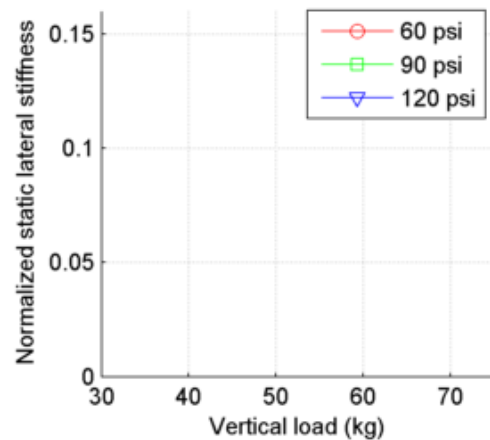
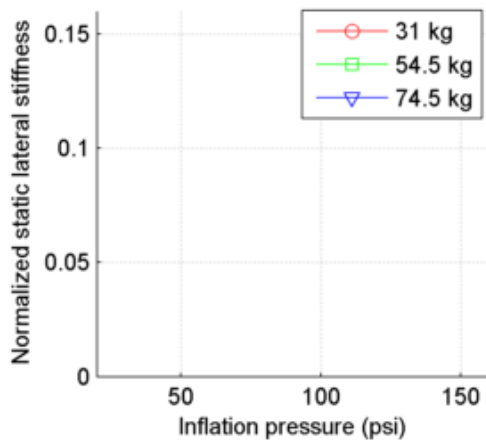
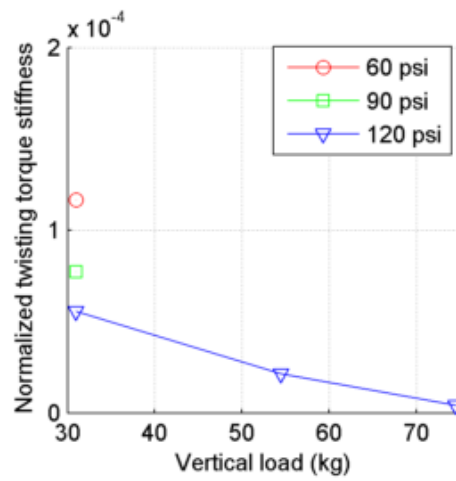
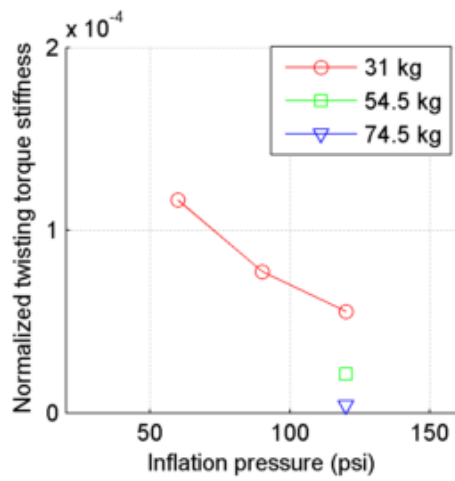
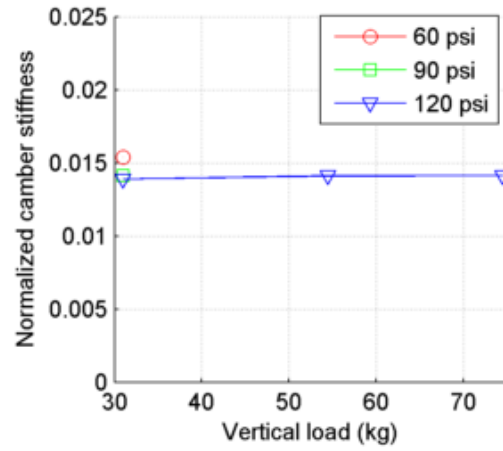
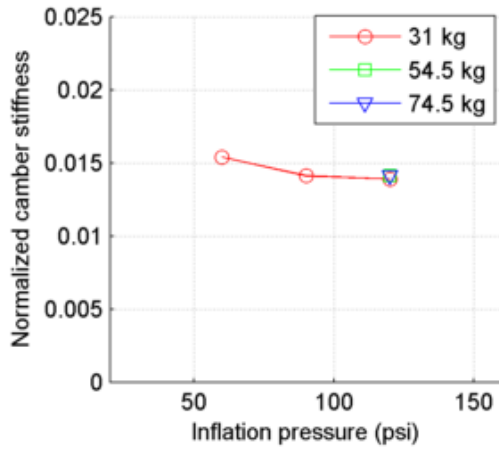
Michelin Dynamic xx-622
 tire radius = 12.5 mm, rim width = 13.4 mm

summary
 part 1 of 2



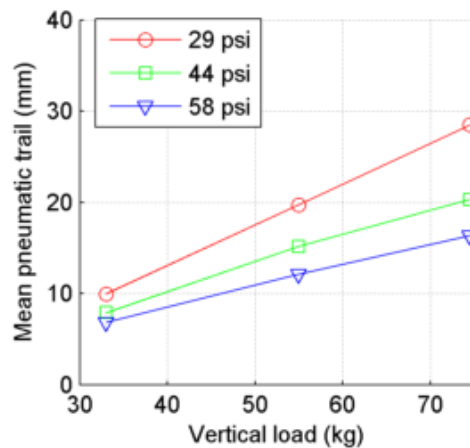
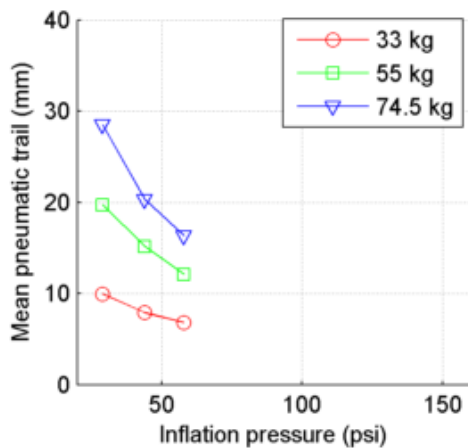
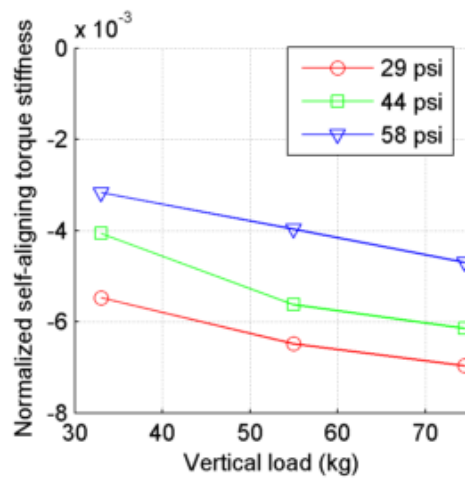
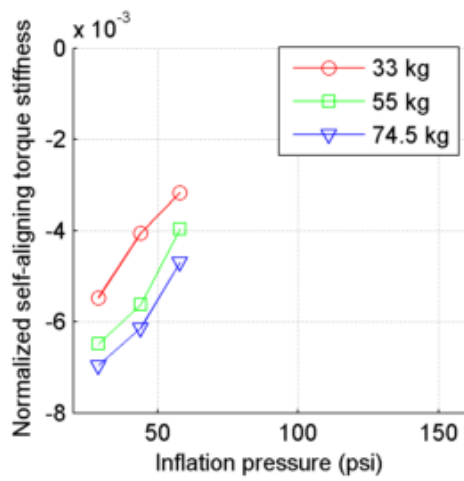
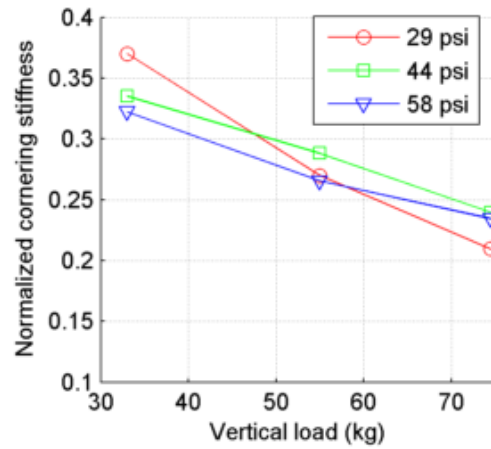
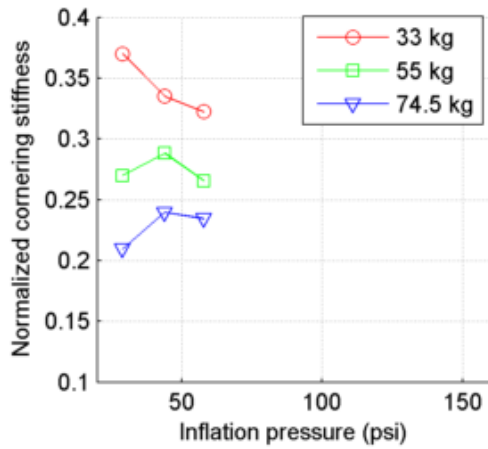
Michelin Dynamic xx-622
 tire radius = 12.5 mm, rim width = 13.4 mm

summary
 part 2 of 2



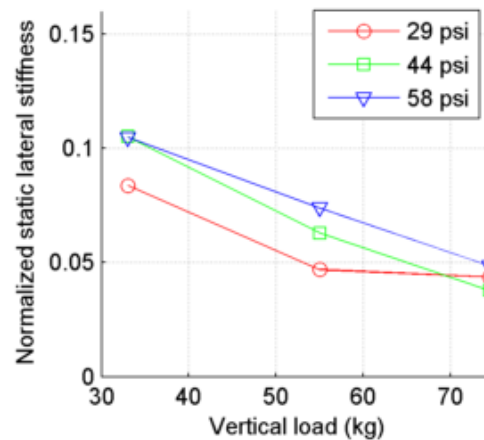
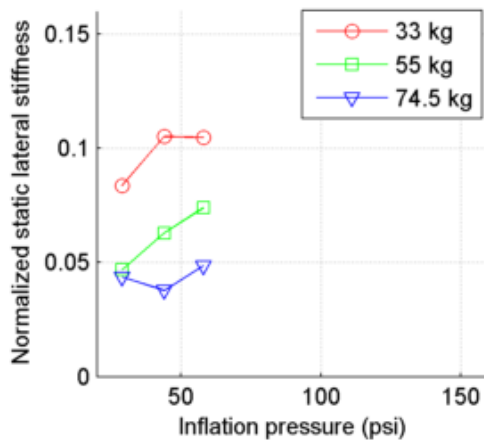
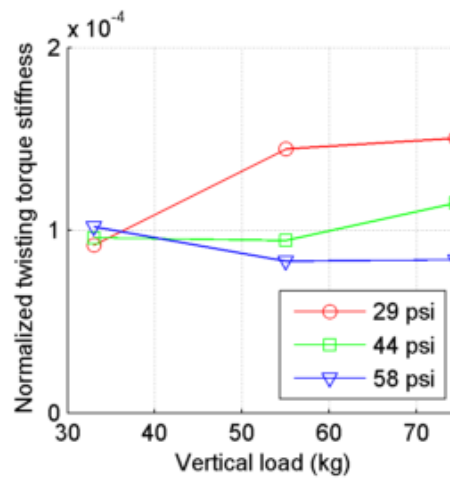
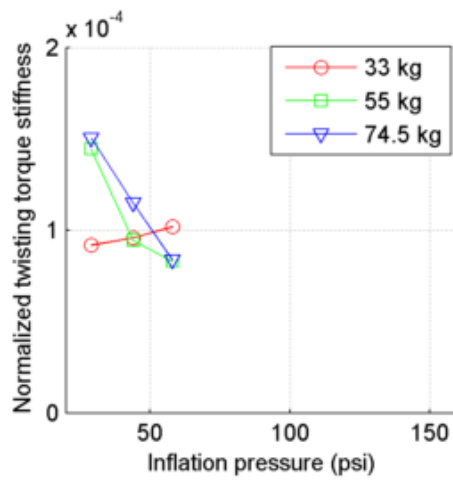
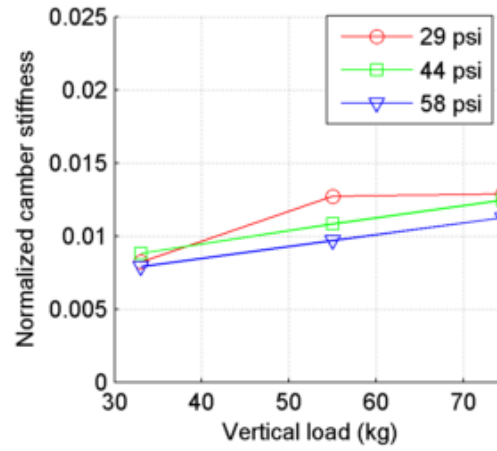
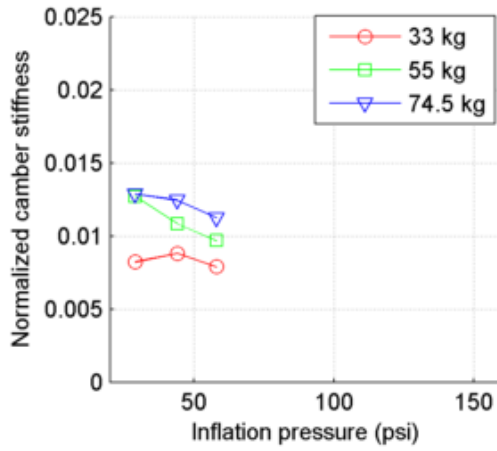
Schwalbe Big Apple 55-622
 tire radius = 23.5 mm, rim width = 18.7 mm

summary
 part 1 of 2



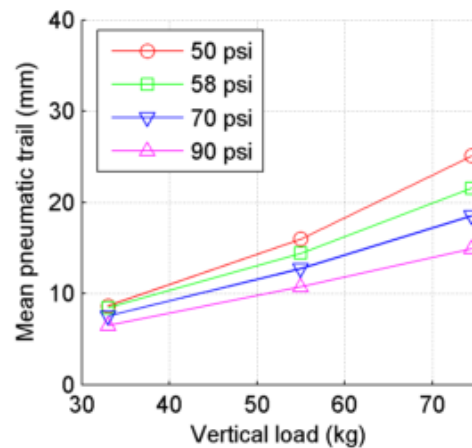
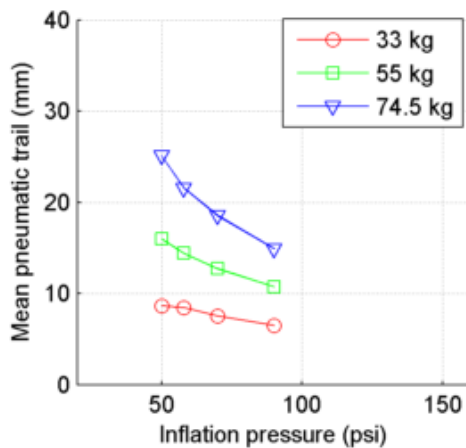
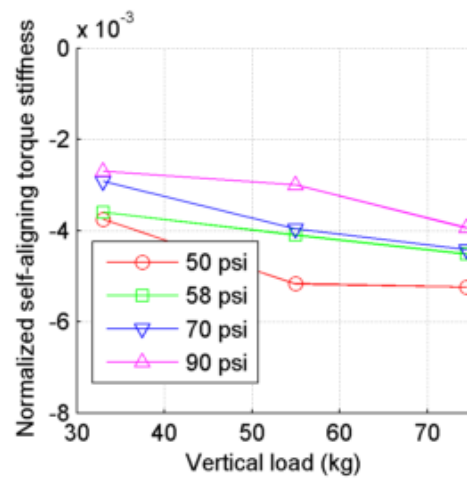
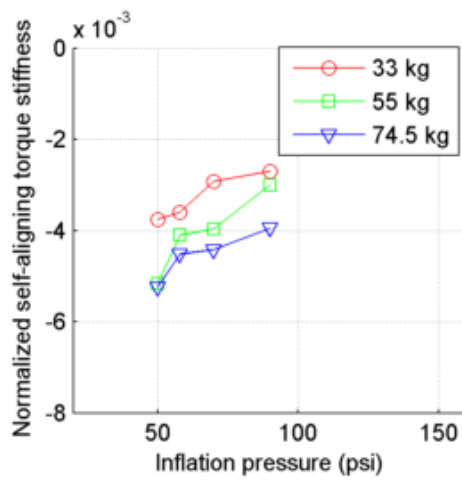
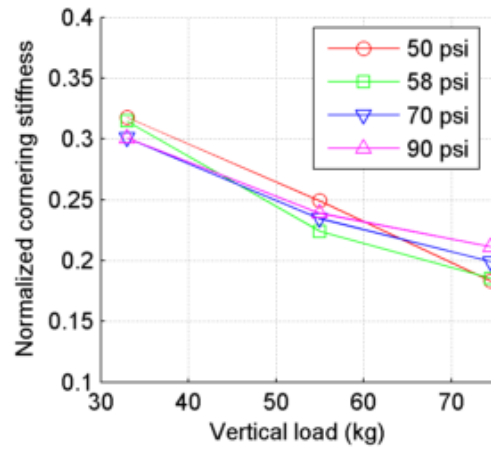
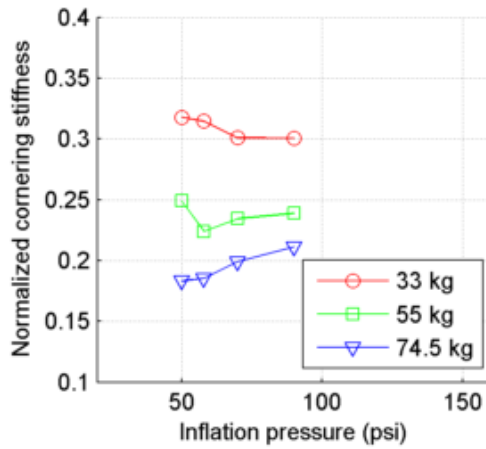
Schwalbe Big Apple 55-622
 tire radius = 23.5 mm, rim width = 18.7 mm

summary
 part 2 of 2



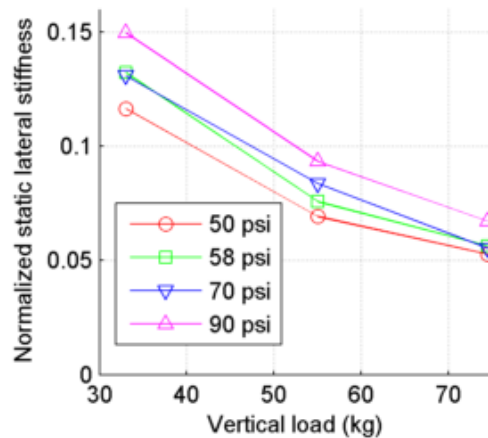
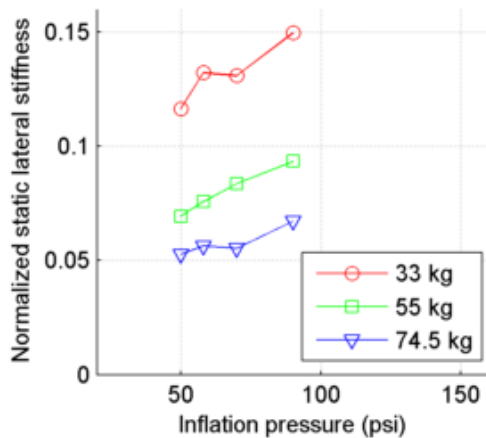
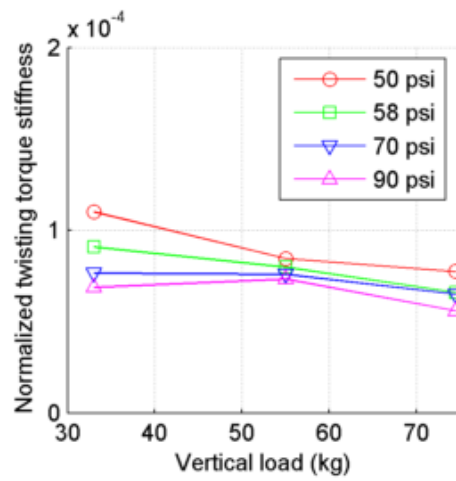
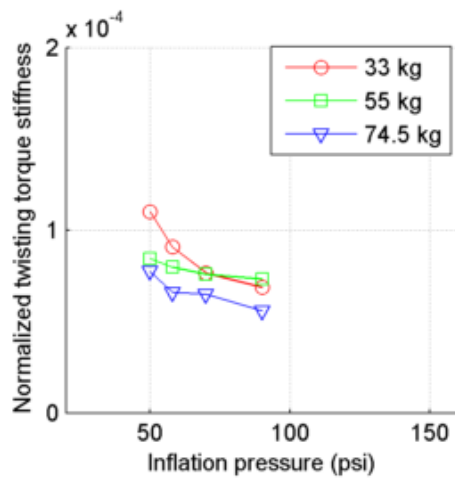
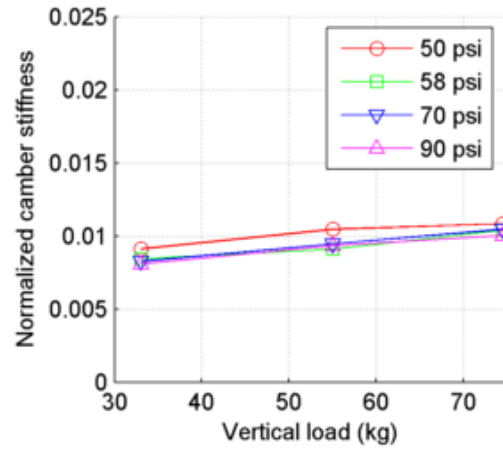
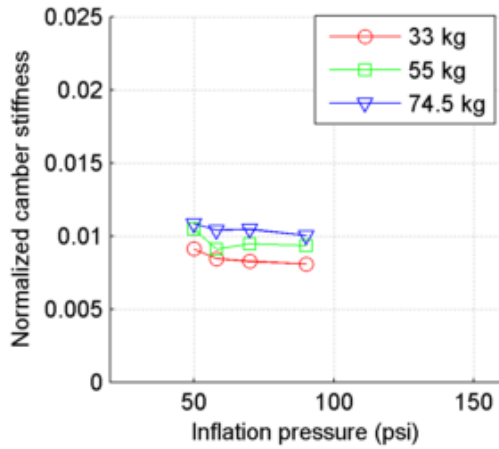
Schwalbe Kojak 35-622
 tire radius = 15.7 mm, rim width = 18.7 mm

summary
 part 1 of 2



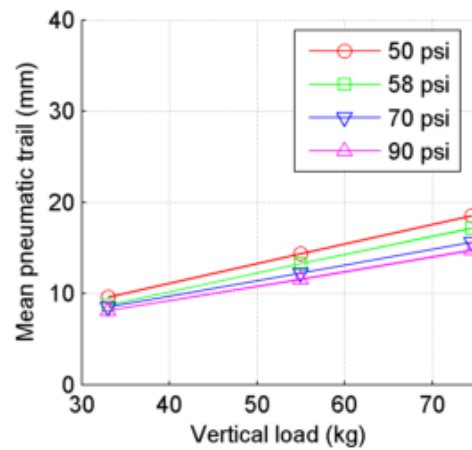
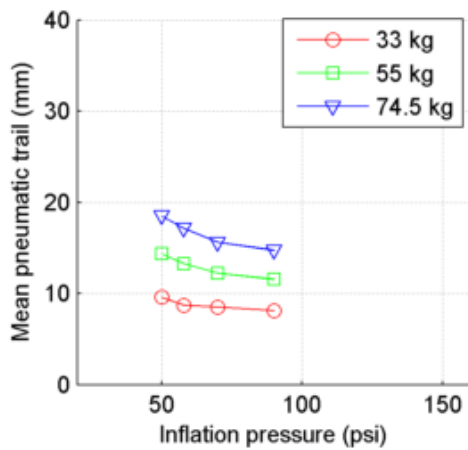
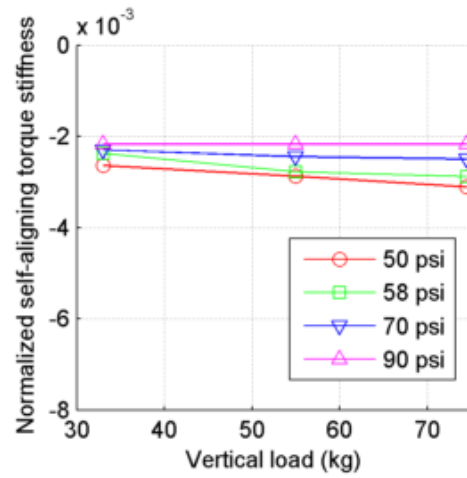
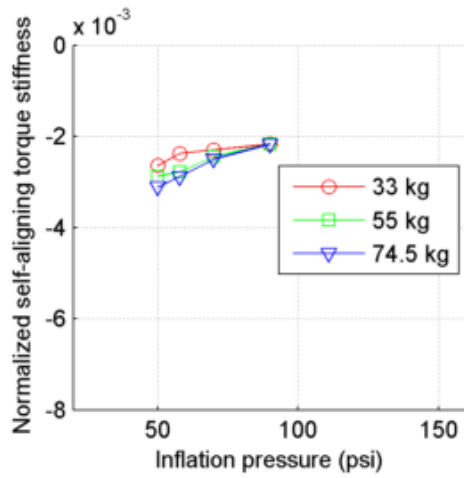
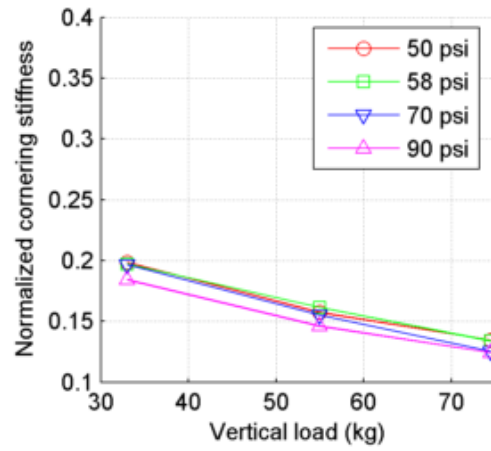
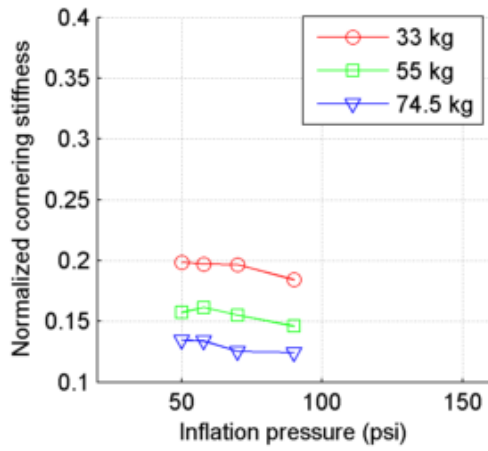
Schwalbe Kojak 35-622
 tire radius = 15.7 mm, rim width = 18.7 mm

summary
 part 2 of 2



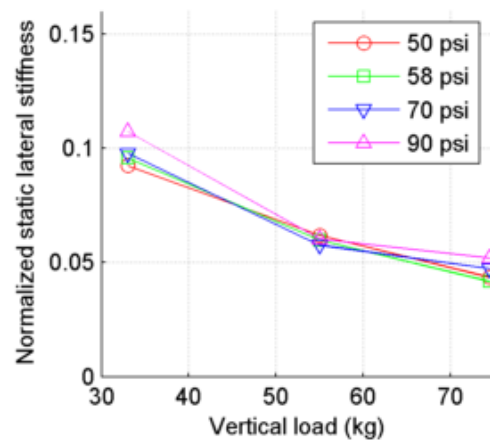
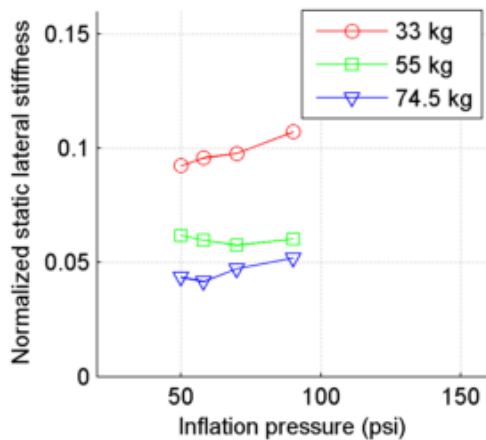
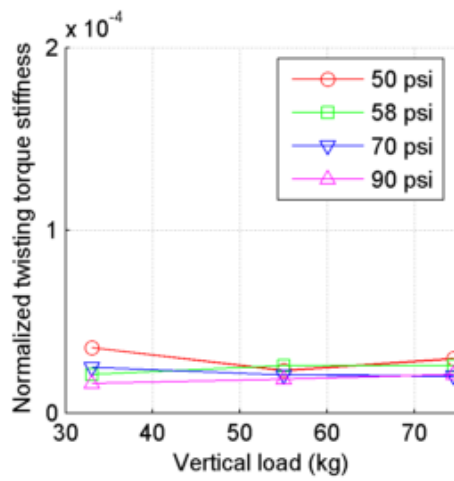
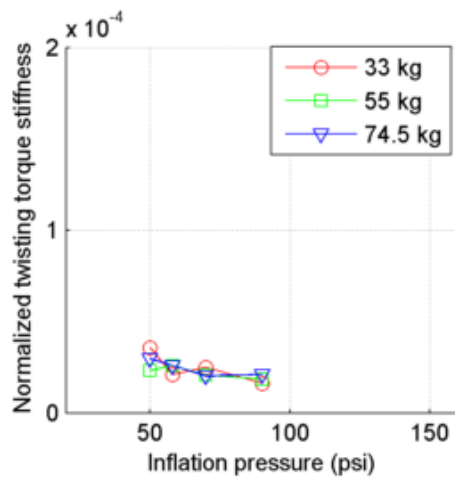
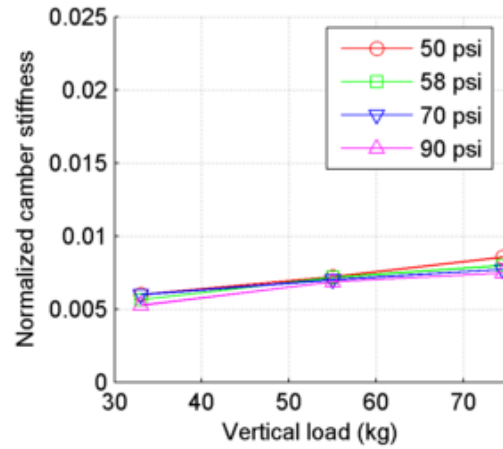
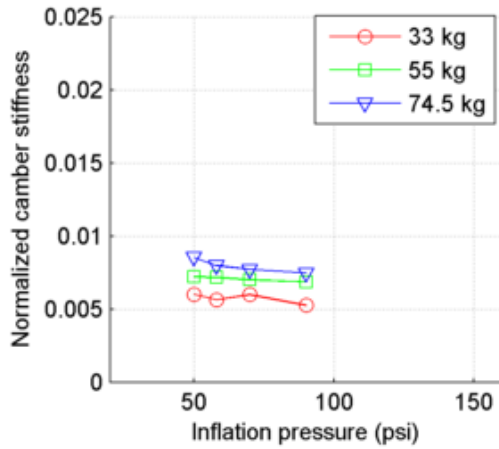
Schwalbe Marathon Plus 37-622
 tire radius = 14.9 mm, rim width = 18.7 mm

summary
 part 1 of 2



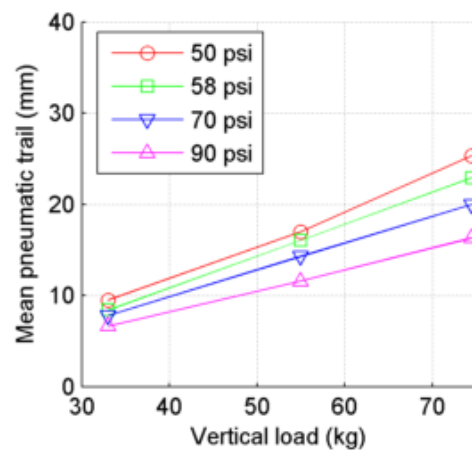
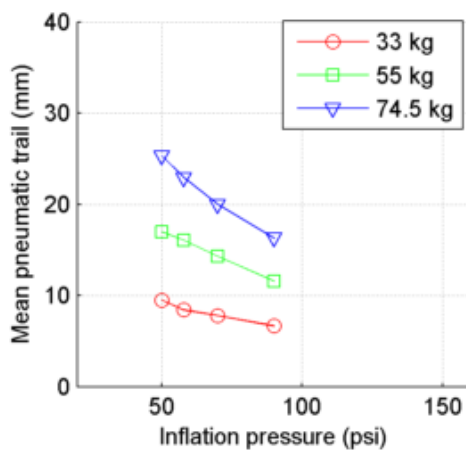
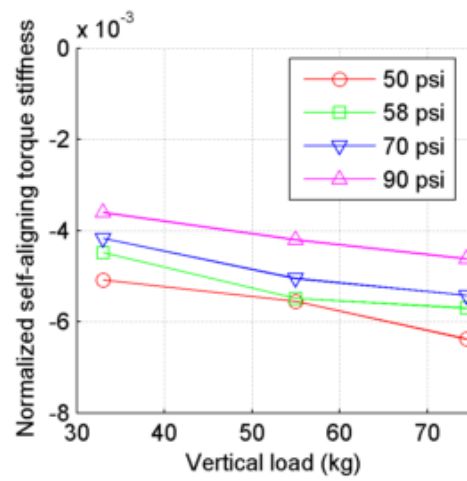
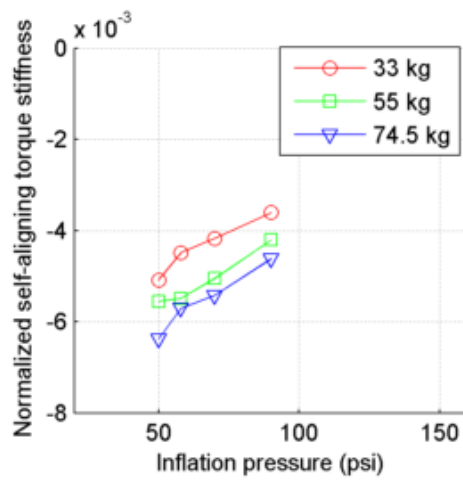
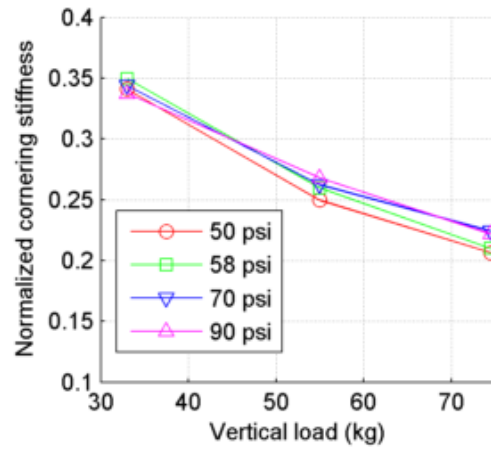
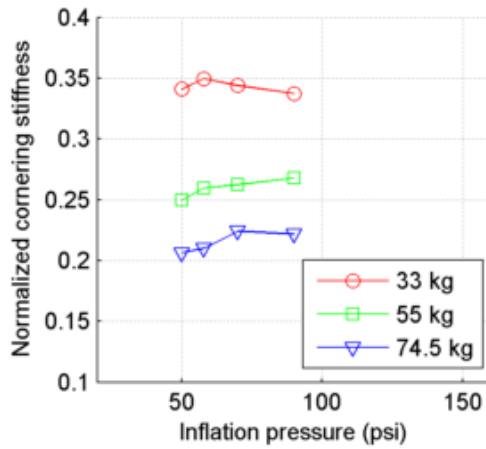
Schwalbe Marathon Plus 37-622
 tire radius = 14.9 mm, rim width = 18.7 mm

summary
 part 2 of 2



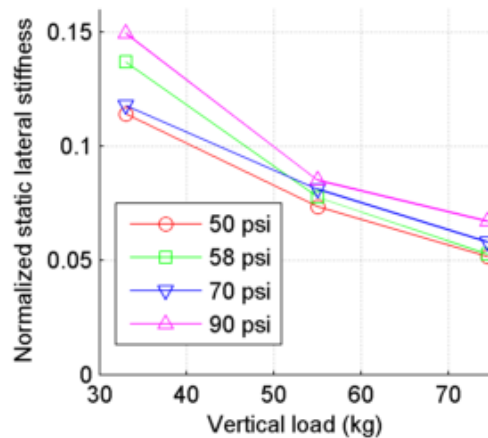
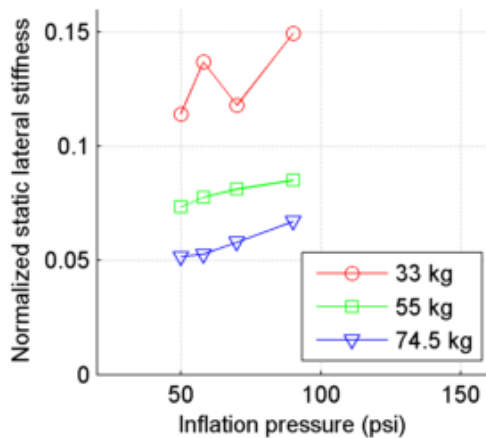
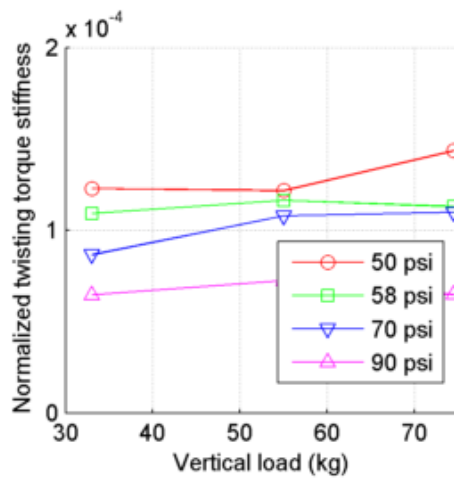
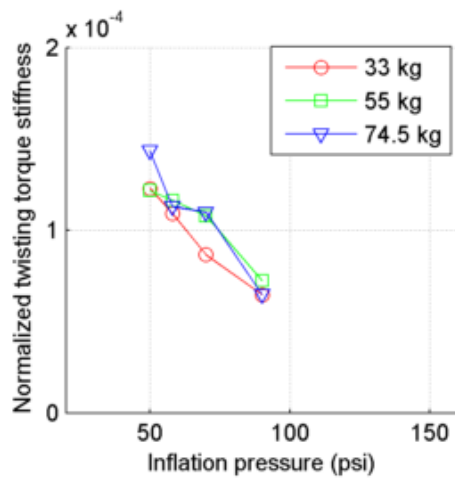
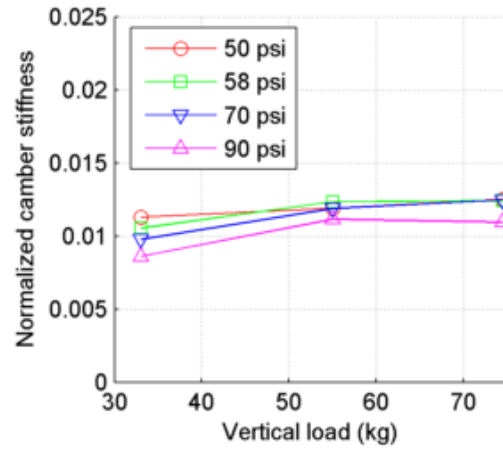
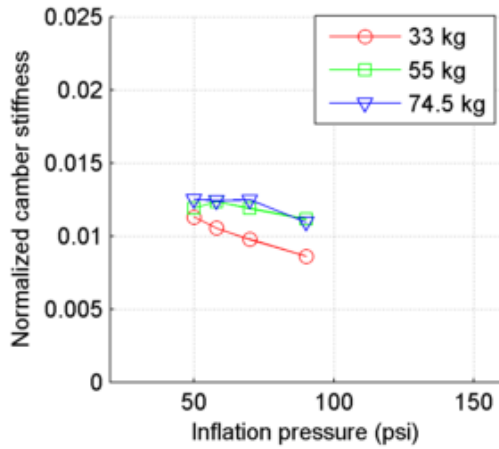
Vittoria Randonneur Hyper 37-622
 tire radius = 17.5 mm, rim width = 18.7 mm

summary
 part 1 of 2



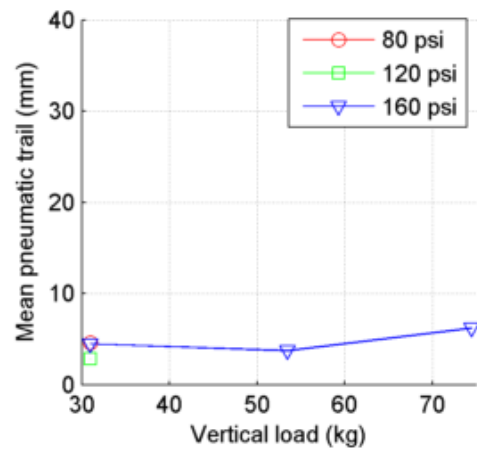
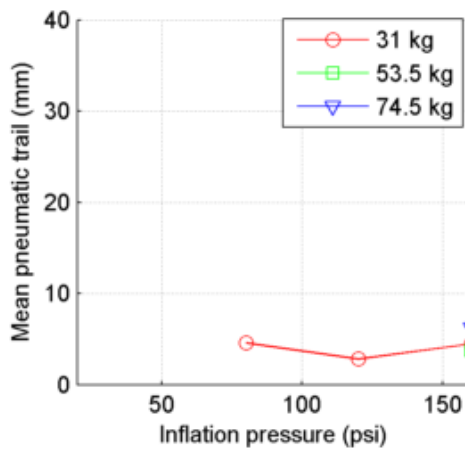
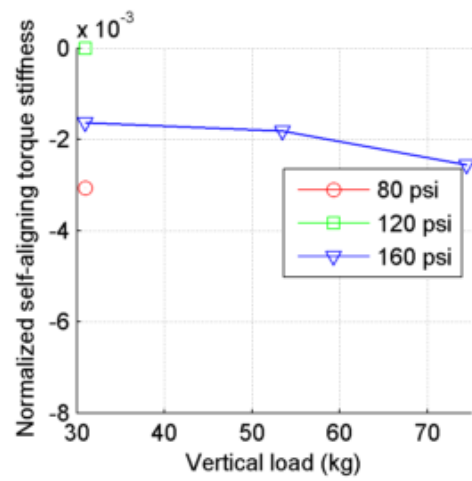
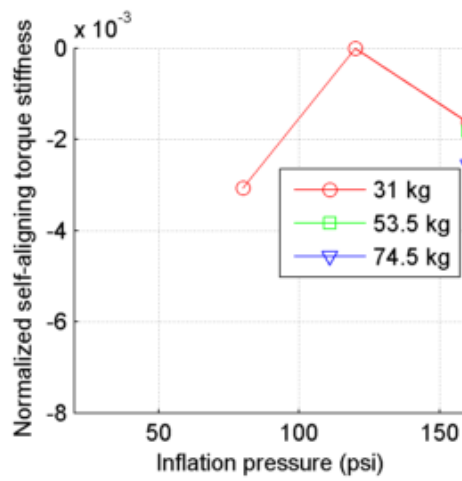
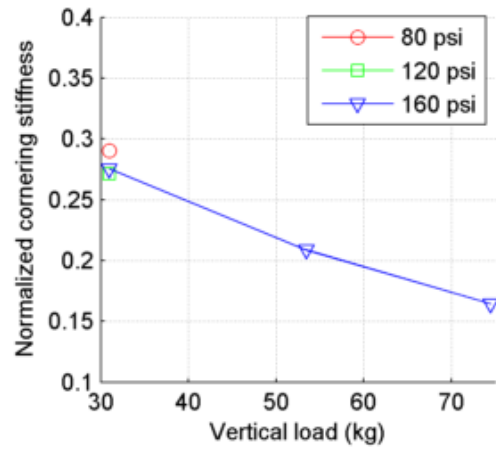
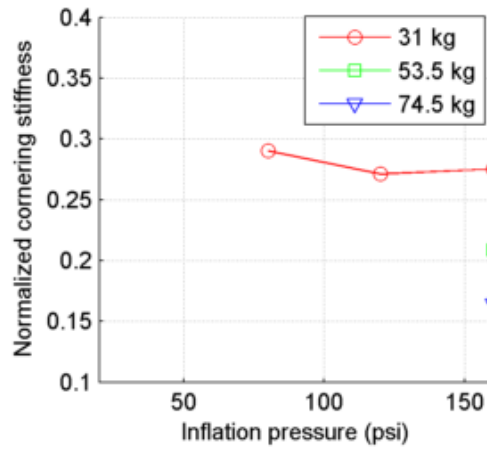
Vittoria Randonneur Hyper 37-622
 tire radius = 17.5 mm, rim width = 18.7 mm

summary
 part 2 of 2



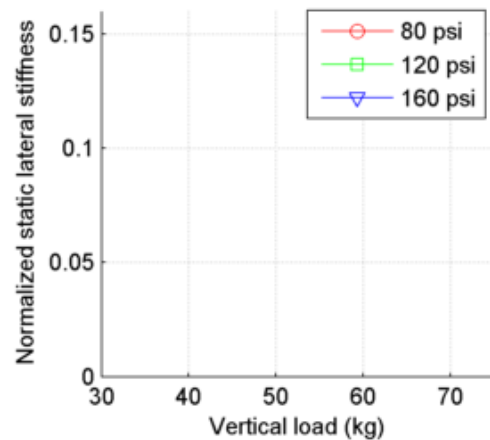
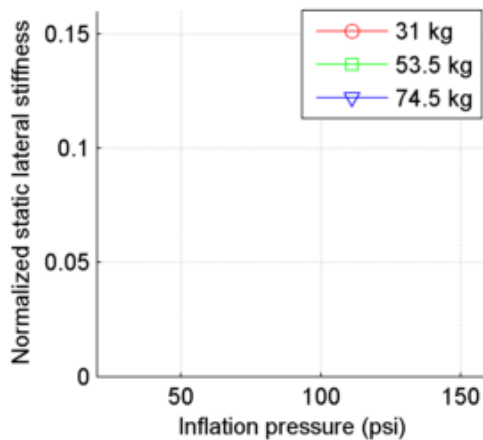
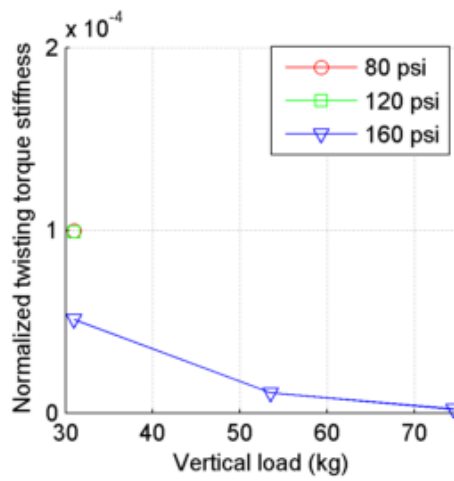
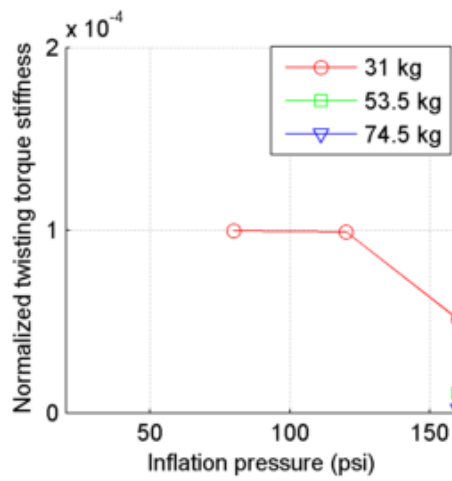
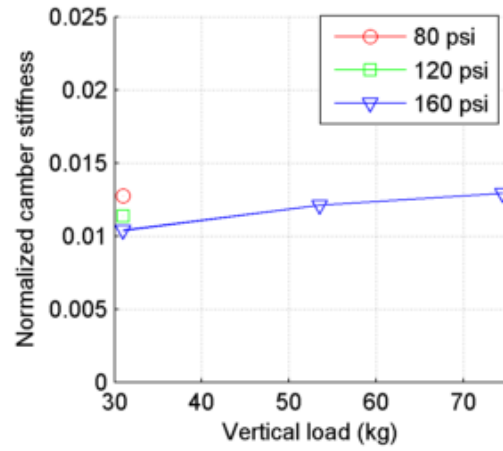
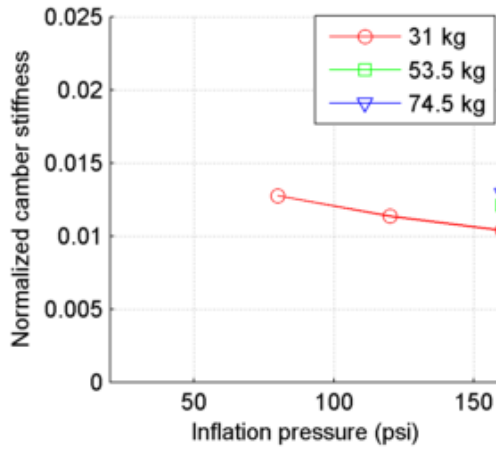
Vredestein Fortezza DuoComp 23-622
 tire radius = 11.5 mm, rim width = 13.4 mm

summary
 part 1 of 2



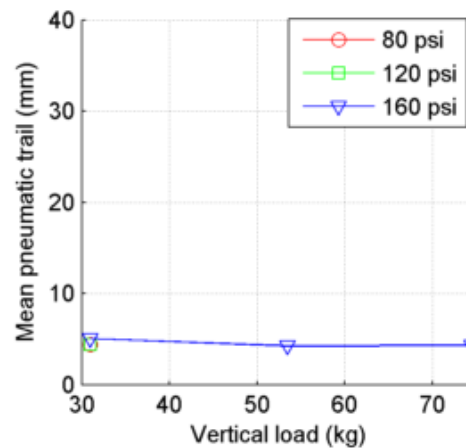
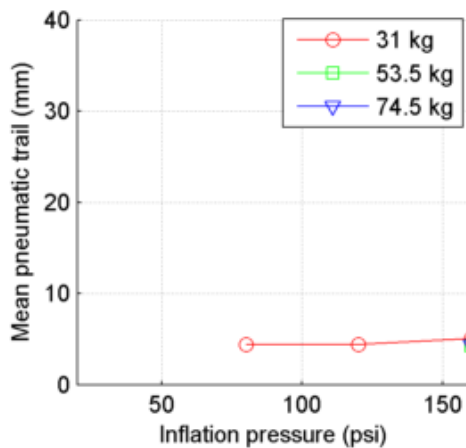
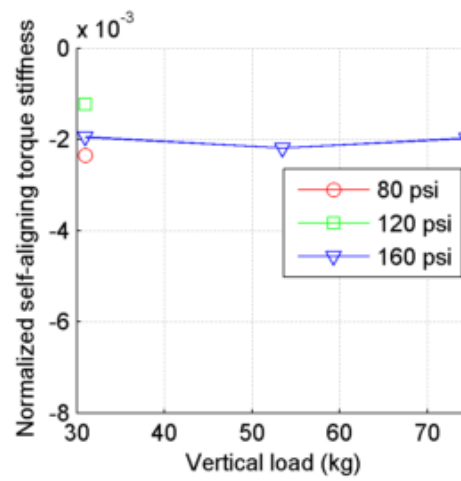
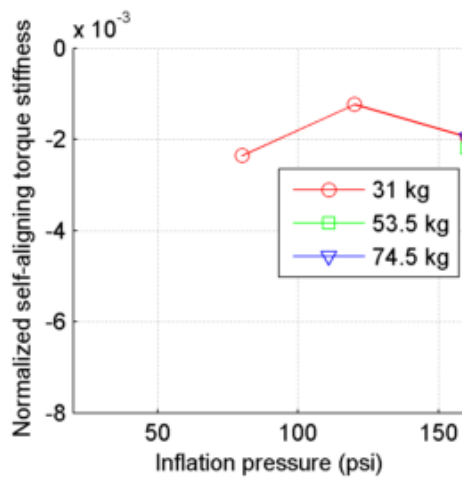
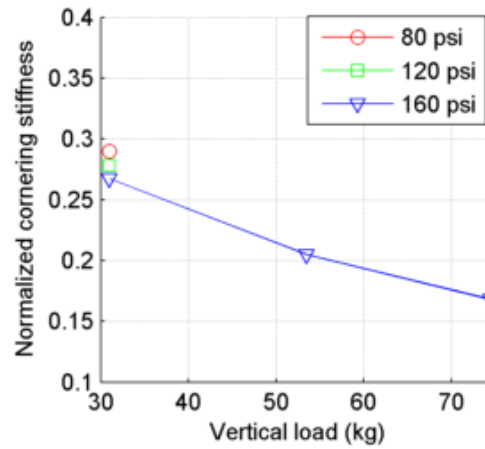
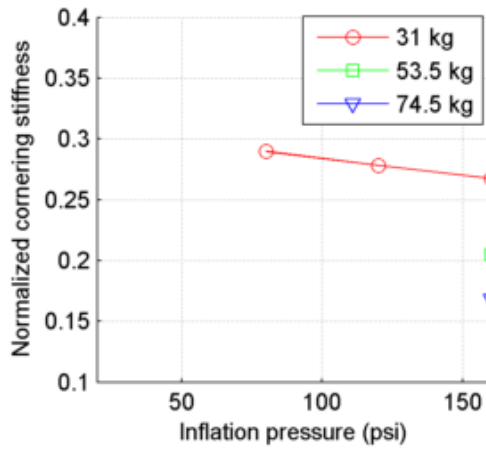
Vredestein Fortezza DuoComp 23-622
 tire radius = 11.5 mm, rim width = 13.4 mm

summary
 part 2 of 2



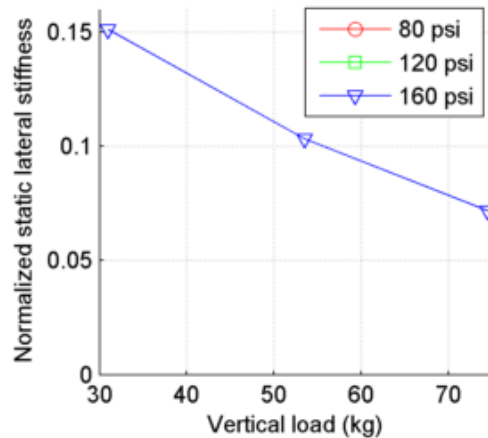
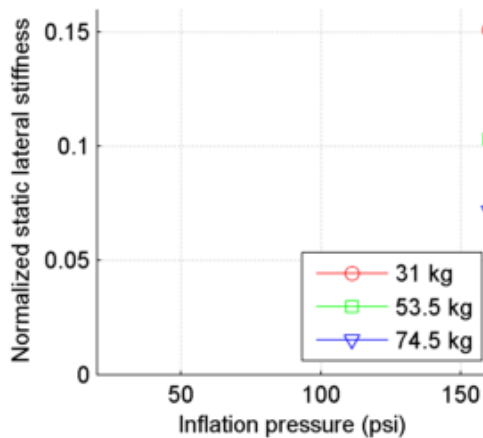
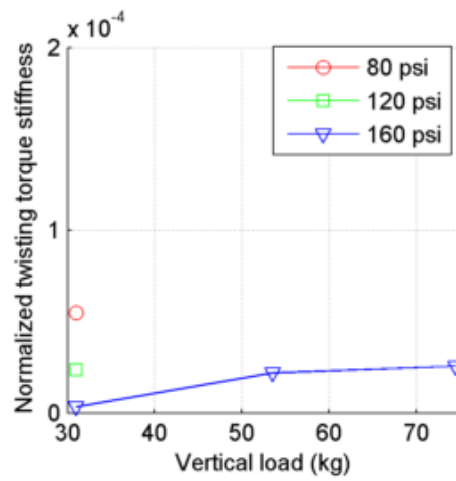
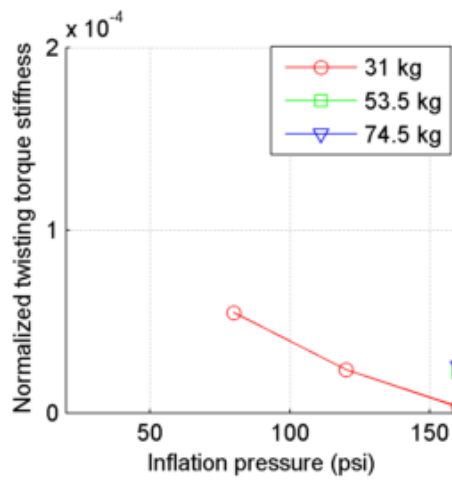
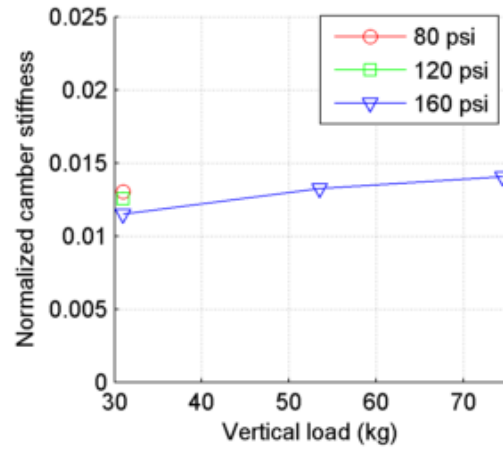
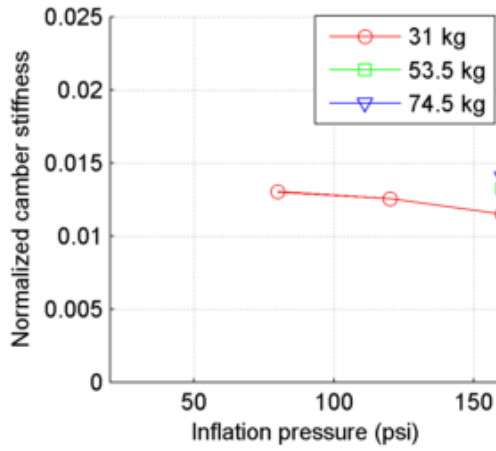
Vredestein Fortezza TriComp 23-622
 tire radius = 11.5 mm, rim width = 13.4 mm

summary
 part 1 of 2



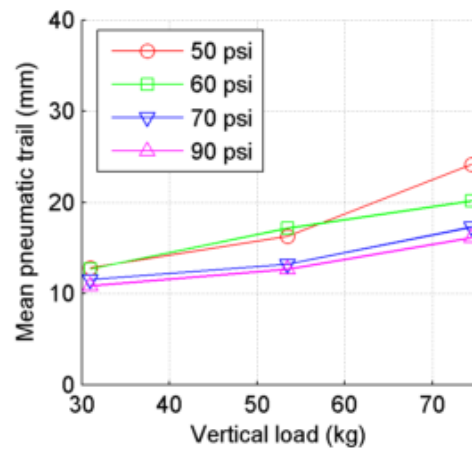
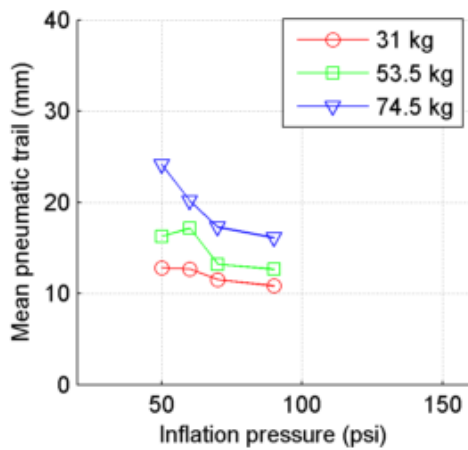
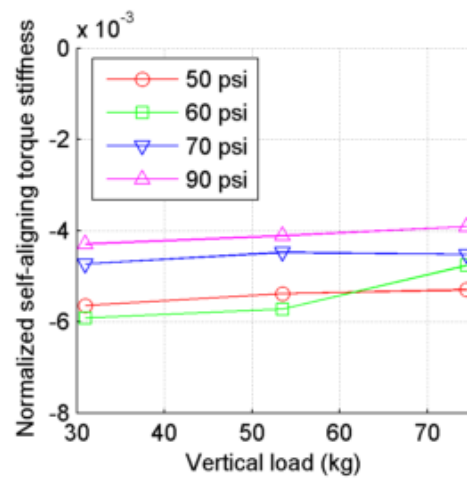
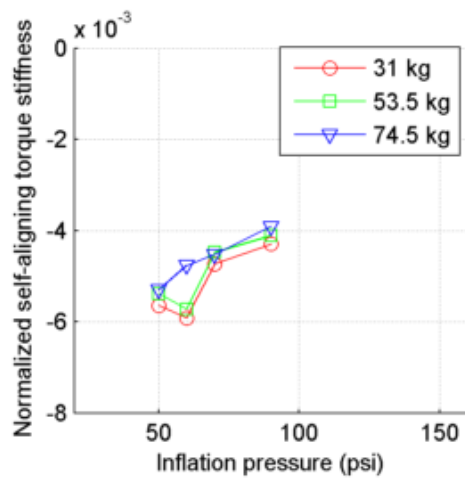
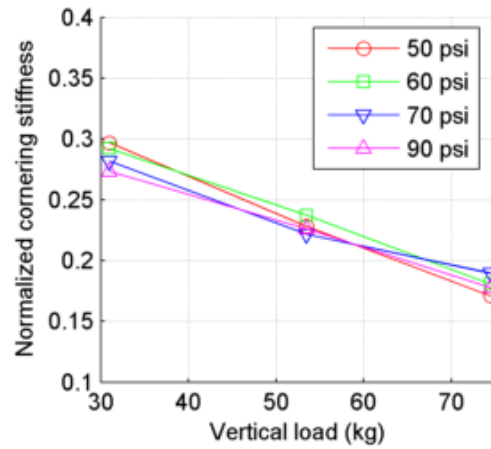
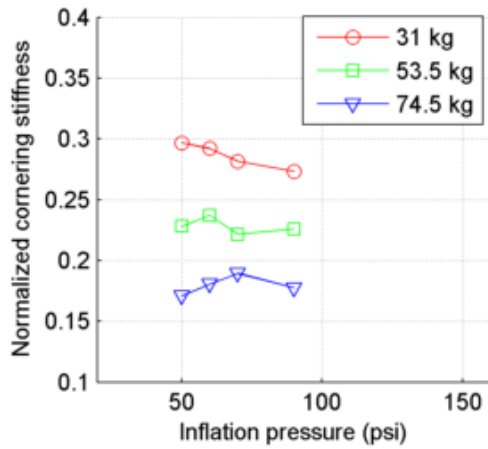
Vredestein Fortezza TriComp 23-622
 tire radius = 11.5 mm, rim width = 13.4 mm

summary
 part 2 of 2



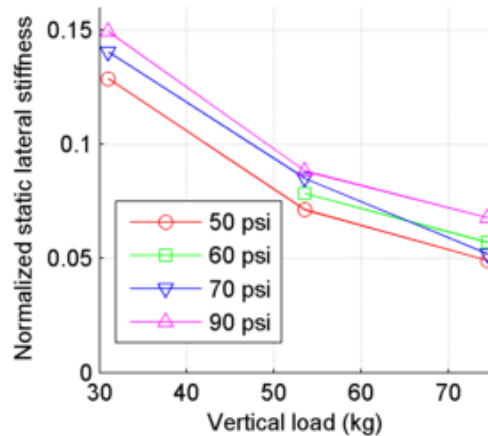
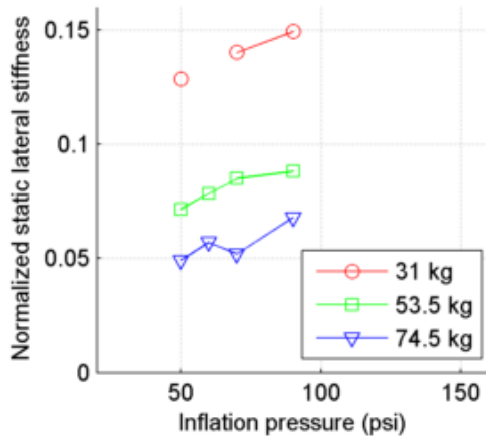
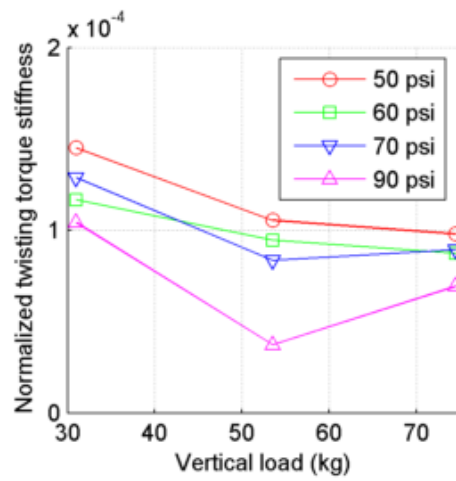
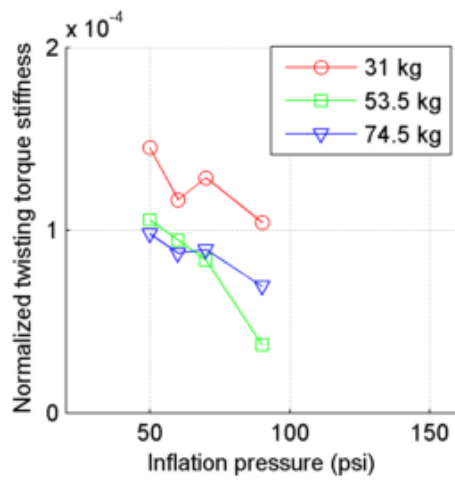
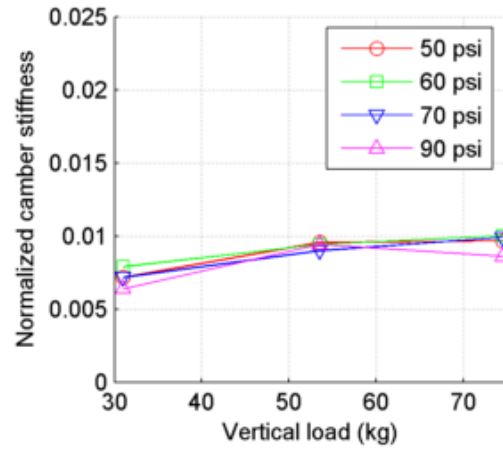
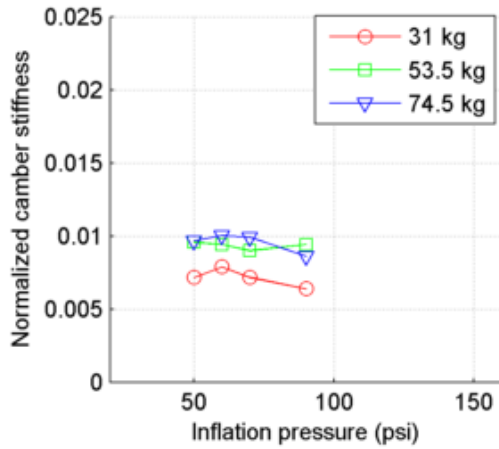
Vredestein Perfect Tour 37-622
 tire radius = 16.8 mm, rim width = 18.7 mm

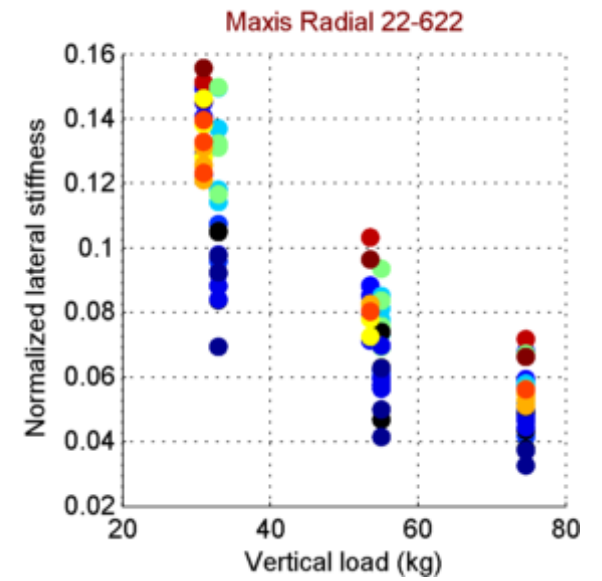
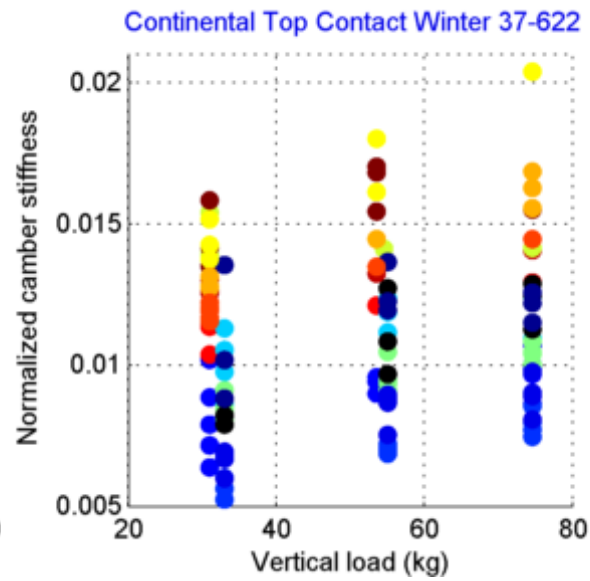
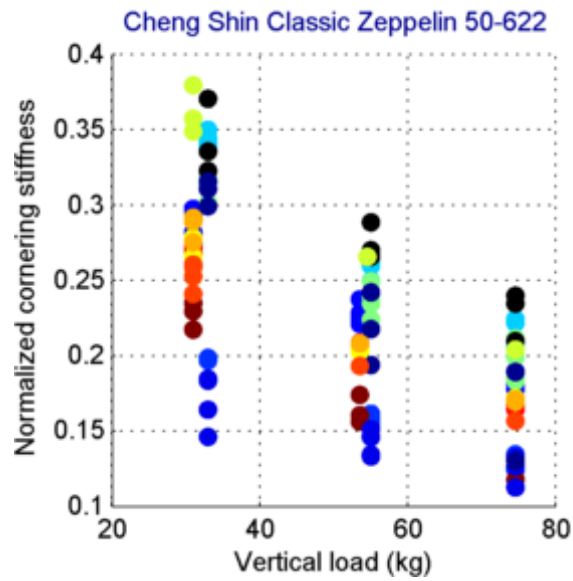
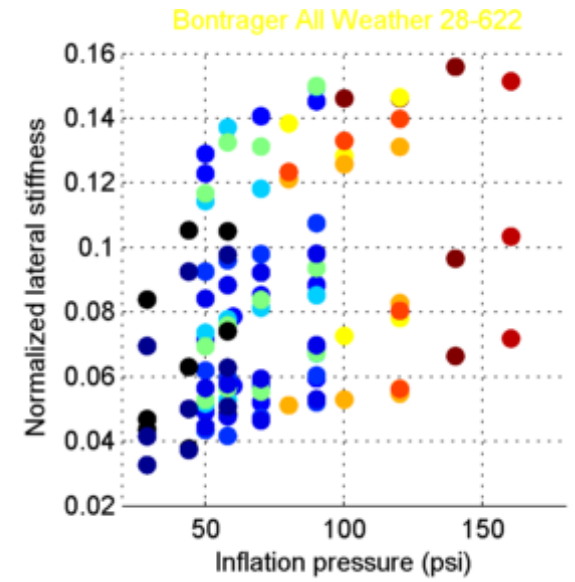
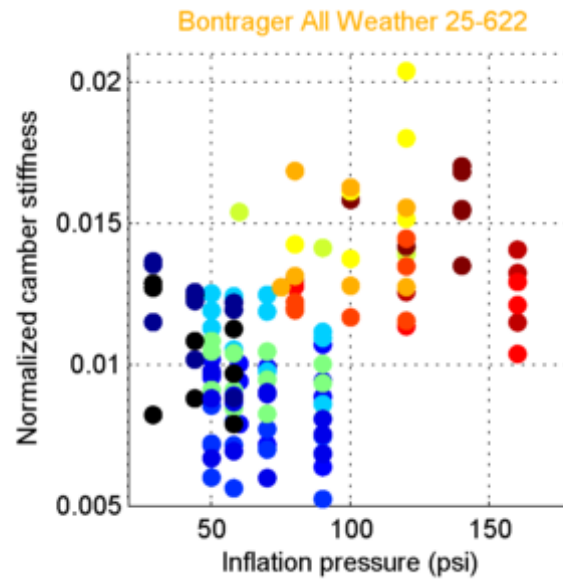
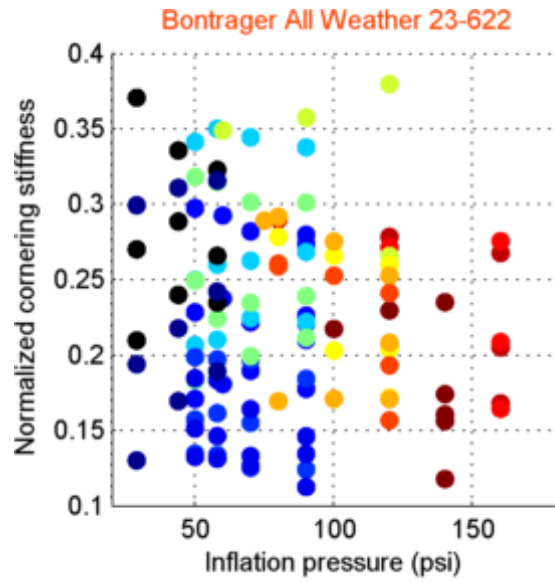
summary
 part 1 of 2

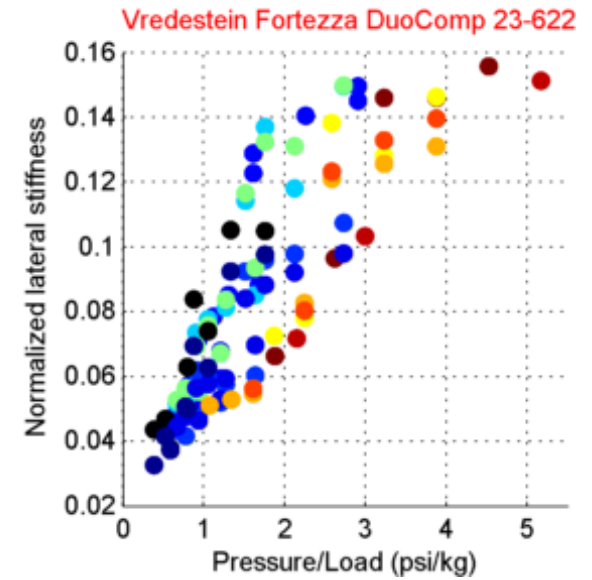
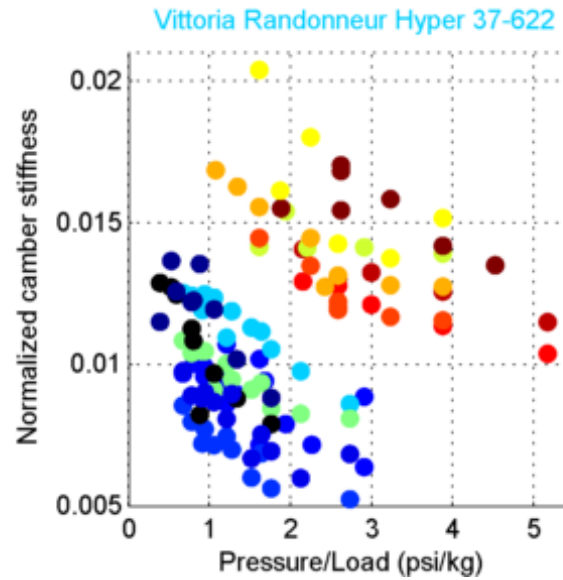
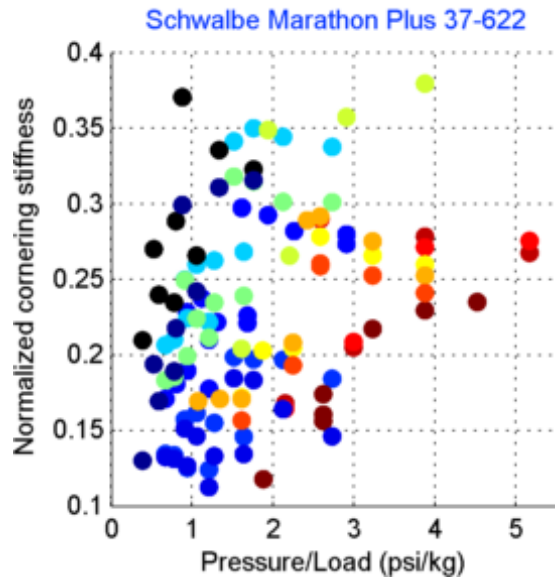
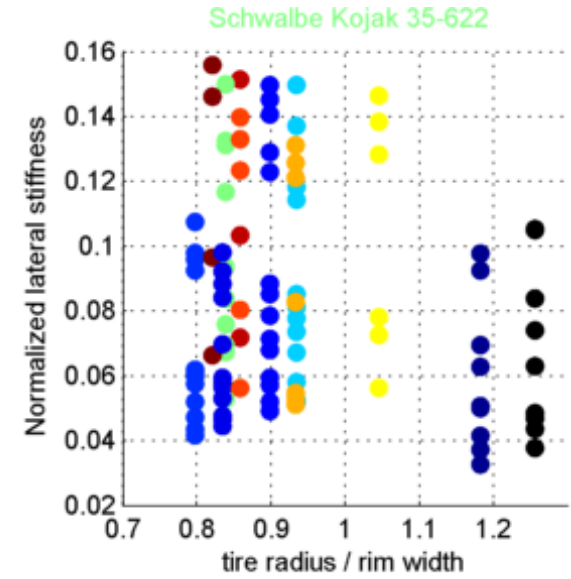
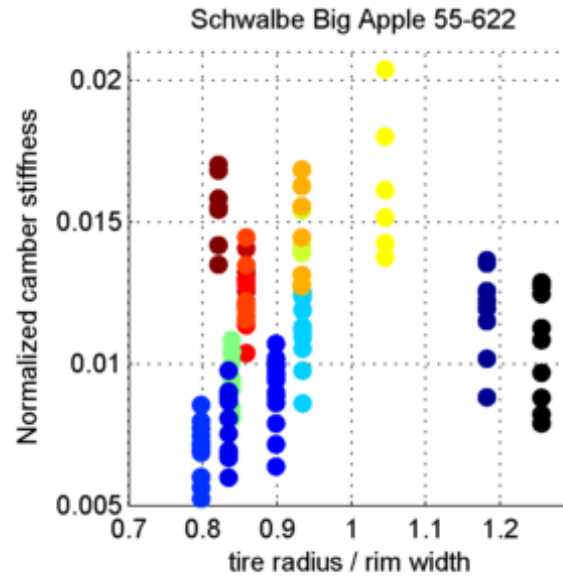
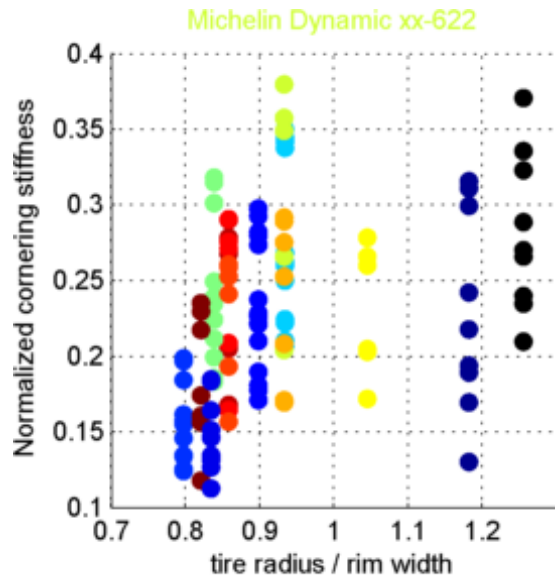


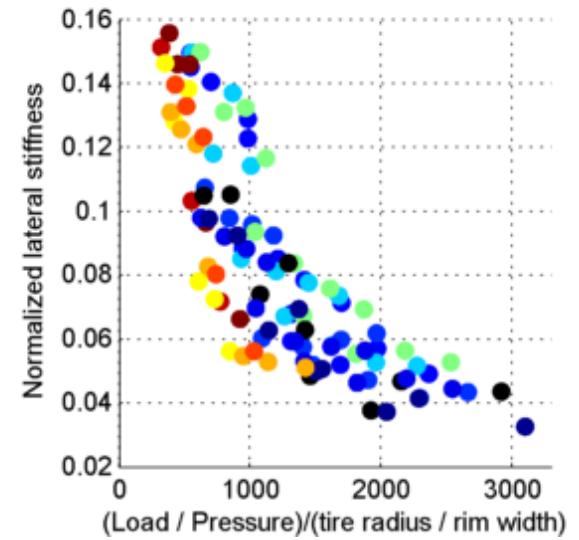
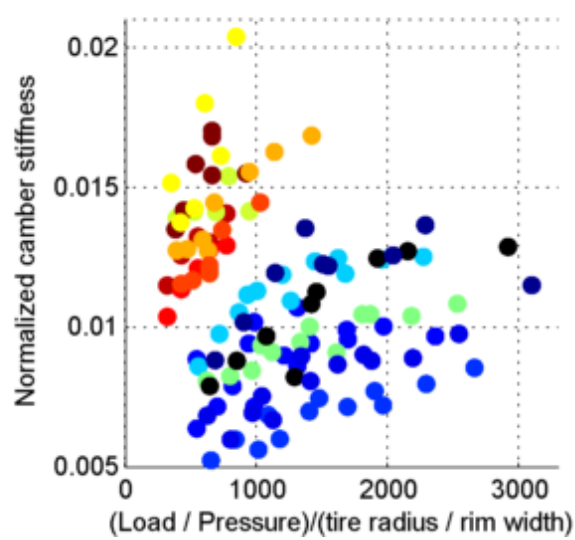
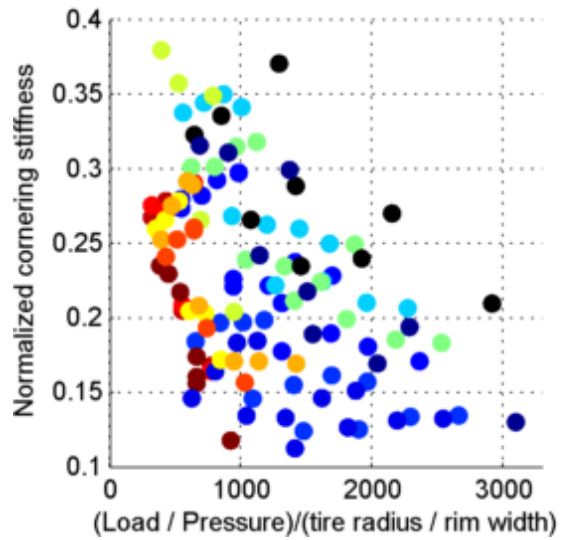
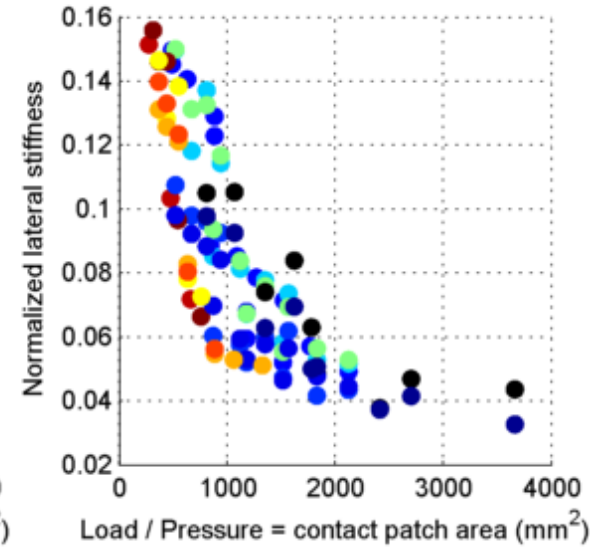
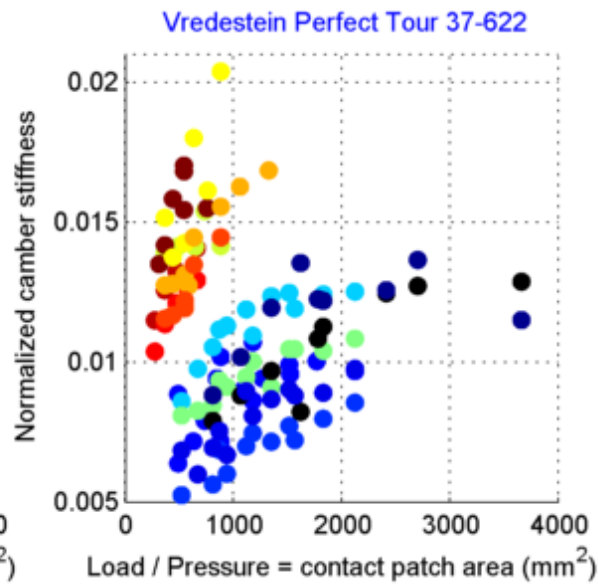
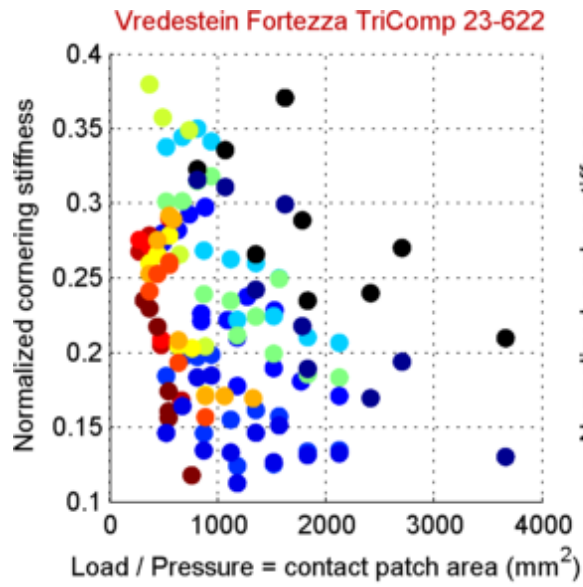
Vredestein Perfect Tour 37-622
 tire radius = 16.8 mm, rim width = 18.7 mm

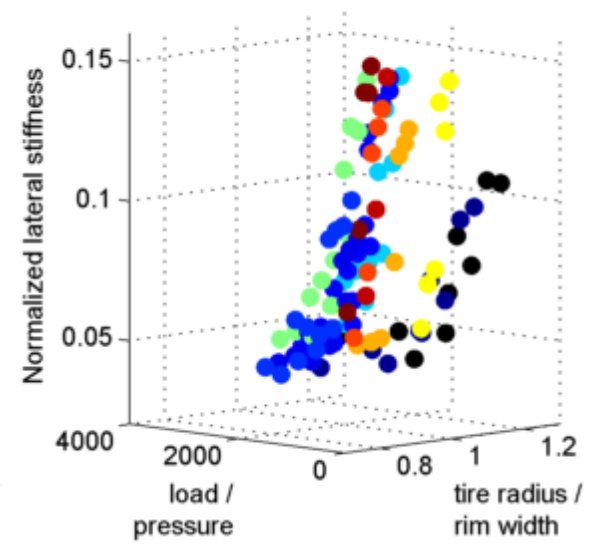
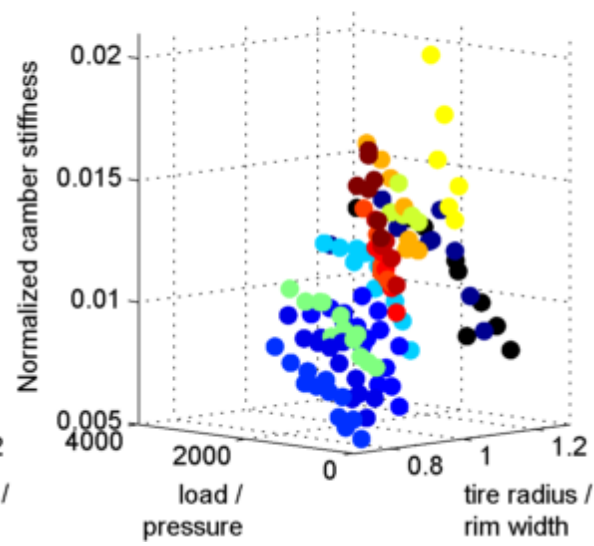
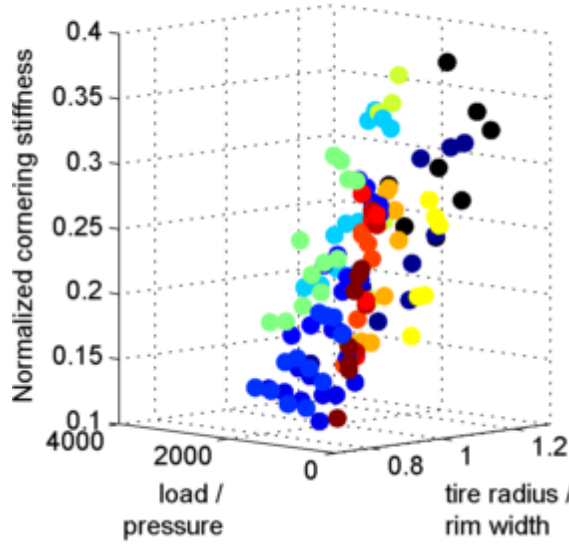
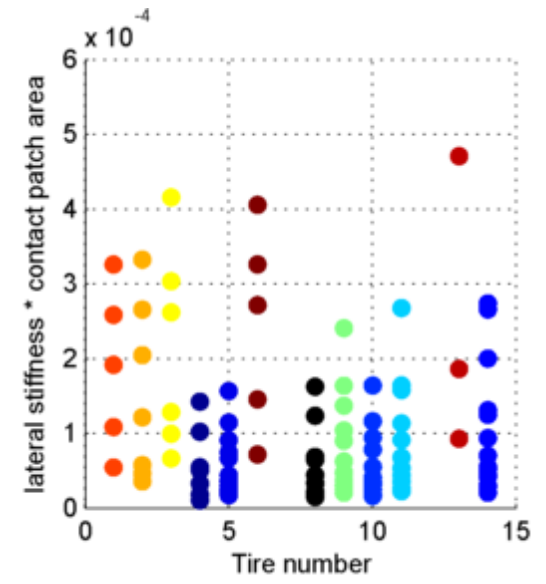
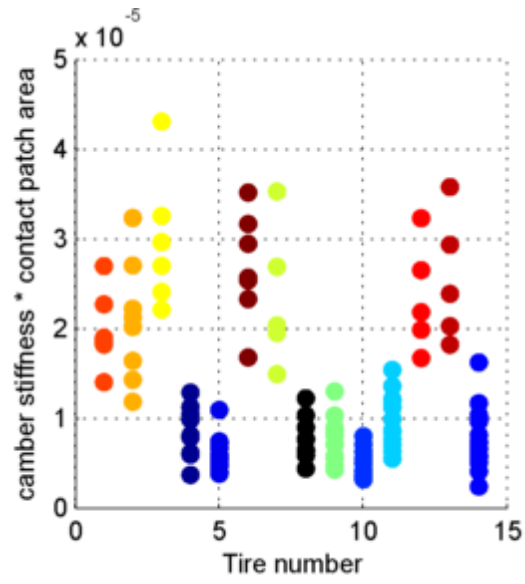
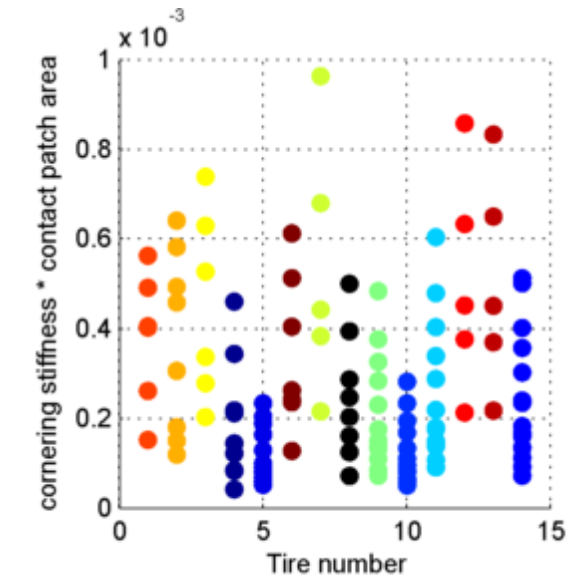
summary
 part 2 of 2











APPENDIX C

MATLAB® SOURCE CODE FOR NUMERICAL MODEL

```
% *****  
% Per Rotta's paper, positive horizontal deflections move the rim towards  
% the left (so tire moves relatively towards the right), and positive  
% camber angles tilt the rim towards the right.  
% *****  
function Rotta_model  
    try  
        tstart = tic;           % keep track of time  
        clc; format compact    % establish desired initial environment  
        disp('Rotta model.')        rc = Rotta_constants;  % define all necessary constants  
  
        % *****  
        % Specify what to do  
        % *****  
        rip.plot_target_vert_force_search_progress = 0;  
        rip.plot_single_tire_config = 1; % plot one set of parameters.  
        rip.plot_wheel_horz_d = 0;  
        rip.run_silent = 0;          % display status after various steps  
        rip.post_patch = 1;         % do calculate tire shape beyond contact patch  
        rip.adjust_wheel_horz_d = 0;  
        read_tire_specs = 0;        % read from a file of tire specs, or not  
        tire_specs_filename = 'Rotta_tire_specs_April_7_format.csv';  
  
        % *****  
        % Specify the number and span of cross sections to define half tire  
        % *****  
        rip.num_slices = 201;      % number of radial slices to evaluate  
        % finding exact end of contact patch and having horz_d -> 0 perfectly  
        % at the end of non-zero camber contact patch is sensitive to this #  
        rip.last_slice_angle = 15*pi/180; % how far around tire to go  
  
        if read_tire_specs == 0  
  
            % *****  
            % Specify slip and camber angles  
            % *****  
            rip.slip_angle = 0.0*pi/180; % angle contact patch center line angle  
            rip.camber_angle = 45*pi/180; % positive = rim tilts to right  
            % positive = contact patch pushed to right, rim to left. Contact patch  
            % front (top of plot) moves right, rear (bottom of plot) moves left  
  
            % *****  
            % Specify the rates at which wheel horizontal displacement decays  
            % once sliding or tire is not longer in contact with ground  
            % *****  
            rip.relaxation_rate_out(2) = 0.993; % before touches ground  
            rip.relaxation_rate_in(2) = 0.993; % just after touching ground  
            rip.relaxation_rate_in(1) = 0.993; % just before leaving ground  
            rip.relaxation_rate_out(1) = 0.993; % after leaving ground  
            rip.relaxation_rate = 0.993;  
  
            rip.friction_coefficient = inf; % inf for no slip  
            rip.friction_coefficient = 1;  % 1 for non-skid tape  
  
            rip.drum_radius = 0;          % flat track at UWM (note use 0 for flat!)  
            rip.drum_radius = 2500/2;    % 2.5 meter diameter drum at TU Delft  
  
            rip.disk_radius = 0;         % straight track at UWM (note use of 0 for straight!)  
            rip.disk_radius = 3*1000/2;  % 3.0 meter diameter disk at Padua
```

```

% *****
% Specify the maximum vertical and horizontal deflections
% *****
rip.wheel_vert_d = 5; % positive = rim sags towards ground
% wheel_vert_d ignored if target_vert_force ~= 0

rip.wheel_horz_d = 0; %
% Positive values push contact patch to the right, or rim to left, and
% positive values reduce camber thrust deficiency.
% *****
% define wheel and tire parameters
% *****
rip.rim_diameter = 622; % 700C has "bead seat diameter" = 622
rip.rim_width = 18.7; % interior width from tire bead to bead
rip.tire_size = 37;
rip.tire_width = 0;%128.2; % estimate this below
rip.inf_press = 4 * rc.MPa_per_bar; % inflation pressue
rip.target_vert_force = 400; % * rc.N_per_kg;
% rip.target_vert_force = 0;

% *****
% try to make a smart first guess
% *****
rip.initial_sinkage_guess = 0.1 * rip.target_vert_force / rc.g;

rows = 1; % just do one, as specified above
else % read_tire_specs == 1

fprintf('Reading tire specs from %s\n', tire_specs_filename');
% *****
% Read in a comma-delimited file of tire specifications, skipping
% first row of text column headers
% *****
tire_specs = csvread(tire_specs_filename, 1, 0);
[rows, cols] = size(tire_specs);
end

% *****
% Default to going as fast as possible when doing more than one
% *****
if rows > 1
rip.plot_target_vert_force_search_progress = 0;
rip.plot_single_tire_config = 0;
rip.plot_wheel_horz_d = 0;
rip.run_silent = 1;
end

% *****
% Evaluate all the tire specifications requested
% *****
tire_specs_evaluated = 0;
for row = 1:rows

if read_tire_specs == 1
% *****
% decide whether to skip or not, and let user know what's up
% *****
do_this_row = tire_specs(row,1);
if read_tire_specs == 1 && do_this_row == 1
fprintf(' Starting row %d of %d\n', row, rows)
elseif read_tire_specs == 1 && do_this_row == 0
fprintf(' Skipping row %d of %d\n', row, rows)
continue
end
% *****
% stuff tire specs from file into parameters expected below
% *****
rip.drum_radius = tire_specs(row,2);
rip.disk_radius = tire_specs(row,3);

```

```

rip.rim_diameter = tire_specs(row,4);
rip.rim_width = tire_specs(row,5);
rip.tire_number = tire_specs(row,6);
rip.tire_size = tire_specs(row,7);
rip.tire_radius = tire_specs(row,8);
rip.tire_width = tire_specs(row,9);
rip.tire_thickness = tire_specs(row,10);
rip.inf_press = tire_specs(row,11) * rc.MPa_per_psi;
rip.target_vert_force = tire_specs(row,12) * rc.N_per_kg;
rip.wheel_vert_d = tire_specs(row,13);
rip.wheel_horz_d = tire_specs(row,14);
rip.slip_angle = tire_specs(row,15)*pi/180;
rip.camber_angle = tire_specs(row,16)*pi/180;
rip.friction_coefficient = tire_specs(row, 17);
rip.relaxation_rate_out(1) = tire_specs(row,18);
rip.relaxation_rate_in(1) = tire_specs(row,19);
rip.relaxation_rate_in(2) = tire_specs(row,20);
rip.relaxation_rate_out(2) = tire_specs(row,21);
rip.relaxation_rate = sum(tire_specs(row,18:21))/4; % average
measured_lateral_stiffness = tire_specs(row,22);
measured_cornering_stiffness = tire_specs(row,23);
measured_camber_stiffness = tire_specs(row,24);
if ~isnan(rip.target_vert_force) && rip.target_vert_force ~= 0
    rip.initial_sinkage_guess = 0.1 * rip.target_vert_force / rc.g;
end
end

% *****
% Calculate additional wheel and tire dimensions
% Note that:
% 1. "rip.rim_width" is distance from one inner rim edge to other
% 2. "rip.rim_angle" is angle swept by tire from rim to rim
% 3. "rip.tire_size" is number printed on the size
% 4. "rip.tire_radius" is actual radius of tire circular arc
% 5. "rip.tire_width" is circumference of tire cross section
% *****
if rip.tire_width == 0 % not yet specified? Estimate from tire size

    rip.tire_radius = rip.tire_size / 2;
    rip.rim_angle = 2 * asin(rip.rim_width / (2 * rip.tire_radius));
    rip.rim_height = rip.tire_radius * (1 + cos(rip.rim_angle / 2));
    rip.tire_width = rip.tire_radius * (2*pi - rip.rim_angle);

else % rip.tire_width ~= 0, use it to calculate tire radius and "size"
    % no closed-form solution, have to iterate. At least let ML do it.
    rip.rim_angle = fzero(@(t) (rip.rim_width/rip.tire_width - ...
        (2*sin(0.5*t))/(2*pi - t)), pi/4);
    rip.tire_radius = rip.rim_width / (2*sin(0.5*rip.rim_angle));
    rip.tire_size = rip.tire_radius * 2;
    rip.rim_angle = 2 * asin(rip.rim_width / (2 * rip.tire_radius));
    rip.rim_height = rip.tire_radius * (1 + sin((pi - rip.rim_angle) / 2));
end

% *****
% calculate all the rotta stuff
% *****
[rop] = Rotta_core(rip);
tire_specs_evaluated = tire_specs_evaluated + 1;

% *****
% If test compatible with stiffnesses,
% calculate those values
% *****
norm_lateral_stiffness = NaN; norm_cornering_stiffness = NaN; ...
    norm_camber_stiffness = NaN;
if rip.wheel_horz_d ~= 0 && rip.camber_angle == 0 && rip.slip_angle == 0
    norm_lateral_stiffness = (rop.horz_force / rop.vert_force) / ...
        rip.wheel_horz_d;
elseif rip.slip_angle ~= 0 && rip.camber_angle == 0
    norm_cornering_stiffness = (rop.horz_force / rop.vert_force) / ...

```

```

                                (rip.slip_angle*180/pi);
elseif rip.slip_angle == 0 && rip.camber_angle ~= 0
    norm_camber_stiffness = (rop.horz_force / rop.vert_force) / ...
                            (rip.camber_angle*180/pi);
end

if read_tire_specs == 1
    tire_specs(row, (cols + 1)) = rop.vert_force;
    tire_specs(row, (cols + 2)) = rop.wheel_vert_d;
    tire_specs(row, (cols + 3)) = 100*rop.wheel_vert_d/rip.rim_height;
    tire_specs(row, (cols + 4)) = rop.wheel_horz_d;
    tire_specs(row, (cols + 5)) = rop.cp_length;
    tire_specs(row, (cols + 6)) = rop.cp_width;
    tire_specs(row, (cols + 7)) = rop.cp_area;
    tire_specs(row, (cols + 8)) = rop.ellipse_cp_length;
    tire_specs(row, (cols + 9)) = rop.ellipse_cp_width;
    tire_specs(row, (cols + 10)) = rop.ellipse_cp_area;
    tire_specs(row, (cols + 11)) = rop.horz_force;
    tire_specs(row, (cols + 12)) = rop.net_force_orientation;
    tire_specs(row, (cols + 13)) = rop.relaxation_length;
    tire_specs(row, (cols + 14)) = rop.pneumatic_trail;
    tire_specs(row, (cols + 15)) = rop.self_aligning_torque;
    tire_specs(row, (cols + 16)) = norm_lateral_stiffness;
    tire_specs(row, (cols + 17)) = norm_cornering_stiffness;
    tire_specs(row, (cols + 18)) = norm_camber_stiffness;
    tire_specs(row, (cols + 19)) = (norm_lateral_stiffness - ...
        measured_lateral_stiffness)/measured_lateral_stiffness;
    tire_specs(row, (cols + 20)) = (norm_cornering_stiffness - ...
        measured_cornering_stiffness)/measured_cornering_stiffness;
    tire_specs(row, (cols + 21)) = (norm_camber_stiffness - ...
        measured_camber_stiffness)/measured_camber_stiffness;
end

end % for row = 1:rows
% *****
% Write tire specs previously read along with new values calculated
% back out to a comma-delimited file
% Pad first row digits to make room for row of text column headings
% that will be overwritten next
% *****
if read_tire_specs == 1
    % read first row of text column headings
    h = fopen(tire_specs_filename, 'rt');
    tire_specs_header = fgetl(h);
    fclose(h);
    % append additional column headings for newly calculated values
    tire_specs_header = [tire_specs_header ...
        ',Rotta vertical force (N),Rotta vertical displacement (mm)' ...
        ',Rotta sinkage (%),Rotta wheel horz disp (mm),Rotta contact patch length (mm)' ...
        ',Rotta contact patch width (mm),Rotta contact patch area (mm^2)' ...
        ',Rotta contact patch ellipse length (mm),Rotta contact patch ellipse width (mm)' ...
        ',Rotta contact patch ellipse area (mm^2),Rotta horz force (N)' ...
        ',Rotta net force orientation (degrees),Rotta relaxation length (mm)' ...
        ',Rotta pneumatic trail (mm),Rotta self aligning torque (N-mm)' ...
        ',Rotta norm lat stiffness (1/mm),Rotta norm corn stiffness (1/deg)' ...
        ',Rotta norm camb stiffness (1/deg)'];
    % write out first row of text column headings
    output_filename = ['out_' tire_specs_filename];
    h = fopen(output_filename, 'wt');
    while h == -1
        beep;
        ButtonName = questdlg(sprintf('Could not open %s\n Retry?', ...
            output_filename), 'Error', ...
            'Yes', 'No', 'Yes');
        switch ButtonName
            case 'Yes'
                h = fopen(output_filename, 'wt');
            case 'No'
                break
        end
    end
end

```

```

end
if h == -1
    fprintf('Could not open %s so no results written\n', ...
            output_filename)
else
    fprintf(h, '%s\n', tire_specs_header);
    fclose(h);
    % write out matrix of values and padded digits
    dlmwrite(output_filename, tire_specs, '-append')
    fprintf('Results written to %s\n', output_filename)
end
end % if read_tire_specs == 1
t = toc(tstart);
fprintf(['All done. Evaluated %d set of tire specs in %0.4g seconds' ...
        ', at a rate of %0.3g seconds per tire spec.\n'], ...
        tire_specs_evaluated, t, t/tire_specs_evaluated)
catch me
    fprintf('\n\nUh oh. Something went wrong.\n\n')
    fprintf('\n%s\n', getReport(me))
    % *****
    % Write tire specs previously read along with new values calculated
    % back out to a comma-delimited file
    % Pad first row digits to make room for row of text column headings
    % that will be overwritten next
    % *****
if read_tire_specs == 1
    fprintf('\n\nWill now try to write results so far.\n\n')
    % read first row of text column headings
    h = fopen(tire_specs_filename, 'rt');
    tire_specs_header = fgetl(h);
    fclose(h);
    % append additional column headings for newly calculated values
    tire_specs_header = [tire_specs_header ...
        ',Rotta vertical force (N),Rotta vertical displacement (mm)' ...
        ',Rotta sinkage (%),Rotta wheel horz disp (mm),Rotta contact patch length (mm)' ...
        ',Rotta contact patch width (mm),Rotta contact patch area (mm^2)' ...
        ',Rotta contact patch ellipse length (mm),Rotta contact patch ellipse width (mm)' ...
        ',Rotta contact patch ellipse area (mm^2),Rotta horz force (N)' ...
        ',Rotta net force orientation (degrees),Rotta relaxation length (mm)' ...
        ',Rotta pneumatic trail (mm),Rotta self aligning torque (N-mm)' ...
        ',Rotta norm lat stiffness (1/mm),Rotta norm corn stiffness (1/deg)' ...
        ',Rotta norm camb stiffness (1/deg)'];
    % write out first row of text column headings
    output_filename = tire_specs_filename;
    h = fopen(output_filename, 'wt');
    while h == -1
        beep;
        ButtonName = questdlg(sprintf('Could not open %s\n Retry?', ...
            output_filename), 'Error', ...
            'Yes', 'No', 'Yes');

        switch ButtonName
            case 'Yes'
                h = fopen(output_filename, 'wt');
            case 'No'
                break
        end
    end
end
if h == -1
    fprintf('Could not open %s so no results written\n', ...
            output_filename)
else
    fprintf(h, '%s\n', tire_specs_header);
    fclose(h);
    % write out matrix of values and padded digits
    dlmwrite(output_filename, tire_specs, '-append')
    fprintf('Results written to %s\n', output_filename)
end
end % if read_tire_specs == 1
t = toc(tstart);
fprintf(['All done. Evaluated %d set of tire specs in %0.4g seconds' ...

```

```

        ', at a rate of %0.3g seconds per tire spec.\n'], ...
        tire_specs_evaluated, t, t/tire_specs_evaluated)
    end
return
% *****
% *****
% Extract everything from Rotta model
%
% rip = Rotta Input Parameters structure
% rop = Rotta Output Parameters structure
%
% *****
% *****
function [rop] = Rotta_core(varargin)
    rc = Rotta_constants;
    % *****
    % Check for correct input arguments, and complain nicely if missing
    % *****
    if size(varargin,2) ~= 1
        clc; fprintf(['Input argument missing.\n' ...
            ' Use "Rotta_model.m" or "Rotta_with_beam_model.m" instead.\n'])
        return
    else
        rip = varargin{1};
        if ~isstruct(rip)
            clc; fprintf(['Input argument incorrect.\n' ...
                ' Use "Rotta_model.m" or "Rotta_with_beam_model.m" instead.\n'])
            return
        end
    end
end

if rip.relaxation_rate == 0 && rip.friction_coefficient ~= inf
    clc; fprintf(['Finite coefficient of friction with zero ...
        'relaxation rate is problematic.\n'])
    rop.cp_horz_force = 0;
    return
end
% *****
% If no displacements specified, make it explicite
% *****
if ~isfield(rip, 'displacements')
    rip.displacements = [];
end

% *****
% Check for and fill in missing parameters
% *****
if ~isfield(rip, 'relaxation_rate_out')
    rip.relaxation_rate_out = [1 1] * rip.relaxation_rate;
end
if ~isfield(rip, 'relaxation_rate_in')
    rip.relaxation_rate_in = [1 1] * rip.relaxation_rate;
end
if ~isfield(rip, 'adjust_wheel_horz_d')
    rip.adjust_wheel_horz_d = 0;
end

% *****
% Define radial cross section orientations for half tire
% *****
rip.slice_angles = linspace(0, rip.last_slice_angle, rip.num_slices);

% *****
% Indicate no known contact patch horizontal force, yet.
% *****
rip.cp_horz_force = 0;

% *****
% Non-zero slip angle with zero horizontal displacement?
% Guess a good enough horizontal displacement to get things going.

```



```

% *****
if rip.wheel_horz_d == 0 && rip.slip_angle ~= 0
    rip.wheel_horz_d = rip.slip_angle*180/pi;
end

% *****
% Search for sinkage value that produces desired vert load
% *****
if ~isnan(rip.target_vert_force) && rip.target_vert_force ~= 0
    % keyboard
    [rop] = find_sinkage(rip);
    % copy found wheel vertical displacement from output struct to input
    rip.wheel_vert_d = rop.wheel_vert_d;
end
sinkage = rip.wheel_vert_d/rip.rim_height;
% *****
% Prepare to iterate if both friction and relaxation rate specified
% *****
if rip.relaxation_rate ~= 0 && rip.friction_coefficient ~= inf
    plot_single_tire_config = rip.plot_single_tire_config; % local copy
    rip.plot_single_tire_config = 0; % suppress plotting for first time
end
iterations = 0; cp_horz_forces = []; horz_forces = [];
while 1
    if iterations == 2 && rip.plot_single_tire_config == 1
        close(gcf);
    end

    % *****
    % Calculate everything for one complete set of tire parameters
    % *****

    [rop] = calculate_tire_contact_patch(rip); % do the work
    fprintf(['\n Rotta predicts horizontal force = %0.3g N with ' ...
        ' wheel_horz_d = %0.3g mm\n'], rop.horz_force, rip.wheel_horz_d)
    iterations = iterations + 1;
    cp_horz_forces(iterations) = rop.cp_horz_force;
    horz_forces(iterations) = rop.horz_force;
    if rip.relaxation_rate ~= 0 && rip.friction_coefficient ~= inf
        if abs(rip.cp_horz_force - rop.cp_horz_force) < 0.1 || ...
            abs(rip.horz_force - rop.horz_force) / ...
            abs(rop.cp_horz_force) < 0.1
            break
        else
            if iterations >= 1 % only after first iteration
                rip.plot_single_tire_config = plot_single_tire_config;
            end
        end
    end
    % *****
    % Check for oscillations and try to damp them out.
    % *****
    if iterations >= 3 && ...
        abs((cp_horz_forces(iterations - 2) - ...
            cp_horz_forces(iterations - 1)) + ...
            (cp_horz_forces(iterations - 1) - ...
            cp_horz_forces(iterations - 0))) < 0.1
        rip.cp_horz_force = (cp_horz_forces(iterations - 1) + ...
            cp_horz_forces(iterations - 0)) / 2;
        rip.horz_force = (horz_forces(iterations - 1) + ...
            horz_forces(iterations - 0)) *2 / 3;
        fprintf(['\n Oscillations detected, trying to damp ' ...
            'them. Reducing horizontal force to %0.3g\n'], ...
            rip.horz_force);
    else % no oscillations detected, continue...
        rip.cp_horz_force = rop.cp_horz_force;
        rip.horz_force = rop.horz_force;
        % *****
        % Attempt to pick "correct" lateral displacement
        % *****
    end
end

```

```

        if rip.adjust_wheel_horz_d == 1
            if rip.slip_angle ~= 0 && rip.camber_angle == 0
                sinkage = (rip.wheel_vert_d/rip.rim_height);
                s_over_p = (sinkage / rip.inf_press);
                rip.wheel_horz_d = (4.4598 * s_over_p + 0.2598)*1.15;
                kludge = (sinkage / rip.inf_press) * rip.tire_width^2.57;
                rip.wheel_horz_d = (7.1515e-05 * kludge + 2.4252e-01)*1.17;
            end
            if rip.slip_angle == 0 && rip.camber_angle ~= 0
                fudge_factor = 50.0 * 0.14 / sinkage * ...
                    (rip.target_vert_force / 31*rc.N_per_kg);
                rip.wheel_horz_d = fudge_factor * ...
                    (max(rop.cp_center_line(1,:)) - ...
                    min(rop.cp_center_line(1,end)));
            end
        end
    end
else % rip.relaxation_rate == 0 || rip.friction_coefficient == inf
    break
end

if iterations == 10
    disp('          Reached 10 iterations, giving up.')
    break
end

end % while 1

% *****
% Set this up for whomever needs it
% *****
if ~isfield(rop, 'wheel_vert_d')
    rop.wheel_vert_d = rip.wheel_vert_d;
    rop.wheel_horz_d = rip.wheel_horz_d;
end

return

% *****
% *****
% Find sinkage necessary for specified inflation pressure and vertical load
% *****
% *****
function [rop] = find_sinkage(rip)
    rc = Rotta_constants;
    if rip.initial_sinkage_guess == 0
        disp('Bad guess of initial sinkage')
        keyboard
    end
    tstart = tic; % keep track of time to see how much we are wasting
    % *****
    % plot progress for debugging purposes
    % *****
    if rip.plot_target_vert_force_search_progress == 1
        figure; hold on; grid on; set(gcf, 'name', 'Rotta');
        xlabel('vertical displacement (mm)'); ylabel('vertical force (N)');
    end
    fprintf(['          Searching for vertical displacement that produces the ' ...
            '%0.4g N target vertical force.\n'], rip.target_vert_force)

    % *****
    % set up for searching
    % *****
    rip.plot_single_tire_config = 0; % no plotting
    rip.post_patch = 0; % don't calculate anything after contact patch
    vert_forces = zeros(1,10); % initialize for speed
    wheel_vert_ds = zeros(1,10); % initialize for speed
    tries = 1;
    wheel_vert_ds(tries) = rip.initial_sinkage_guess; % use given initial guess
    while 1

```

```

% *****
% Calculate everything for one complete set of tire parameters
% *****
rip.wheel_vert_d = wheel_vert_ds(tries);
[rop] = calculate_tire_contact_patch(rip);
vert_forces(tries) = rop.vert_force;
if rip.plot_target_vert_force_search_progress == 1
    plot(wheel_vert_ds(tries), vert_forces(tries), 'k.');
```

drawnow

```

end
if abs(100*(vert_forces(tries) - rip.target_vert_force) / ...
    rip.target_vert_force) <= rc.percent_force_tolerance
    break
end
wheel_vert_ds(tries+1) = wheel_vert_ds(tries) * ...
    rip.target_vert_force / vert_forces(tries);
if tries >= 10
    disp('          Quit after 10 tries.')
```

break

```

end
tries = tries + 1;
end
t = toc(tstart);
str = sprintf(['%d iterations and %0.4g seconds required to find %0.4g N,' ...
    '\n which is within %0.4g%% of target %0.4g N force'], ...
    tries, t, rop.vert_force, ...
    100*(vert_forces(tries) - rip.target_vert_force)/rip.target_vert_force, ...
    rip.target_vert_force);
if rip.plot_target_vert_force_search_progress == 1
    plot(wheel_vert_ds(tries), vert_forces(tries), 'bo');
```

if tries >= 2

```

    plot(wheel_vert_ds(1:2), vert_forces(1:2), 'b');
```

end

```

hold off
title(str);
end
if rip.run_silent == 0
    disp(str)
end
rop.wheel_vert_d = wheel_vert_ds(tries);
return
% *****
% *****
% Find contact patch for one tire
% *****
function [rop] = calculate_tire_contact_patch(rip)
    rc = Rotta_constants; % define all necessary constants

    % *****
    % Calculate additional wheel and tire dimensions
    % *****
    rip.rim_height = rip.tire_radius * (1 + cos(rip.rim_angle / 2));
    axle_height = rip.rim_diameter / 2 + rip.rim_height; % from axle to ground

    % *****
    % Define undeformed tire cross-section
    % *****
    t = linspace(0, 2*pi - rip.rim_angle, rc.tire_fineness) + pi/2 + rip.rim_angle/2;
    x = rip.tire_radius*cos(t); z = rip.tire_radius*sin(t);

    % *****
    % Start plots
    % *****
    tire_colors = {'r', 'm', 'r'}; % tire_lines = {'-', ':', '--'};

    str = sprintf([' Tire radius = %0.4g mm, tire width = %0.4g, rim width = %0.4g' ...
        'rim diameter = %0.4g mm,\n' ...
        ' rim height = %0.4g mm, ' ...
        'inflation pressure = %0.4g N/mm^2 (%0.4g bar, %0.4g psi)\n' ...
        ' vertical displacement = %0.4g mm (%0.4g%% sinkage), ' ...
```

```

        'horizontal displacement = %0.4g mm,\n' ...
        '        camber angle = %0.4g°, ' ...
        'slip angle = %0.4g°, ' ...
        'relaxation rate = %0.4g, ' ...
        'friction coefficient = %0.4g'], ...
    rip.tire_radius, rip.tire_width, rip.rim_width, rip.rim_diameter, ...
    rip.rim_height, rip.inf_press, (rip.inf_press / rc.MPa_per_psi) *...
    rc.bar_per_psi, rip.inf_press / rc.MPa_per_psi, ...
    rip.wheel_vert_d, 100*rip.wheel_vert_d/rip.rim_height, ...
    rip.wheel_horz_d, rip.camber_angle*180/pi, rip.slip_angle*180/pi, ...
    rip.relaxation_rate, rip.friction_coefficient);
if rip.run_silent == 0
    disp(str)
end
if rip.plot_single_tire_config == 1
    figure; set(gcf, 'name', 'Rotta');
    subplot(2,3,1); cla; axis equal; grid on; hold on;
    % plot3([x(1), x(end)], [z(1) z(end)]*0, [z(1) z(end)], 'c', x, z*0, z, 'm');
    xlim([-1 1]* rip.tire_radius * 1.5); zlim([-1 1]* rip.tire_radius * 1.5);
    xlabel('x (mm)'); ylabel('y (mm)'); zlabel('z (mm)')
    title(str); view(-1,1)

    subplot(2,3,2); cla; hold on; axis equal; grid on;
    xlabel('x (mm)'); ylabel('y (mm)');

    subplot(2,3,4); cla; hold on; grid on;
    xlabel('Horizontal displacement (blue in mm), dS (black) and dN (red) (both in N)');
    ylabel('y, distance along long axis of tire and contact patch (mm)');

    subplot(2,3,5); cla; hold on; grid on;
    xlabel('ground reaction force angle, from the vertical (°)');
    ylabel('y, distance along long axis of contact patch (mm)');

    subplot(2,3,[3 6]); cla; hold on; axis equal; grid on;
    xlabel('x (mm)'); ylabel('y (mm)'); zlabel('z (mm)')
end

% *****
% Predefine 2D rotation matrices
% *****
R2z = [ cos(rip.camber_angle) sin(rip.camber_angle);
        -sin(rip.camber_angle) cos(rip.camber_angle)];
uR2z = [ cos(-rip.camber_angle) sin(-rip.camber_angle);
         -sin(-rip.camber_angle) cos(-rip.camber_angle)];

% *****
% Prepare to loop through both halves (ends) of the contact patch
% *****
max_x = NaN; min_x = NaN; max_y = NaN;
min_y = NaN; max_z = NaN; min_z = NaN;

% *****
% Preallocate for speed, but necessary size unknown
% *****
slice_vert_ds = zeros(1, 1); slice_horz_ds = zeros(1, 1);
% can't pre-allocate these because exact size unknown and extra spaces
% screw up subsequent calculations and plotting
cpexs = []; cpeys = [];
rop.horz_force = 0; rop.cp_area = 0;
rop.relaxation_length = NaN;

% *****
% Figure out how many halves are necessary
% *****
if rip.post_patch == 1
    halves = 2;
else
    if rip.slip_angle ~= 0
        halves = 2;
    else

```

```

        halves = 1;
    end
end

% *****
% Format input displacements into expected shape
% *****
if ~isempty(rip.displacements)
    displacements = ...
        [fliplr(rip.displacements(1:length(rip.displacements)/2)); ...
         rip.displacements(length(rip.displacements)/2+1:end)];
end

% *****
% Loop through the necessary halves
% *****
for half = 1:halves
    rip.relaxation_rate = rip.relaxation_rate_out(half);
    % *****
    % Orient slip angle properly for each half of contact patch
    % *****
    half_rip.slip_angle = rip.slip_angle * (-1)^half;

    % *****
    % Prepare to loop through all cross sections (rip.num_slices) in this half
    % *****
    status = 1; % start with everything okay
    relaxing = 0; % not in the range of tire relaxing from cp yet
    told_about_sliding = 0;
    cp_guess = rip.wheel_horz_d * 0.75; % make first guess. This works for
    % vert_d = 5, horz_d < 17, and rip.camber_angle < 50
    % pre-allocate these for speed
    dy(half,:) = zeros(rip.num_slices, 1); da(half,:) = dy(half,:);
    dS(half,:) = dy(half,:); dN(half,:) = dy(half,:);
    cphxs = zeros(1,4); cphys = cphxs;

    % *****
    % Calculate each cross section (slice)
    % *****
    for slice = 1:rip.num_slices
        slice = 0; % need to use while so can manipulate slice number
        while slice < rip.num_slices
            slice = slice + 1;

            % *****
            % Calculate vertical deflection of this cross section (slice).
            % This is close, but not exact.
            % *****
            slice_vert_ds(half, slice) = cos(rip.camber_angle) * ...
                (axle_height - (axle_height - ...
                    rip.wheel_vert_d) / (cos(rip.slice_angles(slice))));
            % *****
            % Calculate effect of drum curvature, if radius ~= 0
            % *****
            if rip.drum_radius ~= 0 % allows for negative radius
                % this is an approximation that should be good enough for
                % large wheel and drum radii compared to wheel vertical
                % deflection, which is the case with narrow bicycle tires
                drum_angle = asin(axle_height * sin(rip.slice_angles(slice)) / ...
                    rip.drum_radius);

                slice_vert_ds(half, slice) = slice_vert_ds(half, slice) - ...
                    rip.drum_radius * (1 - cos(drum_angle)) / ...
                    cos(rip.slice_angles(slice));
            end

            if isnan(slice_vert_ds(half, slice))
                disp('slice_vert_ds(half, slice) = NaN')
                keyboard
            end
        end
    end
end

```

```

% *****
% Still all okay? Then keep on finding contact patch edges
% *****
if status == 1 % everything okay
    if rip.camber_angle ~= 0
        % *****
        % Calculate horizontal deflection of this slice
        % *****
        slice_horz_ds(half, slice) = rip.wheel_horz_d + ...
            tan(rip.camber_angle) * slice_vert_ds(half, slice);
        if slice == 1 && half == 1
            delta = rip.tire_radius * sin(rip.camber_angle);
            % *****
            % Can't make it perfect, iterate instead
            % *****
            correction = 0; % set this just in case
            while 1 % set up to loop through deltas
                % disp('Testing delta')
                [status, rim, tire, cp, ~, ~] = ...
                    calculate_slice_contact_patch(rip, ...
                        slice_vert_ds(half, slice), ...
                        slice_horz_ds(half, slice), cp_guess, delta);
                if status == 1 % everything okay
                    if abs(cp(1,2) - slice_horz_ds(half, slice)) > ...
                        rc.min_lat_disp
                        correction = (cp(1,2) - slice_horz_ds(half, slice));
                        delta = delta + correction;
                    else
                        break
                    end
                end
            end % while 1
        end
    else % rip.camber_angle == 0
        slice_horz_ds(half, slice) = rip.wheel_horz_d;
        delta = 0; % both of these are specific to
        correction = 0; % rip.camber_angle ~= 0
    end
    % *****
    % Calculate effect of disk curvature, if radius ~<= 0
    % *****
    if rip.disk_radius ~= 0 % allows for negative radius
        % this is an approximation that should be good enough for
        % large wheel and disk radii compared to wheel vertical
        % deflection, which is the case with narrow bicycle tires
        disk_angle = asin(axle_height * sin(rip.slice_angles(slice)) / ...
            rip.disk_radius);
        slice_horz_ds(half, slice) = slice_horz_ds(half, slice) + ...
            sign(rip.disk_radius) * 1.4 - ...
            rip.disk_radius * (1 - cos(disk_angle)) / ...
            cos(rip.slice_angles(slice));
    end
    % *****
    % Apply slip angle
    % *****
    slice_horz_ds(half, slice) = slice_horz_ds(half, slice) - ...
        (axle_height - slice_vert_ds(half, slice)) * ...
        sin(rip.slice_angles(slice)) * sin(half_rip.slip_angle);

    friction_repeat = 1; % force the first iteration
    friction_repeat_count = 0;
    while friction_repeat == 1 % set up to loop in case of sliding
        friction_repeat = 0; % default to not repeating
        friction_repeat_count = friction_repeat_count + 1;
        % *****
        % Find contact patch for one cross-sectional slice
        % *****
        phase = 1;

```



```

else
    dS_f = dy(half, slice) * ...
            (rip.horz_force / rip.cp_horz_force);
end

% *****
% check if available friction exceeded
% *****
if friction_repeat_count == 1 && ...
    abs(dS_f) > abs(dN(half, slice) * ...
        rip.friction_coefficient)
    % "periods per year" = "slices per mm"
    n = length(rip.slice_angles) / ...
        (rip.slice_angles(end)*axle_height);
    % calculate slide at the relaxation rate
    slide = slice_horz_ds(half, slice-1) * ...
        (1 + ((rip.relaxation_rate_in(half)-1) / n)) ^ ...
        (n * rip.slice_angles(2) * axle_height);
    % if not too, small go ahead and slide
    if abs(slide) >= 0.1
        slice_horz_ds(half, slice) = slide;
        if told_about_sliding == 0
            if rip.run_silent == 0
                disp('        Sliding...')
            end
            told_about_sliding = 1;
        end
    end
    friction_repeat = 1;
else % if dS_f > dN(half, slice) * ...
    if rip.plot_single_tire_config == 1
        subplot(2,3,4);
        plot(dS(half, slice) / dy(half, slice), ...
            sum(dy(half,:))*(-1)^(half), 'k.', ...
            dN(half, slice), sum(dy(half,:))*(-1)^(half), 'r. ');
        subplot(2,3,5); plot(...
            90 - atan2(dN(half, slice), ...
            dS(half, slice))*180/pi, ...
            sum(dy(half,:))*(-1)^(half), 'k. ');
    end % if rip.plot_single_tire_config == 1
    end % if dS_f > dN(half, slice) * ...
end % if slice > 1
end % if cp(1,1) >= cp(1,4)
end % if status == 1
end % while 1
end % if status == 1
if status ~= 1
    if rip.post_patch ~= 1
        if rip.run_silent == 0
            disp('        Skipping tire calculations beyond contact patch. ')
        end
        break
    else
        % *****
        % Tire is no longer in contact with ground
        % *****
        cp_len = max(max(cphys)) - min(min(cphys));

        % *****
        % Decay displacement back to zero at specified rate
        % *****
        if ~isempty(rip.displacements) || rip.relaxation_rate ~= 0 ...
            && abs(slice_horz_ds(half, slice-1)) > rc.min_lat_disp
            % *****
            % If available, apply beam displacements
            % *****
            if ~isempty(rip.displacements)
                slice_horz_ds(half, slice) = slice_horz_ds(half, slice-1) * ...
                    displacements(half, slice) / displacements(half, slice-1);
                slice_vert_ds(half, slice) = slice_vert_ds(half, slice-1) * ...

```



```

        displacements(half, slice) / displacements(half, slice-1);
else % isempty(rip.displacements)
    if relaxing == 0 % if the first time?
        relaxing = 1; % it won't be the next time

        % keep track of this for calculating relaxation len
        unrelaxed_slice(half) = slice-1;
        if rip.run_silent == 0
            disp('          Relaxing horizontal displacement.')
        end
    end
    % *****
    % Relax vert and horz displacement for this
    % slice, and must do both. This works much
    % better than just relaxing horz disp, and
    % this method is independent of slice width.
    % *****
    % y(i) = y0*exp((r-1)*x(i));
    e = exp((rip.relaxation_rate-1) * ...
            (rip.slice_angles(slice) - ...
             rip.slice_angles(unrelaxed_slice(half))) * ...
            axle_height);

    slice_horz_ds(half, slice) = ...
        slice_horz_ds(half, unrelaxed_slice(half)) * e;
    if ~isreal(slice_horz_ds(half, slice))
        slice_horz_ds(half, slice) = 0;
    end
    slice_vert_ds(half, slice) = ...
        slice_vert_ds(half, unrelaxed_slice(half)) * e;
    if ~isreal(slice_vert_ds(half, slice))
        slice_vert_ds(half, slice) = 0;
    end
    % only do this once
    if half == 1 && isnan(rop.relaxation_length)
        if slice_horz_ds(half, slice) <= ...
            slice_horz_ds(half, unrelaxed_slice(half))/exp(1)
            rop.relaxation_length = ...
                axle_height * ...
                (sin(rip.slice_angles(slice)) - ...
                 sin(rip.slice_angles(unrelaxed_slice(half))));
        end
    end % if half == 1 && isnan(rop.relaxation_length)
end % else % isempty(rip.displacements)

% *****
% Calculate shape for this relaxed horizontal disp
% *****
phase = 2;
[~, rim, tire, cp, radii, ~] = ...
    calculate_slice_contact_patch(rip, slice_vert_ds(half, slice),
    ...
        slice_horz_ds(half, slice), cp_guess, delta);

dy(half, slice) = axle_height * (sin(rip.slice_angles(slice)) - ...
                                sin(rip.slice_angles(slice-1)));
dS(half, slice) = rip.inf_press * (radii(1) - radii(2)) * ...
    dy(half, slice);
da(half, slice) = 0;
dN(half, slice) = rip.inf_press * da(half, slice);
if rip.plot_single_tire_config == 1
    subplot(2,3,4); plot(dS(half, slice) / dy(half, slice), ...
        sum(dy(half,:))*(-1)^(half), 'k.', ...
        dN(half, slice), sum(dy(half,:))*(-1)^(half), 'r.');
```

```

    subplot(2,3,5); plot(...
        90 - atan2(dN(half, slice), dS(half, slice))*180/pi, ...
        sum(dy(half,:))*(-1)^(half), 'k.');
```

```

    end
else % if rip.relaxation_rate ~= 0 && abs(slice_horz_ds(half, slice-1)) > 0.1
    phase = 3;

```

```

rim = [x(1) x(end); z(1) z(end)];
tire = [x; z];
[~, min_tire_z_idx] = min(tire(2,:));
cp = [tire(1, min_tire_z_idx); tire(2, min_tire_z_idx)];
rim = R2z*rim;
tire = R2z*tire;
%cp = R2z*cp;
slice_horz_ds(half, slice) = NaN; % 'NaN' to aid plotting
end % if rip.relaxation_rate ~= 0 && abs(slice_horz_ds(half, slice-1)) > 0.1
end % if rip.post_patch ~= 1
end % if status == 1

% *****
% Plot everything
% *****
if rip.plot_single_tire_config == 1 && half == 1
    subplot(2,3,1);
    y = -axle_height * sin(rip.slice_angles(2)) * slice;
    plot3(rim(1,:), rim(2,:)*0+y, rim(2,:), 'b', ...
          tire(1,:), tire(2,:)*0+y, tire(2,:), ...
          char(tire_colors(phase)), ...
          cp(1,:), cp(2,:)*0+y, cp(2,:), 'k');
    % *****
    % If cp has 4 columns, the middle two are center lines,
    % so don't connect them with lines when they cross outside.
    % *****
    [~,c] = size(cp);
    if c == 4
        if cp(1,2) > cp(1,1) && cp(1,2) < cp(1,4)
            plot3(cp(1,:), cp(2,:)*0+y, cp(2,:), 'g');
        else
            plot3(cp(1,[1 c]), cp(2,[1 c])*0+y, cp(2,[1 c]), 'g');
        end
    else
        plot3(cp(1,:), cp(2,:)*0+y, cp(2,:), 'g');
    end
end % if rip.plot_single_tire_config == 1

% *****
% Un-rotate camber in 2D so that it can be re-rotated in 3D
% *****
rim = uR2z*rim;
tire = uR2z*tire;
cp = uR2z*cp;

% *****
% translate and expand to 3D
% *****
rim3 = [rim(1,:); [0 0]; rim(2,:) - (axle_height - rip.tire_radius)];
tire3 = [tire(1,:); zeros(1,length(tire)); ...
         tire(2,:) - (axle_height - rip.tire_radius)];
cp3 = [cp(1,:); zeros(1,length(cp(1,:))); ...
       cp(2,:) - (axle_height - rip.tire_radius)];
% rotate about x-axis: axle
R3x = [1      0      0;
       0 cos(rip.slice_angles(slice)*(-1)^(half+1)) ...
         sin(rip.slice_angles(slice)*(-1)^(half+1));
       0 -sin(rip.slice_angles(slice)*(-1)^(half+1)) ...
         cos(rip.slice_angles(slice)*(-1)^(half+1))];
% rotate about y-axis: camber (could come out of this loop)
R3y = [cos(rip.camber_angle) 0 sin(rip.camber_angle);
       0 1 0;
       -sin(rip.camber_angle) 0 cos(rip.camber_angle)];
R3 = R3y*R3x;
rim3 = R3*rim3;
tire3 = R3*tire3;
cp3 = R3*cp3;

% *****
% Keep track of contact patch edges

```

```

% *****
if status == 1 % everything okay
    cphxs(slice,:) = cp3(1,:);
    cphys(slice,:) = cp3(2,:);
end

% *****
% Plot rim, tire, and contact patch edges in 3D
% *****
if rip.plot_single_tire_config == 1
    subplot(2,3,[3 6]);
    plot3(rim3(1,:), rim3(2,:), rim3(3,:), 'b');
    plot3(tire3(1,:), tire3(2,:), tire3(3,:), ...
          char(tire_colors(phase)));
    plot3(cp3(1,:), cp3(2,:), cp3(3,:), '.k');

    % *****
    % Extract contact patch edge coordinates from 3D model of tire
    % If cp3 has 4 columns, middle two are center lines,
    % so don't connect them with lines when they cross outside.
    % *****
    [~,c] = size(cp3);
    if c == 4
        if cp3(1,2) > cp3(1,1) && cp3(1,2) < cp3(1,4)
            plot3(cp3(1,:), cp3(2,:), cp3(3,:), 'g');
        else
            plot3(cp3(1,[1 c]), cp3(2,[1 c]), cp3(3,[1 c]), 'g');
        end
    else
        plot3(cp3(1,:), cp3(2,:), cp3(3,:), 'g');
    end

    % *****
    % Keep track of these for setting limits at the end
    % *****
    max_x = max([max_x tire3(1,:)]);
    min_x = min([min_x tire3(1,:)]);
    max_y = max([max_y tire3(2,:)]);
    min_y = min([min_y tire3(2,:)]);
    max_z = max([max_z tire3(3,:)]);
    min_z = min([min_z tire3(3,:)]);
end
end % for slice = 1:rip.num_slices

[r,~] = size(cphxs); % get number of rows
if r > 1 % if results exist, not just first row of zeros
    % *****
    % Assemble complete contact patch boarder to calculate area,
    % from two, assymmetrical halves (created by slip angle)
    % *****
    cph_cl = [cphxs(:,2)'; cphys(:,2)']; % extract center line
    if half == 1
        cphxs = [cphxs(:,1); flipud(cphxs(:,2)); ...
                cphxs(:,3); flipud(cphxs(:,4))];
        cphys = [cphys(:,1); flipud(cphys(:,2)); ...
                cphys(:,3); flipud(cphys(:,4))];
    else
        cphxs = [cphxs(:,1); flipud(cphxs(:,2)); ...
                cphxs(:,3); flipud(cphxs(:,4))];
        cphys = [cphys(:,1); flipud(cphys(:,2)); ...
                cphys(:,3); flipud(cphys(:,4))];
    end
    rop.cp_area = rop.cp_area + polyarea(cphxs, cphys);
    cpexs = [cpexs; cphxs];
    cpeys = [cpeys; cphys];
    if half == 1
        cp_cl = fliplr(cph_cl);
    else
        cp_cl = [cp_cl cph_cl];
    end
end

```

```

% *****
% Sum up lateral force and contact patch length
% *****
cp_half_length = (max(max(cphys)) - min(min(cphys)));
ys(half,:) = cumsum(dy(half,:));

% calculate pneumatic trail for this half of contact patch
rop.pneumatic_trails(half) = (sum(ys(half, ys(half,:) <= cp_half_length) ...
    .* dS(half, ys(half,:) <= cp_half_length)) / ...
    sum(dS(half, ys(half,:) ...
    <= cp_half_length))*(-1)^(half+1);
rop.horz_forces(half) = sum(dS(half,:));
else
    disp('Something went wrong and there are no results to plot.')
    break
end
end % for half = 1:2
if halves == 1 && rip.run_silent == 0
    disp('          Skipping second half of symmetrical contact patch.')
end

% *****
% Put everything into format expected by caller
% *****
rop.dS = [fliplr(dS(1,:)) dS(halves,:)];
rop.dN = [fliplr(dN(1,:)) dN(halves,:)];
rop.slice_horz_ds = [fliplr(slice_horz_ds(1,:)) slice_horz_ds(halves,:)];
rop.slice_vert_ds = [fliplr(slice_vert_ds(1,:)) slice_vert_ds(halves,:)];
rop.horz_force = sum(rop.horz_forces);
% combine pneumatic trails from both halves
rop.pneumatic_trail =
sum(abs(rop.horz_forces).*rop.pneumatic_trails)/sum(abs(rop.horz_forces));
rop.self_aligning_torque = rop.pneumatic_trail * rop.horz_force;
rop.cp_area = rop.cp_area * 2 / halves; % double area if only did one half
rop.cp_length = max(max(cpeys)) - min(min(cpeys)) * 2 / halves;
rop.cp_width = max(max(cpexs)) - min(min(cpexs));
rop.cp_center_line = cp_cl;
rop.axle_height = axle_height;
if halves == 2 % only if we did both sizes
    rop.cp_horz_force = sum(rop.dS(rip.num_slices-cp_end_slice(1) : ...
        rip.num_slices+1+cp_end_slice(2))); % in N
else
    rop.cp_horz_force = 0;
end
rop.cp_end_slice = cp_end_slice;
rop.vert_force = rop.cp_area * rip.inf_press;
rop.net_force_orientation = atan2(rop.horz_force, rop.vert_force) * 180/pi;
str = sprintf(['    Vertical force = %0.4g N (%0.4g kg, %0.4g lb)\n' ...
    '    Horizontal force = %0.4g N (%0.4g kg, %0.4g lb),' ...
    ' which normalizes to %0.4g\n' ...
    '    Resultant force orientation = %0.4g° from' ...
    ' vertical, (%0.4g% of camber angle)\n' ...
    '    Relaxation length = %0.4g mm'], ...
    rop.vert_force, rop.vert_force / rc.g, rop.vert_force / rc.N_per_lb,
    ...
    rop.horz_force, rop.horz_force / rc.g, rop.horz_force / rc.N_per_lb,
    ...
    rop.horz_force/rop.vert_force, ...
    rop.net_force_orientation, ...
    100 * rop.net_force_orientation / (rip.camber_angle*180/pi), ...
    rop.relaxation_length);
if rip.wheel_horz_d ~= 0 && rip.slip_angle == 0 && rip.camber_angle == 0
    static_lateral_stiffness = rop.horz_force/rip.wheel_horz_d;
    str = [str ...
        sprintf(['    Static lateral stiffness = %0.4g N/mm' ...
            ' (%0.4g 1/mm)'], ...
            static_lateral_stiffness, ...
            static_lateral_stiffness/rop.vert_force)];
elseif rip.wheel_horz_d ~= 0 && rip.slip_angle ~= 0 && rip.camber_angle == 0

```

```

cornering_stiffness = rop.horz_force/(rip.slip_angle*180/pi);
str = [str ...
      sprintf(['', Cornering stiffness = %0.4g N/degree' ...
              ' (%0.4g 1/degree)'], ...
              cornering_stiffness, ...
              cornering_stiffness/rop.vert_force)];
elseif rip.wheel_horz_d ~= 0 && rip.slip_angle == 0 && rip.camber_angle ~= 0
camber_stiffness = rop.horz_force/(rip.camber_angle*180/pi);
str = [str ...
      sprintf(['', Camber stiffness = %0.4g N/degree' ...
              ' (%0.4g 1/degree)'], ...
              camber_stiffness, ...
              camber_stiffness/rop.vert_force)];
end
if rip.plot_single_tire_config == 1
subplot(2,3,[3 6]); title(str);

subplot(2,3,4); title(sprintf( ...
['Horizontal (dS) and vertical (dN) force per unit length (N/mm)\n' ...
 'actual horizontal deflections vary from %0.4g to %0.4g mm'], ...
max(max(slice_horz_ds)), min(min(slice_horz_ds))));
cp_force_per_length = rop.horz_force/rop.cp_length;
plot(cp_cl * 0 + cp_force_per_length, cp_cl, 'g. ');
ylim([-1 1] * axle_height * rip.last_slice_angle);

subplot(2,3,5); title(sprintf( ...
['Ground reaction force orientation (from the vertical) '...
 'per contact patch section\n' ...
 'actual vertical deflections vary from %0.4g to %0.4g mm'], ...
max(max(slice_vert_ds)), min(min(slice_vert_ds))));

end
if rip.run_silent == 0
disp(str)
fprintf(['          Contact patch length = %0.4g mm ' ...
        'area = %0.4g mm^2\n'], rop.cp_length, rop.cp_area)
end

% *****
% Fit an ellipse to contact patch with same algorithm used
% for ink prints
% *****
if rip.camber_angle == 0 && rip.slip_angle == 0 && rip.wheel_horz_d == 0
ellipse_t = fit_ellipse(cpexs, cpeys);
t = linspace(0, 2*pi); % redo so it goes all the way around
ellipse_x = ellipse_t.X0_in + ...
            ellipse_t.long_axis/2 * cos(t) * cos(-ellipse_t.phi) - ...
            ellipse_t.short_axis/2 * sin(t) * sin(-ellipse_t.phi);
ellipse_y = ellipse_t.Y0_in + ...
            ellipse_t.long_axis/2 * cos(t) * sin(-ellipse_t.phi) + ...
            ellipse_t.short_axis/2 * sin(t) * cos(-ellipse_t.phi);
ellipse_area = pi*ellipse_t.long_axis*ellipse_t.short_axis/4;
rop.ellipse_cp_length = ellipse_t.long_axis;
rop.ellipse_cp_width = ellipse_t.short_axis;
rop.ellipse_cp_area = ellipse_area;
else
rop.ellipse_cp_length = NaN;
rop.ellipse_cp_width = NaN;
rop.ellipse_cp_area = NaN;
end

if rip.plot_single_tire_config == 1
subplot(2,3,2); fill(cpexs, cpeys, 'g');
xlim([min(min(cpeys)) max(max(cpeys))] * 1.05 + cpexs(1,1));
ylim([min(min(cpeys)) max(max(cpeys))] * 1.05);
title(sprintf(['Contact patch length = %0.4g mm (%0.4g in),\n' ...
              'width = %0.4g mm (%0.4g in),\n' ...
              'area = %0.4g mm^2 (%0.4g in^2)'], ...
              rop.cp_length, rop.cp_length / rc.mm_per_in, ...
              rop.cp_width, rop.cp_width / rc.mm_per_in, ...

```

```

        rop.cp_area, rop.cp_area / rc.mm_per_in^2));

if rip.camber_angle == 0 && rip.slip_angle == 0 && rip.wheel_horz_d == 0
    hold on; plot(ellipse_y, ellipse_x, 'b', 'linewidth', 2);
    xl = xlim;
    text(xl(1)*0.9, 0, ...
        sprintf(['Fitted ellipse(in blue)\n' ...
            'has length = %0.4g mm\n (%0.4g in) %0.4g%%,\n' ...
            'width = %0.4g mm\n (%0.4g in) %0.4g%%,\n' ...
            'area = %0.4g mm^2\n (%0.4g in^2) %0.4g%%'], ...
            ellipse_t.long_axis, ...
            ellipse_t.long_axis / rc.mm_per_in, ...
            100 * ellipse_t.long_axis / rop.cp_length, ...
            ellipse_t.short_axis, ...
            ellipse_t.short_axis / rc.mm_per_in, ...
            100 * ellipse_t.short_axis / rop.cp_width, ...
            ellipse_area, ellipse_area / rc.mm_per_in^2, ...
            100 * ellipse_area / rop.cp_area));
    hold off
end
end
% *****
% Wrap up all plots: hold off, set limits and view angle for 3D
% *****
if rip.plot_single_tire_config == 1
    subplot(2,3,4); xl = xlim; plot(xl, [1 1]*(-rop.pneumatic_trail), 'k');
    text((xl(1) + xl(2))/2.5, -rop.pneumatic_trail+6, ...
        sprintf('Pneumatic trail = %0.3g mm', rop.pneumatic_trail));
    beam_length = 2 * (rip.rim_diameter/2 + rip.tire_radius) * max(rip.slice_angles);
    xint = linspace(0, beam_length/2, rip.num_slices);
    xint = [-fliplr(xint) xint]; % this dupes center point to match rest
    subplot(2,3,4); plot(rop.slice_horz_ds, xint, 'b.');
```

```

% plot measured vs. modeled centerline displacement. matches:
% rip.wheel_vert_d = 2.866; % positive = rim sags towards ground
% rip.wheel_horz_d = 1.1;
% rip.slip_angle = 0.55*pi/180; % angle contact patch center line angle
% rip.camber_angle = 0*pi/180; % positive = rim tilts to right
% rip.relaxation_rate_out(2) = 0.991; % before touches ground
% rip.relaxation_rate_in(2) = 0.991; % just after touching ground
% rip.relaxation_rate_in(1) = 0.98; % just before leaving ground
% rip.relaxation_rate_out(1) = 0.995; % after leaving ground
% rip.relaxation_rate = 1;
% rip.friction_coefficient = 4; % 1 for non-skid tape
% h = gcf;
% load('tire_centerline_lateral_displacement.mat')
% figure; plot(x-530, y, 'g.');
```

```

% hold on; grid on
% plot(-xint, rop.slice_horz_ds, 'b.');
```

```

% plot(-xint(rip.num_slices-unrelaxed_slice(1): ...
%     rip.num_slices+1+unrelaxed_slice(2)), ...
%     rop.slice_horz_ds(rip.num_slices-unrelaxed_slice(1): ...
%     rip.num_slices+1+unrelaxed_slice(2)), 'r.');
```

```

% legend('measured', 'modeled'); set(gcf, 'Position', [38 499 1879 602]);
% xlabel('distance along tire (mm)'); ylabel('lateral deflection (mm)')
% figure(h);

subplot(2,3,1); hold off; subplot(2,3,2); hold off;
subplot(2,3,4); hold off; yl = ylim;
subplot(2,3,5); hold off; ylim(yl);
subplot(2,3,[3 6]); hold off;
% view(90, 0); % perfect side view
view(-10, 15); % nice view into open end of section
xlim([min_x max_x]); ylim([min_y max_y]); zlim([min_z max_z]);
set(gcf, 'Position', [1 1 1920 1124], 'Color', 'white')
end
if rip.plot_single_tire_config == 1 && rip.plot_wheel_horz_d == 1
    figure; set(gcf, 'name', 'Rotta');
    subplot(3,1,1); plot(xint, rop.slice_horz_ds, 'b.-');
    ylabel('Horizontal displacements'); xlabel('Beam location (mm)')
    title(sprintf('Slices = %g, relaxation rate = %g', ...

```

```

        rip.num_slices, rip.relaxation_rate))
        subplot(3,1,2); plot(xint, rop.dS); ylabel('dS')
        subplot(3,1,3); plot(xint, rop.dN); ylabel('dN')
    end
return

% *****
% *****
% Find contact patch and tire shape for one cross-sectional slice
% *****
% *****
function [status, rim, tire, cp, radii, angles] = ...
    calculate_slice_contact_patch(rip, ...
        slice_vert_d, slice_horz_d, cp_guess, delta)

rc = Rotta_constants; % define all necessary constants

slice_horz_d = slice_horz_d - delta;

% *****
% Specify local parameters
% *****
status = 1; % assume success

% *****
% Calculate additional wheel and tire dimensions for use below
% *****
rip.rim_angle = 2 * asin(rip.rim_width / (2 * rip.tire_radius)); % of
rip.rim_height = rip.tire_radius * (1 + cos(rip.rim_angle / 2)); % tire
tire_circumference = rip.tire_radius * (2 * pi - rip.rim_angle); % from
% rim to rim
% *****
% define un-translated and un-rotated rim
% *****
rip.rim_widths = [-1 0 1] * rip.rim_width/2;
rip.rim_heights = [0 0 0] + (rip.rim_height - rip.tire_radius);

% *****
% Origin is at center of undeformed tire cross section. Per Rotta,
% x is horizontal, z is vertical, and y is normal to cross section
% so camber rotates about z-axis in 2D
% *****
R2z = [ cos(rip.camber_angle) sin(rip.camber_angle);
        -sin(rip.camber_angle) cos(rip.camber_angle)];
xy = R2z*[rip.rim_widths; rip.rim_heights];
rip.rim_widths(1) = xy(1,1);
rip.rim_widths(2) = xy(1,3);
rip.rim_widths(3) = xy(1,2);
rip.rim_heights(1) = xy(2,1);
rip.rim_heights(2) = xy(2,3);
rip.rim_heights(3) = xy(2,2);
% note that mid-point gets moved to end so that side 2 is element 2

% *****
% pre-allocate, for speed
% *****
cp_edges = [0 0]; cp_mids = [0 0]; ctr_x = [0 0]; ctr_z = [0 0];
s = [0 0]; r = [0 0]; a = [0 0];

for side = 1:2
    % *****
    % calculate actual side bulge arc length, radius, and theta
    % try using MATLAB's fzero() instead of a while loop
    % Woo Hoo! takes only 25% of time required by while loop
    % first, make sure initial guess is okay. Adjust as necessary
    % *****
    if slice_vert_d > 1
        x0 = [cp_guess rip.rim_width*(-1)^side];
        while 1
            for i = 1:2

```

```

        cp_edge = x0(i);
        y0(i) = (((rip.rim_widths(side) - cp_edge)^2 + ...
            (rip.rim_heights(side) + rip.tire_radius - slice_vert_d)^2) / ...
            (2 * (rip.rim_heights(side) + rip.tire_radius - slice_vert_d)))
* ...
            (pi - asin((rip.rim_widths(side) - cp_edge) * (-1)^(side) / ...
            ((rip.rim_widths(side) - cp_edge)^2 + ...
            (rip.rim_heights(side) + rip.tire_radius - slice_vert_d)^2) / ...
            (2 * (rip.rim_heights(side) + rip.tire_radius - slice_vert_d
)))))) - ...
            (tire_circumference/2 - ...
            cp_edge * (-1)^(side) + ...
            slice_horz_d * (-1)^(side));
    end
    if sign(y0(1)) == sign(y0(2))
        if rip.run_silent == 0
            disp('Shifting range of fzero()')
        end
        x0(1) = x0(1) + (x0(1) - x0(2))/2;
        x0(2) = x0(2) + (x0(2) - x0(1))/2;
    else
        break;
    end
end % while 1
else
    x0 = cp_guess;
end
% *****
% Finally, calculate contact patch edge location
% Origin of coordinate system used is center of undeformed tire
% *****
cp_edges(side) = fzero(@(cp_edge) ...
    (((rip.rim_widths(side) - cp_edge)^2 + ...
    (rip.rim_heights(side) + rip.tire_radius - slice_vert_d)^2) / ...
    (2 * (rip.rim_heights(side) + rip.tire_radius - slice_vert_d))) * ...
    (pi - asin((rip.rim_widths(side) - cp_edge) * (-1)^(side) / ...
    ((rip.rim_widths(side) - cp_edge)^2 + ...
    (rip.rim_heights(side) + rip.tire_radius - slice_vert_d)^2) / ...
    (2 * (rip.rim_heights(side) + rip.tire_radius - slice_vert_d)))))) - ...
    (tire_circumference/2 - ...
    cp_edge * (-1)^(side) + ...
    slice_horz_d * (-1)^(side))), ...
    x0);
% *****
% subtract slice_horz_d from rubber on side one,
% so side one is the left side. Camber angle already
% incorporated in rim location used in next step.
% *****
s(side) = tire_circumference/2 - ...
    cp_edges(side) * (-1)^(side) + ...
    slice_horz_d * (-1)^(side);

% *****
% calculate radius of side bulge via
%  $r^2 = x^2 + (z - r)^2 \Rightarrow r = (x^2 + z^2)/(2z)$  where
%  $x = \text{rip.rim\_width} - \text{cp\_edge}$ 
%  $z = \text{rip.rim\_height} + \text{rip.tire\_radius} - \text{slice\_vert\_d}$ 
% *****
r(side) = ((rip.rim_widths(side) - cp_edges(side))^2 + ...
    (rip.rim_heights(side) + rip.tire_radius - slice_vert_d)^2) / ...
    (2 * (rip.rim_heights(side) + rip.tire_radius - slice_vert_d));

% *****
% calculate angle swept by radius of side bulge
% via  $\theta = \pi - \text{asin}(x/r)$ 
% *****
a(side) = pi - ...
    asin((rip.rim_widths(side) - cp_edges(side)) * (-1)^(side) / ...
    r(side));

```



```

% *****
% See if we have exceeded the tire circumference yet
% *****
if abs(r(side)*a(side) - s(side)) > rc.circumference_tolerance % short?
    disp('          Ran out of tire while calculating bulge arc length.')
    keyboard;
    status = 0; % not okay
end

% *****
% Define tire bulge for this side:
%   First, point at center of curve, straight up from cp edges
% *****
ctr_x(side) = cp_edges(side);
ctr_z(side) = r(side) - rip.tire_radius + slice_vert_d;

% *****
%   Then, define tire arcs about that center point
% *****
t = linspace(0, a(side), rc.tire_fineness/2 + 1) - pi/2;
x = ctr_x(side) + r(side) * cos(t)*(-1)^side;
z = ctr_z(side) + r(side) * sin(t);

% *****
%   Assemble both sides into single long array for drawing
% *****
if side == 1
    tire = [fliplr(x); fliplr(z)]; % flip so pnts end up in order
else
    tire = [tire(1,:) NaN x;
            tire(2,:) NaN z];
end

% *****
% Calculate where bottom-dead-center ended up
% add to edge of contact patch location the difference between
% radius*angle of side bulge and original length of side to bdc
% *****
cp_mids(side) = x(1) + (r(side)*a(side) - rip.tire_radius * ...
    (pi - 0.5*rip.rim_angle - rip.camber_angle*(-1)^side))*(-1)^side;

end % for side = 1:2

% *****
% Format results as expected by calling function
% *****
rim = [rip.rim_widths(1:2); rip.rim_heights(1:2)];
cp = [[cp_edges(1) cp_mids(1) cp_mids(2) cp_edges(2)]; ...
      [1 1 1 1]*(-rip.tire_radius + slice_vert_d)];
radii = r;
angles = a;

% *****
% Check results
% *****
carcass_width = 0;
i = 2;
while i < length(tire)
    if ~isnan(tire(1,i))
        carcass_width = carcass_width + ...
            sqrt((tire(1, i) - tire(1, i-1))^2 + ...
                (tire(2, i) - tire(2, i-1))^2);
        i = i + 1;
    else % jump over, but measure, contact patch
        carcass_width = carcass_width + ...
            sqrt((tire(1, i+1) - tire(1, i-1))^2 + ...
                (tire(2, i+1) - tire(2, i-1))^2);
        i = i + 2;
    end
end
end

```

```

% carcass_width_target = r(1)*a(1)+r(2)*a(2) + cp(1,4) - cp(1,1);
% if abs(carcass_width_target - tire_circumference) > 0.5 || ...
%   abs(carcass_width - tire_circumference) > 0.5
%   str = sprintf(['Uh oh. Tire carcass width came out wrong:\n' ...
%               '   carcass width = %0.4g mm,\n' ...
%               '   tire circumference = %0.4g mm\n' ...
%               '   for a difference = %0.4g mm (%0.4g%%)'], ...
%               carcass_width, tire_circumference, ...
%               (carcass_width - tire_circumference), ...
%               100*(carcass_width - tire_circumference) / ...
%               tire_circumference);
%   if rip.run_silent == 0
%       disp(str)
%   end
% end
% end
return
% *****
% *****
% define some constants for conversion, initialization, etc.
% *****
% *****
function [h] = Rotta_constants

% *****
% Unit conversions
% *****
h.MPa_per_psi = 0.00689475728; % Netwons/mm^2 = MPa
h.MPa_per_bar = 0.1;          % Netwons/mm^2 = MPa
h.bar_per_psi = 0.0689475728; % 1 bar = 0.1 newton/square millimeter
h.N_per_lb = 4.4482216;      % Newtons per pound
h.N_per_kg = 9.81;           % Newtons per kilogram
h.mm_per_in = 25.4;          % millimeters per inch
h.g = 9.81;                  % acceleration of gravity

% *****
% Program constants
% *****
h.circumference_tolerance = 0.01; % total tire circumference tolerance
h.tire_fineness = 1000;          % number of points used to define tire
h.percent_force_tolerance = 0.1; %
h.min_lat_disp = 0.1;           % when to quit relaxing lateral dispacemnt
return

```

APPENDIX D

ADDITIONAL TEST DEVICE DESIGNS

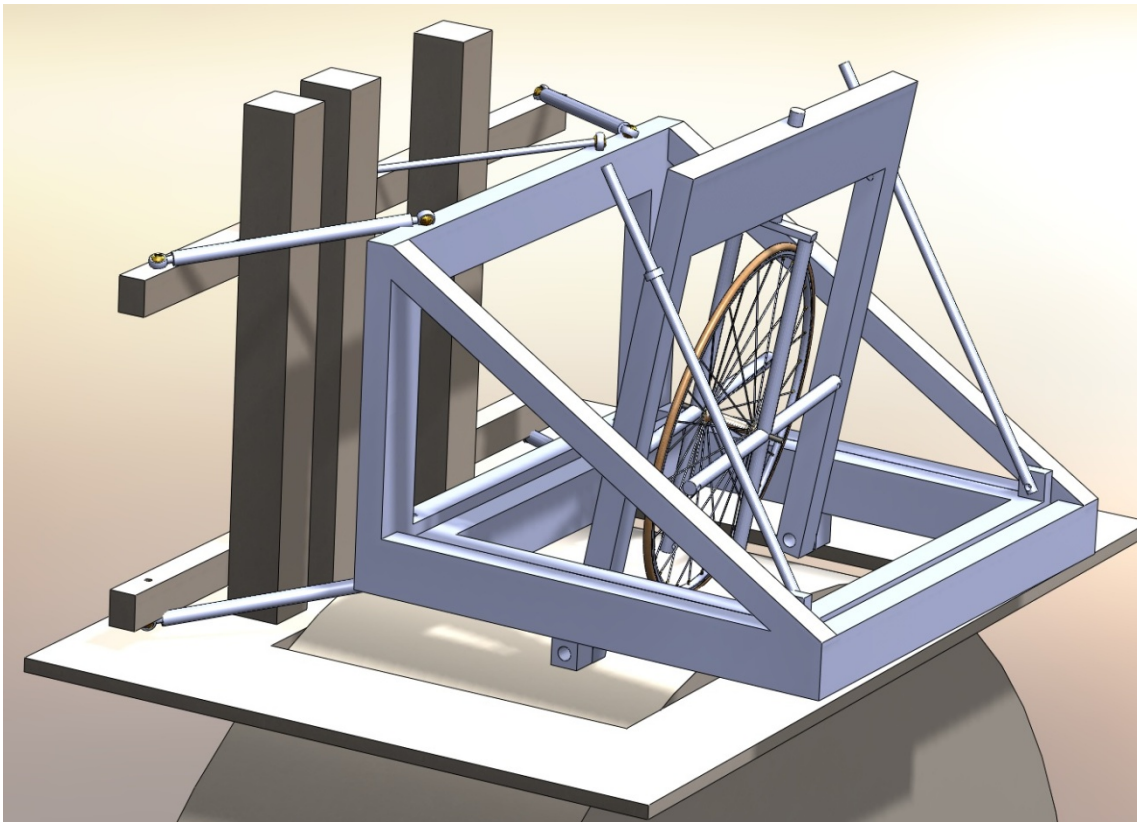


Figure 8-1: Alternate test device design for TU Delft drum

An early design for a test device to mount above the TU Delft 2.5 meter drum was based on a system of links. It was eventually rejected for being likely too complicated for the budget and manufacturing techniques available.

BIBLIOGRAPHY

- [1] Calspan Corporation, "Calspan: Safer Highways, Safer Skies," 2013. [Online]. Available: <http://www.calspan.com/>.
- [2] H. B. Pacejka, *Tyre and Vehicle Dynamics*, Elsevier, 2006.
- [3] V. Cossalter, R. Lot and M. Massaro, "An advanced multibody code for handling and stability analysis of motorcycles," *Meccanica, An international Journal of Theoretical and Applied Mechanics*, 2010.
- [4] A. L. Schwab, J. Papadopoulos, A. Ruina and A. Dressel, "JBike6," Cornell University, 2006. [Online]. Available: http://ruina.tam.cornell.edu/research/topics/bicycle_mechanics/JBike6_web_folder/index.htm.
- [5] V. Cossalter, *Motorcycle Dynamics*, Lulu, 2006.
- [6] J. P. Meijaard, J. M. Papadopoulos, A. Ruina and A. L. Schwab, "Linearized dynamics equations for the balance and steer of a bicycle: a benchmark and review," *Proceedings of the Royal Society A*, vol. 463, p. 1955–1982, 2007.
- [7] R. S. Sharp, "On the Stability and Control of the Bicycle," *Applied Mechanics Reviews*, vol. 61, no. 6, pp. 060803-06080324, 2008.
- [8] M. Plochl, J. Edelmann, B. Angrosch and C. Ott, "On the wobble mode of a bicycle," *Vehicle System Dynamics*, vol. 50, no. 3, pp. 415-429, 2012.
- [9] P. Hawken, A. Lovins and L. H. Lovins, *Natural Capitalism*, First ed., Little, Brown and Company, 1999, p. 272.
- [10] J. D. G. Kooijman, A. L. Schwab and J. P. Meijaard, "Experimental validation of a model of an uncontrolled bicycle," *Multibody System Dynamics*, vol. 19, pp. 115-132, 2008.

- [11] V. Cossalter, A. Doria, R. Lot, N. Ruffo and M. Salvador, "Dynamic Properties of Motorcycle and Scooter Tires: Measurement and Comparison," *Vehicle System Dynamics*, vol. 39, no. 5, pp. 329-352, 2003.
- [12] R. S. Sharp, "The Stability and Control of Motorcycles," *Journal Mechanical Engineering Sciences*, vol. 15, no. 5, pp. 316-329, 1971.
- [13] R. D. Roland, "Computer Simulation of Bicycle Dynamics," in *Proceedings of ASME*, 1973.
- [14] "Human Control of a Bicycle, System Identification," August 2012. [Online]. Available: <http://moorepants.github.com/dissertation/systemidentification.html>. [Accessed March 2013].
- [15] A. E. Dressel and A. Rahman, "Benchmarking Bicycle and Motorcycle Equations of Motion," in *Proceedings of the ASME 2011 International Design Engineering Technical Conferences*, Washington, DC, 2011.
- [16] R. T. Uil, "Non-lagging effect of motorcycle tyres," Eindhoven University of Technology, Eindhoven, 2006.
- [17] H. B. Pacejka and R. S. Sharp, "Shear Force Development by Pneumatic Tyres in Steady State Conditions: A Review of Modelling Aspects," *Vehicle System Dynamics*, vol. 20, pp. 121-176, 1991.
- [18] H. Sakai, O. Kanaya and H. Iijima, "Effect of main factors on dynamic properties of motorcycle tires," Society of Automotive Engineers, Warrendale, Pa, 1979.
- [19] D. R. Roland, "Bicycle Dynamics, Tire Characteristics, and Rider Modeling," CALSPAN, Buffalo, 1972.
- [20] J. A. Davis, "Bicycle tire testing - Effects of Inflation Pressure & Low Coefficient Surfaces," CALSPAN, Buffalo, 1975.
- [21] G. K. Man and T. R. Kane, "790187: Steady Turning of Two-Wheeled Vehicles," Society of Automotive Engineers, 1979.
- [22] P. Basu-Mandal, A. Chatterjee and J. M. Papadopoulos, "Hands-free

- circular motions of a benchmark bicycle," *Proc. R. Soc. A*, vol. 463, p. 1983–2003, 5 June 2007.
- [23] C. R. Kyle, "Gm tire test report on 17" moulton tires. Technical report, General Motors.," 1987.
- [24] C. R. Kyle, "GM Sunraycer case history, chapter 3-3: The Sunraycer, Wheels, Tires and Brakes. Number M-101.," Society of Automotive Engineers, Warrendale, PA, 1988.
- [25] C. R. Kyle, "Abbreviated tire test report, U. S. cycling team. Technical report, General Motors.," 1996.
- [26] C. R. Kyle, "Coast down tests in a university hallway using an instrumented and weighted tricycle. Technical report," University of California, Long Beach, CA, 1996.
- [27] D. J. Cole and Y. H. Khoo, "Prediction of vehicle stability using a 'back to back' tyre test method," *International Journal of Vehicle Design*, vol. 26, no. 5, pp. 573-584, 2001.
- [28] A. Doria, M. Tognazzo, G. Cusimano, V. Bulsink, A. Cooke and B. Koopman, "Identification of the mechanical properties of bicycle tyres for modelling of bicycle dynamics," *Vehicle System Dynamics*, 2012.
- [29] M. Gipser, "FTire Software: Advances in Modelization and Data Supply," in *Tire Science and Technology*, Akron, OH, 2006.
- [30] A. Waheed, "Michelin Power One Race Tire Review," *MotorcycleUSA*, 11 April 2011.
- [31] R. S. Rice, "Accident Avoidance Capabilities of Motorcycles," Calspan Corporation, Buffalo, NY, 1975.
- [32] E. J. H. de Vries and H. B. Pacejka, "Motorcycle Tyre Measurements and Models," *Vehicle System Dynamics*, vol. 29, pp. 280-298, 1998.
- [33] I. Kageyama and S. Kuwahara, "A study on tire modeling for camber thrust and camber torque," *JSAE Review*, vol. 23, no. 3, p. 325–331, 2002.
- [34] R. Berritta, V. Cossalter, A. Doria and N. Ruffo, "Identification of motorcycle tire properties by means of a testing machine," *Proc. 2002 SEM Annual Conference and Exposition on*

Experimental and Applied Mechanics, pp. 116-119, 2002.

- [35] S. Brown and J. Allen, "Tire Sizing Systems," 12 June 2012. [Online]. Available: <http://sheldonbrown.com/tire-sizing.html#dishonest>. [Accessed 20 Feb 2013].
- [36] National Floor Safety Institute, "Certified Products," 17 Sept 2012. [Online]. Available: http://www.nfsi.org/certified_products.php. [Accessed 20 Feb 2013].
- [37] A. Dressel and A. Rahman, "Measuring sideslip and camber characteristics of bicycle tyres," *Vehicle System Dynamics*, 2011.
- [38] PASCO, "PASCO Support Product Manuals," 2013. [Online]. Available: <http://store.pasco.com/manuals/>.
- [39] D. G. Wilson and J. Papadopoulos, *Bicycling Science*, 3rd ed., Cambridge, MA: The MIT Press, 2004.
- [40] Roues Artisanales, "Great wheel test – Part 3 – Stiffness," 27 Oct 2008. [Online]. Available: <http://www.rouesartisanales.com/article-23159755.html>. [Accessed 19 Feb 2013].
- [41] T. Foale, *Motorcycle Handling and Chassis Design*, Tony Foale Designs, 2006.
- [42] G. Baffet, A. Charara and J. Stéphant, "Sideslip angle, lateral tire force and road friction estimation in simulations and experiments," in *Proceedings of the 2006 IEEE, Munich*, 2006.
- [43] C. L. Phillips and R. D. Harbor, *Basic Feedback Control Systems*, Englewood Cliffs: Prentice-Hall Inc., 1991, pp. 116-119.
- [44] Y. Watanabe, "The Mechanism of Camber Thrust Generation in a Bias-ply Motorcycle Tire," *Vehicle System Dynamics*, vol. 13, no. 4, pp. 173-186, 1984.
- [45] V. J. Rotta, "Zur Statik des Luftreifens (For the statics of the tire)," *Ingenieur-Archiv (Engineer Archive)*, vol. XVII, pp. 129-141, 1949.
- [46] L. F. Shampine, I. Gladwell and S. Thompson, *Solving ODEs with MATLAB*, Cambridge University Press, 2003, p. 164.

- [47] S. K. Clark, *Mechanics of Pneumatic Tires*, Washington DC: US Department of Transportation, National Highway Traffic Safety Administration, 1981.
- [48] M. I. Lyasko, "The Determination of Deflection and Contact Characteristics of a Pneumatic Tire on a Rigid Surface," *Journal of Terracechanics*, vol. 31, no. 4, pp. 239-246, 1994.
- [49] C. R. Kyle, "Gm test of tire characteristics on a flat track slow speed steel band," General Motors, 1995.
- [50] R. Carvel and A. N. Beard, *The Handbook Of Tunnel Fire Safety*, Thomas Telford, 2005.

CURRICULUM VITAE

Andrew Erwin Dressel

Born in Meriden, Connecticut

Education

B.S., Rensselaer Polytechnic Institute, May 1985
Major: Computer Science

M. Eng., Cornell University, May 2003
Major: Theoretical and Applied Mechanics

M. S., Cornell University, December 2006
Major: Mechanics

Dissertation Title: Measuring and Modeling the Mechanical Properties of Bicycle Tires

Teaching Experience

Milwaukee School of Engineering, 2010-Present
Statics, Dynamics, Strength of Materials, Finite Element Analysis

University of Wisconsin-Milwaukee, 2008-2011
Statics, Dynamics, Strength of Materials, Finite Element Analysis

Awards/Honors

UWM Chancellors' Award, 2008-2013

UWM Graduate Research Poster Competition
2010: Third Place,
2011: Honorable Mention

Publications

“Comment on ‘On the stability of a bicycle on rollers’”, *European Journal of Physics*, 2012

“Measuring side slip and camber characteristics of bicycle tyres”, *Vehicle System Dynamics*, 2011

“Benchmarking Bicycle and Motorcycle Equations of Motion”, *Proceedings of the ASME 2011 International Design Engineering Technical Conferences & Computers and Information in Engineering Conference*, 2011

“Measuring Dynamic Properties of Bicycle Tires”, *Proceedings of the Bicycle and Motorcycle Dynamics Symposium*, 2010

“Promoting Holistic Problem Solving in Mechanics Pedagogy”, *Proceedings of American Society for Engineering Education Conference*, 2007